



Hashemite Kingdom of Jordan



Jordan Journal of



Biological Sciences

An International Peer-Reviewed Scientific Journal

Financed by the Scientific Research and Innovation Support Fund



<http://jjbs.hu.edu.jo/>

Jordan Journal of Biological Sciences (JJBS) (ISSN: 1995–6673 (Print); 2307-7166 (Online)): An International Peer- Reviewed Open Access Research Journal financed by the Scientific Research and Innovation Support Fund, Ministry of Higher Education and Scientific Research, Jordan and published quarterly by the Deanship of Scientific Research , The Hashemite University, Jordan.

Editor-in-Chief

Professor 'Y g f {cp, 'O qj co o gf C.
Environmental Biochemistry
The Hashemite University

Assistant Editor

Dr. Muhannad, Massadeh I.
Microbial Biotechnology,
The Hashemite University

Editorial Board (Arranged alphabetically)

Professor Al-Eitan, Laith
Biotechnology and Genetic Engineering
Jordan University of Science and Technology

Professor Al-Khateeb , Wesam M.
Plant Genetics and Biotechnology
Yarmouk University

Professor Al-Ghzawi , Abdul Latief A.
Plant biotechnology
The Hashemite University

Professor Al-Najjar , Tariq Hasan Ahmad.
Marine Biology
The University of Jordan/ Aqaba

Professor Khleifat, Khaled M.
Microbiology and Biotechnology
Mutah University

Professor Odat , Nidal
Plant biodiversity
Al Balqa Applied University

Associate Editorial Board

Professor Al-Hindi, Adnan I.
Parasitology
The Islamic University of Gaza, Faculty of Health
Sciences, Palestine

Dr Gammoh, Noor
Tumor Virology
Cancer Research UK Edinburgh Centre, University of
Edinburgh, U.K.

Professor Kasperek, Max
Natural Sciences
Editor-in-Chief, Journal Zoology in the Middle East,
Germany

Professor Krystufek, Boris
Conservation Biology
Slovenian Museum of Natural History,
Slovenia

Dr Rabei, Sami H.
Plant Ecology and Taxonomy
Botany and Microbiology Department,
Faculty of Science, Damietta University, Egypt

Professor Simerly, Calvin R.
Reproductive Biology
Department of Obstetrics/Gynecology and
Reproductive Sciences, University of
Pittsburgh, USA

Editorial Board Support Team

Language Editor
Dr. Shadi Neimneh

Publishing Layout
Eng.Mohannad Oqdeh

Submission Address

Professor Atoum, Manar F
The Hashemite University
P.O. Box 330127, Zarqa, 13115, Jordan
Phone: +962-5-3903333 ext.4147
E-Mail: jjbs@hu.edu.jo

International Advisory Board (Arranged alphabetically)

Professor Abdelaziz M. Hussein
Mansoura University, Egypt

Professor Adnan Bashir Al-Iahham
German Jordanian University, Jordan

Professor Ahmed Amri
genetic resources ICARDA in Morocco, Morocco

Professor Amir Menwer Al-Hroob
Al-Hussein Bin Talal University, Jordan

Professor Elif Demirkan
Bursa Uludag University Turkey, Turkey

Professor Erhan Nurettin ÜNLÜ
Turkey Dicle University, Turkey

Professor Hassan Mohammed M. Abd El-Rahman Awad
National Research Centre, Egypt

Professor Khalid M. Al-Batayneh
Yarmouk University, Jordan

Professor Laith Abd Jalil Jawad
School of Environmental and Animal Sciences, Unitec Institute of
Technology Auckland, New Zealand

Professor Maroof A. Khalaf
Jordan University/ Aqaba, Jordan

Professor Mohammed H. Abu-Dieyeh
Biological and Environmental Sciences, Qatar University, Qatar

Professor Nour Shafik Emam El-Gendy
Egyptian Petroleum Research Institute, Egypt

Professor Omar F. Khabour
Jordan University of Science and Technology, Jordan

Professor Saleem Hmood Aladaileh
Al-Hussein Bin Talal University, Jordan

Professor Walid Al Zyoud
German Jordanian University, Jordan

Professor Abhik Gupta
School of Environmental Sciences, Assam University, India

Professor Ahmed Deaf Allah Telfah
Leibniz-Institut für Analytische Wissenschaften-, Germany

Dr. Amalia A Tsiami
University of West London, London

Professor David Modry
Masaryk University, Science Department, Czech

Professor Emad Hussein Malkawi
Yarmouk University, Jordan

Professor Gottfried Hartmut Richard Jetschke
Friedrich-Schiller-University of Jena, Germany

Professor Ihsan Ali Mahasneh
Al al-Bayt University, Jordan

Professor Khalid Majid Hameed
Dept. of Biological Sciences, Duke University, USA

Dr Maizirwan Bin Muhammad Mel
International Islamic University Malaysia, Malaysia

Professor Mohamed Emara
Chartered Management Institute, UK

Professor Nabil Joseph Awadalla Girgis
King Khalid University, Saudi Arabia

Professor Olga Anne
Marine Technology and Natural Sciences of Klaipėda University,
Lithuania

Dr Roy Hendroko Setyobudi
University of Muhammadiyah, Indonesia

Dr. Salem M Akel
St. Jude's Children's Research Hospital, USA

Professor Yacob Hassan Yacob
Al al-Bayt University, Jordan

Instructions to Authors

Scopes

Study areas include cell biology, genomics, microbiology, immunology, molecular biology, biochemistry, embryology, immunogenetics, cell and tissue culture, molecular ecology, genetic engineering and biological engineering, bioremediation and biodegradation, bioinformatics, biotechnology regulations, gene therapy, organismal biology, microbial and environmental biotechnology, marine sciences. The JJBS welcomes the submission of manuscript that meets the general criteria of significance and academic excellence. All articles published in JJBS are peer-reviewed. Papers will be published approximately one to two months after acceptance.

Type of Papers

The journal publishes high-quality original scientific papers, short communications, correspondence and case studies. Review articles are usually by invitation only. However, Review articles of current interest and high standard will be considered.

Submission of Manuscript

Manuscript, or the essence of their content, must be previously unpublished and should not be under simultaneous consideration by another journal. The authors should also declare if any similar work has been submitted to or published by another journal. They should also declare that it has not been submitted/ published elsewhere in the same form, in English or in any other language, without the written consent of the Publisher. The authors should also declare that the paper is the original work of the author(s) and not copied (in whole or in part) from any other work. All papers will be automatically checked for duplicate publication and plagiarism. If detected, appropriate action will be taken in accordance with International Ethical Guideline. By virtue of the submitted manuscript, the corresponding author acknowledges that all the co-authors have seen and approved the final version of the manuscript. The corresponding author should provide all co-authors with information regarding the manuscript, and obtain their approval before submitting any revisions. Electronic submission of manuscripts is strongly recommended, provided that the text, tables and figures are included in a single Microsoft Word file. Submit manuscript as e-mail attachment to the Editorial Office at: JJBS@hu.edu.jo. After submission, a manuscript number will be communicated to the corresponding author within 48 hours.

Peer-review Process

It is requested to submit, with the manuscript, the names, addresses and e-mail addresses of at least 4 potential reviewers. It is the sole right of the editor to decide whether or not the suggested reviewers to be used. The reviewers' comments will be sent to authors within 6-8 weeks after submission. Manuscripts and figures for review will not be returned to authors whether the editorial decision is to accept, revise, or reject. All Case Reports and Short Communication must include at least one table and/ or one figure.

Preparation of Manuscript

The manuscript should be written in English with simple lay out. The text should be prepared in single column format. Bold face, italics, subscripts, superscripts etc. can be used. Pages should be numbered consecutively, beginning with the title page and continuing through the last page of typewritten material.

The text can be divided into numbered sections with brief headings. Starting from introduction with section 1. Subsections should be numbered (for example 2.1 (then 2.1.1, 2.1.2, 2.2, etc.), up to three levels. Manuscripts in general should be organized in the following manner:

Title Page

The title page should contain a brief title, correct first name, middle initial and family name of each author and name and address of the department(s) and institution(s) from where the research was carried out for each author. The title should be without any abbreviations and it should enlighten the contents of the paper. All affiliations should be provided with a lower-case superscript number just after the author's name and in front of the appropriate address.

The name of the corresponding author should be indicated along with telephone and fax numbers (with country and area code) along with full postal address and e-mail address.

Abstract

The abstract should be concise and informative. It should not exceed **350 words** in length for full manuscript and Review article and **150 words** in case of Case Report and/ or Short Communication. It should briefly describe the purpose of the work, techniques and methods used, major findings with important data and conclusions. No references should be cited in this part. Generally non-standard abbreviations should not be used, if necessary they should be clearly defined in the abstract, at first use.

Keywords

Immediately after the abstract, **about 4-8 keywords** should be given. Use of abbreviations should be avoided, only standard abbreviations, well known in the established area may be used, if appropriate. These keywords will be used for indexing.

Abbreviations

Non-standard abbreviations should be listed and full form of each abbreviation should be given in parentheses at first use in the text.

Introduction

Provide a factual background, clearly defined problem, proposed solution, a brief literature survey and the scope and justification of the work done.

Materials and Methods

Give adequate information to allow the experiment to be reproduced. Already published methods should be mentioned with references. Significant modifications of published methods and new methods should be described in detail. Capitalize trade names and include the manufacturer's name and address. Subheading should be used.

Results

Results should be clearly described in a concise manner. Results for different parameters should be described under subheadings or in separate paragraph. Results should be explained, but largely without referring to the literature. Table or figure numbers should be mentioned in parentheses for better understanding.

Discussion

The discussion should not repeat the results, but provide detailed interpretation of data. This should interpret the significance of the findings of the work. Citations should be given in support of the findings. The results and discussion part can also be described as separate, if appropriate. The Results and Discussion sections can include subheadings, and when appropriate, both sections can be combined

Conclusions

This should briefly state the major findings of the study.

Acknowledgment

A brief acknowledgment section may be given after the conclusion section just before the references. The acknowledgment of people who provided assistance in manuscript preparation, funding for research, etc. should be listed in this section.

Tables and Figures

Tables and figures should be presented as per their appearance in the text. It is suggested that the discussion about the tables and figures should appear in the text before the appearance of the respective tables and figures. No tables or figures should be given without discussion or reference inside the text.

Tables should be explanatory enough to be understandable without any text reference. Double spacing should be maintained throughout the table, including table headings and footnotes. Table headings should be placed above the table. Footnotes should be placed below the table with superscript lowercase letters. Each table should be on a separate page, numbered consecutively in Arabic numerals. Each figure should have a caption. The caption should be concise and typed separately, not on the figure area. Figures should be self-explanatory. Information presented in the figure should not be repeated in the table. All symbols and abbreviations used in the illustrations should be defined clearly. Figure legends should be given below the figures.

References

References should be listed alphabetically at the end of the manuscript. Every reference referred in the text must be also present in the reference list and vice versa. In the text, a reference identified by means of an author's name should be followed by the year of publication in parentheses (e.g.(Brown,2009)). For two authors, both authors' names followed by the year of publication (e.g.(Nelson and Brown, 2007)). When there are more than two authors, only the first author's name followed by "*et al.*" and the year of publication (e.g. (Abu-Elteen *et al.*, 2010)). When two or more works of an author has been published during the same year, the reference should be identified by the letters "a", "b", "c", etc., placed after the year of publication. This should be followed both in the text and reference list. e.g., Hilly, (2002a, 2002b); Hilly, and Nelson, (2004). Articles in preparation or submitted for publication, unpublished observations, personal communications, etc. should not be included in the reference list but should only be mentioned in the article text (e.g., Shtyawy,A., University of Jordan, personal communication). Journal titles should be abbreviated according to the system adopted in Biological Abstract and Index Medicus, if not included in Biological Abstract or Index Medicus journal title should be given in full. The author is responsible for the scuracy and completeness of the references and for their correct textual citation. Failure to do so may result in the paper being withdraw from the evaluation process. Example of correct reference form is given as follows:-

Reference to a journal publication:

Bloch BK. 2002. Econazole nitrate in the treatment of *Candida vaginitis*. *S Afr Med J.* , **58**:314-323.

Ogunseitan OA and Ndoye IL. 2006. Protein method for investigating mercuric reductase gene expression in aquatic environments. *Appl Environ Microbiol.* , **64**: 695-702.

Hilly MO, Adams MN and Nelson SC. 2009. Potential fly-ash utilization in agriculture. *Progress in Natural Sci.*, **19**: 1173-1186.

Reference to a book:

Brown WY and White SR.1985. **The Elements of Style**, third ed. MacMillan, New York.

Reference to a chapter in an edited book:

Mettam GR and Adams LB. 2010. How to prepare an electronic version of your article. In: Jones BS and Smith RZ (Eds.), **Introduction to the Electronic Age**. Kluwer Academic Publishers, Netherlands, pp. 281–304.

Conferences and Meetings:

Embabi NS. 1990. Environmental aspects of distribution of mangrove in the United Arab Emirates. Proceedings of the First ASWAS Conference. University of the United Arab Emirates. Al-Ain, United Arab Emirates.

Theses and Dissertations:

El-Labadi SN. 2002. Intestinal digenetic trematodes of some marine fishes from the Gulf of Aqaba. MSc dissertation, The Hashemite University, Zarqa, Jordan.

Nomenclature and Units

Internationally accepted rules and the international system of units (SI) should be used. If other units are mentioned, please give their equivalent in SI.

For biological nomenclature, the conventions of the *International Code of Botanical Nomenclature*, the *International Code of Nomenclature of Bacteria*, and the *International Code of Zoological Nomenclature* should be followed.

Scientific names of all biological creatures (crops, plants, insects, birds, mammals, etc.) should be mentioned in parentheses at first use of their English term.

Chemical nomenclature, as laid down in the *International Union of Pure and Applied Chemistry* and the official recommendations of the *IUPAC-IUB Combined Commission on Biochemical Nomenclature* should be followed. All biocides and other organic compounds must be identified by their Geneva names when first used in the text. Active ingredients of all formulations should be likewise identified.

Math formulae

All equations referred to in the text should be numbered serially at the right-hand side in parentheses. Meaning of all symbols should be given immediately after the equation at first use. Instead of root signs fractional powers should be used. Subscripts and superscripts should be presented clearly. Variables should be presented in italics. Greek letters and non-Roman symbols should be described in the margin at their first use.

To avoid any misunderstanding zero (0) and the letter O, and one (1) and the letter l should be clearly differentiated. For simple fractions use of the solidus (/) instead of a horizontal line is recommended. Levels of statistical significance such as: * $P < 0.05$, ** $P < 0.01$ and *** $P < 0.001$ do not require any further explanation.

Copyright

Submission of a manuscript clearly indicates that: the study has not been published before or is not under consideration for publication elsewhere (except as an abstract or as part of a published lecture or academic thesis); its publication is permitted by all authors and after accepted for publication it will not be submitted for publication anywhere else, in English or in any other language, without the written approval of the copyright-holder. The journal may consider manuscripts that are translations of articles originally published in another language. In this case, the consent of the journal in which the article was originally published must be obtained and the fact that the article has already been published must be made clear on submission and stated in the abstract. It is compulsory for the authors to ensure that no material submitted as part of a manuscript infringes existing copyrights, or the rights of a third party.

Ethical Consent

All manuscripts reporting the results of experimental investigation involving human subjects should include a statement confirming that each subject or subject's guardian obtains an informed consent, after the approval of the experimental protocol by a local human ethics committee or IRB. When reporting experiments on animals, authors should indicate whether the institutional and national guide for the care and use of laboratory animals was followed.

Plagiarism

The JJBS hold no responsibility for plagiarism. If a published paper is found later to be extensively plagiarized and is found to be a duplicate or redundant publication, a note of retraction will be published, and copies of the correspondence will be sent to the authors' head of institute.

Galley Proofs

The Editorial Office will send proofs of the manuscript to the corresponding author as an e-mail attachment for final proof reading and it will be the responsibility of the corresponding author to return the galley proof materials appropriately corrected within the stipulated time. Authors will be asked to check any typographical or minor clerical errors in the manuscript at this stage. No other major alteration in the manuscript is allowed. After publication authors can freely access the full text of the article as well as can download and print the PDF file.

Publication Charges

There are no page charges for publication in Jordan Journal of Biological Sciences, except for color illustrations,

Reprints

Ten (10) reprints are provided to corresponding author free of charge within two weeks after the printed journal date. For orders of more reprints, a reprint order form and prices will be sent with article proofs, which should be returned directly to the Editor for processing.

Disclaimer

Articles, communication, or editorials published by JJBS represent the sole opinions of the authors. The publisher shoulders no responsibility or liability what so ever for the use or misuse of the information published by JJBS.

Indexing

JJBS is indexed and abstracted by:

DOAJ (Directory of Open Access Journals)

Google Scholar

Journal Seek

HINARI

Index Copernicus

NDL Japanese Periodicals Index

SCIRUS

OAJSE

ISC (Islamic World Science Citation Center)

Directory of Research Journal Indexing
(DRJI)

Ulrich's

CABI

EBSCO

CAS (Chemical Abstract Service)

ETH- Citations

Open J-Gat

SCImago

Clarivate Analytics (Zoological Abstract)

Scopus

AGORA (United Nation's FAO database)

SHERPA/RoMEO (UK)

المجلة الأردنية للعلوم الحياتية
Jordan Journal of Biological Sciences (JJBS)
ISSN 1995- 6673 (Print), 2307- 7166 (Online)

<http://jjbs.hu.edu.jo>

The Hashemite University
Deanship of Scientific Research
TRANSFER OF COPYRIGHT AGREEMENT

Journal publishers and authors share a common interest in the protection of copyright: authors principally because they want their creative works to be protected from plagiarism and other unlawful uses, publishers because they need to protect their work and investment in the production, marketing and distribution of the published version of the article. In order to do so effectively, publishers request a formal written transfer of copyright from the author(s) for each article published. Publishers and authors are also concerned that the integrity of the official record of publication of an article (once refereed and published) be maintained, and in order to protect that reference value and validation process, we ask that authors recognize that distribution (including through the Internet/WWW or other on-line means) of the authoritative version of the article as published is best administered by the Publisher.

To avoid any delay in the publication of your article, please read the terms of this agreement, sign in the space provided and return the complete form to us at the address below as quickly as possible.

Article entitled:-----

Corresponding author: -----

To be published in the journal: Jordan Journal of Biological Sciences (JJBS)

I hereby assign to the Hashemite University the copyright in the manuscript identified above and any supplemental tables, illustrations or other information submitted therewith (the "article") in all forms and media (whether now known or hereafter developed), throughout the world, in all languages, for the full term of copyright and all extensions and renewals thereof, effective when and if the article is accepted for publication. This transfer includes the right to adapt the presentation of the article for use in conjunction with computer systems and programs, including reproduction or publication in machine-readable form and incorporation in electronic retrieval systems.

Authors retain or are hereby granted (without the need to obtain further permission) rights to use the article for traditional scholarship communications, for teaching, and for distribution within their institution.

- I am the sole author of the manuscript
- I am signing on behalf of all co-authors of the manuscript
- The article is a 'work made for hire' and I am signing as an authorized representative of the employing company/institution

Please mark one or more of the above boxes (as appropriate) and then sign and date the document in black ink.

Signed: _____ Name printed: _____

Title and Company (if employer representative) : _____

Date: _____

Data Protection: By submitting this form you are consenting that the personal information provided herein may be used by the Hashemite University and its affiliated institutions worldwide to contact you concerning the publishing of your article.

Please return the completed and signed original of this form by mail or fax, or a scanned copy of the signed original by e-mail, retaining a copy for your files, to:

Hashemite University
Jordan Journal of Biological Sciences
Zarqa 13115 Jordan
Fax: +962 5 3903338
Email: jjbs@hu.edu.jo

EDITORIAL PREFACE

Jordan Journal of Biological Sciences (JJBS) is a refereed, quarterly international journal financed by the Scientific Research and Innovation Support Fund, Ministry of Higher Education and Scientific Research in cooperation with the Hashemite University, Jordan. JJBS celebrated its 12th commencement this past January, 2020. JJBS was founded in 2008 to create a peer-reviewed journal that publishes high-quality research articles, reviews and short communications on novel and innovative aspects of a wide variety of biological sciences such as cell biology, developmental biology, structural biology, microbiology, entomology, molecular biology, biochemistry, medical biotechnology, biodiversity, ecology, marine biology, plant and animal biology, plant and animal physiology, genomics and bioinformatics.

We have watched the growth and success of JJBS over the years. JJBS has published 14 volumes, 60 issues and 800 articles. JJBS has been indexed by SCOPUS, CABI's Full-Text Repository, EBSCO, Clarivate Analytics- Zoological Record and recently has been included in the UGC India approved journals. JJBS Cite Score has improved from 0.7 in 2019 to 1.4 in 2021 (Last updated on 6 March, 2022) and with Scimago Institution Ranking (SJR) 0.22 (Q3) in 2021.

A group of highly valuable scholars have agreed to serve on the editorial board and this places JJBS in a position of most authoritative on biological sciences. I am honored to have six eminent associate editors from various countries. I am also delighted with our group of international advisory board members coming from 15 countries worldwide for their continuous support of JJBS. With our editorial board's cumulative experience in various fields of biological sciences, this journal brings a substantial representation of biological sciences in different disciplines. Without the service and dedication of our editorial; associate editorial and international advisory board members, JJBS would have never existed.

In the coming year, we hope that JJBS will be indexed in Clarivate Analytics and MEDLINE (the U.S. National Library of Medicine database) and others. As you read throughout this volume of JJBS, I would like to remind you that the success of our journal depends on the number of quality articles submitted for review. Accordingly, I would like to request your participation and colleagues by submitting quality manuscripts for review. One of the great benefits we can provide to our prospective authors, regardless of acceptance of their manuscripts or not, is the feedback of our review process. JJBS provides authors with high quality, helpful reviews to improve their manuscripts.

Finally, JJBS would not have succeeded without the collaboration of authors and referees. Their work is greatly appreciated. Furthermore, my thanks are also extended to The Hashemite University and the Scientific Research and Innovation Support Fund, Ministry of Higher Education and Scientific Research for their continuous financial and administrative support to JJBS.

Professor Y gf {cp."O qj co o gf "C0
....."Ugr vgo dgt."4245"

CONTENTS

Original Articles

- 565 – 575 Potential of Bioactive Compounds from Jamblang (*Syzygium Cumini*) And Hanjeli (*Coix Lacryma-Jobi*L.) Essential Oils As SARS-COV-2 Antivirus Targeting NSP5 And ACE2 Receptors
Diky Setya Diningrat , Ayu Nirmala Sari, Kusdianti , Novita Sari Harahap
- 577 – 585 Protective Effects of Secoisolariciresinol Diglucoside on Arsenic-induced Renal Damage and Oxidative Stress in Rats
Tareq Nayef AlRamadneh, Muhannad I. Massadeh, Rania Algroom, Hashem A Abu-Harirah, Kawther Faisal Amawi, Nada S. Daifalla, Hammad Khalifeh Aldal'in, Razan N. AlQuraan, Rajesh Javaraiah
- 587 – 592 Increased Virus Resistance in Transgenic Petunia with Heterologous *ZRNase II* gene
Olga Ovcharenko, Andrii Potrokhov, Daria Sosnovska, Yuliya Hoysyuk, Olha Yaroshko, Tetiana Shevchenko, Iryna Budzanivska, Volodymyr Rudas, Mykola Kuchuk
- 593 – 597 Whole Exome Sequencing in Intellectual Disability Patients Identifies *de novo* Mutations in *KCNB1*, *SHANK2*, and *SYNGAP1* Genes and a Novel Mutation in *PPP1R3F*
Asem M Alkhateeb, Miral Almomani, and Hani H Hammad
- 599 – 609 Studies on Toxicity and Peptic Ulcer Healing Potential of Crude Extract of *Osbeckia crinita* in Swiss Albino Mice
Sanchayeeta Roy, Bishnupada Roy
- 611 – 619 Comprehensive Characterization and Expression Profiling of the GATA Transcription Factor in Sugar Beet (*Beta vulgaris* L.) Suggests Their Potential Roles in Taproot Development and Biotic Stress Response
Le Thi Man, Phi Bang Cao, Thi Thanh Huyen Tran, Nguyen Quoc Trung, Dong Huy Gioi, Ninh Thi Thao, Quynh Thi Ngoc Le, Hong Viet La, Thi Xuan Quyen Vu, Ha Duc Chu
- 621 – 632 Biogenic Silver Nanoparticles by *Pseudomonas aeruginosa* Reduce Expression of Biofilm and Quorum Signaling Genes in Multi-drug Resistant *Acinetobacter baumannii*
Talar Ibrahim Hasan & Akhter Ahmed Ahmed
- 633 – 639 Effects of Reducing Browning on the Somatic Embryogenesis of *Coffea arabica*
Jarinya Hongwiangchanand Noppamart Lokkamlue
- 641 – 647 Renal Calculi Composition in Alkaptonuria: Insights on Etiology
Nesrin Riad Mwafi , Amjad Asri Al-Tarawneh, Ibrahim Naji Tarawneh , Mohannad Fayiz Alqedrh , Ahmad Ibrahim Alsbou' , Lekaa Ja'far Al Mughrabi F , Ali Mohammad Khlaifat, Muhamad Odeh Al-Limoun , Khaled Mohammad khleifat
- 649 – 654 Proximate Composition, Fatty Acid Profile, and Microplastic Contamination of Edible Odonate Larvae (Aeshnidae: *Anax* sp.) in Rice Fields
Witwisitpong Maneechan, Taeng On Prommi
- 655 – 664 Assessing the Immunomodulatory and Hepatoprotective Activities of Aqueous Tuber Extract of *Typhonium flagelliforme* (Lood) Blume in BALB/c Mouse
Wira Eka Putra, Anis Fatayatil Insani, Desi Nurhayati, Arief Hidayatullah3, Muhaimin Rifa'i
- 665 – 672 Evaluation of Antifungal Potential of *Mentha pulegium* Essential oil in Biological Control Against the Pathogen of Inflorescence Rot Disease of Date Palm (*Mauginiella scaettae*)
Hammia Hadjra, Bouatrous Yamina, Kriker Soulef, Ramazan Erenler
- 673 – 685 Cloning and Characterization of Terpene synthase 3 (*SoTPS3*) Gene from Leaves of Garden Sage (*Salvia officinalis*)
Mohammed Ali, El-ramah, F. A., Esraa A. Elsherbeny, Mohamed N.S. Suliman, Mokhtar Said Rizk
- 687 – 692 The Association between Vitamin D Deficiency, Obesity, and Insulin Resistance among the Jordanian Population
Raed A. Halalshah , Linda A. Soufan, and Hosam J. Al-Tamimi
- 693 – 698 The Growth Response and Digestive Enzyme Activity of Juvenile African Catfish (*Clarias gariepinus*) Exposed to Artificial Light at Night (ALAN) Spectral
Gabriel A. Dedeke, Festus O. Kehinde and Ife A. George
- 699 – 704 Generation and Evaluation of Gold-binding Peptide Fused Protein A
Thuy-Dung Doan-Tran, Thanh-Tan Nguyen, and Hieu Tran-Van

- 705 – 715 Evaluating the Mood and Memory-enhancing Effects of *Punicagranatum* Seeds (Pomegranate) Extract using an Animal Model
Abdelrahim Alqudah, Esam Y. Qnais, Omar Gammoh, Mohammed Alqudah
- 717 – 726 Extraction of *Klebsiella pneumoniae* and *Candida albicans* Biofilm and Studying their Cytotoxic Effects on Human Lymphocytes
Batol Imran Dheeb, Sara Najim Abdulla, Safaa AL-Deen Ahmed Shanter AL-Qaysi, Basma M. Al-Sarraj, Mohammed Sami Farhan

Potential of Bioactive Compounds from Jamblang (*Syzygium Cumini*) And Hanjeli (*Coix Lacryma-Jobi*L.) Essential Oils As SARS-COV-2 Antivirus Targeting NSP5 And ACE2 Receptors

Diky Setya Diningrat^{1,*}, Ayu Nirmala Sari², Kusdianti³, Novita Sari Harahap⁴

¹Department of Biology, Faculty of Mathematics and Natural Sciences, Universitas Negeri Medan (Medan State University), Indonesia; ²Biology Study Program, Faculty of Science and Technology, Ar-Raniry State Islamic University (UIN), Banda Aceh, Indonesia; ³Department of Biology, Faculty of Mathematics and Natural Sciences, Universitas Pendidikan Indonesia; ⁴Department of Sports Science, Faculty of Sports Science, Universitas Negeri Medan (Medan State University), Indonesia.

Received: September 28, 2022; Revised: February 10, 2023; Accepted: March 15, 2023

Abstract

This study uses bioactive compounds from jamblang (*Syzygium cumini*) and hanjeli (*Coix lacryma-jobi* L.) essential oils, namely Aziridine-2-carbothioamide and 4-Dibenzofuranamine which are thought to have antiviral activity on MERS-CoV and H3N2 HA. The specific target receptors for current anti-SARS-CoV-2 drugs are NSP5 (nonstructural protein) and ACE2 (angiotensin-converting enzyme 2). The purpose of this study was to determine the antiviral activity of SARS-CoV-2 from compounds of Aziridine-2-carbothioamide and 4-Dibenzofuranamine in silico. The compound was prepared in advance by downloading the PDB ID code, preparing 2D and 3D structures, determining the minimum energy, generating SMILES codes, and predicting physicochemical properties and toxicity. After preparation, the process continued with molecular binding using the PyRx-Vina® application. Docking results were analyzed using PyMOL® software and Discovery Studio Visualizer®. The results of the physicochemical profile showed that the compounds of 4-Dibenzofuranamine and Aziridine-2-carbothioamide had complied with Lipinski's five rules, and each compound had LD50 values of 1350 mg/kg and 340 mg/kg. The docking resulted in interactions of Aziridine-2-carbothioamide at the 2GZ7 receptor and 4-Dibenzofuranamine at the 3D0G, and 1R4L receptors showed significant differences, respectively, to lopinavir and chloroquine with p-value < 0.05 so that these compounds were predicted to have better antiviral potential. This research shows that bioactive compounds from the essential oils of *S. cumini* and *C. lacryma-jobi* can act as SARS-COV-2 antivirals, which have been compared with antivirals used medically in silico. In vivo and in vitro testing needs to be done so that it can be applied medically.

Keywords: COVID-19, essential oil, *Syzygium cumini*, *Coix lacryma-jobi*, Physicochemistry, Toxicity, and In silico.

1. Background

Coronavirus Disease (COVID-19) is caused by the severe acute respiratory syndrome coronavirus-2 (SARSCoV-2). The coronavirus that became the etiology of COVID-19 is included in the betacoronavirus genus (Lai et al, 2020). The results of phylogenetic analysis show that this virus belongs to the same subgenus as the coronavirus that caused the severe acute respiratory illness outbreak (SARS) in 2002-2004, namely Sarbecovirus (Malik et al, 2020; Oglat et al, 2022). The replication process of the COVID-19 virus, namely SARS-CoV-2, binds to the receptors and makes its way into the cell. Then, the glycoprotein contained in the viral spike envelope will bind to the cellular receptor in the form of ACE2 in SARS-CoV-2. SARS-CoV-2 will duplicate genetic material, synthesize the required proteins, and then form new virions that appear on the cell surface (Awaid, 2022; Beyerstedt et al, 2021).

NSP5 plays an indispensable role in SARS-CoV-2 proliferation (Yashvardhini et al, 2022). This research is important to do. This was done to determine the role of

bioactive compounds from *Syzygium cumini* essential oil and *Coix lacryma-jobi* essential oil in their activity against the NSP5 protein and ACE2 inhibitors in their role in preventing SARS-CoV-2 infection.

Aziridine-2-carbothioamide is a small molecule biologic as one of the FDA-approved drugs. These small molecules have been selected to ensure that they meet the five criteria of Lipinski's law. One of the criteria is molecular weight, where if the molecular weight is above 500 Da, the drug cannot diffuse through the cell membrane (Oroojalian et al, 2020). Aziridine-2-carbothioamide has shown a very high IC50 concentration of 0.83 g/ml against Middle East respiratory syndrome coronavirus (MERS-CoV) (Ugwuja and Nwankwo, 2022). Aziridine-2-carbothioamide has been shown to decrease the expression of the pro-inflammatory cytokine IL6 in SARS-CoV-2 infection (Ugwuja and Nwankwo, 2022). In previous research, molecular docking of Aziridine-2-carbothioamide against the Mpro (6LU7) receptor was carried out; 3CLpro (1UK4); ACE2 (6M0J); NSP12 (6NUR) (Fadaka et al, 2022), but this has not been done for NSP5 and other ACE2 receptors.

* Corresponding author. e-mail: dikysd@unimed.ac.id.

One of the other small molecule inhibitors is 4-Dibenzofuranamine. 4-Dibenzofuranamine has been shown to inhibit the low-pH conformational change of hemagglutinin (HA) and block the fusion process (da Silva Hage-Melim et al. 2020). Influenza virus (H3N2) HA has a similar sequence or structure to the SARS-CoV-2 spike glycoprotein (Oroojalian et al, 2020). Previous molecular docking studies have shown that 4-Dibenzofuranamine interacts with the ACE2 receptor (6LZG) so that it can inhibit SARS-CoV-2 membrane fusion into host cells (Sharma et al. 2021). Neither 4-Dibenzofuranamine nor Aziridine-2-carbothioamide is registered in Indonesia based on the Indonesian Food and Drug Supervisory Agency. Therefore, based on the literature regarding indications of 4-Dibenzofuranamine and Aziridine-2-carbothioamide, these two compounds have potential as new drugs in Indonesia.

Another study was conducted on 81 cases (45 cases in the umifenovir/4-Dibenzofuranamine group and 36 cases in the control group) moderate or severe COVID-19 by comparing the results of CT scans after administration, and the results showed that there was no difference in changes in CT values in 1 week, thus indicating that giving umifenovir does not give better results or shorten the duration of treatment in COVID-19 patients. However, because this study is a single center (retrospective study with small sample size), which is biased and with potentially subjective conclusions, further verification in randomized controlled clinical trials is necessary (Sharma et al. 2021).

In this study, two target receptors were used: NSP5 and ACE2. The NSP5 receptor (nonstructural protein) is known as Mpro (Roe et al, 2021) and 3-chymotrypsin-like protease (3CLpro) (Mody et al, 2021). This NSP5 receptor was chosen because of its mechanism in mediating viral protein replication and transcription (Singh et al, 2022). Another receptor is ACE2 (angiotensin-converting enzyme 2) which has three physiological functions, namely as a negative regulator of the renin-angiotensin system, facilitator of amino acid transport, and receptor for the binding site for SARS-CoV and SARS-CoV-2 (Diningrat et al, 2021; Diningrat et al, 2021).

To determine the effectiveness of the tested ligands as new drugs, molecular binding, physicochemical and toxicity tests were carried out in this study. In addition, a comparison of the binding affinity values of the comparator of lopinavir to Aziridine-2-carbothioamide and the comparator of chloroquine to 4-Dibenzofuranamine was carried out. This research is important to do because in the development of COVID-19 drugs, it is necessary to predict properties absorption, distribution, metabolism, excretion (ADME), toxicity, and describe drug interactions with receptors. Physicochemical tests describe the solubility/solubility of a compound, whether it is soluble in water (hydrophobic)/fat (hydrophilic), and this solubility property is required to penetrate cell membranes by the movement of drugs from high to low concentrations (passive diffusion) (Fadaka et al, 2022). Toxicity is the ability of a chemical substance to cause damage to organisms both when used and when in the environment (da Silva Hage-Melim et al, 2020).

2. Materials and Methods

2.1. Materials

The materials used in this study were PyRx 0.8®, Discovery Studio Visualizer®, PyMOL®, and AutoDockTools-1.5.6®.

2.2. Tools

The hardware tools used were a set of laptops with specifications for an Intel® Celeron® CPU N3350 @ 1.10GHz, 2 GB of RAM, and Windows 10 Pro 64-bit operating system software (10.0, Build 19041)(Diningrat et al, 2021).

2.3. Preparation of Ligands and Comparative Compounds

Ligand samples were produced from GCMS analysis of metabolites obtained from essential oils of *S. cumini* and *C. lacryma-jobi*. The bioactive compounds are Aziridine-2-carbothioamide from *S. cumini* essential oil and 4-Dibenzofuranamine from *C. lacryma-jobi* essential oil. Sample preparation began with downloading the ligands and comparison compounds from the Protein Data Bank website <https://www.rcsb.org> in *pdb format. For visualization data in the form of two-dimensional structures, compounds were drawn using the ChemDraw 19.0® program. The ligand preparation process to become a ready-to-use file with a 3D chemical structure format is carried out using the AutoDockTools-1.5.6® conversion facility. The ligands used were Aziridine-2-carbothioamide and 4-Dibenzofuranamine, as well as their comparison compounds, lopinavir and chloroquine. Then, the downloaded ligand complex file will be opened in pdb format. The next step was ligand preparation by eliminating solvent (water), all residues, and small molecules, then storing in the form of pdbqt (Protein Data Bank, Partial Charge (Q), & Atom Type (T))(Diningrat et al, 2021).

2.4. Receptor Preparation

A Receptor preparation was initiated by downloading the NSP5 (7BQY and 2GZ7) and ACE2 (3D0G and 1R4L) receptor structures on the Protein Data Bank (PDB) site in pdb format. Receptor protein preparation was carried out using the PyMOL® application. At this stage, the elimination of solvents (water) and small molecules is carried out. After that, the file was saved in the form of pdbqt (Protein Data Bank, Partial Charge (Q), & Atom Type (T)) (Diningrat et al, 2021; Diningrat et al, 2021).

2.5. Determination of Minimum Energy

The determination of the minimum energy was carried out using the Chem3D 19.0® program. It was replicated three times using the Merck Molecular Force Field 94 (MMFF94) method, but first the three-dimensional structure was downloaded from the <https://pubchem.ncbi.nlm.nih.gov/> site in *sdf format. After that, the minimum energy calculation is carried out through Chem3D 19.0® by importing file > calculation > MMFF94 > Perform MMFF94 Minimization.

2.6. Determination of Grid Box Center and Sizes

The determination of grid box centers and sizes was done with blind docking tools automatically using the CB-Dock® application. CB-Dock® predicts receptor binding

sites, calculates centers and sizes with a curvature-based cavity detection approach (Mills et al, 2015). Ligands and receptors in pdb format were uploaded to the site <http://cao.labshare.cn/cb-dock/> and then calculated. The results obtained were interactions between ligands and receptors in 3D form and a table containing the vina score, cavity size, center, and size. The results were then saved or copied into Microsoft Word.

2.7. Method Validation

The validation process in this *in silico* test was carried out through re-docking of native ligands that have been downloaded through the Protein Data Bank website <https://www.rcsb.org>, and there are several native ligands that were prepared using the Discovery Studio Visualizer® application. Receptor validation was performed three times using the PyRx-Vina® application. The parameter observed at this stage is the root mean square deviation (RMSD) value resulting from the re-docking of the native ligand with its protein (Basu et al. 2020). The method is said to be valid and good if the resulting RMSD value is < 2 (Perrella et al, 2021).

2.8. Binding Process

The binding process was carried out between the ligand and the comparison compound at each receptor through the PyRx-Vina® software. Receptors and compounds that have been prepared were inserted into the PyRx 0.8® application in the form of pdbqt. The receptor was then set to a macromolecule, while the compound is set to a ligand. The ligands and receptors would be saved on the computer automatically and would be listed in the navigator section "AutoDockTools-1.5.6®". Receptors and ligands that have been stored earlier are entered in the control section of the Vina Wizard select molecule selection. Then, the forward button is selected and the grid box center and sizes from the resulting CBDock® application are set.

Then, vina search space information (center and dimension) was recorded, and this data was used for administrative needs, validation, and when analyzing relative positions. Next, Run Vina was selected, and the results were obtained in the form of affinity values and

RMSD values for validation need (Diningrat et al, 2021; Diningrat et al, 2021).

2.9. Prediction of Physicochemical Properties and Toxicity

The prediction of the physicochemical properties of the ligands was carried out by checking the simplified molecular input line entry system (SMILE) code of the ligands and the comparison compounds obtained from the ChemDraw 19.0® application. The SMILE code is uploaded to the SwissADME website <http://www.swissadme.ch/>. The results were analyzed based on Lipinski's five rules. Lipinski contains five rule that must be met by the ligand in order to proceed to the docking simulation stage. Compounds are said to not meet Lipinski's five rules if there are errors of more than one criterion [8], by means of molecular weight analysis (BM), logarithm of partition coefficient (Log P (XLogP3)), hydrogen bond acceptors (HBA), hydrogen bond donors (HBD), and molar refractivity. To predict ligand toxicity based on LD50 values, skin sensitization, AMES toxicity, and hepatotoxicity, the prepared SMILES code was entered through the pkCSM online tools site <https://biosig.unimelb.edu.au/pkcsm/prediction> and the Protox II online site tools https://toxnew.charite.de/protox_II/ to predict the LD50 value.

3. Results

The chemical structure of Aziridine-2-carbothioamide and 4-Dibenzofuranamine compounds as well as the comparison compounds of lopinavir and chloroquine can be seen in Figure 1. The minimum average results obtained for the compounds Aziridine-2-carbothioamide and 4-Dibenzofuranamine were 12,148 kcal/mol and 72,0405667, respectively.

The results of the docking validation can be seen in Table 1.

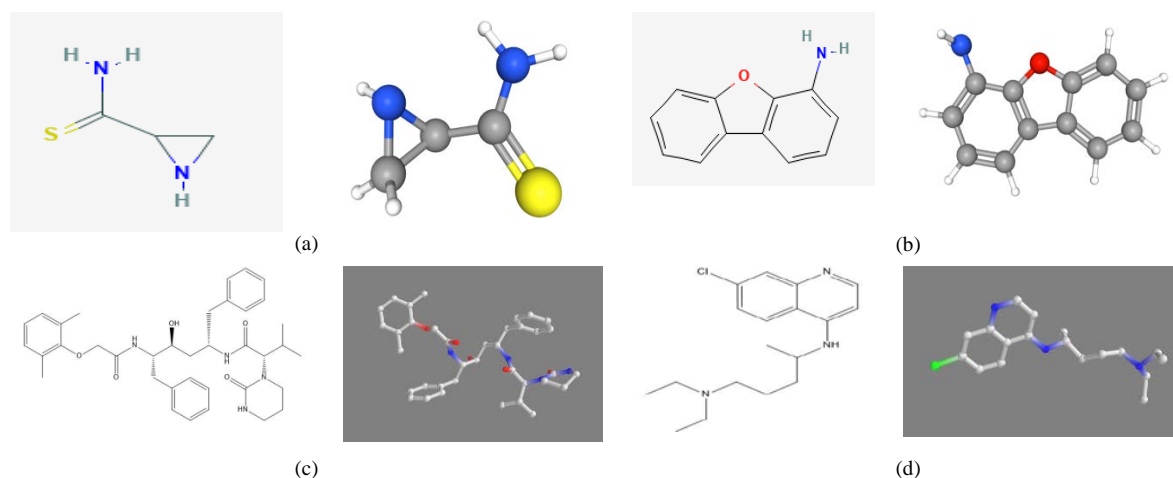


Figure 1. Chemical structure of compounds (a) Aziridine-2-carbothioamide and (b) 4-Dibenzofuranamine, as well as comparison compounds (c) lopinavir and (d) chloroquine

Table 1. The results of the docking validation on RMSD

Receptors	Native Ligand	RMSD Lower (Å)	RMSD Upper (Å)
7BQY	Native ligand 1	1.751±0.060	3.469 ± 0.736
2GZ7	Native ligand 2	0.185 ± 0.009	2.950 ± 0.093
3D0G	Native ligand 3	1.846 ± 0.047	2.202 ± 0.079
	Native ligand 4	1.852 ± 0.029	5.257 ± 0.034
1R4L	Native ligand 5	1.356 ± 0.668	2.279 ± 0.458
	Native ligand 6	1.805 ± 0.157	2.276 ± 0.214

Native ligand 1: n-[(5-methylisoxazol-3-yl)carbonyl]alanyl-l-valyl-n~1~((1r,2z)-4(benzyloxy)-4-oxo-1-[(3r)-2oxopyrrolidin-3-yl]methyl}but-2enyl)-l-leucinamide, Native ligand 2: 2-[(2,4-dichloro-5-methylphenyl)sulfonyl]-1,3-dinitro-5-(trifluoromethyl)Benzene
 Native ligand 3: 2-acetamido-2-deoxy-beta-D-glucopyranose, Native ligand 4: 2-acetamido-2-deoxy-alpha-D-glucopyranose , Native ligand 5: (s,s)-2-[1-carboxy-2-[3-(3,5-dichloro-benzyl)-3h-imidazol-4-yl]-ethylamino]-4-methyl-pentanoic acid

The results of docking using the application of PyRx-Vina® on the compound of Aziridine-2-carbothioamide, the comparison compound of lopinavir, and the native ligand against the 7BQY and 2GZ7 receptors, as well as the 4-Dibenzofuranamine compound, the comparison

compound of chloroquine, and the native ligand against the 3D0G and 1R4L receptors are shown in Figure and Table 2.

The types of interactions in three-dimensional form are shown in Figure 2

Table 2. Results of docking of test compounds, comparison compounds, and native ligands for each receptor

Receptor	Compound	Affinity (kcal/mol)	Center			Size (x*y*z)
			X	Y	Z	
NSP5 (7BQY)	Aziridine-2-carbothioamide*	-5.7 ± 0	-6 ± 0	2 ± 0	9.7 ± 0.929	21*21*21
	Lopinavir (Control Compound)	-5.633 ± 0.058	9 ± 0	3 ± 0	9.2 ± 1.701	26*26*26
	Native ligand 1	-5.467 ± 0.208	9 ± 0	3 ± 0	5.6 ± 3.650	29*29*29
NSP5 (2GZ7)	Aziridine-2-carbothioamide**	-6.667 ± 0.153	-1 ± 0	37 ± 0.058	14.4 ± 2.223	21*21*21
	Lopinavir (Control Compound)	-7.8 ± 0.1	-1 ± 0	-37 ± 0	15 ± 4.114	26*26*26
	Native ligand 2	-5.6 ± 0	-23 ± 0.058	-40 ± 0.058	14.1 ± 0.305	21*21*21
ACE2 (3D0G)	4-Dibenzofuranamine***	-6.567 ± 0.208	19 ± 0.058	39 ± 0.058	68.4 ± 0.889	22*22*22
	Chloroquine (Control Compound)	-4.1 ± 0.1	47 ± 0.058	-11 ± 0.058	77.6 ± 3.980	24*24*24
	Native ligand 3	-3.367 ± 0.058	61 ± 0	17 ± 0	68.2 ± 0.346	18*32*18
ACE2 (1R4L)	4-Dibenzofuranamine***	-6.667 ± 0.115	46 ± 0	5 ± 0	18.7 ± 2.285	35*24*35
	Chloroquine (Control Compound)	-9.167 ± 0.058	46 ± 0	2 ± 0	26.7 ± 1.4	35*23*35
	Native ligand 4	-6,267 ± 0.058	46 ± 0	5 ± 0	27.3 ± 0.153	35*18*35

The significance value between the test compound and the comparison compound at each receptor .

* : 0.114 kcal /mol, ** : 0.000 kcal / mol, *** : 0.000 kcal /mol, **** : 0.034 kcal /mol

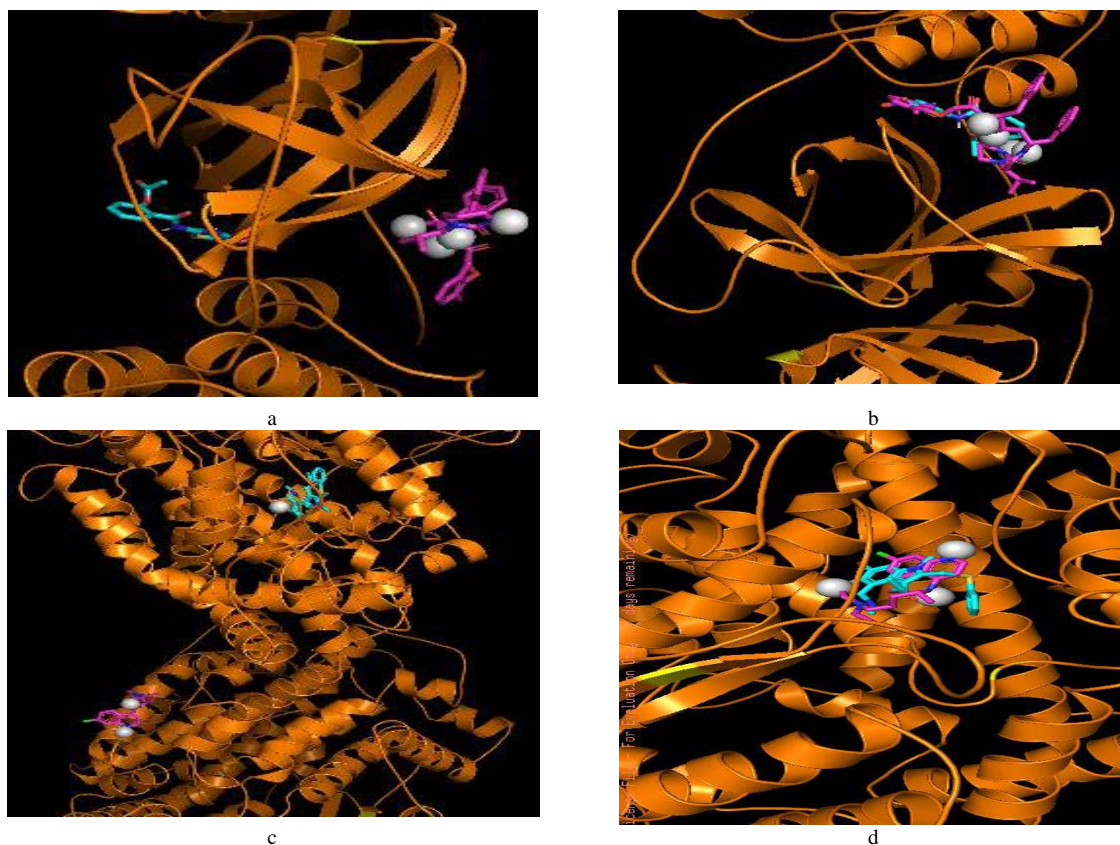
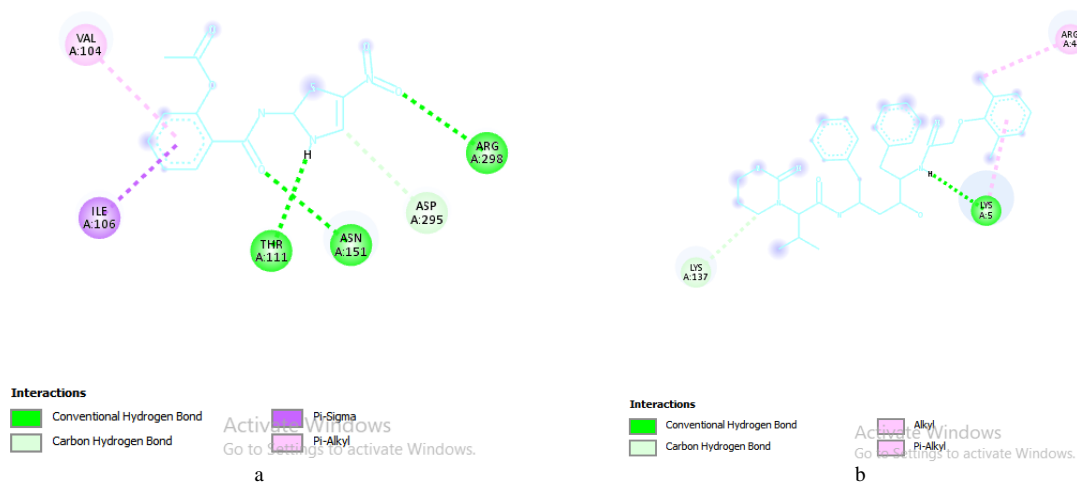


Figure 2. Three-dimensional shape (a) Aziridine-2-carbothioamide (cyan)-lopinavir (purple) against the 7BQY receptor (b) Aziridine-2-carbothioamide (cyan)-lopinavir (purple) against the 2GZ7 receptor (c) 4-Dibenzofuranamine (cyan)-chloroquine (purple) to 3D0G receptors (d) 4-Dibenzofuranamine (cyan)-chloroquine (purple) to 1R4L receptors

The type of interaction in two-dimensional form is shown in Figure 3.



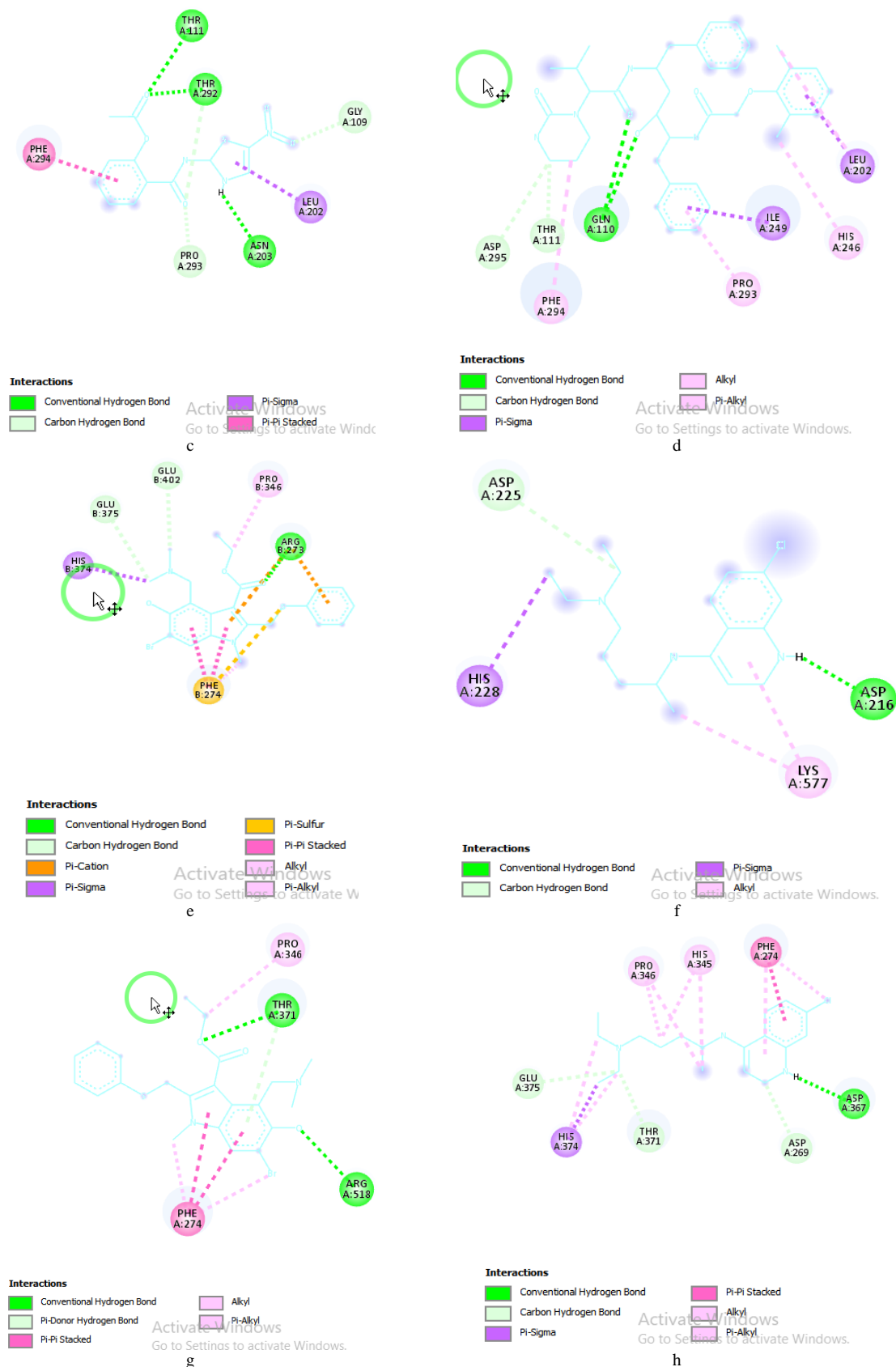


Figure 3. Two-dimensional shape (a) Aziridine-2-carbothioamide-7BQY (b) Lopinavir-7BQY (c) Aziridine-2-carbothioamide-2GZ7 (d) Lopinavir-2GZ7 (e) 4-Dibenzofuranamine-3D0G (f) Chloroquine -3D0G (g) 4-Dibenzofuranamine-1R4L (h) Chloroquine-1R4L

By using the tools, the pharmacokinetic profile of compounds such as absorption, distribution, and ligand metabolism could be evaluated. The results of screening the physicochemical properties of Aziridine-2-

carbothioamide and 4-Dibenzofuranamine compounds, as well as the comparison compounds of lopinavir and chloroquine can be seen in table 3.

Table 3. The results of reading the physicochemical properties by applying Lipinski's five rule to receptor protein compounds

Compound	Lipinski Five Rules					Result
	MW (Dalton)	Log P	NBD	HBA	MR (cm ³ mol ⁻¹ K ⁻¹)	
Aziridine-2-carbothioamide	307.28	2.04	1	6	76.65	Yes
4-Dibenzofuranamine	477.41	4.43	1	4	122.69	Yes
Lopinavir	628.80	5.92	4	5	187.92	No
Chloroquine	319.87	4.63	1	2	97.41	Yes

MW: Molecule Weight < 500 Dalton ,LogP: Coefficient Partition < 5, HBD: Hydrogen Bond Donor < 5 ,HBA: Hydrogen Bond Acceptor < 10, MR: Molar Refractivity (40 < MR < 130)

Many kinds of toxicity assessment were carried out in this test, such as LD50, skin sensitization, Ames toxicity (Ames test devised by a scientist "Bruce Ames" is used to assess the potential carcinogenic effect of chemicals (Pan, 2021)), and hepatotoxicity. The Globally Harmonized System classifies LD50 into 6 classes: class I (fatal if swallowed): LD50 5mg/kg; class II (fatal if swallowed): 5

< LD50 50 mg/kg; class III (toxic if swallowed): 50 < LD50 300 mg/kg; class IV (harmful if swallowed): 300 < LD50 2000 mg/kg; class V (may be harmful if swallowed): 2000 < LD50 5000 mg/kg; and class VI (non-toxic): LD50 > 5000 mg/kg [43]. The results of the predicted toxicity are shown in Table 4.

Table 4. The predicted results of the toxicity properties of the protein compounds of Aziridine-2-carbothioamide and 4-Dibenzofuranamine, as well as the comparison compounds of lopinavir and chloroquine by using pkCSM Online Tools and Prottox II Online Tools receptor protein compounds.

Compounds	Toxicity Category				Results (GHS)
	LD50 (mg/ kg)*	Skin sensitization**	Ames toxicity**	Hepatotoxicity **	
Aziridine-2-carbothioamide	1350	No	Yes	Yes	4
4-Dibenzofuranamine	340	No	No	No	4
Lopinavir	5000	No	No	Yes	5
Chloroquine	750	No	Yes	Yes	4

*Prottox II Online Tools ,** pkCSM Online Tools

4. Discussion

The determination of the minimum energy in the compounds of Aziridine-2-carbothioamide and 4-Dibenzofuranamine was carried out with the aim of obtaining a more accurate calculation of the molecule and a more stable final conformation (Joshi et al. 2020). This energy is the most possibly minimum energy in the stereochemical form and the most stable form for docking. The validation process was carried out with the aim of ensuring the method used was validated and a good method was obtained so that it can be continued in the next research stage. The parameter observed at this stage was the RMSD value resulting from the redocking of native ligand with its protein (Yanagisawa et al. 2022). RMSD is the process of measuring two poses by comparing the atomic positions between the experimental structure and the docked protein structure (Sarathi & Padhi, 2021). The method is said to be valid and good if the resulting RMSD value is < 2 (Yanagisawa et al. 2022).

PyRx-Vina® produces two types of RMSD: RMSD lower and RMSD upper. However, only the value of the lower RMSD was analyzed because the lower RMSD was obtained by searching for all possible atoms in a symmetrical molecule (Shi et al. 2022). That is, the lower RMSD is calculated from the conformational approach of the native ligand in all symmetries. Atoms that cannot be distinguished will give correct results by correcting the symmetry so that the lower RMSD value can be more precise (Prateeksha et al. 2021).

Based on the validation process, the RMSD value was obtained. These values were different, possibly because

the molecules analyzed are symmetrical molecules so that the potential substructures correspond to positions in the molecule (not all with the same position) (Laksmiani et al. 2020). The six native ligands were known to meet the validation standards with RMSD values < 2 so that docking of the test compounds on the respective receptors can be carried out.

The results of molecular docking of molecules in this study include the value of binding affinity and its RMSD. Binding affinity is the strength of the interaction between two or more reversibly bound molecules (Aljahdali et al. 2021). The score is a parameter of the strength of the binding affinity of the test ligand to the receptor (Takaya et al. 2020). The more stable ligand-protein interaction will be reflected by the lower score (minus). If the ligand binding to the receptor is more stable, it can be predicted that its activity will also increase (Morris & Corte, 2021).

Table 2 shows that there were compounds with native ligands that have different binding affinity replication data, and this difference was predicted due to differences in ligand binding to amino acids at the receptor (Aljahdali et al. 2021). At the 7BQY receptor, Aziridine-2-carbothioamide obtained a binding affinity value of -5.7 kcal/mol, lopinavir of -5,633 kcal/mol, and native ligand of -5,467 kcal/mol. From this value, it was known that Aziridine-2-carbothioamide had the best binding affinity value so that the compound was more effective (as a drug) and was able to inhibit the replication process of the SARS-CoV-2 virus better. Meanwhile, at the 2GZ7 receptor, Aziridine-2-carbothioamide obtained a binding affinity value of -6,667 kcal/mol, lopinavir of -7.8 kcal/mol, and a native ligand of 5.6 kcal/mol. From these values, it is known that lopinavir had the best binding

affinity value so that the comparison compound is more effective (as a drug) and was able to better inhibit the replication process of the SARS-CoV-2 virus. However, Aziridine-2-carbothioamide had a better binding affinity value than the native ligand.

At the 3D0G receptor, 4-Dibenzofuranamine obtained a binding affinity value of -6.567 kcal/mol, chloroquine of -4.1 kcal/mol, the first native ligand of -3.367 kcal/mol, and the second native ligand of -5.3 kcal/mol. From this value, it is known that 4-Dibenzofuranamine has the best binding affinity value, so that the compound is predicted to be more effective as a drug and able to inhibit the attachment of the virus to the ACE2 receptor.

Meanwhile, the second native ligand was known to have a better binding affinity value than the first native ligand. Furthermore, at the 1R4L receptor, 4-Dibenzofuranamine obtained a binding affinity value of -8.1 kcal/mol, chloroquine of -6.667 kcal/mol, the first native ligand of -9.167 kcal/mol, and the second native ligand of -6.267 kcal/mol. From this value, it is known that the first native ligand with the name (s,s)-2-([1-carboxy-2-[3-(3,5-dichloro-benzyl)-3imidazole-4-yl]-ethylamino]-4-methyl-pentanoic acid has the best binding affinity value so that the compound is more effective (as a drug) and is able to inhibit the attachment of the virus to the ACE2 receptor better.

However, 4-Dibenzofuranamine had a better binding affinity value than the comparison compound, namely chloroquine. A hydrogen bond is one that occurs between a hydrogen atom (H) in one molecule and one atomic element (F, O, N) in another molecule, which is the strongest dipole-dipole force (Meyer-Almes, 2020). In biological systems, nitrogen or oxygen atoms are donors and acceptors, especially atoms in the amine (-NH₂) and hydroxyl (-OH) groups. Due to the polar nature of the N-H and O-H bonds, the H atoms can hydrogen bond with acceptor atoms (Diningrat et al, 2021). Hydrogen bonds will be stable and have strong bonds if they have a bond length of < 2.7 (Domínguez-Villa et al. 2021; Diningrat et al. 2021).

The smaller the hydrogen bond distance between the ligand and the acid group is, the greater the affinity value is. The smaller the bond distance is, the stronger the bond is and not easily separated or the other way round (Domínguez-Villa et al, 2021). Hydrophobic bonds are nonpolar molecules that do not contain hydrated ions or have a dipole moment. This happens because in water, these molecules are insoluble or almost insoluble (Meyer-Almes et al. 2020). This binding is important in the process of combining the nonpolar region of the ligand with the nonpolar region of the receptor. The nonpolar region of the water-insoluble molecule and the surrounding water molecules will combine through hydrogen bonds to form a quasi-crystalline structure (icebergs) (Zhang et al. 2020). Hydrophobic binding is a parameter of the strong amino acid interaction between the ligand and the receptor which is useful in helping to maintain the binding conformation (Aljahdali et al. 2021) (Figure 2).

Electrostatic bonds describe the forces between polar atoms and are usually represented by the Coulomb potential. In general, there were two grading function approaches for hydrogen bond interactions: (i) using specific force field-based parameters related to van der

Waals and electrostatic energy potentials; (ii) using a directional term, where the hydrogen bond contribution was a function of the deviation of the geometric parameter from the ideal hydrogen bond (Zhang et al. 2020). Hydrophobic interactions and electrostatic interactions can increase conformational stability (Zhang et al. 2020).

The 3D visualization results showed that Aziridine-2-carbothioamide-lopinavir at the 2GZ7 receptor and 4-Dibenzofuranamine-chloroquine at the 1R4L receptor have the same binding position, so it could be predicted that the test compound has inhibitory activity (2GZ7) or attachment (1R4L) of the SARS-CoV virus. -2. Meanwhile, Aziridine-2-carbothioamide-lopinavir at the 7BQY receptor and 4-Dibenzofuranamine-chloroquine at the 3D0G receptor did not have the same position and angle of each atom. The similarity of the ligand pose with the comparison compound could be influenced by the RMSD value, where an RMSD value that was close to zero would cause the pose similarity between the two (Aljahdali et al. 2021).

Figure 3 shows the dotted lines. They are the bond distance (Aljahdali et al. 2021). Hydrogen bonds are indicated by dotted lines in lime green and salted egg green; Electrostatic interactions are indicated by the orange dotted line and hydrophobic interactions are indicated by the purple, neon pink, and pink dotted lines.

In Figures 3(a) and 3(b), it can be seen that the Aziridine-2-carbothioamide compound was more stable, supported by the presence of hydrogen bonds with the amino acids Asn 151, Arg 298, Thr 111, and Asp 295; and hydrophobic interactions with amino acids Ile 106 and Val 104. Meanwhile, the comparison compound lopinavir only had two hydrogen bonds with the amino acids Lys 5 and Lys 137; and hydrophobic interaction with amino acid Arg 4. Meanwhile, in Figures 3(c) and 3(d), the comparison compound of lopinavir was more stable, supported by the presence of hydrogen bonds with amino acids Gln 110 (2), Thr 111, and Asp 295; and hydrophobic interactions with the amino acids Leu 202 (2), Ile 249, His 246, Phe 294, and Pro 293. Aziridine-2-carbothioamide had hydrogen bonds with the amino acids Thr 111, Thr 292, Asn 203, Gly 109, and Pro 293; and had only two hydrophobic interactions with the amino acids Leu 202 and Phe 294.

In Figures 3(e) and 3(f), the 4-Dibenzofuranamine compound was more stable, supported by the presence of hydrogen bonds with amino acids Arg 273, Glu 375, and Glu 402; hydrophobic interactions with the amino acids His 374, Phe 274 (3), and Pro 346; and electrostatic interactions with the amino acid Arg 273 (2). Meanwhile, chloroquine has only two hydrogen bonds with the amino acids Asp 216 and Asp 225 and has only three hydrophobic interactions with the amino acids His 228 and Lys 577 (2).

Furthermore, in Figures 3(g) and 3(h), chloroquine compounds were more stable, supported by the presence of hydrogen bonds with amino acids Asp 367, Asp 269, Thr 371, and Glu 375; and hydrophobic interactions with the amino acids His 374, Phe 274 (3), and Pro 346 (2). Meanwhile, 4-Dibenzofuranamine has only three hydrogen bonds with the amino acids Thr 371 (2) and Arg 518; and has only five hydrophobic interactions with the amino acids Phe 274 (4) and Pro 346.

The prediction of physicochemical properties was carried out by checking the ligands of Aziridine-2-

carbothioamide and 4-Dibenzofuranamine, as well as comparison compounds lopinavir and chloroquine. Compounds are said to not meet if there are errors of more than one criterion, by means of the analysis of Molecular Weight (BM), logarithm of partition coefficient (Log P (XLogP3)), hydrogen bond acceptors (HBA), hydrogen bond donors (HBD), and molar refractivity. SwissADME was chosen because this platform does not incur costs and functions in calculating the molecular properties of ligands based on Lipinski's five rules (Ferdausi et al, 2022).

From Table 3, it can be seen that the compounds of Aziridine-2-carbothioamide, 4-Dibenzofuranamine, and chloroquine had a molecular weight of less than 500 Daltons, a LogP value less than 5, a hydrogen bond donor value less than 5, a hydrogen bond acceptor value less than 10, and the value of the molar refractivity was between 40 and 130. Thus, the compound of 4-Dibenzofuranamine and chloroquine complies with Lipinski's five rules and can be said to be easy to absorb and have high permeability. Therefore, the above compounds can be administered orally (Basu et al. 2020).

Meanwhile, lopinavir did not meet Lipinski's five laws because there were three criteria that were not met that are the molecular weight value of 628.80 Da ($BM < 500$ Da), the LogP value of 5.92, and the molar refractivity value of 187.92 ($40 < MR < 130$). Compounds can be said to not meet if there is more than one criterion that deviates. The condition for the value of LogP (XLogP3) is -0.4-5. The larger or the more positive the log P value is, the more hydrophobic is the molecule. If it is too hydrophobic, the level of toxicity will also be high because it will be retained longer in the lipid bilayer or the base of the cell membrane structure and distributed more widely in the body so that the selectivity of binding to the target enzyme is reduced (Missioui et al. 2022). Molar refractivity that does not meet the requirements would cause nonpolar compounds to be unable to form momentum so that they cannot bind to receptors, and their polar nature cannot excrete residues from compound metabolism (Cheng et al. 2021). Therefore, lopinavir compounds will be difficult to absorb and have low permeability.

Toxicity is the ability of a chemical substance to cause damage to organisms either when used or when in the environment (Upreti et al. 2021). A toxicity test is carried out if it is known that the compound has a better predictive activity than the comparison compound based on the equation of the Quantitative Structure and Activity Relationship (HKSA) (Cheng et al. 2021).

Based on Table 4, the results obtained for all compounds were proven to have no toxicity on skin sensitization analysis so all compounds did not cause skin sensitization. For the results of the Ames toxicity test, there were two positive compounds, Aziridine-2-carbothioamide and chloroquine, which means that both compounds are mutagenic and therefore can act as carcinogens (Ahmad et al. 2021). Then, the hepatotoxicity test showed positive results on the protein compound Aziridine-2-carbothioamide and the comparison compound of lopinavir and chloroquine, so it could be predicted that the three compounds were toxic to the liver. In addition, for oral toxicity in experimental animals (LD50), testing and classification of toxicity are carried out on the Protox II Online Tools website. Lethal dose 50 (LD50) is statistical data of a quantity to express a single dose of a

compound that is estimated to cause death or toxic effects in 50% of experimental animals after treatment. The smaller the toxic value is, the more toxic is the compound, or the other way round (Khaerunnisa et al. 2020).

From these tests, it can be predicted that the compound of Aziridine-2-carbothioamide has an LD50 value of 1350 mg/kg in experimental animals, while the compound of 4-Dibenzofuranamine is 340 mg/kg and the comparison compound of chloroquine is 750 mg/kg so that the three compounds are classified in class 4 GHS ($300 < LD50 < 2000$ mg/kg), which means the compound has a relatively low toxicity effect (Ahmad et al. 2021). Meanwhile, the comparison compound of lopinavir is predicted to have a value of 5000 mg/kg so that the compound is classified in class 5 GHS ($2000 < LD50 < 5000$ mg/kg), which means it has a low acute toxicity effect. The greater the toxic value, the less toxic is a compound or the other way round (Khaerunnisa et al. 2020; Ahmad et al. 2021).

5. Conclusion

The Aziridine-2-carbothioamide compound at the NSP5 receptor (7BQY) did not have a significant difference in binding affinity values with the comparison compound of lopinavir, while Aziridine-2-carbothioamide at the NSP5 receptor (2GZ7); and 4-Dibenzofuranamine at the ACE2 receptors (3D0G and 1R4L) had a significant difference in binding affinity respectively to the comparator lopinavir and chloroquine. However, the binding affinity of 4-Dibenzofuranamine is less effective than the native ligand of the 1R4L receptor, so further research is recommended to test 4-Dibenzofuranamine at the ACE2 receptor with a different code. To develop the antiviral potential of SARS-CoV-2, the ligand needs to be observed through molecular dynamics analysis at a later stage.

6. Conflict of Interest

The authors declare no financial or commercial conflict of interest.

Acknowledgment

This study was financially supported by the Director of Research, Technology and Community Service (DRTPM), Ministry of Education, Research, Technology and Higher Education, Republic of Indonesia. Basic Research of Higher Education with contract number 002/UN33.8/DRTPM/PL/2022.

References

- Lai, C. C., Shih, T. P., Ko, W. C., Tang, H. J., & Hsueh, P. R. (2020). Severe acute respiratory syndrome coronavirus 2 (SARS-CoV-2) and coronavirus disease-2019 (COVID-19): The epidemic and the challenges. *Int. J. Antimicrob. Agents*, 55(3), 105924. <https://doi.org/10.1016/j.ijantimicag.2020.105924>
- Oglat, A. A., Oqlat, M. A., Oqlat, A. A., Alanagreh, L. A., Khaniabadi, P. M., Dheyab, M. A., ... & Althalji, O. (2022). Imaging Aspects (Chest Radiographic and CT Scan Findings) of COVID-19 with Clinical Classifications. *Jordan J. Biol. Sci.*, 15(3). <https://doi.org/10.54319/jjbs/150308>

- Malik, Y. A. (2020). Properties of coronavirus and SARS-CoV-2. *The Malays. J. Pathol.*, *42*(1), 3-11. <http://mjpath.org.my/2020/v42n1/properties-of-coronavirus.pdf>.
- Awaid, H. A. A. (2022). Complications of COVID-19: Correlation between Arrhythmia, Acute Cardiac Injury and COVID-19 Severity. *Jordan J. Biol. Sci.*, *15*(2). <https://doi.org/10.54319/jjbs/150201>
- Beyerstedt, S., Casaro, E. B., & Rangel, É. B. (2021). COVID-19: angiotensin-converting enzyme 2 (ACE2) expression and tissue susceptibility to SARS-CoV-2 infection. *Eur. J. Clin. Microbiol. Infect. Dis.*, *40*(5), 905-919. <https://doi.org/10.1007/s10096-020-04138-6>
- Yashvardhini, N., Kumar, A., & Jha, D. K. (2022). Analysis of SARS-CoV-2 mutations in the main viral protease (NSP5) and its implications on the vaccine designing strategies. *Vacunas*, *23*(1), 1-13. <https://doi.org/10.1016/j.vacune.2022.08.001>
- Ugwuja, E. I., & Nwankwo, J. O. (2022). An Overview of COVID-19 in Sub-Saharan Africa: the Transmissibility, Pathogenicity, Morbidity and Mortality so far. *Jordan J. Biol. Sci.*, *15*(2). <https://doi.org/10.54319/jjbs/150208>
- Oroojalian, F., Haghbin, A., Baradaran, B., Hemmat, N., Shahbazi, MA, Baghi, HB, Mokhtarzadeh, A., & Hamblin, MR (2020). Novel insights into the treatment of SARS-CoV-2 infection: an overview of current clinical trials. *Int. J. Biol. Macromol.*, *165*, 18-43. <https://doi.org/10.1016/j.ijbiomac.2020.09.204>
- Fadaka, A. O., Sibuyi, N. R. S., Madiehe, A. M., & Meyer, M. (2022). Computational insight of dexamethasone against potential targets of SARS-CoV-2. *J. Biomol. Struct. Dyn.*, *40*(2), 875-885. <https://doi.org/10.1080/07391102.2020.1819880>
- Sharma, R., Prajapati, G. K., & Akhoury, G. (2021). Pentagalloylglucose, a phytochemical from Terminalia chebula can efficiently prevent SARS-CoV-2 entry: In Silico study. *Isr. J. Plant Sci.*, *68*(1-2), 124-132. <https://doi.org/10.1016/j.ifs.2020.117963>
- Roe, M. K., Junod, N. A., Young, A. R., Beachboard, D. C., & Stobart, C. C. (2021). Targeting novel structural and functional features of coronavirus protease nsp5 (3CLpro, Mpro) in the age of COVID-19. *J. Gen. Virol.*, *102*(3). <https://doi.org/10.1099/jgv.0.001558>
- Mody, V., Ho, J., Wills, S., Mawri, A., Lawson, L., Ebert, M. C., ... & Taval, S. (2021). Identification of 3-chymotrypsin like protease (3CLPro) inhibitors as potential anti-SARS-CoV-2 agents. *Commun. Biol.*, *4*(1), 1-10. <https://doi.org/10.1038/s42003-020-01577-x>
- Singh, R., Bhardwaj, V. K., Sharma, J., Purohit, R., & Kumar, S. (2022). In-silico evaluation of bioactive compounds from tea as potential SARS-CoV-2 nonstructural protein 16 inhibitors. *J. Tradit. Complementary Med.*, *12*(1), 35-43. <https://doi.org/10.1016/j.jtcm.2021.05.005>
- Diningrat, D. S., Sari, A. N., Harahap, N. S., & Kusdianti, K. (2021). Potential of Hanjeli (Coix lacryma-jobi) essential oil in preventing SARS-CoV-2 infection via blocking the Angiotensin Converting Enzyme 2 (ACE2) receptor. *J. Plant Biotechnol.*, *48*(4), 289-303. <https://doi.org/10.5010/JPB.2021.48.4.289>
- Diningrat, D. S., Sari, A. N., & Harahap, N. S. (2021). In silico study of the toxicity and antiviral activity prediction of jamblang (Syzygium cumini) leaves essential oil as ace2 inhibitor. *Pharmacologyonline*, *13*, 1334-1351. https://pharmacologyonline.silae.it/files/archives/2021/vol3/PhOL_2021_3_A146_Diningrat.pdf
- da Silva Hage-Melim, L. I., Federico, L. B., de Oliveira, N. K. S., Francisco, V. C. C., Correia, L. C., de Lima, H. B., Gomes, S. Q., Barcelos, M. P., & Francischini, I. A. G. (2020). Virtual screening, ADME/Tox predictions and the drug repurposing concept for future use of old drugs against the COVID-19. *Life Sci.*, *256*, 117963.
- Mills, C. L., Beuning, P. J., & Ondrechen, M. J. (2015). Biochemical functional predictions for protein structures of unknown or uncertain function. *Comput. Struct. Biotechnol. J.*, *13*, 182-191. <https://doi.org/10.1016/j.csbj.2015.02.003>
- Perrella, F., Coppola, F., Petrone, A., Platella, C., Montesarchio, D., Stringaro, A., Ravagnan, G., Fuggetta, M.P., Rega, N. & Musumeci, D., 2021. Interference of Polydatin/Resveratrol in the ACE2: Spike recognition during COVID-19 infection. A focus on their potential mechanism of action through computational and biochemical assays. *Biomol.*, *11*(7), 1048. <https://doi.org/10.3390/biom11071048>
- Joshi, T., Sharma, P., Mathpal, S., Joshi, T., Maiti, P., Nand, M., Pande, V. & Chandra, S. (2022). Computational investigation of drug bank compounds against 3C-like protease (3CLpro) of SARS-CoV-2 using deep learning and molecular dynamics simulation. *Mol. Diversity*, *26*(4), 2243-2256. <https://doi.org/10.1007/s11030-021-10330-3>
- Sarathi, P., & Padhi, S. (2021). Insight of the various in silico screening techniques developed for assortment of cocrystal formers and their thermodynamic characterization. *Drug Dev. Ind. Pharm.*, *47*(10), 1523-1534. <https://doi.org/10.1080/03639045.2022.2042554>
- Pan, X. (2021). *Mutagenicity Evaluation of Nanoparticles by the Ames Assay. In Environmental Toxicology and Toxicogenomics: Principles, Methods, and Applications.* Springer. New York, 275-285.
- Yanagisawa, K., Kubota, R., Yoshikawa, Y., Ohue, M., & Akiyama, Y. (2022). Effective Protein-Ligand Docking Strategy via Fragment Reuse and a Proof-of-Concept Implementation. *ACS Omega*, *34*, 30265-30274. <https://doi.org/10.1021/acsomega.2c03470>
- Shi, L., Wen, Z., Song, Y., Wang, J., & Yu, D. (2022). Computational investigation of potent inhibitors against SARS-CoV-2 2'-O-methyltransferase (nsp16): Structure-based pharmacophore modeling, molecular docking, molecular dynamics simulations and binding free energy calculations. *J. Mol. Graphics Modell.*, *108*, 108306. <https://doi.org/10.1016/j.jmgm.2022.108306>
- Prateeksha, G., Rana, T. S., Asthana, A. K., Singh, B. N., & Barik, S. K. (2021). Screening of cryptogamic secondary metabolites as putative inhibitors of SARS-CoV-2 main protease and ribosomal binding domain of spike glycoprotein by molecular docking and molecular dynamics approaches. *J. Mol. Struct.*, *1240*, 130506. <https://doi.org/10.1016/j.molstruc.2021.130506>
- Laksmiani, N. P. L., Larasanty, L. P. F., Santika, A. A. G. J., Prayoga, P. A. A., Dewi, A. A. I. K., & Dewi, N. P. A. K. (2020). Active compounds activity from the medicinal plants against SARS-CoV-2 using in silico assay. *Biomed. Pharmacol. J.*, *13*(2), 873-881. [https://doi.org/10.4209/aaqr.2020.07.0388](https://dx.doi.org/10.13005/bpj/1953Zhang, L., Yang, L., Zhou, Q., Zhang, X., Xing, W., Zhang, H., Toriba, A., Hayakawa, K & Tang, N. (2020). Impact of the COVID-19 outbreak on the long-range transport of particulate PAHs in East Asia. <i>Aerosol Air Qual. Res.</i>, <i>20</i>(10), 2035-2046. <a href=)

- Aljahdali, M. O., Molla, M. H. R., & Ahammad, F. (2021). Compounds identified from marine mangrove plant (*Avicennia Alba*) as potential antiviral drug candidates against WDSV, an in-silico approach. *Mar. Drugs*, **19**(5), 253. <https://doi.org/10.3390/md19050253>
- Takaya, D., Niwa, H., Mikuni, J., Nakamura, K., Handa, N., Tanaka, A., Yokoyama, S., & Honma, T. (2020). Protein ligand interaction analysis against new CaMKK2 inhibitors by use of X-ray crystallography and the fragment molecular orbital (FMO) method. *J. Mol. Graphics Modell.*, **99**, 107599. <https://doi.org/10.1016/j.jmgm.2020.107599>
- Morris, C. J., & Corte, D. D. (2021). Using molecular docking and molecular dynamics to investigate protein-ligand interactions. *Mod. Phys. Lett. B*, **35**(08), 2130002. <https://doi.org/10.1142/S0217984921300027>
- Diningrat, D. S., Harahap, N. S., Risfandi, M., & Sari, A. N. (2021). Antioxidant and antibacterial activities of *Coix lacrymajobi* seed and root oil potential for meningitis treatment. *Jordan J. Biol. Sci.*, **14**(5). <https://doi.org/10.54319/jjbs/140501>
- Domínguez-Villa, F. X., Durán-Iturbide, N. A., & Ávila-Zárraga, J. G. (2021). Synthesis, molecular docking, and in silico ADME/Tox profiling studies of new 1-aryl-5-(3-azidopropyl) indol-4-ones: Potential inhibitors of SARS CoV-2 main protease. *Bioorg. Chem.*, **106**, 104497. <https://doi.org/10.1016/j.bioorg.2020.104497>
- Meyer-Almes, F. J. (2020). Repurposing approved drugs as potential inhibitors of 3CL-protease of SARS-CoV-2: Virtual screening and structure based drug design. *Comput. Biol. Chem.*, **88**, 107351. <https://doi.org/10.1016/j.compbiolchem.2020.107351>
- Zhang, D. H., Wu, K. L., Zhang, X., Deng, S. Q., & Peng, B. (2020). In silico screening of Chinese herbal medicines with the potential to directly inhibit 2019 novel coronavirus. *J. Integr. Med.* **18**(2), 152-158. <https://doi.org/10.1016/j.joim.2020.02.005>
- Ferdausi, N., Islam, S., Rimti, F.H., Quayum, S.T., Arshad, E.M., Ibnat, A., Islam, T., Arefin, A., Ema, T.I., Biswas, P. & Dey, D., 2022. Point-specific interactions of isovitexin with the neighboring amino acid residues of the hACE2 receptor as a targeted therapeutic agent in suppressing the SARS-CoV-2 influx mechanism. *J. Adv. Vet. Anim. Res.*, **9**(2), 230. <https://doi.org/10.5455%2Fjavar.2022.i588>
- Basu, A., Sarkar, A., & Maulik, U. (2020). Molecular docking study of potential phytochemicals and their effects on the complex of SARS-CoV2 spike protein and human ACE2. *Sci. Rep.*, **10**(1), 1-15. <https://doi.org/10.1038/s41598-020-74715-4>
- Missioui, M., Said, M. A., Demirtaş, G., Mague, J. T., Al-Sulami, A., Al-Kaff, N. S., & Ramli, Y. (2022). A possible potential COVID-19 drug candidate: Diethyl 2-(2-(2-(3-methyl-2-oxoquinoxalin-1 (2H)-yl) acetyl) hydrazono) malonate: Docking of disordered independent molecules of a novel crystal structure, HSA/DFT/XRD and cytotoxicity. *Arabian J. Chem.*, **15**(2), 103595. <https://doi.org/10.1016/j.arabjc.2021.103595>
- Cheng, F.J., Huynh, T.K., Yang, C.S., Hu, D.W., Shen, Y.C., Tu, C.Y., Wu, Y.C., Tang, C.H., Huang, W.C., Chen, Y. & Ho, C.Y., 2021. Hesperidin is a potential inhibitor against SARS-CoV-2 infection. *Nutr.*, **13**(8), 2800. <https://doi.org/10.3390/nu13082800>
- Upreti, S., Prusty, J. S., Pandey, S. C., Kumar, A., & Samant, M. (2021). Identification of novel inhibitors of angiotensin-converting enzyme 2 (ACE-2) receptor from *Urtica dioica* to combat coronavirus disease 2019 (COVID-19). *Mol. Diversity*, **25**(3), 1795-1809. <https://doi.org/10.1007/s11030-020-10159-2>
- Ahmad, S., Abbasi, H. W., Shahid, S., Gul, S., & Abbasi, S. W. (2021). Molecular docking, simulation and MM-PBSA studies of nigella sativa compounds: a computational quest to identify potential natural antiviral for COVID-19 treatment. *J. Biomol. Struct. Dyn.*, **39**(12), 4225-4233. <https://doi.org/10.1080/07391102.2020.1775129>
- Khaerunnisa, S., Kurniawan, H., Awaluddin, R., Suhartati, S., & Soetjpto, S. (2020). Potential inhibitor of COVID-19 main protease (Mpro) from several medicinal plant compounds by molecular docking study. *Prepr.*, **2020**, 20200-30226. <https://doi.org/10.20944/preprints202003.0226.v1>

Protective Effects of Secoisolariciresinol Diglucoside on Arsenic-induced Renal Damage and Oxidative Stress in Rats

Tareq Nayef AlRamadneh^{1,*}, Muhannad I. Massadeh², Rania Algroom^{1,3}, Hashem A. Abu-Harirah¹, Kawther Faisal Amawi¹, Nada S. Daifalla⁴, Hammad Khalifeh Aldal'in⁵, Razan N. AlQuraan⁶, Rajesh Javaraiah⁷

¹Department of Medical Laboratory Sciences, Faculty of Allied Medical Sciences, Zarqa University, 132222 Al-Zarqa 13132, JORDAN; ²Department of Biology and Biotechnology, Faculty of science, The Hashemite University 13115 Zarqa Jordan; ³Department of Allied Medical Sciences, Zarqa University College, Al-Balqa Applied University, Zarqa, Jordan, 2000 Zarqa; ⁴Department of Basic Sciences, Deanship of Preparatory Year and Supporting Studies, Imam Abdulrahman Bin Faisal University, P.O. Box 1982, Dammam 34212, SAUDI ARABIA; ⁵Department of Medical Support, Al-Balqa Applied University, Al-Karak University College, Al-Karak 61710, Jordan; ⁶Department of Biological Sciences, Faculty of Science, Yarmouk University, Irbid 21163. JORDAN; ⁷Department of Biochemistry, Yuvaraja's College, University of Mysore, Mysuru-570005, Karnataka, INDIA.

Received: February 20, 2023; Revised: March 14, 2023; Accepted: March 20, 2023

Abstract

The naturally occurring metal Arsenic (AS) poses a hazard to human health as it can generate oxygen free radicals and oxidative stress. The build-up of free radicals may cause chronic renal insufficiency and abrupt renal failure. The significant lignan in flaxseed, secoisolariciresinol diglucoside (SDG), provides various health benefits. The current research investigates the preventive benefits of SDG against Arsenic trioxide (As₂O₃)-induced kidney damage.

Four groups of healthy Wistar rats were equally distributed and received daily injections for 5 days as follows: Group 1 got injections (IP) of saline as a control; Group 2 got subcutaneous (SC) injections of SDG at 10 mg/kg/day; Group 3 got intraperitoneal (IP) injections of Arsenic trioxide (As₂O₃) at 20 mg/kg/day, and Group 4 got 20 mg/kg/day As₂O₃ IP followed by 10 mg/kg/day SDG subcutaneously one hour later. The impact of As₂O₃ on the kidney was measured using a variety of indicators including the Greatest Distributable, ROS levels in renal tissues, and malondialdehyde (MDA), as well as two renal function markers the blood urea nitrogen (BUN) and serum creatinine (CREA). Besides the histological examinations, the antioxidant molecule glutathione was evaluated, and so were the functions of superoxide dismutase (SOD), catalase, and glutathione peroxidase (GSH-Px).

Arsenic trioxide (As₂O₃) enhanced MDA generation, oxygen free radicals, and As₂O₃ levels in kidney tissue while decreasing SOD and GSH-Px activity, and the ratio of reduced glutathione to oxidized glutathione. Moreover, serum As₂O₃ elevated BUN and serum CREA activity. As₂O₃ induced kidney damage, according to histopathological alterations. Interestingly, SDG treatment reduced ROS generation in serum and kidney and restored antioxidant enzyme levels. In addition, the SDG-treated rats showed significant improvement in all nephrotoxic features.

According to the results of this investigation, SDG exhibited an exceptional restorative impact on Arsenic trioxide-mediated kidney cytotoxicity.

Keywords: Secoisolariciresinol diglucoside, Renal toxicity, Antioxidant enzyme, Heavy metal

1. Introduction

Humans and animals are exposed to environmental hazardous metals and compounds like mercury (Hg), lead (Pb), cadmium (Cd), uranium (U), and arsenic (As), which affect the structure and function of several organs. Natural sources of As include air, soil, and water, but it can also be created artificially. There are different types of As which may or may not contain carbon (organic and inorganic, respectively) (Hilal and Ismail, 2008; Sall *et al.*, 2020). The most frequent inorganic types of As that enter the human body from contaminated drinking water are trivalent arsenite (As^{III}) and pentavalent arsenate (As^V) (Health and Services, 1999; Tchounwou *et al.*, 2019). When drinking As-contaminated water regularly, poisoning develops in all

body regions. The kidneys, which are essential for As biotransformation and exclusion, are the most often targeted organ for As deposit. Excessive and continuous exposure to As increases the incidence of kidney cancer in animals (Sotomayor *et al.*, 2020).

Epithelial cells of the kidney have very high reabsorptive power. Because of their anatomical position, they are the prime target for filtered toxicants and hence are highly receptive to As toxicity (Chang and Singh, 2019). Studies carried out on rats treated with arsenate showed an enlargement of mitochondria and reduced respiratory functions (Zhao *et al.*, 2018). The multifactorial mechanisms in metal-induced toxicity involve the metal-induced production of ROS (Hu *et al.*, 2020).

Arsenic metal is a well-studied pro-oxidant. Metabolic abnormalities caused by oxidative stress include amino

* Corresponding author. e-mail : talramadneh@zu.edu.jo.

acid synthesis, methionine cycle (transmethylation), membrane phospholipid degradation, and purine metabolism, contributing to cell toxicity and death. Reduced tricarboxylic acid cycle (TCA cycle), disrupted carbohydrate metabolism, oxidative pentose pathway, and the hexose monophosphate shunt (HMP-shunt) pathway alteration or gluconeogenesis may be responsible for damaging the Brush Border Membrane (BBM) as well as the mitochondria in kidney's proximal tubules (Wang *et al.*, 2017; Al-Groom, 2022). Several researchers have shown that chelating compounds may be utilized to minimize As-induced toxicity (Flora *et al.*, 2007; Bjørklund *et al.*, 2020; Nurchi *et al.*, 2020). However, The role of different antioxidants against As poisoning has been studied widely. These studies have established the fact that the dispensation of antioxidants contributes to the prevention of symptoms of As poisoning and diminution of the absorption of As in tissues (Bjørklund *et al.*, 2020).

As the best plant source of omega-3 fatty acid ALA, flaxseed (*Linum usitatissimum*) has been well known. It also contains minerals such as manganese, which is an essential mineral for bone and blood health. Flaxseed contains several lignans, among which SDG is the major one (Al-Mamoori *et al.*, 2019; Ebrahimi *et al.*, 2021; Al-Mamoori and Aburjai, 2022). In vivo and in vitro studies revealed the antioxidant activity of the SDG in flaxseed (Kezimana *et al.*, 2018). Flaxseed therapy has been shown to slow the progression of atherosclerosis because of its lignan concentration and the antioxidant impact of SDG (Parikh and Pierce, 2019; Bujok *et al.*, 2021; AlRamadneh *et al.*, 2022). When rats with streptozotocin-induced diabetes were given SDG, there was a considerable reduction in glucose and lipid concentrations and an improvement in insulin levels which reduces the chance of developing diabetes (Prasad *et al.*, 2000; Draganescu *et al.*, 2021). SDG is effective against inflammation, lowering reactive oxygen species levels and decreasing apoptosis. Furthermore, SDG has been shown to defend against heavy metal-induced kidney impairment (Aqeel *et al.*, 2019; Aqeel *et al.*, 2020; Zhang *et al.*, 2020; Aqeel *et al.*, 2021). Nevertheless, no studies have been done to test whether SDG can prevent As-induced nephrotoxicity. As a result, the current research looked at the antioxidant status, several biochemical indicators, and histological alterations in rats with As-induced nephrotoxicity to determine whether flaxseed lignan-SDG might protect them.

2. Materials and methods

2.1. Chemicals

Chemicals and reagents utilized in this investigation were purchased from Sigma-Aldrich (Burlington, MA, USA), except the following: Sodium arsenite from Indiamart (Bengaluru, India), Reference SDG from Teco Diagnostics (Anaheim, CA 92807, USA), and Blood urea nitrogen (BUN) and creatinine (CREA) from StressMarq Biosciences (Cadboro Bay Village, Canada).

2.2. Isolation of SDG from flaxseed

As already mentioned, SDG was extracted and refined using HPLC (Aqeel *et al.*, 2019). Lignans were extracted from purified defatted flaxseed flour (200gm) using 50ml of methanol. The mixed components were incubated at

65°C for 4 hours in a circulating water bath, then centrifuged at 3000 rpm for 30 minutes to separate the sediment. The supernatant was acidified with 2M H₂SO₄ at pH 3.0 before being submitted to HPLC analysis using a Water Alliance e26925 model (Waters Corporation, USA) with an RP-C18 column (Sun fire) with a particle size of 5µm, photodiode array detectors (Waters model 2996), and chromatograms recorded at 280 nm. Five percent (v/v) acetonitrile in 0.01 M phosphate buffer at pH 2.8 (solvent A), and acetonitrile were used in the mobile phase (solvent B). All linear-gradient profiles were performed for 32 minutes at 1ml/min, and the temperature of the column was reset to 25°C. Running 0.5mg/ml of standard SDG produced a linear curve.

2.3. Experimental design

Animal experiments followed the guidelines approved by the institution (Approval No. In vivo/IAEC/012/2020). The rodents utilized were 24 male Wistar albino rats weighing 150 - 200 grammes. They were kept in a controlled environment with a temperature of 24° C, 12-hour light-dark cycles, and a humidity of 40 %. A regular pellet diet was provided to the rats (Hindustan Lever, Bangalore, India). Following a week of acclimation, the rats were separated into 4 groups: Group 1 (Control) received daily IP injections of 0.5 ml saline (0.9 % NaCl); Group 2 got SC injections of 10 mg/kg/day SDG in 0.5 ml saline, and Group 3 got IP injections of 20 mg/kg/day As₂O₃ in 0.5 ml saline. Since our objective was to study the acute effects of As exposure, sodium arsenate was injected in 4 doses, over a short period of time. We used a smaller dose of sodium arsenate in our study as compared to the standard value of sodium arsenate LD50 (FRANKE and Moxon, 1936), the amount utilized in prior studies (Hood *et al.*, 1987; Hood *et al.*, 1988).

Animals in Group 4 were given As₂O₃ + SDG. The rats in this group were given As₂O₃ IP injections of 20 mg/kg/day in 0.5 ml saline and SC injections of 10 mg/kg/day SDG in 0.5 ml saline 1 hour later. All animals in each group received their daily medications at a similar time. During the trial, hazardous signs, body mass, and feed consumption were followed. All animals were euthanized 24 hours after completing the experimental phase on the 5th day. Blood and urine samples were collected. The kidneys were extracted and homogenized in 15% (w/v) 0.1 M Tris-HCl, pH 7.5 using a Potter-Elvehjem homogenizer (Remi Motors, Mumbai, India). To eliminate debris from the cells, the homogenized tissues were spun for 15 min at 3000 rpm at 5°C. The supernatants were aliquoted and kept at -20 °C for later use.

2.4. Serum analysis

Jugular vein blood was collected using vacuum blood collection tubes containing the anticoagulant heparin sodium. Blood urea nitrogen (BUN) and creatinine (CREA) were measured by kits from StressMarq Biosciences after the samples were spun at 3,000 rpm for 10 minutes.

2.5. Biochemical examination

Renal tissue homogenates were used to analyze the levels of GSH, and GSSH (Puri and Meister, 1983) along with the antioxidant enzymes activity of CAT, SOD, and GSH-Px based on methods described by Sani, Radák, and

Avissar, respectively (Avissar *et al.*, 1994; Radák *et al.*, 1996; Sani *et al.*, 2006).

2.6. ROS & MDA level measurement in kidney tissue

The procedure of Weiss *et al.* was used to create a single-cell solution of 100gm kidney tissue (Weiss *et al.*, 2008). The amount of ROS produced inside the cells was measured using the oxidation-sensitive fluorometric probe dichloro-dihydro-fluorescein diacetate (DCFH-DA) as described previously (Aranda *et al.*, 2013).

Deng *et al.* approach was used to quantify MDA in kidney tissue (Deng *et al.*, 2012). 0.1 ml liver homogenate, 0.1 mol/L phosphate buffer, and 0.1 mol/L $FeCl_2$. The samples were boiled for 20 minutes with 1.0 ml of 10% TCA and 0.67 %TBA. Finally, the samples were chilled on ice, centrifuged at 3,000 rpm, and the amount of MDA generated in the supernatants was measured spectroscopically at 535 nm and reported as nmol/mg of protein.

2.7. Urine analysis to determine As species

Urine samples from rats were obtained (from 8 a.m. to 8 a.m.) and kept at $-20^{\circ}C$ before being analyzed. After spinning the urine samples for 30 minutes at 12,000 rpm, the supernatants were passed through 0.5- μ m PTFE unlined membrane filters. Analysis of urine was conducted with High-Performance Liquid Chromatography-hydrate generation-atomic fluorescence spectrometry, as previously described, to determine total As, arsenate (V), arsenite (III), and monomethylated metabolites (MMA and DMA, respectively) (Yu *et al.*, 2013). There was a concentration difference between As and As-related compounds in urine samples.

2.8. Estimation of the level of As in kidneys

A total of 0.5g of kidney tissue was digested for 2 days at $130^{\circ}C$ with HNO_3-HClO_4 solution. The samples were

diluted with de-ionized water after the HNO_3 had evaporated. The level of

As in kidney samples was determined using an Atomic Fluorescence Spectrometer (Perkin-Elmer 3100) and expressed as ng/g (Cui *et al.*, 2004).

2.9. Histopathological analysis

For histopathological studies, left kidneys were removed from rats of all groups and were incubated in 10% formalin solution for 30h at room temperature. 5-6 μ m thick sections of the kidneys were prepared, fixed, and paraffin-embedded. The sections were then stained with Hematoxylin and Eosin (H&E) and were examined using BX-FM; ZEISS microscopes (Jena, Germany).

2.10. Statistical analysis

The statistics were presented as mean \pm standard error mean (SEM). A one-way ANOVA was used to determine the statistical differences among the subjects. Statistical significance was calculated using Tukey's post hoc test ($p < 0.05$). The statistical program used for analysis was GraphPad Prism 6 (GraphPad Software, Inc., La Jolla, CA, USA).

3. Results

3.1. High-Performance Liquid Chromatography analysis of SDG

High-Performance liquid chromatogram indicated that SDG was the dominant lignan (2.0 mg/g) of flaxseed extract with the highest absorption at 280nm (Figure 1). SDG had a 34.714-retention time.

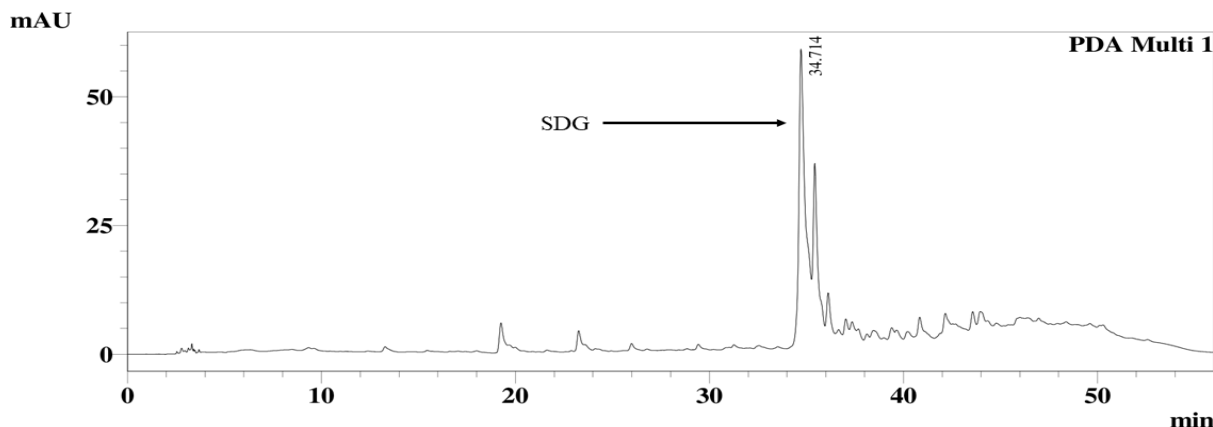


Figure 1. High-Performance Liquid Chromatography chromatograms of compounds in Flaxseed extract with SDG (Rt 34.714).

3.2. SDG attenuated As_2O_3 -induced renal damage

The two most essential indications for determining renal impairment are BUN and CREA. As a result, serum BUN and CREA concentrations were measured to see whether SDG might reduce As_2O_3 -induced kidney tissue damage. The levels of BUN and CREA in the As_2O_3

treated animals were substantially higher compared to the controls ($P < 0.05$). The values of BUN and CREA were not affected in animals receiving SDG alone. In the group that took As_2O_3 followed by SDG, however, BUN and CREA levels were lowered to near-normal levels (Figure 2).

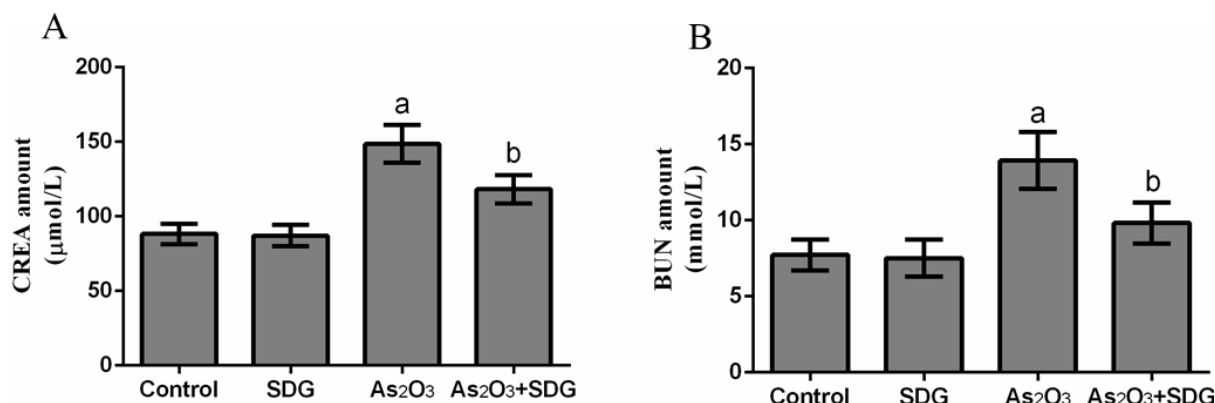


Figure 2. Impacts of SDG on the level of blood serum creatinine (CRET) and level of blood urea nitrogen (BUN) of rats that received As trioxides (As₂O₃), a considerable change at $p < 0.05$ when compared to the control group. ^b Significant change at $P < 0.05$ from the As₂O₃ group.

3.3. SDG restored the production of antioxidant enzymes in kidneys of rats with As₂O₃-induced toxicity

The batch of rats given As₂O₃ showed a considerable drop ($P < 0.05$) in CAT, SOD, and GSH-Px levels, whereas the saline-treated group showed no such changes (Table 1). As₂O₃ considerably reduced the activity of SOD and GSH-Px (24.18 ± 4.53 U per mg protein and 93.82 ± 6.29 mol/min/mg protein, respectively) in the As₂O₃-treated

group relative to the control group (52.775.18 U per mg protein and 139.159.42 mol/min/mg of protein, respectively). Furthermore, compared to the control group (233.1713.39 mol/min/mg of protein), the activity of CAT was significantly lowered (151.1712.77 mol/min/mg protein). However, in the As₂O₃-SDG treated group, concentrations of the measured enzymes were considerably higher ($P < 0.05$).

Table 1. Impact of SDG on antioxidant enzymes in As₂O₃-treated kidney homogenate

Parameters*	Group A	Group B	Group C	Group D
SOD (µmol/min /mg protein)	52.77±5.18	55.14±6.03	24.18±4.53 ^a	40.33±5.13 ^b
GSH-PX (µmol/min /mg protein)	233.17±13.34	227.55±15.77	151.17±12.77 ^a	212.37±17.18 ^b
CAT(µmol/min /mg protein)	139.15±9.61	142.88±8.93	93.82±6.29 ^a	125.14±12.22 ^b

Values are mean ± SEM. ^a Significant change at $p < 0.05$ from group A. ^b Significant change at $P < 0.05$ from group C. (Group A: Control group; Group B: SDG; Group C: As₂O₃ Group; Group D: As₂O₃ + SDG).

3.4. SDG reduced oxidative stress induced by As₂O₃ in kidneys

Kidney tissues exposed to As₂O₃ showed significantly higher levels of ROS and MDA than the controls ($P < 0.05$)

(Figure 3). Yet, following the exposure to As₂O₃, treatment of renal tissues with SDG dramatically lowered ROS and MDA to levels comparable to those of the control group (Figure 3).

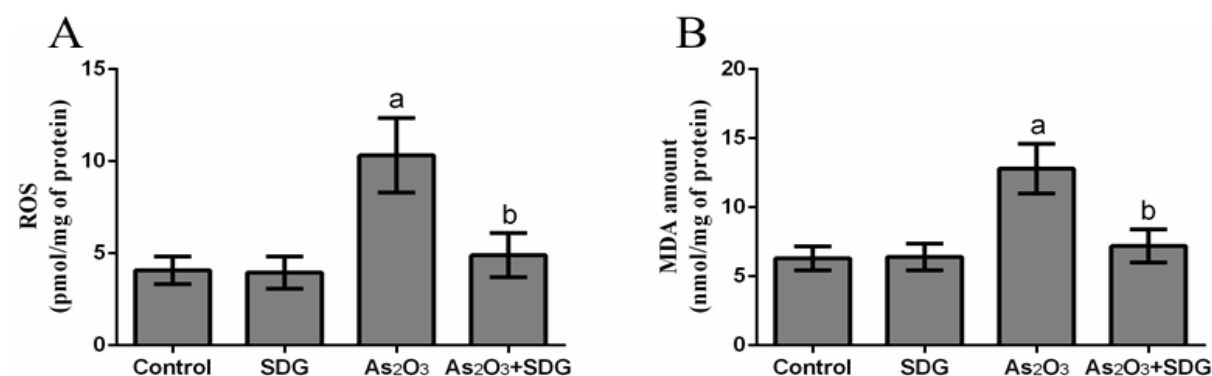


Figure 3. Impacts of SDG on MDA and ROS level in rats kidneys that received Astrioxides (As₂O₃), ^a Considerable change at $p < 0.05$ when compared to the control group. ^b Significant change at $P < 0.05$ from the As₂O₃ group.

3.5. SDG increased GSH and GSH/GSSG ratio in kidney tissues

In addition to ROS and electrophiles, GSH protects condensed protein situations against oxidative stress. Thiol GSH plays a dominant role in the human antioxidant

defence system. Thus, the GSH concentration and GSH/GSSG ratio in rat kidneys were determined. As per the study's findings, As₂O₃ treatment lowered GSH levels and GSH/GSSG ratios. On the other hand, SDG therapy raised GSH levels and the GSH/GSSG ratio in As₂O₃-treated rats, (Figures 4 a & 4b).

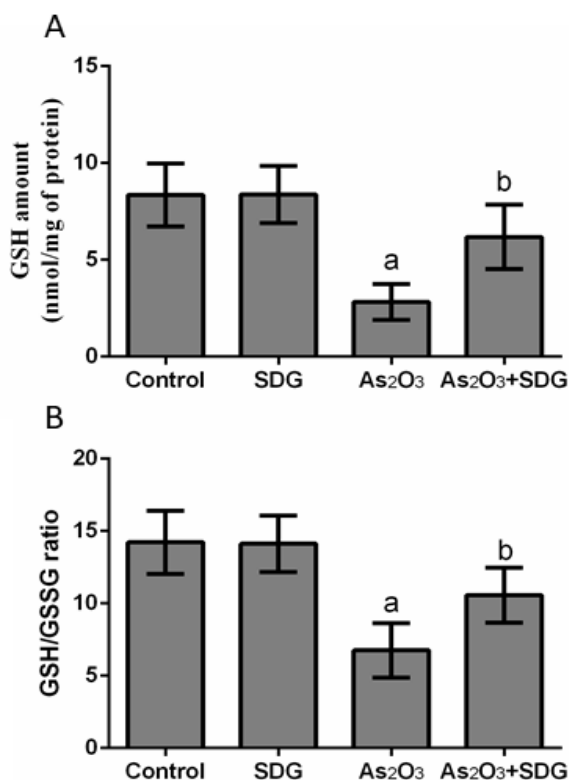


Figure 4. Effect of SDG on GSH level and the ratios of GSH/GSSG levels in rats kidneys that received As trioxides (As₂O₃). ^a Considerable change at p<0.05 compared to the control group. ^b Considerable change at P<0.05 from the As₂O₃ group.

3.6. SDG reduced the concentration of As in the kidneys

The kidneys' ability to retain As was examined to see whether SDG offered any protection against As₂O₃-induced renal damage. For the As₂O₃ group, the As levels in the kidney were significantly greater than those in the controls (Figure 5). Significantly lower As concentration

in the kidney (P<0.05) was achieved after injection of As₂O₃ and treatment with SDG (Figure. 5).

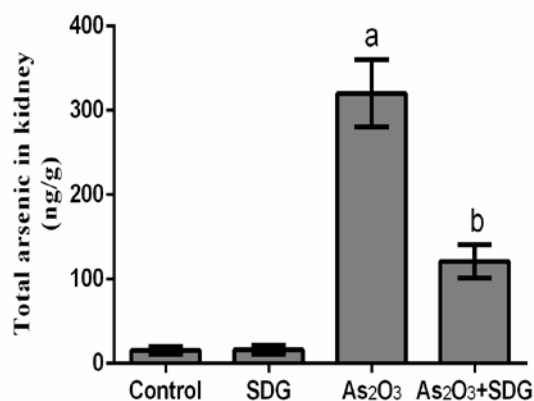


Figure 5. Effect of SDG on the total As accumulation in rat kidneys that received As trioxides (As₂O₃). ^a Significant change at p<0.05 compared to the control group. ^b Significant change at P<0.05 from the As₂O₃ group

3.7. SDG enhanced As excretion in the urine

We looked at the amounts of As excretion in the urine of rats to see whether SDG had any effect. The As levels in the urine of the As₂O₃ + SDG-treated rats rose substantially more than in the As₂O₃ alone-treated individuals (Table 2). Rats administered As₂O₃ + SDG had significantly lower urinary iAs(III) concentrations than rats given As₂O₃ alone (P<0.05).

Table2. Effects of SDG on the urine sample of rats received As₂O₃

Parameters*	Group A	Group B	Group C	Group D
Urine total arsenic (µg/L)	5.19±1.19	6.22±1.58	30.22±6.37 ^a	62.75±12.89 ^b
Permillage of iAs(III) in total arsenic (%)	7.63±2.48	7.97±2.77	48.47±9.79 ^a	57.94±12.81 ^b
Permillage of as(V) in total arsenic (%)	38.14±9.61	35.46±6.48	5.94±1.76 ^a	14.33±4.29 ^b
Permillage of MMA in total arsenic (%)	3.48±1.08	2.91±0.93	18.83±3.19 ^a	29.91±4.67 ^b
Permillage of DMA in total arsenic (%)	10.43±2.09	9.86±2.93	55.84±8.81 ^a	82.73±13.60 ^b

Values are mean ± SEM. ^a Significant change at p<0.05 from group A. ^b Significant change at P<0.05 from group C. (Group A: Control group; Group B: SDG; Group C: As₂O₃ Group; Group D: As₂O₃ + SDG).

3.8. Histopathological observation

The magnitude of kidney injury caused by As was assessed through histopathological examination. SDG-treated kidney tubules appeared normal in all control groups (Fig. 6a) and the SDG-treated group (Fig. 6b). In the group that did not receive SDG, As₂O₃-induced changes in the kidney tissues' histopathology including

epithelial damage, modified tubular cell organization, necrosis and interstitial fibrosis, infiltration of inflammatory cells, and hyperemia of the glomerular capillaries, dilation, as well as a decline and desertion of the Bowman's capsule (Figure.6c). Figure 6d shows that As₂O₃-induced necrosis, interstitial fibrosis, and epithelial degeneration were significantly reduced by SDG therapy.

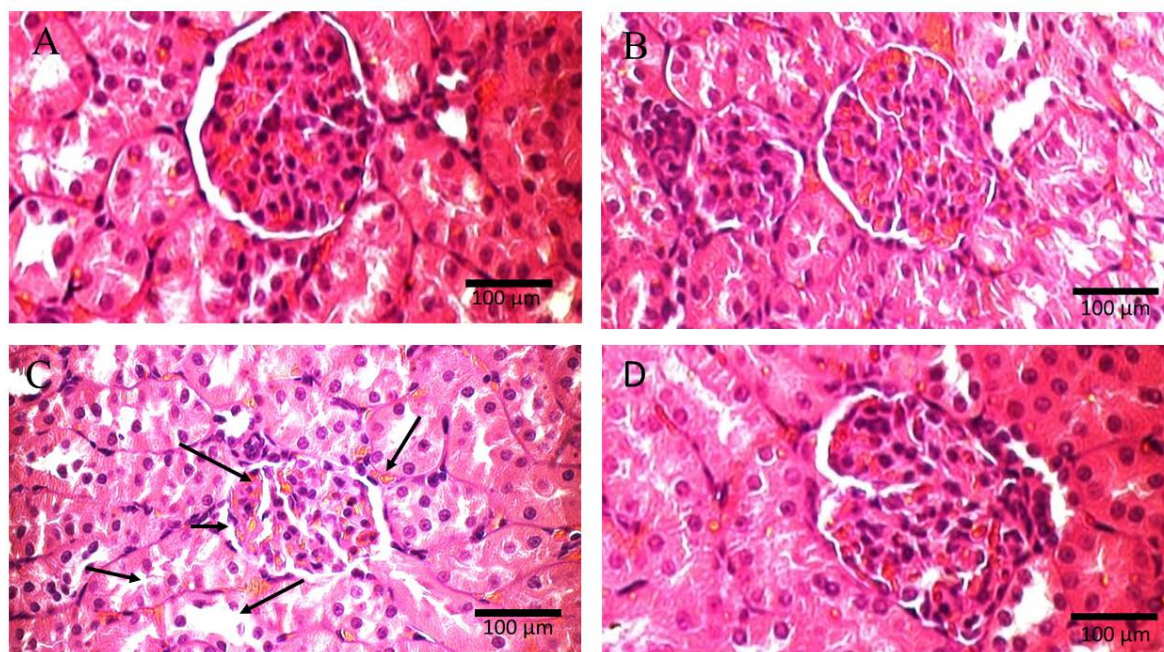


Figure 6. After five days of treatment with As trioxides (As_2O_3) and SDG, histology of rat kidneys. (a) Control group with normal morphology glomeruli and tubules. (b) Normal tubules and glomeruli in the SDG group. (c) As_2O_3 -treated rats' kidneys showing atrophied glomeruli with widened urinary space and de-generated tubules with a disturbed contour in the proximal tubule and distal tubule with some vacuoles inside it plus interstitial blood accumulation with tubular necrosis and glomerular hyperemia. (d) Group As_2O_3 + SDG. In comparison to the control group, renal tubules and glomeruli histology were almost normal.

4. Discussion

Arsenic (As), an ecological and environmental toxin, is associated with an elevated chance of heart disorders and tumours in humans. As compounds have adverse effects on many organs, including the kidneys (Rana *et al.*, 2018; Guo *et al.*, 2020). Due to its propensity to alter ROS configuration, As has a toxic impact on the human body (Guo *et al.*, 2020; Zaid Alkilani *et al.*, 2022). Various elements such as chelating agents were examined for their defensive impending in the toxicity induced by As. However, clinical applications have not been proved safe yet (Bjørklund *et al.*, 2020). The utilization of antioxidant dietary substances, which are naturally occurring to counteract the toxic effects of different environmental agents and toxicants, together with metalloids/ metals, has been gaining importance lately (Pace *et al.*, 2017). SDG enriched with ALA, and phytoestrogenic lignans provide nutritious sources of bioactive components that are co-therapeutic and co-preventative in several disorders (Rizwan *et al.*, 2014). Ameliorate treatment comprises dietary SDG consumption against toxicity induced by lead acetate was investigated (Aqeel *et al.*, 2021). But an in-depth study of the effectiveness of SDG against As_2O_3 nephrotoxicity has not been reported yet. The current study suggests that lipid peroxidation, ROS, and oxidative stress add to the nephrotoxicity caused by As_2O_3 . Prior treatment with SDG would help decrease the oxidative stress induced by As_2O_3 and reduce its damaging effect on kidneys. According to our results, SDG lowered renal As retention and elevated the concentration of distinct species of As and the quantity of methylated As excreted in the urine, which might explain its nephroprotective benefits in rats poisoned with As. Similar As properties related to environmental contact

with arsenicals including renal injury, GSH-Px, CAT, SOD activities, GSH concentration, and the GSH/GSSG ratio were all reduced by As_2O_3 , which caused renal tubule and glomerulus damage. This is in accordance with previous studies where long exposure to As damaged endothelial cell membrane lipids and proteins and nucleic acids, resulting in kidney tubule and glomerular dysfunction (Rizwan *et al.*, 2014).

Arsenic is mainly eliminated by the kidney. Consequently, renal tissues are the chief targets for toxicity due to the accumulation of As. As a result of the nephrotoxic effects of As, it was concluded that oxidative stress played a significant part in As-induced kidney injury (Emadi and Gore, 2010). It is during the cytoplasmic and mitochondrial metabolism of As that the free radicals of hydrogen peroxide (HO), superoxide anion (O_2^-), nitric oxide, hydroxyl radicals, and dimethylarginine oxidation are made (Shi *et al.*, 2004; Robles-Osorio *et al.*, 2015). An additional effect of arsenicals is their ability to slow down the thioredoxin reductase enzyme as well as the antioxidant glutathione synthase (Miodragović *et al.*, 2019).

The formation of free radicals overwhelms the body's antioxidant defense system (comprising antioxidants and antioxidant enzymes), and interrupts the antioxidant or pro-oxidative balance in kidney tissue, leading to OS-induced kidney damage, as evidenced by the increase in ROS and GSH reduction, antioxidant enzyme activity and enhancement of lipid peroxidation in renal tissue. It is possible that cellular energy metabolism is inhibited by As (Fu and Xi, 2020).

Arsenate is a phosphate analogue that can restore phosphate in cellular respiration and glycolytic pathways (Nurchi *et al.*, 2020). Research states that arsenite can interfere with the citric acid cycle and cellular ATP

production by reacting with proteins that include sulfuryl groups. This results in decreased intake of glucose, fatty acid oxidation, glucose production, and the movement of pyruvate dehydrogenase, which results in a decreased ability to generate ATP from citric acid (Bergquist *et al.*, 2009). Chromatin swapping, chromosomal abnormalities, and DNA hypo- and hypermethylation are all consequences of As exposure (Navasumrit *et al.*, 2019). The glomerular filtration membrane is damaged as demonstrated by renal histological abnormalities and higher than usual levels of BUN and CREA due to mitochondrial depolarization, ATP reduction, and angiogenic endothelium mortality. Antioxidant enzyme activity, GSH levels, and GSH/GSSG ratio were significantly restored following dual treatment with SDG and As.

As shown by histological studies, the repair of structural alterations in the renal tissues gave further proof of SDG protective action. Nephron-protecting properties may be attributed to SDG capability to inhibit the activity of radical's species and enhance the antioxidant defence system. Antioxidants, such as coenzyme Q and SDG, remove free radicals and reduce the complicated oxidative chain complex that produces reactive oxygen species. Previous studies have shown that O_2^- radicals produced in the mitochondria stimulate many antioxidant enzymes, including SOD, glutathione reductase, and CAT (Karapehliyan *et al.*, 2014). In a previous study, SDG suppressed NF- κ B, JNK, c-Jun/AP-1, caspase activation, and lipid peroxidation, which resulted in apoptosis (Kutuk *et al.*, 2006). SDGs have also been linked to reduced inflammation, increased cellular respiration, and elevated mitochondrial biogenesis (Tennen *et al.*, 2012). The SDG was found to improve renal microcirculation and guard the tubular epithelium. The antioxidant capacity of plasma, the amount of lipid peroxidation, and the impact of Fenton reaction products on lipid peroxidation were all increased when SDG was administered (Cadenas and Barja, 1999). In a reliability investigation, SDG protected the kidneys against oxidative stress generated by As_2O_3 and DNA destruction (Olson, 2021).

Arsenic accumulation, which is linked to kidney impairment, was observed to be influenced by SDG therapy. To make iAs, pentavalent iAs are reduced to trivalent iAs, which are oxidatively methylated to MMA, then reduced to trivalent MMA, and finally methylated to DMA, which is eliminated in the urine. Since As is not completely methylated, some MMA and iAs are also eliminated in the urine with DMA (Hayakawa *et al.*, 2005). By sticking to protein fragments, iAs, MMA, and DMA may all exist in the kidney simultaneously (Thomas *et al.*, 2001; Kuo *et al.*, 2017). Because of this, biological measures of methylation and exposure capacity such as concentrations of As in kidneys and levels of MMA, As (III), As(V), and DMA in urine are considered appropriate (Chiou *et al.*, 1997; Chanda *et al.*, 2020). DMA and MMA, the primary methylation products, are rapidly eliminated from the body and do not have the same affinity for macromolecules as iAs and are not well absorbed by cells. Due to its ability to enhance exocytosis, As methylation may be considered a detoxification method. The SDG co-administration led to levels of low tissues, augmented levels of different species of As, and a high

percentage of arsenical methylation in urine, showing that the treatment of SDG assuaged - nephrotoxicity induced by As by improving the capacity of methylation and assisting the excretion of As.

The mechanisms mediated by SDG that impact the metabolism of As are: 1. a stimulatory role by GSH is first played in pathways of methylation as a reducing agent or as an undeviating association with arsenicals (Davison *et al.*, 2003; Zhao *et al.*, 2019). SDG provides methylation of As by avoiding the GSH depletion induced by ROS. 2. P-glycoproteins and other multidrug-resistant proteins with ATP-binding transporters move glutathione-conjugated arsenicals between extracellular space and intracellular space (Zhou *et al.*, 2021). SDG may enhance arsenic metabolism by enhancing mitochondrial biogenesis and avoiding ATP depletion, both of which are caused by As, and therefore provide enough energy for As secretion. 3. SDG affects the activity and expression of enzymes that metabolize medicines, according to Patel *et al.* (Patel *et al.*, 2012). Increased As regulation (oxidation state) methyltransferases may have decreased DNA breakage due to their role in the methylation of the toxic metal As as well as the efflux system (De la Rosa *et al.*, 2017; Lin *et al.*, 2018).

5. Conclusion

SDG can prevent renal damage caused by As_2O_3 by alleviating oxidative stress and increasing As methylation metabolism. Hence, it is opined that SDG might be effective in the cure and healing and could serve as an alternative therapy to prevent arsenical toxicity. Nevertheless, in-depth studies are mandated to prove and propose dietary SDG as a therapeutic agent for arsenic nephrotoxicity.

Acknowledgements

A special thanks go out to Zarqa University in Jordan and Yuvaraja's College at the University of Mysore in India for providing the research facilities and Invivo Biosciences in Kodigehalli, Bengaluru, India, for providing the study animals that were used in this work.

Funding

Not applicable.

Ethical approval

Animal experiments followed the guidelines approved by the institution (Approval No. In vivo/IAEC/012/2020). The experimental protocol was approved by Invivo Biosciences, Bangalore, India.

Competing Interests Declaration

The study's authors claim that they have no financial or personal links that might have impacted the findings provided in this study.

References

- Al-Groom RM., 2022. Effectiveness of flower extract of hibiscus sabdariffa l. Against anticancer drug cyclophosphamide induced hepatotoxicity and oxidative stress. *Jordan J Biol Sci*, **15**(5).
- Al-Mamoori F and T Aburjai, 2022. **Medicinal plants for the treatment of nephrolithiasis.**
- Al-Mamoori F A Al-Samydai and TAburjai, 2019. Medicinal plants for the prevention and management of nephrolithiasis: A review. *Int J Sci Res Sci Technol*, **8**: 2700-2705.
- AlRamadneh, T.N., N. AlQurashi, M.S.A. Khan, S.M. Hashimi, R. Javaraiah, F.H. Al-Ostoot and A.A.A. Alhaija, 2022. Flaxseed oil ameliorates mercuric chloride-induced liver damage in rats. *J Trace Elem Med Biol*, **71**: 126965.
- Aqeel, T., S. Chikkalakshmpura Gurumallu, S.M. Hashimi, N. AlQurashi and R. Javaraiah, 2019. Evaluation of protective efficacy of flaxseed lignan-secoisolariciresinol diglucoside against mercuric chloride-induced nephrotoxicity in rats. *Mol Biol Rep*, **46**(6): 6171-6179.
- Aqeel, T., S.C. Gurumallu, A. Bhaskar, S.M. Hashimi, N.C. Lohith and R. Javaraiah, 2021. Protective role of flaxseed lignan secoisolariciresinol diglucoside against lead-acetate-induced oxidative-stress-mediated nephrotoxicity in rats. *Phytomed Plus*, **1**(3): 100038.
- Aqeel, T., S.C. Gurumallu, A. Bhaskar and R. Javaraiah, 2020. Secoisolariciresinol diglucoside protects against cadmium-induced oxidative stress-mediated renal toxicity in rats. *J Trace Elem Med Biol*, **61**: 126552.
- Aranda, A., L. Sequedo, L. Tolosa, G. Quintas, E. Burello, J. Castell and L. Gombau, 2013. Dichloro-dihydro-fluorescein diacetate (dfh-da) assay: A quantitative method for oxidative stress assessment of nanoparticle-treated cells. *In Vitro Toxicol*, **27**(2): 954-963.
- Avissar, N., D.B. Ornt, Y. Yagil, S. Horowitz, R.H. Watkins, E.A. Kerl, K. Takahashi, I.S. Palmer and H.J. Cohen, 1994. Human kidney proximal tubules are the main source of plasma glutathione peroxidase. *Am J Physiol Cell Physiol*, **266**(2): C367-C375.
- Bergquist, E.R., R.J. Fischer, K.D. Sugden and B.D. Martin, 2009. Inhibition by methylated organoarsenicals of the respiratory 2-oxo-acid dehydrogenases. *J Organomet Chem*, **694**(6): 973-980.
- Bjørklund, G., P. Oliinyk, R. Lysiuk, M. Rahaman, H. Antonyak, I. Lozynska, L. Lenchyk and M. Peana, 2020. Arsenic intoxication: General aspects and chelating agents. *Arch Toxicol*, **94**(6): 1879-1897.
- Bjørklund, G., P. Oliinyk, R. Lysiuk, M.S. Rahaman, H. Antonyak, I. Lozynska, L. Lenchyk and M. Peana, 2020. Arsenic intoxication: General aspects and chelating agents. *Arch Toxicol*, **94**(6): 1879-1897.
- Bujok, J., D. Mišta, E. Wincewicz, B. Króliczewska, S. Dzimira and M. Žuk, 2021. Atherosclerosis development and aortic contractility in hypercholesterolemic rabbits supplemented with two different flaxseed varieties. *Foods*, **10**(3): 534.
- Cadenas, S. and G. Barja, 1999. Resveratrol, melatonin, vitamin e, and pbn protect against renal oxidative DNA damage induced by the kidney carcinogen kbro3. *Free Radic Biol Med*, **26**(11-12): 1531-1537.
- Chang, Y.W. and K.P. Singh, 2019. Arsenic induces fibrogenic changes in human kidney epithelial cells potentially through epigenetic alterations in DNA methylation. *J Cell Physiol*, **234**(4): 4713-4725.
- Cui, X., Y. Kobayashi, T. Hayakawa and S. Hirano, 2004. Arsenic speciation in bile and urine following oral and intravenous exposure to inorganic and organic arsenics in rats. *Toxicol Sci*, **82**(2): 478-487.
- Davison, K., S. Cote, S. Mader and W. Miller, 2003. Glutathione depletion overcomes resistance to arsenic trioxide in arsenic-resistant cell lines. *Leukemia*, **17**(5): 931-940.
- De la Rosa, R., C. Steinmaus, N.K. Akers, L. Conde, C. Ferreccio, D. Kalman, K.R. Zhang, C.F. Skibola, A.H. Smith and L. Zhang, 2017. Associations between arsenic (+ 3 oxidation state) methyltransferase (as3mt) and n-6 adenine-specific DNA methyltransferase 1 (n6amt1) polymorphisms, arsenic metabolism, and cancer risk in a chilean population. *Environ Mol Mutagen*, **58**(6): 411-422.
- Draganescu, D., C. Andritoiu, D. Hritcu, G. Dodi and M.I. Popa, 2021. Flaxseed lignans and polyphenols enhanced activity in streptozotocin-induced diabetic rats. *Biology*, **10**(1): 43.
- Ebrahimi, B., Z. Nazmara, N. Hassanzadeh, A. Yarahmadi, N. Ghaffari, F. Hassani, A. Liaghat, L. Noori and G. Hassanzadeh, 2021. Biomedical features of flaxseed against different pathologic situations: A narrative review. *Iran J Basic Med Sci*, **24**(5): 551.
- Emadi, A. and S.D. Gore, 2010. Arsenic trioxide—an old drug rediscovered. *Blood Rev*, **24**(4-5): 191-199.
- Flora, S., S. Bhadauria, G. Kannan and N. Singh, 2007. Arsenic induced oxidative stress and the role of antioxidant supplementation during chelation: A review. *J Environ Biol*, **28**(2): 333.
- FRANKE, K.W. and A.L. Moxon, 1936. A comparison of the minimum fatal doses of selenium, tellurium, arsenic and vanadium. *J Pharmacol Exp Ther*, **58**(4): 454-459.
- Fu, Z. and S. Xi, 2020. The effects of heavy metals on human metabolism. *Toxicol Mech Methods*, **30**(3): 167-176.
- Guo, Q., Z. Sun, R. Niu, R.K. Manthari, M. Yuan, K. Yang, M. Cheng, Z. Gong and J. Wang, 2020. Effect of arsenic and/or fluoride gestational exposure on renal autophagy in offspring mice. *Chemosphere*, **241**: 124861.
- Hayakawa, T., Y. Kobayashi, X. Cui and S. Hirano, 2005. A new metabolic pathway of arsenite: Arsenic–glutathione complexes are substrates for human arsenic methyltransferase cyt19. *Arch Toxicol*, **79**(4): 183-191.
- Health, U.D.o. and H. Services, 1999. **Agency for toxic substances and disease registry-atsdr.**
- Hilal, A.A. and N. Ismail, 2008. Heavy metals in eleven common species of fish from the gulf of aqaba, red sea. *Jordan J Biol Sci.*, **1**(1): 13-18.
- Hood, R.D., G.C. Vedel-Macrandar, M.J. Zaworotko, F.M. Tatum and R.G. Meeks, 1987. Distribution, metabolism, and fetal uptake of pentavalent arsenic in pregnant mice following oral or intraperitoneal administration. *Teratology*, **35**(1): 19-25.
- Hood, R.D., G.C. Vedel, M.J. Zaworotko, F.M. Tatum and R.G. Meeks, 1988. Uptake, distribution, and metabolism of trivalent arsenic in the pregnant mouse. *J Toxicol Environ Health Part A*, **25**(4): 423-434.
- Hu, Y., J. Li, B. Lou, R. Wu, G. Wang, C. Lu, H. Wang, J. Pi and Y. Xu, 2020. The role of reactive oxygen species in arsenic toxicity. *Biomolecules*, **10**(2): 240.
- Karapehliyan, M., M. Ogun, I. Kaya, H. Ozen, H.A. Deveci and M. Karaman, 2014. Protective effect of omega-3 fatty acid against mercury chloride intoxication in mice. *J Trace Elem Med Biol*, **28**(1): 94-99.
- Kezimana, P., A.A. Dmitriev, A.V. Kudryavtseva, E.V. Romanova and N.V. Melnikova, 2018. Secoisolariciresinol diglucoside of flaxseed and its metabolites: Biosynthesis and potential for nutraceuticals. *Front Genet*, **9**: 641.

- Kuo, C.-C., K.A. Moon, S.-L. Wang, E. Silbergeld and A. Navas-Acien, 2017. The association of arsenic metabolism with cancer, cardiovascular disease, and diabetes: A systematic review of the epidemiological evidence. *Environ Health Perspect*, **125**(8): 087001.
- Kutuk, O., G. Poli and H. Basaga, 2006. Resveratrol protects against 4-hydroxynonenal-induced apoptosis by blocking jnk and c-jun/ap-1 signaling. *Toxicol Sci*, **90**(1): 120-132.
- Lin, Y.-C., W.-J. Chen, C.-Y. Huang, H.-S. Shiue, C.-T. Su, P.-L. Ao, Y.-S. Pu and Y.-M. Hsueh, 2018. Polymorphisms of arsenic (+ 3 oxidation state) methyltransferase and arsenic methylation capacity affect the risk of bladder cancer. *Toxicol Sci*, **164**(1): 328-338.
- Miodragović, Đ., E.P. Swindell, Z.S. Waxali, A. Bogachkov and T.V. O'Halloran, 2019. Beyond cisplatin: Combination therapy with arsenic trioxide. *Inorganica Chim Acta*, **496**: 119030.
- Navasumrit, P., K. Chaisatra, J. Promvijit, V. Parnlob, S. Waraprasit, C. Chompoobut, T.T. Binh, D.N. Hai, N.D. Bao and N.K. Hai, 2019. Exposure to arsenic in utero is associated with various types of DNA damage and micronuclei in newborns: A birth cohort study. *Environ. Health Rev*, **18**(1): 1-16.
- Nurchi, V.M., A. Buha Djordjevic, G. Crisponi, J. Alexander, G. Bjørklund and J. Aaseth, 2020. Arsenic toxicity: Molecular targets and therapeutic agents. *Biomolecules*, **10**(2): 235.
- Olson, J.D.L., 2021. **Environmental arsenic exposure in humans: Toxicity and adaptation in the bolivian andes. Karolinska Institutet (Sweden).**
- Pace, C., R. Dagda and J. Angermann, 2017. Antioxidants protect against arsenic induced mitochondrial cardio-toxicity. *Toxics*, **5**(4): 38.
- Parikh, M. and G.N. Pierce, 2019. Dietary flaxseed: What we know and don't know about its effects on cardiovascular disease. *Can J Physiol Pharmacol*, **97**(2): 75-81.
- Patel, D., J. Vaghasiya, S. Pancholi and A. Paul, 2012. Therapeutic potential of secoisolariciresinol diglucoside: A plant lignan. *Int J Pharm Sci Drug Res*, **4**(1): 15-18.
- Prasad, K., S. Mantha, A. Muir and N. Westcott, 2000. Protective effect of secoisolariciresinol diglucoside against streptozotocin-induced diabetes and its mechanism. *Mol Cell Biochem*, **206**(1): 141-150.
- Puri, R.N. and A. Meister, 1983. Transport of glutathione, as gamma-glutamylcysteinylglycyl ester, into liver and kidney. *Proc Natl Acad Sci U S A*, **80**(17): 5258-5260.
- Radák, Z., K. Asano, M. Inoue, T. Kizaki, S. Oh-Ishi, K. Suzuki, N. Taniguchi and H. Ohno, 1996. Superoxide dismutase derivative prevents oxidative damage in liver and kidney of rats induced by exhausting exercise. *Eur J Appl Physiol*, **72**(3): 189-194.
- Rana, M.N., J. Tangpong and M.M. Rahman, 2018. Toxicodynamics of lead, cadmium, mercury and arsenic-induced kidney toxicity and treatment strategy: A mini review. *Toxicol Rep*, **5**: 704-713.
- Rizwan, S., R. Kumar, A.K. Singh, Y. Kusuma, K. Yadav and C.S. Pandav, 2014. Prevalence of hypertension in indian tribes: A systematic review and meta-analysis of observational studies. *PLoS one*, **9**(5): e95896.
- Robles-Osorio, M.L., E. Sabath-Silva and E. Sabath, 2015. Arsenic-mediated nephrotoxicity. *Ren Fail*, **37**(4): 542-547.
- Sall, M.L., A.K.D. Diaw, D. Gningue-Sall, S. Efremova Aaron and J.-J. Aaron, 2020. Toxic heavy metals: Impact on the environment and human health, and treatment with conducting organic polymers, a review. *Environ Sci Pollut Res Int*, **27**: 29927-29942.
- Sani, M., H. Sebaï, W. Gadacha, N.A. Boughattas, A. Reinberg and B.A. Mossadok, 2006. Catalase activity and rhythmic patterns in mouse brain, kidney and liver. *Comp Biochem Physiol B Biochem Mol Biol*, **145**(3-4): 331-337.
- Shi, H., X. Shi and K.J. Liu, 2004. Oxidative mechanism of arsenic toxicity and carcinogenesis. *Mol Cell Biochem*, **255**(1): 67-78.
- Sotomayor, C.G., D. Groothof, J.J. Vodegel, T.A. Gacitúa, A.W. Gomes-Neto, M.C. Osté, R.A. Pol, C. Ferreccio, S.P. Berger and G. Chong, 2020. Circulating arsenic is associated with long-term risk of graft failure in kidney transplant recipients: A prospective cohort study. *J Clin Med*, **9**(2): 417.
- Tchounwou, P.B., C.G. Yedjou, U.K. Udensi, M. Pacurari, J.J. Stevens, A.K. Patlolla, F. Noubissi and S. Kumar, 2019. State of the science review of the health effects of inorganic arsenic: Perspectives for future research. *Environ Toxicol*, **34**(2): 188-202.
- Tennen, R.I., E. Michishita-Kioi and K.F. Chua, 2012. Finding a target for resveratrol. *Cell*, **148**(3): 387-389.
- Thomas, D.J., M. Styblo and S. Lin, 2001. The cellular metabolism and systemic toxicity of arsenic. *Toxicol Appl Pharmacol*, **176**(2): 127-144.
- Wang, Y., H. Zhao, Y. Shao, J. Liu, J. Li and M. Xing, 2017. Copper or/and arsenic induce oxidative stress-cascaded, nuclear factor kappa b-dependent inflammation and immune imbalance, triggering heat shock response in the kidney of chicken. *Oncotarget*, **8**(58): 98103.
- Weiss, T.S., M. Lichtenauer, S. Kirchner, P. Stock, H. Aurich, B. Christ, G. Brockhoff, L.A. Kunz-Schughart, K.-W. Jauch and H.J. Schlitt, 2008. Hepatic progenitor cells from adult human livers for cell transplantation. *Gut*, **57**(8): 1129-1138.
- Zaid Alkilani, A., H. Abu-Zour, A. Alshishani, R. Abu-Huwaij, H.A. Basheer and H. Abo-Zour, 2022. Formulation and evaluation of niosomal alendronate sodium encapsulated in polymeric microneedles: In vitro studies, stability study and cytotoxicity study. *Nanomaterials*, **12**(20): 3570.
- Zhang, S., M. Cheng, Z. Wang, Y. Liu, Y. Ren, S. Rong and X. Wang, 2020. Secoisolariciresinol diglucoside exerts anti-inflammatory and antiapoptotic effects through inhibiting the akt/ikb/nf-kb pathway on human umbilical vein endothelial cells. *Mediators Inflamm*, 2020.
- Zhao, M.-X., J.-L. Wen, L. Wang, X.-P. Wang and T.-S. Chen, 2019. Intracellular catalase activity instead of glutathione level dominates the resistance of cells to reactive oxygen species. *Cell Stress Chaperones*, **24**(3): 609-619.
- Zhao, Y., R. Du, T. Zhou, D. Yang, Y. Huang, Y. Wang, J. Huang, X. Ma, F. He and J. Qiu, 2018. Arsenic trioxide-coated stent is an endothelium-friendly drug eluting stent. *Adv Healthc Mater*, **7**(15): 1800207.
- Zhou, J.R., G. Kaur, Y. Ma, D. Arutyunov, X. Lu, X.C. Le and E.M. Leslie, 2021. Biliary excretion of arsenic by human hepatic cells is stimulated by selenide and mediated by the multidrug resistance protein 2 (mrp2/abcc2). *Biochem Pharmacol*, **193**: 114799.

Increased Virus Resistance in Transgenic Petunia with Heterologous *ZRNase II* gene

Olga Ovcharenko^{1,*}, Andrii Potrokhov¹, Daria Sosnovska², Yuliya Hoysyuk², Olha Yaroshko¹, Tetiana Shevchenko², Iryna Budzanivska², Volodymyr Rudas¹, Mykola Kuchuk¹

¹ Institute of Cell Biology and Genetic Engineering, 148, Zabolotnogo str., Kyiv, Ukraine 03143, +380 44 526-7104; ²ESC “Institute of Biology and Medicine”, Taras Shevchenko National University of Kyiv, 64/13 Volodymyrska Street, City of Kyiv, 01601, Ukraine

Received: October 18, 2022; Revised: February 10, 2023; Accepted: March 19, 2023

Abstract

The production of transgenic petunia plants with heterologous *ZRNase II* gene and the evaluation of resistance to *Tobacco mosaic virus* in the resultant plants was the aim of our research.

We have generated transgenic petunia plants with *ZRNase II* gene via *Agrobacterium*-mediated transformation. The presence of *ZRNase II* gene was confirmed by PCR-analysis. Orcin method revealed that RNase activity in transgenic petunia expressing *ZRNase II* gene was 1.34-2.10 fold higher compared to wild-type plants. RNase activity varied among different transgenic lines. Both petunia varieties used for production of transgenic lines differed in their natural resistance to *Tobacco mosaic virus*. The symptoms of the viral infection in the transgenic plants of the susceptible variety inoculated with the virus were less severe. Indirect ELISA confirmed 3.3 – 4.0 fold lower accumulation of viral antigens in the infected transformed plants compared to the infected wild type ones.

Application of *ZRNase II* gene in creation of transgenic petunia leads to the generation of plants tolerant to *Tobacco mosaic virus*.

Keywords. Genetically engineered plants, disease resistance, *Tobacco mosaic virus*, extracellular ribonucleases.

1. Introduction

Petunia is an economically important ornamental plant, which was traditionally propagated by seeds. The emergence of modern hybrid cultivars called 'Surfinia' led to the increasing of vegetative propagation on petunia market. Introduction of vegetatively propagated *Petunia* hybrids led to an increased risk of virus infections of propagated material (Chung *et al.*, 2007). Nowadays, 26 RNA containing viruses and 4 viroids were identified to infect *Petunia* plants (Sastriy *et al.*, 2019). Among them the most detrimental are *Tobacco mosaic virus* (TMV), *Petunia vein-clearing virus*, *Tomato mosaic virus*, *Potato virus Y*, *Alfalfa mosaic virus*, *Cucumber mosaic virus*, and *Broad bean wilt I virus*. They are often identified in mixed infections (Lasemann, 1996; Chung *et al.*, 2007). Viral infections decrease decorative characteristics of cultivars, which become the source of the virus for uninfected plants.

Except of its direct economic value as an ornamental plant, petunia is attractive as a model system. There is a need in modern plant biology for the model systems (beyond *Arabidopsis*) for different specialized demands. Such advantages of petunia as short generation time, easy cultivation, efficient protocol for genetic transformation, large leaves and flowers suitable for a number of analysis, make it a convenient model for investigations (Vandenbussche *et al.*, 2016). *Petunia* can also be used for testing of various antiviral strategies prior to testing them on recalcitrant species.

Transgenic virus resistant plants can be produced by approaches of modern biotechnology. Antisense RNAs, coat protein mediated resistance, microRNAs, hammerhead ribozyme, plantibodies, replicase mediated resistance, ribosome-inactivating proteins (RIP), RNA dependent RNA polymerase mediated resistance, RNA interference, RNA satellites, and some ribonucleases have been tested as a putative antiviral strategies previously (Sudarshana *et al.*, 2007; Galvez *et al.*, 2014). Sometimes viruses have the capability to suppress plant defense against virus infections (Abdelkhalek and Sanan-Mishra, 2018), so the more antiviral strategies we have, the better is plant disease control.

ZRNase II gene was isolated from *Zinnia elegance*. The gene encodes an extracellular ribonuclease, which hydrolyzes viral RNAs during their penetration into the plant cell (Kochetov and Shummy, 2017). The enzyme digests viral RNAs, thus localizing the infection, retarding and mitigating the severity of infection symptoms in tobacco (Sangaev *et al.*, 2007, Trifonova *et al.*, 2012) and potato (Petrochov *et al.*, 2021).

Production of transgenic petunia plants expressing heterologous extracellular ribonuclease of *Zinnia* and evaluation of virus resistance in obtained plants was the aim of our research.

2. Materials and methods

2.1. Plant material

Petunia cultivars were originated from a pack of mixed commercial seeds and chosen based on floral phenotype. These cultivars, shown in Figure 1, are currently being maintained vegetatively for research purposes in the *in vitro* collection at the Institute of Cell Biology and Genetic Engineering. The varieties with the highest regeneration capacity from leaf explants (M1 and P5) were chosen for *Agrobacterium*-mediated genetic transformation (data not shown). Plants are available upon request.



Figure 1. General appearance of varieties used for genetic transformation. M1 (a) and P5 (b) petunia cultivars.

2.2. *Agrobacterium*-mediated transformation

Transgenic petunia plants were produced according to Lutke (2006). Petunia leaf discs were transformed with *A. tumefaciens* AGL0 strain harboring pBi-RNS vector. T-DNA of pBi-RNS vector included *ZRNase II* gene of *S-like* RNase of *Zinnia elegans* (817 bp, Gene Bank accession number U19923.1) controlled by p35S CaMV, derived from the cauliflower mosaic virus (CaMV) and neomycin phosphotransferase gene (*npt II*), under control of nopaline synthase promoter (pNOS), as shown in Figure 2 (Sangaev *et al.*, 2007). Plants were regenerated and

selected on regeneration MS medium (Murashige and Skoog, 1962) with 1 mg/l of BA, 0.1 mg/l of NAA, 100 mg/l kanamycin and 400 mg/l cefotaxime.

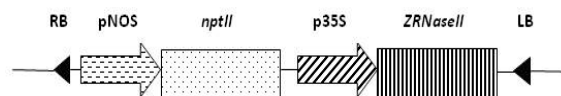


Figure 2. Schematic representation of the T-DNA region of the plasmid pBi-RNS used for petunia transformation. LB, left border; pNOS, nopaline synthase promoter; *npt II*, neomycin phosphotransferase gene; 35S, promoter, derived from the cauliflower mosaic virus (CaMV); *ZRNase II*, S-like RNase gene of *Zinnia elegans*; RB, right border.

2.3. Polymerase chain reaction assays (PCR and RT-PCR)

PCR was used to analyze the presence of gene of interest and selective gene in kanamycin resistant plants.

DNA was isolated from putative transgenic plants, positive and negative controls using a standard kit «NeoPrep100 DNA plant» («Neogene», Ukraine) according to the manufacturer's instructions. The transformation events were confirmed by standard PCR techniques (Sambrook *et al.*, 1989) using «PCR MIX 2-R» kit («Neogene», Ukraine). The primers and expected size of the PCR fragments are shown in the Table 1. The amplification of *ZRNase II* gene fragment was carried out under following conditions: 3 min at 94°C, 42 cycles (30 s at 94°C; 30 s at 55°C; 45 s at 72°C), 10 min at 72°C. The amplification of *npt II* gene fragment was carried out under following conditions: 4 min at 94°C, 8 cycles (30 s at 94°C; 45 s at 68°C; 30 s at 72°C), 25 cycles (30 s at 94°C; 30 s at 60°C; 30 s at 72°C), 1 min at 72°C. The amplification conditions for *virC* fragment were: 3 min at 94°C, 40 cycles (30 s at 94°C; 47 s at 55°C; 30 s at 72°C), 5 min at 72°C. The samples were fractionated in 1% agarose gel in LB (lithium borate) buffer (Brody *et al.*, 2004). Thermo Scientific GeneRuler 1 kb (250 –10000) bp was used as a molecular-weight size marker.

Table 1. The primers used for PCR analyses and expected size of amplified fragments.

Gene	Primers	Annealing temperature, °C	Amplified fragment, bp
<i>ZRNase II</i>	5'-GAATCTAGAAATTTAGAATGAAGGA-3' 5'-ACACTCGAGCACACAAACATGAAGA-3'	55	720 (Sangaev <i>et al.</i> , 2007)
<i>npt II</i>	5'-GAG GCT ATT CGG CTA TGA CTG-3' 5'-ATC GGG AGC GGC GAT ACC GTA-3'	68, 60	700 (Bińka, 2011)
<i>virC</i>	5'-ATC ATT TGT AGC GAC T-3' 5'-AGC TCA AAC CTG CTT C-3'	55	720 (Sawada <i>et al.</i> , 1995)

The transgene expression in petunia plants was examined by RT-PCR analysis. Total RNA was isolated with "RNA isolation kit" ("Zymo Research"). "First strand cDNA synthesis kit" ("Fermentas") was used for cDNA generation according to manufactures manual. Each sample was analyzed with and without addition of reverse transcriptase M-MuLV. The amplification was conducted as described above with the same primers for *ZRNase II*. The amplification products were separated on 1.2% agarose gel in LB buffer.

2.4. Conditions for growing plants in greenhouse and inoculating with virus

Wild type and transgenic (2 of M1 and 3 of P5) lines of petunia were propagated *in vitro* via stem cuttings on MS medium. Rooted plants were acclimated to the greenhouse condition and grown at 24°C under a photoperiod of 16h light and 8 h darkness.

One month after transfer to soil, transgenic and wild type petunia plants were inoculated with 100 µl of TMV in inoculation buffer (the concentration of purified powder-dried virions in 0.05 M sodium phosphate buffer, pH 7.0 was 250 µg/ml). Tomato plants with severe symptoms of viral infection were the source of TMV sample. Upper

fully expanded leaves of experimental petunia plants were dusted with carborundum and inoculated by rubbing with the TMV suspension. Mock-inoculated plants were inoculated with the buffer without virus. After inoculation, plants were rinsed with tap water and incubated in the greenhouse ($20 \pm 5^\circ\text{C}$).

Each experiment involving TMV inoculations was performed in six replicates (a single plant represented one replicate). Afterwards, plants were monitored for the development of viral symptoms.

2.5. RNase activity detection

RNase activity was determined by colorimetric method according to Jain *et al.* (2020).

2.6. Enzyme linked immunosorbent assay (ELISA).

Accumulation of viral antigens was analyzed by indirect ELISA. Primary polyclonal rabbit antibodies to TMV and secondary goat anti-rabbit antibodies (Sigma) were used according to the manufacturer's instructions and Crowther (1995). Upper leaves from six distinct plants per each variant of experiment were drilled, and the probes were tested by ELISA. Samples were considered positive according to condition mentioned in Arli-Sökmen *et al.* (1998).

2.7. Statistical evaluation

Analysis of variance was used to calculate the least significant differences by Statistica 5.5 and MS Excel 2016 software. Data were compared by Mann-Whitney U test in order to evaluate statistical differences between each transgenic line and corresponding non-transgenic controls. Each transgenic line and non-transgenic controls were represented by six plants. Experiments were repeated triple.

3. Results

3.1. Selection of the putative transgenic plants.

Shoots began to regenerate from leaf disks in a month after *Agrobacterium* treatment on regeneration MS medium supplemented with kanamycin sulfate, as shown in Figure 3. Kanamycin-resistant shoots of petunia were rooted spontaneously on MS medium with 100 mg/l of kanamycin sulfate. Only the most vigorous and rooted lines were selected from each variety. Eight putative transgenic lines with pBi-RNS vector of M1 petunia and 10 lines of P5 were analyzed further.

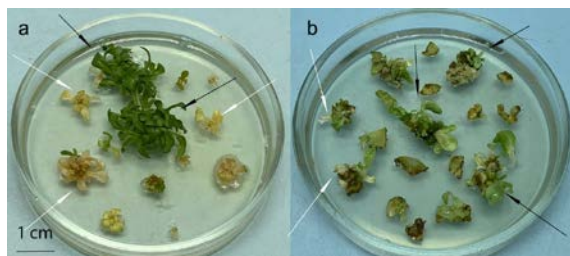


Figure 3. Genetic transformation of *Petunia* using *Agrobacterium tumefaciens* AGL0 with pBi-RNS vector (bar 1 cm). Regeneration of M1 (a) and P5 (b) kanamycin resistant shoots on MS regeneration medium containing 100 mg/l of kanamycin sulfate 8 weeks after cocultivation. Black arrows indicate resistant shoots while white arrows mark the susceptible ones.

3.2. PCR analyses of transgenic plants

Putative transgenic plants were analysed with primers specific to *npt II* and *ZRNase II* genes. Non-transformed M1 and P5 petunia cultivars were PCR tested to confirm the absence of the transgenes. There was no amplification of the tested fragments with primers to both genes in non-transformed plants. All selected kanamycin resistant lines demonstrated the presence of amplified fragments with primers to *npt II* (data not shown) and *ZRNase II* genes as shown in Figure 4. Fragment of *virC* gene, characteristic to *A.tumefaciens* was not found. RT-PCR revealed the expression of gene of interest (Figure 5).

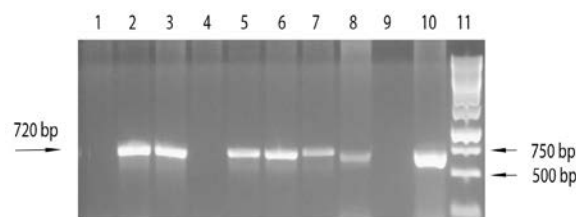


Figure 4. Polymerase chain reaction analysis of transgenic petunia for the *ZRNase II* gene (720 bp). Lanes: 1- M1 non-transgenic plant; 2, 3 - transgenic lines MIT1, MIT2; 4 - P5 non-transgenic plant; 5-8 - transgenic lines P5T1, P5T2, P5T3; 9 - negative control, without DNA; 10 - positive control, total DNA of *A. tumefaciens* AGL0 with pBi-RNS plasmid; 11 - Thermo Scientific GeneRuler 1 kb, 250 -10000 bp.

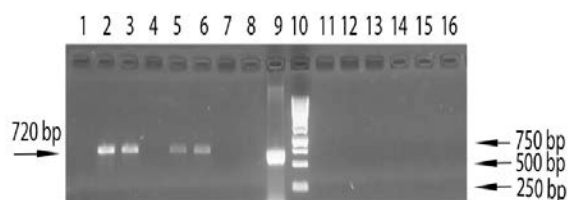


Figure 5. RT-PCR with primers for the *ZRNase II* gene (720 bp) in samples from petunia leaves. Amplification with cDNA (lanes 1-6) and appropriate RNA samples (lanes 11 - 16) isolated from petunia. Lanes: 1, 11 - cultivar M1, wild type; 2, 12 - transgenic line MIT1; 3, 13 -transgenic line MIT2; 4, 14 - cultivar P5, wild type; 5, 15 - transgenic line P5T1; 6, 16 -transgenic line P5T2; 7 - reagent mix without cDNA addition; 8 - reagent mix without RNA addition; 9 - total DNA of *A. tumefaciens* AGL0 with pBi-RNS plasmid; 10 - DNA marker ladder (Thermo Scientific GeneRuler 1 kb, 250 -10000 bp).

For further tests on RNase activity and virus resistance, MIT1, MIT2 transgenic petunia lines of M1 variety and P5T1, P5T2, P5T3 lines of P5 expressing S-like RNase of *Zinnia elegans* were selected. These lines were propagated *in vitro* and transferred to soil.

3.3. RNase activity assay

RNase activity of the transgenic plants significantly ($P \leq 0,05$) exceeded that of non-transgenic ones as shown in Figure 6. Total RNase activity of different transgenic lines of P5 variety exceeded from 1.83 to 2.10 fold the activity of wild type line. The RNase activity in M1 based lines was from 1.34 to 1.85 fold higher than in appropriate wild type variety.

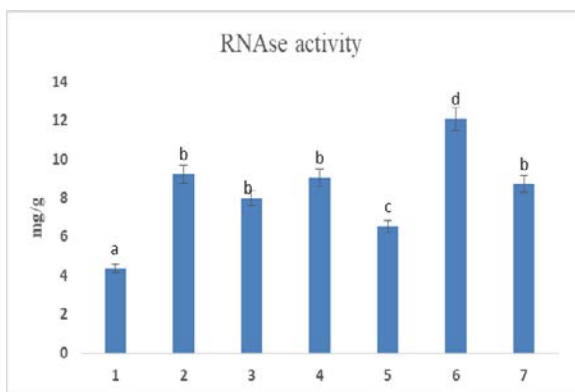


Figure 6. The RNase activity in petunia leaf extracts. The amount of destroyed RNA in mg per g of plant tissue (fresh weight) was estimated. 1, 5 – non-transformed 5P and M1 petunia plants, respectively; 2-4 – P5T1, P5T2, P5T3 transgenic lines of 5P petunia; 6-7 – MIT1 and MIT2, transgenic lines of M1 petunia. The same letters mark bars without significant differences. ($P \leq 0.05$).

3.4. Infection of petunia plants with TMV.

After mechanical inoculation of fully expanded leaves of petunia with TMV inoculum, the systemic signs of viral infection were evaluated. The typical symptoms of TMV infection such as mosaic on leaves, mottling, rugosity of leaf blades appeared on the upper leaves in wild type petunia plants on the third week after inoculation, as shown in Figure 7. The upper leaves of infected non-transgenic M1 plants manifested severe infection symptoms in contrast to the wild type P5 petunia. The latter showed only slight rugosity of leaves. Leaf morphology of infected transgenic cultivars (M1 (Figure 7a, c, e) and P5 varieties) and plants inoculated with buffer was similar.



Figure 7. Systemic signs of infection in TMV inoculated non-transformed and transformed petunia plants expressing S-like RNase of *Zinnia elegans*. Detached petunia leaves (a – c): a – M1 line mock-infected, b – M1 line inoculated with TMV, c – transgenic MIT1 line inoculated with TMV. Development of visual systemic symptoms of viral infection on TMV infected control non-transformed M1 petunia plants (d) versus the transgenic MIT1 petunia plants (e).

3.5. Detection of TMV in plants by ELISA

Systemic TMV infection was investigated in the upper fully expanded young leaves of intact and infected plants by ELISA. The results are presented in Figure 8. Viral antigens were recovered from the upper non-inoculated leaves of infected M1 wild type plants indicating the systemic viral movement. In non-transgenic M1 variety the difference in extinction values was almost 4-fold between mock and infected plants. According to Arli-Sökmen *et al.* (1998) viral particles are considered to be accumulated in plants if there is at least 2-fold difference between the absorbance values (A_{405}) of infected and virus-free samples. In contrast, in the P5 variety (where minor signs of viral infection were observed) the difference was less obvious (1.62 folds). There was the significant difference in the antigen amount between wild type P5 and M1 varieties. Antigen accumulation was higher in M1 than in P5. The absorbance values in samples of infected M1 variety 2.6 fold exceeded those of infected P5. The infected transgenic plants of M1 variety manifested much lower ELISA values than the infected wild type plants (from 3.3 to 4.0 fold). Extinction values of infected P5 and M1 transgenic varieties, compared to mock ones, were lower 1.15-1.32 and 0.98-1.19 fold respectively. These means did not exceed those of the virus-free samples by at least a factor of two (Arli-Sökmen *et al.*, 1998). So, they can be considered undistinguishable from mock treated plants. We can consider that there was no significant accumulation of viral particles in transgenic plants.

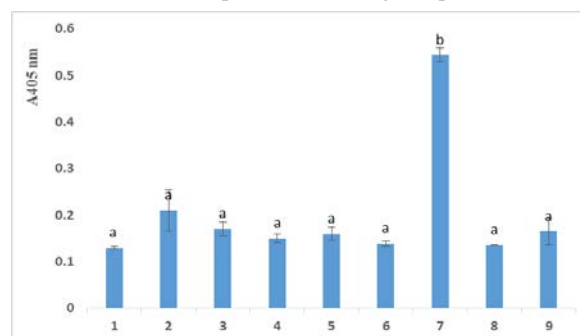


Figure 8. Indirect ELISA extinction values of different petunia lines. 1, 6 – inoculated with buffer non-transformed control P5 and M1 petunia plants, respectively; 2, 7 – inoculated with TMV non-transformed control P5 and M1 petunia plants, respectively; 3-5 – inoculated with TMV transformed lines of P5 petunia - P5T1, P5T2, P5T3; 8-9 – transformed lines of M1 petunia MIT1, MIT2. Samples were considered to be positive when the A_{405} absorbance values exceeded the mean of the virus-free samples by at least a factor of two. The same letters mark bars without significant differences.

4. Discussion

Nowadays, there is an insistent demand for efficient control of pathogens injuring important cultivated species. RNases are involved in the wound response and induction of the defense-related genes. That is one of the ways in which plants respond to mechanical injury and prevent viral infection (LeBrasseur *et al.*, 2002). The effect of heterologous *ZRNase II* gene expression on TMV resistance of transgenic petunia plants was investigated. It is important to note that the transgene expression had no influence on plant morphology in the transgenic petunia

plants grown in the greenhouse. No obvious effect of this gene on transgenic petunia plant growth and development was observed in accordance to similar previous research on tobacco and potato (Sangaev *et al.*, 2007; Potrochov *et al.*, 2021). The absence of negative influence of excessive RNases on transgenic plants can be associated with subcellular compartmentalization of the plant RNases outside the cell (Hugot *et al.*, 2002)

In our experiments, total RNase activity of wild type lines (M1 and P5) differed, due to their genetic background. However, in both cases the RNase activity of transgenic lines, containing the extracellular *ZRNase II* gene, were higher. There were differences also among the transgenic *ZRNase II* petunia lines. The transgenic plants had total RNase activity higher 1.34 – 2.10 fold compared to the control. Gene position effect and the levels of expression could explain the differences in activity. Previously, tobacco plants, which were transformed with a vector containing *ZRNase II* gene, were characterized with RNase activity 1.6 – 3.0 and 3.5 – 14.4 fold higher than in the control, presumably depending on regulatory elements (Sangaev *et al.*, 2007; Trifonova *et al.*, 2012). Transgenic potato plants transformed with pBi-RNS vector manifested total activities of RNases 1.2 times higher as compared to non-transgenic plants (Petrochov *et al.*, 2021). Although the activity of total RNases increased moderately, the transgenic plants tolerated inoculation with the high viral doses, in contrast to non-transgenic ones. This is in accordance with the fact that PR-4 protein, the product of L3 gene from *Capsicum chinense*, with both RNase and DNase activity, protected plants of this species from the most of tobamoviruses, despite the very low contribution to the bulk activity of nucleases in infected plants (Guevara-Morato *et al.*, 2010).

We found that wild type P5 and M1 lines differed in their tolerance to TMV. The visual signs of infection after viral inoculation both with subsequent ELISA demonstrated different susceptibility of wild type M1 and P5 petunia plants to TMV infection, as shown in Figure 8. On the third week after inoculation, we observed 4-fold rise of viral antigens for infected wild type M1 line and no significant increase for P5 line, as compared to the results for mock infected plants. Symptoms of tobamoviruses in naturally infected petunias usually begin to appear from the second week after inoculation and differ among cultivars (Cohen *et al.*, 1999). In the infected plants they can range from the complete absence of detectable symptoms to different severity forms of mottling and mosaic, leaf deformations. Infection can also reduce the number of flowers along with size and cause the break of flower colour. Cohen *et al.* (1999) observed no viral signs developed on the upper leaves of a number of cultivars up to four weeks post inoculation with TMV, but detection of the viral particles from non-inoculated leaves revealed their systemic movement even in symptomless plants. We can consider that P5 line has high natural tolerance to TMV infection for its minor symptoms and low extinction values of ELISA. In contrast, M1 is a susceptible cultivar. The reason of the various susceptibility to virus among the varieties may be due to difference in the genetic background. The difference among the petunias in tolerance to TMV is consistent with the previous findings (Cohen *et al.*, 1999).

The aim of our study was looking at systemic responses to TMV infection in petunia plants. The inoculation dose of 250 µg/ml was used in our experiment in order to obtain the systemic infection. Although we used such high viral concentration for petunia inoculation, the absorbance value in transgenic plants was similar to the mock infected plants. The difference in the observed visual symptoms and antigen accumulation retained after three weeks post inoculation with TMV between wild type plants and two transgenic clones of susceptible petunia variety M1. Absorbance values for infected transgenic P5 clones were similar to those inoculated with buffer. The absorbance values for infected wild type P5 plants (control) exceeded those in transgenic P5 clones, but were not substantial on the third week post inoculation. Previously, systemic responses were observed in experiments when 12.5 times less concentrated TMV inoculum dose with 20 µg/ml of TMV for experimental infection of wild type petunias and 25 times lower viral concentration for inoculation of tobaccos were used (Cohen *et al.*, 1999; Trifonova *et al.*, 2012). It was shown earlier that the response of transgenic tobacco plants (with *ZRNase II* gene) infected with TMV depended on the concentration of virus (Trifonova *et al.*, 2012). These researchers observed that in the case of low (0.01 µg/ml) or medium (0.1 µg/ml) content of the viral particles in the inoculum, the virus accumulation and development of infection symptoms were absent or delayed in transformed plants as compared to the control ones. If the TMV concentration in inoculum was 10 µg/ml, the differences between infected control and transformed plants were less obvious at 3 weeks after inoculation (Trifonova *et al.*, 2012). Thus, our results demonstrate the easier infection course in inoculated transgenic plants that corroborates previous findings (Sangaev *et al.*, 2007; Trifonova *et al.*, 2012; Potrochov *et al.*, 2021).

Heterologous recombinant RNases were demonstrated to increase antiviral resistance in transgenic plants previously (Ishida *et al.*, 2002). However, there is a report that the protection effectiveness of some proteins with RNase activity can be virus specific (Guevara-Morato *et al.*, 2010). Some reports also demonstrate the direct protection of plant RNases against fungal pathogens in the apoplastic compartment (Hugot *et al.*, 2002). Thus, the transgenic *ZRNase II* plants present an interesting model for further investigation of the plant resistance to a number of viruses and fungi.

5. Conclusions

Transgenic petunia plants were transformed with heterologous *ZRNase II* gene. The transgenic plants manifested increased levels of RNase activity and the reduction in virus antigen accumulation in susceptible to *Tobacco mosaic virus* cultivar. Genetic transformation of this ornamental species with extracellular ribonuclease gene resulted in production of plants tolerant to TMV.

6. Data Availability Statement

The data that support the findings of this study are available from the corresponding author, OO, upon reasonable request.

Acknowledgement

We are very grateful to Biotech Initiative, the US-Ukraine foundation for donating equipment for electrophoresis (RunView Real Time Gel Visualization System). This research was supported by target research programs of the Department of General Biology of the National Academy of Sciences of Ukraine "Fundamentals of forecasting and prevention of the negative impact of climate change on the biotic systems of Ukraine" (2017-2021 years) and "Mechanisms of stress adaptation and creation of resistant plant lines by genetic engineering methods" III-5-22.

References

- Abdelkhalek A and Sanan-Mishra N. 2018. A comparative analysis of the suppressor activity of tobacco mosaic virus proteins in the tomato plant. *Jordan J Biol Sci.*, **11**(4): 469 – 473.
- Arli-Sökmen M, Barker H and Torrance L. 1998. Factors affecting the detection of potato mop-top virus in potato tubers and improvement of test procedures for more reliable assays. *Ann Appl Biol.*, **133**: 55–63.
- Bińka A, Orczyk W and Nadolska-Orczyk A. 2011. The *Agrobacterium*-mediated transformation of common wheat (*Triticum aestivum* L.) and triticale (x *Triticosecale* Wittmack): Role of the binary vector system and selection cassettes. *J Appl Genet.*, **53**: 1–8.
- Brody JR, Calhoun ES, Gallmeier E, Creavalle TD, and Kern SE. 2004. Ultra-fast high-resolution agarose electrophoresis of DNA and RNA using low-molarity conductive media. *BioTechniques* **37**(4): 598-602.
- Chung B-N, Kim J-S, Cho J-D, Cheong S-R and Jeong M-I. 2007. Tobacco mosaic virus detected in vegetatively propagated petunia hybrids "Surfinia." *Plant Pathol J.*, **23**(1):34–36.
- Cohen J, Sikron N, Shuval S and Gera A. 1999. Susceptibility of vegetatively propagated petunia to tobamovirus infection and its possible control. *HortScience.*, **34**(2): 292–293.
- Crowther JR. 1995. **ELISA. Theory and practice.** Hamana Press, New York.
- Galvez L C, Banerjee J, Pinar H and Mitra A. 2014. Engineered plant virus resistance. *Plant Sci.*, **228**: 11–25.
- Guevara-Morato MA, de Lacoba MG, García-Luque I and Serra MT. 2010. Characterization of a pathogenesis-related protein 4 (PR-4) induced in *Capsicum chinense* L3 plants with dual RNase and DNase activities. *J Exp Bot.*, **61**(12): 3259–3271.
- Hugot K, Ponchet M, Marais A, Ricci P and Galiana E. 2002. A tobacco S-like RNase inhibits hyphal elongation of plant pathogens. *Mol Plant Microbe Interact: MPMI*, **15** (3): 243–250.
- Ishida I, Tukahara M, Yoshioka M, Ogawa T, Kakitani M and Toguri T. 2002. Production of anti-virus, viroid plants by genetic manipulations. *Pest Manag Sci.*, **58** (11): 1132–1136.
- Jain A, Jain R and Jain S. 2020. Estimation of RNA using orcinol method. In: **Basic Techniques in Biochemistry, Microbiology and Molecular Biology.** Springer Protocols Handbooks. Humana, New York, pp. 73–75.
- Kochetov A and Shumny V. 2017. Transgenic plants as genetic models for studying functions of plant genes. *Russ J Genet Appl Res.*, **7** (4): 421–427.
- LeBrasseur ND, MacIntosh G C, Pérez-Amador MA, Saitoh Mand Green PJ. 2002. Local and systemic wound-induction of RNase and nuclease activities in *Arabidopsis*: RNS1 as a marker for a JA-independent systemic signaling pathway. *Plant J Cell Mol Biol.*, **29**(4): 393–403.
- Lesemann DE. 1996. Viruses recently detected in vegetatively propagated *Petunia*. *Acta Hort.*, **432**: 88–94.
- Lutke, WK. 2006. *Petunia (Petunia hybrida)*. In: Wang, K. (eds) **Agrobacterium Protocols Volume 2. Methods in Molecular Biology 344.** Humana Press, pp. 339–349.
- Murashige T, Skoog F. 1962. A revised medium for rapid growth and bioassays with tobacco tissue cultures. *Physiol Plant.*, **15**:473–497.
- Potrokhov A, Sosnovska D, Ovcharenko O, Budzaniwska I, Rudas V and Kuchuk M. 2021. Increased ribonuclease activity in *Solanum tuberosum* L. transformed with heterologous genes of apolastic ribonucleases as a putative approach for production of virus resistant plants. *Turk J Biol.*, **45** (1): 79–87.
- Sambrook J, Fritsch E, Maniatis T. 1989. **Molecular Cloning.** 2nd ed. New York, Cold Spring Harbor Laboratory.
- Sangaev SS, Trifonova EA, Titov SE, Romanova AV, KolodyazhnayaYaS *et al.* 2007. Effective expression of the gene encoding an extracellular ribonuclease of *Zinnia elegans* in the SR1 *Nicotiana tabacum* plants. *Russ J Genet.*, **43**: 831–833.
- Sastry KS, Mandal B, Hammond J, Scott SW and Briddon RW. 2019. **Encyclopedia of Plant Viruses and Viroids.** Springer, New Delhi Springer Nature India Private Limited, 2936 p.
- Sawada H, Ieki H, Matsuda I. 1995. PCR detection of Ti and Ri plasmids from phytopathogenic *Agrobacterium* strains. *Appl Environ Microbiol.*, **61** (2): 828–831.
- Sudarshana MR, Roy G and Falk BW. 2007. **Methods for engineering resistance to plant viruses. Methods of Molecular Biology 354** Humana Press, pp. 183–195.
- Trifonova E, Romanova A, Sangaev S, Sapotsky M, Malinovsky V *et al.* 2012. Inducible expression of the gene of *Zinnia elegans* coding for extracellular ribonuclease in *Nicotiana tabacum* plants. *Biol Plant*, **56** (3): 571–574.
- Vandenbussche M, Chambrier P, Rodrigues, Bento S, Morel P. 2016. *Petunia*, your next supermodel? *Front Plant Sci.*, **7**: 72.

Whole Exome Sequencing in Intellectual Disability Patients Identifies *de novo* Mutations in *KCNB1*, *SHANK2*, and *SYNGAP1* Genes and a Novel Mutation in *PPP1R3F*

Asem M Alkhateeb^{1,*}, Miral Almomani², and Hani H Hammad¹

¹ Biotechnology and Genetics Department, Jordan University of Science and Technology, Irbid 22110, Jordan; ² Pediatrics Department, Jordan University of Science and Technology, Irbid 22110, Jordan.

Received: November 24, 2022; Revised: December 10, 2022; Accepted: March 19, 2023

Abstract

Intellectual disability etiology still poses a challenge to clinicians and families. Here we aimed to dissect the genes causing intellectual disability in local families from Jordan. We recruited nine trio families with unexplained intellectual disability, and utilized whole exome sequencing to identify causative genes/mutations. Out of nine families, we identified the candidate causative genes in four (44% detection rate). Novel and known mutations were identified in *KCNB1*, *PPP1R3F*, *SYNGAP1*, and *SHANK2*. Mutations in *KCNB1*, *SYNGAP1*, and *SHANK2* were *de novo*, while *PPP1R3F* mutation was X-linked inherited from the mother. With a highly inbred population, it was unexpected to find the majority of our mutations to be *de novo* representing autosomal dominant inheritance as the major pattern for our sample of unexplained intellectual disability. Our data confirm previous data that *de novo* mutations in autosomal dominantly expressed genes represent the major cause of unexplained intellectual disability, even in highly inbred populations that usually shows enrichment of mutations in genes with autosomal recessive mode of inheritance.

Key words: Exome, Intellectual disability, *de novo*, *KCNB1*, *PPP1R3F*, *SHANK2*, *SYNGAP1*

1. Introduction

Intellectual disability (ID) is a complex neurodevelopmental disorder with a range of intellectual delay. It is characterized by intelligence quotient of less than 70 and deficits in adaptive behavior [Buracket *et al.*, 2021]. Prevalence of ID is estimated to be (0.5-2%) with the majority of cases happening in children less than 15 years old (McBride *et al.*, 2021). According to recent estimates, more than 1,000 genes are implicated in causing ID in humans (Leblondet *et al.*, 2021), with an expectation of more than 1000 yet to be discovered (Kaplaniset *al.*, 2020).

Studies in populations with common consanguineous marriages resulted in the discovery of mainly autosomal recessive ID genes (Rasheed *et al.*, 2021) whereas finding such genes is rare in outbred populations (Martin *et al.*, 2018). On the other hand, *de novo* variants were commonly found in studies from mixed and founder populations (Hamdanet *al.*, 2014; Jarvelaet *al.*, 2021). Recent reports show that up to 48% of patients with ID and developmental disorders harbor pathogenic *de novo* mutations in protein-coding genes (Deciphering Developmental Disorders Study 2017; Kaplaniset *al.*, 2020).

Given the scarce studies done on the middle eastern and specifically the Jordanian population, we aimed to decipher the potential genetic etiologies in 9 families

having at least one affected child with nonspecific ID through trio-whole-exome sequencing (trio-WES) and bioinformatic analysis. Even though the Jordanian community is largely inbred with a continuing prevalent consanguinity, most mutations found were *de novo* demonstrating the importance of such mutations even in highly inbred populations.

2. Methods

2.1. Participants

Patients with established perinatal diseases or chromosomal aneuploidies were excluded. We recruited 9 families with at least one child manifesting nonspecific ID as the major phenotype. The study is approved by the ethics committee at Jordan University of Science and Technology (#24/123/2019) and conforms to the declaration of Helsinki. Goals of the study were explained to parents, and written informed consent was obtained before their inclusion in the study. A neuropediatrician examined all patients, and family histories and medical reports were obtained.

2.2. Trio-WES and bioinformatics analysis

Peripheral blood was collected from available family members, followed by DNA extraction using manufactures protocol (QIAamp DNA Blood mini kit, Qiagen, Hilden, Germany). Trio-WES was performed in Centogene laboratory (Rostock, Germany). One microgram of

* Corresponding author. e-mail: asemalkhateeb@just.edu.jo.

fragmented genomic DNA was used to enrich 60 MB of human exons using SureSelect Human All Exon V6 kit (Agilent, Santa Clara, California, USA) targeting >99% of regions in RefSeq, GENCODE, and the consensus coding sequence project (CCDS) databases. Exons were processed on NextSeq platform (Illumina, San Diego, CA, USA), and an average coverage of ~100X was obtained. More than 10X coverage was obtained for approximately 97% of targeted bases. All variants reported in this report had >45X depth of coverage. In-house bioinformatics pipeline was used to call base pairs, align reads to genome assembly GRCh37/hg19, filter out poor quality, and annotate variants. We considered all disease-causing variants in ClinVar (Landrum *et al.*, 2016), HMGD (Stenson *et al.*, 2020), and CentroMD (Trujillano *et al.*, 2016) databases and all variants in gnomAD (Karczewski *et al.*, 2020) (<http://gnomad.broadinstitute.org/>) database with an allele frequency of less than 0.01%. Identified variants in coding exons and their flanking intronic sequences were investigated taking into account multiple inheritance patterns (de novo autosomal dominant, autosomal recessive, and X-linked). Family history and clinical data were considered in evaluating identified variants. Candidate disease variants were confirmed by Sanger sequencing for probands. Deleterious variants were predicted by multiple commonly used algorithms, such as MutationTaster (Schwarz *et al.*, 2014), PolyPhen-2 (Adzhubei *et al.*, 2010), and SIFT (Sim *et al.*, 2012). The pathogenicity of variants was evaluated according to the

American College of Medical Genetics guidelines (Richardson *et al.*, 2015).

3. Results

We recruited 9 families with ID and performed trios for probands and their parents. All patients had normal brain MRI. The sequencing data were filtered by focusing on very rare variants (MAF<0.01%) and giving priority for those with potential effect on protein structure and function such as nonsense, splicing, and non-conservative missense mutations. Variants with low depth of coverage were excluded (Depth of coverage less than 20 readings). Only one of the nine families was consanguineous (family 799), in another family (family 751) the parents were distant relatives. Variants were analyzed in all modes of inheritance including sex-linked mode.

We identified 3 *de novo* mutations in *KCNBI*, *SHANK2*, and *SYNGAP1* genes and a novel mutation in a boy inherited from the mother in X-linked *PPP1R3F* gene, all of which are already in ID etiology. All mutations had zero allele frequency in The Genome Aggregation Database (gnomAD) (Karczewski *et al.*, 2020) until the writing of the manuscript. Albeit, two of the mutations were reported before c.916C>T, p.Arg306Cys, in *KCNBI* (Saitsuet *et al.*, 2015) and c.1735C>T, p.Arg579*, in *SYNGAP1* (Hamdan *et al.*, 2009). The other 2 mutations are novel c.446C>G, p.Pro149Arg, in *PPP1R3F* and c.757C>T, p.Arg253*, in *SHANK2* (Table 1).

Table 1. List of identified mutations.

Family	Gene	Transcript	Variant	Previously published	Genotype	Inheritance	OMIM phenotype	OMIM#
750	<i>KCNBI</i>	NM_004975.2	c.916C>T, p.Arg306Cys	Saitsuet <i>et al.</i> , 2015	Heterozygous	AD/ <i>de novo</i>	Developmental and epileptic encephalopathy 26	616056
751	<i>SYNGAP1</i>	NM_006772.2	c.1735C>T, p.Arg579*	Hamdan <i>et al.</i> , 2009	Heterozygous	AD/ <i>de novo</i>	Mental retardation, autosomal dominant 5	612621
766	<i>PPP1R3F</i>	NM_033215.4	c.446C>G, p.Pro149Arg	-	Hemizygous	X linked/ inherited from mother	-	-
804	<i>SHANK2</i>	NM_133266.4	c.757C>T, p.Arg253*	Berkelet <i>et al.</i> , 2010	Heterozygous	AD/ <i>de novo</i>	Autism susceptibility 17	613436

All mutations are *de novo* with zero allele frequency in gnomAD v2.1.1 database (<https://gnomad.broadinstitute.org/>) (Karczewski *et al.*, 2020). AD, autosomal dominant inheritance.

Mutations in *KCNBI* gene cause Developmental and epileptic encephalopathy 26 (OMIM# 616056) (Torkamani *et al.*, 2014), and mutations in *SYNGAP1* cause Autosomal dominant mental retardation 5 (OMIM# 612621) (Hamdan *et al.*, 2009). *PPP1R3F* variant changes proline to arginine, which is predicted to be damaging/deleterious by MutTaster, Polyphen, and SIFT prediction tools (Table 2). *PPP1R3F* mutations are

reported in patients with autism spectrum disorder (Piton *et al.*, 2011; Doostparastorshizet *et al.*, 2018). *SHANK2* variant creates a termination codon at position 253 that is expected to produce a nonfunctional gene product. *SHANK2* mutation has been reported to cause autism spectrum disorder and mental retardation (Berkelet *et al.*, 2010).

Table 2. Prediction software results and read depth for the identified mutations.

Gene	Variant	Chromosomal coordinates	MutationTaster	Polyphen-2	SIFT	Read depth
<i>KCNBI</i>	c.916C>T, p.Arg306Cys	chr20:47991181	Disease causing	Probably damaging	Deleterious	183
<i>SYNGAP1</i>	c.1735C>T, p.Arg579*	chr6:33408564	-	-	-	158
<i>PPP1R3F</i>	c.446C>G, p.Pro149Arg	chrX:49126778	Disease causing	Probably damaging	Deleterious	46
<i>SHANK2</i>	c.757C>T, p.Arg253*	Chr11:70336411	-	-	-	239

4. Discussion

In this study, we recruited 9 families affected with ID from Jordan. After doing trio whole exome sequencing for patients and their parents, we found 4 mutations in 4 genes associated with ID. Two of these mutations were reported before while the other two are novel. All 4 mutations are extremely rare, and none of them is listed in the gnomad database (Karczewskiet al., 2020). Molecular diagnostic yield attained in this study (44%) was similar to other recent studies utilizing trio WES to ascertain the genetic etiology of ID (Pode-Shakked et al., 2021; Sheth et al., 2021; Xiang et al., 2021).

PPP1R3F is an X-linked gene, whose mutations have been associated with autism spectrum disorder. Mutations include c.733T>C (p.Phe245Leu) which was found in a child diagnosed with seizures and Asperger Syndrome. This mutation was inherited from the mother who suffered from learning disabilities and seizures herself (Piton et al., 2011). Another mutation, c.2161A>G (p. Arg375Gly), was found in childhood-onset schizophrenia (Ambalavanan et al., 2019). *PPP1R3F* is predominantly expressed in various brain regions such as cerebellum and frontal cortex and is a master regulator of 177 genes, 89 of which are highly expressed in various brain regions compared to other tissues (DoostparastTorshiziet al., 2018). In this study, we found a novel mutation in a boy affected with ID. This mutation was classified as damaging/deleterious by several prediction tools. It changes a proline to Arginine c.446C>G, p.Pro149Arg. Proline is the only amino acid creating a ring with the polypeptide backbone, and it has very firm structure which curves the core chain of the protein in a distinctive way (Khan and Vihinen 2007). No other candidate disease-causing mutations were found in this patient.

Mutations in *SHANK2* are present in 0.17% of patients with ASD and mild ID (Leblond et al., 2014). Many truncating mutations were reported in patients such as c.1384C>T (p.Arg462*) (Berkelet al., 2010), c.1896dupA (p.Asp633Argfs) (Bowling et al., 2017), and multiple-exon deletions (Leblond et al., 2014). Additionally, many single point mutations were found in ASD, ID and Schizophrenia patients (reviewed in Eltokhiet al., 2018). We found a *de novo* truncating mutation early in the gene that is expected to have a detrimental effect on gene product. It is novel and not reported before. No other candidate mutations were found in this patient. All this supports the candidacy of this mutation in causing the phenotype.

In conclusion, we have studied 9 families by trio-WES. The families came from a highly inbred population. We suspected having homozygous mutations prevalent in our sample. However, we found 4 mutations in 4 families (44% detection rate), and 3 of these mutations were *de novo* and all extremely rare. This supports previous reports (Al-Mubarak et al., 2017; Järveläet al., 2021; Wang et al., 2019) pointing to the private and heterogeneous nature of the genetic architecture of ASD and ID even in highly inbred populations. Functional analysis is needed to confirm the role of the mutations found in causing disease. Whole genome sequencing and robust bioinformatic analysis might be needed to solve the genetic cause of disease in the other unresolved families.

Acknowledgement

We kindly thank our participating families. This work was supported by grant number Bas/2/1/2017 from Scientific Research and Innovation Support Fund, Ministry of Higher Education and Scientific Research, Jordan.

Details of the contribution of individual authors

AA designed the study, analyzed data, and wrote manuscript; MA recruited patients, made full clinical assessment; HH helped in collecting samples and helped carry out experimental work. All authors reviewed and corrected the manuscript.

Compliance with ethical standards

Informed consent

Informed consent is obtained from guardians of all patients. Institutional review board (IRB) approval is obtained from the Jordan University of Science and Technology. All procedures followed are in accordance with the IRB approval and with the Helsinki Declaration of 1975, as revised in 2000. Consent to publish is obtained, and the manuscript does not contain any individual person's data in any form.

Conflict of interest

Authors declare no conflict of interest.

Funding

This work was supported by grant number Bas/2/1/2017 from Scientific Research and Innovation Support Fund, Ministry of Higher Education and Scientific Research, Jordan.

Availability of data

Detailed whole exome data in the manuscript are available upon request.

References

- Adzhubei IA, Schmidt S, Peshkin L, Ramensky VE, Gerasimova A, Bork P, Kondrashov AS, Sunyaev SR. 2010. A method and server for predicting damaging missense mutations. *Nat Methods.*, **7(4)**:248-9.
- Al-Mubarak B, Abouelhoda M, Omar A, AlDhalaan H, Aldosari M, Nester M, Alshamrani HA, El-Kalioby M, Goljan E, Albar R, Subhani S, Tahir A, Asfahani S, Eskandrani A, Almusaib A, Magrashi A, Shinwari J, Monies D, Al Tassan N. 2017. Whole exome sequencing reveals inherited and *de novo* variants in autism spectrum disorder: a trio study from Saudi families. *Sci Rep.*, **7(1)**:5679.
- Ambalavanan A, Chaumette B, Zhou S, Xie P, He Q, Spiegelman D, Dionne-Laporte A, Bourassa CV, Therrien M, Rochefort D, Xiong L, Dion PA, Joobor R, Rapoport JL, Girard SL, Rouleau GA. 2019. Exome sequencing of sporadic childhood-onset schizophrenia suggests the contribution of X-linked genes in males. *Am J Med Genet B Neuropsychiatr Genet.*, **180(6)**:335-340.

- Berkel S, Marshall CR, Weiss B, Howe J, Roeth R, Moog U, Endris V, Roberts W, Szatmari P, Pinto D, Bonin M, Riess A, Engels H, Sprengel R, Scherer SW, Rappold GA. 2010. Mutations in the *SHANK2* synaptic scaffolding gene in autism spectrum disorder and mental retardation. *Nat Genet.*, **42(6)**:489-91.
- Bowling KM, Thompson ML, Amaral MD, Finnila CR, Hiatt SM, Engel KL, Cochran JN, Brothers KB, East KM, Gray DE, Kelley WV, Lamb NE, Lose EJ, Rich CA, Simmons S, Whittle JS, Weaver BT, Nesmith AS, Myers RM, Barsh GS, Bebin EM, Cooper GM. 2017. Genomic diagnosis for children with intellectual disability and/or developmental delay. *Genome Med.*, **9(1)**:43.
- Burack JA, Evans DW, Russo N, Napoleon JS, Goldman KJ, Iarocci G. 2021. Developmental Perspectives on the Study of Persons with intellectual disability. *Annu Rev Clin Psychol.*, **17**:339-363.
- Deciphering Developmental Disorders Study. 2017. Prevalence and architecture of *de novo* mutations in developmental disorders. *Nature.*, **542(7642)**:433-438.
- DoostparastTorshizi A, Duan J, Wang K. 2018. Transcriptional network analysis on brains reveals a potential regulatory role of *PPP1R3F* in autism spectrum disorders. *BMC Res Notes.*, **11(1)**:489.
- Eltokhi A, Rappold G, Sprengel R. 2018. Distinct Phenotypes of *Shank2* Mouse Models Reflect Neuropsychiatric Spectrum Disorders of Human Patients with *SHANK2* Variants. *Front Mol Neurosci.*, **11**:240.
- Hamdan FF, Gauthier J, Spiegelman D, Noreau A, Yang Y, Pellerin S, Dobrzyńska S, Côté M, Perreau-Linck E, Carmant L, D'Anjou G, Fombonne E, Addington AM, Rapoport JL, Delisi LE, Krebs MO, Mouaffak F, Joobor R, Mottron L, Drapeau P, Marineau C, Lafrenière RG, Lacombe JC, Rouleau GA, Michaud JL; Synapse to Disease Group. 2009. Mutations in *SYNGAP1* in autosomal nonsyndromic mental retardation. *New Eng. J. Med.*, **360**: 599-605.
- Hamdan FF, Srour M, Capo-Chichi JM, Daoud H, Nassif C, Patry L, Massicotte C, Ambalavanan A, Spiegelman D, Diallo O, Henrion E, Dionne-Laporte A, Fougere A, Pshzhetsky AV, Venkateswaran S, Rouleau GA, Michaud JL. 2014. *De novo* mutations in moderate or severe intellectual disability. *PLoS Genet.*, **10(10)**:e1004772.
- Järvelä I, Määttä T, Acharya A, Leppälä J, Jhangiani SN, Arvio M, Siren A, Kankuri-Tammilehto M, Kokkonen H, Palomäki M, Varilo T, Fang M, Hadley TD, Jolly A, Linnankivi T, Paetau R, Saarela A, Kälviäinen R, Olme J, Nouel-Saied LM, Cornejo-Sanchez DM, Llaci L, Lupski JR, Posey JE, Leal SM, Schrauwen I. 2021. Exome sequencing reveals predominantly *de novo* variants in disorders with intellectual disability (ID) in the founder population of Finland. *Hum Genet.*, **140(7)**:1011-1029.
- Kaplanis J, Samocha KE, Wiel L, Zhang Z, Arvai KJ, Eberhardt RY, Gallone G, Lelieveld SH, Martin HC, McRae JF, Short PJ, Torene RI, de Boer E, Danecek P, Gardner EJ, Huang N, Lord J, Martincorena I, Pfundt R, Reijnders MRF, Yeung A, Yntema HG; Deciphering Developmental Disorders Study, Vissers LELM, Jussola J, Wright CF, Brunner HG, Firth HV, FitzPatrick DR, Barrett JC, Hurles ME, Gilissen C, Retterer K. 2020. Evidence for 28 genetic disorders discovered by combining healthcare and research data. *Nature.*, **586(7831)**:757-762.
- Karczewski KJ, Francioli LC, Tiao G, Cummings BB, Alföldi J, Wang Q, Collins RL, Laricchia KM, Ganna A, Birnbaum DP, Gauthier LD, Brand H, Solomonson M, Watts NA, Rhodes D, Singer-Berk M, England EM, Seaby EG, Kosmicki JA, Walters RK, Tashman K, Farjoun Y, Banks E, Poterba T, Wang A, Seed C, Whiffin N, Chong JX, Samocha KE, Pierce-Hoffman E, Zappala Z, O'Donnell-Luria AH, Minikel EV, Weisburd B, Lek M, Ware JS, Vittal C, Armean IM, Bergelson L, Cibulskis K, Connolly KM, Covarrubias M, Donnelly S, Ferreira S, Gabriel S, Gentry J, Gupta N, Jeandet T, Kaplan D, Llanwarne C, Munshi R, Novod S, Petrillo N, Roazen D, Ruano-Rubio V, Saltzman A, Schleicher M, Soto J, Tibbetts K, Tolonen C, Wade G, Talkowski ME; Genome Aggregation Database Consortium, Neale BM, Daly MJ, MacArthur DG. 2020. The mutational constraint spectrum quantified from variation in 141,456 humans. *Nature.*, **581(7809)**:434-443.
- Khan S, Vihinen M. 2007. Spectrum of disease-causing mutations in protein secondary structures. *BMC Struct Biol.*, **7**:56.
- Landrum MJ, Lee JM, Benson M, Brown G, Chao C, Chitipiralla S, Gu B, Hart J, Hoffman D, Hoover J, Jang W, Katz K, Ovetzky M, Riley G, Sethi A, Tully R, Villamarin-Salomon R, Rubinstein W, Maglott DR. 2016. ClinVar: public archive of interpretations of clinically relevant variants. *Nucleic Acids Res.*, **44(D1)**: D862-8.
- Leblond CS, Nava C, Polge A, Gauthier J, Huguet G, Lumbroso S, Giuliano F, Stordeur C, Depienne C, Mouzat K, Pinto D, Howe J, Lemièrre N, Durand CM, Guibert J, Ey E, Toro R, Peyre H, Mathieu A, Amsellem F, Rastam M, Gillberg IC, Rappold GA, Holt R, Monaco AP, Maestrini E, Galan P, Heron D, Jacqueline A, Afenjar A, Rastetter A, Brice A, Devillard F, Assouline B, Laffargue F, Lespinasse J, Chiesa J, Rivier F, Bonneau D, Regnault B, Zelenika D, Delepine M, Lathrop M, Sanlaville D, Schluth-Bolard C, Edery P, Perrin L, Tabet AC, Schmeisser MJ, Boeckers TM, Coleman M, Sato D, Szatmari P, Scherer SW, Rouleau GA, Betancur C, Leboyer M, Gillberg C, Delorme R, Bourgeron T. 2014. Meta-analysis of *SHANK* Mutations in Autism Spectrum Disorders: a gradient of severity in cognitive impairments. *PLoS Genet.*, **10(9)**:e1004580.
- Leblond CS, Le TL, Malesys S, Cliquet F, Tabet AC, Delorme R, Rolland T, Bourgeron T. 2021. Operative list of genes associated with autism and neurodevelopmental disorders based on database review. *Mol Cell Neurosci.*, **113**:103623.
- McBride O, Heslop P, Glover G, Taggart T, Hanna-Trainor L, Shevlin M, Murphy J. 2021. Prevalence estimation of intellectual disability using national administrative and household survey data: The importance of survey question specificity. *Int J Popul Data Sci.*, **6(1)**:1342.
- Piton A, Gauthier J, Hamdan FF, Lafrenière RG, Yang Y, Henrion E, Laurent S, Noreau A, Thibodeau P, Karemera L, Spiegelman D, Kuku F, Duguay J, Destrois-maisons L, Jolivet P, Côté M, Lachapelle K, Diallo O, Raymond A, Marineau C, Champagne N, Xiong L, Gaspar C, Rivière JB, Tarabeux J, Cossette P, Krebs MO, Rapoport JL, Addington A, Delisi LE, Mottron L, Joobor R, Fombonne E, Drapeau P, Rouleau GA. 2011. Systematic resequencing of X-chromosome synaptic genes in autism spectrum disorder and schizophrenia. *Mol Psychiatry.*, **16(8)**:867-80.
- Pode-Shakked B, Barel O, Singer A, Regev M, Poran H, Eliyahu A, Finezilber Y, Segev M, Berkenstadt M, Yonath H, Reznik-Wolf H, Gazit Y, Chorin O, Heimer G, Gabis LV, Tzadok M, Nissenkorn A, Bar-Yosef O, Zohar-Dayana E, Ben-Zeev B, Mor N, Kol N, Nayshool O, Shimshoviz N, Bar-Joseph I, Marek-Yagel D, Javasky E, Einy R, Gal M, Grinshpun-Cohen J, Shohat M, Dominissini D, Raas-Rothschild A, Rechavi G, Pras E, Greenbaum L. 2021. A single center experience with publicly funded clinical exome sequencing for neurodevelopmental disorders or multiple congenital anomalies. *Sci Rep.*, **11(1)**:19099.
- DoostparastTorshizi A, Duan J, Wang K. 2018. Transcriptional network analysis on brains reveals a potential regulatory role of *PPP1R3F* in autism spectrum disorders. *BMC Res Notes.*, **11(1)**:489.
- Rasheed M, Khan V, Harripaul R, Siddiqui M, Malik MA, Ullah Z, Zahid M, Vincent JB, Ansar M. 2021. Exome sequencing identifies novel and known mutations in families with ID. *BMC Med Genomics.*, **14(1)**:211.

- Richards S, Aziz N, Bale S, Bick D, Das S, Gastier-Foster J, Grody WW, Hegde M, Lyon E, Spector E, Voelkerding K, Rehm HL; ACMG Laboratory Quality Assurance Committee. 2015. Standards and guidelines for the interpretation of sequence variants: a joint consensus recommendation of the American College of Medical Genetics and Genomics and the Association for Molecular Pathology. *Genet Med.*, **17(5)**:405-24.
- Saitou, H., Akita, T., Tohyama, J., Goldberg-Stern, H., Kobayashi, Y., Cohen, R., Kato, M., Ohba, C., Miyatake, S., Tsurusaki, Y., Nakashima, M., Miyake, N., Fukuda, A., & Matsumoto, N. 2015. *De novoKCNB1* mutations in infantile epilepsy inhibit repetitive neuronal firing. *Scientific reports.*,**5**:15199.
- Schwarz JM, Cooper DN, Schuelke M, Seelow D. MutationTaster2: mutation prediction for the deep-sequencing age. *Nat Methods.* 2014; 11(4):361-2.
- Sheth H, Pancholi D, Bhavsar R, Mannan AU, Ganapathy A, Chowdhury M, Shah S, Solanki D, Sheth F, Sheth J. 2021. Assessing Utility of Clinical Exome Sequencing in Diagnosis of Rare Idiopathic Neurodevelopmental Disorders in Indian Population. *Neurol India.*, **69(6)**:1729-1736.
- Sim NL, Kumar P, Hu J, Henikoff S, Schneider G, Ng PC. 2012. SIFT web server: predicting effects of amino acid substitutions on proteins. *Nucleic Acids Res.*, **40**(Web Server issue): W452-7.
- Stenson PD, Mort M, Ball EV, Chapman M, Evans K, Azevedo L, Hayden M, Heywood S, Millar DS, Phillips AD, Cooper DN. 2020. The Human Gene Mutation Database (HGMD®): optimizing its use in a clinical diagnostic or research setting. *Hum Genet.*, **139(10)**:1197-1207.
- Torkamani A, Bersell K, Jorge BS, Bjork RL Jr, Friedman JR, Bloss CS, Cohen J, Gupta S, Naidu S, Vanoye CG, George AL Jr, Kearney JA. 2014. *De novoKCNB1* mutations in epileptic encephalopathy. *Ann Neurol.*, **76(4)**:529-540.
- Trujillano D, Oprea GE, Schmitz Y, Bertoli-Avella AM, AbouJamra R, Rolfs A. 2016. A comprehensive global genotype-phenotype database for rare diseases. *Mol Genet Genomic Med.*, **5(1)**:66-75.
- Wang W, Corominas R, Lin GN. 2019. *De novo* Mutations from Whole Exome Sequencing in Neurodevelopmental and Psychiatric Disorders: From Discovery to Application. *Front Genet.*, **10**:258.
- Xiang J, Ding Y, Yang F, Gao A, Zhang W, Tang H, Mao J, He Q, Zhang Q, Wang T. 2021. Genetic Analysis of Children with Unexplained Developmental Delay and/or intellectual disability by Whole-Exome Sequencing. *Front Genet.*, **12**:738561.

Studies on Toxicity and Peptic Ulcer Healing Potential of Crude Extract of *Osbeckia crinita* in Swiss Albino Mice

Sanchayeeta Roy, Bishnupada Roy*

Parasitology and Toxicology Laboratory, Department of zoology North-Eastern Hill University, Shillong- 793022, Meghalaya, India

Received: November 17, 2022; Revised: March 21, 2023; Accepted: March 29, 2023

Abstract

Background: For gastrointestinal diseases *Osbeckia crinita* (*O. crinita*) has been traditionally used among different parts of Northeast India. The present study aims to evaluate the toxicity and antiulcer activity of *O. crinita* methanolic leaf extract.

Method: For sub-acute toxicity study, repeated oral doses of 150 mg, 300 mg and 600 mg extract of the plant *O. crinita* per kg body weight of mice were administered for 28 days, and analyzed the hematological and biochemical parameters. The effect of crude methanolic extract of the plant on ethanol-induced peptic ulcer was studied using repeated dosing (200 mg/kg bw) for 6, 10 and 14 days, respectively. Ranitidine (30 mg/kg bw) was used as standard drug. Antiulcer activity was assessed by measuring Ulcer index, healing percentage, gross macroscopic lesions, protein and carbohydrate content along with histopathology and ultra-structural observation.

Result: LD₅₀ value was found to be more than 2000 mg/kg body weight. The sub-acute toxicity study showed that at a dose of 600 mg/kg bw of mice significant changes were observed in hematological and biochemical parameters. Six, ten and fourteen day's treatment with the plant extract exhibited significant increase in ulcer protection by 62.09%, 81.04% and 90.06%, respectively. As compared to negative ulcerated mice, *O. crinita* treated mice showed higher level of protein and carbohydrate content. The histological and scanning electron microscopic observations showed treatment with *O. crinita* resulted in comparatively better gastric healing in a time dependent manner.

Conclusion: Based on the results, it was concluded that *O. crinita* extract possesses peptic ulcer protective potency comparable to ranitidine, which justifies the use of this plant for ulcer treatment.

Keywords: *Osbeckia crinita*; antiulcer; toxicity; Ranitidine; ethanol; methanol; protein.

1. Introduction

Peptic ulcer is a lesion of gastric or duodenal mucosa that occurs due to imbalance between the aggressive factors (acid, pepsin, free radicals, etc) and the mucosal protective factors, (mucus, prostaglandins) and is responsible for high rate of morbidity affecting up to 10% of the world's population (Kuna *et al.*, 2019). Various factors are implicated that play a pivotal role in the pathogenesis of the ulceration like exposure to *Helicobacter pylori*, smoking, consumption of alcohol, poor diet, stress, and the abuse of non-steroidal anti-inflammatory drugs (NSAIDs) (Tijani *et al.*, 2021 and Mahmoud *et al.*, 2023). The epidemiology revealed that infection with *Helicobacter pylori* is the primary cause of peptic ulcers. It causes 70% of stomach ulcers and 95% of duodenal ulcers (Tripathi *et al.*, 2021). The protective gastric mucosal factors are a group of several neurohormonal and physiological systems which prevent the mucosa against noxious and harmful stimuli (Yandrapu and Sarosiek, 2015). The ethanol-induced gastric ulcer model has been frequently utilized to test anti-ulcer activity in the laboratory because of its close resemblance to acute gastric ulcer in humans (Song *et al.*, 2018). Excessive alcohol consumption is the most prevalent cause

of ulcer which damages the gastric mucosal integrity through lowering gastric mucosal blood flow (Yu *et al.*, 2020)

Drug therapy of peptic ulcer has been commonly targeted at either counteracting the aggressive factors or stimulating the defensive ones. Various synthetic antiulcer drugs presently available in the market include antacids, proton pump inhibitors, anticholinergics, H₂- receptor antagonists and cytoprotective agents which are being used to prevent and treat various types of ulcers. However, most of the drugs confer simpler to several side effects like arrhythmias, impotence, hematopoietic changes etc. (Freedberg *et al.*, 2017; Sharifi-Rad *et al.*, 2018); these complications enforce for the development of new antiulcer drug and search for novel molecules from drug basket of nature, which are the herbal resources.

Traditionally used natural plant products and their derivatives have long been recognized as a viable alternative source of therapeutic agents (Koparde *et al.*, 2019). *O. crinita* belongs to the family Melastomataceae, known to possess wound healing property and being used for treatment of snake bites and nose bleeding (Rao *et al.*, 1981). Methanolic leaf extract of *O. crinita* exhibits anti-inflammatory and anti-oxidant properties. In addition, the plant is reported to contain a plenty of phytochemicals such as alkaloids, flavonoids, tannin and saponin etc.

* Corresponding author. e-mail: bishnuroy9@gmail.com.

(Kalita *et al.*, 2022). Local people of Nagaland use this plant to cure gastrointestinal disease. Since scientific validation of the plant is not carried out, the present study aims to assess the anti-peptic ulcer activity of methanolic crude extract of *O. crinita* leaves against ethanol induced peptic ulcer in mice. Acute and sub-acute tests were also carried out to assess the extent of toxicity of the methanolic crude extract of *O. crinita* leaves.

2. Materials and method

2.1. Experimental Animals

Healthy Swiss albino mice (males and females) of 8-12 weeks old and weighing 25-30 grams were used for this study. The animals were procured from the Pasteur Research Institute, Shillong, Meghalaya, and maintained under housing conditions: lighting cycles of 12 h light/12 h dark and temperature of 22-25°C. They were fed with a standard laboratory Rodents' diet and an unlimited supply of drinking water was allowed. The animals were acclimatized for five days before conducting the experiments. The final approval to carry out the study was granted by the Institutional Animal Ethics Committee (IEC), North-Eastern Hill University, Shillong, Meghalaya, India (IEC/MS/Misc./05)

2.2. Plant collection and preparation of methanolic extract

The plant *O. crinita* was collected during the months of July to August, 2019, from Nagaland and was identified and authenticated by a taxonomist from the Botanical Survey of India, Shillong (Accession No. of *O. crinita*: NEHU – 98166). For preparation of the crude extract, the leaves were separated from the plant, washed with water, dried under shade and then grinded into fine powder using a blender. The powder was then soaked in 90% methanol (100 g/l) for 10 days, filtered using Whatman filter paper No.1 and the solvent from the solution was separated out using a rotary evaporator. The methanolic crude extract of leaves yielded 12.7% and was stored at 4°C until further use. Before treatment, the doses were prepared by dissolving the extract in 0.9% Phosphate Buffer Saline (PBS, pH 7.2-7.4).

2.3. Phytochemical analysis of plant extracts

The plant materials were subjected to various qualitative tests to detect the presence of different phytochemicals such as alkaloids, terpenoids, tannins, saponins, flavonoids etc. using standard protocols (Obiamine and Uche, 2008).

2.4. Acute toxicity study

Acute oral toxicity study was conducted according to the guidelines of Organization for Economic Co-operation and Development (OECD, 2002). Fifteen mice were divided into three groups with five animals in each group. Following an overnight fasting, the mice were administered with different concentrations (500, 1000, 2000 mg/kg bw) of crude plant extract only once (on day 0), and cage side observations were carried out to document any sign of toxicity (tremors, convulsions, salivation, diarrhea, lethargy, sleep and coma) and mortality, if any, for next 14 days. Number of dead mice

was recorded and used for calculation of the median lethal dose (LD₅₀).

2.5. Sub-acute toxicity study

Sub-acute toxicity study was conducted according to the guidelines of Organization for Economic Co-operation and Development (OECD, 2008). Twenty four animals were divided into four groups of six animals each. Before the experiments mice were fasted for 24 h. Group I (control) was administered orally with vehicle (PBS) only, and the remaining three groups (Group II, III and IV) were administered orally with different desired sub-acute concentrations (150, 300, 600 mg/kg bw) of crude plant extracts daily for 28 days. Food and water intake was recorded daily, whereas body weight was recorded once in a week throughout the study period.

2.5.1. Hematological and biochemical analysis

Twenty four hours after termination of experiment, the blood sample was drawn from the vein of hind leg of mice with a syringe under anesthesia and collected into vials containing the anticoagulant to count RBCs, WBCs, and platelets and to determine haemoglobin content (Davie and Lewis, 1975). Biochemical indices for liver function test and renal function test was carried out using a semi-automated biochemical analyzer using standard kits. Organs like liver, kidney, stomach, heart and spleen were excised and washed with 0.9% saline and weighed. The relative organ weight (ROW) was calculated as follows:

$$\text{ROW} = \frac{\text{Absolute organ weight (g)} \times 100}{\text{Body weight (g) on the day of sacrifice}}$$

(Geetha and Vijayalakshmi, 2013).

2.6. Anti-peptic ulcer study

Swiss albino mice were randomly divided into four groups of six animals each. Ulcer was induced in all the animals by administration of ethanol following Oates and Hakkinen, (1988) with slight modification. All animals were fasted for 24 hours with free excess to water, and then 80% ethanol was administered at a dose of 1 ml/100 g of mice orally. Group I was considered as ulcerated group, where animals were sacrificed one hour after induction of ulcer, Group II, considered as negative control, received only distilled water; Group III considered as positive control, received ranitidine (30 mg/kg bw). The reference drug was procured from Cadila pharmaceuticals limited. Group IV, considered as treated group, received methanolic crude extract of *O. crinita* (200 mg/kg bw). At the end of the 6th, 10th and 14th day, animals were kept for 24h fasting and then were sacrificed under ether anesthesia.

2.6.1. Scoring of ulcers

Stomach of each animal was opened along the greater curvature, rinsed in water and examined to assess the formation of ulcer (Photographs were obtained using digital camera). Scoring of ulcer was recorded following Dashputre and Naikwade, (2011), as mentioned below:

Normal colored stomach = 0, Red coloration = 0.5, Spot ulcer = 1, Hemorrhagic streak = 1.5, Deep ulcer = 2, Perforation = 3. Mean ulcer score for each animal was expressed as ulcer index. The percentage of ulcer healing was determined as follows:

Ulcer index (U_I) was measured by using following formula: $U_I = U_N + U_S + U_P \times 10^{-1}$

Where, U_1 = Ulcer Index; U_N = Average number of ulcers per animal; U_S = Average number of severity score; U_P = Percentage of animals with ulcers. Percentage inhibition of ulceration was calculated as given below:

$$\text{Percentage of ulcer healing} = [(UI_{\text{control}} - UI_{\text{treated}}) / UI_{\text{control}}] \times 100$$

2.6.2. Histopathological examination

After dissection, the tissues (stomach) of the experimental groups were collected and fixed in Bouin's fixative and were processed for microtomy followed by staining the sections in hematoxylin and eosin, mounting in DPX and viewed under compound microscope (Leica DM1000)

2.6.3. Ultrastructural studies

For observation of fine surface alterations, scanning electron microscopy was carried out where specimens were fixed in neutral buffer formalin, dehydration was carried out in acetone grades followed by air drying in tetramethylsilane following Dey *et al.*(1989) modified by Roy and Tandon, (1991). The gold coated specimens were viewed in the JEOL JSM 6360 scanning electron microscope at 25 kV.

2.6.4. Estimation of protein and carbohydrate

For estimation of protein and carbohydrate content the stomach tissues were collected after 6, 10 and 14 days of treatment, and 5% homogenate was prepared in PBS (pH-7.4) using homogenizer. Total Protein and carbohydrate content of the different groups were estimated following Bradford, (1976) and Albalasmeh *et al.* (2013).

2.7. Statistical analysis

Data were analyzed using SPSS software and were expressed as mean \pm Standard Error Mean, and analyzed using one-way analysis of variance (ANOVA). Tukey's test was applied for post hoc analysis. $p < 0.05$ was considered as statistically significant.

3. Results

3.1. Preliminary phytochemical test

Preliminary phytochemical analysis of the *O. crinita* leaves extract revealed the presence of alkaloids, flavonoids, saponins, steroids, glycosides, terpenoids and tannin (Fig 1)

Alkaloids (Dragendroffs reagent)		Alkaloids (Mayer's reagent)		Anthroquinone		Terpenoids (salkowski test)		Steroids		Glycoside (keller- kilani test)		Glyceroids (libersmens test)		Tanins	
C	+	C	+	C	-	C	+	C	+	C	+	C	+	C	+
Flavonoids (Fecl3 test)		Flavonoids (Alkaline reagent test)		Saponin		Phlobatanins		Reducing sugars							
C	+	C	+	C	+	C	-	C	-						

Figure 1. Photograph showing phytochemical analysis of methanolic leaves extract of *Osbeckia crinita*. C: control, "+": present, "-": absent

3.2. Effect of plant extracts on acute toxicity studies

The result of the acute toxicity study recorded zero mortality of mice receiving 2000 mg/kg bw methanolic extract of *O. crinita*. No lethal effects were noted

throughout the short and long-term observation period. Therefore, the extract was revealed to be safe at a dose level 2000 mg/kg bw of mice and LD_{50} was considered to be more than 2000 mg/kg bw (Table 1).

Table 1. Clinical sign of acute toxicity test of methanolic leaves extract of *O. crinita* treated mice at dose 2000 mg/kg bw

Observation on the mice	30mins		4 hrs		24 hrs		72 hrs		1week		2 weeks	
	C	T	C	T	C	T	C	T	C	T	C	T
Skin and fur	N	N	N	N	N	N	N	N	N	N	N	N
eyes	N	N	N	N	N	N	N	N	N	N	N	N
Mucus membrane	N	N	N	N	N	N	N	N	N	N	N	N
Salivation	N	X	N	N	N	N	N	N	N	N	N	N
Lethargy	N	X	N	N	N	N	N	N	N	N	N	N
Sleep	N	X	N	N	N	N	N	N	N	N	N	N
convulsion	N	X	N	N	N	N	N	N	N	N	N	N
Tremors	N	X	N	N	N	N	N	N	N	N	N	N
Diarrhea	N	N	N	N	N	N	N	N	N	N	N	N
Mortality	N	N	N	N	N	N	N	N	N	N	N	N

Where C= Control, T= Treated, N= Normal and X=Change

3.3. Effect of plant extracts on sub-acute toxicity studies

All the treated mice of both sexes at the doses of 150, 300 and 600 mg/kg survived throughout the 28 days of treatment. No observable toxicity signs were noticed in the extract treated mice compared to the control.

3.3.1. Body weight and relative organ weight

The mean body weight changes of tested mice for 28 days of treatment are shown in Table 2. At the end of the 28 days study period, there was no significant change

observed between control and treated mice at doses 150 and 300 mg/kg body weight; however, a significant reduction in mean body weight was observed at 600mg/kg body weight, although after 28 days of sub-acute treatment, significant changes were not recorded in the organ's weight compared to control group (Table 3).

Table 2. Effect of methanolic leaves extract of *Osbeckia crinita* on Body weight in sub-acute toxicity (28 days)

Body weight (g)	control	150mg/kg	300mg/kg	600mg/kg
Initial	29.26±0.37	30.88±0.46	30.59±0.68	29.31±0.67
Final	32.68±1.35	32.78±1.09	31.70±1.82	27.39±1.39
Mean weight change	3.42±1.15	1.89±1.38	1.11±1.15	-1.92±0.44*

Values are expressed as mean ±S.E.M. (n=6) * significantly different from control ($p<0.05$).

Table 3. Effect of methanolic leaves extract of *Osbeckia crinita* on Relative Organ Weight (ROW) in sub-acute toxicity (28 days)

ROW (g)	Control	150mg/kg	300mg/kg	600mg/kg
Liver	4.39 ± 0.11	4.44 ± 0.25	4.59±0.19	4.67±0.09
Kidney	1.22 ± 0.08	1.32± 0.05	1.32±0.06	1.35±0.08
Stomach	1.22 ± 0.16	1.27 ± 0.06	1.24±0.18	1.43±0.11
Heart	0.54 ± 0.04	0.62 ± 0.05	0.52±0.03	0.58±0.02
Spleen	0.37 ± 0.04	0.46 ± 0.02	0.35±0.04	0.41±0.07

Values are expressed as mean ±S.E.M. (n=6)

3.3.2. Hematological and biochemical studies

Table 4. represents the results of hematological parameters of control and *O. crinita* treated groups for 28 days. After 28 days, the results revealed that there is a significant increase in blood parameters such as Hb and RBC at dose 150 mg/kg bw when compared with the

control group. *O. crinita* treatment at 300 mg/kg caused no significant changes in the blood parameters. However, when the dose of plant extract was increased to 600 mg/kg bw a significant decline in Hb, RBC and WBC count was recorded.

Table 4. Effect of methanolic leaves extract of *Osbeckia crinita* on hematological parameters in sub acute toxicity (28 days)

Parameters	control	150mg/kg	300mg/kg	600mg/kg
Hb (g%)	14.48±0.25	15.78±0.28*	14.13±0.46	12.24±0.47*
RBC (10 ⁵ /mm ³)	8.57±0.28	9.78±0.29*	8.06±0.16	6.93±0.18*
WBC (10 ³ /mm ³)	5.80±0.12	6.36±0.27	6.54±0.29	4.1±0.23*
Plt (10 ⁵ /mm ³)	9.15±0.51	8.47±0.54	8.35±0.39	7.65±0.51

Values are expressed as mean ±S.E.M. (n=6) * significantly different from control ($p<0.05$). Hb: Hemoglobin, RBC: Red Blood Cells, WBC: White Blood Cells, Plt: Platelets.

Table 5. represents the results on biochemical parameters of control and *O. crinita* treated groups for 28 days. Interestingly, after 28 days of treatment, results showed the changes in ALT and ALP level in all *O. crinita* treatment group but were not significant from that of the control group, while there was a significant increase in AST at dose 600 mg/kg bw compared to control group. Treatment with *O. crinita* at a dose of 600 mg/kg bw for 28 days, showed a significant increase in bilirubin(T)

level. On the other hand, no significant changes were observed in the levels of bilirubin(D) in mice treated with 150, 300 and 600 mg *O. crinita*/ kg bw. The creatinine level increased significantly in experimental groups treated with *O. crinita* at concentration of 150 and 600 mg/kg bw. Treatment with *O. crinita* showed a significant elevation in urea level in both 300 and 600 mg/kg bw treated mice groups.

Table5. Effect of methanolic leaves extract of *Osbeckia crinita* on biochemical parameters in sub acute toxicity (28 days)

Parameters	control	150mg/kg	300mg/kg	600mg/kg
ALT (U/L)	17.53±0.38	18.58±1.85	17.97±1.08	15.38±0.58
AST (U/L)	32.69±0.84	32.49±1.04	30.70±0.85	44.46±0.31*
ALP (U/L)	64.73±0.32	59.58±3.53	62.20±1.54	66.73±0.52
Bilirubin(T) (mg/dl)	0.68±0.01	0.68±0.03	0.69±0.02	0.82±0.02*
Bilirubin(D) (mg/dl)	0.34±0.02	0.34±0.04	0.35±0.03	0.39±0.02
Creatinine (mg/dl)	0.43±0.01	0.52±0.02*	0.47±0.01	0.53±0.01*
Urea (mg/dl)	70.49±0.53	70.21±0.89	79.78±0.86*	82.07±1.18*

Values are expressed as mean ±S.E.M. (n=6) * significantly different from control ($p<0.05$). ALT: Alanine transaminase, AST: Aspartate transaminase, ALP: Alkaline phosphatase, Bilirubin(T): bilirubin total, Bilirubin(D): bilirubin direct

3.4. Anti-ulcer activity of the plant extract

3.4.1. Ulcer scoring

Table 6. represents the ulcer index and healing activity of control, negative control, ranitidine and *O. crinita* treated groups. Treatment with *O. crinita* extract at 200

mg/kg and with ranitidine 30 mg/kg bw significantly ($p<0.05$) reduced the ulcer index when compared with negative control group. Consequently, it also stimulated the healing process of peptic ulcers provoked by 80% ethanol. However, ranitidine (30 mg/kg bw) treated mice showed highest healing property.

Table 6. Effect of treatment with *Osbeckia crinita* methanolic leave extract in the ulcer index and healing activity in ethanol induced peptic ulcer in mice

Groups	Ulcer index		Healing %			
	6 days		10 days		14 days	
	Ulcer index	Healing %	Ulcer index	Healing %	Ulcer index	Healing %
Ulcerated	1.53±0.03		-			
NC	0.95±0.02 ^{a*}	37.90	0.75±0.03 ^{a*}	51	0.57±0.02 ^{a*}	62.15
PC (30 mg/kg)	0.52±0.02 ^{a*b*}	66.01	0.20±0.06 ^{a*b*}	86.47	0.07±0.03 ^{a*b*}	95.09
<i>O. crinita</i> (200 mg/kg)	0.58±0.04 ^{a*b*}	62.09	0.29±0.06 ^{a*b*}	81.04	0.15±0.04 ^{a*b*}	90.06

Values are expressed as mean ± S.E.M. (n=6), a* $p<0.05$, when compared with ulcerated group b* $p<0.05$, when compared with negative control group. Statistically analyzed by one way analysis of variance (ANOVA) followed by tukey's test. NC: Negative control, PC: positive control, *O. crinita*: *Osbeckia crinita*

Macroscopic view of gastric mucosa of control and experimental groups of mice were presented in Fig 2. Gastric mucosa of healthy mice showed clear and proper arrangement of cells. Whereas ethanol induced gastric ulcerated mice mucosa showed several reddish lesions

with hemorrhagic streaks. Total stomach signs of mice administered with *O. crinita* and ranitidine showed remarkable decrease in reddish lesion and hemorrhagic streaks as compared to negative control and ulcerated mice.

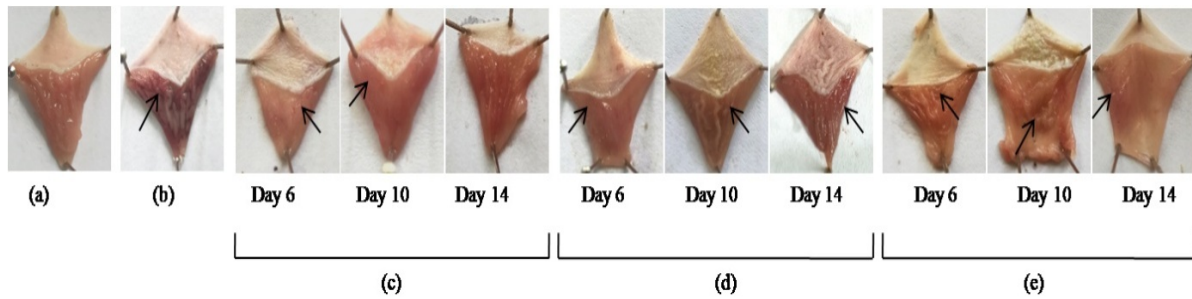


Figure 2. Photographs showing ethanol induced ulceration in the stomach of mice. Gastric mucosa of (a) Healthy normal animals showing absence of ulcer; (b) ethanol administered mice showing severe ulceration as a reddish lesions (c) Ranitidine (30 mg/kg bw) treated animals showing less intense ulcer as compared to ulcerated mice in 6,10 and 14 days respectively; (d) *O. crinita* (200 mg/kg bw) treated mice showing moderate ulcers in 6 days and minor mucosa lesion in 10 and 14 days as compared to ulcerated animals; (e) animals treated with normal saline (negative control) showing major mucosa lesion in day 6, however lesion reduces in day 10 and 14 respectively.

3.4.2. Evaluation of total protein and carbohydrate

After 6, 10, and 14 days of treatment, the amount of protein and carbohydrate in the stomach tissues were measured quantitatively. The analysis of total protein revealed that in *O. crinita* and ranitidine treated groups, total protein content was found to be significantly higher ($p < 0.05$) than in the ulcerated groups. Administration of *O. crinita* (200 mg/kg bw) and ranitidine (30 mg/kg bw) for 6, 10 and 14 days to ethanol induced ulcerated mice showed significant ($p < 0.05$) elevation in protein and carbohydrates levels when compared with ulcerated groups. No changes were observed in protein levels in *O. crinita* and ranitidine treated mice when compared with healthy mice. Fourteen days of treatment with *O. crinita* depicts the elevation of protein concentration to the normal level as that of healthy mice (Fig 3 and Fig 4).

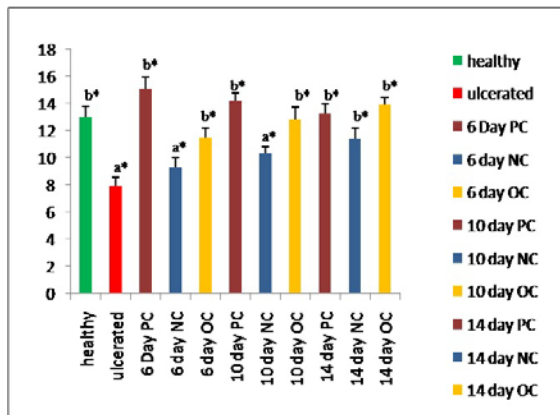


Figure 3. Effect of *O. crinita* on protein concentration in the stomach tissue after ulcer induction. Values are expressed as mean SEM (n=6), $a^*p < 0.05$, when compared with control group, $b^*p < 0.05$ when compared with healthy group. Statistically analyzed by one way analysis of variance (ANOVA) followed by tukey's test. PC: Positive control, NC: Negative control, OC: *Osbeckia crinita*

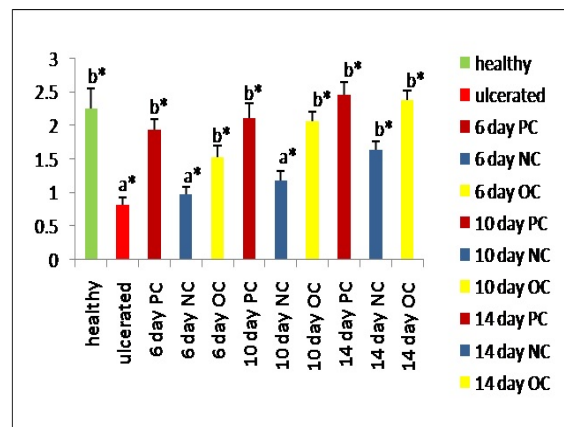


Figure 4. Effect of *O. crinita* on carbohydrate concentration in the stomach tissue after ulcer induction. Values are expressed as mean SEM (n=6), $a^*p < 0.05$, when compared with healthy group, $b^*p < 0.05$, when compared with ulcerated group. Statistically analyzed by one way analysis of variance (ANOVA) followed by tukey's test. PC: Positive control, NC: Negative control, OC: *Osbeckia crinita*

3.4.3. Histological and ultrastructure Observations

Histology of a healthy stomach showed intact gastric epithelium with normal architecture of stomach. Contrary in the ulcerated group, histological analysis revealed fairly substantial damage to the stomach mucosa, with necrotic lesions which penetrate deeply into the mucosa and extensive edema along with leukocyte infiltration. Compared to negative control group, treatment with ranitidine (30 mg/kg) and *O. crinita* (200 mg/kg), a significant reduction of mucosal damage in a time dependent manner was recorded. It also reduced inflammatory cell infiltration in sub mucosal region as well. However, ranitidine (30 mg/kg) restores the mucosal injury faster than *O. crinita*. Furthermore, *O. crinita* (200 mg/kg) and ranitidine (30 mg/kg) allowed regeneration in time dependent manner (Fig 5).

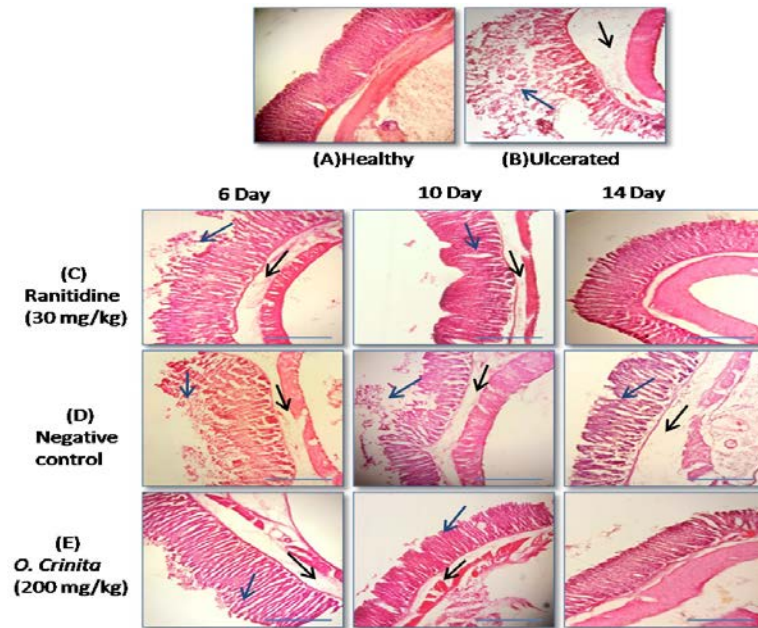


Figure 5. Effect of methanolic leave extract of *O. crinita* on histology of gastric epithelium in ethanol induced peptic ulcer damage in swiss albino mice. Healthy mice (A) showing normal stomach's architecture or morphology of the stomach. Stomach of ulcerated (B) mice showing several mucosal injury (blue arrow) edema with leucocytes and inflammation of sub mucosal layer (black arrow). (C) represents ranitidine (30mg/kg) treated mice in 6, 10 and 14 day respectively. (D) represents negative mice in 6, 10 and 14 days respectively. (E) represents *O. crinita* treated mice in 6, 10 and 14 days. Scale bar: 100µm.

Scanning electron microscopy of healthy group depicted intact epithelial cells with perfect arrangement. Ulcerated groups showed damaged epithelial cells along with erosion and damaged gastric pits. Treatment with *O.*

crinita (200 mg/kg) revealed a normal epithelium with slight erosion. However, ranitidine (30 mg/kg) treated showed intact epithelium like normal group (Fig 6).

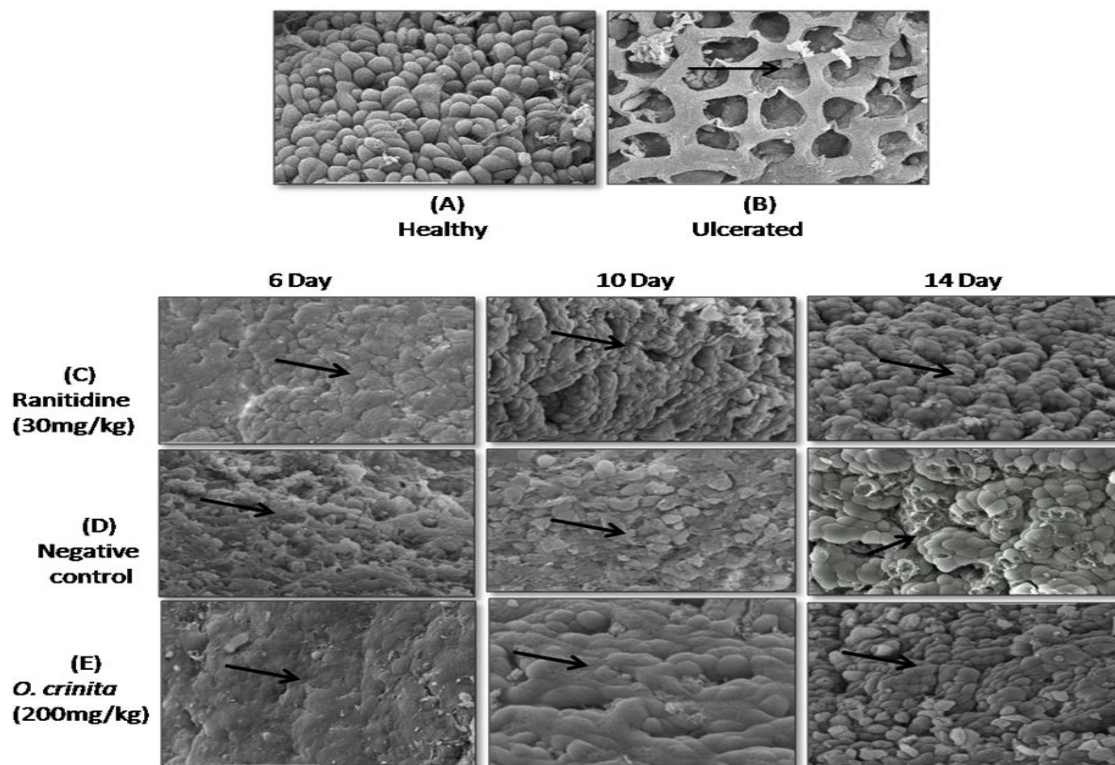


Figure 6. Scanning electron micrographs of (A) Healthy normal mice showing uniform epithelium with no damage (B) Ulcerated mice showing damaged epithelium with several erosions. (C) Ranitidine (30mg/kg) treated mice in 6, 10 and 14 days, respectively, showing time dependent regeneration to normal architecture of epithelium. (D) Negative control (treated with saline only) mice in 6, 10 and 14 days. (E) *O. crinita* (200 mg/kg) treated mice in 6, 10 and 14 days showing recovered normal structural features of the epithelium. (Magnification: 20kv x 500, 50 µm)

4. Discussion

Acute toxicity study revealed that the crude extract of the plant *O. crinita* is safe in mice at a limit dose of 2000 mg/kg bw. The doses employed in sub-acute toxicity study were selected on the basis of LD₅₀ calculated in the acute toxicity study.

Sub-acute toxicity study at low dose (150 mg/kg bw) revealed a significant increase in Hb and RBC. This suggests that the plant extract may include phytochemicals that induce erythropoietin synthesis or secretion in animal's stem cells. This observation agrees with the report of Oyedemi *et al.* (2011), who reported that *Azela africana* extract increases RBC levels when treated the diabetic wistar rats. However, Hb, RBC and WBC levels were significantly declined when the concentration of plant extract was increased to 600 mg/kg bw. This observation agrees with the several scientists who reported a reduction in the blood parameters (RBCs, WBCs, and hemoglobin) in animals exposed to different plant extracts (Sule *et al.*, 2012; Ladokun *et al.*, 2015). Platelets play a major role in blood clotting and our present study does not show any significant alteration in platelets level, which suggests that the plant extract may have positive response in blood vessel and homeostasis.

The levels of three enzymes (ALT, AST, and ALP) in the blood serum are frequently employed as clinical biochemical indicators for liver disease (Yun *et al.*, 2018; Bencheikh *et al.*, 2019). Among these enzymes, AST level showed significant increase at higher dose (600 mg/kg bw) of *O. crinita*, indicating occurrence of cellular damage in liver. Similar kind of results was also recorded by Obakiro *et al.* (2021) where AST level was increased on administration of higher doses of *Entada abyssinica* to Wistar albino rats, and they suggested the hepatoprotective effect of the extract at lower doses. Elevation in AST activity is related to the number of affected hepatocytes and does not reflect the severity or reversibility of the lesion on a pathological basis (Wang *et al.*, 2019). In the present study, no significant changes were recorded in both ALT and ALP levels, which indicates that the plant extract has negligible effects on liver function at lower doses (150 mg/kg bw and 300 mg/kg bw). Bilirubin (total and direct) act as an essential indicator to assess liver excretory function and hemolytic anaemia (Saidu *et al.*, 2007). The present study showed that *O. crinita* increased total bilirubin levels of the mice administered with 600mg/kg body weight; however, direct bilirubin levels remained in normal range. The observation suggests that the extract may be responsible for haemolytic anaemia. This kind of result was also reported by Njinga *et al.* (2020), where extract of *Hibiscus sabdariffa* administration increased the total bilirubin levels in wistar rats. The end products of protein metabolism are creatinine and urea, and a rise in their blood levels suggests the extent of renal damage (Gowda *et al.*, 2010). As an outcome, a rise in these indicators implies that extracts administered at 600 mg/kg bw have an adverse effect on the renal tissue's integrity and function.

The phytochemical analysis of methanolic leaf extract of *O. crinita* demonstrated the presence of alkaloids, steroids, glycosides, flavonoids, saponins, tannins, and terpenoids. In a previous Study, Jain *et al.* (2016), reported

that secondary plant metabolites specifically, alkaloids, flavonoids and terpenoids have a major impact on peptic ulcer treatment. However, flavonoids are claimed to be the most important secondary metabolites that are employed as an antiulcer agent and protect the gastric mucosa through multiple mechanisms. These mechanisms includes: free radical scavenging, increase in mucosal prostaglandin content, improvement in gastric tissue microcirculation and cytoprotection (Mota *et al.*, 2009; Serafim *et al.*, 2020). Flavonoids maintains gastric cytoprotective effects through modulating prostaglandins (PG's) and nitric oxide synthase (NOS) pathways, which serves to maintain stomach mucosal integrity, mediates gastric blood flow, inhibits gastric acid secretion and accelerates mucosal healing (Zhang *et al.*, 2020).

Ethanol intake predominantly damages the glandular portion of the stomach since it penetrates rapidly in to the gastric mucosa and leads to gastric lesion such as extensive submucosal edema, hemorrhage, desquamation of epithelial cells and infiltration of inflammatory cells (Mousa *et al.*, 2019; Ciciliato *et al.*, 2022; Sadek, 2022). The repeated oral dose study for ethanol-induced ulcer model showed a significant reduction in ulcer index ($p < 0.05$) in 6, 10 and 14 days treatment with *O. crinita* at dose 200mg/kg. Besides this, the percentage of ulcer healing significantly increased in a time dependent manner from 6 days to 14 days treatment. However, ranitidine (30mg/kg bw) showed a strong healing effect in ethanol induced peptic ulcer. The obtained result indicates that the ulcer healing efficacy of the plant extract is somehow similar with the reference drug (Abebaw *et al.*, 2017). Further, the extract's antiulcer activity is mostly owing to its anti-secretory properties, in addition to cytoprotective effects or plant mucosal tissue regeneration due to the presence of active photochemical (Mekonnen *et al.*, 2020). Protein which supplies nutritional factor, increases the resistance of the stomach wall against the combined attack of pepsin and hydrochloric acid in ulcerated condition (Qin *et al.*, 2018). In the present study, repeated treatment of ulcerated mice with *O. crinita* (200 mg/kg bw) showed significant time dependent increase in the protein level in 6, 10 and 14 days. Previously, a significant increase in total protein content upon treatment with Schiff base derived dibromo compound was reported in rats with acute superficial hemorrhagic mucosal lesions (Saremi *et al.*, 2019). One of the essential criteria to determine the status of the mucosal resistance/barrier is the state of mucus secretion in the stomach. The increase in carbohydrate content in *O. crinita* treated and ranitidine treated groups over that of the negative ulcerated group appears to be due to stimulation of mucus secretion by the phytoproducts and drugs. Increased mucus secretion by gastric mucosa can inhibit gastric ulceration by preventing back-diffusion of H⁺ ions and by buffering of the acid gastric juice (Ribeiro *et al.*, 2016). Hereby, it is suggested that the antiulcer activity of *O. crinita* observed in the present study could be due to restoration of the mucosal barrier system as observed in the histopathological study. Similarly, Gopinathan and Nija, (2014), also found that the elevating total carbohydrate content significantly increased the antiulcer efficacy by preserving the mucosal barrier system.

Gastric mucosa plays an important role in defensive mechanism. It maintains the structural integrity of stomach and protects the gastric wall from the aggressive and

noxious agents by producing mucous-bicarbonate barrier (Sidahmed *et al.*, 2019). Saleh *et al.* (2016) reported that Gastric motility changes are crucial in the development and prevention of experimental gastric lesions. Results of microscopic analysis revealed that the plant extract at the dose of 200 mg/kg bw showed significant reduction in necrotic lesions than the negative control group and healing ability is comparable to that of the positive control group. This suggests that the extract shows healing action by reducing the stomach motility. These findings are found to be consistent with earlier work carried out by Halabi *et al.* (2014), where new schiff based derived complex showed flatter of mucosal folds by decreasing the gastric motility in ethanol induced gastric ulcer. Histological study further confirmed that treatment with *O. crinita* (200 mg/kg) restore the damage gastric mucosa with a clear reduction of sub mucosal edema, leukocyte infiltration, and with the epithelium lining being protected almost to the appearance of the normal control group. This suggests that extract might stimulate the mucus secretion which enables to heal the damage mucus layer. Similar observation has been reported by Takayama *et al.* (2011) and Halabi *et al.* (2014). In the current study, scanning electron microscopy of gastric mucosa of ethanol induced ulcerated group exhibited damaged epithelial cells, erosions with widened gastric pits. On the contrary, Scanning electron micrographs of *O. crinita* (200 mg/kg bw) 14 day treated groups showed an intact epithelium with negligible erosion; thus, the present finding has also been supported by histological and surface topographical studies to establish the ulcer healing potential of the plant *O. crinita*.

5. Conclusions

The findings from this study showed that methanolic crude extract of *O. crinita* exerts antiulcer activity via gastric mucin secretion, which could be possibly attributed to phytochemicals present in the plant extract. Further research is required to isolate the active elements involved for the anti-ulcer efficacy and to determine the specific mechanism of action in gastric ulcer healing.

Acknowledgement

The authors would like to thank the University Grant of Commission (UGC, New Delhi) for providing financial support (NEHU NON- NET Fellowship to SR). Department of Zoology and Sophisticated Analytical Instruments Facility (SAIF), North-Eastern Hill University, Shillong is also acknowledged for providing infrastructural facilities.

Author contribution

BR designed the work, corrected and finalized the manuscript. SR carried out the experiment, wrote the manuscript and prepared the final draft. All authors read and approved the final manuscript.

Funding:

This study did not receive any external funding.

References

- Abebaw M, Mishra B and Gelayee DA. 2017. Evaluation of anti-ulcer activity of the leaf extract of *Osyris quadripartita* Decne. (Santalaceae) in rats. *J Exp Pharmacol.*, **9**:1-11.
- Akhtar MS, Akhtar AH and Khan MA.1992. Antiulcerogenic Effects of *Ocimum basilicum* Extracts, Volatile Oils and Flavonoid Glycosides in Albino Rats. *Int. j. Pharmacogn.*, **30**(2):97-104.
- Albalasmeh AA, Berhe AA and Ghezzehei TA. 2013. A new method for rapid determination of carbohydrate and total carbon concentrations using UV spectrophotometry. *Carbohydr Polym.*, **97**(2):253-261.
- Bencheikh N, Bouhrim M, Kharchoufa L, Choukri M, Bnouham M and Elachouri M. 2019. Protective Effect of *Zizyphus lotus* L. (Desf.) Fruit against CCl4-Induced acute liver injury in rat. *Evid Based Complement Alternat Med.*, 6161593.
- Bradford MM. 1976. A rapid and sensitive method for the quantitation of microgram quantities of protein utilizing the principle of protein-dye binding. *Anal Biochem.*, **72**:248-54.
- Ciciliato MP, de Souza MC, Tarran CM, de Castilho ALT, Vieira AJ and Rozza AL. 2022. Anti-Inflammatory Effect of Vanillin Protects the Stomach against Ulcer Formation. *Pharmaceutics.*, **14**(4):755.
- Dashputre NL and Naikwade NS. 2011. Evaluation of anti-ulcer activity of methanolic extract of *Abutilon indicum* Linn leaves in experimental rats. *Int J Pharm Sci Drug Res.*, **3**(2):97-100.
- Davie JV and Lewis SM. 1975. **Practical Haematology**, 5th edition. Edinburgh, Churchill.
- Dey S, Basubaul TS, Roy B and Dey D. 1989. A new rapid method of air drying for scanning electron microscopy using tetramethylsilane. *J Microsc.*, **156**(2): 259-261.
- Freedberg DE, Kim LS and Yang YX. 2017. The Risks and Benefits of Long-term Use of Proton Pump Inhibitors: Expert review and best practice advice from the American Gastroenterological Association. *Gastroenterology.*, **152**(4):706-715.
- Geetha M and Vijayalakshmi A. 2013. Acute and sub-acute toxicity studies of the ethanolic extract of the anti-psoriatic plant *Givotia rottleriformis* Griff. Ex Wight. bark. *Journal of Pharma Research.*, **2**:6-9.
- Gopinathan S, and Nija S. 2014. Gastric ulcer curative potential of *Mollugo oppositifolia* Linn. extract—A preclinical study. *World J Pharm Res.*, **3**(7): 929-948.
- Gowda S, Desai PB, Kulkarni SS, Hull VV, Math AA and Vernekar SN. 2010. Markers of renal function tests. *N Am J Med Sci.*, **2**(4):170-173.
- Halabi MF, Shakir RM, Bardi DA, Al-Wajeeh NS, Ablat A, Hassandarvish P, Hajrezaie M, Norazit A and Abdulla MA. 2014. Gastroprotective activity of ethyl-4-[(3,5-di-tert-butyl-2-hydroxybenzylidene) amino]benzoate against ethanol-induced gastric mucosal ulcer in rats. *PLoS One.*, **9**(5):e95908.
- Jain P. 2016. Secondary metabolites for antiulcer activity. *Nat Prod Res.*, **30**(6):640-656.
- Kalita P, Medhi S, Borah S, Bhargav GK, and Alam F. 2022. Evaluation of Anti Inflammatory and Anti Oxidant Activities of *Osbeckia crinita*. *J Pharm Res Int.*, **34**(8B): 38–46.
- Koparde AA, Dojjad RC, and Magdum CS. 2019. Natural products in drug discovery. **Pharmacognosy-medicinal plants**. IntechOpen publisher, PP. 14
- Kuna L, Jakab J, Smolic R, Raguz-Lucic N, Vcev A and Smolic M. 2019. Peptic Ulcer Disease: A Brief Review of Conventional Therapy and Herbal Treatment Options. *J Clin Med.*, **8**(2):179.

- Ladokun O, Ojezele M and Arojojoye O. 2015. Comparative study on the effects of aqueous extracts of *Viscum album* (mistletoe) from three host plants on hematological parameters in albino rats. *Afr Health Sci.*, **15**(2):606-612.
- Mahmoud MF, Abdo W, Nabil M, Drissi B, El-Shazly AM, Abdelfattah MAO and Sobeh M. 2023. Apple (*Malus domestica* Borkh) leaves attenuate indomethacin-induced gastric ulcer in rats. *Biomed Pharmacother.*, 160:114331.
- Mekonnen AN, Asrade Atnafie S, and Wahab Atta MA. 2020. Evaluation of antiulcer activity of 80% methanol extract and solvent fractions of the root of *Croton macrostachyus* Hochst: Ex Del. (Euphorbiaceae) in rodents. *Evid -based Complement Altern Med.*, 2020.
- Mota KS, Dias GE, Pinto ME, Luiz-Ferreira A, Souza-Brito AR, Hiruma-Lima CA, Barbosa-Filho JM and Batista LM. 2009. Flavonoids with gastroprotective activity. *Molecules.*, **14**(3):979-1012.
- Mousa AM, El-Sammad NM, Hassan SK, Madboli AENA, Hashim AN, Moustafa ES, Bakry SM and Elsayed EA. 2019. Antiulcerogenic effect of *Cuphea ignea* extract against ethanol-induced gastric ulcer in rats. *BMC Complement Altern Med.*, **19**(1):345.
- Njinga NS, Kola-Mustapha AT, Quadri AL, Atolani O, Ayanniyi RO, Buhari MO, Amusa TO, Ajani EO, Folaranmi OO, Bakare-Odunola MT, Kambizi L, Oladiji AT and Ebong P. 2020. Toxicity assessment of sub-acute and sub-chronic oral administration and diuretic potential of aqueous extract of *Hibiscus sabdariffa* calyces. *Heliyon.*, **6**(9):e04853.
- Oates PT and Hakkinen JP. 1988. Studies on the mechanism of ethanol-induced gastric damage in rats. *Gastroenterology.*, **94**(1): 10-21.
- Obakiro SB, Kiprof A, Kigundu E, K'owino I, Kiyimba K, Drago Kato C and Gavamukulya Y. 2021. Sub-Acute Toxicity Effects of Methanolic Stem Bark Extract of *Entada abyssinica* on Biochemical, Haematological and Histopathological Parameters in Wistar Albino Rats. *Front Pharmacol.*, **12**:740305.
- Obiamine AW and Uche FI. 2008. The phytochemical screening and effects of methanolic extract of *Phyllanthus amarus* leaf on the biochemical parameters of male Guinea pigs. *J Appl SCI Environ Manag.*, **12**(4): 73-77.
- OECD. 2002. Test No. 423: Acute oral toxicity – acute toxic class method, OECD guidelines for the testing of chemicals, Section 4. OECD Publishing, Paris.
- Organization for Economic Cooperation and Development (OECD). 2008. Guideline 407. Repeated-dose 28-day Oral Toxicity Study in Rodents. Adopted by the Council on 3rd October, 2008, Paris. 1-13.
- Oyedemi SO, Adewusi EA, Aiyegoro OA and Akinpelu DA. 2011. Antidiabetic and haematological effect of aqueous extract of stem bark of *Azelia africana* (Smith) on streptozotocin-induced diabetic Wistar rats. *Asian Pac J Trop Biomed.*, **1**(5):353-358.
- Qin Z, Wang Y, Zhao W, Zhang Y, Tian Y, Sun S, and Li X. 2018. Pressure ulcer healing promoted by adequate protein intake in rats. *Exp Ther Med.*, **15**(5): 4173-4178.
- Rao RR. 1981. Ethnobotany of Meghalaya: medicinal plants used by Khasi and Garo tribes. *Economic Botany.*, **35**(1):4-9.
- Ribeiro ARS, do Nascimento Valença JD, da Silva Santos J, Boeing T, da Silva LM, de Andrade SF, Albuquerque-Júnior RL and Thomazzi SM. 2016. The effects of baicalein on gastric mucosal ulcerations in mice: Protective pathways and anti-secretory mechanisms. *Chem Biol Interact.*, **260**:33-41.
- Roy B and Tandon V. 1991. Usefulness of Tetramethylsilane in the preparation of helminth parasites for scanning electron microscopy. *Revista di Parasitologia.*, **8**(3): 405-413.
- Sadek SA. 2022. *Sepia officinalis* ink mitigates gastric ulcer via modulation of antioxidant/anti-inflammatory pathways. *Beni-Suef Univ J Basic Appl Sci.*, **11**(1):1-12.
- Saleh MM, Qader SW and Thaker AA. 2016. Gastroprotective activity of *Eruca sativa* leaf extract on ethanol-induced gastric mucosal injury in *Rattus norvegicus*. *Jordan J Biol Sci.*, **147**(3384): 1-6.
- Saidu Y, Bilbis LS, Lawal M, Isezuo SA, Hassan SW and Abbas AY. 2007. Acute and sub-chronic toxicity studies of crude aqueous extract of *Albizzia chevalieri* harms (leguminosae). *Asian J Biochem.*, **2**(4):224-236.
- Saremi K, Rad SK, Tayeb F, Abdulla MA, Karimian H and Majid NA. 2019. Gastroprotective activity of a novel Schiff base derived dibromo substituted compound against ethanol-induced acute gastric lesions in rats. *BMC Pharmacol Toxicol.*, **20**(1):1-13.
- Serafim C, Araruna ME, Júnior EA, Diniz M, Hiruma-Lima C, and Batista L. 2020. A review of the role of flavonoids in peptic ulcer (2010–2020). *Molecules.*, **25**(22):5431.
- Sharifi-Rad M, Fokou PVT, Sharopov F, Martorell M, Ademiluyi AO, Rajkovic J, Salehi B, Martins N, Iriti M and Sharifi-Rad J. 2018. Antiulcer agents: From plant extracts to phytochemicals in healing promotion. *Molecules.*, **23**(7):1751.
- Sidahmed HMA, Vadivelu J, Loke MF, Arbab IA, Abdul B, Sukari MA, and Abdelwahab SI. 2019. Anti-ulcerogenic activity of dentatin from *Clausena excavata* Burm. f. against ethanol-induced gastric ulcer in rats: Possible role of mucus and anti-oxidant effect. *Phytomedicine.*, **55**:31-39.
- Song SH, Kim JE, Sung JE, Lee HA, Yun WB, Lee YH, Song H and Hwang D. 2018. Anti-ulcer effect of Gallarhois extract with anti-oxidant activity in an ICR model of ethanol/hydrochloride acid-induced gastric injury. *J Tradit Complement Med.*, **9**(4):372-382.
- Sule OJ, Elekwa I and Ayalogu EO. 2012. Effect of *Acalypha Wilkesiana* Muell Arg. On Haematological Parameters in Wistar Albino Rats. *Int j biol med res.*, **3**(1):1234-1237.
- Takayama C, de-Faria FM, de Almeida AC, Valim-Araújo Dde A, Rehen CS, Dunder RJ, Socca EA, Manzo LP, Rozza AL, Salvador MJ, Pellizzon CH, Hiruma-Lima CA, Luiz-Ferreira A and Souza-Brito AR. 2011. Gastroprotective and ulcer healing effects of essential oil from *Hyptis spicigera* Lam. (Lamiaceae). *J Ethnopharmacol.*, **135**(1):147-155.
- Tijani AS, Farombi EO, and Olaleye SB. 2021. Mechanisms underlying the healing potentials of the methanol extract of *Chasmanthera dependens* stem on indomethacin-induced gastric ulcer. *Egypt j basic appl sci.*, **8**(1):17-31.
- Tripathi A, Singh S, and Mukerjee A. 2021. Antiulcer activity of ethanolic leaf extract of *Capparis zeylanica* against chemically induced ulcers. *Futur J Pharm Sci.*, **7**: 211
- Wang W, Dong Z, Zhang J, Zhou X, Wei X, Cheng F, Li B and Zhang J. 2019. Acute and Subacute Toxicity Assessment of Oxyclozanide in Wistar Rats. *Front Vet Sci.*, **6**:294.
- Yandrapu H and Sarosiek J. 2015. Protective Factors of the Gastric and Duodenal Mucosa: An Overview. *Curr Gastroenterol Rep.*, **17**:24
- Yu L, Li R, Liu W, Zhou Y, Li Y, Qin Y, Chen Y, Xu Y. 2020. Protective Effects of Wheat Peptides against Ethanol-Induced Gastric Mucosal Lesions in Rats: Vasodilation and Anti-Inflammation. *Nutrients.*, **12**(8):2355.
- Yun JW, Kwon E, Kim YS, Kim SH, You JR, Kim HC, Park JS, Che JH, Lee SK, Jang JJ, Kim HH and Kang BC. 2018. Assessment of acute, 14-day, and 13-week repeated oral dose toxicity of Tiglium seed extract in rats. *BMC Complement Altern Med.*, **18**(1):251.

Zhang W, Lian Y, Li Q, Sun L, Chen R, Lai X, Lai Z, Yuan E and Sun S. 2020. Preventative and Therapeutic Potential of Flavonoids in Peptic Ulcers. *Molecules*, **25(20)**:4626.

Ethical statement

The experimental study was carried out by in compliance with the ethical guidelines issued by the

committee for the purpose of control and supervision on experiments on animals (CPCSEA), Government of India. The experimental protocol was approved (IEC/MS/Misc./05) by the Institutional Ethics Committee (Animal models), North Eastern Hill University, Shillong, Meghalaya, India on 28th

Comprehensive Characterization and Expression Profiling of the GATA Transcription Factor in Sugar Beet (*Beta vulgaris* L.) Suggests Their Potential Roles in Taproot Development and Biotic Stress Response

Le Thi Man¹, Phi Bang Cao¹, Thi Thanh Huyen Tran², Nguyen Quoc Trung³, Dong Huy Gioi³, Ninh Thi Thao³, Quynh Thi Ngoc Le⁴, Hong Viet La⁵, Thi Xuan Quyen Vu¹, Ha Duc Chu^{6,*}

¹Faculty of Natural Sciences, Hung Vuong University, Phu Tho Province 35000, Vietnam; ²Faculty of Biology, Hanoi National University of Education, Xuan Thuy Road, Cau Giay District, Hanoi City 122300, Vietnam; ³Faculty of Biotechnology, Vietnam National University of Agriculture, Gia Lam District, Hanoi City 122300, Vietnam; ⁴Department of Biotechnology, Thuyloi University, Tay Son Street, Dong Da District, Hanoi City 122300, Vietnam; ⁵Institute of Research and Application, Hanoi Pedagogical University 2, Phuc Yen City, Vinh Phuc Province 280000, Vietnam; ⁶Faculty of Agricultural Technology, University of Engineering and Technology, Vietnam National University Hanoi, Xuan Thuy Road, Cau Giay District, Hanoi City 122300, Vietnam;

Received: November 29, 2022; Revised: March 31, 2023; Accepted: April 3, 2023

Abstract

GATA transcription factors (TFs) are well-characterized as major regulators whose DNA-binding domain is a type IV zinc finger motif. In this present study, we identified and characterized the GATA TFs in sugar beet (*Beta vulgaris*). A total of 16 BvGATA TFs from sugar beet has been reported. Based on the web-based tools, our analysis indicated that the BvGATA TFs exhibited a high variation in their physico-chemical features and gene structure. Four segmental duplication events that occurred in the BvGATA gene family have been predicted. The phylogeny analysis demonstrated that the BvGATA TFs could be classified into four clades. Interestingly, the transcriptional changes of the BvGATA genes were analyzed according to three available transcriptome databases. We found that a majority of the BvGATA genes showed significant transcriptional changes in major tissues under adverse environmental conditions. To sum up, our findings could provide a cornerstone to deeply understand the GATA TFs in sugar beet.

Keywords: Characterization, expression profiles, GATA, identification, sugar beet, transcription factor.

1. Introduction

Sugar beet (*Beta vulgaris* L.) has been regarded as the major sugar-yielding crop that is cultivated commercially in the world. Providing 30 - 35% of annual sugar production in the world (Monteiro *et al.*, 2018), sugar beet was reported to be the second-largest source of sugar (Zhang *et al.*, 2016). This crop could be used as human food and cattle feed (Evans and Messerschmidt, 2017; Monteiro *et al.*, 2018; Zhang *et al.*, 2016) and raw materials for bioethanol production (Mall *et al.*, 2021; Pavlečić *et al.*, 2017). Interestingly, containing various natural pigments (Chhikara *et al.*, 2019), sugar beet is believed to offer beneficial physiological effects as a functional food (Chen *et al.*, 2021; Mirmiran *et al.*, 2020). It, accordingly, would be more significant to investigate the growth and development processes in this important sugar-producing crop on a molecular basis.

In higher plant species, transcription factors (TFs) could play crucial roles in various biological pathways, particularly related to unfavorable condition stimulate

(Baillio *et al.*, 2019; Fujita *et al.*, 2011). Among them, GATA, a group of highly conserved type IV zinc finger motifs is well-characterized as one of the general eukaryotic-specific TFs (Schwechheimer *et al.*, 2022). Structurally, GATA TFs include a single domain that specifically binds to a conserved DNA motif, like -WGATAR- in the promoter regions (Behringer and Schwechheimer, 2015; Schwechheimer *et al.*, 2022; Teakle *et al.*, 2002). To date, the GATA TFs have been identified in a variety of higher plant species, including dicotyledonous plants, like *Arabidopsis thaliana* (Teakle *et al.*, 2002), soybean (*Glycine max*) (Zhang *et al.*, 2015), apple (*Malus domestica*) (Chen *et al.*, 2017), grape (*Vitis vinifera*) (Zhang *et al.*, 2018), cotton (*Gossypium* spp.) (Zhang *et al.*, 2019), chickpea (*Cicer arietinum*) (Niu *et al.*, 2020), pepper (*Capsicum annuum*) (Yu *et al.*, 2021), cucumber (*Cucumis sativus*) (Zhang *et al.*, 2021), potato (*Solanum tuberosum*) (Yu *et al.*, 2021) and Rosaceae species (Manzoor *et al.*, 2021), and monocotyledonous plants, like rice (*Oryza sativa*) (Reyes *et al.*, 2004), purple false brome (*Brachypodium distachyon*) (Peng *et al.*, 2021), *Populus* spp. (Kim *et al.*, 2021) and wheat

* Corresponding author. e-mail: cd.ha@vnu.edu.vn.

(*Triticum aestivum*) (Feng *et al.*, 2022). Unfortunately, the GATA TFs in sugar beet remain poorly understood, even though the genome of this important crop has been published recently (Dohm *et al.*, 2014).

In this current study, we performed a systematic analysis of the GATA TFs in sugar beet by using computational approaches. We first screened and identified all putative members of the GATA TFs in sugar beet. The general characteristics of the GATA TFs in sugar beet have been analyzed. Additionally, the gene duplication events and gene structures have been predicted in the GATA TFs in sugar beet. Finally, we carried out a re-analysis of the expression profiles of the *GATA* genes under numerous conditions in sugar beet.

2. Materials and Methods

2.1. 2.1. Database searches for the GATA TFs in sugar beet

The GATA TFs in sugar beet were searched by using various well-known databases. Briefly, the PlantTFDB v4.0 (Jin *et al.*, 2017) was firstly used to screen all putative GATA amino acid (aa) sequences in the sugar beet proteome (Dohm *et al.*, 2014) as previously reported (Chu *et al.*, 2018; La *et al.*, 2022; Niu *et al.*, 2020). The Pfam database (Mistry *et al.*, 2021) was then employed to confirm the existence of the GATA TF conserved domains as previously described (Schwechheimer *et al.*, 2022). The GATA TFs were annotated by BlastP-ing against the sugar beet assemblies (Dohm *et al.*, 2014) available from the NCBI and Phytozome v12.0 (Goodstein *et al.*, 2012) as previously guided (La *et al.*, 2022).

2.2. 2.2. Estimation of protein features of the GATA TFs in sugar beet

The aa sequences of the GATA TFs were used to analyze the general features of proteins as previously reported (Chu *et al.*, 2018; La *et al.*, 2022; Niu *et al.*, 2020). Particularly, five properties, including protein size (aa residues), protein mass (kilo Dalton, kDa), isoelectric point (pI), aliphatic index (AI) and grand average of hydropathicity (GRAVY) were calculated by the ExPaSy tool (Gasteiger *et al.*, 2003; Gasteiger *et al.*, 2005).

2.3. 2.3. Prediction of the subcellular localization of the GATA TFs in sugar beet

The full-length aa sequences of the GATA TFs in sugar beet were used as seed sequences to query in the YLOC tool (Briesemeister *et al.*, 2010) as previously described (La *et al.*, 2022; Niu *et al.*, 2020). Organelle-specific signal peptides were screened in the full-length aa sequences of each protein. Ten major organelles were investigated for the plant model as previously reported (Briesemeister *et al.*, 2010).

2.4. 2.4. Generation of phylogenetic tree of the GATA TFs in sugar beet

To generate the phylogenetic tree of the GATA TFs in sugar beet, full-length aa sequences were analyzed in various tools as previously described (La *et al.*, 2022). Firstly, ClustalX 2.0 software (Larkin *et al.*, 2007) was used to align the full-length aa sequences. An unrooted phylogenetic tree of the GATA TFs in sugar beet was then generated by using the Maximum likelihood (ML)

estimation with 1000 times bootstrap and other default parameters in the MEGA tool (Kumar *et al.*, 2016). We also collected 29 well-established members of the GATA TFs in *A. thaliana* from the previous study (Teakle *et al.*, 2002) for other ML- phylogenetic tree by the MEGA tool. All phylogenetic trees were then visualized by using the Adobe Illustrator software.

2.5. 2.5. Investigation of gene features of the GATA TFs in sugar beet

The structural information on the GATA TFs in sugar beet was analyzed as previously described (La *et al.*, 2022; Niu *et al.*, 2020). Briefly, the full-length nucleotide sequences of each gene encoding the GATA TFs obtained in the previous *in silico* analyses were used to apply in the Gene Structure Display Server (GSDS) website (Hu *et al.*, 2015). The order of exon/intron structures of genes encoding the GATA TFs was then constructed based on the ML phylogenetic tree (Kumar *et al.*, 2016). To carry out enrichment analysis on gene sets, the aa sequences of the GATA TFs were analyzed by using the Blast2GO software (Conesa *et al.*, 2005)

2.6. 2.6. Prediction of gene duplication of the GATA TFs in sugar beet

To analyze the gene duplication in the *GATA* gene family in sugar beet, the full-length nucleotide sequences were used as templates for *in silico* prediction by following the previous studies (La *et al.*, 2022; Niu *et al.*, 2020) with minor adjustment. Particularly, the identity matrix of all aligned nucleotide sequences of *GATA* genes was constructed by the BioEDIT software (Hall, 1999). All duplication events were then applied in the DNASp tool (Roza *et al.*, 2017) to calculate the ratio between non-synonymous substitutions per non-synonymous site (Ka) and synonymous substitutions per synonymous site (Ks) as previously described (La *et al.*, 2022; Niu *et al.*, 2020).

2.7. 2.7. Analysis of the expression profiles of the GATA TFs in sugar beet

To investigate the transcriptional changes of the *GATA* TFs, we performed a re-analysis of four transcriptome datasets available from the NCBI Gene expression omnibus (NCBI GEO) (Barrett *et al.*, 2013). Particularly, GSE107627 provided a dataset related short-term and long-term treatment of alkaline solution in leaves (Zou *et al.*, 2020). We also analyzed GSE114968 dataset, which provided expression data of salt- treated (1 day and 7 days) roots at seedling stages (Liu *et al.*, 2020). Finally, we re-analyzed the third microarray dataset (GSE135555) related to the beet cyst nematode inoculation in roots (Ghaemi *et al.*, 2020). Responsive gene was defined by a fold-change cut-off (fold-change ≥ 1.5 -fold or ≤ -1.5 -fold).

3. Results and Discussion

3.1. Identification and annotation of the GATA TFs in sugar beet

To find all members of the GATA TFs in sugar beet, we explored the PlantTFDB (Jin *et al.*, 2017) and the newest sugar beet assembly (Dohm *et al.*, 2014) from NCBI and Phytozome (Goodstein *et al.*, 2012). After validating by the Pfam (Mistry *et al.*, 2021), we explored a total of 16 conserved GATA aa sequences in the sugar beet

proteome (Table 1). The annotations, like ProteinID and locusID, were accordingly retrieved from the NCBI and Phytozome databases (Goodstein *et al.*, 2012), respectively and showed in Table 1. Finally, according to the physical

location on genome, we assigned whole 16 identified GATA aa sequences from BvGATA01 to BvGATA16 (Table 1).

Table 1. Summary of the BvGATA TFs in sugar beet

#	Gene	Phytozome locus	NCBI Protein ID	Gene size	Protein size	MW (kDa)	pI	AI	GRAVY	SCL
1	BvGATA01	EL10Ac1g00497	XP_010671518.1	5793	297	32.88	5.94	62.29	-0.74	Nucleus
2	BvGATA02	EL10Ac1g00493	XP_010671467.1	6631	346	37.72	5.74	69.05	-0.67	Nucleus
3	BvGATA03	EL10Ac2g03883	XP_010667257.2	3488	318	35.72	8.94	60.19	-0.85	Cytoplasm
4	BvGATA04	EL10Ac2g04003	XP_010668515.1	1794	375	41.53	6.52	60.85	-0.67	Cytoplasm
5	BvGATA05	EL10Ac3g04929	XP_010670911.1	667	155	16.7	10.02	64.84	-0.82	Cytoplasm
6	BvGATA06	EL10Ac4g09843	XP_010674149.1	580	146	16.76	9.26	48.08	-0.94	Nucleus
7	BvGATA07	EL10Ac5g12284	XP_010677131.2	6317	548	61.06	5.72	65.84	-0.66	Nucleus
8	BvGATA08	EL10Ac7g16992	XP_010683872.2	2977	308	33.88	8.41	65.58	-0.54	Cytoplasm
9	BvGATA09	EL10Ac6g14415	XP_010681549.2	3862	491	55.57	8.89	57.56	-0.93	Cytoplasm
10	BvGATA10	EL10Ac7g17612	XP_010684625.1	673	138	14.99	9.56	70.00	-0.6	Cytoplasm
11	BvGATA11	EL10Ac7g18179	XP_010696086.2	10707	299	32.89	5.94	55.75	-0.82	Nucleus
12	BvGATA12	EL10Ac9g21650	XP_010690771.1	2553	320	35.22	8.36	58.78	-0.54	Cytoplasm
13	BvGATA13	EL10Ac9g22059	XP_010691384.1	10336	353	38.85	4.97	66.86	-0.60	Nucleus
14	BvGATA14	EL10Ac9g22099	XP_010691426.1	1228	309	33.85	6.43	47.96	-0.75	Cytoplasm
15	BvGATA15	EL10As8g23860	XP_010679831.2	957	281	31.63	8.73	46.16	-0.93	Cytoplasm
16	BvGATA16	EL10Ac6g15556	XP_010679730.1	1203	259	28.39	7.61	35.48	-0.92	Cytoplasm

Note: -: No information, AI: Aliphatic index, pI: Iso-electric point, GRAVY: Grand average of hydropathicity, SCL: Sub-cellular localization

Recently, great efforts have been recorded in order to identify and intensively analyze the GATA TFs in numerous plant species. The numbers of the GATA TFs in dicotyledonous plants were varied from 19 (in grape) (Zhang *et al.*, 2018) to 64 members (in soybean) (Zhang *et al.*, 2015). Another case in cotton species, a total of 46, 46 and 87 members of the GATA TFs has been reported in *G. arboreum*, *G. raimondii* and *G. hirsutum* (Zhang *et al.*, 2019). In four Rosaceae species, 92 members of the GATA TFs were found, with 32 members from *Pyrus bretschneideri*, 18 members from *Prunus avium*, 20 members from *Prunus mume* and 22 members from *Prunus persica* (Manzoor *et al.*, 2021). In monocotyledonous plants, the amounts of the GATA TFs were also variable. For example, the GATA TFs in rice have been reported to contain 28 members (Reyes *et al.*, 2004), as similar as the members in purple false brome (Peng *et al.*, 2021). Additionally, 79 members of the GATA TFs have been investigated in wheat (Feng *et al.*, 2022). To sum up, 16 members of the BvGATA TFs found throughout the whole genome of sugar beet is close to which is close to the 18, 19 and 20 GATA TFs identified in grape (Zhang *et al.*, 2018), *P. avium* and *P. mume* (Manzoor *et al.*, 2021), respectively, but greatly less than the GATA TFs identified in other dicots, like *P. persica* (22 members) (Manzoor *et al.*, 2021), chickpea (25 members) (Niu *et al.*, 2020), *A. thaliana* (29 members) (Teakle *et al.*, 2002), *P. bretschneideri* (32 members) (Manzoor *et al.*, 2021), apple (35 members) (Chen *et al.*, 2017), seven *Populus* spp. (33 to 40 members) (Kim *et al.*, 2021), *G. arboreum* (46 members) (Zhang *et al.*, 2019), *G. raimondii* (46 members) (Z. Zhang *et al.*, 2019), potato (49 members) (Yu *et al.*, 2021), soybean (64 members) (C. Zhang *et al.*, 2015) and *G. hirsutum* (87 members) (Zhang

et al., 2019). Our comparisons revealed that the number of GATA TF members varies greatly between higher plant species.

3.2. Analysis of the physical and chemical features of the GATA TFs in sugar beet

In this study, the ExPaSy ProtParam tool (Gasteiger *et al.*, 2003; Gasteiger *et al.*, 2005) was applied to analyze full-length aa sequences of 16 BvGATA members in sugar beet. As a result, the physical and chemical properties of the BvGATA TFs in sugar beet were provided in Table 1. Particularly, the amounts of aa residues encoded by 16 BvGATA TFs ranged from 138 (BvGATA10) to 548 aa residues (BvGATA07), with an average of nearly 309 aa (Table 1). Next, the weights of BvGATA TFs were distributed between 14.99 (BvGATA10) and 61.06 kDa (BvGATA07), with an average of approximately 34.23 kDa (Table 1). The theoretical pI scores of the BvGATA TFs were recorded to be acidic, ranging from 4.97 (BvGATA13) to 6.52 (BvGATA04) and base, ranging from 7.61 (BvGATA16) to 10.02 (BvGATA05), with an average of approximately 7.56 (Table 1). Additionally, the AI values of the BvGATA TFs were varied from 35.48 (BvGATA16) to 70.00 (BvGATA10), with an average of nearly 58.45 (Table 1). Finally, the GRAVY scores of all members of the BvGATA TFs in sugar beet were < 0, with average of approximately -0.75 (Table 1), suggesting that BvGATA TFs belonged to hydrophilic proteins.

Previously, the general characteristics of the GATA TFs were also comprehensively analyzed and reported in other higher plant species. The sizes of the GATA TFs in legumes, like soybean and chickpea ranged from 80 to 551 aa residues (9.1 to 60.8 kDa) (Zhang *et al.*, 2015) and from 133 to 541 aa residues (14.9 to 60.2 kDa) (Niu *et al.*, 2020), respectively, while the protein lengths of the GATA

TFs in grape were varied from 109 to 386 aa residues (Zhang *et al.*, 2018). The aa residues of the GATA TFs in potato were 118 and the largest was 380 (13.15 to 60.63 kDa) (R. Yu *et al.*, 2021), while the numbers of aa residues of the GATA TFs in apple were varied from 90 to 1161 (9.9 to 129.74 kDa) (Chen *et al.*, 2017). In cotton species, the predicted GATA sequences consisted of 119 to 584 aa residues, with an average of 306 aa residues (Zhang *et al.*, 2019). Next, the pI values of the GATA TFs in higher plant species were confirmed to range from acidic to base. For example, the pI scores of the GATA TFs in soybean and chickpea have been reported to range from 4.63 to 9.66 (Zhang *et al.*, 2015) and 4.27 to 10.27 (Niu *et al.*, 2020), respectively. Interestingly, all members of the GATA TFs in apple and chickpea were reportedly < 0 (Chen *et al.*, 2017; Niu *et al.*, 2020), suggested that the GATA TFs in these plants, or perhaps in other plant species were hydrophilic (Schwechheimer *et al.*, 2022). To sum up, our results indicated that the BvGATA TFs in sugar beet, perhaps in many plant species showed high variation in their physical and chemical properties.

3.3. Subcellular localization and gene ontology analysis of the GATA TFs in sugar beet

The determination of the subcellular localization of proteins may suggest their potential function in the cellular metabolism (Goodin, 2018). Here, we predicted the subcellular localization of the BvGATA TFs in sugar beet by using the YLOC tool (Briesemeister *et al.*, 2010). As a result, a large amount of the BvGATA TFs (10 out of 16) was localized in the cytoplasm, while the remaining members of the BvGATA TFs (six out of 16) were predicted to distribute on the nucleus (Table 1).

Furthermore, the potential functions of the BvGATA TFs were annotated by using the gene ontology (GO) annotation analysis in sugar beet. As a result, 16 members of the BvGATA TFs in sugar beet were classified into three ontologies, like molecular function, biological process and subcellular localization. These BvGATA TFs were assigned with 15 GO terms belonging to the molecular function (Figure 1). Under the molecular function category, all BvGATA proteins were confirmed to act as TFs (Figure 1). Under the biological process category, all BvGATAs were involved in regulation of biological processes and 15 out of 16 members of the BvGATA TFs were predicted to play a role in response to stimulus (GO:0050896), regulation of nitrogen compound metabolic process (GO:0051171), regulation of metabolic process (GO:0019222) and regulation of cellular metabolic process (GO:0031323) (Figure 1). The GO analysis also indicated that all BvGATA TFs were localized in the nucleus, which is also confirmed by the YLoc prediction (Briesemeister *et al.*, 2010).

These findings were also confirmed in the previous reports. Particularly, a member of the GATA TFs in purple false brome, namely in BvGATA13, was investigated to localize in the nucleus by green fluorescent protein tagging method (Peng *et al.*, 2021). Previously, the green fluorescent protein::GmGATA58 (a member of the GATA TFs in soybean) fusion protein driven by the CaMV 35S promoter exhibited a strong green fluorescent signal in the nucleus (Zhang *et al.*, 2020). It suggested that the GmGATA58 protein was indeed localized in nucleus (Zhang *et al.*, 2020). Moreover, the Gene Ontology annotation analysis predicted that a majority of the GATA TFs in four Rosaceae species anticipated their function into nuclear (Manzoor *et al.*, 2021).

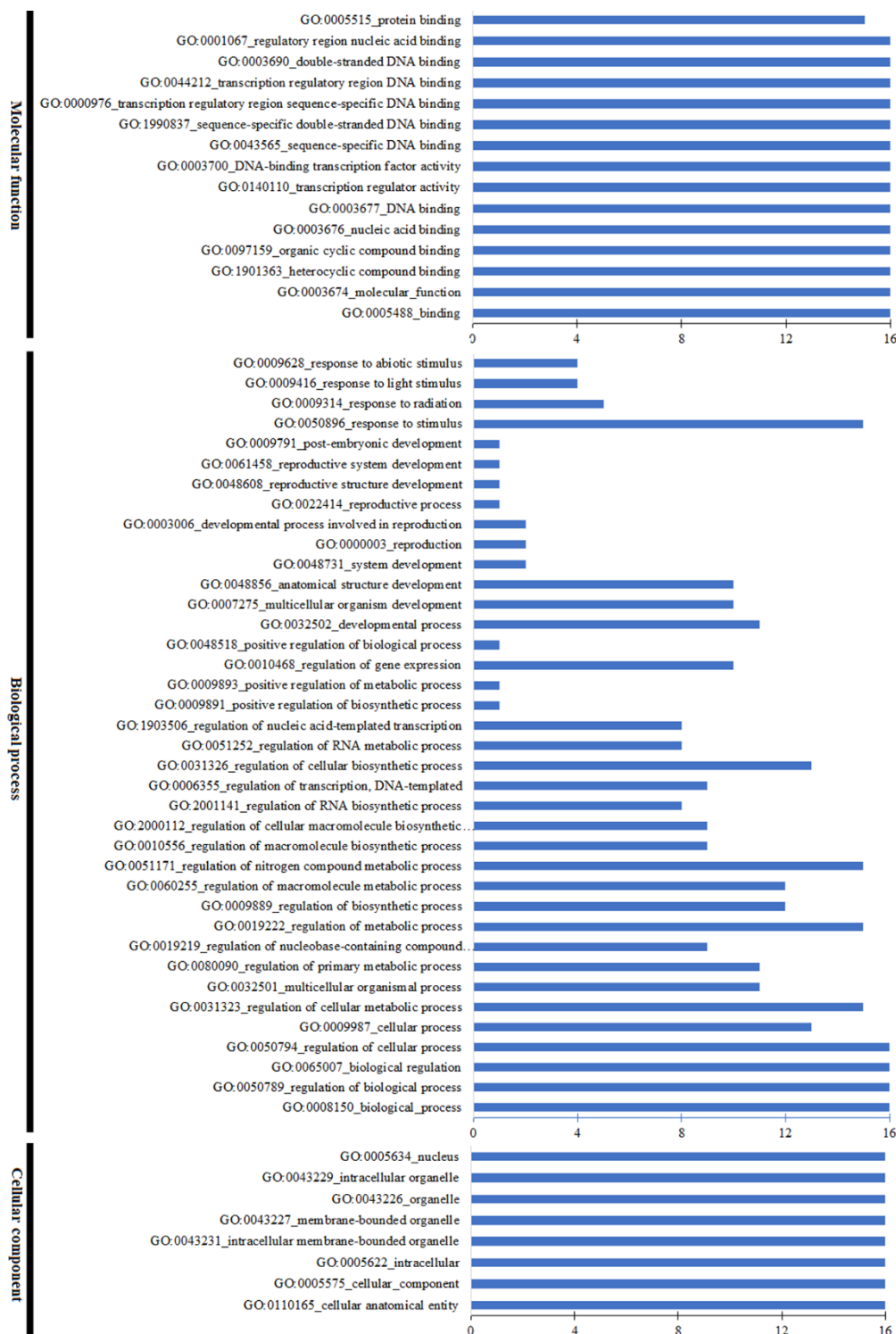


Figure 1. GO analysis involving in molecular function, biological processes, and cellular component of BvGATA investigated by NETGO 2.0

3.4. Phylogenetic analysis of the GATA TFs in sugar beet

In order to elucidate the phylogenetic relationships of the BvGATA TFs in sugar beet, an unrooted phylogenetic tree of whole 16 BvGATA TFs and well-characterized GATA TFs from *A. thaliana* (Teakle *et al.*, 2002) has been built. Based on the ML estimation, 16 BvGATA proteins were classified into four different sub-groups (Figure 2).

Particularly, clade 1 contained six (out of 16) members, including BvGATA04, 09, 10, 11, 14 and 16 (Figure 2). Clade 2 and 3 had four (out of 16), like BvGATA01, 02, 12 and 15, and five (out of 16), members, like BvGATA03, 05, 06, 08 and 12, respectively (Figure 2). Finally, only one (out of 16) member of the BvGATA TFs, like BvGATA07 was distributed in the clade 4 (Figure 2). Phylogenetic tree strongly indicated that the categorization of the BvGATA TFs in sugar beet exhibited a similar trend when comparing with *A. thaliana*.

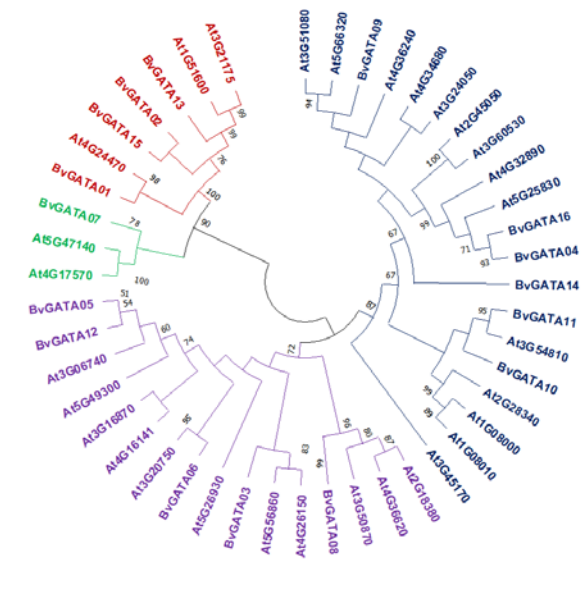


Figure 2. Phylogenetic tree of GATA family from sugar beet (Bv) and Arabidopsis (At).

Previously, the classification of the GATA TFs has been demonstrated in various higher plant species. Briefly, an unrooted phylogenetic tree between all members of the GATA TFs from *A. thaliana* (Teakle *et al.*, 2002) and four

Rosaceae species revealed that these GATA TFs were also classified into four clades (Manzoor *et al.*, 2021). This result was confirmed in the report of the GATA TFs in *Populus* spp. (Kim *et al.*, 2021). Particularly, a phylogenetic tree of the GATA TFs from *Populus* spp. and *A. thaliana* (Teakle *et al.*, 2002) has been built in order to reveal sub-families (Kim *et al.*, 2021). As expected, four sub-families have been identified; particularly clade I and IV contained the largest and smallest number of the GATA TFs from *Populus* spp., respectively (Kim *et al.*, 2021). This phenomenon was confirmed in the GATA TFs in other plant species, like *A. thaliana* (Teakle *et al.*, 2002), soybean (Zhang *et al.*, 2015) and grape (Zhang *et al.*, 2018).

3.5. Physical distribution, gene organization and gene duplication of the GATA TFs in sugar beet

In this study, we examined the chromosomal distributions of the 16 *BvGATA* genes. The *BvGATA* gene family was found to randomly localize on the sugar beet genome. For example, two members of the *BvGATA* gene family were located in chromosome 1 (Figure 3). Chromosome 2 also contained two *BvGATA* genes, while only one member from the *BvGATA* gene family has been found in each of chromosome 3, 4 and 5 (Figure 3). Next, three *BvGATA* genes were mapped on each of chromosome 6, 7 and 9 (Figure 3). Additionally, no *BvGATA* gene was found in chromosome 8 (Figure 3).

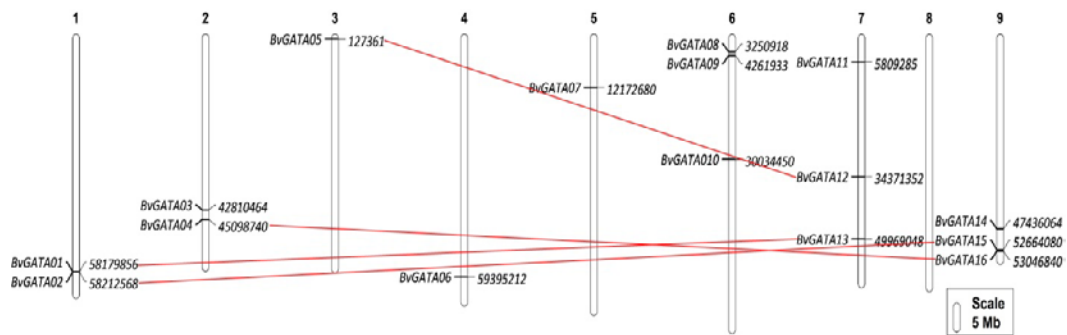


Figure 3. The chromosomal distribution of *BvGATA* genes in the sugar beet genome. The red lines indicated the duplication events. The chromosome number is indicated to the above of each chromosome

Next, we analyzed the exon/intron configuration of the *BvGATA* genes in sugar beet. Our results revealed the variable features of the four sub-groups (Figure 4). Particularly, five (out of six) members in clade 1 contained two exons, whereas only *BvGATA14* in clade 1 had three exons (Figure 4). Similarly, a majority member from clade

3 had three exons and only two (out of five) members in this clade, particularly *BvGATA06* and *08* contained two exons. Interestingly, *BvGATA01* and *13* from clade 2 had seven exons, while *BvGATA02* and *15* from clade 2 contained 10 exons (Figure 4). *BvGATA07* from clade 4 contained eight exons (Figure 4).

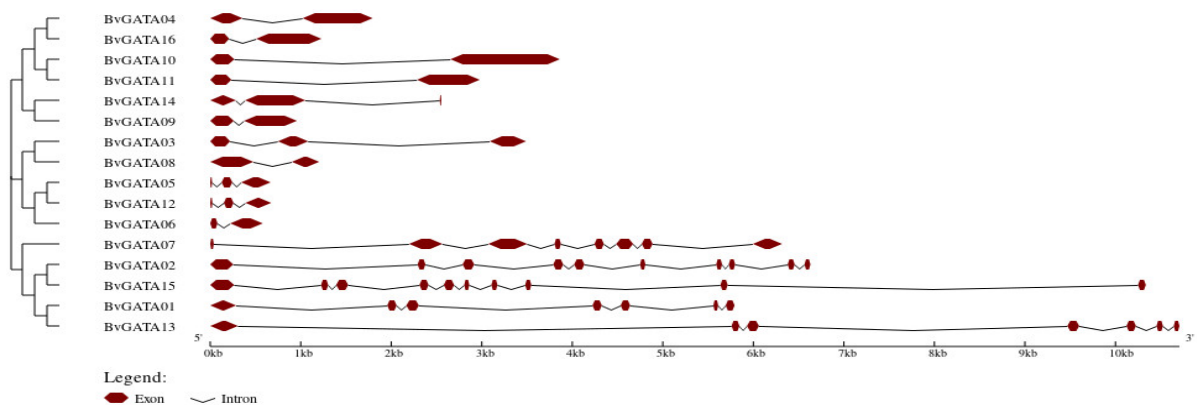


Figure 4. Gene exon/intron organizations of the GATA TF family in sugar beet

As an interesting part of this study, we also predicted the duplication events occurred in the *BvGATA* gene family in sugar beet by using various tools (Hall, 1999; Rozas *et al.*, 2017) as previously described (La *et al.*, 2022; Niu *et al.*, 2020). As well-described in Figure 3 and Table 2, a total of four duplicated genes has been reported in the *BvGATA* family. The similar levels at the nucleotide scale of whole events were varied from 50.0 (*BvGATA02* and *15*) to 57.5% (*BvGATA05* and *12*) (Table 2).

Table 2. Prediction of the duplication events in the *BvGATA* gene family in sugar beet

Duplicated genes	Mechanism	Similar level (%)	Ka	Ks	Ka/Ks
<i>BvGATA04</i> and <i>16</i>	Segmental duplication	53.7	0.3760	0.6451	0.58
<i>BvGATA05</i> and <i>12</i>	Segmental duplication	57.5	0.3913	0.6446	0.61
<i>BvGATA01</i> and <i>13</i>	Segmental duplication	52.9	0.4880	1.3361	0.36
<i>BvGATA02</i> and <i>15</i>	Segmental duplication	50.0	0.5717	1.5408	0.37

3.6. Expression patterns of the sugar beet GATA TFs under abiotic and biotic stress

In this study, of our interest, we explored the expression patterns of the *BvGATA* genes in various organs/tissues under different conditions. As a result, a heatmap was constructed by using R script. We realized that all *BvGATA* genes showed their variable expression in various main tissues under different conditions.

Under the alkaline treatment, a large number of the *BvGATA* genes has been reported to differentially express in leaves. Two genes (out of 16), like *BvGATA02* and *07* were up-regulated in treated leaves, whereas eight genes (out of 16), including *BvGATA03*, *04*, *05*, *06*, *08*, *09*, *12* and *16* were down-regulated in short-term- and/or long-term- alkaline treated leaves (Figure 5). These remaining *BvGATA* genes (six out of 16) were not differentially expressed in leaves under any alkaline treatments (Figure 5).

Under the salt treatment, only seven (out of 16) *BvGATA* genes were found to be responsive in roots. Particularly, three (*BvGATA03*, *11* and *16*) and three (*BvGATA02*, *06* and *14*) genes were up- and down-regulated in salt-treated roots, respectively (Figure 5). Interestingly, *BvGATA04* was induced (~4.00-fold) and reduced (~-15.26-fold) in one-day and seven-day salt-treated root tissues (Figure 5). The expression levels of nine remaining *BvGATA* genes were not significantly changed in roots under salt treatments (Figure 5).

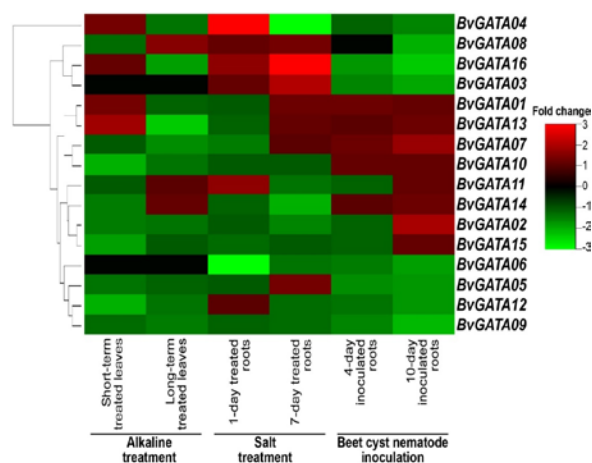


Figure 5. Expression patterns of the *BvGATA* gene family under abiotic and biotic stress

Interestingly, we realized that all duplicated genes were localized in different chromosomes of the sugar beet genome (Figure 3). This finding revealed that the segmental duplication events were major reasons for the expansion of the *BvGATA* gene family. Furthermore, the rates of Ka/Ks of four duplicated genes were recorded to be less than 1, ranging from 0.36 (*BvGATA01* and *13*) to 0.61 (*BvGATA05* and *12*) (Table 2).

Next, our re-analysis of the microarray related to the nematode inoculation in sugar beet's roots indicated that seven (out of 16) *BvGATA* genes were down-regulated in tested tissues (Figure 5). Particularly, three genes, like *BvGATA10*, *12* and *15* were reduced in roots under four days of nematode inoculation, while three genes, including *BvGATA07*, *08* and *16* were reduced in roots under 10 days of nematode treatment (Figure 5). Interestingly, *BvGATA13* were reduced in roots under both four and 10 days of nematode inoculation (Figure 5). Our re-analysis revealed that the *BvGATA* genes were differentially expressed in major organs/tissues under treatments, which may suggest their roles during growth and development processes. In the further studies, these *BvGATA* genes would be used for functional characterization via CRISPR/Cas system to obtain the stress-resistant sugar beet lines.

4. Conclusions

In this present study, we comprehensively identify and characterize 16 *BvGATA* TFs in sugar beet. By using various tools, the sizes, weights, pI and AI scores of the *BvGATA* TFs were greatly variable, whereas all these proteins were hydrophilic. We predicted that the *BvGATA* TFs were localized in the cytoplasm and nucleus. Our phylogeny analysis demonstrated that the *BvGATA* TFs could be categorized into four distinct groups, with a majority of *BvGATA* genes contained two and three exons. We also re-analyzed the available microarray datasets and indicated that the *BvGATA* genes were significantly changed in major organs/tissues under various treatments. Taken together, our study could provide valuable information and candidate *BvGATA* genes for further functional characterization of the *BvGATA* TFs in sugar beet plants.

Acknowledgments

This work was funded by the fundamental research program of Hung Vuong University under the project grant No. 16/2022/HĐKH (HV16.2022).

Author Contributions

Conceptualization: P.B.C., H.D.C., T.M.L., Data collection: H.V.L., T.T.H.T., Q.T.N., T.T.N., Q.T.N.L., T.X.Q.V., T.M.L., H.G.D., Guidance of data analysis: P.B.C., D.H.C., V.H.L., T.M.L., Manuscript writing: P.B.C., D.H.C. All authors discussed the results and contributed to the final manuscript.

References

- Baillo EH, Kimotho RN, Zhang Z and Xu P. 2019. Transcription Factors Associated with Abiotic and Biotic Stress Tolerance and Their Potential for Crops Improvement. *Genes*, **10(10)**: doi:10.3390/genes10100771
- Barrett T, Wilhite SE, Ledoux P, Evangelista C, Kim IF, Tomashevsky M, Marshall KA, Phillippy KH, Sherman PM, Holko M, Yefanov A, Lee H, Zhang N, Robertson CL, Serova N, Davis S and Soboleva A. 2013. NCBI GEO: archive for functional genomics data sets—update. *Nucleic Acids Res.*, **41(D1)**: D991-D995. doi:10.1093/nar/gks1193
- Behringer C and Schwecheimer C. 2015. B-GATA transcription factors—insights into their structure, regulation, and role in plant development. *Front Plant Sci.*, **6**: 90. doi: 10.3389/fpls.2015.00090
- Briesemeister S, Rahnenführer J and Kohlbacher O. 2010. YLoc—an interpretable web server for predicting subcellular localization. *Nucleic Acids Res.*, **38**(Web Server issue): W497-502. doi:10.1093/nar/gkq477
- Chen H, Shao H, Li K, Zhang D, Fan S, Li Y and Han M. 2017. Genome-wide identification, evolution, and expression analysis of GATA transcription factors in apple (*Malus x domestica* Borkh.). *Gene*, **627**: 460-472. doi:10.1016/j.gene.2017.06.049
- Chen L, Zhu Y, Hu Z and Wu S. 2021. Beetroot as a functional food with huge health benefits: Antioxidant, antitumor, physical function, and chronic metabolomics activity. *Food sci nutr.*, **9(11)**: 6406-6420. doi:10.1002/fsn3.2577
- Chhikara N, Kushwaha K, Sharma P, Gat Y and Panghal A. 2019. Bioactive compounds of beetroot and utilization in food processing industry: A critical review. *Food Chem.*, **272**: 192-200. doi:10.1016/j.foodchem.2018.08.022
- Chu HD, Nguyen KH, Watanabe Y, Le DT, Pham TLT, Mochida K and Tran LP. 2018. Identification, structural characterization and gene expression analysis of members of the nuclear factor-Y family in chickpea (*Cicer arietinum* L.) under dehydration and abscisic acid treatments. *Int J Mol Sci.*, **19(11)**: E3290. doi:10.3390/ijms19113290
- Conesa A, Götz S, García-Gómez JM, Terol J, Talón M and Robles M. 2005. Blast2GO: a universal tool for annotation, visualization and analysis in functional genomics research. *Bioinformatics*, **21(18)**: 3674-3676. doi:10.1093/bioinformatics/bti610
- Dohm JC, Minoche AE., Holtgräwe D, Capella-Gutiérrez S, Zakrzewski F, Tafer H, Rupp O, Sörensen TR., Stracke R, Reinhardt R, Goesmann A, Kraft T, Schulz B, Stadler PF, Schmidt T, Gabaldón T, Lehrach H, Weisshaar B and Himmelbauer H. 2014. The genome of the recently domesticated crop plant sugar beet (*Beta vulgaris*). *Nature*, **505(7484)**: 546-549. doi:10.1038/nature12817
- Evans E and Messerschmidt U. 2017. Review: Sugar beets as a substitute for grain for lactating dairy cattle. *J Anim Sci Biotechnol.*, **8**: 25. doi:10.1186/s40104-017-0154-8
- Feng X, Yu Q, Zeng J, He X and Liu W. 2022. Genome-wide identification and characterization of GATA family genes in wheat. *BMC Plant Biol.*, **22(1)**: 372. doi:10.1186/s12870-022-03733-3
- Fujita Y, Fujita M, Shinozaki K and Yamaguchi-Shinozaki K. 2011. ABA-mediated transcriptional regulation in response to osmotic stress in plants. *J Plant Res.*, **124(4)**: 509-525. doi:10.1007/s10265-011-0412-3
- Gasteiger E, Gattiker A, Hoogland C, Ivanyi I, Appel RD and Bairoch A. 2003. ExPASy: The proteomics server for in-depth protein knowledge and analysis. *Nucleic Acids Res.*, **31(13)**: 3784-3788. doi:10.1093/nar/gkg563
- Gasteiger E, Hoogland C, Gattiker A, Wilkins MR, Appel RD and Bairoch A. 2005. Protein identification and analysis tools on the ExPASy server. In: Walker JM (Eds.) The Proteomics Protocols Handbook. Springer Protocols Handbooks. Humana Press. pp. 571-607. doi: 10.1385/1-59259-890-0:571.
- Ghaemi R, Pourjam E, Safaie N, Verstraeten B, Mahmoudi SB, Mehrabi R, De Meyer T and Kyndt T. 2020. Molecular insights into the compatible and incompatible interactions between sugar beet and the beet cyst nematode. *BMC Plant Biol.*, **20(1)**: 483. doi:10.1186/s12870-020-02706-8
- Goodin MM. 2018. Chapter Six - Protein Localization and Interaction Studies in Plants: Toward Defining Complete Proteomes by Visualization. In Kielian M, Mettenleiter TC and Roossinck MJ (Eds.), *Adv Virus Res.* **100**, Academic Press. pp. 117-144.
- Goodstein DM, Shu S, Howson R, Neupane R, Hayes RD, Fazo J, Mitros T, Dirks W, Hellsten U, Putnam N and Rokhsar DS. 2012. Phytozome: A comparative platform for green plant genomics. *Nucleic Acids Res.*, **40(Database issue)**: D1178-D1186. doi:10.1093/nar/gkr944
- Hall TA. 1999. BioEdit: A user-friendly biological sequence alignment editor and analysis program for Windows 95/98/NT. *Nucleic Acids Symp Ser.*, **41**: 95-98.
- Hu B, Jin J, Guo AY, Zhang H, Luo J and Gao G. 2015. GSDS 2.0: An upgraded gene feature visualization server. *Bioinformatics*, **31(8)**: 1296-1297. doi:10.1093/bioinformatics/btu817
- Jin J, Tian F, Yang D-C, Meng Y-Q, Kong L, Luo J and Gao G. 2017. PlantTFDB 4.0: toward a central hub for transcription factors and regulatory interactions in plants. *Nucleic Acids Res.*, **45(D1)**: D1040-D1045. doi:10.1093/nar/gkw982
- Kim M, Xi H, Park S, Yun Y and Park J. 2021. Genome-wide comparative analyses of GATA transcription factors among seven *Populus* genomes. *Scientific Reports*, **11(1)**: 1-15.
- Kumar S, Stecher G and Tamura K. 2016. MEGA7: Molecular evolutionary genetics analysis version 7.0 for bigger datasets. *Mol Biol Evol.*, **33(7)**: 1870-1874. doi:10.1093/molbev/msw054
- La HV, Chu HD, Ha QT, Tran TTH, Tong VH., Tran VT, Le TNQ, Bui THT and Cao PB. 2022. SWEET Gene Family in Sugar Beet (*Beta vulgaris*): Genome-Wide Survey, Phylogeny and Expression Analysis. *Pak J Biol Sci.*, **25(5)**: 387-395.
- Larkin MA, Blackshields G and Brown NP. 2007. Clustal W and clustal X version 2.0. *Bioinformatics*, **23**. doi:10.1093/bioinformatics/btm404
- Liu L, Wang B, Liu D, Zou C, Wu P, Wang Z, Wang Y and Li C. 2020. Transcriptomic and metabolomic analyses reveal mechanisms of adaptation to salinity in which carbon and nitrogen metabolism is altered in sugar beet roots. *BMC Plant Biol.*, **20(1)**: 138. doi:10.1186/s12870-020-02349-9

- Mall AK, Misra V, Santeshwari, Pathak AD and Srivastava S. 2021. Sugar Beet Cultivation in India: Prospects for Bio-Ethanol Production and Value-Added Co-Products. *Sugar tech.*, **23(6)**: 1218-1234. doi:10.1007/s12355-021-01007-0
- Manzoor MA, Sabir IA, Shah IH, Wang H, Yu Z, Rasool F, Mazhar MZ, Younas S, Abdullah M and Cai Y. 2021. Comprehensive Comparative Analysis of the GATA Transcription Factors in Four Rosaceae Species and Phytohormonal Response in Chinese Pear (*Pyrus bretschneideri*) Fruit. *Int J Mol Sci.*, **22(22)**: 12492. doi:10.3390/ijms222212492
- Mirmiran P, Houshialsadat Z, Gaeini Z, Bahadoran Z and Azizi F. 2020. Functional properties of beetroot (*Beta vulgaris*) in management of cardio-metabolic diseases. *Nutr Metab (Lond)*, **17**: 3. doi:10.1186/s12986-019-0421-0
- Mistry J, Chuguransky S, Williams L, Qureshi M, Salazar GA, Sonnhammer ELL, Tosatto SCE, Paladin L, Raj S, Richardson LJ, Finn RD and Bateman A. 2021. Pfam: The protein families database in 2021. *Nucleic Acids Res.*, **49(D1)**: D412-D419. doi:10.1093/nar/gkaa913
- Monteiro F, Frese L, Castro S, Duarte MC, Paulo OS, Loureiro J and Romeiras MM. 2018. Genetic and Genomic Tools to Assist Sugar Beet Improvement: The Value of the Crop Wild Relatives. *Front Plant Sci.*, **9**: 74. doi:10.3389/fpls.2018.00074
- Niu L, Chu HD, Tran CD, Nguyen KH, Pham HX, Le DT, Li W, Wang W, Le TD and Tran L-SP. 2020. The GATA gene family in chickpea: Structure analysis and transcriptional responses to abscisic acid and dehydration treatments revealed potential genes involved in drought adaptation. *J Plant Growth Regul.*, **39(4)**: 1647-1660. doi:10.1007/s00344-020-10201-5
- Pavlečić M, Rezić T, Šantek MI, Horvat P and Šantek B. 2017. Bioethanol production from raw sugar beet cosettes in horizontal rotating tubular bioreactor. *Bioprocess Biosyst Eng.*, **40(11)**: 1679-1688. doi:10.1007/s00449-017-1823-x
- Peng W, Li W, Song N, Tang Z, Liu J, Wang Y, Pan S, Dai L and Wang B. 2021. Genome-Wide Characterization, Evolution, and Expression Profile Analysis of GATA Transcription Factors in *Brachypodium distachyon*. *Int J Mol Sci.*, **22(4)**: 2026. doi:10.3390/ijms22042026
- Reyes JC, Muro-Pastor MI and Florencio FJ. 2004. The GATA family of transcription factors in *Arabidopsis* and rice. *Plant Physiol.*, **134(4)**: 1718-1732. doi:10.1104/pp.103.037788
- Rozas J, Ferrer-Mata A, Sanchez-DelBarrio JC, Guirao-Rico S, Librado P, Ramos-Onsins SE and Sanchez-Gracia A. 2017. DnaSP 6: DNA Sequence Polymorphism Analysis of Large Data Sets. *Mol Biol Evol.*, **34(12)**: 3299-3302. doi:10.1093/molbev/msx248
- Schwechheimer C, Schroder PM and Blaby-Haas CE. 2022. Plant GATA Factors: Their biology, phylogeny, and phylogenomics. *Annu Rev Plant Biol.*, **73**: 123-148. doi:10.1146/annurev-arplant-072221-092913
- Teakle GR., Manfield IW, Graham JF and Gilmartin PM. 2002. *Arabidopsis thaliana* GATA factors: organisation, expression and DNA-binding characteristics. *Plant Mol Biol.*, **50(1)**: 43-57. doi:10.1023/a:1016062325584
- Yu C, Li N, Yin Y, Wang F, Gao S, Jiao C and Yao M. 2021. Genome-wide identification and function characterization of GATA transcription factors during development and in response to abiotic stresses and hormone treatments in pepper. *J Appl Genet.*, **62(2)**: 265-280. doi:10.1007/s13353-021-00618-3
- Yu R, Chang Y, Chen H, Feng J, Wang H, Tian T, Song Y and Gao G. 2021. Genome-wide identification of the GATA gene family in potato (*Solanum tuberosum* L.) and expression analysis. *J Plant Biotech Biochem.*, **31(1)**: 37-48. doi:10.1007/s13562-021-00652-6
- Zhang C, Hou Y, Hao Q, Chen H, Chen L, Yuan S, Shan Z, Zhang X, Yang Z, Qiu D, Zhou X and Huang W. 2015. Genome-wide survey of the soybean GATA transcription factor gene family and expression analysis under low nitrogen stress. *PLoS One*, **10(4)**: e0125174. doi:10.1371/journal.pone.0125174
- Zhang C, Huang Y, Xiao Z, Yang H, Hao Q, Yuan S, Chen H, Chen L, Chen S, Zhou X and Zhou X. 2020. A GATA transcription factor from soybean (*Glycine max*) regulates chlorophyll biosynthesis and suppresses growth in the transgenic *Arabidopsis thaliana*. *Plants (Basel)*, **9(8)**: 1036. doi:10.3390/plants9081036
- Zhang K, Jia L, Yang D, Hu Y, Njogu MK and Wang P. 2021. Genome-Wide Identification, Phylogenetic and Expression Pattern Analysis of GATA Family Genes in Cucumber (*Cucumis sativus* L.). *Plants (Basel, Switzerland)*. **10(8)**: 1626. doi:10.3390/plants10081626
- Zhang Y, Nan J and Yu B. 2016. OMICS Technologies and Applications in Sugar Beet. *Front Plant Sci.*, **7**: 900-900. doi:10.3389/fpls.2016.00900
- Zhang Z, Ren C, Zou L, Wang Y, Li S and Liang Z. 2018. Characterization of the GATA gene family in *Vitis vinifera*: genome-wide analysis, expression profiles, and involvement in light and phytohormone response. *Genome*, **61(10)**: 713-723. doi:10.1139/gen-2018-0042
- Zhang Z, Zou X, Huang Z, Fan S, Qun G, Liu A, Gong J, Li J, Gong W, Shi Y, Fan L, Zhang Z, Liu R, Jiang X, Lei K, Shang H, Xu A and Yuan Y. 2019. Genome-wide identification and analysis of the evolution and expression patterns of the GATA transcription factors in three species of *Gossypium* genus. *Gene*, **680**: 72-83. doi:10.1016/j.gene.2018.09.039
- Zou C, Wang Y, Wang B, Liu D, Liu L, Gai Z and Li C. 2020. Long non-coding RNAs in the alkaline stress response in sugar beet (*Beta vulgaris* L.). *BMC Plant Biol.*, **20(1)**: 227. doi:10.1186/s12870-020-02437-w.

Biogenic Silver Nanoparticles by *Pseudomonas aeruginosa* Reduce Expression of Biofilm and Quorum Signaling Genes in Multi-drug Resistant *Acinetobacter baumannii*

Talar Ibrahim Hasan & Akhter Ahmed Ahmed*

Department of Biology, College of Science, Salahaddin University- Erbil, Iraq

Received: December 30, 2022; Revised: March 1, 2023; Accepted: April 4 2023

Abstract

Discovery of antibiotics is regarded as one of the critical moments in the history of medicine; however, irrational use caused the emergence of a phenomenon known as drug resistance. Once considered benign, *Acinetobacter baumannii* (*A. baumannii*) evolved to become a challenging pathogen threatening the current antibiotic era. In 2017, WHO appointed *A. baumannii* as the most critical pathogen towards which the development of novel antibiotics is keenly required. The current study intends to explore the silver nanoparticles (AgNPs) role in the weakening of virulence and biofilm through reducing the expression of outer membrane protein-A (*OmpA*), biofilm-associated protein (*Bap*), *Acinetobacter baumannii* autoinducer-I (*abaI*) and *Acinetobacter baumannii* receptor (*abaR*) genes in the multi-drug resistant (MDR) *A. baumannii*. All bacterial isolates were capable to form biofilm and exhibited high resistance levels to the antibiotics used including (ampicillin/sulbactam, ceftazidime, tobramycin, amikacin, gentamicin, levofloxacin, imipenem, ciprofloxacin, meropenem, piperacillin/tazobactam, cefepime, ceftriaxone, doxycycline, and trimethoprim/sulfamethoxazole). AgNPs were biologically synthesized by *Pseudomonas aeruginosa* (*P. aeruginosa*) (PA-AgNP) and characterized via FTIR, UV-vis, EDX, XRD, and SEM. Results of characterization tools supported the successful formation of crystalline AgNPs. Minimum-inhibitory concentrations of the harvested AgNPs were determined to study their antibiofilm and quorum quenching potential at sub-inhibitory concentrations (SIC). RT PCR was utilized to estimate the influence of PA-AgNPs on the quorum sensing (QS) and biofilm at level of gene expression. Exposure of the tested isolates to PA-AgNP at SIC values decreased their biofilm fabrication capacity and significantly downregulated candidate genes expression. The results show that *P. aeruginosa* can be used to bio-fabricate AgNPs capable of interrupting bacterial-growth and biofilm progress in the MDR *A. baumannii* through the downregulation of QS and biofilm-associated genes.

Keywords: Quorum sensing, biofilm, virulence, silver nanoparticle, *Acinetobacter baumannii*

1. Introduction

Last century witnessed the revelation of antibiotics which is regarded as one of the most prominent inventions in the history of medicine (Ghosh *et al.*, 2020). For more than 70 years later, antibiotics enabled the treatment of previously lethal bacterial infections and saved millions of lives (Uddin *et al.*, 2021; Laws *et al.*, 2019, Ventola, 2015). However, prolonged overuse and misuse of antibiotics, ineffective infection control strategies, and lack of new drug development have led to the occurrence of a phenomenon known as antibiotic resistance (Aslam *et al.*, 2021; Ventola, 2015). According to a report issued by World Health Organization (WHO) in 2019, antimicrobial resistance was deemed to be responsible for the annual death of at least 700,000 people worldwide and that figure is expected to increase up to 10 million by 2050 if the current situation is left untreated (Nji *et al.*, 2021). As over 70% of the pathogenic bacteria are currently resistant to at least one type of antibiotics, novel approaches should be considered to tackle this global crisis (Uddin *et al.*, 2021;

Laws *et al.*, 2019). Bacteriophages or phage-derived proteins, organic or inorganic nanomaterials in particular gold and silver nanoparticles, probiotics, antimicrobial peptides, repurposing drugs and combination therapy, quorum quenching, and anti-biofilm development are investigated extensively to be used as a possible alternative strategy against superbug infections (García-Contreras *et al.*, 2022).

Acinetobacter baumannii (*A. baumannii*) is an ESCAPE pathogen of great concern regarding both hospital and community-acquired infections and accounts for up to 20% of infections in ICUs globally (Lee *et al.*, 2017). Estimated number of the infectious cases range from 600,000 up to 1,400,000 cases per year throughout the world with fatality rates varying from 20-80% (Havenga *et al.*, 2022). *A. baumannii* is considered the most critical pathogen in the first ever antibiotic resistant priority pathogen list published by WHO in 2017 (Mancuso *et al.*, 2021). Furthermore, disease control and prevention center (CDC) also declared *A. baumannii* as the most urgent in its 2019 antibiotic resistance threat report (CDC, 2019). What makes this pathogen dreadful is a

* Corresponding author. e-mail: akhter.ahmed@su.edu.krd.

repertoire of virulence factors and immense aptitude to withstand stressful environmental settings and multiple classes of antibiotics including “carbapenem” (Ayoub Moubareck and Hammoudi Halat, 2020). Formation of biofilm and virulence factors are sustained by quorum sensing (QS) (Saipriya *et al.*, 2020). Many bacteria use QS as a communication mechanism among each other to sustain population density via production of small diffusible signal-molecules termed autoinducers (Tang *et al.*, 2020; Saipriya *et al.*, 2020).

QS is employed by both gram-positive and gram-negative bacteria where oligopeptides in gram-positive bacteria and acyl-homoserine lactones (AHLs) in gram-negative bacteria are used as the primary autoinducers (Papenfort and Bassler, 2016). Concentration of signaling molecules increases in parallel with the increase in number of bacterial cells, and once a certain threshold has been reached a cascade of reactions will be triggered in response to the binding of autoinducers to their cognate receptors which in turn changes the expression of QS target genes in the bacterial cell (Saipriya *et al.*, 2020; Tang *et al.*, 2020). Recently, a number of reports indicated that two components *Acinetobacter baumannii* autoinducer-I (*abaI*), *Acinetobacter baumannii* receptor (*abaR*) make up the QS regulatory system of *A. baumannii* where the *abaI* is the AHL synthase with 3-hydroxy-C12 homoserine being the primary AHL synthesized and *abaR* is the transcriptional regulator that functions as a receptor for the signal molecules (Cui *et al.*, 2022; Tang *et al.*, 2020). A complex will be formed upon binding of AHL and *abaR* receptor, which in turn attaches to the specific promoter-sequence of the respective genes and modulate their expression (Cui *et al.*, 2022). Quorum quenching refers to various methods used to combat quorum sensing (Ibrahim *et al.*, 2021). Over years a number of synthetic and natural quorum sensing inhibitors have been suggested (Saipriya *et al.*, 2020). Nowadays, the production of nanomaterials has increased (Kumar *et al.*, 2020) and recent developments in nanotechnology made it easier to find use cases for the technology in medicine, electronics, agricultural, renewable energy, and other fields (Pavani *et al.*, 2020). Nanomedicine managed to receive a great deal of recognition from scientists as a possible approach for the drug resistance catastrophe (Uddin *et al.*, 2021). Large amounts of nanoparticles can be manufactured via conventional physical or chemical routes; however, these methods are complicated, expensive, non-ecofriendly, energy-consuming, and require the use of toxic chemicals which limits their biomedical applications (Busi and Rajkumari, 2019). Hence, green-approach for the synthesis of nanoparticles continues to attract more attention because it is simple, requires less energy, cost-efficient, eco-friendly, and is nontoxic (Ball *et al.*, 2019). Among the biological routes, bacteria are considered the best candidate due to their abundance, adaptability, and impressive ability to reduce heavy metal-ions viz, (*Bacillus cereus*, *Pseudomonas stutzeri*, *Bacillus subtilis* and *Pseudomonas aeruginosa*) (Busi and Rajkumari, 2019; Irvani, 2014). Green-synthesized silver nanoparticles targeting bacterial quorum sensing and biofilms are being reported as a novel approach against drug-resistant bacteria (Zhong and He, 2021; Shah *et al.*, 2019). Despite the availability of multiple studies devoted to the effect of inhibitors on *A. baumannii* growth (Raorane *et al.*, 2020;

Singh *et al.*, 2018), none of them has investigated the effect on the level of QS and virulence-related gene expression.

To investigate the role of biogenic silver nanoparticles (AgNPs) in the weakening of QS related virulence and biofilm of the MDR *A. baumannii* through reducing the expression of outer membrane protein-A (*OmpA*), biofilm-associated protein (*Bap*), *abaI* and *abaR* genes, this study was executed.

2. 2. Materials and Methods

2.1. Sample collection and *Acinetobacter baumannii* (*A. baumannii*) identification

This study was conducted in accordance with the principles of the Helsinki Declaration and was approved by the Human Ethics Committee of the Science College at Salahaddin University Erbil (No:4S/478; date, September 9, 2021; Erbil, Iraq).

A total of 26 *A. baumannii* isolates were collected from various bacteriology laboratories of hospitals in the city of Erbil, Kurdistan Region, Iraq. An ATCC strain of *A. baumannii* (19606) was purchased from Medya Diagnostic center to be used as control throughout the study. The clinical isolates were recultivated onto MacConkey (MA, Merck, Germany) agar petri-plates and subjected to aerobic incubation overnight at 37°C. Based on previously described standard techniques in (Tille, 2021), a series of biochemical and conventional diagnostic assays were carried out to establish identification of the individual colonies as *A. baumannii*. Automated Vitek-2 (Biomerieux, France) was employed to validate the identification process. Pure cultures were periodically cultivated on Muller Hinton agar slants and stored at -70°C in nutrient broth supplemented with 25% glycerol for further study.

2.2. Antibiotic susceptibility assay

Guidelines provided by Clinical and Laboratory Institute (CLSI) were considered in the selection of antimicrobial agents to evaluate the sensitivity or susceptibility of the bacterial isolates through disc-diffusion technique (CLSI, 2022). Prior to inoculation onto the Muller Hinton agar (MHA, Biomark Laboratories, India) plates, turbidity or clarity of the bacterial suspensions was accommodated to 0.5 McFarland by a spectrophotometer. Following lawn plating, the plates were then subjected to the following antibiotics: ampicillin/sulbactam (10/10 µg, Himedia), ceftazidime (30 µg, Bioanalyse), tobramycin (10 µg, Bioanalyse), amikacin (10 µg, Bioanalyse), gentamicin (10 µg, Bioanalyse), levofloxacin (5 µg, Bioanalyse), imipenem (10 µg, Bioanalyse), ciprofloxacin (10 µg, Bioanalyse), meropenem (10 µg, Bioanalyse), piperacillin/tazobactam (100/10 µg, Himedia), cefepime (10 µg, Bioanalyse), ceftriaxone (10 µg, Bioanalyse), doxycycline (10 µg, Bioanalyse), and trimethoprim/sulfamethoxazole (25 µg, Himedia).

For data analysis, The CLSI diameter breakpoints shown in table (1) were employed, and data were interpreted as susceptible, intermediate and resistant. The most resistant strains were selected to test the inhibitory effect of PA-AgNPs. Two biological replicates were considered on different occasions.

Table 1. Antibiotic inhibition zone interpretive standard for *A. baumannii* according to clinical and laboratory institute

Antibiotic Agents	Code	Inhibition Zone Diameter (mm)		
		Sensitive	Intermediate	Resistant
Amikacin	AK	≥17	15-16	≤14
Ampicillin – Sulbactam	A/S	≥15	12-14	≤11
Cefepime	CEF	≥18	15-17	≤14
Ceftazidime	CAZ	≥18	15-17	≤14
Ceftriaxone	CRO	≥21	14-20	≤13
Ciprofloxacin	CIP	≥21	16-20	≤15
Doxycycline	DO	≥13	10-12	≤9
Gentamicin	GEN	≥15	13=14	≤12
Imipenem	IPM	≥22	19-21	≤18
Levofloxacin	LEV	≥17	14-16	≤13
Meropenem	MER	≥18	15-17	≤14
Piperacillin – Tazobactam	P/T	≥21	18-20	≤17
Tobramycin	TOB	≥15	13-14	≤12
Trimethoprim - sulfamethoxazole	T/S	≥16	11-15	≤10

2.3. Static biofilm assay

The microplate technique described by (Limban *et al.*, 2011) was adopted with slight modifications to examine the ability of the identified *A. baumannii* isolates to form biofilm. In brief, 15 µl of the overnight cultures of the desired bacteria were inoculated into wells of the microtiter plate (MTP, Citotest Labware, China) containing 200 µl of sterile Nutrient broth (NB, Neogen, USA) supplemented with 2% glucose. Wells containing NB only served as control. Then, the inoculated MTP was incubated for 24 hours in a static condition at 37°C. Following the incubation period, the cavities were rinsed thrice with sterile phosphate buffer saline (PBS) after disposal of the supernatant. The wells were dried at 55°C by oven (memmert, Germany), 200 µl of 1% crystal-violet staining solution was allocated into each of the cavities and incubated for (10 minutes) at ambient temperature. Lastly, the wells of the microplate were carefully rinsed thrice with sterilized PBS and eluted with 95% ethanol solvent to quantify the biofilms produced spectrophotometrically by mean of ELISA (BioTek Instruments, USA) at a wavelength of 490 nm. Three biological replicates were considered on different occasions.

2.4. Bio-fabrication of biogenic silver nanoparticles

The method described by (Nirmala and Sridevi, 2021) with slight modifications was employed for the bio-fabrication of PA-AgNPs by an ATCC strain of *Pseudomonas aeruginosa* (*P. aeruginosa*) (50126). First, a loopful of the *P. aeruginosa* inoculum was placed in 500 ml of sterile NB and incubated overnight at 37°C. Following incubation, the broth was centrifuged for 10 minutes at 6000 rpm to obtain a cell-free broth. The later was mixed with 500 ml of 4 mM silver-nitrate and incubated in the dark for 72 hours at 60°C. After the incubation period, a transition in the color of the reaction-mixture to dark brown was regarded as the initial indicator for AgNPs synthesis. The stronger biofilm producers were selected to test the antibacterial effect of PA-AgNPs.

Three biological replicates were considered, and standard errors were measured.

2.5. Characterization of biogenic silver nanoparticles

The existence of the formed PA-AgNPs was confirmed via using Ultraviolet-visible spectroscopy (UV-1900i, Shimadzu, Japan). Energy-Dispersive X-Ray analysis (EDS), Scanning-Electron Microscopy (SEM), X-ray Diffraction (XRD), and Fourier-Transform Infrared-Spectroscopy (FTIR) (Jasco, Japan) were employed to further characterize the harvested PA-AgNPs (Nirmala and Sridevi, 2021).

2.6. Minimum and sub-minimum inhibitory concentration (MIC and SIC) determination of PA-AgNPs

CLSI instructions were utilized accordingly to assess MIC of the prepared PA-AgNPs against ten of the clinical MDR and the most frequent biofilm producers along with an *A. baumannii* ATCC 19606 through broth-microdilution technique (CLSI, 2018). 200µL NB containing different concentrations (80, 40, 20, 10, 5, 2.5, 1.25 mg/ml) of PA-AgNPs were administered to the wells of MTP. Then 10 µl of overnight *A. baumannii* culture adjusted to the standard 0.5 McFarland was added to the wells and incubated overnight aerobically in the rotating incubator (150 rpm) at 37°C. The wells with no evident growth were determined as MIC. SIC values were ruled as the measures below the MIC values and were employed to appraise anti-biofilm/anti-QS activity of the PA-AgNPs.

2.7. SIC effect of PA-AgNPs on the biofilm

The protocol described by (Ahmed and Salih, 2019) was considered to evaluate the impact of the PA-AgNPs on biofilm fabrication by the ten clinical MDR and strongest strains along with an *A. baumannii* ATCC 19606 at SIC. Briefly, 15 µl from the sub-MICs wells of the previous procedure (MIC) were allocated into wells of flat-bottom MTP containing 200 µl of nutrient broth supplemented with 2% glucose. Then, the inoculated MTP was placed in the incubator at 37°C for 24 hours under a static condition. Wells containing NB with bacterium inoculum only used as control. Following the incubation period, 1% crystal-violet was applied to stain the microplate after disposal of the liquid-cultures from the wells and rinsing with PBS thrice. After the staining procedure, the wells were rinsed with PBS, eluted with 95% ethanol, and subjected to ELISA in order to quantify the biofilm produced at the wavelength of 490 nm.

2.8. RNA extraction and quantification of QS and biofilm related genes

Real-time PCR instrument (RT-PCR) was operated to assess the PA-AgNPs effect at the SIC value on the expression extent of the outer membrane protein-A (*OmpA*), biofilm-associated protein (*Bap*), *Acinetobacter baumannii* autoinducer-I (*abaI*) and *Acinetobacter baumannii* receptor (*abaR*) genes. Total RNA was extracted from both untreated bacteria which were used as control and bacteria exposed to PA-AgNPs following guidance provided by the manufacturer (total RNA kit, Favorgen Biotech, Taiwan). cDNA was synthesized through reverse transcription of the isolated RNA using the AddScript cDNA synthesis kit coinciding with the manufacturer protocol (addbio, Korea). RT-PCR reactions

were executed utilizing “RealQ-Plus 2x Master-Mix Green” (Ampliqon, Denmark) in the PCRmax Eco 48 RT-PCR system. Primer sequences listed in Table (2) were

used to analyze candidate genes via (RT-PCR) and the procured results were calculated using the $\Delta\Delta C_t$ method (Ahmed and Salih, 2019).

Table 2. List of genes and their primer sequences

Gene	Primer Sequence (5'-3')		Product size(bp)	Ref.
	Forward	Reverse		
<i>abaI</i>	AAAGTTACCGCTACAGGG	CACGATGGGCACGAAA	435	(Tang <i>et al.</i> , 2020)
<i>abaR</i>	TCCTCGGGT CCCAATA	AAATCTACCGCATCAA	310	(Tang <i>et al.</i> , 2020)
<i>ompA</i>	ATGAAAAAGACAGCTATCGCGATTGCA	CACCAAAAAGCACCCAGCGCCAGTTG	136	(Amin <i>et al.</i> , 2019)
<i>Bap</i>	AATGCACCGGTACTTGATCC	TATTGCCTGCAGGGTCAGTT	205	(Amin <i>et al.</i> , 2019)

2.9. Statistical analysis

The obtained results were analyzed through GraphPad Prism 8.0 software. Two-way analysis of variance (ANOVA) method was selected for multiple comparisons. Data presented as mean \pm SE.

3. Results

3.1. *Acinetobacter baumannii* (*A. baumannii*) isolates

A total of 27 *A. baumannii* isolates including ATCC (19606) were obtained from various hospitals in Erbil governorate to conduct the current study. The bacterial isolates were identified as gram-negative coccobacilli, catalase-positive, oxidase-negative, indole-negative, citrate-positive, non-fermentative bacteria capable of growth on MacConkey agar. To confirm their identification, Vitek-2 system was employed to identify the isolates as *A. baumannii* with a probability rate of 96 to 99%. Following specimen type analysis, it was found that (58%) of the clinical isolates were recovered from sputum followed by wound (27%), blood (12%), and CSF (4%) as seen in figure (1).

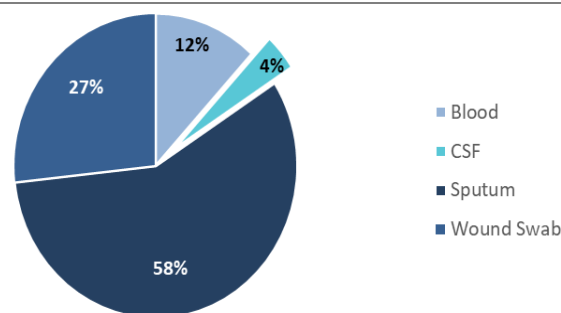


Figure 1. Different clinical specimens recovered from patients with *A. baumannii* including sputum, wound, blood, and CSF

3.2. Antibiotic sensitivity pattern

Kirby-Bauer test was employed to evaluate the susceptibility of the isolates to the antibiotics included in this study and the results indicated that all isolates showed 100% resistance to cefepime and ceftazidime followed by 96% resistance to amikacin, 93% resistance to (ceftriaxone, ciprofloxacin, gentamicin, levofloxacin), 78% imipenem, 74% meropenem, 70% doxycycline, 67% tobramycin, 63% trimethoprim/sulfamethoxazole, 33% piperacillin/tazobactam and least resistance was shown to ampicillin/sulbactam with a percentage of only 26% as shown in figure (2).

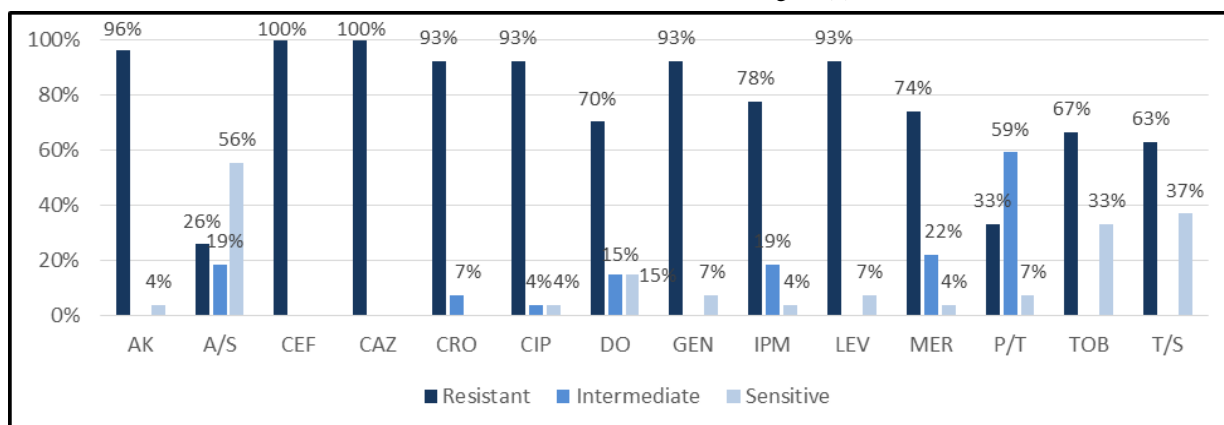


Figure 2. Percentage of sensitive, intermediate, and resistant *A. baumannii* isolates obtained from antibiotic sensitivity assay: AK (Amikacin); A/S (ampicillin/sulbactam); CEF (cefepime); CAZ (ceftazidime); CRO (ceftriaxone); CIP (ciprofloxacin); DO (doxycycline); GEN (gentamicin); IPM (imipenem); LEV (levofloxacin); MER (meropenem); P/T (piperacillin/tazobactam); TOB (tobramycin); T/S (trimethoprim/sulfamethoxazole).

Furthermore, based on the antibiotic susceptibility test results *A. baumannii* isolates were categorized into three groups (MDR, XDR, and non-MDR). It was calculated that the majority of isolates were XDR with a whopping percentage of 67%, 30% were MDR and around 4% were observed to be non-MDR as illustrated in figure (3).

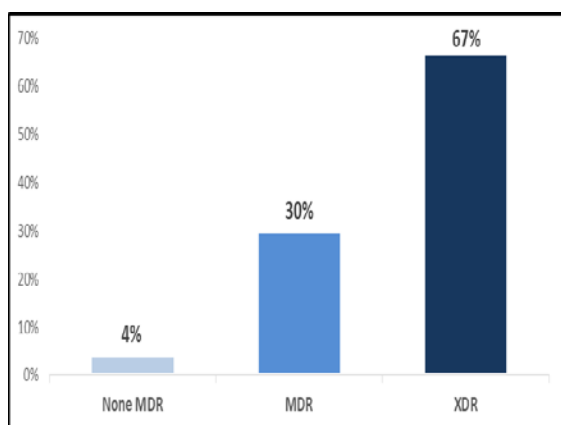


Figure 3. Distribution of *A. baumannii* isolates according to their pattern of resistance

3.3. Biofilm analysis

The microplate method was considered to evaluate capability of the *A. baumannii* strains to form biofilms. Results indicated that while 11% of the strains were marked as potent biofilm producers, 48% and 41% were labeled as moderate and weak biofilm formers as presented in figure (4).

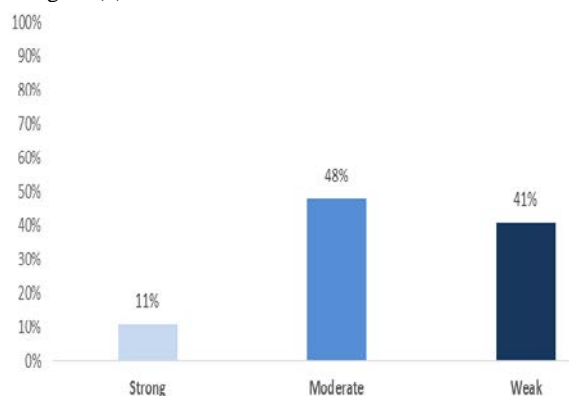


Figure 4. Percentage of the biofilm development status of isolates based on results obtained from the microtiter plate method.

3.4. Biosynthesis and characterization of nano-silvers

The standard strain of *Pseudomonas aeruginosa* ATCC 50126 was utilized to manufacture the AgNPs biologically. Following incubation at 60 °C for 72 hours, a switch in the reaction-mixture color from pale yellow to deep brown manifested was viewed as the initial indicator for the presence of nano-silver. UV-vis spectroscopy was employed to confirm the bio-reduction of AgNO₃ to AgNPs. Absorption peak at 268 nm was observed for the silver-nitrate solution solely; however, after 72 hours of incubation with the cell-free supernatant this peak vanished, and a new peak was observed at 420 nm indicating the formation of PA-AgNPs as observed in figure (5).

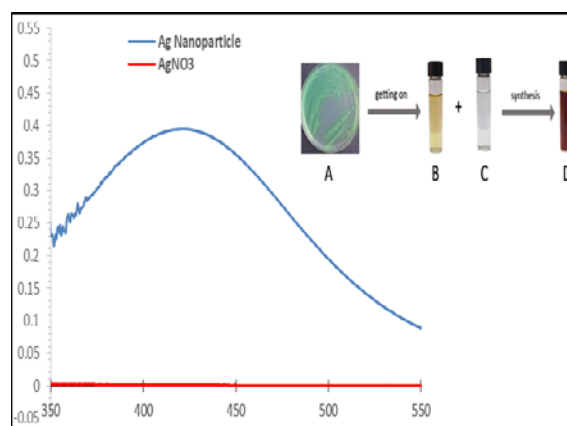


Figure 5. UV-Vis spectrum of bio-fabricated AgNPs and demonstration of AgNPs bio-fabrication: (A) *P. aeruginosa* ATCC 50126; (B) cell-free supernatant; (C) AgNO₃; (D) reduction of silver ion to nanoparticle.

3.5. FTIR analysis

FTIR measurements in the range of 400 to 4000 cm⁻¹ were conducted in order to identify functional groups in the biological compounds that may be implicated in the bio-reduction of AgNO₃, and bio-capping of nano-silver. FTIR spectra of the biosynthesized PA-AgNPs were compared with the standard values to detect functional groups. Hence, obtained bands at 3266, 2136, 1735, 1635, 1369, and 1218 cm⁻¹ were analogous to the O-H (alcohol), C≡C (alkyne), C=O (carbonyl), C double bond (alkene), C-H (alkane) and C-O for (carboxylic acids, ethers, alcohols, esters) stretching vibrations (Figure 6).

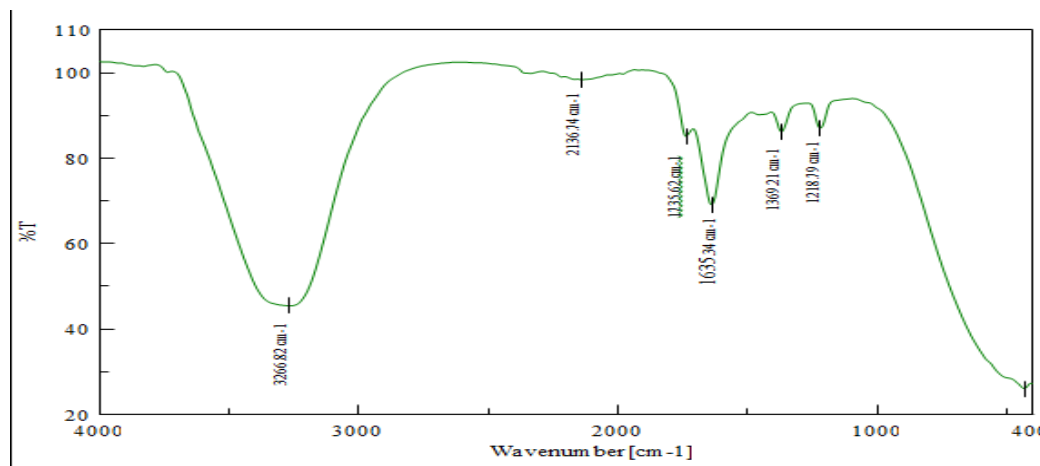


Figure 6. FTIR spectra of *P. aeruginosa* synthesized silver nanoparticles.

3.6. XRD

Crystal-like nature of the PA-AgNPs was confirmed via XRD analysis. Figure (7) represents XRD pattern of our sample which shows 8 distinct peaks at 2θ of 27.219, 31.674, 45.707, 54.333, 56.954, 66.941, 74.025 and 76.242 corresponding to 111, 200, 311, 222, 400, 331, 420 and 422 planes of face-centered-cubic silver nanoparticles respectively. These findings were further supported by the international center for diffraction data (JCPDS no. 98-005-6538). The Debye-Scherrer formula was employed to calculate crystallite size from the XRD data, and the average crystallite size was 28.32nm.

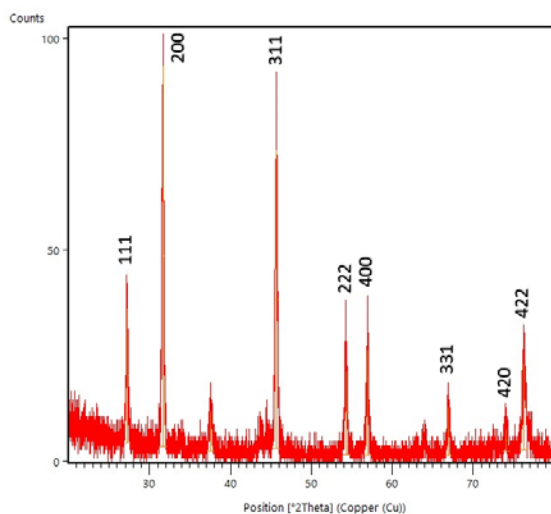


Figure 7. XRD spectra of biosynthesized silver nanoparticle.

3.7. SEM and EDAX

SEM instrument was utilized to study the surface morphology and size of PA-AgNPs which appeared to be spherically shaped and polydispersed with a size range of 45nm to 50 nm (Figure 8).

Furthermore, EDAX was operated to inspect the elemental makeup of the bio-fabricated PA-AgNPs. From figure (9), we can observe an intense absorption peak at 3 KeV suggesting the presence of metallic AgNPs. In addition to silver, we can also observe chlorine peak. Total weight of the element silver was found to be 84.15% whereas chlorine was 15.85%.

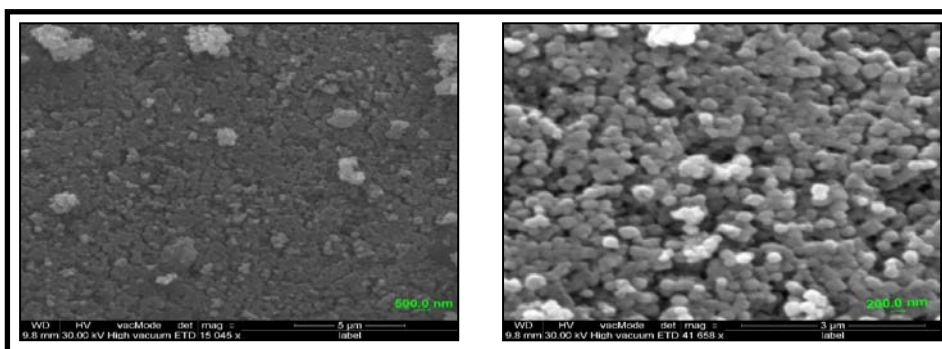


Figure 8. SEM micrograph of biosynthesized PA-AgNPs.

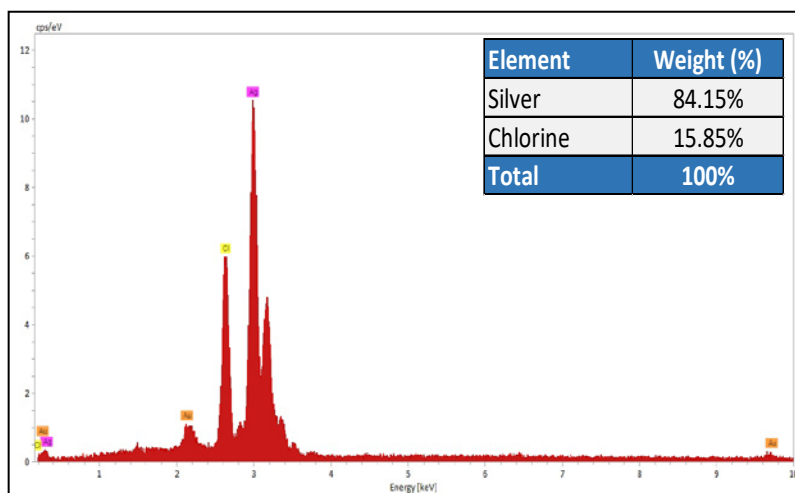


Figure 9. EDAX profile of green synthesized AgNPs.

3.8. Effect of biogenic silver nanoparticle on the isolates at SIC

To analyze antibiofilm potential of the bacteriogenic nano-silvers in the tested isolates at SIC, we first needed to unveil the MIC values of the bio-fabricated AgNPs via broth-microdilution technique. For this purpose, 10 of the strongest biofilm-producing isolates along with an ATCC strain were employed and the results showed MIC values between 10 to 20 mg/ml along with respective SIC values of 5 to 10 mg/ml as detailed in table (3).

Table 3. Minimum-inhibitory concentrations (MICs) and Sub-MICs of biogenic PA-AgNPs of MDR *A. baumannii*.

Bacterial isolates	MIC (mg/ml)	Sub-MIC (mg/ml)
3	10	5
5	20	10
6	20	10
11	20	10
13	20	10
14	10	5
16	10	5
20	20	10
21	20	10
23	20	10
ATCC (19606)	20	10

The influence of the bio-formulated AgNPs on the capacity of the selected strains to develop biofilm at SIC values was elucidated via microplate protocol, and the results indicated that exposure to the PA-AgNPs significantly ($P < 0.0001$) lowered biofilm production in all of the selected isolates as observed in figure (10).

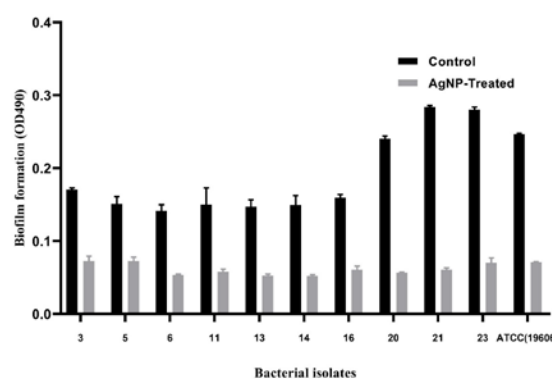


Figure 10. Quantitative measurement of *Acinetobacter baumannii* biofilm reduction by SIC of biogenic PA-AgNPs. Data are displayed as (mean±SE). All data are significant at $P < 0.0001$.

3.9. Impact of PA-AgNPs on biofilm and virulence related gene expression of *A. baumannii*

The level of gene-expression for each of the candidate genes was evaluated in the selected isolates in the presence and absence of PA-AgNPs using qPCR. Following analysis of the obtained results, we indicated that PA-AgNPs affected the tested isolates differently as observed in figure (11). The expression level of all candidate genes in samples A2 and A3 were down-regulated significantly following exposure to PA-AgNPs. However, the *Bap* gene was not affected in sample A1. Interestingly, neither QS genes nor *OmpA* gene were down-regulated in the ATCC sample treated with PA-AgNPs.

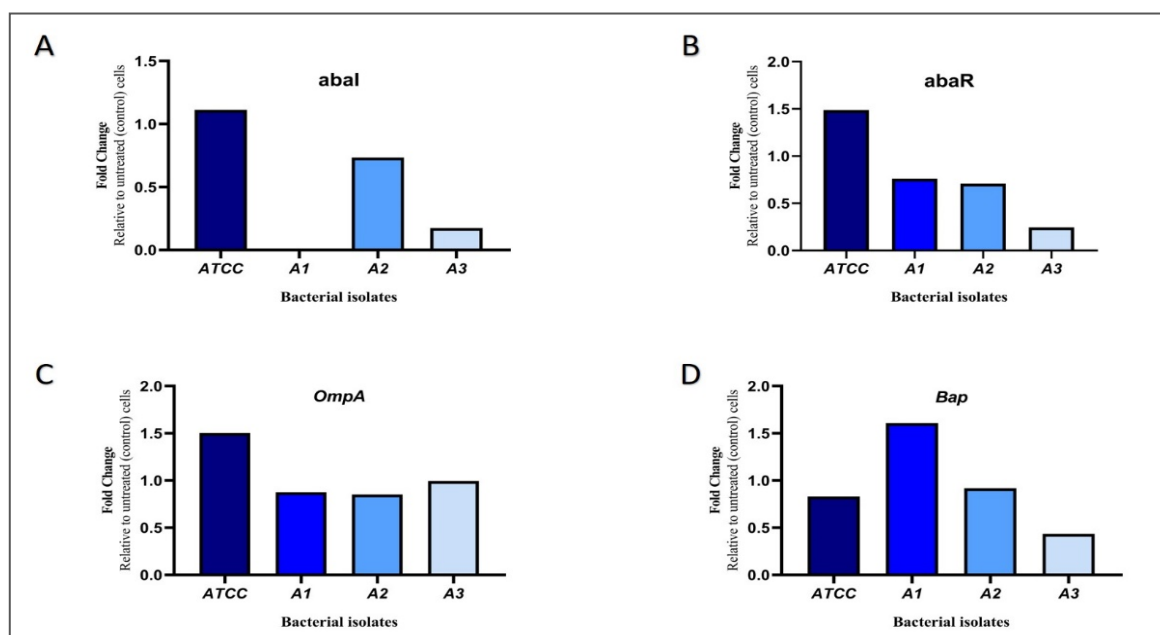


Figure 11. Fold change in the expression level of candidate genes (*abaI*, *abaR*, *OmpA*, *Bap*) in the treated bacterial isolates relative to untreated control cells.

4. Discussion

Currently, drug resistance is regarded as a major problem posing threat to not just global health but also to development and food security (Nji *et al.*, 2021). *Acinetobacter baumannii* (*A. baumannii*) is equipped with a repertoire of virulence factors that enable the bacteria to cause a series of life-threatening infections and resist stressful environmental circumstances (Ayoub Moubareck and Hammoudi Halat, 2020). They can cause infections in various sites in the body such as urinary-tract infections, wound infections, pneumonia, meningitis, and septicemia (Hetta *et al.*, 2021; Ayoub Moubareck and Hammoudi Halat, 2020). In the current study, we collected 26 clinical isolates in which the majority were recovered from sputum followed by wound, blood, and CSF specimens as observed in figure (1). Similarly in a recent study from Iraq 38 *A. baumannii* isolates were collected out of which 32% were recovered from sputum followed by 29% swabs, 21% urine, 13% blood, and 5% fluid (Muhsin *et al.*, 2022). The reason for the isolation of the bacteria from sputum at a higher percentage could be due to the tendency of the pathogen to infect the respiratory-tract most commonly (Li *et al.*, 2017). Various adhesins and the ability to develop biofilm participate greatly in their pathogenesis and resistance to antibiotics (Ghasemian *et al.*, 2019). Also, it is well-known that the bacteria living in biofilm are able to resist antibiotics 1000 fold higher than the free-living or planktonic bacteria, which in turn minimizes our choices for an effective antibiotic therapy (Hall and Mah, 2017). In this regard, all of our isolates produced biofilm and showed resistance to the tested antibiotics at varying degrees. Forty-eight percentage of our isolates were recorded as moderate biofilm producers while 11% and 41% were strong and weak biofilm producers as illustrated in figure (4). These observations agree with the findings of another study in which 100% of the isolates produced biofilm and the majority were reported to be moderate biofilm producers (Sherif *et al.*, 2021). In the present

study, 67% of the strains were categorized as XDR as seen in figure (3). A similar resistance pattern was reported by Maspi *et al* where 71.2% of the confirmed *A. baumannii* isolates were XDR (Maspi *et al.*, 2016). Among the 14 tested antibiotics, highest level of resistance was observed against cefepime and ceftazidime where all isolates exhibited 100% resistance followed by 96% to amikacin and maximum susceptibility (56%) was shown against ampicillin/sulbactam as seen in figure (2). Our antibiotic susceptibility results are in line with a study from Tehran that reported the isolates to be resistant to majority of antibiotics including 100% resistance to cefepime and ceftazidime along with 90% resistance to amikacin (Khoshnood *et al.*, 2017). WHO has appointed *A. baumannii* as the most critical pathogen towards which investigation, discovery and development of new antibiotics are eagerly required (Ayoub Moubareck and Hammoudi Halat, 2020). In this regard, a number of reports have been issued in the last few decades highlighting the successful use of nanoparticles in particular AgNPs as an effective antibacterial agent (Kaur *et al.*, 2021). Compared to other nanoparticles, AgNPs are less toxic and are more effective in combating microorganisms; hence, they are studied more extensively and are viewed as the upcoming antibiotic generation. AgNPs are cytotoxic to microbes due to their ability to increase cell permeability by damaging both cell wall and cell membrane and cause internal damage through release of silver-ions that trigger oxidative stress and cell death through production of reactive-oxygen and interfering with vital processes of the cell (Mba and Nweze, 2021).

Bacteria synthesize biogenic nanoparticles either intracellularly or extracellularly in the presence of enzymes; however, extracellular production does not require added purification steps and is considered more cost-efficient (Nirmala and Sridevi, 2021). C-type cytochromes, reducing-cofactors, Ag-resistant genes,

peptides, and enzymes such as nitrate reductase empower the bacteria to reduce and stabilize silver ions to AgNPs (Singh *et al.*, 2015). In this aspect, studies were conducted by Oza *et al.* (2012) and Paul and Sinha (2014) where *Pseudomonas aeruginosa* (*P. aeruginosa*) was successfully used to synthesize well-dispersed AgNPs. In another part of the study, they confirmed the involvement of nitrate reductase as the reducing agent. Furthermore, Peiris and coworkers conducted a research where they compared the antimicrobial effect of nano-silvers synthesized by each of “*Escherichia coli*, *A. baumannii*, *Staphylococcus aureus*, *P. aeruginosa*” and they indicated most stable AgNPs were bio-fabricated by *P. aeruginosa* that showed broad antimicrobial effect (Peiris *et al.*, 2018). Consequently, we chose *P. aeruginosa* for extracellular synthesis of AgNPs. From figure (5), we can observe the shade of the reaction-mixture swapped from pale yellow to dark brown following incubation which is thought to be due to a phenomena known as surface plasmon resonance and is regarded as an initial indicator for reduction of Ag-ion to nanoparticles (Nirmala and Sridevi, 2021). Occurrence of this characteristic brown color has also been reported previously by (Sunkar and Nachiyar, 2012). Spherically-shaped AgNPs with sizes ranging from 2 to 100 nm would be expected in case a single UV spectral band between 410 and 440 nm was observed (Haji *et al.*, 2022). In our study, we observed a single UV band at 420nm for our PA-AgNPs suggesting that our particles were spherical and parallel to SEM images. Similar observations were made by (Bhatt *et al.*, 2018) where they reported a single UV peak at 430 nm using cell free extract of *P. aeruginosa*. SEM observations indicate that our nanoparticles are uniform, spherical with little to no aggregation and size was ranged from 45 to 50 nm (Figure 8). Our findings reveal smaller particle sizes and better dispersity compared to (Peiris *et al.*, 2017) where majority of nanoparticles had size range of 50 to 100nm. Elemental-composition of the PA-AgNPs was investigated via EDX where we noticed intense absorption peak for silver at 3 Kev confirming formation of AgNPs (Ibrahim *et al.*, 2019). The results of EDX indicate higher distribution of silver element with a percentage of 84.15% in the green PA-AgNPs as demonstrated in figure (9). Presence of chlorine could be due to emissions from enzymes or proteins in the culture-supernatant (Kumar and Mamidyala, 2011). In agreement with our results, intense absorption peak at 3 Kev was observed by EDX analysis of *Pseudomonas* spp AgNPs (Punjabi *et al.*, 2017). FTIR was used to detect functional groups that could have led to bio-reduction of silver-ions. FTIR results seen in figure (6) revealed 6 peaks at 3266, 2136, 1735, 1635, 1369 and 1218 cm^{-1} parallel to O-H (alcohol), C≡C (alkyne), C=O (carbonyl), C double bond (alkene), C-H (alkane) and C-O for (carboxylic acids, ethers, alcohols, esters) stretching vibrations (Bhatt *et al.*, 2018). Overall, FTIR analysis indicated presence of a number of biomolecules that might have reduced and capped the green PA-AgNPs (Yang *et al.*, 2020). Fernando *et al.* also revealed presence of carbonyl and alkene groups following FTIR spectrum analysis of AgNPs synthesized by means of *P. aeruginosa* indicating stabilization of the nanoparticles with aid of proteins (Peiris *et al.*, 2017). In accordance with standard data, XRD analysis confirmed PA-AgNPs to be face-centered-cubic crystals. According to Ahmed *et al.*,

(2020), the intense labeled peaks observed in figure (7) are thought to be brought about by capping agents that stabilized the nanoparticle. In a recent study, XRD was also used to confirm AgNPs Crystalline nature synthesized by a *P. aeruginosa* strain (Yang *et al.*, 2020). Based on XRD data profile we ascertained average crystallite size of 28.32 nm using Scherer formula ($D=K\lambda/\beta\text{hklCos}\theta$) (Bindu and Thomas, 2014). Average crystallite size in this study was much smaller compared to a previous report that made use of Scherer formula to calculate crystallite size (Abootalebi *et al.*, 2021).

Recently, numerous studies delineated the antimicrobial effect of nanosized silver (Urnukhsaikhan *et al.*, 2021; Ali *et al.*, 2020). However, studies regarding the inhibitory impact of silver-based nanoparticles bio-fabricated by bacteria on biofilm formation and quorum signaling (QS) are scarce. The expression of numerous virulence factors is under the control of QS; hence, any interference with this system can lead to the downregulation of the virulence genes (Zhong and He, 2021).

Our results showed the antibiofilm ability of silver where SIC of PA-AgNPs greatly decreased the competency of the tested strains to construct biofilms as shown in figure (10). Accordant with our results, earlier reports also emphasized the role of AgNPs as a potent biofilm inhibitor (Slavin *et al.*, 2021). The anti-biofilm and anti-QS effect of our PA-AgNPs were evaluated using relative RT-PCR. We observed that exposure of the tested isolates to SIC values of PA-AgNPs greatly affected the expression of the candidate genes as observed in figure (11). A number of genes including *Bap*, *abal*, and *OmpA* are believed to participate in the development of biofilm in *A. baumannii* (Dolma *et al.*, 2022). Downregulation of each of *Bap*, *abal*, and *OmpA* genes may lead to the inhibition of biofilm (Nie *et al.*, 2020; Alejandro *et al.*, 2018). Moreover, a number of reports previously stated a decrease in the ability of the bacteria to develop biofilm following inhibition of *abaR* gene (Sun and Xiang, 2021). Hence, the decline observed in the ability of our clinical isolates to develop biofilm maybe due to disruption in the expression of *Bap*, *OmpA*, and QS genes. Inhibition of QS genes by means of a chemical AgNPs was lately reported in a study (Hetta *et al.*, 2021). However, the current study represents the first report regarding the anti-biofilm/anti-QS effect of green AgNPs synthesized by means of *P. aeruginosa* in opposition to clinical *A. baumannii*. Due to time limitations, economic burden and shortage in the quantity of the nanoparticles, we could not operate transmission electron microscopy (TEM) for our nanoparticles since it needed to be sent abroad; nor could we include more strains to examine the AgNPs effect on level of gene expression.

5. Conclusion

Reinforced by the experimental outcomes of this study, we conclude that *P. aeruginosa* can be used to bio-fabricate AgNPs (PA-AgNPs) in an efficient and cost-effective manner. The majority of our clinical isolates portrayed elevated resistance to the selected antimicrobials and were all competent to construct biofilms at varying degrees. Exposure of the isolates to PA-AgNPs at SIC greatly reduced their ability to form biofilm. Furthermore,

PA-AgNPs treated isolates exhibited pronounced reduction in the level of QS, *OmpA* and *Bap* genes expression which are culpable for the development of resistance and biofilm in *A. baumannii*. Hence, anti-QS anti-biofilm results of the green AgNPs obtained from the current study could pave the way for their use as a promising nanomaterial in the battle against the critical pathogen *A. baumannii* through interfering with their QS mechanism.

Author contribution

AA outlined research; TI & AA conducted research and analyzed data; TI wrote the paper; AA superintended the study and edited the paper. TI & AA read and approved the final version of the manuscript.

Data Availability

The data used to support the findings of this study are included within the article.

Conflict of interest

All authors declared no conflict of interest in the present manuscript.

Funding Statement

No funding.

References

- Abootelebi S, Mousavi SM, Hashemi SA, Shorafa E, Omidifar N & Gholami A. 2021. Antibacterial effect of green synthesized silver nanoparticles using ferula assafoetida against *Acinetobacter baumannii* isolated from the hospital and their cytotoxicity on the human cell line. *J. Nanomater*, **2021**: 1-12.
- Ahmed AA and Salih FA. 2019. Quercus infectoria gall extracts reduce quorum sensing-controlled virulence factors production and biofilm formation in *Pseudomonas aeruginosa* recovered from burn wounds. *BMC Complement Altern Med*, **19** (1): 1-11.
- Ahmed FY, Aly UF, Abd El-Baky RM and Waly NG. 2020. Comparative study of antibacterial effects of titanium dioxide nanoparticles alone and in combination with antibiotics on mdr *Pseudomonas aeruginosa* strains. *Int J Nanomedicine*, **15**: 3393-3404.
- Alejandro H-MD, Humberto M-OM, Fidel G-L, Antonio G-LM and Eduardo S-G. 2018. Inhibition of *Acinetobacter baumannii* biofilm formation by methanolic extract of *Nothoscordum bivalve*. *Adv Microbiol*, **8**(5): 422-438.
- Ali Z, Mirani DZ, Urooj S, Khan M, Khan AB, Shaikh I, Siddiqui A and Za M. 2020. An effective weapon against biofilm consortia and small colony variants of MRSA. *Iran J Basic Med Sci*, **23**: 1494-1498.
- Amin M, Navidifar T, Shooshtari FS, Rashno M, Savari M, Jahangirmehr F and Arshadi M. 2019. Association between biofilm formation, structure, and the expression levels of genes related to biofilm formation and biofilm-specific resistance of *Acinetobacter baumannii* strains isolated from burn infection in ahvaz, iran. *Infect Drug Resist*, **12**: 3867-3881.
- Aslam B, Khurshid M, Arshad MI, Muzammil S, Rasool M, Yasmeen N, Shah T, Chaudhry TH, Rasool MH, Shahid A, Xueshan X and Baloch Z. 2021. Antibiotic resistance: One health one world outlook. *Front Cell Infect Microbiol*, **11**: 1-20.
- Ayoub Moubareck C and Hammoudi Halat D. 2020. Insights into *Acinetobacter baumannii*: A review of microbiological, virulence, and resistance traits in a threatening nosocomial pathogen. *Antibiotics (Basel)*, **9**(3): 1-28.
- Ball AS, Patil S and Soni S. 2019. Introduction into nanotechnology and microbiology. *Methods Microbiol*, **46**: 1-18.
- Bhatt D, Gupta E, Kaushik S, Srivastava VK, Saxena J and Jyoti A. 2018. Bio-fabrication of silver nanoparticles by *Pseudomonas aeruginosa*: Optimisation and antibacterial activity against selected waterborne human pathogens. *IET Nanobiotechnol*, **12**(7): 981-986.
- Bindu P and Thomas S. 2014. Estimation of lattice strain in ZnO nanoparticles: X-ray peak profile analysis. *J Theor Appl Phys*, **8**(4): 123-134.
- Busi S and Rajkumari J. 2019. **Microbially synthesized nanoparticles as next generation antimicrobials: Scope and applications**, in *Nanoparticles in Pharmacotherapy*, William Andrew Publishing.
- CDC. 2019. **Antibiotic resistance threats in the united states**. *Centers for Disease Control and Prevention*. Available: <https://www.cdc.gov/drugresistance/biggest-threats.html>.
- CLSI. 2018. **Methods for dilution antimicrobial susceptibility tests for bacteria that grow aerobically; approved standard. eleventh Edition**. *CLSI document M07*. Wayne, PA: Clinical and Laboratory Standards Institute.
- CLSI. 2022. **Performance standards for antimicrobial susceptibility testing**. Informational Supplement. *CLSI document M100Ed32E*. Wayne, PA: Clinical and Laboratory Standards Institute.
- Cui B, Chen X, Guo Q, Song S, Wang M, Liu J and Deng Y. 2022. The cell-cell communication signal indole controls the physiology and interspecies communication of *Acinetobacter baumannii*. *Microbiol Spectr*, **10**(4): 1-12.
- Dolma KG, Khatri R, Paul AK, Rahmatullah M, De Lourdes Pereira M, Wilairatana P, Khandelwal B, Gupta C, Gautam D, Gupta M, Goyal RK, Wiart C and Nissapatorn V. 2022. Virulence characteristics and emerging therapies for biofilm-forming *Acinetobacter baumannii*: A review. *Biology*, **11**(9): 1-20.
- García-Contreras R, Martínez-Vázquez M, González-Pedrajo B and Castillo-Juárez I. 2022. Editorial: Alternatives to combat bacterial infections. *Front Microbiol*, **13**: 1-5.
- Ghasemian A, Mobarez AM, Peerayeh SN and Bezmin Abadi AT. 2019. The association of surface adhesion genes and the biofilm formation among *Klebsiella oxytoca* clinical isolates. *New Microbes New Infect*, **27**: 36-39.
- Ghosh D, Veeraraghavan B, Elangovan R and Vivekanandan P. 2020. Antibiotic resistance and epigenetics: More to it than meets the eye. *Antimicrob Agents Chemother*, **64**(2): 1-27.
- Haji SH, Ali FA and Aka STH. 2022. Synergistic antibacterial activity of silver nanoparticles biosynthesized by carbapenem-resistant gram-negative bacilli. *Sci Rep*, **12**(1): 1-13.
- Hall CW and Mah T-F. 2017. Molecular mechanisms of biofilm-based antibiotic resistance and tolerance in pathogenic bacteria. *FEMS Microbiol Rev*, **41**(3): 276-301.
- Havenga B, Reyneke B, Waso-Reyneke M, Ndlovu T, Khan S and Khan W. 2022. Biological control of *Acinetobacter baumannii*: In vitro and in vivo activity, limitations, and combination therapies. *Microorganisms*, **10**(5): 1-25.
- Hetta HF, Al-Kadmy IMS, Khazaal SS, Abbas S, Suhail A, El-Mokhtar MA, Ellah NHA, Ahmed EA, Abd-Ellatif RB, El-Masry EA, Batiha GE, Elkady AA, Mohamed NA and Algamal AM. 2021. Antibiofilm and antivirulence potential of silver nanoparticles against multidrug-resistant *Acinetobacter baumannii*. *Sci Rep*, **11**(1): 1-11.

- Ibrahim E, Fouad H, Zhang M, Zhang Y, Qiu W, Yan C, Li B, Mo J and Chen J. 2019. Biosynthesis of silver nanoparticles using endophytic bacteria and their role in inhibition of rice pathogenic bacteria and plant growth promotion. *RSC Adv*, **9(50)**: 1-7.
- Ibrahim S, Al-Saryi N, Al-Kadmy IMS and Aziz SN 2021. Multidrug-resistant *Acinetobacter baumannii* as an emerging concern in hospitals. *Mol Biol Rep*, **48(10)**: 1-11.
- Iravani S. 2014. Bacteria in nanoparticle synthesis: Current status and future prospects. *Int Sch Res Notices*, **2014**: 1-19.
- Kaur K, Reddy S, Barathe P, Shriram V, Anand U, Proćków J and Kumar V. 2021. Combating drug-resistant bacteria using photothermally active nanomaterials: A perspective review. *Front Microbiol*, **12**: 1-18.
- Khoshnood S, Eslami G, Hashemi A, Bahramian A, Heidary M, Yousefi Nojookambari N, Mohammadi F and Gholami M. 2017. Distribution of aminoglycoside resistance genes among *Acinetobacter baumannii* strains isolated from burn patients in tehran, iran. *Iran Arch Pediatr Infect Dis*, **5(3)**: 1-5.
- Kumar CG and Mamidyala SK. 2011. Extracellular synthesis of silver nanoparticles using culture supernatant of *pseudomonas aeruginosa*. *Colloids Surf B Biointerfaces*, **84(2)**: 462-466.
- Kumar G, Srivastava A and Singh R. 2020. Impact of nanoparticles on genetic integrity of buckwheat (*fagopyrum esculentum moench*). *Jordan J Biol Sci*, **13(1)**: 13-17.
- Laws M, Shaaban A and Rahman KM. 2019. Antibiotic resistance breakers: Current approaches and future directions. *FEMS Microbiol Rev*, **43(5)**: 490-516.
- Lee C-R, Lee JH, Park M, Park KS, Bae IK, Kim YB, Cha C-J, Jeong BC and Lee SH. 2017. Biology of *Acinetobacter baumannii*: Pathogenesis, antibiotic resistance mechanisms, and prospective treatment options. *Front Cell Infect Microbiol*, **7**: 1-35.
- Li YJ, Pan CZ, Fang CQ, Zhao ZX, Chen HL, Guo PH and Zhao ZW. 2017. Pneumonia caused by extensive drug-resistant *Acinetobacter baumannii* among hospitalized patients: Genetic relationships, risk factors and mortality. *BMC Infect Dis*, **17(1)**: 1-10.
- Limban C, Marutescu L and Chifiriuc MC. 2011. Synthesis, spectroscopic properties and antipathogenic activity of new thiourea derivatives. *Molecules*, **16(9)**: 7593-7607.
- Mancuso G, Midiri A, Gerace E and Biondo C. 2021. Bacterial antibiotic resistance: The most critical pathogens. *Pathogens*, **10(10)**: 1-14.
- Maspi H, Mahmoodzadeh Hosseini H, Amin M and Imani Fooladi AA. 2016. High prevalence of extensively drug-resistant and metallo beta-lactamase-producing clinical *Acinetobacter baumannii* in iran. *Microb Pathog*, **98**: 155-159.
- Mba IE and Nweze EI. 2021. Nanoparticles as therapeutic options for treating multidrug-resistant bacteria: Research progress, challenges, and prospects. *World J Microbiol Biotechnol*, **37(6)**: 1-30.
- Muhsin SS, Bakir WaE and Sabbah MA. 2022. Identification and sequencing of isaba2 of *Acinetobacter baumannii* isolated from baghdad hospitals. *Mustansiriyah Med J*, **21(1)**: 29-36.
- Nie D, Hu Y, Chen Z, Li M, Hou Z, Luo X, Mao X and Xue X. 2020. Outer membrane protein a (ompA) as a potential therapeutic target for *Acinetobacter baumannii* infection. *J of Biomed Sci*, **27(1)**: 1-8.
- Nirmala C and Sridevi M. 2021. Characterization, antimicrobial and antioxidant evaluation of biofabricated silver nanoparticles from endophytic *Pantoea anthophila*. *J Inorg Organomet Polym Mater*, **31(9)**: 3711-3725.
- Nji E, Kazibwe J, Hambridge T, Joko CA, Larbi AA, Dampthey LaO, Nkansa-Gyamfi NA, Stålsby Lundborg C and Lien LTQ. 2021. High prevalence of antibiotic resistance in commensal *Escherichia coli* from healthy human sources in community settings. *Sci Rep*, **11(1)**: 1-11.
- Oza G, Pandey DS, Shah R and Sharon M. 2012. Extracellular fabrication of silver nanoparticles using *Pseudomonas aeruginosa* and its antimicrobial assay. *Adv Appl Sci Res*, **3**: 1776-1783.
- Papenfort K and Bassler BL. 2016. Quorum sensing signal-response systems in gram-negative bacteria. *Nat Rev Microbiol*, **14(9)**: 576-588.
- Paul D and Sinha SN. 2014. Extracellular synthesis of silver nanoparticles using *Pseudomonas aeruginosa* kupsb12 and its antibacterial activity. *Jordan J Biol Sci*, **7(4)**: 245-250.
- Pavani K, Poojitha GS and Beulah M. 2020. Phytotoxicity of zinc-oxide nanoparticles on seedling growth and antioxidant activity of red gram (*Cajanus cajan* L.) seed. *Jordan J Biol Sci*, **13**: 153-158.
- Peiris MK, Gunasekara CP, Jayaweera PM, Arachchi ND and Fernando N. 2017. Biosynthesized silver nanoparticles: Are they effective antimicrobials? *Mem Inst Oswaldo Cruz, Rio de Janeiro*, **112**: 537-543.
- Peiris MMK, Fernando N, Jayaweera P, Hegoda Arachchi N and Gunasekara C. 2018. Comparison of antimicrobial properties of silver nanoparticles synthesized from selected bacteria. *Indian J Microbiol*, **58**: 1-11.
- Punjabi K, Yedurkar S, Doshi S, Deshapande S and Vaidya S. 2017. Biosynthesis of silver nanoparticles by *Pseudomonas* spp. Isolated from effluent of an electroplating industry. *IET Nanobiotechnol*, **11(5)**: 584-590.
- Raorane CJ, Lee JH and Lee J. 2020. Rapid killing and biofilm inhibition of multidrug-resistant *Acinetobacter baumannii* strains and other microbes by iodoindoles. *Biomolecules*, **10(8)**: 1-13.
- Saipriya K, Swathi CH, Ratnakar KS and Sritharan V. 2020. Quorum-sensing system in *Acinetobacter baumannii*: A potential target for new drug development. *J Appl Microbiol*, **128(1)**: 15-27.
- Shah S, Gaikwad S, Nagar S, Kulshrestha S, Vaidya V, Nawani N and Pawar S. 2019. Biofilm inhibition and anti-quorum sensing activity of phytosynthesized silver nanoparticles against the nosocomial pathogen *Pseudomonas aeruginosa*. *Biofouling*, **35(1)**: 34-49.
- Sherif MM, Elkhatib WF, Khalaf WS, Elleboudy NS & Abdelaziz NA. 2021. Multidrug resistant *Acinetobacter baumannii* biofilms: Evaluation of phenotypic–genotypic association and susceptibility to cinnamic and gallic acids. *Front Microbiol*, **12**: 1-15.
- Singh R, Shedbalkar UU, Wadhvani SA and Chopade BA. 2015. Bacteriogenic silver nanoparticles: Synthesis, mechanism, and applications. *Appl Microbiol Biotechnol*, **99(11)**: 4579-4593.
- Singh R, Vora J, Nadhe SB, Wadhvani SA, Shedbalkar UU and Chopade BA. 2018. Antibacterial activities of bacteriogenic silver nanoparticles against nosocomial *Acinetobacter baumannii*. *J Nanosci Nanotechnol*, **18(6)**: 3806-3815.
- Slavin YN, Ivanova K, Hoyo J, Perelshtein I, Owen G, Haegert A, Lin Y-Y, Lebiha S, Gedanken A, Häfeli UO, Tzanov T and Bach H. 2021. Novel lignin-capped silver nanoparticles against multidrug-resistant bacteria. *ACS Appl Mater Interfaces*, **13(19)**: 22098-22109.
- Sun X and Xiang J. 2021. Mechanism underlying the role of luxR family transcriptional regulator abar in biofilm formation by *Acinetobacter baumannii*. *Curr Microbiol*, **78(11)**: 3936-3944.
- Sunkar S and Nachiyar CV. 2012. Biogenesis of antibacterial silver nanoparticles using the endophytic bacterium *Bacillus cereus* isolated from *Garcinia xanthochymus*. *Asian Pac J Trop Biomed*, **2(12)**: 953-959.

Tang J, Chen Y, Wang X, Ding Y, Sun X and Ni Z. 2020. Contribution of the *abaI/abaR* quorum sensing system to resistance and virulence of *Acinetobacter baumannii* clinical strains. *Infect Drug Resist*, **13**: 4273-4281.

Tille PM. 2021. **Bailey & Scott's Diagnostic Microbiology**, 15th edition. Elsevier/Mosby, China.

Uddin TM, Chakraborty AJ, Khusro A, Zidan BMRM, Mitra S, Emran TB, Dhama K, Ripon MKH, Gajdács M, Sahibzada MUK, Hossain MJ and Koirala N. 2021. Antibiotic resistance in microbes: History, mechanisms, therapeutic strategies and future prospects. *J Infect Public Health*, **14(12)**: 1750-1766.

Urnuksaikhon E, Bold B-E, Gunbileg A, Sukhbaatar N and Mishig-Ochir T. 2021. Antibacterial activity and characteristics of silver nanoparticles biosynthesized from *carduus crispus*. *Sci Rep*, **11(1)**: 1-12.

Ventola CL. 2015. The antibiotic resistance crisis: Part 1: Causes and threats. *P T*, **40(4)**: 277-283.

Yang J, Wang Q, Wang C, Yang R, Ahmed M, Kumaran S, Velu P and Li B. 2020. *Pseudomonas aeruginosa* synthesized silver nanoparticles inhibit cell proliferation and induce *ros* mediated apoptosis in thyroid cancer cell line (tpc1). *Artif Cells Nanomed Biotechnol*, **48(1)**: 800-809.

Zhong S and He S. 2021. Quorum sensing inhibition or quenching in *Acinetobacter baumannii*: The novel therapeutic strategies for new drug development. *Front Microbiol*, **12**: 1-7.

Effects of Reducing Browning on the Somatic Embryogenesis of *Coffea arabica*

Jarinya Hongwiangchanand Noppamart Lokkamlue*

Department of Science and Bioinnovation, Faculty of Liberal Arts and Science, Kasetsart University Kamphaeng Saen Campus, Nakhon Pathom 73140, Thailand

Received: November 29, 2022; Revised: March 6, 2023; Accepted: April 6, 2023

Abstract

The browning of plant tissues is a major constraint in plant tissue culture. This is especially true for embryogenic cells grown on a culture medium to produce true-to-type hybrid coffee via somatic embryogenesis. There is very little information in the current literature of the rate of browning intensity involved in the development stage of coffee callus. We investigated the use of the antioxidant cysteine (Cys) and activated charcoal (AC) to induce callus formation, reduce browning of the callus, and induce somatic embryos of *Coffea arabica*. Explants were cultured on MS media supplemented with Cys and AC. The study involved varying the Cys rates in the order of 30, 35, and 40 mg/L, as well as varying the AC rates in the order of 0.008%, 0.01%, and 0.08% (w/v). The statistical analysis of the results was performed using the Statistical Package for Social Sciences (SPSS) version 14, with a significance level set at $p < 0.05$. Neither anti-browning agent increased the rate of callus induction. The use of MS+1 μM 2,4-dichlorophenoxyacetic acid (2,4-D) +5 μM 6-benzyl adenine (BA) media supplemented with 30 or 35 mg/L Cys or 0.008% AC reduced the rate of tissue browning and induced a high rate of somatic embryo (SE) induction (80%, 84.21%, and 65%, respectively). SE treated with 30 mg/L Cys could be germinated to the asynchronous developmental stages within six months. They could be converted to mature plantlets on MS without plant growth regulator hormones. Therefore, the use of Cys and AC could be valuable for the propagation of *Coffea arabica* L. cv. Catimor CIFC 7963.

Keywords: Activated charcoal, Antioxidants, Callus, Somatic embryo, Catimor CIFC 7963, Phenolic compounds, Leaf explant, Cysteine

1. Introduction

Coffee (*Coffea arabica* L.) is one of the main agricultural exports of Thailand. Seed propagation results in uncontrolled genetic variation due to heterozygosity of coffee. The conventional method of coffee propagation, using vegetative grafting or rooting of cuttings, produces greater genetic uniformity, but this approach is the high production cost of plantlets for large-scale production (Etienne *et al.*, 2018). Somatic embryogenesis technique is used to mass-produce hundreds of thousands of hybrid plantlets that are true-to-type, reducing production costs compared to conventional methods (Landey *et al.*, 2013; Etienne *et al.*, 2016). *In vitro* propagation, the darkening of culture medium is a problem. Darkening of the culture medium has been attributed to phenolic compounds exuded from the excised portion of explants and accumulated in the culture medium. Phenolic compounds are secondary metabolites possessing one or more aromatic rings, with one or more hydroxyl groups. Many plants have developed defense mechanisms to protect themselves from microbial infection. One such mechanism is the production of antibacterial compounds found in phenolic compounds of medicinal plants (de León and Montesano, 2013; Al-Ghamdi *et al.*, 2020). Phenolic compounds are exuded in

tissue culture protocols that involve wounding during explant transfer and culturing in stressful environments (Jones and Saxena, 2013). The medium in which explants are grown becomes colored. The browning developed during the culture of callus is due to the quinones (browning pigments), which are toxic to plant tissues leading to the death of tissue. This process involves the polyphenol oxidase (PPO) catalyzing the oxidation of phenolic compounds by oxygen to give the quinones (Schieber, 2018; Wen *et al.*, 2020). PPO activity is affected by the type and amounts of endogenous phenolic compounds, the presence of oxygen, and the pH in the plant cell (Moon *et al.*, 2020). This enzyme is most abundant in young plant cells, which are removed from young mother plants for somatic embryogenesis production (Beena *et al.*, 2014; Taranto *et al.*, 2017).

At present, *C. arabica* cv. Catimor CIFC 7963 has been reported exhibiting the characteristics of leaf rust resistance in Thailand (Rittisang and Lokkamlue, 2020). However, coffee has a long seed-breeding cycle of up to five years and the tissue culture method allows easy maintenance of the desirable traits of coffee. The somatic embryogenesis might be the most effective technique because of its potential for producing the highest rate of multiplication. In a previous experiment, we found that most coffee calli were dark brown during culture, resulting in a 61% rate of somatic embryo (SE) induction (Rittisang

* Corresponding author. e-mail: faasnmlo@ku.ac.th.

and Lokkamlue, 2020). Therefore, phenolic compound accumulation is a serious concern for coffee cell development if a callus with minimized phenolic compound accumulation is necessary for the successful induction of coffee SE.

Most strategies for controlling tissue browning involve either the inhibition of PPO activity or the conversion of quinones to colorless adducts. The chemicals used to inhibit PPO activity are classified as competitive inhibitors, chelating agents, or acidulants, while the antioxidants prevent the formation of browning pigment by binding to intermediates (Brütsch *et al.*, 2018).

Cysteine (2-amino-3-mercaptopropionic acid), a thiol compound, has been investigated as an anti-browning agent, which reduces quinones to their phenol precursors or colorless adducts, and is dependent on environment factors (Ioannou and Ghol, 2013; Ali *et al.*, 2015; Ali *et al.*, 2016). The cysteinyl-catechol conjugate directly inhibits PPO and produces some browning inhibition by forming peptide side chains (Ali *et al.*, 2015). Therefore, cysteine may act as a PPO inhibitor, or may react with quinone to give a colorless adduct (Cabezas-Serrano *et al.*, 2013; Ali *et al.*, 2015). Cysteine acts as a competitive PPO inhibitor at low concentrations, while at high concentrations it can react with the assay product, quinone, to produce a colorless adduct (Ali *et al.*, 2015).

Activated charcoal (AC) is frequently added to culture medium to reduce the concentration of toxic compounds or improve the morphogenic responses of explants. The use of AC as a component of the culture medium reduces the incidence of tissue browning, which can lead to loss of explants, and its omission has been shown to seriously compromise the efficiency of the process. Furthermore, the excised explants significantly increased phenolic compound excretion (Jones and Saxena, 2013). AC also absorbs the phenolic compounds, which initially leach into the medium from the excised portions of the explants (Sashikesh *et al.*, 2023).

Coffee contains a high concentration of phenolic compounds that cause the browning process (Ahmad *et al.*, 2013). Therefore, understanding the processes contributing to the oxidation of phenolic compounds, and the way in which these processes can be minimized when initiating explants is critical for successful induction of somatic embryogenesis. Gallego Rúa *et al.* (2016) found that SEs were able to regenerate effectively in a medium-low level of polyphenols, and polyphenols were distributed in the periphery of the embryo epidermal layer. In the non-regenerating variety, embryogenic calli were compact, and contained polyphenols randomly distributed across all tissues. Therefore, the embryogenic capacity seems to be associated with a balanced concentration and distribution of polyphenols (Gallego Rúa *et al.*, 2016). At the end of the embryo induction step, high concentrations of polyphenols lead to a non-regenerating response of SEs (Gallego Rúa *et al.*, 2016). The occurrence of browning in plant tissue culture is unpredictable due to genotypic variation (Jones and Saxena, 2013). There are few reports related to *C. arabica* cv. Catimor CIFIC 7963 grown in *in vitro* culture. Moreover, considering that the biochemical alterations during cell differentiation have not yet been studied, very little information is available on whether the optimum accumulation of phenolics under low light intensity is associated with the developmental stage of *C. arabica* cv.

Catimor CIFIC 7963. The objective of this study was to determine the concentration of AC required for the adsorption of phenolic compounds and cysteine to reduce the browning of callus in *C. arabica* cv. Catimor CIFIC 7963, and evaluate its effects on callus formation and somatic embryogenesis.

2. Materials and Methods

2.1. Culture of explants on callus induction medium

Somatic embryogenesis of *Coffea arabica* cv. Catimor CIFIC 7963 purchased from Chiang Mai Royal Agricultural Research Center, Chiang Mai, Thailand, was induced from second leaves derived from the apices of the coffee plant *in vitro*. The leaves were cut into 40 pieces of 1 cm² and cultured on callus induction medium (CIM): MS medium (Calibre scientific company, Kansas, Lenexa, USA): 1 μM 2,4-D (Plant research institute Inc., Delaware, USA), 5 μM BA (Plant research institute Inc, Delaware, USA) solidified with 10 mg/L gelrite (Calibre scientific company, Kansas, Lenexa, USA). Before autoclaving, the pH was adjusted to a range of 5.7 to 5.8. Six treatments were used to evaluate the effect of concentrations of cysteine (Merck KGaA, Darmstadt, Germany) and activated charcoal (Calibre scientific company, Kansas, Lenexa, USA): 30 mg/L Cys, 35 mg/L Cys, 40 mg/L Cys, 0.008% w/v AC, 0.01% w/v AC, and 0.08% w/v AC. All media were adjusted to pH 5.7 to 5.8 before autoclaving for 15 min at 394.15 K. Petri dishes with 20 mL of culture media containing ten explants and five replicates were used. The cultures were incubated in the dark at 298.15 K ± 275.15 K and subcultured every four weeks for three months.

2.2. Evaluation of callus browning

After two months of culture, the calli were evaluated for browning using a protocol modified from Modeste *et al.* (2017). The browning intensity was assessed on an arbitrary scale of 1 to 4, where 1 = white callus without browning; 2 = 1% to 33% white callus higher than browning (low level); 3 = 34% to 66% browning callus higher than white callus (moderate to high level); 4 = 67% to 100% browning callus (highest level). The average value of browning rate was determined as equation (1)

Average scale of browning = sum of browning rating / total number of calli (1)

2.3. Evaluation of callus and SE induction

After two months of culturing, the calli were counted to calculate the rate of callus induction (RCI). For SE induction, the calli were subsequently cultured on CIM for one month. The rate of SE induction was determined and calculated for the rate of a somatic embryo (RSE). The RCI and RSE were calculated using equation (1) (Modeste *et al.*, 2017), and equation (2), respectively.

$$RCI = (\text{no. of the explants that induced calli} / \text{total no. of the explants cultured}) \times 100 \quad (1)$$

$$RSE = (\text{no. of the explant with SE} / \text{total no. of the explant with callus}) \times 100 \quad (2)$$

2.4. SE development of *C. arabica* cv. Catimor CIFIC 7963

During the development of SE, we transferred the embryogenic calli to embryogenic callus induction medium (ECIM): half-strength MS medium (1/2MS), 30

mg/L sucrose (Bio Basic Inc., Toronto, Canada), 20 mg/L thymine (Ajax Finechem Pty. Ltd., Taren Point, Australia), 20 mg/L glycine (Ajax Finechem Pty. Ltd., Taren Point, Australia), 1 mg/L niacin (Ajax Finechem Pty. Ltd., Taren Point, Australia), 200 mg/L myo-inositol (Himedia Laboratories Pvt. Ltd., Maharashtra, India), 40 mg/L L-cysteine, 200 mg/L casein hydrolysate (Himedia Laboratories Pvt. Ltd., Maharashtra, India), 800 mg/L malt extract (Becton, Dickinson and Company, Sparks, MD, USA) 60 mg/L adenine sulfate (Johnson Matthey Company, Istanbul, Turkey), 0.1 μ M BA, and solidified with 8 mg/L gelrite, for three months.

2.5. Germination and conversion of SEs into plantlets

The six-month-old 105 cotyledonary-stage embryos were cultured on MS medium without plant growth regulators (PGRs). All cultures were placed in a growth room for six months at $298.15 \pm 275.15 \text{ K}$ under light radiation of $30 \mu\text{mol.m}^{-2}.\text{s}^{-1}$ for a 16-hr photoperiod.

2.6. Statistical analysis

The results were analyzed using analysis of variance (ANOVA) with the Statistica 14.0 software. For unequal numbers, analysis of variance was performed using a generalized linear model. When a significant difference was observed between treatments, multiple range tests using one way ANOVAs at a 5% ($p < 0.05$) threshold were used to separate the averages.

3. Results

3.1. Callus induction in *C. arabica* cv. *Catimor C1FC 7963* leaf explants

One week after the leaf explant culture, cell division was induced in the leaf section in groups of small cells. The groups of small cells showed continuous development to callus after one month on MS media supplemented with 1

μM 2,4-D and 5 μM BA (CIM, control medium) with cysteine application of 30, 35, and 40 mg/L, and AC application of 0.008% and 0.01% (w/v). We obtained two-month-old compact and friable calli. However, it was observed that the CIM produced compact, rather than friable callus, while only CIM containing cysteine and AC improved friable callus induction (Figs. 1A–1C).

In the CIM containing 0.08% AC none of the groups of small cells showed development to callus (Fig. 1D). The experimental values of callus induction rate, addition of cysteine, and AC, showed no significant differences among the different concentrations or the CIM, but did have a significant effect on the 0.08% AC (Table 1). Increasing the concentration of AC beyond 0.01% resulted in decreased callus formation. AC appears to eliminate both undesirable compounds, thereby facilitating adsorption of hormones through the culture media. The highest induction rate (100%) was significantly improved over the rate derived from different media (37.5%) (Table 1).

Table 1. Effect of cysteine and AC on two-month-old callus in *C.*

Supplements	Concentration	Rates of callus induction (%RCI)
Control(CIM)	0	100 ^a
Cysteine	30 mg/L	100 ^a
	35 mg/L	100 ^a
	40 mg/L	100 ^a
AC	0.008%	100 ^a
	0.01%	100 ^a
	0.08%	37.5 ^{b*}

arabica cv. *Catimor C1FC 7963* leaf explants

Note: * Groups of small cells. ^{a,b} represent differences among treatment means within the same column ($p < 0.05$).

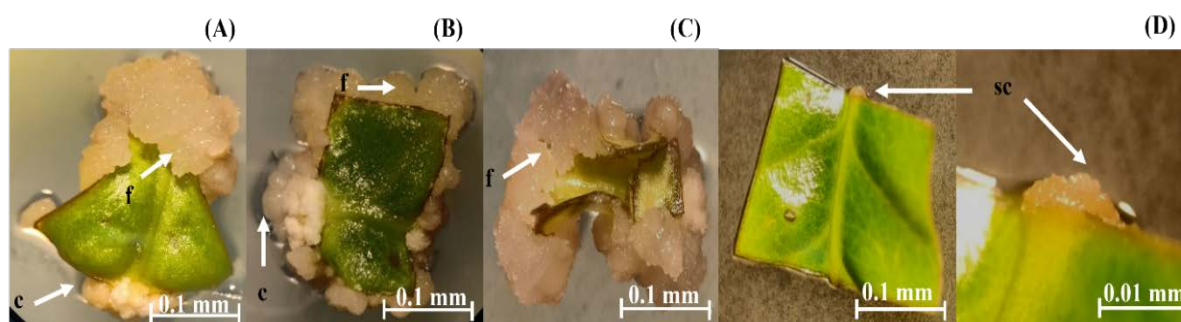


Figure 1. Friable callus (f), compact callus (c) and groups of small cells (sc) in *C. arabica* cv. *Catimor C1FC 7963* leaf explants on media after two months. (A) CIM (B) CIM + 30 mg/L cysteine (C) CIM + 0.008% AC (D) CIM + 0.08% AC.

3.2. Tissue browning intensity in *C. arabica* cv. *Catimor C1FC 7963* callus from leaf explants

All calli were cultured on media for two to three months. At the end of the second month, some yellowish calli had a brownish color, and green colored leaves presented as yellowish to brownish in the different types and concentrations of supplements (Fig. 2). The scale of browning of tissue was classified as 1 to 4, as described in Fig. 2. The reduction of callus browning depended on the type and the concentration of supplements. We found that the two-month-old calli derived from *C. arabica* cv. *Catimor C1FC 7963* leaf explants produced on

CIM containing no supplements exhibited the highest intensity of browning, and the callus browning rate was recorded as 3 on the scale discussed above. Concentrations of 30 and 35 mg/L cysteine and 0.008% AC produced a significant reduction of the callus browning rate, to scale 2. Among the concentrations of cysteine used, 40 mg/L resulted in an increase of callus browning intensity to scale 3. Similarly, the increased concentration of AC from 0.01% to 0.08%, had no effect on the reduction of browning callus. CIM containing 0.08% AC had the highest effect on the calli, reaching a scale of 4 (Table 2). High phenolic compounds may minimize the growth and stop embryonic development in non-differentiating callus. The number of

declining and dying cells increased in parallel with the increase in browning.

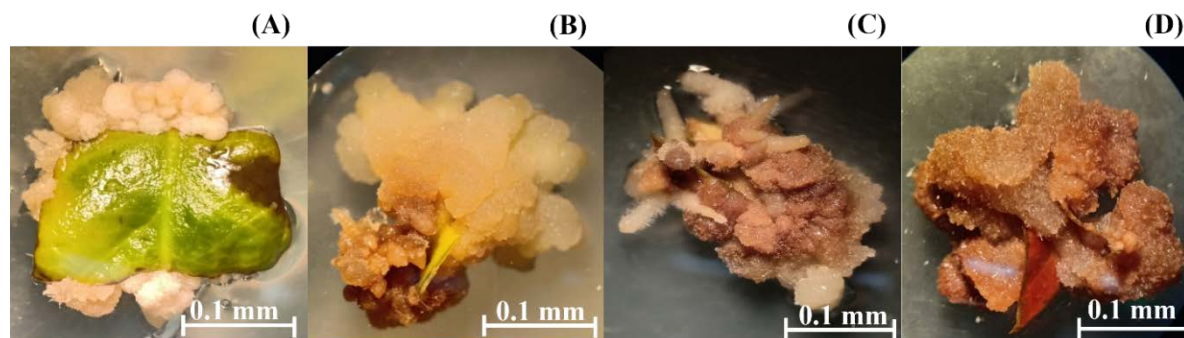


Figure 2. Two-month-old calli of *C. arabica* cv. Catimor CIFC 7963 leaf used for browning intensity assessment. (A) Without browning. (B) Browning intensities 1% to 33%. (C) Browning intensities 34% to 66%. (D) Browning intensities 67% to 100%.

Table 2. Browning intensity of two-month-old callus in *C. arabica* cv. Catimor CIFC 7963 leaf explants

Supplements	Concentration	Callus browning scale*
Control(CIM)	0	3
Cysteine	30 mg/L	2
	35 mg/L	2
	40 mg/L	3
AC	0.008%	2
	0.01%	3
	0.08%	4

*In column three, 2 corresponds to calli with 1% to 33% browning, 3 corresponds to calli with 34% to 66% browning, and 4 corresponds to calli with 67% to 100% browning.

3.3. Effect of cysteine and AC on SE induction in *C. arabica* cv. Catimor CIFC 7963 calli

Three months after explant culture, the induction of SEs was observed on CIM supplemented with anti-browning agents, followed by subsequent development of SEs on the ECIM. The results showed that after three to six months of culture, the SEs were characterized by asynchronous developmental stages (globular, heart, torpedo, and cotyledonary stages) and some calli produced

roots (Figs. 3A and 3B). The highest percentage of SE induction (84.21%) was observed on CIM supplemented with 35 mg/L cysteine, followed by CIM supplemented with 30 mg/L cysteine (80%). However, there was no significant difference in the RSE (Table 3). CIM and CIM supplemented with 0.008% AC also produced SE, but did induce lower percentages of RSE, at 61.54 and 65, respectively. AC appears to have been included as a component of the culture medium to prevent high incidences of tissue browning, which consequently leads to loss of cells in callus. Furthermore, it was shown that its omission mainly compromised the efficiency of the SE process. Increased concentrations of cysteine beyond 40 mg/L cysteine and 0.01% AC decreased the percentage of RSE (Table 3). We found that only SEs from CIM supplemented with 30 mg/L cysteine developed into differential sizes of cotyledonary embryos on ECIM after six months (Fig. 1B). The six-month-old cotyledonary embryos germinated, and 50 out of 105 embryos produced roots on MS without PGRs within one month (Fig. 1C), and then produced true leaves (Fig. 1D). We found that about half of the embryos lacked roots. This result indicated that most cotyledonary embryos were monopolar.

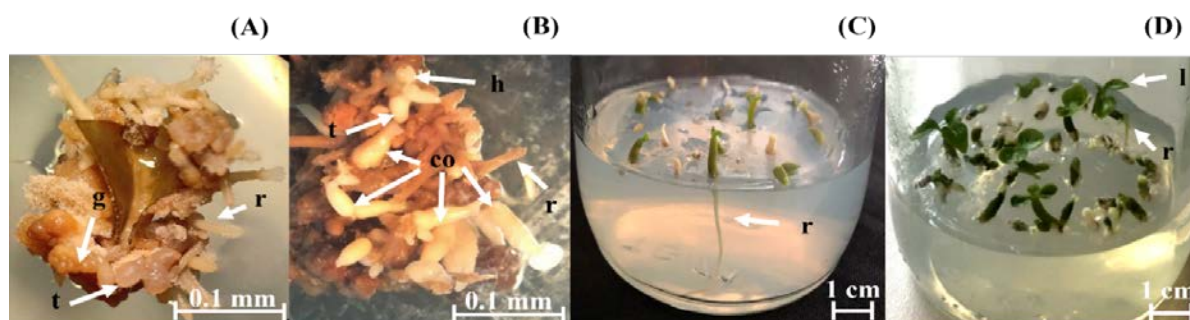


Figure 3. Somatic embryogenesis of *C. arabica* cv. Catimor CIFC 7963 embryogenic calli with roots (r). (A) stages of embryo: globular (g) and torpedo (t) embryos at three months. (B) Development of somatic embryos: torpedo (t), heart (h), and cotyledonary (co) embryos at six months. (C) Germination of six-month-old cotyledonary embryos at one month. (D) Regenerated plantlet with root and leaf (l) at two months.

Table 3.Rate of somatic embryo induction in *C. arabicacv.* Catimor C1FC 7963 calli at three months

Supplements	Concentration	Rate of somatic embryo (% RSE)
Control(C1M)	0	61.54 ^{ab}
Cysteine	30 mg/L	80 ^a
	35 mg/L	84.21 ^a
	40 mg/L	51.28 ^b
AC	0.008%	65 ^{ab}
	0.01%	12.5 ^c
	0.08%	0 ^c

Note: a,ab,b,c represent differences among treatment means within the same column ($p < 0.05$).



Figure 4. Mature plants of *C. arabicacv.* Catimor C1FC 7963 on MS medium from six-month-old cotyledonary embryos. (A) At six months. (B) At 12 months.

4. Discussion

We investigated total friable callus induction on culture medium with 0.008% AC. Adding 0.08% AC to the medium did not significantly promote the formation of callus. The addition of 0.01% to 0.08% AC decreased the number of SEs. It seems that the effect of AC is mainly due to the adsorption of substances such as 2,4-D and BA from the medium. Although AC has been reported to have a positive effect in other works (Abdulwahed, 2013), its presence may reduce the effectiveness of the medium for *in vitro* growth of the jojoba plant (*Simmondsia chinensis* L.) (Hassanein *et al.*, 2015).

There are also other factors that influence the SE response to AC concentration, such as plant species, cell density, cell cluster size, and cell lines used that modify the effect of AC adsorbing nutrient components from the culture medium (Das and Srivastav, 2015). However, AC also adsorbs high phenolic compounds (Gholizadeh *et al.*, 2013) produced by plant tissues that may inhibit embryogenesis and further embryo development. These results indicated that the embryogenesis of *C. arabicacv.* Catimor C1FC 7963 was dependent on the AC concentration in the medium.

We found both compact and friable callus induction on culture medium with cysteine. The culture medium supplemented with 35 mg/L cysteine had a balanced phenolic compound concentration, and produced the highest number of SEs. The total phenolic compound content was found to be highest in light roasted arabica coffee beans (de Souza *et al.*, 2020). However, the phenolic compounds produced from young leaf tissue showed browning of the callus, and the different stages of leaves showed significant differences in total phenolic compounds (Chen

3.4. Conversion of SEs into plantlets in *C. arabica cv.* Catimor C1FC 7963

In the present study, six-month-old cotyledonary embryos were converted into mature plantlets on MS medium without PGRs after six months. Our results showed that *C. arabicacv.* Catimor C1FC 7963 mature plantlets had well-developed shoot and root systems, and showed normal leaves (Fig. 4A). The plantlets showed varied growth due to the size of the cotyledonary embryos. The plantlets were cultured for a further six months, and the 12-month-old plantlets showed different developmental stages (Fig. 4B).

et al., 2018; Ngamsuk *et al.*, 2019). The possible role of these compounds in plant improvement via somatic embryogenesis has been examined in various plants, such as *Theobroma cacao* L. (Modeste *et al.*, 2017) and *Salacca sumatrana* Becc. (Elimasni *et al.*, 2020). The differential accumulation of phenolic compounds, in the culture medium of *C. arabica* could be a major cause of the interruption to the cell division pattern, affecting cellular proliferation and the process of somatic embryogenesis (Nic-Can *et al.*, 2015). The balanced concentration and distribution of polyphenols induces embryogenesis (Gallego Rúa *et al.*, 2016). Therefore, the reduced browning of coffee callus resulted from the secretion of phenolic compounds in scale 2 (callus with 1% to 33% of browning) affected SE induction (Tables 2 and 3). This result is consistent with those of Modeste *et al.* (2017), who reported that cocoa (*Theobroma cacao* L.) callus could be derived from petals. They also observed that somatic embryogenesis was more successful when calli were cultured in media supplemented with 8, 16, or 24 mg/L cysteine. We found that the browning rate of coffee callus treated with 35 mg/L cysteine appeared to reduce in comparison with that of the untreated control. Therefore, although the effect of 35 mg/L cysteine may be inhibiting the browning reaction caused by the formation of a colorless compound, it did not involve a direct inhibition on the PPO active site. Consistent with the report, cysteine's nucleophilic reactivity towards quinones inhibits enzymatic browning reactions, resulting in colorless products (Ali *et al.*, 2015). Furthermore, in the previous experiment, we discovered that secondary SEs developed from primary SEs. This is a valuable technique for regenerating embryo cells during plant gene transformation (Rittisang and Lekkamlue, 2020). During the gene transformation process in plant cells, wounding

occurs which leads to exudation of phenolic compounds. This phenomenon is a concern for transgenic cell development as accumulation of phenolic compounds can hinder the successful induction of transgenic coffee SEs and further study of genes involved in SE. Therefore, it is important to minimize phenolic compound accumulation in callus during the gene transformation protocol to achieve successful transgenic SE induction.

We found that only treatment with 30 mg/L cysteine resulted in the conversion of SEs to plantlets. We found that half of the embryos lacked roots, a lower rate than the two-thirds found in previous research (Rittisang and Lekkamlue, 2020). We should further culture these embryos on a suitable rooting medium to produce more coffee plants. The rooting process of SEs in *C. arabica* cv. Catimor CIFC 7963 can be improved by using an optimum concentration of cysteine. The conversion of six-month-old cotyledonary embryos into mature plantlets takes about six months, which is in line with previous research that also found a conversion time of around seven months (Rittisang and Lekkamlue, 2020). We identified different developmental stages of plantlets, with more leave and roots, after culture at 12 months as all embryonic stages were observed simultaneously in the same callus since the differentiation occurred asynchronously (Figs. 3A and 3B). This result suggested that plantlets with well-developed leaves and roots had more efficient photosynthesis and a better supply of water and nutrients from the environment under such drought conditions (Yao et al., 2017; Saghiaesh and Souri, 2018).

5. Conclusion

The addition of the anti-browning agents cysteine and ACToMS + 1 μ M 2,4-D + 5 μ MBA medium had no significant effect on callus induction in *C. arabica* cv. Catimor CIFC 7963. Callus browning was reduced in the presence of anti-browning agents, to different extents. The best results for reducing the browning intensity of callus at scale 2 (amount of brown callus < that of white callus) were obtained at concentrations of cysteine of 30 or 35 mg/L and 0.008% AC. This intensity level of browning releases a balanced amount of phenolic compounds, promoting somatic embryogenesis. Moreover, treatment with 30 mg/L cysteine improved the rate of somatic embryogenesis and produced embryos of different stages. This protocol could improve *in vitro* propagation and reduce the cost of producing *C. arabica* cv. Catimor CIFC 7963 plantlets by increasing the reliability of the rooting process in coffee SEs without rooting hormones on culture medium.

Acknowledgements

The authors gratefully acknowledge the grant provided by the Faculty of Liberal Arts and Science and Kasetsart University Kamphaeng Saen Campus, Thailand, and the necessary facilities provided by the Department of Science and Bioinnovation.

References

- Abdulwahed MS. 2013. Identification of the effect of different levels of activated charcoal and sucrose on multiplication shoots of date palm *Phoenix dactylifera* L. cv. Sufedy *in vitro*. *J Horticult For.*, **5**: 139–145. <https://doi.org/10.5897/JHF2013.0299>
- Ahmad I, Hussain T, Ashraf I, Nafees M, Nafees M, Rafay M and Iqbal M. 2013. Lethal effects of secondary metabolites on plant tissue culture. *Am-Eurasian J Agric Environ Sci.*, **13**: 539–547. <https://doi.org/10.5829/idosi.ajeaes.2013.13.04.1975>
- Al-Ghamdi AY, Fadlilmula AA and Abdalla MOM. 2020. Total phenolic content, antioxidant and antimicrobial activity of *Ruta chalepensis* L. leaf extract in Al-Baha area, Saudi Arabia. *Jordan JBiolSci.*, **13**: 675–680.
- Ali HM, El-Gizawy AM, El-Bassiouny REL and Saleh MA. 2015. Browning inhibition mechanisms by cysteine, ascorbic acid and citric acid, and identifying PPO–catechol–cysteine reaction products. *J Food Sci Technol.*, **52**: 3651–3659. <https://doi.org/10.1007/s13197-014-1437-0>
- Ali HM, El-Gizawy AM, El-Bassiouny REL and Saleh MA. 2016. The role of various amino acids in enzymatic browning process in potato tubers, and identifying the browning products. *Food Chem.*, **192**: 879–885. <https://doi.org/10.1016/j.foodchem.2015.07.100>
- Beena MR, Winter S and Makesh Kumar T. 2014. Influence of age of explants and genotype on somatic embryogenesis in African and Indian cassava cultivars. *J Root Crops*, **40**: 21–27.
- Brütsch L, Rugiero S, Serrano SS, Städeli C, Windhab EJ, Fischer P and Kuster S. 2018. Targeted inhibition of enzymatic browning in wheat pastry dough. *J Agric Food Chem.*, **66**: 12353–12360. <https://doi.org/10.1021/acs.jafc.8b04477>
- Cabezas-Serrano AB, Amodio ML and Colelli G. 2013. Effect of solution pH of cysteine-based pre-treatments to prevent browning of fresh-cut artichokes. *Postharvest Biol Technol.*, **75**: 17–23. <https://doi.org/10.1016/j.postharvbio.2012.07.006>
- Chen XM, Ma Z and Kitts DD. 2018. Effects of processing method and age of leaves on phytochemical profiles and bioactivity of coffee leaves. *Food Chem.*, **249**: 143–153. <https://doi.org/10.1016/j.foodchem.2017.12.073>
- Das P and Srivastav AK. 2015. To study the effect of activated charcoal, ascorbic acid and light duration on *in vitro* micropropagation of *Aloe vera* L. *Int J Innov Res Sci Eng Technol.*, **4**: 17–23. <https://doi.org/10.15680/IJIRSET.2015.0405091>
- de León IP and Montesano M. 2013. Activation of defense mechanisms against pathogens in mosses and flowering plants. *Int J Mol Sci.*, **14**: 3178–3200. <https://doi.org/10.3390/ijms14023178>
- de Souza LS, Hortaa IPC, de Souza Rosaa L, Lima LGB, da Rosa JS, Montenegro J, da Silva Santos L, de Castro RBN, Freitas-Silva O and Teodoro AJ. 2020. Effect of the roasting levels of *Coffea arabica* L. extracts on their potential antioxidant capacity and antiproliferative activity in human prostate cancer cells. *RSC Adv.*, **10**: 30115–30126. <https://doi.org/10.1039/D0RA01179G>
- Elimasni I, Haryati I, Nurwahyuni I and Gusvani V. 2020. The role of cysteine in improving somatic embryos of salak sidempuan (*Salacca sumatrana* Becc.). *J Phys Conf Ser.*, **1116**: 052019. <https://doi.org/10.1088/1742-6596/1116/5/052019>
- Etienne H, Bertrand B, Déchamp E, Maurel P, Georget F, Guyot R and Breitler J-C. 2016. Are genetics and epigenetic instabilities of plant embryogenic cells a fatality? The experience of coffee somatic embryogenesis. *Hum Genet Embryol.*, **61**: 10000136. <https://doi.org/10.4172/2161-0436.1000136>

- Etienne H, Breton D, Breidler J-C, Bertrand B, Déchamp E, Awada R, Marraccini P, Lérain S, Alpizar E, Campa C, Courtel P, Georget F and Ducos J-P. 2018. Coffee somatic embryogenesis: How did research, experience gained and innovations promote the commercial propagation of elite clones from the two cultivated species?. *Front Plant Sci.*, **9**:1–21. <https://doi.org/10.3389/fpls.2018.01630>
- Gallego Rúa AM, Henao Ramírez AM, Urrea Trujillo AI and Atehortúa Garcés L. 2016. Polyphenols distribution and reserve substances analysis in cocoa somatic embryogenesis. *Acta Biol Colomb.*, **21**:335–345. <https://doi.org/10.15446/abc.v21n2.50196>
- Gholizadeh A, Kermani M, Gholami M and Farzadkia M. 2013. Kinetic and isotherm studies of adsorption and biosorption processes in the removal of phenolic compounds from aqueous solutions: Comparative study. *J Environ Health Sci Eng.*, **11**: 29.
- Hassanein AM, Galal A, Soltan DM and Saad GK. 2015. Effect of medium strength and activated charcoal on *in vitro* shoot multiplications and growth of jojoba. *J Environ Stud.*, **14**: 81–90. <https://doi.org/10.21608/jesj.2015.196828>
- Ioannou I and Ghoul M. 2013. Prevention of enzymatic browning in fruit and vegetables. *Eur J Lipid Sci Technol.*, **9**: 310–341.
- Jones AMP and Saxena PK. 2013. Inhibition of phenylpropanoid biosynthesis in *Astemisia annua* L.: A novel approach to reduce oxidative browning in plant tissue culture. *PLoS One*, **8**: e76802. <https://doi.org/10.1371/journal.pone.0076802>
- Landey RB, Cenci A, Georget F, Bertrand B, Camayo G, Dechamp E, Herrera JC, Santoni S, Lashermes P, Simpson J and Etienne H. 2013. High genetic and epigenetic stability in *Coffea arabica* plants derived from embryogenic suspensions and secondary embryogenesis as revealed by AFLP, MSAP and the phenotypic variation rate. *PLoSOne*, **8**:e56372. <https://doi.org/10.1371/journal.pone.0056372>
- Modeste KK, Eliane MT, Daouda K, Brahim SA, Tchoa K, Kouablan KE and Mongomaké K. 2017. Effect of antioxidants on the callus induction and the development of somatic embryogenesis of cocoa [*Theobroma cacao* (L.)]. *Aust J Crop Sci.*, **11**: 25–31. <https://doi.org/10.21475/ajcs.2017.11.01.pne174>
- Moon KM, Kwon EB, Lee B and Kim CY. 2020. Recent trends in controlling the enzymatic browning of fruit and vegetable products. *Molecules*, **25**:2754. <https://doi.org/10.3390/molecules25122754>
- Ngamsuk S, Huang TC and Hsu JL. 2019. Determination of phenolic compounds, procyanidins, and antioxidant activity in processed *Coffea arabica* L. leaves. *Foods*, **8**:389. <https://doi.org/10.3390/foods8090389>
- Nic-Can GI, Galaz-Ávalos RM, De-la-Peña C, AlcazarMagaña A, Wrobel K and Loyola-Vargas VM. 2015. Somatic embryogenesis: Identified factors that lead to embryogenic repression. A case of species of the same genus. *PLoS One*, **10**:e0126414. <https://doi.org/10.1371/journal.pone.0126414>
- Rittisang S and Lekkamlue N. 2020. Induction of somatic embryos of *Coffea arabica* cv. Catimor C1FC 7963 using spirulina extract. *Maejo Int J Sci Technol.*, **14**:43–55. <https://doi.org/10.12982/CMUJNS.2020.0027>
- Saghaiesh SP and Souri MK. 2018. Root growth characteristics of khatouni melon seedlings as affected by potassium nutrition. *Acta Sci Pol Hortorum Cultus*, **17**:191–198. <https://doi.org/10.24326/asphc.2018.5.17>
- Sashikesh G, Anushkaran P, Praveena Y, Arumukham M, Kugamoorthy V and Kandasamy V. 2023. A comparison study of the efficacy of different activated charcoals derived from palmyra kernel shell in removing phenolic compounds. *Curr Opin Green Sustain Chem.*, **6**: 100355. <https://doi.org/10.1016/j.crgsc.2023.100355>
- Schieber A. 2018. Reactions of quinones, mechanisms, structures, and prospects for food research. *J Agric Food Chem.*, **66**: 13051–13055. <https://doi.org/10.1021/acs.jafc.8b05215>
- Taranto F, Pasqualone A, Mangini G, Tripodi P, Miazzi MM, Pavan S and Montemurro C. 2017. Polyphenol oxidases in crops: Biochemical, physiological and genetic aspects. *Int JMol Sci.*, **18**: 377. <https://doi.org/10.3390/ijms18020377>
- Wen B, Li D, Tang D, Huang Z, Kedbanglai P, Ge Z, Du X and Supapvanich S. 2020. Effects of simultaneous ultrasonic and cysteine treatment on antibrowning and physicochemical quality of fresh-cut lotus roots during cold storage. *Postharvest Biol Technol.*, **168**:111294. <https://doi.org/10.1016/j.postharvbio.2020.111294>
- Yao X-Y, Liu X-Y, Xu Z-G and Jiao X-L. 2017. Effects of lights intensity on leaf microstructure and growth of rape seedlings cultivated under a combination of red and blue LEDs. *J Integr Agric.*, **16**: 97–105. [https://doi.org/10.1016/S2095-3119\(16\)61393-X](https://doi.org/10.1016/S2095-3119(16)61393-X)

Renal Calculi Composition in Alkaptonuria: Insights on Etiology

Nesrin Riad Mwafi^{1,2*}, Amjad Asri Al-Tarawneh³, Ibrahim Naji Tarawneh⁴,
Mohannad Fayiz Alqedrh⁵, Ahmad Ibrahim Alsbou⁶, Lekaa Ja'far Al Mughrabi F⁶,
Ali Mohammad Khlaifat⁷, Muhamad Odeh Al-Limoun⁸, Khaled Mohammad khleifat⁸

¹ Department of Biochemistry and Molecular Biology, Faculty of Medicine, Mutah University, Al-karak 61710, Jordan; ² Faculty of Allied Medical Sciences, Mutah University, Al-karak 61710, Jordan; ³ Prince Faisal Center for Dead Sea, Environmental and Energy Research, Mutah University, Al-karak 61710, Jordan; ⁴ Department of Chemistry, Faculty of Science, Al-Balqa Applied University, Al-Salt 19117, Jordan; ⁵ Department of general surgery, Albasheer hospital, Amman 11151, Jordan; ⁶ Faculty of medicine, Mutah University, Al-karak 61710, Jordan; ⁷ Department of Nursing, Faculty of Prince Aysha for Applied Health and Nursing, Al-Hussein Bin Talal University, Ma'an 71111, Jordan; ⁸ Department of Biological Sciences, Faculty of Science, Mutah University, Al-karak 61710, Jordan.

Received: October 5, 2022; Revised: April 6, 2023; Accepted: April 12, 2023

Abstract

Alkaptonuria is a rare genetic disease caused by defect in the phenylalanine and tyrosine metabolism due to a deficiency in homogentisate 1,2-dioxygenase enzyme. The formation of ochronotic brownish-black pigment is the hallmark of the disease and at later stage AKU patients complain of recurrent renal calculi formation. In this report, we describe the case of 48 years old man who is previously diagnosed with alkaptonuria and is suffering from recurrent renal stones formation. We analysed the chemical composition of his AKU-stones by Fourier transform infrared spectroscopy (FTIR) and Inductively coupled plasma-mass spectrometry (ICP-MS) respectively and compared them with non-AKU stones obtained from 48 years old non-AKU man. Our results showed that sulphur content was 33 folds higher in AKU stones compared to non-AKU sample. This provides an evidence that sulphur-rich protein is a critical component for stone formation and growth from calcium oxalate monohydrate (COM) crystals. Accordingly, a model was proposed for the formation and growth of ochronotic renal stones in AKU patients with protein stimulated COM aggregation based on the generation of adducts between benzoquinone acetate and sulphur-rich proteins. Overall, the outcomes of this study shed a new light on the disease pathogenesis at the molecular level and opened new perspective which might orient the physicians to find a convenient therapeutic intervention or at least prophylactic measures to avoid recurrent formation of calculi in AKU patients.

Keywords: Alkaptonuria, Homogentisate 1,2-dioxygenase enzyme, Ochronosis, Renal stones.

1. Introduction

Alkaptonuria (AKU), also called the black bone disease, was originally defined as an inborn error of metabolism by Garrod in 1902 (Garrod, 1902; Phornphutkul *et al.*, 2002). It is an autosomal metabolic disease inherited in a recessive mode and characterized by generation and accumulation of homogentisic acid (HGA) in the blood and urine due to abnormal metabolism of phenylalanine and tyrosine (Alsbou and Mwafi, 2013; Mwafi *et al.*, 2021b). This happens due to mutations in homogentisate 1,2-dioxygenase (HGD) gene located on the long arm of chromosome 3 and subsequent deficiency in functional HGD enzyme (Khalil *et al.*, 2021; Mwafi *et al.*, 2021a). Although AKU is globally classified as a rare disease (incidence of 1:250,000), its prevalence is considered high in certain ethnicity such as Slovakian, Dominican, Indian and Jordanian population (Alsbou and Mwafi, 2013; Al-Shagahin *et al.*, 2019).

The bluish-black discoloration of the connective tissues, a phenomenon called ochronosis, is the hallmark of the disease which occurs due to the deposition of the

oxidized polymeric products of homogentisic acid in tendons, ligaments, heart valves, sclera, auricular and articular cartilages, bone of large joints and intervertebral discs (Albatayneh *et al.*, 2019). Consequently, multiple degenerative changes, inflammation and calcification will occur resulting in severe spondyloarthropathy and osteoarthritis (Wu, 2018). Rarely patients are recognised in early childhood due to diaper black staining and the disease diagnosis remains delayed until the patient is referred to orthopaedic clinic complaining of severe low backache, pain in the knee, hip and/or shoulder joints (da Silva Martins Ferreira *et al.*, 2014; Mirzashahi, 2016). These symptoms usually start in the third or fourth decades of life depending on the degree of the disease severity score (Kohet *et al.*, 1994). As a general rule, the disease is suspected in the presence of the triad of: brownish-black turning of urine if left standing or upon alkalization, ochronosis and extensive degenerative changes and arthritis in the large joints and spine of young adults (Raina *et al.*, 2008; Doganavsargilet *et al.*, 2015; Gil *et al.*, 2016). In later stages of the disease, AKU patients complain of recurrent kidney stones formation with the function of kidneys being conserved (Wolff *et al.*, 2015; Al-Tarawneh

* Corresponding author. e-mail: dnesrin@mutah.edu.jo.

et al., 2023). Few studies reported the chemical composition of AKU renal calculi and the analysis of stones with efficient physical methods such as ICP-MS are poorly documented in the literature. The aim of this study is to investigate the composition of renal stones collected from AKU patient and compare them with renal stones obtained from non-AKU patient. The calculi were analysed using FTIR and ICP-MS techniques. Our results afford insight into stone etiology and pathogenesis in AKU patients and suggest a critical role of sulphur-containing proteins in the growth and formation of kidney stones in AKU compared to non-AKU patient.

2. Materials and Methods

2.1. Sample collection

Renal stones were obtained from AKU (48 years male) and non-AKU (48 years male) patients after submission to the process of lithotripsy in the King Hussein Medical City. Both patients were matched in gender and age. Informed consents were obtained from patients and the study was approved by the Research Ethics Committee in faculty of medicine/ Mutah University. The study protocol was in accordance with the Declaration of Helsinki and its contemporary amendments. AKU patient was diagnosed based on family history and clinical examination. The black urine was confirmed by overnight standing of urine sample and by black ring formation upon addition of few drops of 10% FeCl_3 solution to fresh urine sample collected from the AKU patient (Figure 1, C-H). Moreover, the existence of homogentisic acid was confirmed by measuring urinary homogentisic acid level (1.2g/24h) using gas chromatography-mass spectrometry (GC-MS) analysis.

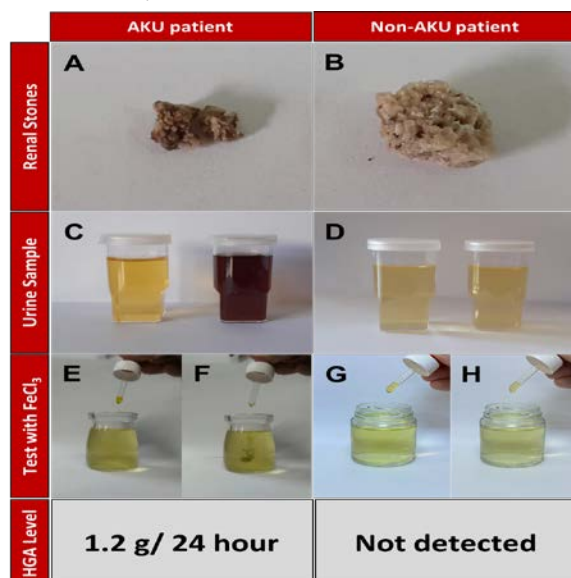


Figure 1. The black colour of renal stones and urine sample collected from AKU patient compared to non-AKU patient. (A) COM category of AKU calculi with budding appearance compared to (B) COD crystals with beige colour. (C) In AKU patient, the urine turns black in colour on 24-48 hours of standing (D) but the colour is not changed in non-AKU urine. (E) upon addition of few drops of 10% FeCl_3 solution to fresh AKU urine sample, (F) a black ring will appear due to the oxidation of HGA, (G,H) a phenomenon which is not detected in non-AKU sample. HGA level measured by GC-MS was detected only in AKU urine sample.

2.2. FTIR spectroscopy

Fourier transform infrared spectroscopy (FTIR) was performed using Bruker FTIR spectrometer (Bruker, Bremen-Germany) equipped with OPUS 7.5 program. The spectra were acquired in the middle IR range (i.e. 400 to 4000 cm^{-1}). The concentration of potassium bromide (KBr) was in the range of 0.2-1% of the sample through the preparation process of the pellets. The dried FTIR grade potassium bromide was transferred from the oven into a mortar in which 1-2 % of the powdered AKU, and non-AKU samples were mixed separately and again grounded into a fine powder. Finally, the pellet of the homogenous sample and potassium bromide were obtained. The pellets were placed in the transmission holder in front of the IR beam. Finally, the AKU and non-AKU renal stone components were evaluated according to the absorbed wavelength.

2.3. Elemental analysis using ICP-MS

One ml of external standard (Bismuth 200 ppm) was added to 0.1 g of each sample into teflon vials. The samples were digested by concentrated HNO_3 , HCl , and HF with mixing ratio of 2:6:2 (v/v) respectively for 5 min at 75 °C, 10 min at 100 °C, 10 min at 120 °C, 10 min at 150 °C, and 20 min at 200 °C using hotplate. The samples were filtered with syringe filters of 0.45 μm pore size (Sartorius, Göttingen/Germany). The filtrate was diluted to 50 ml with 2% nitric acid and then analyzed for elements by means of inductively coupled plasma-mass spectrometry abbreviated as ICP-MS (ELAN 9000, Perkin-Elmer SCIEX).

2.4. Kidney stones analysis

The stones were analyzed by kidney stones kit "URISTONE3" (Ben Biochemical Enterprise, Italy) for semiquantitative colorimetric determination of the chemical class of the collected calculi. Initially, the stones were crushed in a mortar. The well mixed powder was transferred to a sample tube. Five drops of Reagent 1 (H_2SO_4) were added to dissolve the powder. Then, 10 ml distilled water was added. After gentle mixing, the sample was transferred to 50 ml tube and distilled water is added up to the mark of 50 ml. The sample was distributed in 7 test tubes, and the colorimetric reaction was performed according to the instructions of URISTONE3 kit.

3. Results

3.1. Renal stones morphology and colour

In the current study, renal calculi were collected from AKU and non-AKU patients. It was observed that there are differences both in colour and morphology between AKU and non-AKU kidney stones (Figure 1, A & B). AKU stones are dark brown to black in colour due to the presence of the ochronotic pigment supposed to be composed of the oxidation product of HGA. However, non-AKU renal stones featured brighter colour ranging from white to beige. Surprisingly, chemical analysis of stones by URISTONE3 kit revealed that both are majorly composed of calcium oxalate salt. The non-AKU renal stone is classified as II based on the classification previously reported in literature (Daudon *et al.*, 2008a ; Daudon *et al.*, 2016a). However, the dissimilarity in the morphology could be related to the other components in

stone composition as well as the mechanism involved in the stone formation. Therefore, the stones were analysed by means of physical methods namely FTIR spectroscopy and ICP-MS for elemental analysis to identify the nature of chemical constituents and to semi-quantify their respective proportion within the calculi.

3.2. FTIR spectroscopy

Fourier transform infrared spectroscopy represents a conventional analytical technique from which information about the composition of renal stones of AKU patient could be achieved rapidly. Infrared spectra give information about kind of functional groups involved in

the structural formula rather than defining the exact chemical composition. Samples of AKU and non-AKU renal stones were analysed using FTIR spectrum, in which the band assignment was done according to peer-reviewed papers (George, 2004). Figure 2(A & B) shows the recorded mid-infrared spectra of AKU and non-AKU samples, respectively. The two main observed differences between AKU and non-AKU FTIR transmittance spectra are the downstream peak shift from 1644 cm^{-1} to 1621 cm^{-1} and the shape and strength of peak detected around 3477 cm^{-1} .

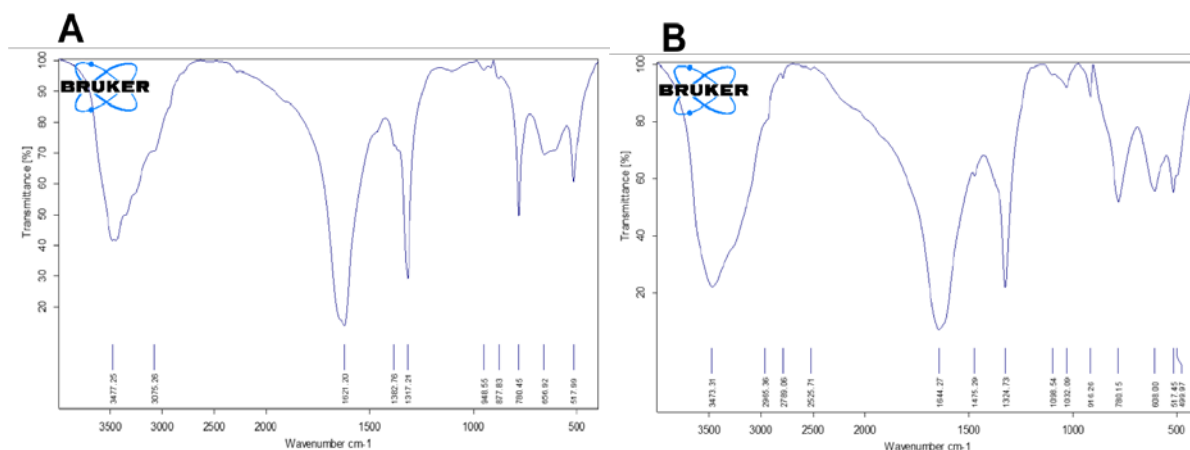


Figure 2. FTIR transmittance spectrum for AKU (A) and non-AKU (B) renal stones. (A) The peak appeared at 3477 cm^{-1} with transmittance of 40% and two spikes is indicative of N-H bond and the second distinctive peak at 1621 cm^{-1} indicates Amide I rich with β -Sheet aggregates. (B) The peak appeared at 3473 cm^{-1} is strong (with transmittance of 20%) broad, smooth and it is indicative of alcoholic O-H bond. Moreover, there is an upstream shift in the second distinctive peak from 1621 cm^{-1} to 1644 cm^{-1} indicates less β -Sheet aggregates.

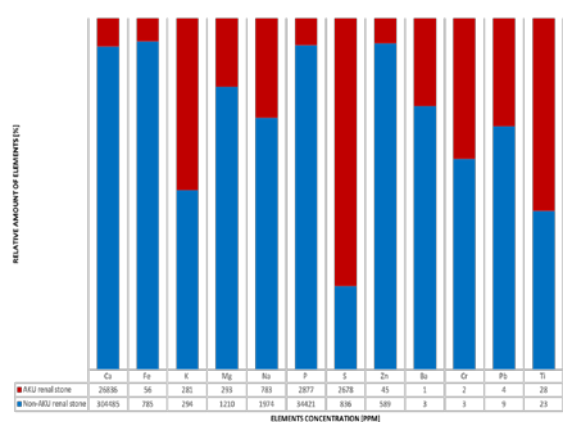
3.3. Elemental analysis by ICP-MS

To measure the trace level of elements (range: ppm = parts per million) found in biological samples such as kidney stones, inductively coupled plasma-mass-spectrometry (ICP-MS) was used. ICP-MS is rapid and sensitive technique with minimal elemental interference. It is a suitable method for elemental analysis of very small sample size such as renal stones. The sample was prepared according to the standard protocol of solid ICP-MS sample preparation. After digestion, the sample was converted to aerosol and transported directly to the plasma with inert

gas. The results are illustrated in Table 1 and Figure 3. The concentrations of twelve elements in AKU and non-AKU renal stone samples were expressed in ppm (horizontal line) and the relative amount in percentage (vertical line) as depicted in Figure 3. Additionally, the ratio of each element to the total amount was calculated in both types of renal stone samples (Table 1). The obtained results showed a marked difference of approximately 33 times in sulphur content between AKU and non-AKU samples.

Table 1. Ratio of elements in AKU and non-AKU renal stones calculated by dividing each element concentration on total elements quantity.

Element Name	non-AKU renal stones		AKU renal stones	
	Element Conc. [Mean±SD]	Element ratio [%]	Element Conc. [Mean±SD]	Element ratio [%]
Ca	304485 ± 44333	88.35	26836 ± 3907	79.12
Fe	785 ± 85	0.23	56 ± 6	0.17
K	294 ± 27	0.085	281 ± 26	0.83
Mg	1210 ± 190	0.35	293 ± 46	0.87
Na	1974 ± 177	0.57	783 ± 70	2.31
P	34421 ± 4027	9.99	2877 ± 337	8.49
S	836 ± 94	0.24	2678 ± 300	7.90
Zn	589 ± 59	0.17	45 ± 4	0.13
Ba	3 ± 0.3	0.0009	1 ± 0.1	0.003
Cr	3 ± 0.5	0.0009	2 ± 0.3	0.006
Pb	9 ± 0.6	0.003	4 ± 0.3	0.012
Ti	23 ± 2	0.007	28 ± 3	0.083
Total	344632	100%	33884	100%

**Figure 3.** Comparison between the elements content in renal stones of AKU and non-AKU patients using ICP-MS method of analysis

4. Discussion

The comparison between AKU and non-AKU renal stones reveals differences both in color and morphology. In fact, 80% of renal stones are primarily composed of calcium oxalate crystals of two main types: calcium oxalate monohydrate (COM) known as whewellite and calcium oxalate dihydrate (COD) known as weddellite (Zhang *et al.*, 2021). Studies reported that COM stones are formed in hyperoxaluria condition and when calcium to oxalate ratio is low (Giordani *et al.*, 2003; Trinchieri *et al.*, 2005). On the other hand, hypercalciuria and higher calcium to oxalate ratio are predominately associated with COD class of calcium oxalate stones (Bazin *et al.*, 2016; Daudon *et al.*, 2016b). Our results demonstrated that AKU and non-AKU stones fall under the categories of COM and COD crystals, respectively. AKU stones are distinguished with the budding appearance and dark-brown rough surface. The dark color can be explained due to the incorporation of HGA-oxidized pigments within the stones during their growth and formation process. Several studies stated that the color of the stones generally reflects the lithogenic activity of the disease in which light colour stones are generated when crystallization process is very active (Daudon *et al.*, 2008a; Daudon *et al.*, 2008b).

Consequently, the dark colour of AKU stones indicates that the lithogenic mechanism is slow and intermittent in AKU patients. This is in agreement with the mechanism implicated in the development and appearance of AKU symptoms as it is accumulative process highly dependent on the build-up of HGA level in various tissues of human body (Zatkova *et al.*, 2020). In the study of evaluation of factors that affect COM and COD fragmented calculi regrowth, Costa-Bauzá and his co-authors found that COM and COD are formed under pH conditions of 5.5 and 6.5 respectively (Costa-Bauzá *et al.*, 2006). In AKU patients, homogentisic acid is normally excreted in the urine by renal glomerular filtration and tubular secretion leading to slightly acidic urine in AKU patients with average pH = 5.6 (Tokuhara *et al.*, 2018; Ranganath *et al.*, 2020). In addition to the stone colour and morphology, AKU acidic urine condition provides another evidence that AKU renal stones fall under the category of COM crystals compared to COD stones formed in non-AKU calculi.

To identify the chemical composition of renal stones, FTIR was performed, and the obtained peaks were compared to infrared spectroscopy correlation tables as functional groups give different peaks in different substances (George, 2004). Regarding the fingerprint region of IR spectrum located between 500 and 1500 cm^{-1} , both AKU and non-AKU stones exhibit partial similarity and matching in some peaks. It is known that fingerprint region of certain compound is unique and can be used to distinguish it from other compounds. Additionally, AKU-renal stone spectrum displays a lower intensity at 517 and 780 cm^{-1} (O-C=O bending) compared to the healthy renal stone. This was in agreement with the study of Bazinet *et al.*, 2016 who found a difference between IR spectrum of COM and COD crystals of renal stones (Bazin *et al.*, 2016). The authors reported differences in peaks strength and shape at the region of 517-780 cm^{-1} with COD spectrum at this region being similar to our non-AKU spectrum and COM spectrum being identical to our AKU spectrum (Bazin *et al.*, 2016). These results additionally confirm the previous morphology findings in which AKU and non-AKU stones were classified as COM and COD crystals, respectively.

The discrete formation of these bands is important for distinguishing AKU from non-AKU renal stones.

However, few information can be extracted from fingerprint region to differentiate between the types of functional groups in the two kinds of renal stones included in this study. Therefore, the diagnostic region located between 1500-4000 cm^{-1} is more informative. In this study, the most important spectral characteristic has been chosen to give a good distinguishing bands between the two different categories of stones. In fact, the five bands between 3477 – 3047 cm^{-1} and the band at 1380 cm^{-1} , which are due to symmetric and asymmetric OH, stretch and out of plane OH bending respectively, are not found in a healthy renal stone spectrum (Figure 2). This finding could be explained by the presence of higher amounts of HGA and its oxidized products in AKU sample. In general, by comparing the peaks in Figure 2, two preliminary information are extracted. Firstly, in non-AKU sample, the peak at 3470 cm^{-1} is smooth, broad and strong (20% transmittance). This peak is indicative of alcoholic OH. On the other hand, similar peak appears in AKU sample, but it is broad with two spikes and weaker than that appeared in non-AKU sample (40% transmittance). This peak is typical for amide N-H group rather than alcoholic O-H group. Secondly, there was a downstream shift in the peak appearing at wave number of 1644 cm^{-1} in non-AKU to wave number of 1621 cm^{-1} in AKU sample. This downstream shift is indicative of Amide I and representative for protein secondary structure (Barth, 2007). As a matter of fact, the downshift from 1644 (Figure 2 B) to 1621 cm^{-1} (Figure 2 A) indicates the presence of more β -Sheet aggregates in AKU-renal stone (Giorgini *et al.*, 2010 ; Miller *et al.*, 2013; Boulet-Audet *et al.*, 2014). β -Sheets consist of extended polypeptide strands (β -strands) connected by a network of hydrogen bonds and occur widely in proteins. Although the importance of β -sheets in the folded structures of proteins has long been recognized, there is a growing recognition of the importance of intermolecular interactions among β -sheets. Intermolecular interactions between the hydrogen-bonding edges of β -sheets constitute a fundamental form of biomolecular recognition and are involved in protein quaternary structure, protein-protein interactions, and peptide and protein aggregation. The importance of β -sheet interactions in biological processes makes them potential targets for intervention in diseases such as AIDS, cancer, Alzheimer's (Nowick, 2008; Miller *et al.*, 2013) and could be for AKU disease.

However, AKU renal stones are expected to be rich with protein which is precipitated and participated in the growth and formation of AKU renal stones. To get more evidence of this suspicion, elemental analysis was performed for both samples using ICP-MS technique.

Our results detected a marked difference in sulphur content which is 33 folds higher in AKU stones compared to non-AKU sample. Similarly, Millucci *et al.*, 2014 reported the presence of sulphur in ochronotic cardiac valve tissue obtained from AKU patient compared to non-AKU sample (Millucci *et al.*, 2014). This finding strongly supports our result and suggests sulphur as one of several components of AKU ochronotic pigment. Although ochronosis or the black discoloration of tissues is the hallmark of AKU, the nature of this pigment and the exact mechanism implicated in the dark colour appearance of biological samples (e.g. ligament, tendon, bone, cartilage, renal stones, etc) obtained from AKU patients are still

ambiguous (Braconi *et al.*, 2015). Preliminary studies suggested the spontaneous oxidation of homogentisic acid (HGA) into 1,4-benzoquinone-2-acetic acid (BQA) followed by polymerization and subsequent formation of melanin-like pigment (Zannoni *et al.*, 1969; Hegedus and Nayak 1994). It was found that BQA is highly reactive metabolite and can form adducts with compounds containing free sulfhydryl or amino groups (Lustberg *et al.*, 1971) such as cysteine thiols and lysine amines; the nucleophilic sites on proteins (Fisher *et al.*, 2014; Li *et al.*, 2005). Indeed, BQA can bind single amino acids as well as whole protein (Morrison *et al.*, 1969). Moreover, BQA-protein binding induces structural and functional modification of the bound proteins enhancing their aggregation and subsequent precipitation, a mechanism proposed to contribute to ochronotic pigment formation in AKU patients (Nicolis *et al.*, 2013; Millucci *et al.*, 2014). Our finding is in agreement with Wolff *et al.*, 2015 who detected high protein content among the chemical composition of AKU renal stones analysed by X-ray diffraction (Wolff *et al.*, 2015) and Ranganath *et al.*, 2019 who proposed the presence of HGA-bound protein in the ochronotic pigment deposited in tissues (Ranganath *et al.*, 2019).

Our data recognised a quite similar ratio of calcium and phosphate both in AKU and non-AKU samples. This can be justified because ochronotic pigment is known to induce damage of connective tissues (e.g. cartilages, joints, bone) and enhance bone resorption process (Wolff *et al.*, 2015). Consequently, higher amounts of calcium and phosphate will be excreted in the renal filtrate of AKU patients. In addition, our results reported higher percentages of Na^+ and K^+ elements in AKU compared to non-AKU samples. Accordingly, our study suggests a stone formation model in AKU patients based on the precipitation of HGA as Na^+ and K^+ salts in the kidney followed by auto-oxidation to the corresponding BQA molecules which subsequently co-precipitate with free cysteine amino acids, cysteine-containing proteins or any free sulfhydryl containing compounds found in the renal system and resulting in the formation and development of renal stones (see Figure 4). This model is strongly supported by finding that AKU stones are highly enriched in sulphur (33 folds).

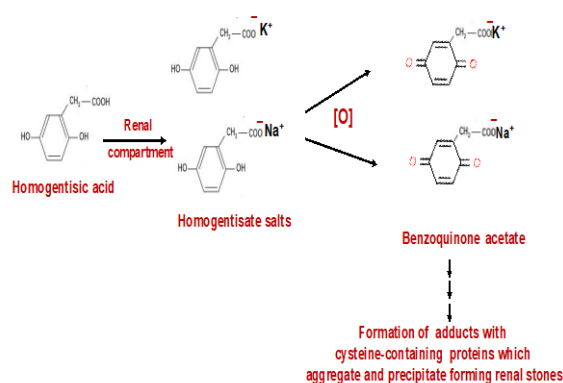


Figure 4. The proposed mechanism for the formation of ochronotic renal stones in AKU patients. The homogentisate salts in renal compartment undergo spontaneous oxidation to the corresponding benzoquinone acetate which can bind sulphur containing proteins resulting in precipitation of the modified adducts and subsequent formation of stones.

5. Conclusion

The identification of ochronotic pigment constituents is challenging, and further work is required to understand how does circulating HGA in AKU patients can interact with biological molecules to uncover the exact molecular mechanism underlying renal stones formation. Our findings show that sulphur-rich proteins are major components of AKU renal stones. However, knowing the composition of the calculus is fundamental because the nature of AKU stones in fact helps the physicians to find a convenient therapeutic interventions or at least guide the development of more effective stone preventive measures to avoid recurrent formation of calculi. Further studies are needed to understand the influence of sulphur-containing proteins on calcium oxalate (COM) stone formation and growth in AKU patients.

Acknowledgments

This study was Funded by the Deanship of Scientific Research, Mutah University, Al-Karak 61710, Jordan. Grant Number (422/2021).

Competing interests

The authors declare no competing interests.

References

- Albatayneh EM, Al-Sbou MS, Mahgoub SS, Mwafi NR and Alnawaiseh NA. 2019. Serum oxidative-antioxidative status in patients with alkaptonuria. *J Clin Med Res.* **11(5)**:337-344.
- Alsbou M and Mwafi N. 2013. A previously undiagnosed case of alkaptonuria: a case report. *Arch Rheumatol.* **28(2)**:132-135.
- Al-Shagahin H, Mwafi N, Khasawneh M, Al Zubi K and Alsbou M. 2019. Ear, nose, and throat manifestations of alkaptonuria patients from Jordan. *J Otol.* **25**:109-113.
- Al-Tarawneh A, Al-Limoun M, Khlaifat AM, Tarawneh I, Mwafi N, Khleifat K, Alqaraleh M and Mizher H. 2023. Bacterial quality of urinary tract in patients with alkaptonuria. *Am J Med Sci.* **365(4)**: 368-374.
- Barth A. 2007. Infrared spectroscopy of proteins. *Biochim Biophys Acta* **1767(9)**: 1073-1101.
- Bazin D, Leroy C, Tielsens F, Bonhomme Ch, Bonhomme-Courry L, Damay F, Le Denmat D, Sadoine J, Rode J, Frochot V, Emmanuel L, Haymann JP and Daudon M. 2016. Hyperoxaluria is related to whewellite and hypercalciuria to weddellite: What happens when crystalline conversion occurs? *C R Chim.* **19(11)**:1492-1503.
- Boulet-Audet M, Byrne B and Kazarian SG. 2014. High-throughput thermal stability analysis of a monoclonal antibody by attenuated total reflection FT-IR spectroscopic imaging. *Anal Chem.* **86(19)**: 9786-9793.
- Braconi D, Millucci L, Bernardini G and Santucci A. 2015. Oxidative stress and mechanisms of ochronosis in alkaptonuria. *Free Radic Biol Med.* **88** (Pt A): 70-80.
- Costa-Bauzá A, Perelló J, Isern B, Sanchis P and Grases F. 2006. Factors affecting calcium oxalate dihydrate fragmented calculi regrowth. *BMC Urol.* **6(16)**: 1-7.
- da Silva Martins Ferreira AM, Santosa FL and Costaa AM. 2014. Knee osteoarthritis secondary to ochronosis - clinical case. *Rev Bras Ortop.* **49(6)**:675-680.
- Daudon M, Jungers P, and Bazinc D., 2008 (a). Stone morphology: implication for pathogenesis. AIP Conference Proceedings, Indianapolis (Indiana), USA.
- Daudon M, Jungers P and Bazin D. 2008 (b). Peculiar morphology of stones in primary hyperoxaluria. *N. Engl. J. Med.* **359(1)**: 100-102.
- Daudon M, Dessombz A, Frochot V, Letavernie E, Haymann JP, Jungers P and Bazin D. 2016 (a). Iconography: comprehensive morpho-constitutional analysis of urinary stones improves etiological diagnosis and therapeutic strategy of nephrolithiasis. *C. R. Chimie.* **19(11-12)**:1470-1491.
- Daudon M, Letavernier E, Frochot V Haymann JP, Bazin D and Jungers P. 2016 (b). Respective influence of calcium and oxalate urine concentration on the formation of calcium oxalate monohydrate or dihydrate crystals. *C. R. Chim.* **19(11-12)**: 1504-1513.
- Doganavarsgil B, Pehlivanoglu B, Bicer EK, Argin M, Bingul KB, Sezak M, Kececi B, Coker M and Oztop F. 2015. Black joint and synovia: histopathological evaluation of degenerative joint disease due to ochronosis. *Pathol Res Pract.* **211(6)**:470-477.
- Fisher AA, Labenski MT, Malladi S, Chapman JD, Bratton SB, Monks TJ and Lau SS. 2011. The frequency of 1,4-benzoquinone-lysine adducts in cytochrome c correlate with defects in apoptosome activation. *Toxicol Sci.* **122(1)**: 64-72.
- Garrod AE. 1902. The incidence of alkaptonuria: a study in chemical individuality. *Lancet.* **160(4137)**: 1616-1620.
- George S. 2004. **Infrared and Raman Characteristic Group Frequencies: Tables and Charts.** Third ed. Wiley, New Jersey.
- Gil J, Wawrzynski J and Waryasz G. 2016. Orthopedic manifestations of ochronosis: pathophysiology, presentation, diagnosis, and management. *Am J Med.* **129(5)**:536.e1-536.e 6
- Giordani P, Modenesi P and Tretiach M. 2003. Determinant factors for the formation of the calcium oxalate minerals, weddellite and whewellite, on the surface of foliose lichens. *Lichenologist.* **35(3)**:255-270.
- Giorgini E, Conti C, Ferraris P, Sabbatini S, Tosi G, Rubini C, Vaccari L, Gioacchini G and Carnevali O. 2010. Effects of Lactobacillus rhamnosus on zebrafish oocyte maturation: an FTIR imaging and biochemical analysis. *Anal Bioanal Chem.* **398(7-8)**: 3063-3072.
- Hegedus ZL and Nayak U. 1994. Homogentisic acid and structurally related compounds as intermediates in plasma soluble melanin formation and in tissue toxicities. *Arch Int Physiol Biochim Biophys.* **102(3)**: 175-181
- Khalil R, Ali D, Mwafi N, Alsaraireh A, Obeidat L, Albsoul E and Al-Sbou A. 2021. Variant Analysis of Alkaptonuria Families with Significant Founder Effect in Jordan. *International BR.* **2021**:1-8.
- Koh KB, Low EH, Ch'ng SL and Zakiah I. 1994. A case of alkaptonuria with root canal stenosis. *Singapore Med J.* **35(1)**:106-107.
- Li WW, Heinze J and Haehnel W. 2005. Site-specific binding of quinones to proteins through thiol addition and addition-elimination reactions. *J. Am. Chem. Soc.* **127(17)**: 6140-6141.
- Lustberg TJ, Schulman JD and Seegmiller JE. 1971. The preparation and identification of various adducts of oxidized homogentisic acid and the development of a new sensitive colorimetric assay for homogentisic acid. *Clin Chim Acta.* **35(2)**: 325-333.
- Miller LM, Bourassa MW and Smith RJ. 2013. FTIR spectroscopic imaging of protein aggregation in living cells. *Biochim Biophys Acta.* **1828(10)**: 2339-2346.

- Millucci L, Ghezzi L, Paccagnini E, Giorgetti G, Viti C, Braconi D, Geminian Mi, Soldani P, Lupetti P, Orlandini M, Benvenuti Ch, Perfetto F, Spreafico A, Bernardini G and Santucci A. 2014. Amyloidosis, inflammation, and oxidative stress in the heart of an alkaptonuric patient. *Mediators Inflamm.*, **2014**: 258471.
- Mirzashahi B, Tafakhori A, Najafi A and Farzan M. 2016. Neglected alkaptonuric patient presenting with steppage gait. *Arch Bone Jt Surg.*, **4(2)**:188-191.
- Morrison M, Steele W and Danner DJ. 1969. The reaction of benzoquinone with amines and proteins. *Arch Biochem Biophys.*, **134(2)**: 515–523.
- Mwafi N, Ali D, Khalil R, Alsou I and Saraireh A. 2021 (a). Novel R225C variant identified in the *HGD* gene in Jordanian patients with alkaptonuria. *AIMS Molecular Science*, **8(1)**:60-75.
- Mwafi N, Alasmari A, Al-Momani M, Alazaydeh S, Alajoulin O, Alsalem M and Kalbouneh H. 2021 (b). Alkaptonuria with extensive ochronotic degeneration of the Achilles tendon and its surgical treatment: a case report and literature review. *Asian Biomed.*, **15(2021)**:129-136.
- Nicolis S, Monzani E, Pezzella A, Ascenzi P, Sbardella D and Casella L. 2013. Neuroglobin modification by reactive quinone species. *Chem. Res. Toxicol.*, **26(12)**: 1821–1831.
- Nowick JS. 2008. Exploring β -Sheet Structure and Interactions with Chemical Model Systems. *Acc. Chem. Res.*, **41(10)**: 1319-1330.
- Phornphutkul Ch, Introne WJ, Perry MP, Bernardini I, Murphey MD, Fitzpatrick DL, Anderson PD, Huizing M, Anikster Y, Gerber LH and Gahl WA. 2002. Natural history of alkaptonuria. *N Engl J Med.*, **347(26)**: 2111–2121.
- Raina S, Mahesh DM, Kaushal SS, Gupta D, Dhiman DS, Negi A and Sharma S. 2008. Alkaptonuria and intramedullary calcification. *J Assoc Physicians India.*, **56**:552-555.
- Ranganath LR, Norman BP and Gallagher JA. 2019. Ochronotic pigmentation is caused by homogentisic acid and is the key event in alkaptonuria leading to the destructive consequences of the disease-A review. *J Inherit Metab Dis.*, **42(5)**: 776–792.
- Ranganath LR, Milan AM, Hughes AT, Khedr M, Davison AS, Shwehdi E, Norman BP, Hughes JH, Bygott H, Luangrath E, Fitzgerald R, Psarelli EE, Kan Ch, Laan D, Olsson B, Rudebeck M, Mankowitz L, Sireau N, Arnoux JP, Sang KL, Jarvis JC, Genovese F, Braconi D, Santucci A, Zatkova A, Glasova H, Stančík R, Imrich R, Rhodes NP and Gallagher JA. 2020. Homogentisic acid is not only eliminated by glomerular filtration and tubular secretion but also produced in the kidney in alkaptonuria. *J Inherit Metab Dis.*, **43(4)**: 737-747.
- Tokuhara Y, Shukuya K, Tanaka M, Sogabe K, Ejima Y, Hosokawa Sh, Ohsaki, Morinishi T, Hirakawa E, Yatomi Y and Shimosawa T. 2018. Absorbance measurements of oxidation of homogentisic acid accelerated by the addition of alkaline solution with sodium hypochlorite pentahydrate. *Sci Rep.*, **8(1)**: 11364.
- Trinchieri A, Castelnovo C, Lizzano R and Zanetti G. 2005. Calcium stone disease: A multiform reality. *Urol. Res.*, **33(3)**:194–198.
- Wolff F, Biao I, Koopmansch K, Bossche MV, Pozdzik A, Roumeguère Th and Cotton F. 2015. Renal and prostate stones composition in alkaptonuria: a case report. *Clin Nephrol.*, **84(6)**:339-342.
- Wu K, Bauer E, Myung G and Fang MA. 2018. Musculoskeletal manifestations of alkaptonuria: A case report and literature review. *Eur J Rheumatol.*, **6(2)**:98-101.
- Zannoni VG, Lomtevas N and Goldfinger S. 1969. Oxidation of homogentisic acid to ochronotic pigment in connective tissue. *Biochim Biophys Acta.*, **177(1)**: 94-105.
- Zatkova A, Ranganath L and Kadasi L. 2020. Alkaptonuria: Current Perspectives. *Appl Clin Genet.*, **13**:37-47.
- Zhang J, Wang L, Zhang W and Putnis CV. 2021. Role of hyperoxaluria/hypercalciuria in controlling the hydrate phase selection of pathological calcium oxalate mineralization. *Crystal Growth & Design.*, **21(1)**:683-691.

Proximate Composition, Fatty Acid Profile, and Microplastic Contamination of Edible Odonate Larvae (Aeshnidae: *Anax* sp.) in Rice Fields

Witwisitpong Maneechan¹, Taeng On Prommi^{2,*}

¹ Program of Bioproducts Science, Department of Science and Bioinnovation, Faculty of Liberal Arts and Science, Kasetsart University, Kamphaeng Saen Campus, Nakhon Pathom, 73140, THAILAND; ² Department of Science and Bioinnovation, Faculty of Liberal Arts and Science, Kasetsart University, Kamphaeng Saen Campus, Nakhon Pathom Province, 73140, THAILAND

Received: October 10, 2022; Revised: December 7, 2022; Accepted: April 14, 2023

Abstract

Although the human consumption of edible insects is a culturally well documented practice, the nutritional literature of aquatic insects has not been completely covered. The present study was conducted with the aim of evaluating the proximate composition, fatty acid profiles, and microplastic contamination of edible odonate larvae (Aeshnidae: *Anax* sp.). Nutrient analysis showed that the proximate composition was a good source of protein (65.70 g/100g dry weight). The major fatty acids were oleic (1.08 g/100g DW) and palmitic acid (1.01 g/100g DW). The long-chain polyunsaturated fatty acid profile showed an abundance of linoleic, alpha-linolenic, and eicosapentaenoic acids. Total microplastics content found 694 items in the gastrointestinal tract, with a mean abundance of 11.57 items/individual. Five distinct polymers, including polyethylene, polyamide, polypropylene, polyethylene terephthalate, and cellulose, were identified through chemical analysis of FTIR spectra. Future research should be conducted regarding a comprehensive nutritional study to as method for a nutritional reference on food safety and security.

Keywords: Edible aquatic insect, Odonata, Proximate composition, Fatty acid, Microplastics, Rice field

1. Introduction

Food security concerns are rising due to the expected increase in the world population growing to 9.6 billion by the year 2050 (UN, 2019). These concerns are influencing research into several alternate human dietary sources. From this perspective, edible insects as early as 1975 (Meyer-Rochow, 1975) were considered to contribute to the food security of the world based on their nutritional value and sustainability of the production system. Globally, approximately 2,000 insect species of 14 orders are considered edible (Mitsuhashi, 2008; Kouřimská and Adámková, 2016). Insects are one of the most diverse and abundant groups in the ecosystem because they are able to exist in and adapt to a variety of terrestrial and aquatic ecosystems. They also have a high reproductive capacity (Das and Hazarika, 2019). The consumption of insects has been recorded throughout history and throughout the world (FAO, 2013). Consuming insects, also known as entomophagy, is a good source of amino acids and fatty acid profiles as well as protein (20–76% of dry matter), fat (2–50% of dry matter) (Kouřimská and Adámková, 2016), including minerals and vitamins (Chakravorty *et al.*, 2011; Ghosh *et al.*, 2017). Beetles (Coleoptera) (31%) are the most widely consumed edible insects in the world, followed by caterpillars (Lepidoptera) (18%), bees, wasps,

and ants (Hymenoptera) (14%) (van Huis, 2013; Macadam and Stockan, 2017).

Prior research has recorded the nutrient composition of dragonfly larvae (Odonata) (Feng *et al.*, 2001; Mozhui *et al.*, 2020; Narzari and Sarmah, 2017; Xiaoming *et al.*, 2010), but only a few species have been investigated. In Thailand, Odonata is a common insect found throughout the country, especially in rice paddies and other wetlands. The practice of consuming dragonfly larvae is common throughout Thailand, particularly in the north and northeast. Odonata species eaten in Northeast Thailand are Aeshnidae (*Aeshna* sp.), Coenagrionidae (*Ceriagrion* sp.), Corduliidae (*Epophtalmiavittigera bellicose*), and Libellulidae (*Rhyothemis* sp.) (Hanboonsong, 2010). In other regions of the world, the most common edible odonata species are *Lestespraemorsus* (Lestidae), *Gomphuscuneatus*, and *Crocothemisservilia* (Libellulidae) (Feng *et al.*, 2001). Protein, fat, amino acids, and trace elements are present in these larvae. Protein, fat, and amino acid levels are on average 58.92%, 25.37%, and 46.03%, respectively. The average content of the eight different types of amino acids required by the human body is 16.41%, or 35.69%, of the total amount of amino acids. Potassium, zinc, calcium, and iron concentrations are 2,960 mg.kg⁻¹, 125.4 mg.kg⁻¹, 2,7616.9 mg.kg⁻¹, and 796.2 mg.kg⁻¹, respectively. Consequently, one of the most nutritious edible insect resources is the dragonfly larva (Feng *et al.*, 2001).

* Corresponding author. e-mail: faastop@ku.ac.th.

Microplastics (MPs) are an issue of concern as they can be found in the larvae that are consumed by humans. This is problematic because if these MPs enter the food chain, they have the potential to negatively impact both human health and the environment (Erren *et al.*, 2013; Muhdhar *et al.*, 2021; Kallenbach *et al.*, 2022). Microplastics are all small plastic particles with range size 1 μm to 5 mm (Hale *et al.*, 2022). These may be degradation products originating from primary MPs (manufactured for addition to certain products) or secondary MPs (derived by physical, chemical, and/or biological degradation from larger plastics) and can be readily dispersed in the natural environment (Wang *et al.*, 2018). A variety of aquatic animals can either ingest microplastics from bottom sediments, suspended particulate material from the water column, or even ingest organisms of lower trophic levels containing these particles (Chaukura *et al.*, 2021). Monitoring of these contaminants can provide useful information on the degree of contamination in aquatic ecosystems. Thus, the aim of the study was to confirm the proximate composition of aquatic dragonfly larvae, *Anax* sp., including quantifying the microplastic accumulation in the gastrointestinal tract of the odonatan *Anax* sp.

2. Materials and Methods

2.1. Sample collection and preparation for nutrition analysis

In November 2021, an aquatic dip net was used to collect aquatic insects from the rice plots' margins. The location of the rice plot was in Nakhon Pathom Province, in the central part of Thailand (N14° 0' 31.964", E99° 58' 53.3838"). The collected odonata specimens were placed in white trays for sorting and screening (Figure 1a). The samples were transferred to containers for identification in the laboratory. Odonata larvae were identified using taxonomic keys (Dudgeon, 1999; Yule and Sen, 2004) under a stereomicroscope (Olympus SZ51). Approximately 1,555 mostly final instar larvae, *Anax* sp., were rinsed, sun-dried for one day, and kept until further biochemical analysis. The descriptive detail of the final instars is the long, spread-apart wing buds. The larvae of *Anax* sp. (Figure 1b), approximately 60 individuals, were preserved in vials properly containing 80% ethanol for microplastic analysis.



Figure 1. a) Photograph of *Anax* sp. (Odonata: Aeshnidae) (red arrow) with other aquatic insect organisms, and b) *Anax* sp. (Odonata: Aeshnidae) characteristic.

2.2. Nutrition analysis

Due to limited sample sizes, this study was unable to conduct triplicate analyses for proximate composition. The sampling technique used was composite sampling (pooling the sample). For the biochemical analysis, 1,555 *Anax* sp. larvae were used. The proximate composition was analyzed based on the contents of moisture (AOAC method 925.45), protein (AOAC method 991.20), fat (AOAC method 2003.05), and ash (AOAC method 923.03). Briefly, the protein content (N X 6.25) was determined by the AOAC Kjeldahl method. The fat content was determined by the Soxhlet extraction technique. Total carbohydrate was determined by calculating the percent remaining after all the other components had been measured: %carbohydrates = 100-(%moisture + %protein + %lipid + %ash). The energy value per 100 g was calculated by multiplying the grams of fat by 9.0 (Sullivan and Carpenter, 1993). The total energy (Kcal/100 g dry matter) was estimated according to FAO (2003). The fatty acid profile was performed using gas chromatograph with a flame ionization detector (FID) (7890-B, Agilent Technologies) and modified Compendium of Methodology for Food Analysis methods (2003). Each parameter of the biochemical analysis was determined only once due to the limited number of specimens.

2.3. Microplastics extraction and identification

A total of 60 dragonfly larvae, *Anax* sp., were rinsed three times with distilled water to get rid of a variety of contaminants. Then, respective larval lengths and weights were determined by calipers (accuracy 0.05 mm) and analytical balance readings (accuracy 0.0001 g). Ten specimens (six replicates) were pooled to measure microplastics in the gastrointestinal tract (GT). The GT of *Anax* sp. was removed from the individuals' guts using metal forceps and weighed using an analytical scale (accuracy 0.0001 g). Then they were placed in separate 30 mL Erlenmeyer flasks with aluminium foil immediately covering the flasks. Prior to microplastics examination, the GT was dried at 40°C for 4 hours in a drying cabinet. Each flask was then filled with 10 mL of a 30% hydrogen peroxide (H_2O_2) solution, immediately covered in parafilm, and placed in an ES-20 environmental shaker incubator, then incubated for 7 days at 150 rpm. After tissue breakdown, the microplastic particles were separated from the remaining matrix using density floatation with a 1.6 g/mL potassium formate (HCOOK) solution. The particles were vacuum-pumped onto 0.45 μm pore size and 47 mm diameter membrane filters. The filters were placed in glass Petri dishes with covers and dried for two days at 50 °C in a drying chamber. To identify MP particles based on their physical properties, each filter paper was visually examined, and images were taken using a stereomicroscope (Leica EZ4E). With the help of an attenuated total reflection-Fourier transform infrared spectrometer (ATR-FTIR), the selected particles were examined to confirm the types of polymers. The spectral range was 4,000 to 500 cm^{-1} , with a 32 cm^{-1} spectral resolution and 32 co-scans for each measurement. The spectra of polymers were matched against a commercial spectral library (Bruker ATR-FTIR Complete Library), with a quality index ≥ 0.7 being accepted (Woodall *et al.*, 2014).

As methods to prevent contamination, special gloves (nitrile), glass, and metal equipment were used. When not in use, all the glass and metal were immediately covered with aluminium foil after being cleaned three times with deionized water. Parallel to the process used for the samples, a procedural blank without tissues was run. The process was completed as quickly as possible.

2.4. Data analysis

The nutritional value was recorded. The abundance, types, and colors of MPs were counted. The data was represented as mean \pm standard deviation (SD).

3. Results and Discussion

The proximate composition is shown in Table 1. The larvae of Odonata, *Anax* sp. were high in protein content (65.7 %). However, the data on the protein content of *Anax* sp. were lower than those for *Sympetrum* sp. (Odonata: Libellulidae) reported by Narzari and Sarmah (2017). However, aquatic insects like Odonata tend to be excellent sources of protein, 40–65% (Williams and Williams, 2017). The fat content in *Anax* sp. was 4.88%. The macronutrient (protein and fat) composition in these edible insects reflects their gross energy value, which is also influenced by other factors, e.g., sex (Kulma *et al.*, 2019), life stages (Ghosh *et al.*, 2021), and diet (Ooninx and Finke, 2021). The total energy content was 360.52 Kcal/100 g and was similar to that found in the great diving beetle (*Dytiscus marginalis*) (Choudhury *et al.*, 2020). However, the obtained energy values for *Anax* sp. are comparably lower than the 431 Kcal/100g reported for the Odonata (Dragonflies and Damselflies), the main order of edible insects commonly consumed worldwide (Ordóñez-Araque *et al.*, 2022). The energy levels of edible insects depend mainly on their fat content. Kouřimská and Adámková (2016) state that because larvae have more lipid stored in their bodies than adults, they are often higher in energy. In contrast, insect species rich in protein contain fewer calories.

Table 1. Proximate compositions and fatty acid compositions of dragonfly larvae, *Anax* sp., g/ 100g dry weight

Proximate composition	
Moisture	10.81
Ash	5.16
Fat	4.88
Protein	65.70
Total carbohydrate	13.45
Total energy, (Kcal/ 100 g)	360.52
Energy from fat, (Kcal/ 100 g)	43.92

Table 2 presents the fatty acid composition of *Anax* sp. Palmitic acid (1.01 g/100 g) was the main saturated fatty acid found in the fatty acids. Oleic acid made up the majority of monounsaturated fatty acids (MUFA), contributing 1.08 g/100 g. Alpha-Linolenic acid (C18:3n3) was the most abundant n-3 polyunsaturated fatty acid (PUFA), while linoleic acid (C18:2n6c) and arachidonic acid (C20:4n6) were the two most abundant n-6 PUFA. These findings were similar to those reported previously regarding common edible dragonfly larvae in Yunnan and Guizhou Provinces, China (Jiang *et al.*, 2017). Long-chain

PUFAs, particularly omega-3 and omega-6 fats such as alpha-linolenic acid and linolenic acid, present in aquatic insects, which are similar to freshwater fish (Zhao *et al.*, 2021). Aquatic insects typically consume small aquatic organisms and algae, which are sources of long-chain PUFAs, or they synthesize PUFAs by expressing the enzymes delta-5 and delta-6 desaturases (D5D and D6D) (Sprecher, 2000).

Table 2. Fatty acid composition of dragonfly larvae, *Anax* sp., g/ 100g dry weight

Fatty acid profile	
Saturated fatty acid (SFA)	
Lauric acid (C12:0)	0.02
Myristic acid (C14:0)	0.05
Pentadecanoic acid (C15:0)	0.04
Palmitic acid (C16:0)	1.01
Heptadecanoic acid (C17:0)	0.13
Stearic acid (C18:0)	0.66
Arachidic acid (C20:0)	0.08
Behenic acid (C22:0)	0.06
Total SFA	2.05
Unsaturated fatty acid	
Palmitoleic acid (C16:1)	0.17
cis-10-Heptadecenoic acid (C17:1n10)	0.06
cis-9-Oleic acid (C18:1n9c)	1.08
Total MUFA	1.31
Linoleic acid (C18:2n6c)	0.53
gamma-Linolenic acid (C18:3n6)	0.02
alpha-Linolenic acid (C18:3n3)	0.28
cis-11,14-Eicosadienoic acid (C20:2)	0.03
cis-8,11,14-Eicosatrienoic acid (C20:3n6)	0.02
Arachidonic acid (C20:4n6)	0.21
Eicosapentaenoic acid (C20:5n3)	0.20
Total PUFA	1.29

Note: MUFA (monounsaturated fatty acids); PUFA (polyunsaturated fatty acids).

In the assessment of microplastic contamination, odonate larvae, *Anax* sp., with comparable weights were used for analysis. The average wet weight of the gastrointestinal tract was 0.1082 \pm 0.0492 g (range 0.0395-0.3056 g). *Anax* sp. had a mean body weight of 0.8046 \pm 0.3736 g (range 0.4112-1.9151 g) and a body length of 40.35 \pm 5.92 mm (range 32.40-55.10 mm). There was no MP contamination in the procedure blank samples. The findings demonstrated that all samples had microplastic particles in their gastrointestinal tracts. Microplastics were discovered in a variety of shapes in the organisms, including fibers, fragments, films, and spheres (Figure 2). Six replicates of pooled samples had microplastics, and the total numbers were 694 items (81-208 items). The average abundance of microplastics in the gastrointestinal tract was 11.57 \pm 4.32 items/GT individual (wet weight) (Table 3). The majority of the particles (87.18%, 605 items) were small (<100 μ m), while 5.48%

(38 items), 3.46% (24 items), and 3.89% (27 items) were in the 200-250 μm , 250-500 μm , and >500 μm size ranges, respectively (Figure 3). Most abundant were fragments (85.59%), followed by fiber (7.78%), sphere (4.90%), and film (1.73%) (Figure 4). The contamination of microplastics in the gastrointestinal tract of *Anax* sp. revealed a wide range of colors. The dominant color was violet (70.89%), followed by orange (12.54%), pink (9.95%), blue (4.76%), transparent colorless (0.86%), brown (0.58%), green (0.43%), and multicolored (0.29%) (Figure 5). As shown in Figure 6, the Fourier transform infrared (FT-IR) spectra revealed that polyethylene, cellulose, polyamide (nylon), polypropylene, and polyethylene terephthalate were the polymers found in the GT of *Anax* sp. Three kinds of polymers, i.e. polyethylene terephthalate, polyethylene, and polypropylene, are similar to those previously reported in freshwater insects (Akindele *et al.*, 2020; Maneechan and Prommi, 2022), while cellulose is similar to that reported by Bertoli *et al.* (2022). Biological organisms are receptors for microplastics and are exposed to microplastics through the air, water, and food they consume (Kallenbach *et al.*, 2022). Odonate larvae like *Anax* sp. are predators (Dudgeon, 1999). They encounter and consume a variety of prey types, with the consequence that the diet is broad. It is possible to state that they might absorb microplastics that are attached to prey with ease or might mistake MP particles for prey and consume MPs (Windsor *et al.*, 2019). This finding is sensitive because MP pollutants can be passed on to other predators like fish, birds, and humans. Because it is impossible to remove insects' intestines before eating the insects, indigestible particles, such as microplastics, enter the trophic chain (Panebianco *et al.*, 2019).

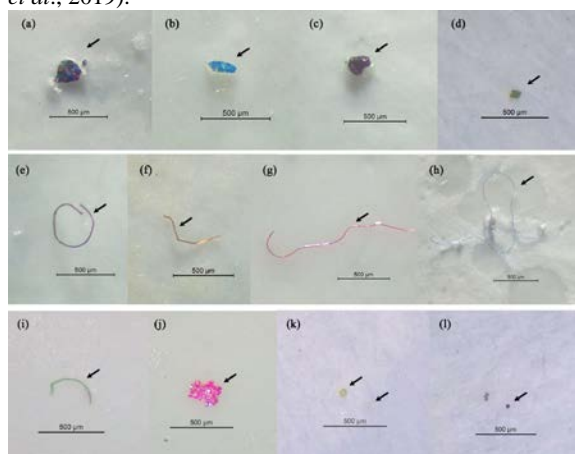


Figure 2. Examples of MPs in biological samples comprise different shapes, colors, and sizes. The arrows indicate fragments (a-d), fibers (e-i), film (j) and spheres (k-l).

Table 3. Basic data and microplastic contamination in *Anax* sp.

Species	Body weight (g)	Body length (mm)	Gastrointestinal tract (GT) wet weight (g)	MP items	
				Total MPs	Average MPs/GT individual
<i>Anax</i> sp.	0.8046±0.3736	40.35±5.92	0.1082±0.0492	694	11.57±4.32
(n = 60)	(0.4112-1.9151)	(32.40-55.10)	(0.0395-0.3056)		

Average ± standard deviation. Minimum and maximum values in parentheses

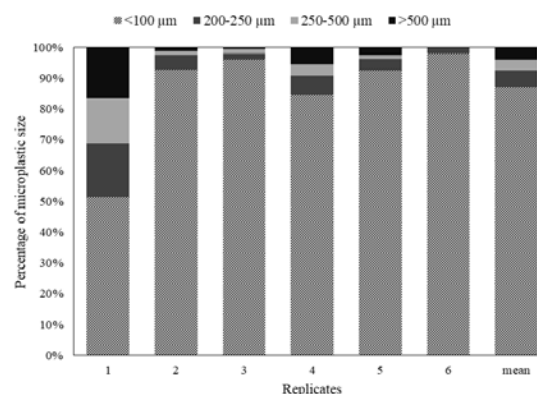


Figure 3. Microplastic size distribution (six replicates)

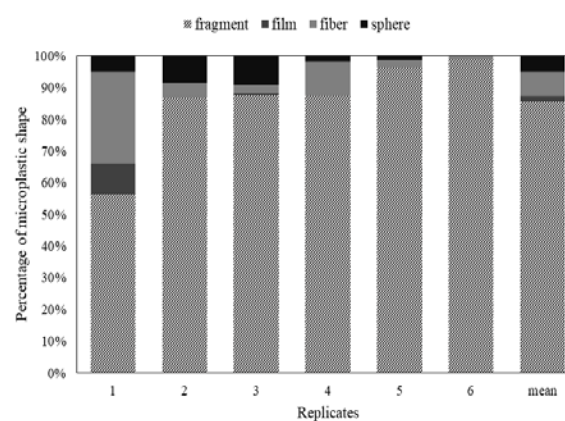


Figure 4. Percent of different microplastic shapes (fiber, sphere, film, and fragment) found in *Anax* sp.

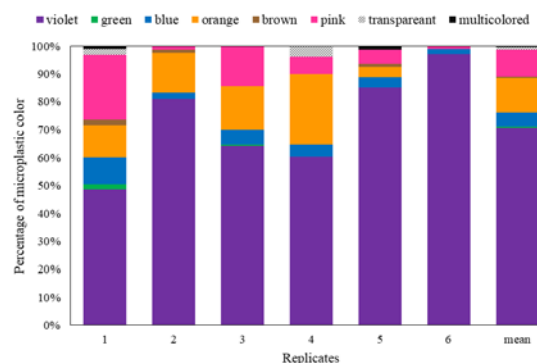


Figure 5. Percent of MPs by colors

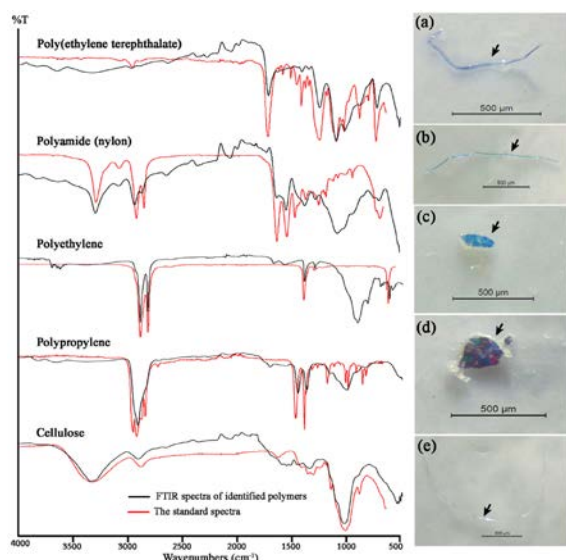


Figure 6. Transmittance spectra of observed microplastics and comparable standard spectra from the spectral library. The black arrows in the photographs indicate a) polyethylene terephthalate, b) polyamide (nylon), c) polyethylene, d) polypropylene, and e) cellulose.

4. Conclusion

In conclusion, odonata larvae (*Anax* sp.) are a good source of protein and fatty acids. The long-chain polyunsaturated fatty acid profile shows an abundance of linoleic acid, alpha-linolenic acid, and eicosapentaenoic acid. Although the odonata larvae were found to be a good source of nutrition, especially protein, a high possibility of microplastic contamination exists, as the current study revealed, and therefore the ingestion of contaminated insects could have some negative consequences on human health. As a result, there are concerns about the potential negative effects of eating these insects. Furthermore, because MPs are a relatively new kind of pollutant with complex and unique properties, more research into their possible effects on edible insects and their vertebrate consumers, such as fish, is strongly recommended.

Acknowledgements

This research project is supported by the National Research Council of Thailand (NRCT): NRCT5-RGJ63002-041 and a part of the Kasetsart University Research and Development Institute, KURDI (FF(KU)37.65).

References

Akindele EO, Ehlers SM and Koop JHE. 2020. Freshwater insects of different feeding guilds ingest microplastics in two Gulf of Guinea tributaries in Nigeria. *Environ. Sci. Pollut. Res.* **27**(26): 33373-33379. <https://doi.org/10.1007/s11356-020-08763-8>

Bertoli M, Pastorino P, Lesa D, Renzi M, Anselmi S, Prearo M and Pizzul E. 2022. Microplastics accumulation in functional feeding guilds and functional habit groups of freshwater macrobenthic invertebrates: Novel insights in a riverine ecosystem. *Sci. Total Environ.* **804**: 150207. <https://doi.org/10.1016/j.scitotenv.2021.150207>

Chakravorty J, Ghosh S and Meyer-Rochow VB. 2011. Chemical Composition of *Aspongopus nepalensis* Westwood 1837 (Hemiptera; Pentatomidae), a Common Food Insect of Tribal People in Arunachal Pradesh (India). *Int. J. Vitam. Nutr. Res.* **81**(1): 1-14.

<https://doi.org/10.1024/0300-9831/a000050>

Chaukura N, Kefeni KK, Chikurunhe I, Nyambiya I, Gwenzi W, Moyo W, Nkambule TT, Mamba BB and Abulude FO. 2021. Microplastics in the aquatic environment—the occurrence, sources, ecological impacts, fate, and remediation challenges. *Pollutants*, **1**(2): 95-118.

<https://doi.org/10.3390/pollutants1020009>

Choudhury K, Sarma D, Saprana PJ and Soren AD. 2020. Proximate and mineral compositions of *Samia cynthia ricini* and *Dytiscus marginalis*, commonly consumed by the Bodo tribe in Assam, India. *Bull. Natl. Res. Cent.* **44**(1): 152. <https://doi.org/10.1186/s42269-020-00411-y>

Das JK and Hazarika AK. 2019. Study on the diversity of aquatic edible insects in Baksa district of Assam with reference to Hemipteran species (Belostomatidae and Nepidae). *The Clarion-International Multidisciplinary Journal*, **8**(1): 15-21.

<https://doi.org/10.5958/2277-937x.2019.00002.9>

Dudgeon D. 1999. **Tropical Asian streams: zoobenthos, ecology and conservation.** Hong Kong University Press.

Erren T, Zeuss D, Steffany F and Meyer-Rochow VB. 2013. Oceans of plastics: possible risks of cancer in marine wildlife and humans. In S. Allodi & E. M. Nazari (Eds.). **Exploring themes on aquatic toxicology** (pp. 51-74): Research Signpost Publ., Trivandrum, India.

FAO. 2003. **Food energy—Methods of analysis and conversion factors.** FAO Food and Nutrition paper 77. Rome, Italy.

Feng Y, Chen X, Wang SY, Ye SD and Chen Y. 2001. Three edible odonata species and their nutritive value. *Forest Research*, **14**(4): 421-424.

Fontaneto D, Tommaso-Ponzetta M, Galli C, Rise P, Glew RH and Paoletti MG. 2011. Differences in fatty acid composition between aquatic and terrestrial insects used as food in human nutrition. *Ecol. Food Nutr.* **50**(4): 351-367.

<https://doi.org/10.1080/03670244.2011.586316>

Ghosh S, Herren P, Meyer-Rochow VB and Jung C. 2021. Nutritional Composition of Honey Bee Drones of Two Subspecies Relative to Their Pupal Developmental Stages. *Insects*, **12**(8): 759.

<https://doi.org/10.3390/insects12080759>

Ghosh S, Lee SM, Jung C and Meyer-Rochow VB. 2017. Nutritional composition of five commercial edible insects in South Korea. *J. Asia Pac. Entomol.* **20**(2): 686-694.

<https://doi.org/10.1016/j.aspen.2017.04.003>

Hale RC, Seeley ME, King AE and Yu LH. 2022. Chapter 2 Analytical Chemistry of Plastic Debris: Sampling, Methods, and Instrumentation. In E. R. Bennett (Ed.), **Microplastic in the Environment: Pattern and Process.** Springer Nature.

Hanboonsong Y. 2010. Edible insects and associated food habits in Thailand. In: Durst P B Johnson DV Leslie RN and Shono K (eds). **Forest insects as food: humans bite back.** Proceedings of a workshop on Asia-Pacific resources and their potential for development, Chiang Mai, Thailand, 19-21 February, 2008 2010 pp.173-182 ref.8

Jiang Y, He Z, Zhao M, Wang C, Sun L and Feng Y. 2017. Oil content and fatty acid composition of six kinds of common edible dragonfly naiads. *China Oils Fats*, **42**(3): 135-139.

Kallenbach EMF, Rødland ES, Buenaventura NT and Hurley R. 2022. Microplastics in Terrestrial and Freshwater Environments.

- In E. R. Bennett (Ed.), **Microplastic in the Environment: Pattern and Process** (pp. 87-130). Springer Nature.
- Kanphaet KW and National Bureau of Agricultural Commodity and Food Standards. 2003. **Compendium of Methods for Food Analysis /cDepartment of Medical Sciences and National Bureau of Agriculture Commodity and Food Standards (1st ed.)**. Thai Industrial Standards Institute: Bangkok, Thailand.
- Kouřimská L and Adámková A. 2016. Nutritional and sensory quality of edible insects. *NFS Journal*, **4**: 22-26. <https://doi.org/10.1016/j.nfs.2016.07.001>
- Kulma M, Kouřimská L, Plachý V, Božik M, Adámková A and Vrabec V. 2019. Effect of sex on the nutritional value of house cricket, *Acheta domestica* L. *Food Chem.* **272**: 267-272. <https://doi.org/10.1016/j.foodchem.2018.08.049>
- Macadam CR and Stockan JA. 2017. The diversity of aquatic insects used as human food. *J. Insects Food Feed.* **3(3)**: 203-209. <https://doi.org/10.3920/jiff2016.0046>
- Meyer-Rochow VB. 1975. Can insects help to ease the problem of world food shortage? *Search*, **6(7)**: 261-262.
- Mitsubishi J. 2008. **Sekai konchu shoko taizen**. Tokyo, Japan.
- Mozhui L, Kakati LN, Kiewhuo P and Changkija S. 2020. Traditional Knowledge of the Utilization of Edible Insects in Nagaland, North-East India. *Foods*, **9(7)**: 852. <https://doi.org/10.3390/foods9070852>
- Muhdhar MHI AI, Sumberartha IW Hassan Z Rahmansyah MS and Tamalene MN. 2021. Examination of Microplastic Particles in Reef Fish Food in Ternate Island Waters, Indonesia. *Jordan J. Biol. Sci.* **14(4)**: 853–858. <https://doi.org/10.54319/jjbs/140427>
- Narzari S and Sarmah J. 2017. Nutritional aspects of an aquatic edible insect *Sympetrum* sp. (Odonata: Libellulidae) of Assam, northeast India. *Int. J. Food Sci. Nutr.* **2(4)**: 38-42.
- Ooninx DGAB and Finke MD. 2021. Nutritional value of insects and ways to manipulate their composition. *J. Insects Food Feed.* **7(5)**: 639-659. <https://doi.org/10.3920/jiff2020.0050>
- Ordóñez-Araque R, Quishpillo-Miranda N and Ramos-Guerrero L. 2022. Edible Insects for Humans and Animals: Nutritional Composition and an Option for Mitigating Environmental Damage. *Insects*, **13(10)**: 944. <https://doi.org/10.3390/insects13100944>
- Panbianco A, Nalbone L, Giarratana F and Ziino G. 2019. First discoveries of microplastics in terrestrial snails. *Food Control*, **106**: 106722. <https://doi.org/10.1016/j.foodcont.2019.106722>
- Sprecher H. 2000. Metabolism of highly unsaturated n-3 and n-6 fatty acids. *Biochim. Biophys. Acta.* **1486**: 219-231. [https://doi.org/10.1016/S1388-1981\(00\)00077-9](https://doi.org/10.1016/S1388-1981(00)00077-9)
- Sullivan DM and Carpenter DE. 1993. **Methods of analysis for nutrition labeling chapter 6 p. 106**. AOAC International, Arlington, Virginia USA.
- UN (United Nations). 2019. **World Population Prospects 2019: highlights (ST/ESA/SER.A/423)**. Department of Economic and Social Affairs, Population Division: Department of Economic and Social Affairs, Population Division. New York, UN. 46 pp.
- van Huis A. 2013. Potential of insects as food and feed in assuring food security. *Annu. Rev. Entomol.* **58**: 563-583. <https://doi.org/10.1146/annurev-ento-120811-153704>
- Wang Z, Taylor SE, Sharma P and Flury M. 2018. Poor extraction efficiencies of polystyrene nano- and microplastics from biosolids and soil. *PLoS One*, **13(11)**: e0208009. <https://doi.org/10.1371/journal.pone.0208009>
- Williams DD and Williams SS. 2017. Aquatic Insects and their Potential to Contribute to the Diet of the Globally Expanding Human Population. *Insects*, **8(3)**: 72. <https://doi.org/10.3390/insects8030072>
- Windsor FM, Tilley RM, Tyler CR and Ormerod SJ. 2019. Microplastic ingestion by riverine macroinvertebrates. *Sci. Total Environ.* **646**: 68-74. <https://doi.org/10.1016/j.scitotenv.2018.07.271>
- Woodall LC, Sanchez-Vidal A, Canals M, Paterson GL, Coppock R, Sleight V, Calafat A, Rogers AD, Narayanaswamy BE and Thompson RC. 2014. The deep sea is a major sink for microplastic debris. *R. Soc. Open Sci.* **1(4)**: 140317. <https://doi.org/10.1098/rsos.140317>
- Xiaoming C, Ying F, Hong Z and Zhiyong C. 2010. Review of the nutritive value of edible insects. In **Forest insects as food: humans bite back** (pp. 85-92).
- Yule CM and Sen YH. 2004. **Freshwater Invertebrates of the Malaysian Region**, Acad. Sci. Malaysia, 2004.
- Zhao M, Wang CY, Sun L, He Z, Yang PL, Liao HJ and Feng Y. 2021. Edible Aquatic Insects: Diversities, Nutrition, and Safety. *Foods*, **10(12)**: 3033. <https://doi.org/10.3390/foods10123033>

Assessing the Immunomodulatory and Hepatoprotective Activities of Aqueous Tuber Extract of *Typhonium flagelliforme* (Lood) Blume in BALB/c Mouse

Wira Eka Putra¹, Anis Fatayatil Insani², Desi Nurhayati², Arief Hidayatullah³,
Muhaimin Rifa'i^{2,*}

¹Biotechnology Study Program, Department of Applied Sciences, Faculty of Mathematics and Natural Sciences, Universitas Negeri Malang, East Java, Indonesia; ²Department of Biology, Faculty of Mathematics and Natural Sciences, Brawijaya University, East Java, Indonesia;

³Health Governance Initiative, United Nations Development Programme Indonesia, Eijkman-RSCM Building, Jakarta, Indonesia

Received: February 10, 2023; Revised: April 14, 2023; Accepted: April 26, 2023

Abstract

Immune cells play a very significant role in the body due to their capacity to preserve homeostasis. They function primarily in the quick elimination of potentially harmful substances from the system. There is a trend towards the increased utilization of the therapeutic potential of medicinal plants to treat a wide range of diseases through the regulation of immunomodulatory mechanisms. In this present work, our objective was to determine the extent to which *Typhonium flagelliforme*, also known as rodent tuber, has an immunomodulatory effect in vivo in BALB/c mice. Four treatment groups were used in this investigation on BALB/c mice, including the control group with each group receiving 0, 50, 100 and 500 mg/kg BW of the plant extract respectively. After fourteen days of treatment, the mice were sacrificed for further analysis. The spleen was isolated for flow cytometry study, and it was then stained with antibodies against CD4, CD8, CD4CD62L, and CD4CD25. The relative number of each immune cell subgroup to be monitored was calculated using the BD FACS Calibur flow cytometer. The liver was also subjected to histological examination using hematoxylin-eosin staining. Our findings indicated the increasing number of CD8⁺ T cells and CD4⁺CD62L⁺ naive T cells in the spleen. Similarly, the relative number of CD8⁺ T and CD4⁺ T cells in thymus were elevated. This findings suggest that the *T. flagelliforme* extract (TFE) exerted the immunomodulatory activity which promote some certain of immune cells.

Keywords: Flow cytometry, immunomodulatory, rodent tuber, T cell, *Typhonium flagelliforme*.

1. Introduction

The immune system has been the main hotspot in biological and medical research in recent years, particularly during the current pandemic outbreak. It is a highly critical and complex system responsible for distinguishing the body's cells and other harmless material from foreign and particularly dangerous material, protecting the body against infections and foreign substances (Childs *et al.*, 2019; Huntington and Gray, 2018). It is a delicate system composed of cells, chemicals, pathways, and tissues that interact to generate an immune response to prevent or eradicate infections as quickly as possible while leaving the body's cells unharmed (Horwitz *et al.*, 2019; Nicholson, 2016). Because humans are always surrounded by hazardous pathogens, toxins, and even cancer cells, it constantly evolves while maintaining vigilance for any signs of invasion or an impending threat. This ability makes it the most crucial element of our species' survival throughout the evolutionary history (Childs *et al.*, 2019; Hurst and Magiorkinis, 2019).

The target of immune cells is to swiftly destroy and eradicate any potentially dangerous materials and cells

while also being able to control themselves to operate within a reasonable operating window (Nicholson, 2016). This capability, however, might be extremely harmful if it either puts the immune system into a hyperdrive condition where it attacks healthy cells and tissues or seriously undermines its capacity and capability, that lowers the body's state of defense and makes the individual more prone to diseases (Kitcharoensakkul and Cooper, 2020; Lotfi *et al.*, 2019). Therefore, the capacity of immune cells to continuously self-regulate and interact with one another, mostly through a variety of cytokines, is of utmost importance. However, some of the regulation mechanisms are still incompletely understood (Cicchese *et al.*, 2018; Tourkochristou *et al.*, 2021). The immune system often steers clear of these extremities of immune response spectrum through a control mechanism known as immunological homeostasis (Huntington and Gray, 2018). Various regulatory components normally carry out this mechanism, both in innate and adaptive immune systems, such as regulatory T cells (Tregs), regulatory B cells (Bregs), M2-like macrophages, mesenchymal stromal cells (MSCs), myeloid-derived suppressor cells (MDSCs), and complement regulatory proteins (CRPs) (Cao *et al.*, 2019; Carvajal *et al.*, 2019; Papp *et al.*, 2017; Tao *et al.*, 2019). It

* Corresponding author. e-mail: rifa123@ub.ac.id.

involves maintaining a balanced response to protect against infection and disease while avoiding overreaction and autoimmune reactions. Disruptions in immune homeostasis can lead to autoimmune disorders and increased susceptibility to infection.

The regulation of homeostasis by the immune system is not only dependent on internal factors including types of transcription factors like FOXO and Myb (Dias *et al.*, 2017; Zaiss and Coffey, 2018), but it is an intriguing mechanism which is also highly influenced by external factors such as diet (Tourkochristou *et al.*, 2021). Numerous herbs and spices, especially their essential oils, have been researched for their potential as immunomodulators. They include quercetin, kaempferol, rutin, genistein, hesperidin, ascorbic acid, and menthol. They can suppress the synthesis of TNF- α , IL-1, IL-2, IL-6, IL-8, and IL-1 β while also stimulating the proliferation of human peripheral blood mononuclear cells (PBMC) and the expression of IFN- γ (Lee *et al.*, 2021; Putra and Rifa'i, 2019; Bian *et al.*, 2019; Cheng *et al.*, 2019; Xiao *et al.*, 2018; Orhan *et al.*, 2016). Most of the well-studied immunomodulatory compounds came from well-known sources, such as herbs like *Leptadenia pyrotechnica*, *Zingiber officinale*, *Curcuma longa*, *Mentha* \times *piperita*, and some fruits like *Citrus limon* and *Muntingia calabura* (Amorim *et al.*, 2016; Dash *et al.*, 2018; Karthikeyan *et al.*, 2021; Miles and Calder, 2021; Orhan *et al.*, 2016; Sujono *et al.*, 2020; Yuandani *et al.*, 2021; Mahassni and Alshafi, 2022). These sources are highly abundant and commercially available all over the globe. Other less well-known indigenous species are also expected to have a similar advantage as immunomodulators; *T. flagelliforme*, sometimes referred to as rodent tuber, is one of them. It is native to Indonesia and belongs to the Araceae family. It is known for its distinctive long, slender, and whip-like leaves and has been investigated for its potential anti-cancer properties (Laurent *et al.*, 2015). Various studies suggest that the *T. flagelliforme* extract could inhibit the proliferation of breast cancer cells, increase the expression of p21 and caspase-3 on MCF-7 cells, and stimulate apoptotic pathways on P388 and NCI-H23 cells (Crystalia and Hillary, 2022; Lai *et al.*, 2008; Maher *et al.*, 2021; Mohan *et al.*, 2011). Although *T. flagelliforme* has a long history of use in traditional medicine, more research is needed to fully understand the mechanisms of action and potential therapeutic uses of the plant and its bioactive components. In this study, we examine the effect of rodent tuber extract in increasing the immune response as measured by the number of CD4⁺, CD8⁺, CD4⁺CD62L⁺, and CD4⁺CD25⁺ cells.

2. Materials and Methods

2.1. Experimental Animals Preparation

The mice (*Mus musculus*) utilized in this study were BALB/c strain, 8 weeks old, and in good health (active movement, no hair loss, no structural anomalies). They were then given food and water, *ad libitum*, and acclimatized for 7 days. The use of experimental animals has received an ethical certificate No. 72-KEP-UB from the Brawijaya University Ethics Committee. This study included four treatments and three replications for a total of twelve mice.

2.2. Water Fraction of Rodent Tuber Preparation and Injection on Mice

The rodent tuber suspension was made by diluting rodent tuber extract powder with water. The rodent tuber powder was obtained by cutting the roots into little pieces, drying them in direct sunlight, and then grounded until they become powder. Meanwhile, the powdered roots are mixed with water according to the dose injected to produce herbal suspensions. The prepared suspension was administered orally to mice twice daily for 14 days, at doses of up to 50 mg/kg BW in treatment group I, 100 mg/kg BW in treatment group II, and 500 mg/kg BW in treatment group III.

2.3. Spleen Isolation Procedure

The isolation procedure was carried out in accordance with our previous studies (Putra *et al.*, 2021; Putra *et al.*, 2016). The spleen was separated from the dissected organs of the mice, washed in sterile PBS and filtered using a 100 μ m BD nylon cell strainer. Then, it was homogenized by compressing it with the syringe's base in one direction from top to bottom, about 2-3 times, until the suspension could be filtered in a petri dish. The filtered suspension was placed in a sterile microtube with sterile PBS and then centrifuged for 5 minutes at 4°C at 1500 rpm. The supernatant was discarded, and the pellet was resuspended and homogenized with 100-1000 μ l PBS. The suspension was repeatedly centrifuged until it formed a white pellet.

2.4. Cells Quantitative Analysis using Flow cytometry

The pellet was resuspended in 1 ml of sterile PBS. A 100 μ l homogenate was transferred to a fresh microtube. It was centrifuged again for three minutes at 2500 rpm and 4°C, and the supernatant was discarded. Anti-CD4⁺, anti-CD8⁺, anti-CD62L⁺ and anti-CD25⁺ antimouse antibodies were then applied to the pellets. The flow cytometer cuvette was loaded with the sample and 400 μ l of sterile PBS was added. The cuvette was connected to the BD FACS Calibur flow cytometer nozzle. The BD Cell Quest Pro software was used for the analysis, set in acquiring mode (Putra *et al.*, 2020; Putra *et al.*, 2015).

2.5. Liver Slide Preparations and Histopathological Observations

The histopathological examination was conducted according to the previous study with few minor adjustments (Putra and Rifa'i, 2020; Putra *et al.*, 2017). The liver was isolated from dissected mice and then cleansed of any remaining blood with PBS before being placed in a 4% PFA fixative solution in PBS at room temperature for 1-7 days. The paraffin technique was used to prepare the liver slides. To remove the paraffin, the preparations were deparaffinized with xylol twice for 4 minutes each and then soaked with graded alcohol (100%, 95%, 90%, 80%, 70%, 60%, 50%, and 30%) for 3 minutes each. After washing with distilled water for 5 minutes, the slides were stained with hematoxylin for 1 minute, rinsed for 5 minutes with distilled water, and submerged in graded ethanol (30%, 60%, 70%) each for 5 minutes. After 10 minutes of eosin, it was rehydrated in graded ethanol (70%, 60%, 30%) for 5 minutes each, cleaned with xylol for 3 \times 5 minutes, and mounted with entellanTM. An Olympus BX51 microscope coupled with an Olympus DP20 digital camera was used to make the observations.

2.6. Observation Parameter

This study investigated both qualitative and quantitative factors. In control and treated animals, changes in the number of CD4⁺, CD8⁺, CD4⁺CD62L⁺, and CD4⁺CD25⁺ cells were evaluated quantitatively using flow cytometry (Figure 1). The impact of injecting rodent tuber extract on the histological microstructure of the liver with hematoxylin-eosin staining was the qualitative parameter evaluated using a light microscope. The existence or absence of damage to the liver as an antitoxic organ was the focus of the observations. The presence of bleeding, congestion, and necrosis of the hepatocytes following the treatments was used to determine the degree of liver injury.

2.7. Data Analysis

This study employed a completely randomized design (CRD) and the 95% confidence interval ANOVA test. The data was collected in changes in the number of CD4⁺, CD8⁺, CD4⁺CD62L⁺, and CD4⁺CD25⁺ cells, which were statistically assessed using normality and variance homogeneity tests. A two-way ANOVA with $\alpha=0.05$ significance level was used to evaluate normally distributed data with homogenous variance. If $p<0.05$ indicates a substantial difference between the tested treatments and vice versa. The Tukey HSD test was then used as a post-hoc test. All of the statistical analysis was carried out by SPSS 16.0 for Windows.

3. Results and Discussion

3.1. The Analysis of the Relative Number of CD4⁺ and CD8⁺ Cells in Thymus

The flow cytometry results of the relative amount of CD4⁺ cells on the thymus are shown in figure 2. The TFE100 group exhibited a significant increase in the relative number of CD4⁺ T cells at 29.10%. It was significantly higher than the TFE50 group at 10.64%. Meanwhile, the flow cytometry results on the relative amount of CD8⁺ cells on the thymus are shown in figure 2. The TFE500 group had a cell count of 3.72%, while the TFE50 group had about 2.79%. Both are statistically insignificant compared to the normal group at 2.05%. However, the TFE100 group's results show a different trajectory by significantly increasing the CD8⁺ cell number to 14.14%.

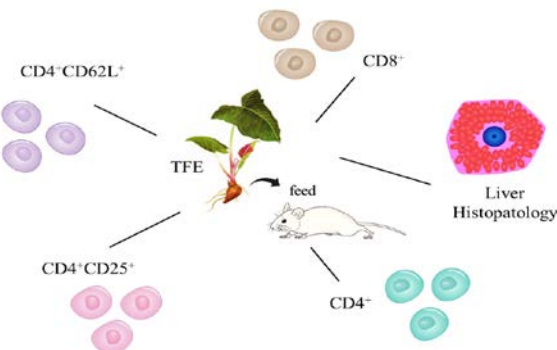


Figure 1. Major immune cell subsets assessed following TFE treatment.

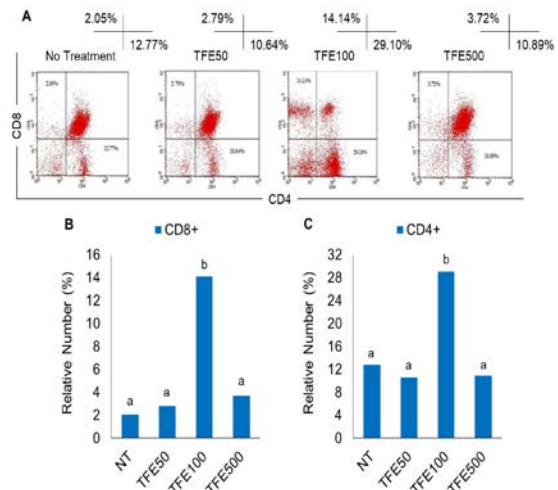


Figure 2. Immunomodulatory assessment of the effect of TFE on CD8 and CD4 T cells in thymus. (A). Flow cytometry graph of CD8⁺/CD4⁺; (B). Bar graph of CD8⁺; and (C). Bar graph of CD4⁺. The different alphabets indicate statistical significance compared to the other groups with p -values < 0.05 .

The increased relative number of naïve CD4⁺ and CD8⁺ cells could be attributed to the content of various fatty acids, including oleic acid, palmitic acid, butyric acid, linoleic acid, 9-hexadecanoic acid, cis-13-octadecenoic acid, and stigmaterol (Lai *et al.*, 2010; Mohan *et al.*, 2011; Sianipar *et al.*, 2016; Sianipar *et al.*, 2019). Accordingly, a study has shown that *T. flagelliforme* contains two rare fatty acids namely benzenetri-decanoic acid and benzenetri-decanoic acid methyl ester (Chen *et al.*, 1997). This suggest *T. flagelliforme* might exert the immunomodulatory activity by interfering the number of naïve CD4⁺ and CD8⁺ cells through its active metabolites. However, up-to-date, the molecular pathway by which those fatty acids affect the number of naïve CD4⁺ and CD8⁺ T cells in the thymus is not fully understood (Hidalgo *et al.*, 2021). The thymocytes migrate from bone marrow to the thymus to undergo the maturational stages. They undergo several stages until the culminating stages become single positive for either CD4 or CD8 (Mothe-Satney *et al.*, 2016).

During those processes, we suggest that one of the possible ways oleic acid, linoleic acid, and other unsaturated fatty acids may increase the number of naïve CD4⁺ and CD8⁺ T cells in the thymus is by increasing their survival rate during the thymic selection process. However, its exact mechanism is still highly unclear. One of our suspected pathways involved is the peroxisome proliferator-activated receptor (PPAR) pathway because it is activated by fatty acids including oleic acid and linoleic acid, and regulates the T cells' survival during its developmental process in the thymus (Le Menn and Neels, 2018; Mothe-Satney *et al.*, 2016). Those studies, however, suggested opposite results. The activation of PPAR β decreases the proliferation rate of CD4-CD8- double-negative stage 4 thymocytes caused by increasing fatty acid oxidation. Other in vitro studies suggest that those unsaturated fatty acids could interfere with T cells' signal transduction before any antigen stimulation, resulting in reduced proliferation capabilities of naïve T cells. In high doses, oleic acid could induce apoptosis by activating the

caspase-3 pathway (Radzikowska *et al.*, 2019; Reilly *et al.*, 2021).

3.2. The Analysis of the Relative Number of CD4⁺ and CD8⁺ Cells on Spleen

We examined the body's immunological response to rodent tuber extract administration and investigated the association between multi-dose dosages and changes in the relative numbers of CD4⁺ and CD8⁺ T cells in the mice. As the proportions of CD4⁺ and CD8⁺ T cell counts in the spleen were calculated using flow cytometry, there was a substantial shift in the relative number of CD4⁺ and CD8⁺ cells in all dosage treatments compared to the control. The results in figure 3 depict the proportion of the relative amount of CD4⁺ T cells in each treatment dosage. The relative number of CD4⁺ T cells in the control group was 18.63%. The relative number of CD4⁺ T cells in TFE50 was increased by 1.33% to 19.96%, although the increase was statistically insignificant. Meanwhile, the relative number of CD4⁺ T cells reduced significantly to 12.3% at TFE100 and 11.065% at TFE500. On the other hand, the same flow cytometry results showed an increase in the number of CD8⁺ T cells, with 11.79%, 9.25%, and 10.7% for TFE50, 100, and 500 groups, respectively, compared to the control group with 7.37%.

With increasing treatment doses, fewer CD4⁺ T cells were present; however, more CD8⁺ T cells were prevalent. The first one could appear counterintuitive because it can result in immunodeficiency. We have not been able to come up with a reasonable explanation for whether *T. flagelliforme* extract's bioactive compounds would have this impact because of limited studies on the medicinal plants, and given that it is frequently brought on by liver-related dysregulation of lipid metabolism (Tran and Sitia, 2016). However, a study found that linoleic and oleic acids could cause murine CD4⁺ T cells to undergo apoptosis, slow down their proliferation rate, and block the T cells' activation and differentiation. Particularly oleic acid inhibits the expression of IL-2 and IFN- γ (Hidalgo *et al.*, 2021). The increased number of apoptotic cells may be brought on by PPAR α activation, which causes an increase in carnitine palmitoyltransferase (CPT) on the mitochondrial membrane and impairs the function of the electron transport chain. One of the critical properties of CD4⁺ T cells is that they have more mitochondria than CD8⁺ T cells, which makes them more susceptible to oxidative stress brought on by the production of ROS, which increases the rate of apoptosis (Brown *et al.*, 2018; Reilly *et al.*, 2021). On the other hand, phytol also decreases the number of CD4⁺ T cells, particularly Th1 cells, through NOX2-induced ROS generation (Blum *et al.*, 2018).

The number of CD8⁺ T cells has been seen to rise with increasing treatment doses, in contrast to its counterpart. The concern is that not each of the major bioactive components in *T. flagelliforme* extract has been properly examined for its impact on the number of CD8⁺ T cells in the spleen. A study suggests that *T. flagelliforme* extract could increase the number of CD8⁺ T cells in immunocompromised mice after cyclophosphamide induction (Nurrochmad *et al.*, 2015). According to one study on autoimmune uveitis, phytol may enhance the CD8⁺ T effector/memory cells, a particular subset of CD8⁺ T cells, in the spleen (Daudin *et al.* 2011). However,

according to another study, neither palmitic acid, linoleic acid, nor oleic acid have any real impact on the population of cells (Medrano *et al.*, 2022). Other research suggests that palmitic acid may reduce CD8⁺ T cell numbers by interfering with mitochondrial function (Manzo *et al.*, 2020).

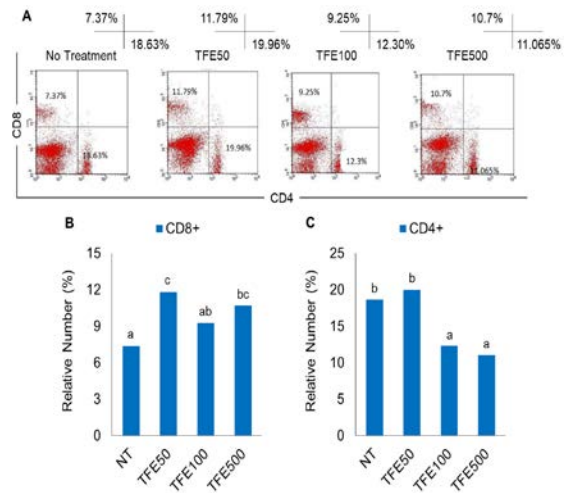


Figure 3. Immunomodulatory assessment of the effect of TFE on CD8 and CD4 T cells in spleen. (A). Flow cytometry graph of CD8⁺/CD4⁺; (B). Bar graph of CD8⁺; and (C). Bar graph of CD4⁺. The different alphabets indicate statistical significance compared to the other groups with p-values < 0.05.

The CD4⁺/CD8⁺ ratio, on the other hand, revealed that the ratios for the control, TFE50, 100, and 500 groups, respectively, were 2.520, 1.693, 1.330, and 1.034. The CD4/CD8 ratio refers to the relative number of CD4⁺ T cells and CD8⁺ T cells, including their respective subsets in the immune system (Golubovskaya and Wu, 2016). It is a crucial factor in determining whether the immune function has been altered. It also serves as a marker for chronic inflammation, particularly that brought on by HIV (Aiello *et al.*, 2019; McBride and Striker, 2017). It is still unclear what the precise CD4⁺/CD8⁺ ratio normal range should be. However, several research showed the acceptable normal ratio, higher than 1.0 (McBride and Striker, 2017; Tang *et al.*, 2015). The control group in this study exhibited the highest ratio, yet as the treatment dose increased, the ratio plummeted to virtually 1.0, which did not progress as we expected.

3.3. The Flow Cytometry Analysis of the Relative Number of CD4⁺CD62L⁺ Cells

The flow cytometry results of CD4⁺CD62L⁺ T cells revealed a substantial reduction in the relative number of CD4⁺CD62L⁺ T cells in TFE50 and TFE100 compared to the control (Figure 4). The relative number of CD4⁺CD62L⁺ T cells in the TFE50 group was down to 3.55%, the TFE100 group was down to 5.78% after the oral treatment, while the control group was maintained at 7.67%.

Our chosen markers are meant to identify the naive T helper cell population, which frequently expresses both markers but more significantly, CD62L, a cell adhesion marker that aids the naive cells in homing to secondary lymphoid organs (Putra *et al.*, 2023; Rahayu *et al.*, 2022; Watson *et al.*, 2019; Sckisel *et al.*, 2017; Yang *et al.*, 2011).

Previously, we made the assertion that the influence of the extract's predominant bioactive constituents, unsaturated fatty acids, on the population of naïve T helper cells is yet unclear. However, the second conceivable reason for this phenomenon may be related to unsaturated fatty acids' capacity to affect CD62L expression. According to a study, unsaturated fatty acids may inhibit its expression on murine naïve T helper cells (Anderson and Fritsche, 2004) making it undetectable by the designated antibody. While we are still looking for an explanation for this occurrence, it is hypothesized that it is related to the Akt pathway's activation by linoleic and oleic acids, which suppress CD62L expression (Crompton *et al.*, 2015; Marcial-Medina *et al.*, 2019; Serna-Marquez *et al.*, 2017). It might have an impact on how naïve T helper cells are conveyed. However, the same publication makes the case that adding polyunsaturated fatty acids may assist naïve T helper cells survive in the short term in the absence of immunological activation (Anderson and Fritsche, 2004). Conversely, it has been demonstrated that saturated fatty acids, such as palmitic acid, can encourage the development of effector T cells into a proinflammatory subset by upregulating the expression of SLAMF3 and IFN- γ , but this impact was seen when mice were fed a high-fat diet (Zhou *et al.*, 2019). Another hypothesis is that the phytol in the extract decreased the proportion of T cells expressing CD4⁺CD62L⁺ because it stimulated the activation of PPAR α , a crucial regulator of IL-4 release and a catalyst for the differentiation of naïve T helper cells into type 2 T helper cells (Th2) (Choi and Bothwell, 2012; Gloerich *et al.*, 2005; Lai *et al.*, 2008).

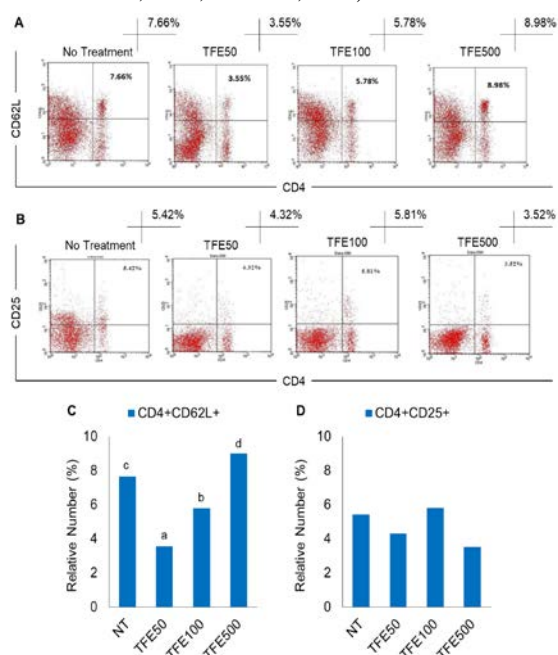


Figure 4. Immunomodulatory assessment of the effect of TFE on CD4CD62L naïve T cell and CD4CD25 regulatory T cell in spleen. (A). Flow cytometry graph of CD4⁺CD62L⁺; (B). Flow cytometry graph of CD4⁺CD25⁺; (C). Bar graph of CD4⁺CD62L⁺; and (D). Bar graph of CD4⁺CD25⁺. The different alphabets indicate statistical significance compared to the other groups with p-values < 0.05.

In contrast, providing the rodent tuber extract at a dosage of 500 mg/kg BW resulted in a substantial rise in the relative number of CD4⁺CD62L⁺ cells to 8.985% as

opposed to a decrease when compared to the control. Unfortunately, given the kind and quantity of bioactive chemicals in the extract, we are unable to come up with a solid explanation for this behavior. It is suggested that the treatments reduced the number of T cells expressing CD4⁺CD62L⁺ because the naïve T cells were promoted into effector cells, such as CD4⁺ T cells expressing CD8⁺, CD69⁺, CD25⁺, and CD44⁺. A reduction in the number of CD4⁺CD62L⁺ T cells reflects the activity of naïve cells, which transform into a subset of CD4⁺ T cells, such as regulatory T cells, as a result of antigen exposure.

3.4. The Analysis of the Relative and Absolute Number of CD4⁺CD25⁺ Cells

The spleen flow cytometry results in figure 4 showed the relative number of CD4⁺CD25⁺ T cells among the total lymphocyte cells. It was demonstrated that mice treated with TFE100 significantly increased CD4⁺CD25⁺ cells' number to 5.81% compared to the control group with 5.42%, while the TFE500 group's cell number exhibited a significant drop to 4.32%. The most significant reduction in CD4⁺CD25⁺ cell number was observed in the TFE50 group, which dropped as low as 3.53% (Figure 4).

One of the possible explanations for the low number of CD4⁺CD25⁺ T cells, better known as regulatory T cells (Tregs), was that the mice models were unexposed to any form of infections or antigens. Because of the nature of the study, which did not expose any antigen to the mouse model; we assumed that the Tregs population measured is categorized under naturally occurring Treg cells. Normally, the population number of naturally occurring Treg cells in the spleen for both human and murine is around 5-10% (Ali and Rosenblum, 2017; Lourenço and La Cava, 2011), which is importantly critical for modulating peripheral tolerance and preventing autoimmune disease (Rocamora-Reverte *et al.* 2021). This number, however, indicates that the population of CD4⁺CD25⁺ T cells in this study is in the lower band of the normal range. Nonetheless, autoimmune research suggests that the normal percentage range of circulating CD4⁺CD25⁺ T cells is from 0.6% to 7.9% (Nurrochmad *et al.*, 2015), making the results completely in the acceptable range.

A study suggests that supplementing polyunsaturated fatty acid could increase the number of Tregs because PPAR γ has a higher affinity for it (Kurniawan *et al.*, 2020). Also, short-chain fatty acids such as butyric acid could induce the expression of FOXP3 by increasing the acetylation of histone H3 in the promoter region and promoting Treg formation (Kempkes *et al.*, 2019). Oleic acid and 9-hexadecenoic acid are suggested to increase Tregs population number through promoting the expression of FOXP3 (Passos *et al.*, 2016; Pompura *et al.*, 2021). We found that almost no study depicted a decreased number of Tregs caused by bioactive compounds in *T. flagelliforme* extract, shown at TFE50 and TFE500 administration. However, it is important to note that the research on their effect on Tregs is still in the early stages, and more studies are needed to fully understand the mechanisms underlying this effect and determine whether similar effects can be observed in humans.

We predominantly suggest that the subset of T cells we studied is Tregs, or naturally occurring Tregs, to be exact, because we assumed that it also expressed FOXP3⁺.

However, it is worth noting that the CD4⁺CD25⁺ T cells could behave as effector cells in addition to being regulatory cells because they lack FOXP3 protein (CD4⁺CD25⁺FOXP3⁻), which is a determinant of their activity as regulators. They were conventional cells activated to become effector cells after exposure to allergens (Wing *et al.*, 2002). Further research is needed to precisely determine the exact function of CD4⁺CD25⁺ T cells in this study because CD4⁺ T cells expressing CD25 surface marker can serve as either conventional cells triggered by allergens or regulatory T cells. As a result, the involvement of CD4⁺CD25⁺ cells must be explored in future research focused on FOXP3. Because this study did not utilize an anti-Foxp3 antibody, the role of CD4⁺CD25⁺ T cells in the results cannot be simply justified.

3.5. Liver Toxicity Analysis After Rodent Tuber Extract Administration

The cytotoxic impact of the rodent tuber extract on liver histopathology with hematoxylin-eosin staining revealed that the control group has hexagonal hepatocytes with a single nucleus, but some have two nuclei (binucleate) in its center. A cell's nucleus undergoing karyorrhexis may be noticed in the liver of TFE50 treatment mice (Figure 5). Administration of TFE100 and TFE500 might induce liver injury by necrosis (marked by an arrow) during the karyorrhexis stage, where nuclear cells in hepatocytes are fragmented or undergo cell lysis. Necrosis is a manifestation of liver damage caused by toxic compounds, including high-level of saponins, or induced by certain diseases caused by viruses and bacteria. This term could be further categorized as drug-induced liver injury (DILI), a common side effect of all drug supplementations, including herbal, particularly as an effect of inhibiting critical enzymes, such as cytochromes and alanine aminotransferase (Mega *et al.*, 2021; Navarro *et al.*, 2017). The results found no statistically significant difference between the treatment groups, implying that all doses did not exert any harmful effect on hepatocytes nor trigger necrosis.

Although we cannot find plenty of research mentioned about the side effect of *T. flagelliforme* extract administration, we found research that has contradicting results, stating that it could have toxic effects on hepatocytes, defined by increased levels of Serum Glutamate Oxaloacetate Transferase (SGOT) and Serum Glutamate Pyruvate Transferase (SGPT) in the blood caused by damaged cells (Isturingrum, 2010; Linasari, 2010). These effects are predicted to be an effect of high-concentration exposure to saponins because they could disrupt the integrity of the liver cell membrane. Saponins have been shown to have detergent-like properties, which can disrupt the lipid bilayer of the cell membrane. This phenomenon can cause leakage of intracellular contents and ultimately lead to cell death (Sudji *et al.*, 2015). The detergent-like properties of saponins are thought to be due to their structural features, specifically the presence of a hydrophobic triterpene or steroidal sapogenin and a hydrophilic carbohydrate moiety (Mugford and Osbourn, 2012; Xu and Yu, 2021). The hydrophobic region of the saponin molecule can interact with the lipid bilayer of the cell membrane, disrupting its integrity and leading to cell death. In addition, saponins may also contribute to liver cell death by altering the absorption and metabolism of other substances. Saponins have been shown to interfere with the absorption of nutrients, particularly fat-soluble

vitamins, which can lead to deficiencies that may contribute to liver injury and cell death (Pathaw *et al.*, 2022; Samtiya *et al.*, 2020). They may also alter the metabolism of certain drugs, potentially leading to liver injury and cell death. However, because we cannot identify any significant hepatocyte damage, it is safe to assume that the saponin content in the tested extract was well below the critical limit because a low concentration of saponins could have a hepatoprotective effect (Juszczak *et al.*, 2021; Qu *et al.*, 2012). Other than that, we cannot find any data on any toxic effect on hepatocytes caused by oleic acid, palmitic acid, butyric acid, linoleic acid, 9-hexadecanoic acid, cis-13-octadecenoic acid, and stigmasterol at possible concentration contained in the *T. flagelliforme* extract.

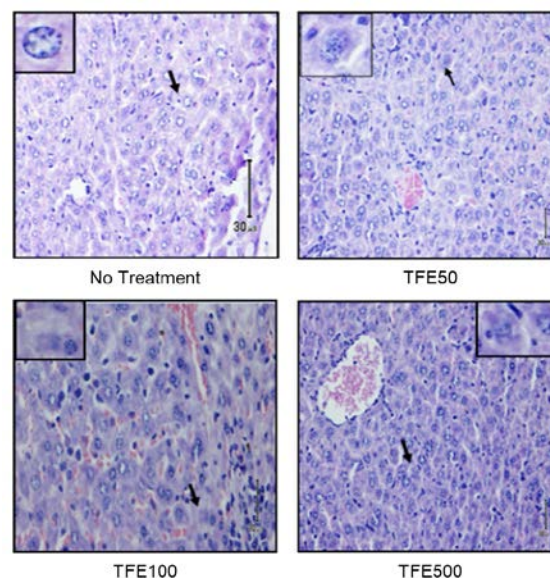


Figure 5. Representative microphotograph of liver section from experimental mice model (HE staining, M = 400×).

Although the common perception towards medicinal plants have far less concerning side effects than its commercial counterparts, it is not fully risk-free either. One of the most utilized herbals, turmeric, is thought to be the main cause of acute liver injury, particularly when combined with black pepper, because piperine in the black pepper increases the curcumin absorption up to 20 fold, causing hepatotoxicity effect (Halegoua-DeMarzio *et al.*, 2022; Sohal *et al.*, 2021).

T. flagelliforme extract, in addition to the immune cells mentioned previously, may influence other types of immune cells, according to various studies. In immunocompromised mice, the extract could increase the levels of various cytokines such as TNF- α and IL-1 α , as well as the number and activity of macrophages, particularly their phagocytic index and capacity. However, in higher doses, the effect could also be reversed (Nurrochmad *et al.*, 2015; Sagala and Murwanti, 2020). It also upregulates the heat shock protein-70 (Hsp-70) in the tumor associated macrophages, which then change their polarization towards pro-inflammatory M1-like macrophages, promoting cancer cell apoptosis via an extrinsic apoptotic pathway (Ibrahim *et al.*, 2022; Lai *et al.*, 2008). *T. flagelliforme* extract has been studied for its apoptosis activity or anti-proliferative effects on numerous of cancer cells (Table 1). For example, in the WEHI-3 leukemia model case, the extract administration also impacted the number of peripheral immature granulocytes

and monocytes by lowering their numbers (Mohan *et al.*, 2010).

Overall, the data point to immune-modulating properties of *T. flagelliforme* extract, which may be helpful in the treatment of a range of immune-related conditions. To cover its effects on a wider spectrum of immune cells and completely comprehend the processes underlying these effects, further research is required due to its limited availability.

Table 1. Several distinct biological activities attributed to *T. flagelliforme* have been observed

No.	Experimental target	Biological activity	Reference
1	CSCC cells	↑ antiproliferation activity	Prisoeryanto <i>et al.</i> , 2020
	Rabbit endothelial cells	↑ antiangiogenesis activity	
2	DMBA-Induced Rats Breast Tumor	↑ Cancer chemopreventive effect ↓ tumor incidence, tumor size, and tumor weight	Maysarah <i>et al.</i> , 2020
3	RBL-2H3 cells	↑ anti-allergic activity	Korinek <i>et al.</i> , 2017
4	HeLa and T47D cells	↓ telomerase expression	Purwaningsih <i>et al.</i> , 2016
5	WiDr cells	↑ apoptosis activity ↓ COX-2 expression	Setiawati <i>et al.</i> , 2016
6	CEMss cells	↑ cytotoxicity ↑ cellular DNA breaks ↑ apoptosis activity	Mohan <i>et al.</i> , 2011
7	WEHI-3 cells BALB/c leukemia mice model	↓ proliferation activity ↓ immature granulocytes and monocytes	Mohan <i>et al.</i> , 2010
8	CEMss cells	↑ apoptosis via ↑ activation of caspase-9, PARP cleavage and cytochrome c release	Mohan <i>et al.</i> , 2010
9	NCI-H23 cells	↓ cancer cell growth ↑ induces apoptosis	Lai <i>et al.</i> , 2008

4. Conclusion

Based on our findings, there was an increase in the number of CD8⁺ T cells as well as CD4⁺CD62L⁺ naïve T cells in the spleen. Additionally, there was an increase in the relative number of CD8⁺ T cells and CD4⁺ T cells in the thymus. Based on these observations, it seems likely that TFE are responsible for the immunomodulatory function that helps particular immune cells thrive.

Acknowledgement

The authors thank Brawijaya University for support and provide the research grant (Muhaimin Rifa'i) for this study.

Conflict of Interest

No conflict of interests.

References

- Aiello A, Farzaneh F, Candore G, Caruso C, Davinelli S, Gambino CM, Ligotti ME, Zareian N, and Accardi G. 2019. Immunosenescence and its hallmarks: How to oppose aging strategically? A review of potential options for therapeutic intervention. *Front. Immunol.*, **25**: 1-19.
- Ali N, and Rosenblum MD. 2017. Regulatory T cells in skin. *Immunol.*, **152**: 372–381.
- Amorim JL, Simas DLR, Pinheiro MMG, Moreno DSA, Alviano CS, da Silva AJR, and Dias Fernandes P. 2016. Anti-inflammatory properties and chemical characterization of the essential oils of four citrus species. *PLoS One*, **11**: 1–18.
- Anderson MJ, and Fritsche KL. 2004. Dietary polyunsaturated fatty acids modulate in vivo, antigen-driven CD4⁺ T-cell proliferation in mice. *J Nutr.*, **134**:1978–1983.
- Bian Y, Liu P, Zhong J, Hu Y, Fan Y, Zhuang S, and Liu Z. 2019. Kaempferol inhibits multiple pathways involved in the secretion of inflammatory mediators from LPS-induced rat intestinal microvascular endothelial cells. *Mol. Med. Rep.*, **19**: 1958–1964.
- Blum L, Tafferfer N, Spring I, Kurz J, deBruin N, Geisslinger G, Parnham MJ, and Schiffmann S. 2018. Dietary phytol reduces clinical symptoms in experimental autoimmune encephalomyelitis (EAE) at least partially by modulating NOX2 expression. *J. Mol. Med.*, **96**: 1131–1144.
- Brown ZJ, Fu Q, and Ma C. 2018. Carnitine palmitoyltransferase gene upregulation by linoleic acid induces CD4⁺ T cell apoptosis promoting HCC development. *Cell Death Dis.*, **9**: 1–14.
- Cao T, Shao S, Fang H, Li B, and Wang G. 2019. Role of regulatory immune cells and molecules in autoimmune bullous dermatoses. *Front. Immunol.*, **10**: 1–11.
- Carvajal JJ, Avellaneda AM, Salazar-Ardiles C, Maya JE, Kalergis AM, and Lay MK. 2019. Host components contributing to respiratory syncytial virus pathogenesis. *Front. Immunol.*, **10**: 1–19.
- Chen SX, Goh CJ, and Kon OL. 1997. Fatty acids from *Typhonium flagelliforme*. *Planta Med.*, **63**: 580-581.
- Cheng S-C, Huang W-C, S. Pang J-H, Wu Y-H, and Cheng C-Y. 2019. Quercetin inhibits the production of IL-1β-induced inflammatory cytokines and chemokines in ARPE-19 cells via the MAPK and NF-κB signaling pathways. *Int. J. Mol. Sci.*, **20**:1–24.
- Childs CE, Calder PC, and Miles EA. 2019. Diet and immune function. *Nutrients*, **11**: 1–9.
- Choi J-M, and Bothwell ALM. 2012. The nuclear receptor PPARs as important regulators of T-cell functions and autoimmune diseases. *Mol. Cells*, **33**: 217–222.
- Cicchese JM, Evans S, and Hult C. 2018. Dynamic balance of pro- and anti-inflammatory signals controls disease and limits pathology. *Immunol. Rev.*, **285**: 147–167.
- Crompton JG, Sukumar M, and Roychoudhuri R. 2015. Akt inhibition enhances expansion of potent tumor-specific lymphocytes with memory cell characteristics. *Cancer Res.*, **75**: 296–305.
- Crystalia AA, and Hillary H. 2022. Anticancer activity of *Typhonium flagelliforme*: A systematic review. *IJLS*, **4**: 100–119.
- Dash S, Ray M, Parida R, Achary KG, Nayak S, and Singh S. 2018. Edible plant-derived essential oils synergistically enhance the Th1, Th2 and anti-inflammatory cytokines in neonatal cord blood monocytic cell line. *Food Agric Immunol.*, **29**: 346–357.

- Daudin J-B, Monnet D, and Kavian N. 2011. Protective effect of pristane on experimental autoimmune uveitis. *Immunol. Lett.*, **141**: 83–93.
- Dias S, D'Amico A, and Cretney E. 2017. Effector regulatory T cell differentiation and immune homeostasis depend on the transcription factor Myb. *Immunity*, **46**: 78–91.
- Gloerich J, van Vlies N, Jansen GA, Denis S, Ruiter JPN, van Werkhoven MA, Duran M, Vaz FM, Wanders RJA, and Ferdinandusse S. 2005. A phytol-enriched diet induces changes in fatty acid metabolism in mice both via PPAR α -dependent and -independent pathways. *J. Lipid Res.*, **46**: 716–726.
- Golubovskaya V, and Wu L. 2016. Different subsets of T cells, memory, effector functions, and CAR-T immunotherapy. *Cancers (Basel)*, **8**: 36.
- Halegoua-DeMarzio D, Navarro V, and Ahmad J. 2022. Liver injury associated with turmeric-a growing problem: Ten cases from the drug-induced liver injury network. *Am. J. Med.*, **9343**: 740–9.
- Hidalgo MA, Carretta MD, and Burgos RA. 2021. Long chain fatty acids as modulators of immune cells function: Contribution of FFA1 and FFA4 receptors. *Front. Physiol.*, **12**: 1–18.
- Horwitz DA, Fahmy TM, and Piccirillo CA, Cava AL. 2019. Rebalancing immune homeostasis to treat autoimmune diseases. *Trends Immunol.*, **40**: 888–908.
- Huntington ND, and Gray DH. 2018. Immune homeostasis in health and disease. *Immunol. Cell Biol.*, **96**: 451–452.
- Hurst TP, and Magiorkinis G. 2019. Editorial: The past and the future of human immunity under viral evolutionary pressure. *Front. Immunol.*, **10**: 1–3.
- Ibrahim S, Putra A, Amalina ND, and Nasution IPA. 2022. Heat shock protein-70 expression in CSCs tumor-associated macrophages induced by *Typhonium flagelliforme* tuber extract. *J. Appl. Pharm. Sci.*, **12**: 146–152.
- Isturiningrum D. 2010. **Pengaruh lama pemberian suspensi herbal keladi tikus (*Typhonium flagelliforme*) terhadap kadar SGOT dan SGPT pada tikus putih (*Rattus norvegicus*)**. Thesis, Universitas Airlangga, Surabaya.
- Juszczak M, Kluska M, Skalski B, Żuchowski J, Stochmal A, Olas B, and Woźniak K. 2021. Multidirectional effects of saponin fraction isolated from the leaves of sea buckthorn *Elaeagnus rhamnoides* (L.) A. Nelson. *Biomed. Pharmacother.*, **137**: 111395.
- Karthikeyan A, Kim HH, Preethi V, Moniruzzaman M, Lee KH, Kalaiselvi S, Kim GS, and Min T. 2021. Assessment of anti-inflammatory and antioxidant effects of citrus unshiu peel (CUP) flavonoids on LPS-stimulated RAW 264.7 Cells. *Plants (Basel)*, **10**: 1–15.
- Kempkes RWM, Joosten I, Koenen HJPM, and He X. 2019. Metabolic pathways involved in regulatory T cell functionality. *Front. Immunol.*, **10**: 1–13.
- Kitcharoensakkul M, and Cooper MA. 2020. **Chapter 28 - autoimmunity in primary immunodeficiency disorders**. In: Rose NR, Mackay IR (eds) *The autoimmune diseases* (Sixth Edition). Academic Press, pp 513–532.
- Korinek M, Tsai YH, El-Shazly M, Lai KH, Backlund A, Wu SF, Lai WC, Wu TY, Chen SL, Wu YC, Cheng YB, Hwang TL, Chen BH, and Chang FR. 2017. Anti-allergic hydroxy fatty acids from *Typhonium blumei* explored through ChemGPS-NP. *Front. Pharmacol.*, **8**: 1-17.
- Kurniawan H, Soriano-Baguet L, and Brenner D. 2020. Regulatory T cell metabolism at the intersection between autoimmune diseases and cancer. *Eur. J. Immunol.*, **50**: 1626–1642.
- Lai C-S, Mas RHM, Nair NK, Majid MIA, Mansor SM, and Navaratnam V. 2008. Typhonium flagelliforme inhibits cancer cell growth in vitro and induces apoptosis: an evaluation by the bioactivity guided approach. *J. Ethnopharmacol.*, **118**: 14–20.
- Lai C-S, Mas RHM, Nair NK, Mansor SM, and Navaratnam V. 2010. Chemical constituents and in vitro anticancer activity of *Typhonium flagelliforme* (Araceae). *J. Ethnopharmacol.*, **127**: 486–494.
- Laurent D, Sianipar NF, Chelen, Listiari, and Wantho A. 2015. Analysis of genetic diversity of Indonesia rodent tuber (*Typhonium flagelliforme* Lodd.) cultivars based on RAPD marker. *KnE Life Sci.*, **2**:139–145
- Le Menn G, and Neels JG. 2018. Regulation of immune cell function by PPARs and the connection with metabolic and neurodegenerative diseases. *Int. J. Mol. Sci.*, **19**:1–16.
- Lee AJ, Lim JW, and Kim H. 2021. Ascorbic acid suppresses house dust mite-induced expression of interleukin-8 in human respiratory epithelial cells. *J. Cancer Prev.*, **26**: 64–70.
- Linasari N. 2010. **Uji toksitas sub kronis suspensi keladi tikus (*Typhonium flagelliforme*) terhadap gambaran histopatologi hati tikus putih (*Rattus norvegicus*) Jantan**. Thesis, Universitas Airlangga, Surabaya.
- Lotfi N, Thome R, Rezaei N, Zhang G-X, Rezaei A, Rostami A, and Esmail N. 2019. Roles of GM-CSF in the pathogenesis of autoimmune diseases: An update. *Front. Immunol.*, **10**: 1–14.
- Lourenço EV, and La Cava A. 2011. Natural regulatory T cells in autoimmunity. *Autoimmun.*, **44**: 33–42.
- Mahassni SH, and Alsaifi BS. 2019. A pilot study: Ground and aqueous extract of *Leptadenia pyrotechnica* modulate the immune system affecting white blood cell counts and increasing red blood cell counts. *Jordan J. Biol. Sci.*, **15**: 413-421.
- Maher T, Ahmad Raus R, Daddiouaissa D, Ahmad F, Adzhar NS, Latif ES, Abdulhafiz F, and Mohammed A. 2021. Medicinal plants with anti-leukemic effects: A review. *Molecules*, **26**: 1–25.
- Manzo T, Prentice BM, and Anderson KG. 2020. Accumulation of long-chain fatty acids in the tumor microenvironment drives dysfunction in intrapancreatic CD8⁺ T cells. *J. Exp. Med.*, **217**: e20191920.
- Marcial-Medina C, Ordoñez-Moreno A, Gonzalez-Reyes C, Cortes-Reynosa P, and Perez Salazar E. 2019. Oleic acid induces migration through a FFAR1/4, EGFR and AKT-dependent pathway in breast cancer cells. *Endocr. Connect.*, **8**: 252–265
- Maysarah H, Faradilla M, Sari Irma, and Illian DN. 2022. Cancer chemopreventive effect of rodent tuber (*Typhonium flagelliforme* (Lood) Bl) against DMBA-induced rats breast tumor. *Res J Pharm Technol.*, **13**: 1-5.
- McBride JA, and Striker R. 2017. Imbalance in the game of T cells: What can the CD4/CD8 T-cell ratio tell us about HIV and health? *PLOS Pathogens*, **13**: e1006624.
- Medrano M, Lemus-Conejo A, and Lopez S. 2022. CD4⁺ and CD8⁺ T-cell responses in bone marrow to fatty acids in high-fat diets. *J. Nutr. Biochem.*, **107**: 109057.
- Mega A, Marzi L, Kob M, Piccin A, and Floreani A. 2021. Food and nutrition in the pathogenesis of liver damage. *Nutrients*, **13**: 1–13.
- Miles EA, and Calder PC. 2021. Effects of citrus fruit juices and their bioactive components on inflammation and immunity: A narrative review. *Front. Immunol.*, **12**: 1–18.
- Mohan S, Abdul AB, Abdelwahab SI, Al-Zubairi AS, Aspollah Sukari M, Abdullah R, Taha MME, Beng NK, and Isa NM. 2010. *Typhonium flagelliforme* inhibits the proliferation of murine leukemia WEHI-3 cells in vitro and induces apoptosis in vivo. *Leuk. Res.*, **34**: 1483–1492.

- Mohan S, Abdul AB, Abdelwahab SI, Al-Zubairi AS, Sukari MA, Abdullah R, Elhassan Taha MM, Ibrahim MY, and Syam S. 2010. *Typhonium flagelliforme* induces apoptosis in CEMss cells via activation of caspase-9, PARP cleavage and cytochrome c release: its activation coupled with G0/G1 phase cell cycle arrest. *J. Ethnopharmacol.*, **131**: 592-600.
- Mohan S, Bustamam A, Ibrahim S, Al-Zubairi AS, Aspollah M, Abdullah R, and Elhassan MM. 2011. *In vitro* ultramorphological assessment of apoptosis on CEMss induced by linoleic acid-rich fraction from *Typhonium flagelliforme* tuber. *Evid Based Complement Alternat Med.*, **421894**: 1-13
- Mothe-Satney I, Murdaca J, and Sibille B. 2016. A role for peroxisome proliferator-activated receptor beta in T cell development. *Sci. Rep.*, **6**: 1-12.
- Mugford ST, and Osbourn A. 2012. Saponin Synthesis and Function. *ISPM*, **28**: 405-424
- Navarro VJ, Khan I, Björnsson E, Seeff LB, Serrano J, and Hoofnagle JH. 2017. Liver injury from herbal and dietary supplements. *Hepatology*, **65**: 363-373.
- Nicholson LB. 2016. The immune system. *Essays Biochem.*, **60**: 275-301.
- Nurrochmad A, Ikawati M, Sari IP, Murwanti R, and Nugroho AE. 2015. Immunomodulatory effects of ethanolic extract of *Typhonium flagelliforme* (Lodd) Blume in rats induced by Cyclophosphamide. *Evid. Based Complementary Altern.*, **20**: 167-172.
- Orhan IE, Mesaik MA, Jabeen A, and Kan Y. 2016. Immunomodulatory properties of various natural compounds and essential oils through modulation of human cellular immune response. *Ind Crops Prod.*, **81**: 117-122.
- Papp G, Boros P, Nakken B, Szodoray P, and Zeher M. 2017. Regulatory immune cells and functions in autoimmunity and transplantation immunology. *Autoimmun. Rev.*, **16**: 435-444.
- Passos MEP, Alves HHO, Momesso CM, Faria FG, Murata G, Cury-Boaventura MF, Hatanaka E, Massao-Hirabara S, and Gorjão R. 2016. Differential effects of palmitoleic acid on human lymphocyte proliferation and function. *Lipids Health Dis.*, **15**: 1-11.
- Pathaw N, Devi KS, Sapam R, Sanasam J, Monteshori S, Phurailatpam S, Devi HC, Chanu WT, Wangkhem B, and Mangang NL. 2022. A comparative review on the anti-nutritional factors of herbal tea concoctions and their reduction strategies. *Front. nutr.*, **9**: 1-14.
- Pompura SL, Wagner A, Kitz A, LaPerche J, Yosef N, Dominguez-Villar M, and Hafler DA. 2021. Oleic acid restores suppressive defects in tissue-resident FOXP3 Tregs from patients with multiple sclerosis. *J. Clin. Investig.*, **131**: 1-16.
- Priosoeryanto BP, Rostantinata R, Harlina E, Nurcholis W, Ridho R, and Sutardi LN. 2020. *In vitro* antiproliferation activity of *Typhonium flagelliforme* leaves ethanol extract and its combination with canine interferons on several tumor-derived cell lines. *Vet. World.*, **13**: 931-939.
- Purwaningsih E, Suciati Y, and Widayanti E. 2016. *Typhonium flagelliforme* decreases telomerase expression in HeLa cervical cancer cells. *Universa Medic.*, **35**: 1-7.
- Putra WE, Agusinta AK, Ashar MSAA, Manullang VA, Rifa'i M. 2023. Immunomodulatory and ameliorative effect of *Citrus limon* extract on DMBA-induced breast cancer in mouse. *Karbala Int. J. Mod. Sci.*, **9**: 1-14.
- Putra WE, Maulana AR, Ramadhan ATK, and Rifa'i M. 2020. T cells regulation modulated by *Sambucus javanica* extracts in DMBA-exposed mice. *J. HerbMed Pharmacol.*, **9**: 408-411.
- Putra WE, Rifa'i M. 2019. Immunomodulatory activities of *Sambucus javanica* extracts in DMBA exposed BALB/c mouse. *Adv. Pharm. Bull.*, **9**: 619-623.
- Putra WE, Rifa'i M. 2020. Assessing the immunomodulatory activity of ethanol extract of *Sambucus javanica* berries and leaves in Chloramphenicol-induced aplastic anemia mouse model. *Trop. Life Sci. Res.*, **31**: 175-185.
- Putra WE, Rifa'i M, Lestari SR, Susanto H, Gofur A. 2021. Evaluating the granzyme production from CD8 T cells and NK1.1 natural killer cell after treating by the combination of *Momordica charantia* and *Averrhoa bilimbi* extract in STZ induced mice. *AIP Conf Proc.* **2353**, **030075**: 1-5.
- Putra WE, Soewondo A, Rifa'i M. 2016. Effect of dexamethasone administration toward hematopoietic stem cells and blood progenitor cells expression on BALB/c mice. *J. pure appl. chem. res.*, **4**: 100-108.
- Putra WE, Soewondo A, Rifa'i M. 2015. Expression of erythroid progenitor cells and erythrocytes on dexamethasone induced-mice. *Biotropika*, **3**: 42-45.
- Putra WE, Waffareta E, Ardiana O, Januarisasi ID, Soewondo A, Rifa'i M. 2017. Dexamethasone-administrated BALB/c mouse promotes proinflammatory cytokine expression and reduces CD4⁺CD25⁺ regulatory T cells population. *Biosci. Res.*, **14**: 201-213.
- Qu L, Xin H, Zheng G, Su Y, and Ling C. 2012. Hepatoprotective activity of the total saponins from *Actinidia valvata* Dunn root against carbon tetrachloride-induced liver damage in mice. *Evid. Based Complementary Altern.*, **2012**: 1-13.
- Radzikowska U, Rinaldi AO, Çelebi Sözen Z, Karaguzel D, Wojcik M, Cypriak K, Akdis M, Akdis CA, and Sokolowska M. 2019. The influence of dietary fatty acids on immune responses. *Nutrients*, **11**: 1-52.
- Rahayu S, Rifa'i M, Qosimah D, Widyarti D, Lestari ND, Jatmiko YD, Putra WE, and Tsuboi H. 2022. Benefits of *Coriandrum sativum* L. seed extract in maintaining immunocompetent cell homeostasis. *Sains Malays.*, **51**: 2425-2434.
- Reilly NA, Lutgens E, Kuiper J, Heijmans BT, and Wouter Jukema J. 2021. Effects of fatty acids on T cell function: Role in atherosclerosis. *Nat. Rev. Cardiol.*, **18**: 824-837.
- Rocamora-Reverte L, Melzer FL, Würzner R, and Weinberger B. 2021. The complex role of regulatory T cells in immunity and aging. *Front. immunol.*, **11**: 1-12.
- Sagala RJ, and Murwanti R. 2020. The combination of ethanol extracts of *Phyllanthus niruri* Linn, *Typhonium flagelliforme* and *Piper crocatum* increase the macrophage phagocytosis in vitro. *MOT*, **25**: 67-75.
- Samtiya M, Aluko RE, and Dhewa T. 2020. Plant food anti-nutritional factors and their reduction strategies: an overview. *Food Prod. Process. Nutr.*, **2**: 1-14.
- Skisel GD, Mirsoian A, Minnar CM, Crittenden M, Curti B, Chen JQ, Blazar BR, Borowsky AD, Monjabez AM, and Murphy WJ. 2017. Differential phenotypes of memory CD4 and CD8 T cells in the spleen and peripheral tissues following immunostimulatory therapy. *J. Immunother. Cancer.*, **5**: 1-11.
- Serna-Marquez N, Diaz-Aragon R, Reyes-Urbe E, Cortes-Reynosa P, and Salazar EP. 2017. Linoleic acid induces migration and invasion through FFAR4- and PI3K-/Akt-dependent pathway in MDA-MB-231 breast cancer cells. *Med. Oncol.*, **34**: 1-12.
- Setiawati A, Immanuel H, and Utami MT. 2016. The inhibition of *Typhonium flagelliforme* Lodd. Blume leaf extract on COX-2 expression of WiDr colon cancer cells. *Asian Pac. J. Trop. Biomed.*, **6**: 251-255.
- Sianipar NF, Assidqi K, Purnamaningsih R, and Herlina T. 2019. In vitro cytotoxic activity of rodent tuber mutant plant

- (*Typhonium flagelliforme* Lodd.) against to MCF-7 breast cancer cell line. *Asian J. Pharm. Clin. Res.*, **12**: 185–189.
- Sianipar NF, Purnamaningsih R, Darwati I, and Laurent D. 2016. Gas chromatography-mass spectrometry (GC-MS) analysis of phytochemicals of first generation gamma-irradiated *Typhonium flagelliforme* Lodd. mutants. *J Teknol.*, **78**: 1–7.
- Sohal A, Alhankawi D, Sandhu S, and Chintanaboina J. 2021. Turmeric-induced hepatotoxicity: report of 2 cases. *Int. Medical Case Rep. J.*, **14**: 849–852.
- Sowjanya K, Girish C, Bammigatti C, and Prasanna Lakshmi N. 2021. Efficacy of *Phyllanthus niruri* on improving liver functions in patients with alcoholic hepatitis: A double-blind randomized controlled trial. *Indian J. Pharmacol.*, **53**: 448.
- Sudji IR, Subburaj Y, Frenkel N, García-Sáez AJ, and Wink M. 2015. Membrane disintegration caused by the steroid saponin digitonin is related to the presence of cholesterol. *Molecules*, **20**: 20146–20160.
- Sujono TA, Kusumowati ITD, and Munawaroh R. 2020. Immunomodulatory activity of *Muntingia calabura* L fruits using carbon clearance assay and their total flavonoid and phenolic contents. *Asian J. Pharm. Clin. Res.*, **13**: 140–145.
- Tang J, Li X, and Price MA. 2015. CD4: CD8 lymphocyte ratio as a quantitative measure of immunologic health in HIV-1 infection: Findings from an African cohort with prospective data. *Front. Microbiol.*, **6**: 1–9.
- Tao L, Liu H, and Gong Y. 2019. Role and mechanism of the Th17/Treg cell balance in the development and progression of insulin resistance. *Mol. Cell Biochem.*, **459**: 183–188.
- Tourkochristou E, Triantos C, and Mouzaki A. 2021. The influence of nutritional factors on immunological outcomes. *Front. Immunol.*, **12**: 1–17.
- Tran NL, and Sitia G. 2016. New players in non-alcoholic fatty liver disease induced carcinogenesis: Lipid dysregulation impairs liver immune surveillance. *Hepatobiliary Surg. Nutr.*, **5**: 511.
- Watson HA, Durairaj RRP, and Ohme J. 2019. L-selectin enhanced T cells improve the efficacy of cancer immunotherapy. *Front. Immunol.*, **10**: 1–20.
- Wing K, Ekmark A, Karlsson H, Rudin A, and Suri-Payer E. 2002. Characterization of human CD25⁺CD4⁺ T cells in thymus, cord and adult blood. *Immunol.*, **106**: 190–199.
- Xiao S, Liu W, Bi J, Liu S, Zhao H, Gong N, Xing D, Gao H, and Gong M. 2018. Anti-inflammatory effect of hesperidin enhances chondrogenesis of human mesenchymal stem cells for cartilage tissue repair. *J. Inflamm-Lond.*, **15**: 1–8.
- Xu P, and Yu B. 2021. **Chapter one - chemical synthesis of saponins: An update.** In: Baker DC (ed) *Advances in Carbohydrate Chemistry and Biochemistry*. Academic Press, pp 1–62.
- Yang S, Liu F, Wang QJ, Rosenberg SA, and Morgan RA. 2011. The shedding of CD62L (L-selectin) regulates the acquisition of lytic activity in human tumor reactive T lymphocytes. *PLoS One*, **6**: 1–10.
- Yuandani, Jantan I, Rohani AS, and Sumantri IB. 2021. Immunomodulatory effects and mechanisms of curcuma species and their bioactive compounds: A review. *Front. Pharmacol.*, **12**: 1–26.
- Zaiss DMW, and Coffey PJ. 2018. Forkhead box transcription factors as context-dependent regulators of lymphocyte homeostasis. *Nat. Rev. Immunol.*, **18**: 703–715.
- Zhou T, Wang G, and Lyu Y. 2019. Upregulation of SLAMF3 on human T cells is induced by palmitic acid through the STAT5-PI3K/Akt pathway and features the chronic inflammatory profiles of type 2 diabetes. *Cell Death Dis.*, **10**: 1–10.

Evaluation of Antifungal Potential of *Mentha pulegium* Essential oil in Biological Control Against the Pathogen of Inflorescence Rot Disease of Date Palm (*Mauginiella scaettae*)

Hammia Hadjra^{1,*}, Bouatrous Yamina¹, Kriker Soulef¹, Ramazan Erenler²

¹ Department of Nature and Life Sciences, Faculty of Exact Sciences and Nature and Life Sciences, Mohamed khider University, 07000;

² Department of Chemistry, Faculty of Art and Science, Tokat Gaziosmanpasa University, Turkey.

Received: February 20, 2023; Revised: April 12, 2023; Accepted: April 26, 2023

Abstract

In desert environments, the date palm is a vital component of the oasis ecosystem. Despite its importance to the local community and the national economy, date palm agriculture in Algeria faces a number of challenges. One of the biggest obstacles is infectious diseases, such as the fungus *Mauginiella scaettae*'s date palm inflorescence rot. While fungicides play an important role in controlling this disease, their use can have negative consequences for human health and the environment due to the presence of residues. In the context of this growth, there is an increasing interest in moving from pesticides to ecologically benign disease management methods. Thus, it is necessary to study innovative methods for the effective and safe control of inflorescence rot. Due to their antifungal qualities, it appears that using the essences of some aromatic and medicinal herbs is one of the most efficient methods for preventing fungal illnesses. In this regard, the latest research evaluates the efficacy of an alternative technique to synthetic fungicides, specifically the examination of *Mentha pulegium* essential oils' antifungal activity "in vitro". Therefore, the purpose of this research consisted of the identification of chemical components involved in *Mentha pulegium* as well as investigation of its possible antifungal activity against *Mauginiella scaettae*. *In vitro* testing was done to determine the antifungal effects of volatile oil at selected doses (0.25, 0.5, and 1) $\mu\text{l/ml}$ against *Mauginiella scaettae*. The obtained data show a yield of $0.99 \pm 0.041\%$ for the essential oil. Seventeen components were identified in the essential oil studied. Isomenthone (19.31%), Thymol (11.39%), Piperone (5.37%), Piperitone (3.04%), and p-Menthan-3-one (4.76%) are the principal constituents detected. The results demonstrated a considerable influence on mycelial growth, with inhibition rates ranging from $92.90 \pm 12.28\%$ to 100%. In addition, it was discovered that the essential oil concentration of $0.5\mu\text{l/ml}$ totally eliminated pathogen growth. This concentration was also the MIC (minimal inhibitory concentration) of *Mauginiella scaettae*. Our investigation revealed that *Mentha pulegium* essential oil possesses antifungal efficacy against the pathogen examined. It can, therefore, be utilized as an alternate antifungal agent.

Keywords: Antifungal activity; GC-MS analysis, Inhibition, *Mauginiella scaettae*; *Mentha pulegium*.

1. Introduction

In the Algerian Sahara region, the production of palms is considered one of the essential agro-activities of the country, date palms being the key plant in the socio-economic context of the region (Benzouche and Chriet, 2012). Algeria's agriculture is based on the date palm sector, which constitutes the country's second-largest export after hydrocarbons and the primary means of livelihood for those who live in desert oasis regions (Abdelmalek, 2023). Algeria is distinguished by several date varieties, which are characterized by their nutritional value and high yield; their production in 2019 was estimated at 1.4 million tons, and among the most important of these varieties, we cite the Deglat Nour, which accounts for 49% of total date production and is regarded as the most demanded variety locally and internationally (AlFaris *et al.*, 2022).

Yet the tree is plagued with numerous pathogens and parasites. One of the most serious fungal diseases is the inflorescence rot (Khamedj), which can infect a palm's male or female in regions with favorable climatic circumstances, such as excessive humidity. Khamedj disease is an important factor limiting productivity. Disease losses are around 2-15%, but can exceed 50-80% in severe epidemics. (Alvanipour *et al.*, 2020; Bouhlali *et al.*, 2021). Significant yield losses attributable to this disease contribute to its economic significance and might even result in genetic degradation (Bounaga and Djerbi, 1990; Dakhia *et al.*, 2013). Inflorescence rot (Khamedj) has been documented in North African date-growing regions (Egypt, Sudan, Libya, Tunisia, Algeria, and Morocco), and its proliferation has been detected not only in North Africa but also in other regions where palms are cultivated, such as Iraq, Palestine, Mauritania, Saudi Arabia, and Italy (Chabrolin, 1928; Hussain, 1958; Michael and Sabet, 1970; Munier, 1955; Al- Ani *et al.*, 1971;). In contrast, Alvanipour *et al.* (2020) demonstrate

* Corresponding author. e-mail: hadjra.hammia@univ-biskra.dz.

that this malady is among the most major date palm diseases in the Iranian province of Khuzestan, where a substantial number of palm trees are infected. In fact, it was caused by the pathogen *Mauginiella scaettae*, which Cavara discovered in Libya in 1925 for the first time (Hussain, 1958; Al-Ani *et al.*, 1971; Abdullah *et al.*, 2005). Several control measures have been established to combat this disease, including the elimination of affected inflorescence portions and their quick burning after harvest, as well as the use of several fungicides on palms (Carpenter and Elmer, 1978). Due to toxicological and ecotoxicological hazards, some pesticides might also have negative effects affecting people as well as the natural world. Considering all these negative effects, it is necessary to investigate alternatives to chemical control. In fact, a great deal of research has been carried out to create novel alternatives for controlling pathogen-caused diseases (Youssef *et al.*, 2012).

Due to their antibacterial activity, which is reliant on their chemical composition, especially the type of their primary volatile components, the natural product of plant extracts, like as essential oils, have been of great importance as biocontrol agents (Cailliet and Lacroix, 2007; Bouhlali *et al.*, 2021). This research has focused on the utilisation of a wide variety of antifungal agents, including natural compounds. Owing to its antifungal qualities, the use of plant essences derived from particular therapeutic and aromatic herbs looks to be one of the highly efficient methods for combating this condition. On the basis of microbiological and antifungal properties, it was determined that *Mentha pulegium* essential oils contain diverse naturally occurring compounds with biological activity (Belghazi *et al.*, 2002). It is widely dispersed around the world, particularly in Europe, the Middle East, Asia and North Africa. Historically, it was utilized for its antiseptic, anticholera, antitubercular, and anti-inflammatory properties. In addition, the essential oil has antifungal, insecticide, antiparasitic, antispasmodic, and antioxidant properties (Teixeira *et al.*, 2012; Marzouk *et al.*, 2008). Yet, the essential oil's antifungal effectiveness against the fungus responsible for date palm inflorescence rot has never been investigated. Therefore, identifying their chemical components as well as the study of the antifungal properties of *Mentha pulegium* essential oil towards *Mauginiella scaettae* were the aims of our current research, with the objective of discovering active natural compounds for a potential biological control of this disease.

2. Materials and methods

2.1. Plant material

Mentha pulegium herb has been gathered in March 2019 from the Besbes region, South East Algeria (34°09'00"N and 4°59'27" E). This one was identified at the University of Biskra's Centre for Scientific and Technical Research on Arid Regions (CRSTRA). The *Mentha pulegium* species' aerial parts (stems and leaves) were air-dried and preserved until extraction in sterile paper sacks.

2.1.1. Extraction of *Mentha pulegium* essential oil

Hydrodistillation was used to extract the *Mentha pulegium* oil using the Clevenger apparatus. A Pyrex glass

bottle containing 100 g of the dry plant material was used to extract the oil, for three hours with 1000 ml of distilled water. Once obtained, the gathered oil was kept out of the light at a temperature of 4 °C (Ismaily *et al.*, 2014).

2.1.2. Determination of the *Mentha pulegium* essential oil yield

Afnor standard (1986) was used to define the essential oil yield. It really is estimated using the following formula in percentage form (Afnor, 1986).

$$Y_{eo} = W_{eo}/W_{dh} \cdot 100$$

Y_{eo} (%): essential oil yield

W_{eo}: weight of the essential oil obtained (g)

W_{dh}: weight of powdered plant material (g)

2.1.3. Gas chromatography- mass analysis

Mass Spectrometer with an ISQ single Quadrupole attached to Trace 1310 Gas Chromatograph was utilised in the analysis (Thermo Fisher Scientific, Austin, Texas). The initial temperature for the treatment was 60 °C for 6 minutes, followed by a ramp to 230 °C at a rate of 2 °C/min, and then 30 minutes at 230 °C. Both the detector and ion source temperatures were 250 °C. We filtered the sample through a disposable syringe filter (0.22 µm). 1 µl was injected into the split-less model. The analyzed sample was separated using Thermo TG-WAXMS GC column (60 m x 0.25 mm ID x 0.25 µm) with 1.2 ml/min of Helium being used as the carrier gas. The range of the mass spectral scan has been adjusted between 55 and 550 (amu). Peaks were identified using NIST Demo components Wiley7, Wiley 9, redlip, mainlip, and WinRI, as well as Wiley7, Wiley 9, redlip, and mainlip (Adams, 2001).

2.2. Collection and purification of pathogens

The 2 cm long fragments of the contaminated inflorescence have been sterilized for 3 minutes using 2% sodium hypochlorite, followed by 3 rinses in sterile distilled water for 3 minutes, then dried on autoclaved filter paper. The samples were subsequently dried on sterile pads then transported in sterilized humid filter paper placed in Petri plates, three pieces in each dish. They would be incubated for seven days under dark conditions at 25±2°C. When the different colonies were clearly distinct, they were re-inoculated repeatedly into novel Petri plates that contained medium PDA to isolate pure colonies. Following obtaining pure strains, macro and microscopic examinations have been carried out to identify them (Abdullah *et al.*, 2005; Rattan and Al-Dboon, 1980).

2.3. Evaluation of antifungal activity of essential oil

The activity of the essential oils was determined using the directed contact technique by diluting the essential oil with Tween 20 (0.1%) (v/v) followed by adding it to 20 ml PDA. Three concentrations were obtained: 0.25, 0.5, and 1 µl/ml PDA. 20 ml of PDA medium was placed in each Petri plate, and after that 1 ml of each concentration has been added, homogenisation of the culture medium was carried out by mixing for 5 minutes. Once the medium had solidified, a mycelial disc with a diameter of 0.5 cm was cut from the edge of a 7-day-old culture and placed in the center of each PDA plate. The plates were then incubated in the dark at 25 ± 2°C for 7 days. The negative control consisted of 20 ml (PDA + Tween 20) but no essential oil. Triplicates were utilised for both the examined and control

oils (Remmal *et al.*, 1993). The mean of two diameters perpendicular to each other across the middle of the box was used to calculate the daily radial spread of cultured explant. The following formulas were used to determine the inhibitory potential (Leroux and Credet, 1978) and mycelial growth rate (Howell, 2003) for each concentration.

- Mycelial growth inhibition rate (MGI)

$$\text{MGI} = [(C - c) / C] \times 100$$

MGI (%): Mycelial growth inhibition rate;

C: the control colony's diameter in (cm);

c: the experimental colony's size in (cm).

- Rate of mycelial growth

To measure colony growth, the following formula was applied:

$$\text{MGR} = \text{Dc-dex} / 2$$

MGR: mycelial growth rate (cm)

Dc: is the colony's diameter (cm)

dex : the diameter of explant (cm)

2.4. Determining the minimum inhibition concentrations (MIC)

The lowest concentration of an essential oil at which no growth is evident to the naked eye is referred to as the "minimum inhibitory concentration." The minimal inhibitory concentration was calculated based on the complete absence of microbiological growth at the various essential oil doses examined (MIC) (Remmal *et al.*, 1993).

2.5. The statistical study of the experimental results

The acquired data were subjected to one-way analysis of variance (ANOVA), and any significant differences between doses of essential oil tested were identified using the Newman-Keuls test. The means are also presented in the form of (mean \pm SD) with $p < 0.05$ as the level of significance. This analysis was performed with the XLSTAT 2014.5.03 analysis software.

3. Results and Discussion

3.1. Essential oil Yield

Essential oil yield from hydrodistillation was 0.99 ± 0.041 %. This extracted oil had a pleasing aroma and was pale yellow in colour (mentholated).

Our results accord with those reported by Zwaving and Smith (1971), who indicated that the yield of oils from the same species in Austria is approximately 0.95 %. On the other hand, the essential oil yield exceeds those cited by Zekri *et al.* (2013) and Hmiri *et al.* (2011) who acquired yields of (5.29–6.2%) and 3.30%, respectively.

3.2. The chemical constitution of the essential oil

Using gas chromatography-mass spectrometry (GC-MS), 17 constituents were identified in the essential oil of *Mentha pulegium* extracted from the Biskra region, which comprised the entire chemical constitution. The analyzed oil had a high concentration of oxygenated monoterpenes (82.43%), including p-Menth-4(8)-en-3-one (36.01%), Isomenthone (19.31%), Thymol (11.39%), Piperitenone

(5.37%), Piperitone (3.04%), and p-Menthan-3-one (4.76%). In addition, there are smaller amounts of the following: isopulegone (0.28%), neo-menthol (0.27%), phenol, 4methyl-2-(2propenyl) (0.96%), Camphor (0.43%), and carvacrol (0.61%). On the other hand, D-Limonene (1.26 %), Ç-Terpinen (4.89 %), and Cymol (5.27 %) are the most abundant hydrocarbon monoterpenes found in this oil (Table 1 and Figure 1).

Based on the investigation's results, it appears that the *Mentha pulegium* essential oil is very different from those cited in the literature and reveals a distinct chemotype due to the presence of the three compounds p-Menth-4(8)-en-3-one, Isomenthone, and Thymol in significant concentrations and the absence of pulegone. The presence of pulegone in substantial amounts in the essential oil of *Mentha pulegium* has been demonstrated by numerous authors: Boukhebt *et al.* (2011) in Setif (Algeria) (38.815%), Stoyanova *et al.* (2005) in Bulgaria (42.9-45.4%), and Mkaddem *et al.* (2007) in Tunisia (41.8%). Moreover, in the Kazeron region (Fars Province, Iran) those same oils are rich in piperitone (38%) and piperenone (33%), while pulegone levels are low (2.3%) (Mahboubi and Haghi, 2008). However, the essential oil of the identical plant, harvested in the Boulmane area (Morocco), was analysed and found to have the piperitone chemotype (35.56%) (Derwich *et al.*, 2010).

Several variables can affect the chemical characteristics and yield of *Mentha pulegium* essential oil, including geographic position, period and location of drying, temperature, methodology and duration of distillation, the type of soil, environmental factors, illness brought on by external factors, post - harvest and extraction procedures, as well as vegetative plant phase (Atailia and Djahoudi, 2015; Bergheul, 2018; Daoudi *et al.*, 2016).

Table 1. Composition of *Mentha pulegium*'s essential oil (%)

Components	Retention Time	(%)
dl-Limonene	15.34	1.26
Ç-Terpinen	17.93	4.89
Cymol	19.43	5.27
Ethyl amylcarbinol	26.86	1.16
Isomenthone	31.14	19.31
p-Menthan-3-one	32.80	4.76
Camphor	34.21	0.43
(+)-Menthylacetate	35.14	0.42
Isopulegone	37.77	0.28
Thymylmethylether	38.24	4.57
neo-Menthol	41.04	0.27
p-Menth-4(8)-en-3-one	42.04	36.01
Piperitone	46.69	3.04
Piperitenone	57.32	5.37
Phenol, 4methyl-2-(2propenyl)	61.18	0.96
Carvacrol	69.54	0.61
Thymol	70.28	11.39
Total		100
Monoterpene hydrocarbons		11.42
Oxygenated monoterpenes		82.43

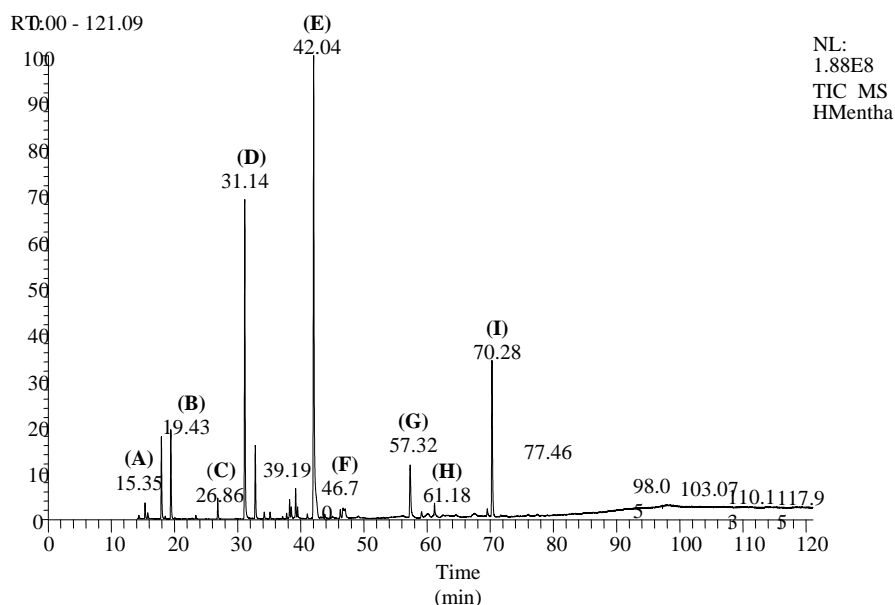


Figure 1. Chromatographic profile of the essential oil *Mentha pulegium*. (A) dl-Limonene; (B) Cymol; (C) Ethyl amylcarbinol; (D) Isomenthone; (E) p-Menth-4(8)-en-3-one; (F) Piperitone; (G) Piperitenone; (H) Phenol, 4methyl-2-(2propenyl); (I) Thymol.

3.3. The essential oil's antifungal activity

3.3.1. Pathogen identification

After 7 days of growth, *Mauginiella scaettae* colonies on PDA were white on the front and creamy to pale brown on the back. They were 3 to 5 cm in diameter and looked powdery (Figure 2 a). According to the observed results, the mycelium consists of branched hyaline and septate hyphae measuring between 15 μm and 80 μm long and 3 to 10 μm wide. Arthroconidia are unicellular or multicellular. Mature spores are uni, bi, tri, or multicellular (Figure 2 b). Our findings validate those of Rattan and Al-Dboon (1980) and Abdullah et al. (2005) who indicated that these characteristics are typical of *Mauginiella scaettae*.



(a)



(b)

Figure 2. Isolation of *Mauginiella scaettae* from diseased date palm spathes. (a) The growth of the fungus on PDA. (b) The fungus' hyphae and conidia.

3.3.2. The mycelial growth inhibition rate

The three doses of oil tested (0.25, 0.5, and 1) $\mu\text{l/ml}$ have a potent antifungal effect on *Mauginiella scaettae*. In fact, the tested strain is extremely sensitive to these concentrations, with the respective inhibition rates of $92.90 \pm 12.28\%$, 100%, and $99.71 \pm 0.49\%$.

The results of the concentration-dependent rate of inhibition of mycelial growth were then subjected to a variance analysis. According to ANOVA, there was no difference between doses, as demonstrated by $p=0.43$ ($P>0.05$) for the non-significant difference analysis. In addition, they are placed in the same group (A) (Figure 3).

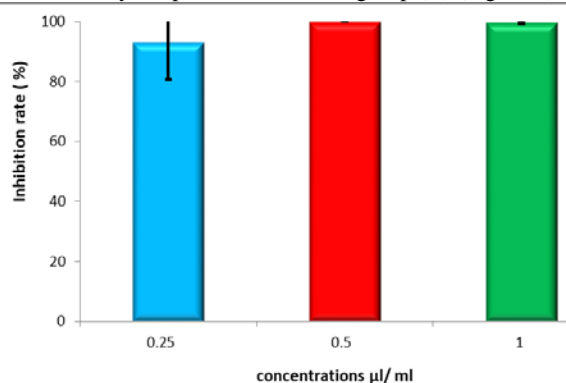


Figure 3. Growth inhibition Rate of fungi tested with *Mentha pulegium* oil

3.3.3. Growth Rate of mycelial

Regarding *Mauginiella scaettae* mycelial growth in relation to different concentrations of essential oil tested, a relatively close linear distribution was observed for three studied doses.

Complete suppression of *Mauginiella scaettae* growth was observed at concentrations of 0.5 and 1 $\mu\text{l/ml}$, to the extent that no development occurs after the application of *Mentha pulegium* oil. Furthermore, it is observed that even with the lowest concentration (0.25 $\mu\text{l/ml}$), mycelial growth progresses very slowly from the first day of the test (0.03 ± 0.06 cm) until the fifth day, when it stabilises and reaches a maximum value of (0.08 ± 0.14 cm) estimated (Figure 4).

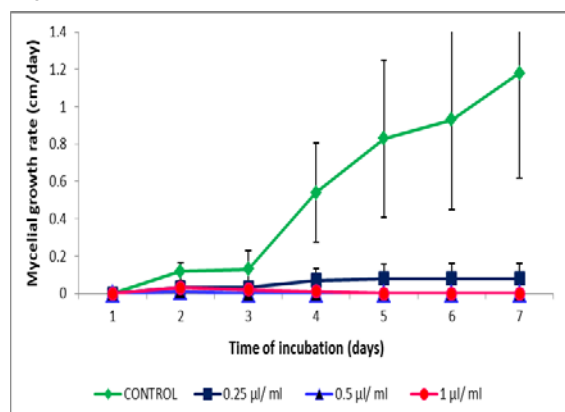


Figure 4. The variation in *Mauginiella scaettae* mycelial growth at various *Mentha pulegium* volatile oil doses.

The phytopathogen *Mauginiella scaettae* has not been the subject of any published research on the effects of essential oils, so a comparison with previous research is

difficult. The first mention of the fungicidal efficacy of *Mentha pulegium* essential oils is, in fact, in this study.

In light of the findings of the study, the tested essential oil examined was found to have a significant antifungal effect against the strain *Mauginiella scaettae*. In terms of the kinetics of mycelial growth, as the incubation period advanced, the growth of control was observed to accelerate. Nonetheless, an inverse relationship was reported between mycelial growth and essential oil concentration. Consequently, the mycelia diameter diminished as essential oil concentration grew. Regarding effectiveness, the *Mauginiella scaettae* strain had a greater sensitivity to essential oil concentrations than the tested species. Depending on our findings, at 0.5 $\mu\text{l/ml}$, the *Mentha pulegium* essential oil completely inhibits the growth of the strain of fungus *Mauginiella scaettae*. These results are consistent with earlier research on the antimicrobial characteristics of the same species' volatile oil. However, Uwineza *et al.*, (2018) demonstrated a total suppression of fungal growth of *Fusarium culmorum* in 1.25 ml/l concentration. In contrast, Hmiri *et al.* (2011) found that 10 μl of *Mentha pulegium* oil completely eliminated the growth of mycelia of two fungi *Alternaria alternata* and *Penicillium expansum*. Hmiri *et al.* (2013) confirmed his findings and demonstrated that *A. alternata* was most sensitive at 156 $\mu\text{l/l}$, whereas *P. expansum* and *B. cinerea* have been totally inhibited at 300 $\mu\text{l/l}$ and above. Hajlaoui *et al.* (2009) mentioned the interesting antifungal activity of this oil against *Fusarium oxysporum*, *Trichoderma* sp., *Aspergillus flavus*, *Aspergillus niger*, *Fusarium culmorum*, and *B. Cinerea* with a volume of 10 μl . Indeed, the powerful fungicidal efficacy of *Mentha pulegium* essential oils may correlate with the high level of oxygenated monoterpene compounds and the synergistic effect with minor compounds. Several studies have shown that oxygenated monoterpenes are effective agents against microbial diseases (Lucini *et al.*, 2006; Kordali *et al.*, 2003). Many studies have shown that the chemical components of *Mentha pulegium*, including phenols (carvacrol, octanol, etc.), aldehydes and ketones (camphor, etc.) alcohols (terpinen-4-ol, terpineol), are recognized to be effective antibacterial agents (Celiktas *et al.*, 2007). Moreover, even at low concentrations, the synergistic impact seen with carvacrol and thymol provides a large spectrum of antimicrobial activity (Didry *et al.*, 1993). However, Dorman and Deans (2000) assert that the observed bioactivity of essential oils is attributable not just to its major constituents but additionally to various minority elements that might collaborate synergistically or antagonistically to provide a powerful antibacterial impact. In a similar vein, a study (Cárdenas-Ortega *et al.*, 2005) showed that modest amounts of piperitone completely reduced *Aspergillus flavus* strains. In fact, Lucini *et al.* (2006) demonstrated that camphor, 1,8 -cineole, linalool, and menthol slowed sclerotic development the most. Sharma and Tripathi (2006) report that the deterioration of mycelium, which appears to be devoid of cytoplasm, as well as the reduction of the rigidity and integrity of their cell walls, are brought on by the usage of essential oils. Many investigations have demonstrated that the toxicity of phenols toward molds is due to the inactivation of fungal enzymes with the SH group at their active site. Consequently, Phenolic terpenes actively bind to hydroxylamine and amine groups in the membrane

proteins of microorganisms, resulting in a disturbance of permeability and a loss of intracellular components (Farag *et al.*, 1989; Celimene *et al.*, 1999; Cowan, 1999; Ultee *et al.*, 1999; Knowles *et al.*, 2005; Lopez-Malo *et al.*, 2005).

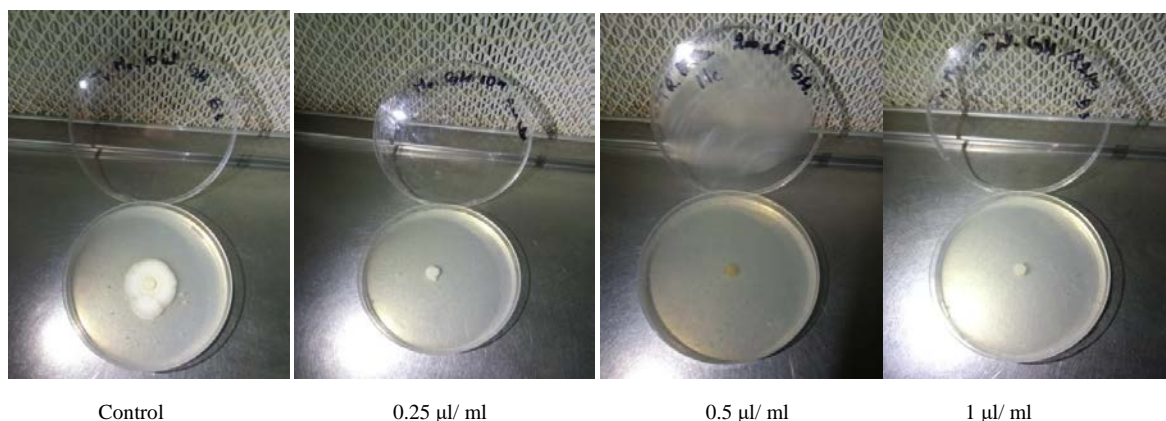


Figure 5. Photograph of *Mauginiella scaettae* mycelial growth in relation to different concentrations of *Mentha pulegium* oil during seven days of incubation

4. Conclusion

In summary, this research demonstrated the anti-fungal power of *Mentha pulegium* essential oil harvested in Besbes (Biskra - Algeria) to control the growth of *Mauginiella scaettae* strains, a pathogen responsible for date palm Khamedj disease. The findings of this research showed that the oil may serve as an important agent for controlling fungal infections. Indeed, compound analysis of *Mentha pulegium* essential oil has revealed that it contains oxygenated monoterpenes. Their effect on the fungal strain tested was very significant. The essential oil evaluated has completely limited the growth of *Mauginiella scaettae* in comparison with control. Furthermore, the results of this research have made it possible to develop a means of biological control of this major date palm pest, through the use of the essential oil of *Mentha pulegium*.

Acknowledgement

Our acknowledgments are due to the staff of the NIVP (National Institute for Vegetal Protection- Biskra, Algeria), particularly Mrs Kardi Karima, for allowing us to use the experimental laboratory for our research. Special thanks go to Prof. Dr. R. ERENLER (Department of Chemistry, Faculty of Arts and Sciences, Gaziosmanpasa University, Tokat, Turkey) for his contribution to the analysis of the essential oil.

References

Abdelmalek H. 2023. La contribution du secteur agricole à la diversification des exportations en Algérie: Cas de la filière dattes (1995-2017). *El-Tawassol*, **29** (6) : 26-42.

Abdullah SK, Asensio L, Monfort E, Gomez-Vidal S, Palma-Guerrero J, Salinas J, Lopez- Lorca LV, Jansson HB and Guarro J. 2005. Occurrence in Elx, SE Spain of inflorescence rot disease of date palms caused by *Mauginiella scaettae*. *J Phytopathol*, **153**: 417-422.

3.4. Minimum inhibition concentration (MIC)

According to observations, the fungal strain *Mauginiella scaettae* is extremely sensitive to the *Mentha pulegium* essential oils, exhibiting a 100% inhibition rate at 0.5 µl/ml concentration (Figure 5).

Adams RP. 2001. **Identification of essential oil components by gas chromatography /quadrupole mass spectroscopy**. Allured publishing corporation, USA.

Afnor .1986. **Huiles essentielles. Recueil de normes françaises**, 2e édition éd. s.l.:Edition Tech& Doc Lavoisier.

Al-Ani HY, El-Behadili A, Majeed HA and Majeed M. 1971. Reaction of date palm cultivars to inflorescence rot and persistency and spreading of the disease. *Phytopathol Mediterr.*, **10**:57-62.

AlFaris NA, Al Tamim JZ, Al Mousa LA, Al Ghamidi FA and Al barid NA. 2022. Date-derived industries: a review of common products, manufacturing methods, and leading countries. *Emir J Food Agric.*, **34** (2): 86-97.

Alvanipour H, Aminian H, Alami-Saeid K, Sorkheh K, Farrokhinejad R, Nejati A and Javan-Nikkhah M. 2020. Cross-transferability of SSR loci of *Phaeosphaeria nodorum* to *Mauginiella scaettae*. *Mycologia Iranica.*, **7** (1): 135-142.

Atilia I and Djahoudi A. 2015. Chemical composition and antibacterial activity of geranium essential oil (*Pelargonium graveolens* L'Hér.) cultivated in Algeria. *Phytotherapie.*, **13**: 156-162.

Belghazi L, Lahlou N, Alaoui Ismaili M, Abousaouir T, Habti N, Tantaoui Iraki A, Talbi M, Blaghen M and Fellat-Zarrouch K. 2002. Extraction et analyse par chromatographie en phase gazeuse de l'huile essentielles de menthe pouliot. Test antifongique [Extraction and analysis by gas chromatography of essential oil of pennyroyal mint tested as antifungal]. *Congrès de biochimie. Casablanca. Biochimie et santé.*, 38-40.

Benziouche SE and Cheriet F. 2012. Structure et contraintes de la filière dattes en Algérie. *New Medit.*, **4** : 49-57.

Bergheul S. 2018. Etude de l'activité antimicrobienne et bioinsecticide de *Ruta chalepensis* L., *R. Angustifolia* Pers. Et *Haplophyllum tuberculatum* (Forsk.) A.Juss.vis-à-vis de quelques bioagresseurs de la culture de tomate (*Lycopersicum esculentum* Mill). Doctorat Thèse, Université Abdelhamid Ibn Badis, Mostaghanem, Algérie, p: 256.

Bouhlali EDT, Ben-Amar H, Meziani R and Essarioui A. 2021. Development of a fungicide-based management strategy of inflorescence rot disease caused by *Mauginiella scaettae* Cavar on date palm (*Phoenix dactylifera* L.) in Morocco. *J Saudi Soc Agricole Sci.*, **20** (3): 173-179.

- Boukhebt H, Chaker AN, Belhadj H, Sahli F, Ramdhani M, Laouer H and Harzallah D. 2011. Chemical composition and antibacterial activity of *Mentha pulegium* L. and *Mentha spicata* L. essential oils. *Der Pharmacia Lettre.*, **3**: 267-275.
- Bounaga N and Djerbi M. 1990. Pathologie du palmier dattier. *Les systèmes agricoles oasiens.*, 127-132.
- Cailliet S and Lacroix M. 2007. **Les huiles essentielles : leurs propriétés antimicrobiennes et leurs applications potentielles en alimentaire.** INRS-institu Armand-Frappier, pp. 1-8.
- Cárdenas- Ortega NC, Pérez Gutiérrez S, Zavala Sánchez MA, Aguirre Rivera JR and Pérez González C. 2005. Antifungal Activity of Six Plants on *Aspergillus flavus* Link. *Rev Mex Cienc Farm.*, **36**: 21-26.
- Carpenter JB and Elmer HS. 1978. **Pests and diseases of the date palm.** (United States Department of Agriculture, Washington, DC: United States Department of Agriculture.
- Celiktas OY, Kocabas EH, Bedir E, Sukan FV, Ozek T and Baser KHC. 2007. Antimicrobial activities of methanol extracts and essential oils of *Rosmarinus officinalis*, depending on location and seasonal variations. *Food Chem.*, **100** (2) : 553-559.
- Celimene CC, Micales JA, Ferge L and Young RA. 1999. Efficacy of pinosylvins against white-rot and brown-rot fungi. *Holzforschung.*, **53**: 491-497.
- Chabrolin C. 1928. La pourriture de inflorescence du palmierdattier. *Ann Epiphyt.*, **14**:377-414.
- Cowan MM. 1999. Plant products as antimicrobial agents. *Clin Microbiol Rev.*, **12**: 564-582.
- Dakhia N, Bensalah MK, Romani M, Djoudi AM and Belhamra M. 2013. Etat phytosanitaire et diversité variétale du palmier dattier au bas Sahara-Algérie. *Journal Algérien des Régions Arides.*, N° Spécial : 5-17.
- Daoudi A, Harouk H, Belaidi R, Slimani I, Ibjibjen J and Nassiri L. 2016. Valorisation de *Ruta montana* et *Ruta chalepensis*: Etude ethnobotanique, Screening phytochimique et pouvoir antibactérien. *J Master Environ Sci.*, **7** (3): 926-935.
- Derwich E, Benziane Z and Boukir A. 2010. GC/MS analysis and antibacterial activity of the essential oil of *Mentha pulegium* grown in Morocco. *Res J Agric Biol Sci.*, **6** (3): 191-198.
- Didry N, Dubreuil L and Pinkas M. 1993. Antimicrobial activity of thymol, carvacrol and cinnamaldehyde alone or in combination. *Pharmazie.*, **48**: 301-304.
- Dorman HJD and Deans SG. 2000. Antimicrobial agents from plants: antibacterial activity of plant volatile oils. *J Essent Oil Res.*, **88**: 308-316.
- Farag RS, Daw ZY, Hewedi FM and El-Baroly GSA. 1989. Antimicrobial activity of some Egyptian spice essential oils. *J Food Prot.*, **52**: 665-667.
- Hajlaoui H, Trabelsi N, Noumi E, Snoussi M, Fallah H, Ksouri R and Bakhrouf A. 2009. Biological activities of the essential oils and methanol extract of two cultivated mint species (*Mentha longifolia* and *Mentha pulegium*) used in the Tunisian folkloric medicine. *World J Microbiol Biotechnol.*, **25**: 2227-2238.
- Hmiri S, Rahouti M, Habib Z, Satrani B, Ghanmi M and El Ajjouri M. 2011. Évaluation du potentiel antifongique des huiles essentielles de *Mentha pulegium* et d'*Eucalyptus camaldulensis* dans la lutte biologique contre les champignons responsables de la détérioration des pommes enconservation. *Bulletin de la Société Royale des Sciences de Liège.*, **80** : 824-836.
- Hmiri S, Amrani N and Rahouti M. 2013. Détermination *in vitro* de l'activité antifongique des vapeurs d'eugénol et d'huiles essentielles de *Mentha pulegium* L. et de *Tanacetum annuum* L. vis-à-vis de trois champignons responsables de la pourriture des pommes en post-récolte. *Acta Bot Gallica.*, **158** (4): 609-616.
- Howell CR. 2003. Mechanisms employed by *Trichoderma* species in the biological control of plant diseases: the history and evolution of current concepts. *Plant Dis.*, **87**: 4-10.
- Hussain F. 1958. Occurrence of date palm inflorescence rots in Iraq. *Plant Dis Rept.*, **42**:555.
- Ismaily AK, El Hajjaji F, Azaroual MA, Taleb M, Chetouani A, Hammouti B, Abrigach F, Khoutoul M, Abboud Y, Aouniti A and Touzani R. 2014. Experimental and quantum chemical studies on Corrosion inhibition performance of pyrazolic derivatives for mild steel in hydrochloric acid medium, correlation between electronic structure and inhibition efficiency. *J Chem Pharm Res.*, **6** (7) :63-81.
- Knowles JR, Roller S, Murray DB and Naidu AS. 2005. Antimicrobial action of carvacrol at different stages of dual-species biofilm development by *Staphylococcus aureus* and *Salmonella enterica* Serovar Typhimurium. *Appl Environ Microbiol.*, **71**: 797-803.
- Kordali S, Cakir A, Zengin H and Duru ME. 2003. Antifungal activities of the leaves of three Pistacia species grown in Turkey. *Fitoterapia.*, **74** : 164-167.
- Leroux P and Credet A. 1978. **Document sur l'étude de l'activité des fongicides.** INRA, Versailles, France.
- Lopez-Malo A, Alzamora SM and Palou E. 2005. *Aspergillus flavus* growth in the presence of chemical preservatives and naturally occurring antimicrobial compounds. *Int J Food Microbiol.*, **99**: 119-128.
- Lucini EI, Zunino MP, López ML and Zygadlo JA. 2006. Effect of monoterpenes on lipid composition and sclerotial development of *Sclerotium cepivorum* Berk. *J Phytopathol.*, **154**: 441-446.
- Mahboubi M and Haghi G. 2008. Antimicrobial activity and chemical composition of *Mentha pulegium* L. essential oil. *J Ethnopharmacol.*, **119**: 325-327.
- Marzouk B, Fredj MBH, Chraief I, Mastouri M, Boukef K and Marzouk Z. 2008. Chemical composition and antimicrobial activity of essential oils from Tunisian *Mentha pulegium* L. *J Food Agric Environ.*, **6** (1): 78-82.
- Michael IF and Sabet KA. 1970. Biology and control of *Mauginiella scaettae* Cav., the pathogen of Khamedj disease in the United Arab Republic. *Ann Date Grower's Inst.*, **47**: 5-8.
- Mkaddem M, Bousaid M and Ben Fadhel N. 2007. Variability of volatiles in Tunisian *Mentha pulegium*L. (Lamiaceae). *J Essent Oil Res.*, **19**: 211-214.
- Munier P. 1955. Le palmier dattier en Mauritanie. *Ann Inst Fruits et Agrumes Coloniaux.*, 12:66.
- Rattan SS and Al-Dboon AHA. 1980. Notes on fungi associated with Date-Palm I. *Sydowia.*, **32**: 246-273.
- Remmal A, Bouchikhi T, Rhayour K, Ettayebi M and Tantaoui-Elaraki A.1993. Improved method for the determination of antimicrobial activity of essential oils in agar medium. *J Essent Oil Res.*, **5** (2): 179-184.
- Stoyanova A, Georgie V, Kula J and Majda T. 2005. Chemical composition of the essential oil of *Mentha pulegium* from Bulgaria. *J Essent Oil Res.*, **17**: 475-477.
- Sharma N and Tripathi A. 2006. Fungitoxicity of the essential oil of *Citrus sinensis* on post-harvest pathogens. *World J Microbiol Biotechnol.*, **22** : 587-593.
- Teixeira B, Marques A, Ramos C, Batista I, Serrano C, Matos O, Neng NR, Nogueira JMF, Saraiva JA and Nunes ML. 2012. European pennyroyal (*Mentha pulegium*) from Portugal: chemical composition of essential oil and antioxidant and antimicrobial properties of extracts and essential oil. *Ind Crops Prod.*, **36**: 81-87.

Ultee A, Kets EPW and Smid EJ. 1999. Mechanisms of action of carvacrol on the food-borne pathogen *Bacillus cereus*. *Appl Environ Microbiol.*, **65**: 4606-4610.

Uwineza MS, El Yousfi B and Lamiri A. 2018. Activités antifongiques *in vitro* des huiles essentielles de *Mentha pulegium*, *Eugenia aromatica* et *Cedrus atlantica* sur *Fusarium culmorum* et *Bipolaris sorokiniana*. *Revue Marocaine de Protection des Plantes.*, **12**: 19-32.

Youssef K, Ligorio A, Sanzani SM, Nigro F and Ippolito A. 2012. Control of storage diseases of citrus by pre-and postharvest application of salts. *Postharvest Biol Technol.*, **72**: 57-63.

Zekri N, Amalich S, Boughdad A, El Belghiti MA and Zair T. 2013. Phytochemical study and insecticidal activity of *Mentha pulegium* L. oils from Morocco against *Sitophilus oryzae*. *Med J Chem.*, **2(4)**: 607-619.

Zwaving JH and Smith D. 1971. Composition of the essential oil of Austrian *Mentha pulegium*. *Phytochemistry.*, **10**: 1951-1953.

Cloning and Characterization of Terpene synthase 3 (*SoTPS3*) Gene from Leaves of Garden Sage (*Salvia officinalis*)

Mohammed Ali*, El-ramah, F. A., Esraa A. Elsherbeny, Mohamed N.S. Suliman, Mokhtar Said Rizk

Genetic Resources Department, Desert Research Center (DRC), Cairo, Egypt.

Received: February 4, 2023; Revised: April 10, 2023; Accepted: May 16, 2023

Abstract

Salvia officinalis plant produce various terpene compounds have many roles and useful biological properties in plants. In different salvia species structure of sesquiterpenes was remarked to be the main group of compounds at various tissues and development stages. However, some genes responsible for sesquiterpene synthase in *S. officinalis* remain unclear. In this study, we clone the full-length of sesquiterpene synthase (*SoTPS3*) gene from *S. officinalis*. The full-length cDNA of *SoTPS3* contains a 1668-bp open reading frame that putatively encoded a protein of 555 amino acids which resembled a sesquiterpene synthase in sequence. The deduced *SoTPS3* shared an overall homology with other known sesquiterpene genes from other plants. Analysis of *SoTPS3* amino acid sequence revealed that it contained two domains and four types of motifs such as, DDxxD, NSE/DTE, RRx8W and RXR. Bioinformatics and phylogenetic analyses revealed that *SoTPS3* clustered in clade subfamily TPS-a, and the genes that belong to this subfamily can encode mono- and sesquiterpene. Functional complementation of *SoTPS3* in *Arabidopsis thaliana* demonstrates that *SoTPS3* is responsible for the production of Germacrene D-4 α -ol. Overexpression of *SoTPS3* in *A. thaliana* enhanced flower formation in transgenic plants compared with wild type. Our study will provide a basis for understanding the role of *SoTPS3* in the biosynthesis of sesquiterpene in *S. officinalis*.

Key words: Essential oils - *S. officinalis* - Terpene synthase - *Arabidopsis* - Functional characterization

1. Introduction

Terpenoids, the largest group of natural products, are secondary metabolites that are discovered in the Kingdom plantae with ~40,000 structures (Nema and Omimah, 2013; Abdul-Rahim and Taha, 2011; Ibrahim, 2011; Bohlmann *et al.* 1998). Isopentenyl diphosphate (IPP), the backbone molecule for terpenoids, consists of five carbon atoms (C₅) (Xi *et al.* 2016; Abbas *et al.* 2019). Some terpenes play a solemn role in the plant metabolism (e.g. plant hormone gibberellin, pigments, Steroid, tryptophan, Brassinosteroid, Carotenoid, unsaturated fatty acids; hence, they affect plant growth, flowering and development (Trapp and Croteau, 2001; Gershenzon, 1999). However, most non-volatile and volatile terpenes are categorized as secondary metabolites, and they are crucial for the processes of protection against biotic and abiotic stresses (Sujatha and Bollipo, 2013; Dorothea *et al.* 2006)

The *Salvia* genus belongs to the Lamiaceae family and encompasses about 1,000 species of small shrubs. The members of this family are cultivated around the world for their medicinal and volatile oil properties. *Salvia* plant species have a sub-cosmopolitan distribution, and are largely present in three areas of the world such as Central

and South America (about 500 species), Mexico (about 250 species), West Asia (about 200 species), East Asia (about 100 species) and Southern Africa (about 30 species) and includes several culinary, medicinal and ornamental plant species. In the low-lying tropical areas *e.g.*, the Amazon, other *Salvia* species are widespread (Ali *et al.* 2018; Ali *et al.* 2017; Sarrou *et al.* 2017; Kamatou *et al.*, 2008; Alziar, 1988–1993). Moreover, Chinese folk medicine utilizes numerous *salvia* species as sedative, antibacterial, anti-inflammatory, antioxidant, antiseptic, cardiovascular, anti-cholinesterase activities, antitumor activities spasmolytic, analgesic and antidiabetic. (Zhenqing *et al.* 2018; Li *et al.* 2015; Wang *et al.* 2015a; Takano and Okada, 2011; Kamatou *et al.*, 2008).

The main composites of *salvia*'s fragrant oil are monoterpenes and sesquiterpenes. The monoterpenes and sesquiterpenes composition in *salvia* species vary depending on the type of tissues on *salvia* species (Makris *et al.*, 2007; Aziz *et al.* 2008; Loizzo *et al.* 2010; Atsuko and Hiroshi 2011; Hua *et al.* 2011; Nadaf *et al.* 2012; Fateme *et al.* 2013; Ali *et al.* 2017; Ali *et al.* 2018). In *S. officinalis*, the main sesquiterpenes are alpha-caryophyllene, isocaryophyllene, (-)-germacrene D and caryophyllene oxide, though, their biological or physiological function is unclear (Ali *et al.* 2017). To our knowledge, many genes responsible for synthesizing

* Corresponding author. Tel.: +0-000-000-0000 ; fax: +0-000-000-0000 ; e-mail: author@institute.xxx .

** **Abbreviations:** OE: Overexpression; EOs: Essential oils; FPP: Farnesyl diphosphate (FPP); TPS: Terpene synthase; *SoTPS3*: *S. officinalis* Germacrene D-4 α -ol synthase; Semi-RT-PCR: Semiquantitative RT-PCR.

sesquiterpenes in salvia are still obscure. In our study, we cloned a full-length cDNA of *SoTPS3* from *S. officinalis*. A following step was established using the *Arabidopsis* floral-dip transformation method to clarify its role in sesquiterpene biosynthesis. The aforementioned strategies revealed that *SoTPS3* synthase gene actively catalyzed the Farnesyl pyrophosphate (FPP) substrate to Germacrene D-4 α -ol. Taken together, these results will enhance our understanding of *SoTPS3* and its role in the biosynthesis of sesquiterpene in *S. officinalis* at the biologically level.

2. Materials and Methods

2.1. Plant materials.

S. officinalis seeds were donated by the Egyptian Desert Gene Bank (EDGB), Desert Research Center (DRC), Egypt. Seeds were grown in the greenhouse at National Research Centre, Cairo, Egypt. Three leaves from 2-years- old plants were used for RNA isolation and gene cloning.

2.2. Sequence characterization of *SoTPS3*.

The sequence of *SoTPS3* gene was selected on the basis of the highest sequence similarity found with the known plant sesquiterpene synthases genes (see Appendix S1). The physical and chemical property of the *SoTPS3* was assessed using PROTPARAM Server (<http://web.expasy.org/protparam/>). Putative transit peptide for open-reading-frames (ORF) of *SoTPS3* was analyzed by iPSORT prediction tool (<http://ipsort.t.hgc.jp/>). NCBI BLASTX tool was used for comparative protein sequence analysis of *SoTPS3* (<http://blast.ncbi.nlm.nih.gov/>). Clustal Omega Online software with default tool parameters was used for analyzing the sequence alignments (<https://www.ebi.ac.uk/Tools/msa/clustalo/>). To predict the 3D protein structure of *SoTPS3*, we used the SWISS-MODEL Server for build the 3D structure based on other homology-modules that have been stored on the site (<https://swissmodel.expasy.org/>). To determine the quality of our predicted 3D structure, we used PROCHECK tool (<http://www.ebi.ac.uk/thornton-srv/software/PROCHECK/>). The evolutionary relationships of *SoTPS3* protein and other plant TPS proteins were inferred using the PhyML Server without changing the tool parameters (<http://www.phylogeny.fr/>) (Dereeper *et al.* 2008; Mehmood *et al.*, 2021).

2.3. Putative tissue expression pattern of *SoTPS3* gene and its subcellular localization.

Tissue-specific expression data from thirty six tissues were analyzed based on *Arabidopsis thaliana* transcript expression database. We used Arabidopsis eFP browsers (<http://bar.utoronto.ca/efp/cgi-bin/efpWeb.cgi>) to generate expression profiles, while, the putative sub-cellular localizations of *SoTPS3* gene from *S. officinalis* was analyzed using the Cell-eFP browsers (http://bar.utoronto.ca/cell_efp/cgi-bin/cell_efp.cgi) as described by (Makhadmeh *et al.*, 2022a and 2022b). The arrow points the expression scale (e.g. red color= high expression & yellow color = low expression).

2.4. RNA extraction and cDNA synthesis

Six tissues with three replicates from two-year-old of *S. officinalis* were used for RNA extraction using TransZOL Reagent for gene cloning and qRT-PCR. Also, leaves from wild and transgenic *A. thaliana* were used for RNA extraction for semi-quantitative RT-PCR. For cDNA Synthesis 1 μ g from each RNAs was used to synthesize the first-strand cDNA using reverse transcriptase TransScript® First-Strand cDNA Synthesis Super Mix kit as described by (Ali *et al.* 2017; Hussain *et al.*, 2017)

2.5. Isolation of full-length *S. officinalis* sesquiterpene synthase gene (*SoTPS3*).

The entire *SoTPS3* cDNA was used as a template to magnify the full-length by short-gene-specific forward (5'-ATGGCTCAAATATATGCATCGG-3') and reverse (5'-AGTTCACGGGCTCTACGAGC-3') primers and KOD-polymerase enzyme and amplification was done at 3 min at 96°C; 33 cycles for 10 s at 98°C; 30 s at 60 °C; 90 s at 68°C, and then 10 min at 68°C. The first PCR product was used as a model for the second PCR using long-gene-specific forward (5'-GGGGACAAGTTTGTACAAAAAAGCAGGCTTCATG GCTCAAATATATGCA-3') and reverse (5'-GGGGACCACTTTGTACAAGAAAGCTGGGTAGTTC ACGGGCTCTACGA-3') primers with the same polymerase enzyme and PCR program conditions to clone into Gateway vectors. The successful amplicon was purified and cloned into a pDONR221vector (Invitrogen, Carlsbad, CA, USA), then pB2GW7 vector (Invitrogen, Carlsbad, CA, USA) and sent for sequencing as depicted by (Ali *et al.* 2017 and Ali *et al.*, 2018).

2.6. Growth conditions of *Arabidopsis* plants and transformation using *Agrobacterium*.

Arabidopsis thaliana seeds from ecotype Columbia-0 (Col-0) were grown in our Lab growth chamber as reported by (Ali *et al.*, 2018). After 2 months from the growth, healthy plants at pre-flowering stage were selected for floral-dip transformation experiment. Moreover, to characterize the function of *SoTPS3* gene, the vector pB2GW7-*SoTPS3* and pB2GW7 (empty vector) were transformed into *Agrobacterium tumefaciens* strain GV101. *A. tumefaciens* GV101 containing pB2GW7-*SoTPS3* was grown in selective solid LB media supplier with rifampin (Rif) and spectinomycin (Spc) as antibiotics. One positive colony was selected and inoculated into 0.8 ml of liquid-LB-media with Rif and Spc, after one day from incubation period at 28°C the bacterial culture was sub-cultured to conical flask containing about 60 ml LB media and incubation at incubator with shaker until the optical density of *Agrobacterium* cells reached to 0.75 (OD 600) according to (Ali *et al.*, 2017; Ali *et al.*, 2018 and Darwish *et al.*, 2022). On the next day, cell suspension was collected, and the bacteria was re-suspended in fresh-inoculation-medium (5.2% sucrose and 0.055% Silwet). The plasmids pB2GW7-*SoTPS3* and pB2GW7 (control) were introduced separately into *A. thaliana* plant by directly immersing the axis of bud flowers in the fresh floral-dip medium with pressing gently to ensure intake of *A. tumefaciens* GV101 harbouring the pB2GW7-*SoTPS3* and pB2GW7 (control) plasmids into the flower gynaecium (Aharoni *et al.* 2003; Su-Fang *et al.* 201.). A total of 12 *A. thaliana* transgenic lines were obtained and

survived the successive subculture process under BASTA resistance. The leaf morphology, flowering time and terpene metabolic of the previous lines were subjected to assessment.

2.7. Semi-Quantitative RT-PCR (sqRT-PCR) analysis

To ensure the success of our gene transfer process qRT-PCR was implemented using a PCR system from Biometra. The *At-B-actin* gene forward primer 5'-GGCTGAGGCTGATGATATTC-3' and reverse primer 5'-CCTTCTGGTTCATCCCAAC-3' were used as housekeeping with 155 bp, and *SoTPS3* forward primer 5'-ACGTCTAGGAGTTGCCTATC-3' and reverse primer 5'-CGGTAACCTTGCTGTCTAAG-3' with 150 bp length. We used IDTdna online website (<http://www.idtdna.com/scitools/Applications/RealTimePCR/>) to design our target primers. The qRT-PCR conditions program as follows: 94°C for 5 min, 33 cycles of 95°C for 30 s, 60°C for 30 s and 72°C for 1 min, 72°C for 10 min. PCR products were screening on 1.4 % agarose gel to determine our genes expression levels.

2.8. Terpenoids extraction and GC-MS analysis.

For a rapid survey of terpenoids in transgenic and non-transgenic *A. thaliana* plants, intact leaves of various lines were frozen in liquid nitrogen (LN₂), powdered with a ceramic mortar and pestle, and directly inundation in n-hexane as a solvent for 72 h to ensure complete removal of terpenoids leave contents as previously described (Ali *et al.* 2017; Ali *et al.* 2018; Ali *et al.*, 2022a, 2022b, 2022c). And an approximately 1µl aliquot of each extract was analyzed by Shimadzu-GC-MS system with three replicates. Terpene component identification was made by reference to Wiley GC/MS Library, the Volatile Organic Compounds (VOC) Analysis S/W software, and the NIST Library as previously described (Ali *et al.* 2017; Ali *et al.* 2018).

2.9. Quantitative real-time PCR (qRT-PCR) analyses.

To analyze the expression of *SoTPS3* in various *S. officinalis* tissues (e.g., flowers, bud flowers, stems, young leaves, old leaves and roots), tissues were collected with three biological replicates. QRT-PCR was performed to represent the scale of *SoTPS3* transcript involved in the production of sesquiterpene. A 157 and 150 bp fragments in the 3' region of *SoACTIN* and *SoTPS3* were amplified using the following couple of primers: for *SoACTIN* forward 5'-GGCAGTCTCTCCCTCTAT-3' and reverse 5' GAGGTGGTCGGTGAGAT-3' was used as a housekeeping gene, and *SoTPS3* forward 5'-ACGTCTAGGAGTTGCCTATC-3' and reverse 5'-CGGTAACCTTGCTGTCTAAG-3. The qRT-PCR experiments were performed using IQTM5 System, SYBR Green and the cycler program as follows (95°C for 10s, 60°C for 30s, and 72°C for 20s), then 65°C for 5s and 95°C for 5s). The expression levels were enumerated by comparing our target gene cycle thresholds (CTs) with the housekeeping gene *SoACTIN* using the ^{2-ΔΔCt} method (Wise *et al.*, 1998; Anders & Huber, 2010; Hussain *et al.*, 2017; Rehman *et al.*, 2017;). Values are offered as means ± SE of three different RNA pools replicates.

3. Results

3.1. Full-length isolation of Terpene synthase 3 (*SoTPS3*) gene and sequence characterization

The full-length-ORF of *SoTPS3* gene with 1668 bp encoded a 555 amino acid protein with a predicted theoretical isoelectric point (pI) of 5.52 and molecular mass of 64.24 kDa. The amino-acid of *SoTPS3* have stumpy signal peptide compare with monoterpene synthases (600–650 aa) and matched with a lot of sesquiterpene synthases of 550–580 aa in the thirty amino acid existence at N-terminal sequence. Using 'iPSORT' program revealed that *SoTPS3* is localized in the chloroplast (plastid) where FPP originates, and biosynthesis takes place. NCBI-BLASTX analysis in (Table 1) indicated that *SoTPS3* shared 79.35% identity and ≤76.12% identity with its homologue sesquiterpene synthase protein from *Salvia splendens* and other plants respectively. The sequence alignment of *SoTPS3* gene with putative and recognized TPS genes from Lamiaceae and other plants aided the prediction of its putative function. Based on this prediction, *SoTPS3* protein have various motifs such as: spartate-rich-DDxxD (residues 313–317), NSE/DTE (residues 457–465) motifs, RXR motif (residues 276–278), RR (X8) W (residues 22–32) and GTLxEL (residues 320–325) region that are predominant in similar sesquiterpene synthases involved in (-)-germacrene D synthesis (Abbas *et al.* 2019; Su-Fang *et al.* 2014; Degenhardt *et al.* 2009; Ali *et al.* 2017; Ali *et al.* 2018; Ali *et al.*, 2022a, 2022b) (Figure 1). Comparable to other sesquiterpene synthases, *SoTPS3* has two domains, which were specified by InterPro database. So, *SoTPS3* protein has three terpene synthase family domains, N-terminal-domain (IPR001906: from 32-207 aa), C-terminal-domain (IPR005630: from 238-499 aa) and metal-binding-domain (IPR034741: from 233-554aa) (Figure 2). The *SoTPS3* was tabulated to the TPS-a subfamily of angiosperm sesquiterpene synthases based on the phylogenetic analysis results (Figure 3).

Table 1. BLASTX analysis of *SoTPS3* was compared with the NCBI protein database for gene identification purposes.

NCBI Accession	^a Description	Organism	E value	Identity (%)
TEY90111.1	(-)-germacrene D synthase	<i>Salvia splendens</i>	0.0	79.35%
ADK73619.1	Terpene synthase 3	<i>Origanum vulgare</i>	0.0	76.12%
Q5SBP6.1	Germacrene-D synthase;	<i>Ocimum basilicum</i>	0.0	69.01%
RVW14969.1	(-)-germacrene D synthase	<i>Vitis vinifera</i>	0.0	56.85%
TEY69656	(-)-germacrene D synthase	<i>Salvia splendens</i>	0.0	53.36%

^a Description—homology search using BLASTX.

3.2. 3D modeling and analysis of active site

The 3D protein model for *SoTPS3* was constructed using (+)-δ-cadinene synthase from *Gossypium arboreum* [PDB accession: 3g4f] as a template (Gennadios *et al.* 2009) (Figure 4). We used Ramachandran plot analysis to check the quality of *SoTPS3*-3D protein model (Laskowski *et al.* 1993) (Figure 4). The model showed a valid fit

versus the reference geometry (Resolution: 2.65Å, R-factor: 0.206 and R-free: 0.256). Accordingly, *SoTPS3* entirely consisted of α -helices with loops, turns, long and short connecting. Both of the C- and N-terminal conserved domains were manifested in the 3D model that was foretell

using SWISS-MODEL server (https://swissmodel.expasy.org). This model illustrates the active site that catalyzes the FPP substrate. (Köllner *et al.* 2008) (Figure 4).

		RR (X8) W	
NsGDS	-----MDFSKGLPV-----	GVHEVSRPSANYHRSIWGD	28
VvGDS	-----MSVQSSVLLA-----	PSKNLSPGAHV	23
ADR74196.1	-----MSGQVLASPLGQFPELENRPVVQYHPSIWGD		31
ADR74197.1	MELAKLFLSYLPIHHSRYSAVLSLSQGINMSTQVSACS LAQIPKPKNRPVTFNHPNIWGD		60
TEY69656.1	---MEMCA-----	PHVSAMKNGKSLDEIRKSATFHPSIWGD	33
sp Q5SBP6.1	--MTNMFA-----	SAAPISTNNTTVEDMRSSVTYHPSVWIKD	34
ADK73619.1	--MAEICA-----	SAAPISTKNTSVEELRSSVTYHPSVWRD	34
SoTPS3	--MAQIYA-----	SAVPISTKNTNVDNIRSSVTYHPSVWRD	34
TEY90111.1	-----	-----	0
NsGDS	YFLDCVS-DSTIINPLERKQVQDLREEVRKMLMAVHDTSSSEKVELIDKIQR LGVSYHFEE		87
VvGDS	YFINCLNLTQNTDDHLKQHVQQLKKEEVRKMLMAADDDSAQKLLLDIAIQR LGVAYHFES		83
ADR74196.1	QFLSYT-PEDEVTRACKEQLEDLKEEIRRKLMNTAGNTSQQLKFIDAVQR LGVAYHFER		90
ADR74197.1	QFITYT-PEDKVTRACKVEQIEDLKKEVKRKLTAATANHSLLLNFIDAVQR LGVAYHFQ		119
TEY69656.1	FFLKYS-NNTKITDAEQEELAKHKEMVRKMLSQTPNDSTCKLELIDEIQR LGVEYHFEE		92
sp Q5SBP6.1	HFLDYAS-GITE--VEMEQLOKQKERIKTLLAQTLDDFVLKIELIDAIQR LGVGYHFEE		90
ADK73619.1	HFLSYTN-DVTEITAAEKELEKQEKVKNLDDQTPNDSTLKI ELIDAIQR LGFGYHFEE		93
SoTPS3	HFLKYTD-DVTKITTAEQEELKQEEVKLLAQTPDDSKVKMELIDAIQR LGVAYHFESK		93
TEY90111.1	-----MLEKQKVEVKLLAQTPDDSTLKM DLINAIQR LGVAYHFESK		41
NsGDS	EIEASLQRMYEAYRE--CNMYGDDLVLVAIGFRLLRQQGHFVSCDVFKKFKDNEGNFDKA		145
VvGDS	EIDEVLKHMFDGSV---VSAEEDVYTASLRFRLLRQQGYHVSCDLEFNNFKDNEGNFKES		139
ADR74196.1	EIEEVLQHIYDSYPN--GDDMEGD IYNVALQFRLLRQAGFNISCGLFNEFKDEKGNFKKA		148
ADR74197.1	EIEEALQHIYESFHD--LNDIDGDLYNVALGFRLLRQQGYSISCGILKKTDERGRFKEV		177
TEY69656.1	EIEESLKHIIHDSYMQRNCKD-NDDLHIVALFRLLRQQGYNVPCGVFCFTDSEGNYEAS		151
sp Q5SBP6.1	EINHSLRQIYDTFQISSK---DNDIRVVALFRLLRQHGYPVPSDVFKKFIDNQRGLDES		147
ADK73619.1	VIDESLGEVYDRYEMPSGKDDDEDIRVRSRFRLLRQQGYRVPDVFKEKLLDDKGNFKDS		153
SoTPS3	EIDESLRKIHDTYQIQSR TD-KDDARVLALFRLLRQQGYRVS DVFENGLVDEEGLNKEW		152
TEY90111.1	EIDDSLRLKIHNNYESQSSKD-KNNVGLVALFRLLRQHG YRVS DVFENGLVDKEGNLKE		100
NsGDS	LTSNVPAMLSLYEAHMVRVHGEDI LEEALVFISNHLKSM-IPILSDSFRVQV LHALNQPI		204
VvGDS	LSSDVRGMLSLEYEATHFRVHGEDI LDEALFTTTHLQSA-TKYSNPLAEQV VHALKQPI		198
ADR74196.1	LVSDVRGMLGLYEAHLRVHGEDI LAKALFTTTHLKAM-VESLGYHLAEQVAHALNRPI		207
ADR74197.1	LITNVRGLLGLYEAHLRVHGEDI LAEALFTTTHLKAM-VESLGYPLAEQV VHALNRPI		236
TEY69656.1	LQNDVEGLLNL YEAHLLTHDEGILENAIEFCSSHLHASLHKLDDVSLSKRVGEALEMPN		211
sp Q5SBP6.1	VMNNVGMLSLEYASNYGMEGEDILDKALEISTSHLEPL-----ASRRSRINEALEMPI		201
ADK73619.1	LITDVEGLLSLEYASNYGINGEEMDKALKFSSSHLEGSIH-KMPTSLSRVKEALDMP		212
SoTPS3	LISDVEGMLSLEYASNYGINGEILEKVLQFTSSHLES-LLPQMSTSLSNRVKEALEMPI		211
TEY90111.1	LIDDVEGMLSLEYASNYGINGEILDKALEFSSSHLRNSLHKTMSTSLSNRVKEALEMPI		160
NsGDS	HMSLTRVEARRFLSTYQSYDTKNELLEFAKLD FNLLQKVHRKELSSITRWWKDLIVTK		264
VvGDS	RKGLPRLEARHYFSVYQADDSHNKALLKLA KLDFNLLQKLHQKELSDISA WKKDLDFAHK		258
ADR74196.1	RKGLERLEARWYISVYQDEAFHDKTLLELAKLDFNLVQSLHKEELSNLARW WKELD FATK		267
ADR74197.1	RKGLERLEARWYISVYQDEAFHDKTLLELAKLDFNLVQSLHREELSNLARW WKELD FATK		296
TEY69656.1	RWSLARLGARKFISAYQDEAHNEILLNFAKLD FNLLQKMHQRELSDATRWWKLDVANK		271
sp Q5SBP6.1	SKTLVRLGARKFISYIEEDES RDELLKFAKLD FNILQKIHQEELTHIARW WKELD LGNK		261
ADK73619.1	SKTLTRLGARKFISLYQEDES HNELLLKFAKLD FNIVQKMHQRELHHTIRW WEGLEFGKK		272
SoTPS3	SKTLMRLGARKFISYIQEIES HNELLLNFAKLD FNVMQKIHQRELHHTIRW WVDLEFGKK		271
TEY90111.1	SKSLIRLGAKKFTSMYQLDESHNQTLNFAKLD FNIVQKIHQRELHHTIRW WVDLEFGKK		220
NsGDS	CPFARDRLVESYFWALGVYFEPK FVIARRMLAKVIALATIIDDDIYDAYS YDEHMCFTEA		324
VvGDS	LPFARDRVVECYFWILGVYFEPQ FFFARRILTKVIAMTSIIDDIYDVYPTIESELFTEA		318
ADR74196.1	LPFARDRLVECYFWMLGVYFEPQ YLRARRILTKVIAMTSIIDDIYDAYS YGTPEELKLFIEA		327
ADR74197.1	LPFARDRLVEGYFWILGVYFEPQ YLRARRILTKVIAMTSIIDDIYDAYS YGNPEELKLFTEA		356
TEY69656.1	IPHARDRIAELYLWVLGVFFEP CYAKARRILKCI SMASIA DDTYE-YATLEIRILTDA		330
sp Q5SBP6.1	LPFARDRVVECYFWILGVYFEPQ YNIARRFMTKVIAMTSIIDDIYDVHPTIEELQRFTDA		321
ADK73619.1	LPFARDRVVECFWILGVYFEPK YEIARRFLTKVISMTS IIDDIYDVYGS LDEARRLTHA		332
SoTPS3	LSFARDRMVECYFWILGVYFEPQ YATARIFLTKVIALTSTLDDIYDVYPTIEELRCFTDA		331
TEY90111.1	LPFARDRVAECYFWIVGVYFEPQ YD TARVMTKVIALTSTIIDDIYDVYPTIEELRFLTHA		280

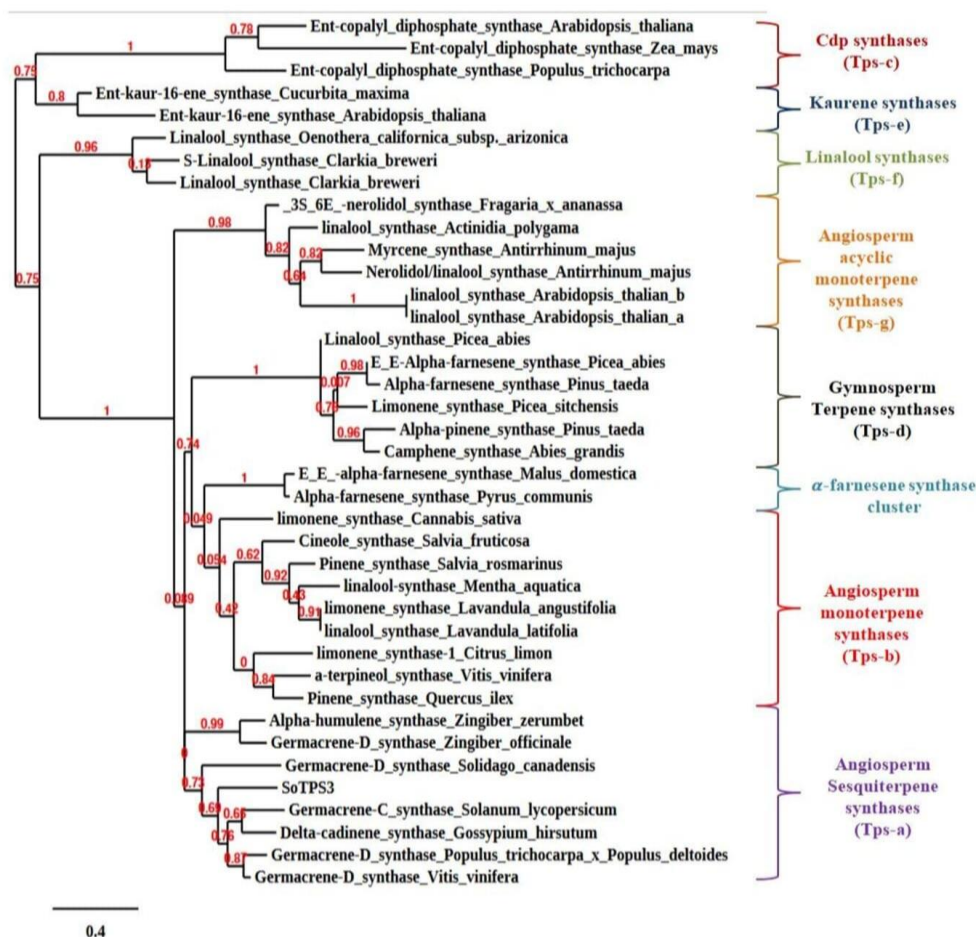


Figure 3. Phylogenetic tree of *SoTPS3* with selected terpene synthases from other plants. Based on the knowledge gained from the work of Bohlmann et al., 1998 and Danner et al., 2011, seven TPS subfamilies (Tps-a to Tps-g) were chosen. However, the Tps-c and Tps-e subfamilies were chosen as out-groups. Those are composed of the copalyl diphosphate (cdp) synthases and kaurene synthases and are involved in primary metabolism. The alignment was performed using the PhyML server. The numbers indicated are the actual bootstrap values of the branches.

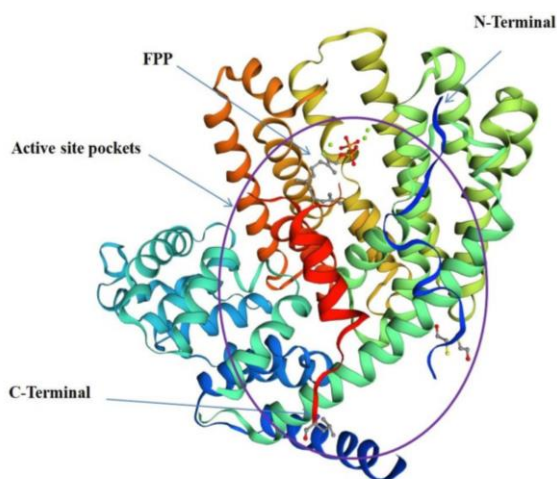


Figure 4. Predicted 3D model of *SoTPS3* generated by the SWISS-MODEL software. The active site pocket with predicted FPP binding residues are indicated through arrows along with the N-terminal domain and the C-terminal domain. Prediction of 3D protein structure and binding residues were generated using online SWISS-MODEL server. An illustration that clarifies the binding between the substrate (FPP) and the active site residues is depicted at the center of the active site in *SoTPS3* 3D proteins.

3.3. Putative tissue expression and subcellular localization of *SoTPS3* gene

To examine the putative tissue expression pattern of *SoTPS3* in the *A. thaliana* genomics, a BlastP search against the *A. thaliana* genomics at Phytozome database (https://phytozome.jgi.doe.gov/pz/portal.html#!search?show=BLAST&method=Org_Athaliana) was conducted with the protein sequence of *SoTPS3* as a query. This research identified several proteins closely related to the *SoTPS3* sequences specially (AT5G23960) with a high BLAST score and e-Value (351.7 and 3E-113), respectively. The tissue expression of *SoTPS3* gene in Arabidopsis uncovered by our data was analysed across forty seven tissue using BAR database (<http://bar.utoronto.ca/efp/cgi-bin/efpWeb.cgi>) and the Arabidopsis Electronic Fluorescent Pictograph Browsers (eFP browsers (<http://bar.utoronto.ca/efp/cgi-bin/efpWeb.cgi>) (Figure 5a and b).

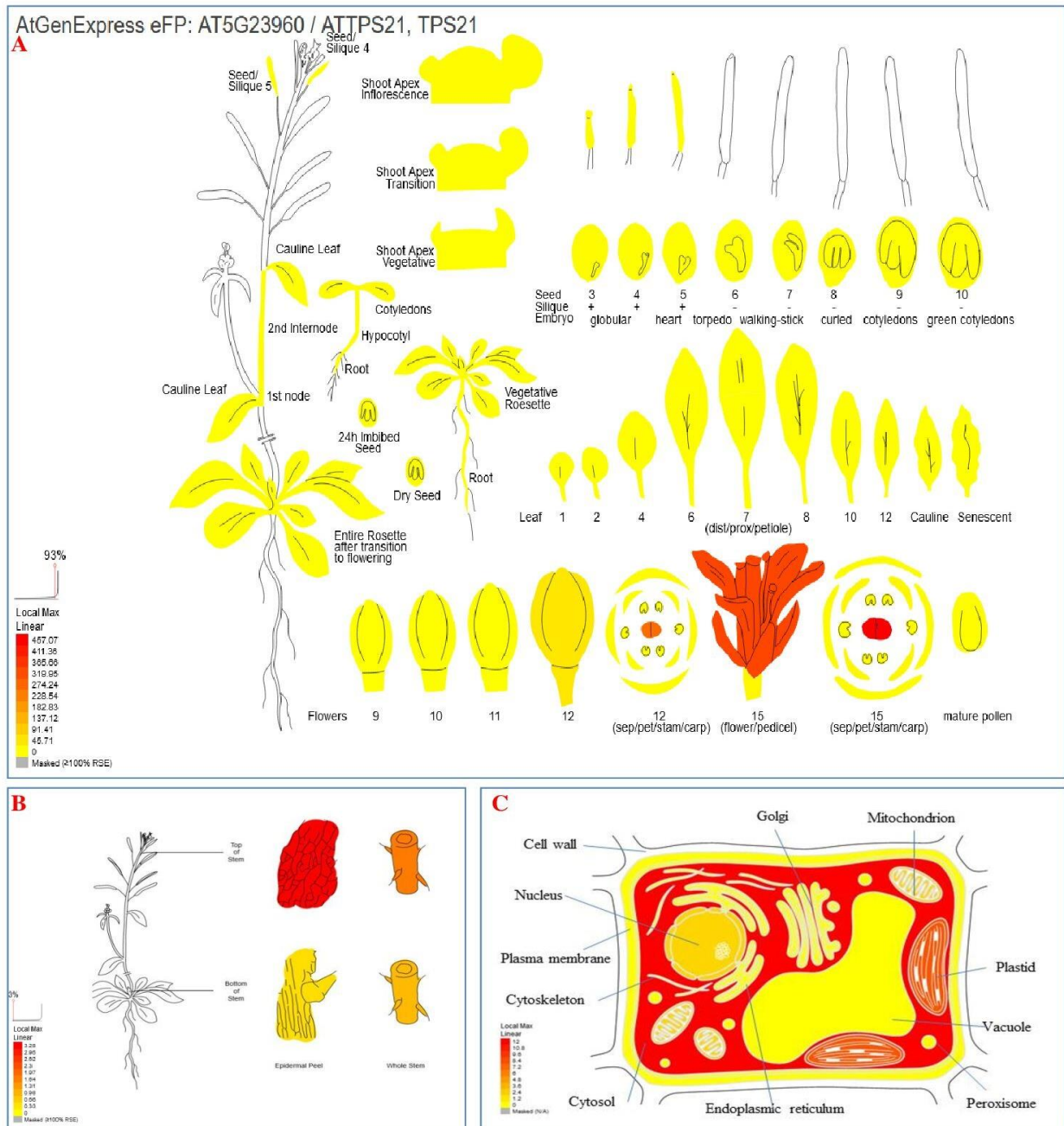


Figure 5. Visualization of the putative tissue expression and cell localization of *SoTPS3* (AT5G23960.1) gene using “electronic fluorescent pictograph” browsers, based on known Arabidopsis gene expression and protein localization. **a** Expression data at different tissues ranging from seedling to flowering stages. **b** Expression data of tissue specific stem epidermis at top and bottom. **c** Expression data at different cell organelles. The color box points the expression scale (the more intense red color, the more gene expression).

The Arabidopsis eFP Browsers clearly showed that (*SoTPS3* gene: AT5G23960) was present in most of the tissues with highly expressed in flower-stage-15-carpels (457.06), flower-stage-15 (332.31), flower-stage-12-carpels (263.98) and flower-stage-12 (43.26) (Figure 5a and Supplementary Table S1). Moreover, putative subcellular localization built using ePlant and cell eFP (http://bar.utoronto.ca/cell_efp/cgi-bin/cell_efp.cgi) for (*SoTPS3*: AT5G23960) gene was present with different expression levels at the fourteen cell organelles see (Figure 5c).

3.4. Screening the expression of *SoTPS3* gene using qRT-PCR.

qPCR-PCR was used to inspect the transcription levels of *SoTPS3* at various tissues of *S. officinalis* (e.g. flowers, bud flowers, stems, young leaves, old leaves and roots) (Figure 6). And from our qPCR-PCR analysis results, we found the highest expression levels were observed in flowers, then in bud flowers, young leaves, stems, old leaves and roots (Figure 6).

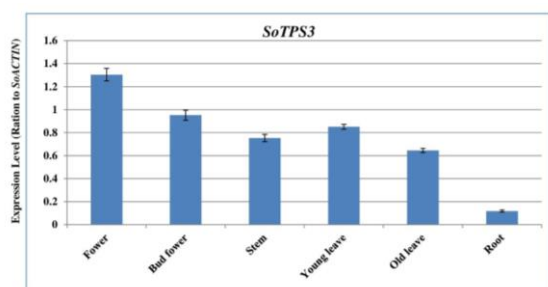


Figure 6. Quantitative RT-PCR validation of *SoTPS3* gene expression from *S. officinalis*. Total RNAs were extracted from flower, bud flower, stem, young leaves, old leaves and bud flower roots samples and the expression of *SoTPS3* gene was analysed using quantitative real-time. We used *SoACTIN* as an internal reference. The values are means \pm SE of three biological replicates.

3.5. Functional expression of *SoTPS3* gene in non- and transgenic *A. thaliana* plants

To study the effect of *SoTPS3* gene on *A. thaliana* plants phenotypes after 33 days of growth, this gene was cloned from *S. officinalis*. Thereafter, *A. thaliana* was utilized as a transient expression system to overexpress the isolated *SoTPS3* gene. We used *A. tumefaciens* strain GV101 harbouring the vector pB2GW7-*SoTPS3* controlled by 35S promoter to generate transgenic *A. thaliana* plants overexpressing *SoTPS3* gene constitutively (Figure 7a). The positive transformants were further verified using BASTA reagent and sqRT-PCR of the genomic cDNA (Figure 7b). Transgenic *A. thaliana* plants showed a decrease in leaf diameter, while the flowering stems start growth earlier when compared to the GUS control

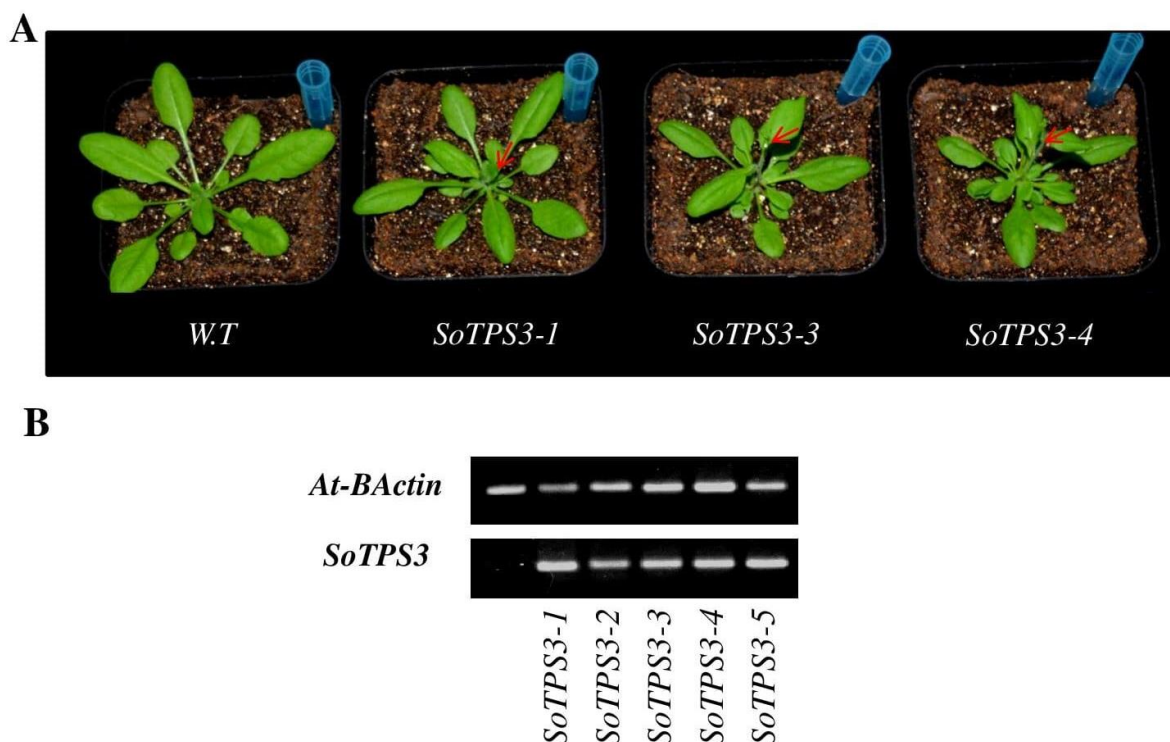


Figure 7. Overexpression of *SoTPS3* gene in transgenic Arabidopsis. (A) The phenotypes of the transgenic *A. thaliana* compared with the wild type *A. thaliana*. (B) Confirmation of the expression of terpeneoid genes via Semiquantitative RT-PCR.

3.6. Overexpression of *SoTPS3* gene altered the terpene profiles in transgenic *A. thaliana* leaves.

To examine the effect of overexpressing *SoTPS3* gene in *A. thaliana* leaves, we analysed the changes of terpene metabolic in transgenic *A. thaliana* leaves using GC-Mass. The results revealed that a variety of terpenes significantly increased in transgenic *A. thaliana* leaves overexpressing *SoTPS3* gene in parallel with control as we notified in Table 2 and Supplementary figure S1. In leaves of *A. thaliana* plants overexpressing *SoTPS3*, Germacrene D-4 α -ol appeared as the main sesquiterpene compound (75.25%), followed by Cis-Caryophyllene epoxide (1.31%), and Topanol (0.97%), whereas 3-Thujen-2-one (1.57%) and Phytol compound (2.05%) were observed as the major monoterpene and diterpene compounds, respectively.

4. Discussion

4.1. Cloning and sequence analysis of *SoTPS3* gene from *S. officinalis*.

The full-length cDNA of *SoTPS3* gene was recognized and isolated from leaves of *S. officinalis*, based on the highly conserved sequence similarity between our query sequence and the other sequences detected in different plant species such as (*Salvia splendens*, *Origanum vulgare*, *Ocimum basilicum* and *Vitis vinifera*). When compared to other sesquiterpene synthases, *SoTPS3* protein has three domains, which were specified by the InterPro database. The first domain is the N-terminal-domain (IPR001906: from 32-207 aa), and the second is the C-terminal-domain (IPR005630: from 238-499 aa), while the third is the metal-binding-domain (IPR034741: from 233-554aa) (Figs 1 and 2).

Table 2. The major terpenoid composition in transgenic *A. thaliana* leave over-expressing of *SoTPS3*.

N	Compound name	R.T (min.)	Formula	Molecular Mass (g mol ⁻¹)	Terpene Type	% Peak area	
						W.T	<i>SoTPS-3</i>
1	Acetic acid, [o-(trimethylsiloxy) phenyl]-, trimethylsilyl ester	29.591	C14H24O3Si2	296.5096		-	0.42
2	Topanol	31.135	C15H24O	220.3505	Sesqui	-	0.97
3	Cyclooctasiloxane, hexadecamethyl-	34.467	C16H48O8Si8	593.2315		-	0.31
4	Lauryl ethoxylate	35.598	C14H30O2	230.3868		1.52	-
5	3-Thujen-2-one	36.075	C10H14O	150.2176	Mono	-	1.57
6	Narceol	36.955	C9H10O2	150.1745		1.57	-
7	2-Methyldecane	38.48	C11H24	156.3083		1.48	-
8	Cyclohexasiloxane, dodecamethyl-	38.649	C12H36O6Si6	444.9236		-	0.38
9	6-Octen-1-ol, 3,7-dimethyl-, acetate	40.625	C12H22O2	198.3019		-	0.82
10	Phytan	41.196	C20H42	282.5475	Diter	2.39	-
11	Dodecamethylcyclohexasiloxane	42.353	C12H36O6Si6	444.9236		-	0.37
12	Oleic Acid	43.799	C18H34O2	282.468		3.29	-
13	Pentadecylic acid	44.721	C15H30O2	242.3975		-	0.86
14	Palmitic acid	45.31	C16H32O2	256.4241		27.86	-
15	Cis-Caryophyllene epoxide	46.055	C15H24O	220.3505	Sesqui	-	1.31
16	2-Methyldodecane	46.257	C13H28	184.3614		3.37	-
17	Palmitic acid, trimethylsilyl ester	47.316	C19H40O2Si	328.6052		6.33	-
18	Phytol	47.572	C20H40O	296.531	Diter	-	2.05
19	Heneicosane	48.625	C21H44	296.5741		3.02	-
20	4,8,13-Duvatriene-1,3-Diol	49.158	C20H34O2	306.4828		-	5.34
21	Trans-Elaidic acid	49.488	C18H34O2	282.4614		26.79	-
22	Germacrene D-4 α -ol	49.898	C15H26O	222.3663	Sesqui	-	75.25
23	Heptadecane, 8-methyl-	50.911	C17H36	240.4677		2.41	-
24	Hexadecamethylcyclooctasiloxane	51.877	C16H48O8Si8	593.2315		-	0.72
25	Cadinane	51.916	C20H41Cl	316.993		10.23	-
26	8,11,14-Eicosatrienoic acid, methyl ester	53.502	C21H36O2	320.5093		-	1.51
27	Oleamide	54.178	C18H35NO	281.4766		-	0.42
28	Hexasiloxane, tetradecamethyl-	56.117	C14H42O5Si6	458.9933		-	1.3
29	N-Pentatriacontane	58.321	C35H72	492.9462		-	0.61
30	Phthalic acid dioctyl ester;	59.765	C24H38O4	390.5561		-	0.57
31	Mandelic acid di(tert butyldimethylsilyl)-	60.91	C20H36O3Si2	380.669		-	0.29
32	Octadecamethyl-cyclononasiloxane	62.357	C18H54O9Si9	667.3855		-	0.75
33	9-Methylnonadecane	63.294	C20H42	282.5475		-	0.46
34	N-Nonacosane	68.714	C29H60	408.7867		-	1.03
35	Hexasiloxane, tetradecamethyl-	69.697	C14H42O5Si6	458.9933		-	0.57
36	2,6,10-Dodecatrien-1-ol, 3,7,11-trimethyl-	74.561	C15H26O	222.3663		-	0.75
37	Octadecamethyl-cyclononasiloxane	77.334	C18H54O9Si9	667.3855		-	0.6
38	N-Nonacosane	78.147	C29H60	408.7867		-	0.77
39	Tetrapentacontane	78.973	C54H110	759.4512		9.74	-
Total % Peak area						% 100	% 100

A comparison between our putative *SoTPS3* protein sequence and other plant sesquiterpene synthase revealed various highly conserved motifs. Two of these motifs are called aspartate-rich-DDxxD motif (residues 313–317) and NSE/DTE motif (residues 457–465); they were reported to be surrounding the doorway to the active site position, and most likely responsible for coordination of divalent metal ion co-factors and substrate binding (Rebecca *et al.* 2020; Lima *et al.* 2013; L'opez-Gallego *et al.* 2010; Abbas *et al.* 2019; Su-Fang *et al.* 2014; Degenhardt *et al.* 2009; Ali *et al.* 2017; Ali *et al.* 2018) (Figure 2). Moreover, they are also known for their role in binding a tri-nuclear-magnesium cluster, two-magnesium-ions and one-magnesium-ion (Christianson, 2006; Lima *et al.* 2013; Abbas *et al.* 2019). This magnesium cluster binds and

interacts with the diphosphate moiety of farnesyl diphosphate (FPP), hence catalyzing the C15-substrate-FPP formation at the hydrophobic substrate binding pocket (Davis and Croteau, 2000; Degenhardt *et al.* 2009; Abbas *et al.* 2019). Moreover, we detected another conserved region RXR motif (residues 276–278) in the *SoTPS3* protein, which is needed for product cyclization in class-III-TPS proteins (Rebecca *et al.* 2020; Su-Fang *et al.* 2014; Whittington *et al.* 2002; Hyatt *et al.* 2007) (Figure 2). Our analysis revealed further conserved region motifs in the *SoTPS3* protein that are dominant in other sesquiterpene synthases, namely, RR (X8) W (residues 22–32) and GTLxEL (residues 320–325) region. Eventually, each protein sequence that belongs to the family of terpene synthase has one or two of these conserved domains and

motifs (Ali *et al.*, 2017, 2018, 2022, 2022a). A phylogenetic tree was generated to analyze the evolutionary relationship between SoTPS3 and other plant sesquiterpene synthase genes, and the evolutionary tree was constructed in a good way by the neighbor-joining method parameters. Based on our classification results, the SoTPS3 protein was classified into the TPS-a subfamily that can encode mono- and sesquiterpene, which explains the ability of SoTPS3 to produce various types of terpenes as previously mentioned by (Ali *et al.*, 2017 and 2018) (Figure 3).

4.2. 3D molecular modeling of SoTPS3

The 3D protein model for SoTPS3 was constructed depending on the crystal structure of (+)- δ -cadinene synthase from *G. arboreum* as depicted in Figure 4. The sequence similarities between our target sequence and (+)- δ -cadinene synthase were about 79% with 2.65Å as a root-mean-square deviation values, which indicates that the SoTPS3 sequence is very similar and well compatible with the (+)- δ -cadinene synthase X-ray template from *G. arboreum*. Moreover, our target sequence has a C-terminal-domain, a N-terminal-domain and the active site to catalyse the substrate FPP as shown in the active site pockets. These results suggest that SoTPS3 possesses similar mechanisms to that (+)- δ -cadinene as a sesquiterpene synthase gene from *G. arboreum*.

4.3. Putative tissue expression pattern and subcellular localizations of SoTPS3 gene

To identify the physiological roles of *SoTPS3*, we explored its putative expression in forty-seven tissues. This was aided by the high resemblance between *SoTPS3* and AT5G23960 gene from *A. thaliana*. *SoTPS3* gene was recognized in the tested tissues, and this result lines up with Ali *et al.*, 2017, 2018, 2022a, who reported that most TPS genes (e.g. *SoFLDH*, *SgTPSV*, *SgGERIS*, *SoLINS2*, *GmTPS21*, *SgFARD*, *SoNEOD* and *SoHUMS*) from *S. officinalis*, *Glycine max.*, and *S. guaranitica* showed an increased expression in leaves, roots and seeds. Furthermore, the putative subcellular localization for SoTPS3 protein revealed that our gene is present at most in the Cytosol, then Plastid, Mitochondria and Nucleus. Our gained results are similar with Ali *et al.*, Taniguchi *et al.*, Chen *et al.*, and Wang *et al.*, (Ali *et al.*, 2017, 2018, 2022a; Wang *et al.*, 2015b; Taniguchiet *al.*, 2014; Chen *et al.*, 2018; Makhadmeh *et al.*, 2022a and 2022b) who found that various TPSs genes were localized in the plastid, mitochondria and nucleus (Figure 5).

4.4. Effectiveness of qRT-PCR for analysis the SoTPS3 gene expression.

We used qRT-PCR to measure the expressed levels of *SoTPS3*. Therefore, qPCR data revealed that *SoTPS3* is highly expressed in flowers then at bud flowers, young leaves and stems. This fits with the information provided previously that found various TPS syntheses genes were highly expressed in bud flowers, young leaves, stems, and old leaves (Sabin *et al.*, 2012; Croteau *et al.*, 1981; Ali *et al.*, 2017; Ali *et al.*, 2018). The low expression of *SoTPS3* gene in old leaves and roots is probably due to many reasons such as: gene-regulatory mechanisms (possible posttranscriptional and/or post-translational) (Figure 6). It is also possible that the expression levels of *SoTPS3* is associated with tissue-developmental-stages, which

strongly influences the expression of terpene synthase in salvia (Sabin *et al.*, 2012; Croteau *et al.*, 1981; Ali *et al.*, 2017; Ali *et al.*, 2018)

4.5. Overexpression of SoTPS3 gene changed the *A. thaliana* plants phenotypes

To evaluate the function of *SoTPS3* in *A. thaliana* (Col-0: Columbia-0) plants, we overexpressed *SoTPS3* in *A. thaliana* through the use of Agrobacterium bacteria harboring the overexpression vector pB2GW7-*SoTPS3*. Thereafter, sqRT-PCR confirmed the expression of our target gene in positive transgenic lines (Figure 7). The transgenic lines showed higher expression level of the *SoTPS3* gene in parallel with the wild-type, which indicated the existence of our target gene in the transgenic plants. After that, we chose three transgenic plants (named; OE-*SoTPS3*-1, OE-*SoTPS3*-3 and OE-*SoTPS3*-4) for terpene analysis. The morphological analysis showed that the previous transgenic plants had an accelerated rate of flowering stem formation unlike the wild type plants (Figure 7). Our earned positive results are in line with Ali *et al.* 2017, 2018 and 2022, where the overexpression of TPS synthesis and terpenoids genes, such as *SgGPS*, *SgLINS*, *SgFPPS*, *SoTPS6*, *SoCINS*, *SoLINS*, *SoFLDH*, *SoSABS*, *SgGPS* and *SoNEOD* from *S. guaranitica* and *S. officinalis* in *A. thaliana* and *Nicotiana tabacum*, accelerated the growth and flower formation when compared to wild type plants. In previous results, numerous TPSs family genes played a key role in different cell-specific processes, such as: 1, 8-cineole, Z- γ -bisabolene, Rhizathalene, β -amyrin and thalianol synthesis as a mono-, sesqui-, di- and triterpene, respectively (Field and Osbourn, 2008; Field *et al.* 2011; Kampranis *et al.* 2007; Wang *et al.* 2016; Ro *et al.* 2006; Vaughan *et al.* 2013; Chen *et al.* 2011; Chen *et al.* 2004). This indicates that these genes can initially co-express in a variety of cells, tissues, and organs to produce distinct plant phenotypes, confirming the function of TPSs-genes in plant development, growth, and blooming. (Field and Osbourn, 2008; Field *et al.* 2011; Kampranis *et al.* 2007; Wang *et al.* 2016; Ro *et al.* 2006; Vaughan *et al.* 2013; Chen *et al.* 2011; Chen *et al.* 2004). The metabolites were analyzed by GC-MS-system to recognize the specific terpenes synthesized after introducing the *SoTPS3* gene into Arabidopsis plants and generating over expressing transformant lines. The mono-, sesqui- and diterpene peaks were easily visible; the percentage of peak area (% peak area) demonstrated the type and amount of the compounds. To identify these terpenes in our transgenic Arabidopsis plants, we used the libraries of mass spectra, the previous extracts of wild-type Arabidopsis as a reference, which produce different quantitative and qualitative of terpenoids. Per the results shown in Table 2 and Supplementary figure S1, a clear alteration was observed in the transgenic plants, and a new peak at retention time (49.898) was detected. This peak was identified as Germacrene D-4 α -ol, based on the matched mass with the Wiley GC/MS, NIST Library and VOC Analysis S/W software. The production of Germacrene D-4 α -ol as a sesquiterpene by the overexpression of *SoTPS3* gene in *A. thaliana* was described formerly by Ali *et al.* 2018; Su-Fang *et al.* 2014. Various terpene synthase genes are known to synthesize various products in unison, e.g. carene, (\pm)-linalool, cineole, myrcene, β -amyrin and

terpinolene synthases (Yoko *et al.*, 2004; Shimada *et al.* 2005; Abbas *et al.* 2019; Lucker *et al.* 2002; Fahrnich *et al.* 2011; Xi *et al.* 2016; Faldt *et al.* 2003). We believe that *SoTPS3* was responsible for the production of Germacrene D-4 α -ol via isoprenoid pathway which is common in sesquiterpene biosynthesis.

5. Conclusions

S. officinalis is a significant Egyptian medicinal herb with unique pharmacological properties. Hence, the cloning and characterization of many genes related to secondary metabolic pathway will aid the success of metabolic engineering in *S. officinalis* and other medicinal plants. In this study, we have cloned a plant Germacrene D-4 α -ol biosynthesis gene from *S. officinalis* and named it *SoTPS3*. Overexpression of *SoTPS3* in *A. thaliana* accelerated the flowering in *OE-SoTPS3-1*, *OE-SoTPS3-3* and *OE-SoTPS3-4* transgenic lines. These previous lines showed a high production of Germacrene D-4 α -ol compared with control. The Germacrene D-4 α -ol produced in these transgenic lines reveals that the *A. thaliana* plants have the ability to synthesize the same product through the common mevalonate-pathway (MVK) of sesquiterpene biosynthesis. Moreover, the putative expression patterns and subcellular localization results revealed that the *SoTPS3* gene was highly expressed in various flower tissues and mainly localized in the cytosol, which underscores the possible role of this gene in yielding various types of terpenes, especially the sesquiterpene Germacrene D-4 α -ol. This study revealed that the *A. thaliana* as a model plant can robustly use as suitable model for study the sesquiterpene gene that can be used for improving essential oil composition in *S. officinalis* and other plant species through metabolic engineering.

6. Ethics approval and consent to participate

No investigations were undertaken using humans/human samples in this study. No experimental animals were used to conduct any of the experiments reported in this manuscript. Our study did not involve endangered or protected species.

7. Competing interests

The authors declare that they have no competing interests.

8. Funding

This study was supported by the Department of Genetic Resources, Desert Research Center (DRC), Egypt.

9. Author's contributions

MA conceived and designed the study; MA, FAE, EAE, MNSS and MSR performed experiments, MA wrote the paper. All authors discussed the results and commented on the manuscript and participated in the analysis of the data. All authors participated in reading and approving the final manuscript.

10. Availability of data and materials

All data supporting my findings can be available and found in the supplementary data.

Acknowledgements

The authors thank Professor Dr. Osama Ezzat Elsayed and Dr. Aamir Hamid Khan for proof-reading the manuscript. We also owe thanks to Dr. Wael Moussa, for constructive comments and help. We also owe thanks to all Molecular Genetic lab (Prof. Dr. Osama Ezzat Elsayed lab) members at National Research Centre, Dokki, Cairo, Egypt for facilitating the practical work at all levels of the experiments; the first author would like to thank the Desert Research Center labs.

References

- Abdul-Rahim A and Taha A.2011. Effects of Rosemary (*Rosmarinus officinalis*) on Lipid Profile of Diabetic Rats. *Jordan J. Biol. Sci.* **4**(4): 199 - 204.
- Abbas F, Yanguo K, Rangcai Y, Yanping F. 2019. Functional characterization and expression analysis of two terpene synthases involved in floral scent formation in *Lilium* 'Siberia.' *Planta.*, **249**:71–93.
- Aharoni A, Giri AP, Deurlein S, Griepink F, de Kogel WJ, Verstappen FW, Verhoeven HA, Jongsma MA, Schwab W, Bouwmeester HJ. 2003. Terpenoid metabolism in wild-type and transgenic Arabidopsis plants. *Plant Cell.*, **15**(12):2866-84.
- Ali M, Alshehri D, Alkhaibari AM, Elhalem NA, Darwish DBE.2022a. Cloning and Characterization of 1,8-Cineole Synthase (*SgCINS*) Gene From the Leaves of *Salvia guaranitica* Plant. *Front Plant Sci.*, **(13)**:869432.
- Ali M, Hussain RM, Rehman NU, She G, Li P, Wan X, Guo L, Zhao J. 2018. De novo transcriptome sequencing and metabolite profiling analyses reveal the complex metabolic genes involved in the terpenoid biosynthesis in Blue Anise Sage (*Salvia guaranitica* L.). *DNA Res.*, **25**(6):597-617.
- Ali M, Li P, She G, Chen D, Wan X, Zhao J. 2017. Transcriptome and metabolite analyses reveal the complex metabolic genes involved in volatile terpenoid biosynthesis in garden sage (*Salvia officinalis*). *Sci Rep.*, **7**(1):16074.
- Ali M, Miao L, Hou Q, Darwish DB, Alrdahe SS, Ali A, Benedito VA, Tadege M, Wang X, Zhao J. 2021. Overexpression of Terpenoid Biosynthesis Genes From Garden Sage (*Salvia officinalis*) Modulates Rhizobia Interaction and Nodulation in Soybean. *Front Plant Sci.*, **(12)**:783269.
- Ali M, Miao L, Soudy FA, Darwish DBE, Alrdahe SS, Alshehri D, Benedito VA, Tadege M, Wang X, Zhao J. 2022c. Overexpression of Terpenoid Biosynthesis Genes Modifies Root Growth and Nodulation in Soybean (*Glycine max*). *Cells.*, **11**(17):2622.
- Ali M, Nishawy E, Ramadan WA, Ewas M, Rizk MS, Sief-Eldein AGM, El-Zayat MAS, Hassan AHM, Guo M, Hu GW, Wang S, Ahmed FA, Amar MH, Wang QF. 2022b. Molecular characterization of a Novel NAD⁺-dependent farnesol dehydrogenase *SoFLDH* gene involved in sesquiterpenoid synthases from *Salvia officinalis*. *PLoS One.*, **17**(6): e0269045.
- Alziar G (1988–1993). Catalogue synonymique des *Salvia* L. dumonde (Lamiaceae). I–VI. *Biocosme Mesogéen.*, **5** (3–4): 87–136; **6**(1–2, 4): 79–115, 163–204; **7**(1–2): 59–109; **9**(2–3): 413–497; **10**(3–4): 33–117.

- Anders S, Huber W. 2010. Differential expression analysis for sequence count data. *Genome Biol.*, **11**(10):R106.
- Atsuko T, Hiroshi O. 2011. Phylogenetic relationships among subgenera, species, and varieties of Japanese *Salvia* L. (Lamiaceae). *J Plant Res.*, **(124)**: 245–252.
- Aziz RA, Hamed FK, Abdulah NA. 2008. Determination of the main components of the essential oil extracted from *Salvia fruticosa* by sing GC and GC-MS DAMASCUS. *J Agr Sci.*, **(24)**:223–236.
- Bohlmann J, Meyer-Gauen G, Croteau R. 1998. Plant terpenoid synthases:molecular biology and phylogenetic analysis. *Proceedings of the National Academy of Sciences of the United States of America.* **(95)** 8:4126–4133.
- Chen X, Chen H, Yuan JS, Kollner TG, Chen Y, Guo Y, et al. 2018. The rice terpene synthase gene *OsTPS19* functions as an (S)-limonene synthase in planta, and its overexpression leads to enhanced resistance to the blast fungus *Magnaporthe oryzae*. *Plant Biotechnol J.*, **16**(10):1778–1787.
- Chen, F.; Ro, D.K.; Petri, J.; Gershenzon, J.; Bohlmann, J.; Pichersky, E.; Tholl, D. 2004. Characterization of a root-specific Arabidopsis terpene synthase responsible for the formation of the volatile monoterpene 1, 8-cineole. *Plant Physiol.*, (135) 1956–1966.
- Chen, F.; Tholl, D.; Bohlmann, J.; Pichersky, E. 2011. The family of terpene synthases in plants: A mid-size family of genes for specialized metabolism that is highly diversified throughout the kingdom. *Plant J.*, **(66)**: 212–229.
- Christianson DW. 2006. Structural biology and chemistry of the terpenoid cyclases. *Chemical Reviews.*, **(106)** 8:3412–3442.
- Croteau, R., Felton, M., Karp, F. and Kjonaas, R. 1981. Relationship of camphor biosynthesis to leaf development in sage *Salvia officinalis*. *Plant Physiol.*, **(67)**: 820–4.
- Darwish DBE, Ali M, Abdelkawy AM, Zayed M, Alatawy M, Nagah A. 2022. Constitutive overexpression of *GsIMaT2* gene from wild soybean enhances rhizobia interaction and increase nodulation in soybean (*Glycine max*). *BMC Plant Biol.*, **22**(1):431.
- Davis EM, Croteau R. 2000. Cyclization enzymes in the biosynthesis of monoterpenes, sesquiterpenes, and diterpenes. in *Biosynthesis: Aromatic Polyketides, Isoprenoids, Alkaloids*, J. C. Vederas and F. J. Leeper, Eds., pp. 53–95, Springer, Berlin, Germany.
- Degenhardt J, Köllner TG, Gershenzon J. 2009. Monoterpene and sesquiterpene synthases and the origin of terpene skeletal diversity in plants. *Phytochemistry.*, **(70)**:1621–1637.
- Dereeper A, Guignon V, Blanc G, Audic S, Buffet S, Chevenet F, Dufayard JF, Guindon S, Lefort V, Lescot M, Claverie JM, Gascuel O. 2008. Phylogeny.fr: robust phylogenetic analysis for the non-specialist. *Nucleic Acids Res.*, **(36)**:W465–W469.
- Dorothea T, Wilhelm B, Armin H, Francesco L, Ursula SRR, Jörg-Peter S. 2006. Practical approaches to plant volatile analysis. *The Plant Journal.*, **(45)**: 540–560.
- Fahnrich A, Krause K, Piechulla B. 2011. Product variability of the 'cineole cassette' monoterpene synthases of related *Nicotiana* species. *Mol Plant.*, **(4)**:965–984.
- Faldt J, Martin D, Miller B, Rawat S, Bohlmann J. 2003. Traumatic resin defense in Norway spruce (*Picea abies*): methyl jasmonate-induced terpene synthase gene expression, and cDNA cloning and functional characterization of (+)-3-carene synthase. *Plant Mol Biol.*, **(51)**:119–133.
- Fateme AM, Mohammad HF, Abdolhossein R, Ali Z, Maryam S. 2013. Volatile Constituents of *Salvia compressa* and *Logochilus macranthus*, two Labiatae Herbs Growing wild in Iran. *Res J Recent Sci.*, **(2)**: 66–68.
- Field, B.; Fiston-Lavier, A.S.; Kemen, A.; Geisler, K.; Quesneville, H.; Osbourn, A.E. 2011. Formation of plant metabolic gene clusters within dynamic chromosomal regions. *Proc. Natl. Acad. Sci. USA.*, **(108)**:16116–16121.
- Field, B.; Osbourn, A.E. 2008. Metabolic diversification-independent assembly of operon-like gene clusters in different plants. *Science.*, **(320)**:543–547.
- Gennadios HA, Gonzalez V, Di Costanzo L, Li A, Yu F, Miller DJ, Allemann RK, Christianson DW. 2009. Crystal structure of (+)-delta-cadinene synthase from *Gossypium arboreum* and evolutionary divergence of metal binding motifs for catalysis. *Biochemistry.*, **(48)**: 6175– 6183.
- Gershenzon J, Kreish W.1999. Biochemistry of terpenoids: monoterpenes, sesquiterpenes, diterpenes, sterols, cardiac glycosides and steroid saponins. In: Wink M, editor. Biochemistry of plant secondary metabolism. Florida: CRC Press., :222–299.
- Ibrahim Mohammad Al-Rawashdeh. 2011. Molecular Taxonomy Among *Mentha spicata*, *Mentha longifolia* and *Ziziphora tenuior* Populations using the RAPD Technique. *Jordan J. Biol. Sci.* **4**(2): 63- 70.
- Hua WP, Zhang Y, Song J, Zhao LJ, Wang ZZ. 2011. *De novo* transcriptome sequencing in *Salvia miltiorrhiza* to identify genes involved in the biosynthesis of active ingredients. *Genomic.s* **(98)**:272–279.
- Hussain RM, Ali M, Feng X, Li X. 2017. The essence of NAC gene family to the cultivation of drought-resistant soybean (*Glycine max* L. Merr.) cultivars. *BMC Plant Biol.* ,**17**(1):55.
- Hyatt DC, Youn B, Zhao Y, Santhamma B, Coates RM, Croteau RB, Kang C. 2007. Structure of limonene synthase, a simple model for terpenoid cyclase catalysis. *Proc Natl Acad Sci.*, **(104)**:5360–5365.
- Köllner TG, Held M, Lenk C et al. 2008. A maize (E)- β -caryophyllene synthase implicated in indirect defense responses against herbivores is not expressed in most American maize varieties. *Plant Cell.*, **(20)** 2: 482–494.
- Kamatoua G.P.P., N.P. Makungab, W.P.N. Ramogolab, A.M. Viljoen. 2008. South African *Salvia* species: A review of biological activities and phytochemistry. *Journal of Ethnopharmacology.*, **(119)**: 664–672.
- Kampranis SC, Ioannidis D, Purvis A, Mahrez W, Ninga E, Katerelos NA, Anssour S, Dunwell JM, Degenhardt J, Makris AM, Goodenough PW, Johnson CB. 2007. Rational conversion of substrate and product specificity in a *Salvia* monoterpene synthase: structural insights into the evolution of terpene synthase function. *Plant Cell.*, **19**(6):1994-2005.
- L'opez-Gallego F, Wawrzyn GT, Schmidt-Dannert C. 2010 Selectivity of fungal sesquiterpene synthases: role of the active site's H-1 α loop in catalysis. *Appl Environ Microbiol.*, **(76)** 23: 7723–7733.
- Laskowski RA, MacArthur MW, Moss DS, Thornton JM. 1993. PROCHECK: a program to check the stereochemical quality of protein structures. *J Appl Crystallogr.*, **(26)**: 283–291.
- Li D, Shao F, Lu S. 2015. Identification and characterization of mRNA-like noncoding RNAs in *Salvia miltiorrhiza*. *Planta.*, **(241)**:1131–1143.
- Lima AS, Jette S, Brigitte L, Johannes N, Jose´ GB, Figueiredo A C, Luis GP, Jo´rg D, Helena T. 2013. Genomic characterization, molecular cloning and expression analysis of two terpene synthases from *Thymus caespititius* (Lamiaceae). *Planta.*, **(238)**:191–204.
- Loizzo MR1, Menichini F, Tundis R, Bonesi M, Nadjafi F, Saab AM, Frega NG, Menichini F. 2010. Comparative chemical composition and antiproliferative activity of aerial parts of *Salvia lerifolia* Benth. And *Salvia acetabulosa* L. essential oils against human tumor cell *in vitro* models. *J Med Food.*, **(13)**: 62–69.
- Lucker J, El Tamer MK, Schwab W, Verstappen FW, van der Plas LH, Bouwmeester HJ et al. 2002. Monoterpene biosynthesis in lemon (*Citrus limon*). *FEBS J.*, **(269)**:3160–3171.
- Makhadmeh I, Albalasmeh AA, Ali M, Thabet SG, Darabseh WA, Jaradat S, Alqudah AM. 2022b. Molecular Characterization of Tomato (*Solanum lycopersicum* L.) Accessions under Drought Stress. *Horticulturae.*, **8**(7):600.

- Makhadmeh IM, Thabet SG, Ali M, Alabbadi B, Albalasmeh A, Alqudah AM. 2022a. Exploring genetic variation among Jordanian *Solanum lycopersicon* L. landraces and their performance under salt stress using SSR markers. *J Genet Eng Biotechnol.*, **20(1)**:45.
- Makris, A.M.; et al. 2007. Rational conversion of substrate and product specificity in a *Salvia* monoterpene synthase: Structural insights into the evolution of terpene synthase function. *Plant Cell.*, **(19)**:1994–2005.
- Mehmood N, Yuan Y, Ali M, Ali M, Iftikhar J, Cheng C, Lyu M, Wu B. 2021. Early transcriptional response of terpenoid metabolism to *Colletotrichum gloeosporioides* in a resistant wild strawberry *Fragaria nilgerrensis*. *Phytochemistry.*, **(181)**:112590.
- Nadaf M, Nasrabadi M, Halimi M. 2012. GC-MS analysis of n-hexane extract from aerial parts of *Salvia nemorosa*. *Middle-East Journal of Scientific Research.*, **(11)**: 1127–1130.
- Nema A. Mohamed and Omimah A. Nassier. 2013. The Antihyperglycaemic Effect of the Aqueous Extract of *Origanium vulgare* Leaves in Streptozotocin-Induced Diabetic Rats. *Jordan J. Biol. Sci.* **6(1)**: 31 - 38.
- Rebecca S W, Ayelign MA, Lina B, Elaheh N, Soheil SM. 2020. Cloning and functional characterization of a floral repressor gene from *Lavandula angustifolia*. *Planta.*, **(251)**:41.
- Rehman NU, Ali M, Ahmad MZ, Liang G, Zhao J. 2017. Strigolactones promote rhizobia interaction and increase nodulation in soybean (*Glycine max*). *Microb Pathog.*, **(114)**:420-430.
- Ro, D.-K.; Ehlting, J.; Keeling, C.I.; Lin, R.; Mattheus, N.; Bohlmann, J. 2006. Microarray expression profiling and functional characterization of AtTPS genes: Duplicated *Arabidopsis thaliana* sesquiterpene synthase genes At4g13280 and At4g13300 encode root-specific and wound-inducible (Z)- γ -bisabolene synthases. *Arch. Biochem. Biophys.*, **(448)**: 104–116.
- Sabine, G.-G., Corinna, S., Ralf, S. and Johannes, N. 2012. Seasonal influence on gene expression of monoterpene synthases in *Salvia officinalis* (Lamiaceae). *J. Plant Physiol.*, **1(69)**: 353–9., 45.
- Sarrou E, Ioannis G, Aliko X, Domenico M, Stefan M, Panagiotis M, Athanasios M, Paschalina C. 2017. Genetic diversity and metabolic profile of *Salvia officinalis* populations: implications for advanced breeding strategies. *Planta.*, **(246)**:201–215.
- Shimada T, Endo T, Fujii H, Hara M, Omura M. 2005. Isolation and characterization of (E)-beta-ocimene and 1, 8 cineole synthases in *Citrus unshiu* Marc. *Plant Sci.*, **(168)**:987–995.
- Su-Fang E, Zeti-Azura M, Roohaida O, Noor AS, Ismanizan I, Zamri Z. 2014. Functional Characterization of Sesquiterpene Synthase from *Polygonum minus*. *The Scientific World Journal.*, 10.1155/2014/840592.
- Sujatha Govindaraj and Bollipo D. Ranjitha Kumari. 2013. Composition and Larvicidal Activity of *Artemisia vulgaris* L. Stem Essential Oil Against *Aedes aegypti*. *Jordan J. Biol. Sci.* **6(1)**: 1 - 16
- Takano A, Okada H. 2011. Phylogenetic relationships among subgenera, species, and varieties of Japanese *Salvia* L. (Lamiaceae). *J Plant Res.*, **(124)**: 245–52.
- Taniguchi S, Miyoshi S, Tamaoki D, Yamada S, Tanaka K, Uji Y, et al. 2014. Isolation of jasmonate-induced sesquiterpene synthase of rice: product of which has an antifungal activity against *Magnaporthe oryzae*. *J. Plant Physiol.*, **(171)**: 625–632.
- Trapp S and Croteau R. 2001. Defensive resin biosynthesis in conifers. *Annu Rev Plant Physiol Plant Mol Biol.*, **(52)**:689-724.
- Vaughan, M.M.; Wang, Q.; Webster, F.X.; Kiemle, D.; Hong, Y.J.; Tantillo, D.J.; Coates, R.M.; Wray, A.T.; Askew, W.; O'Donnell, C.; et al. 2013. Formation of the unusual semivolatile diterpene rhizathalene by the Arabidopsis class I terpene synthase TPS08 in the root stele is involved in defense against belowground herbivory. *Plant Cell.*, **(25)**: 1108–1125.
- Wallach O. 1887. Zur Kenntniss der Terpene u. d. d. atherischen Oele. *Liebig's. Ann Chem.*, **239**: 1-54.
- Wang B, Sun W, Li Q, et al. 2015a. Genome-wide identification of phenolic acid biosynthetic genes in *Salvia miltiorrhiza*. *Planta.*, **241(3)**:711–725.
- Wang B, Wei S, Qiushi L, Ying L, Hongmei L, Jingyuan S, Chao S, Jun Q, Yingjie Z, Alice H, Haibin X, Shilin C. 2015b. Genome-wide identification of phenolic acid biosynthetic genes in *Salvia miltiorrhiza*. *Planta.*, **(241)**:711–725.
- Wang, Q.; Jia, M.; Huh, J.H.; Muchlinski, A.; Peters, R.J.; Tholl, D. 2016. Identification of a Dolabellane Type Diterpene Synthase and other Root-Expressed Diterpene Synthases in Arabidopsis. *Front. Plant Sci.*, **(7)** 1761.
- Whittington DA, Wise ML, Urbansky M, Coates RM, Croteau RB, Christianson DW. 2002. Bornyl diphosphate synthase: structure and strategy for carbocation manipulation by a terpenoid cyclase. *Proc Natl Acad Sci USA.*, **(99)**:15375–15380.
- Wise ML, Savage TJ, Katahira E, Croteau R. Monoterpene synthases from common sage (*Salvia officinalis*). 1998. cDNA isolation, characterization, and functional expression of (+)-sabinene synthase, 1,8-cineole synthase, and (+)-bornyl diphosphate synthase. *J Biol Chem.*, **273(24)**:14891-9.
- Xi i, Lorenzo R, Xiuli L, De-Yu X. 2016. Overexpression of a synthetic insect-plant geranyl pyrophosphate synthase gene in *Camelina sativa* alters plant growth and terpene biosynthesis. *Planta.*, **(244)**:215–230.
- Yoko I, David RG, Eyal F, Efraim L, Eran P. 2004. Characterization of Geraniol Synthase from the Peltate Glands of Sweet Basil. *Plant Physiology.*, **(134)**: 370–379.
- Zhenqing B, Wenrui L, Yanyan J, Zhiyong Y, Jie J, Wenli H, Pengguo X, Zongsuo L. 2018. The ethylene response factor SmERF6 co-regulates the transcription of SmCPS1 and SmKSL1 and is involved in tanshinone biosynthesis in *Salvia miltiorrhiza* hairy roots. *Planta.*, **(248)**: 243–255.

The Association between Vitamin D Deficiency, Obesity, and Insulin Resistance among the Jordanian Population

Raed A. Halalsheh^{1,*}, Linda A. Soufan¹, and Hosam J. Al-Tamimi²

¹Department of Medical Laboratory Sciences, Faculty of Applied Medical Sciences, The Hashemite University, Zarqa, Jordan; ²Animal Production Department, Faculty of Agriculture, Jordan University of Science and Technology, Irbid, Jordan

Received: March 16, 2023; Revised: May 10, 2023; Accepted: May 16, 2023

Abstract

Vitamin D deficiency is a worldwide health concern that is linked to a wide range of chronic diseases such as cardiovascular diseases, hypertension, autoimmune diseases, and type 1 and 2 diabetes mellitus. Low levels of vitamin D may result in an increase in body fat (obesity), which has been widely identified as a risk factor for developing type 2 diabetes. The purpose of this study was to investigate the relationship between vitamin D deficiency, body mass index, and insulin resistance among the Jordanian population. A cross-sectional study design was conducted with a sample size of 205 participants (63 males and 142 females) from the Hashemite University, Jordan. Blood serum was obtained and the 25-hydroxy vitamin D, fasting glucose, and insulin levels were measured for all participants. Height, weight, waist, and hip measurements were also taken. Results showed that vitamin D deficiency is significantly ($P < 0.05$) associated with an increase in BMI. 115 individuals (57%) had a BMI below 25 kg/m², and 85 individuals (43%) had a BMI above 25 kg/m². While 134 individuals (65.4%) had normal vitamin D levels, vitamin D deficiency was found to be present in 71 individuals (34.6%). Furthermore, Vitamin D deficiency was significantly ($P < 0.05$) associated with an increase in HOMA-IR. HOMA-IR index results were elevated in 107 individuals (52.2%), and normal in 98 individuals (47.8%) in which 23 individuals (11%) were vitamin D deficient with normal HOMA-IR, while 48 individuals (23%) with vitamin D deficiency had elevated HOMA-IR. Moreover, in the studied population, vitamin D deficiency prevalence (25-hydroxy vitamin D < 25 nmol/l) was 34.6%, with the prevalence being higher in females (48.6%) than males (1.6%). In conclusion, these results showed that vitamin D deficiency is associated with an increase in body mass index and insulin resistance.

Keywords: Vitamin D, Obesity, Insulin resistance.

1. Introduction

Vitamin D is a fat soluble vitamin (Vanlint, 2013). It can be obtained from diet, but its major source of synthesis is the skin from the precursor 7-dehydrocholesterol after exposure to ultraviolet light (Melmed, 2016). Vitamin D deficiency is now considered a worldwide public health issue (Wacker and Holick, 2013). Currently, around 1 billion people worldwide are considered to have vitamin D deficiency and insufficiency (Pfothner and Shubrook, 2017). The Jordanian population is no exception, as shown by a study conducted on women and their children in northern Jordan, the results of which showed that 97.8% of the women and 39% of the children had 25(OH)D levels less than 50 nmol/L (Gharaibeh and Stoecker, 2009). Another study on women of child-bearing age resulted in a prevalence of 95.7% (Nichols *et al.*, 2012), a finding that is compatible with the previous study. A study of preschool children found that the prevalence of vitamin D deficiency among this age group is 56.5% (Nichols *et al.*, 2015). Batiha *et al.* (2011) reported in his study that the prevalence of vitamin D deficiency among adults is 37.3% in females, compared to 5.1% in males.

Many factors might cause low levels of vitamin D, including limited sun exposure, concealing clothing, sunscreen use, degree of skin pigmentation, aging, certain medications, and chronic illnesses. Added to that is the limited dietary sources of the vitamin (Tsiaras and Weinstock, 2011). Many studies suggest that vitamin D might have a protective role in preventing several chronic diseases, such as cardiovascular diseases, hypertension, certain types of cancer, autoimmune diseases, type 1 and type 2 diabetes, and obesity (Earthman *et al.*, 2012; Pfothner and Shubrook, 2017). Vitamin D deficiency is associated with increased risk of developing these diseases (DeLuca, 2004).

It is well-known that obesity is considered a risk factor for type 2 diabetes (Shoelson *et al.*, 2007). Additionally, insulin resistance is a major condition that leads to type 2 diabetes mellitus (Teegarden and Donkin, 2009). Since vitamin D deficiency seems to be associated with obesity and insulin resistance, it is likely that vitamin D deficiency indirectly contributes to an increased risk of type 2 diabetes (Holick, 2012).

Many studies have discussed an inverse relationship between body fat content and vitamin D concentrations. This negative correlation is found in all age groups and ethnicities (Drincic *et al.*, 2012; Hyppönen and Boucher,

* Corresponding author. e-mail: halalsheh@hu.edu.jo.

2018). Several mechanisms have been proposed to explain this relationship, such as limited sun exposure of the skin in overweight and obese people due to social stigma, elevated levels of 1.25(OH)₂D and parathyroid hormone leading to reduced synthesis of 25(OH)D in the liver through negative feedback, and reduced skin ability to synthesize vitamin D from 7-dehydrocholesterol (Drincic *et al.*, 2012; Looker, 2005). Another proposed explanation for the reduced levels of 25(OH) D is the sequestration of vitamin D in the adipose tissue which reduces its availability for the body (Earthman *et al.*, 2012; Lagunova *et al.*, 2009). A study by Tzotzas *et al.* (2010) supports this mechanism, showing that 10% weight loss in obese women raised their 25-hydroxyvitamin D levels by 34%. Another study on obese children also reported an increase in 25-hydroxyvitamin D levels after weight loss (Reineh *et al.*, 2007).

However, low levels of vitamin D might be causing an increase in body fat. This is supported by the studies that have shown that 1.25-dihydroxyvitamin D inhibits adipocyte differentiation and adipogenesis in vitro (Bouillon *et al.*, 2008; Kong and Li, 2006).

Given the roles that vitamin D plays in the secretion of insulin and the function of pancreatic β cells, several studies tried to investigate the effect of low vitamin D on insulin sensitivity and the development of type 2 diabetes mellitus. Chiu *et al.* (2004) carried out a study on healthy adults and concluded that vitamin D deficiency is associated with increased risk of insulin resistance and type 2 diabetes. The same study also evaluated the function of β cells in the pancreas, and results showed that the function of β cells was affected in the case of low vitamin D levels. There is growing evidence suggesting that low levels of 25-hydroxyvitamin D are a risk factor for type 2 diabetes (Mathieu *et al.*, 2005; Wimalawansa, 2018). Several cross-sectional studies reported that diabetes mellitus patients have lower concentrations of 25-hydroxyvitamin D (Liu *et al.*, 2008). The interactive relationship between vitamin D and diabetes might rise from different possible contributors. It might be that obesity, usually associated with vitamin D deficiency, is the cause of diabetes, because it is well-known that obesity is a strong contributor to type 2 diabetes (Shoelson *et al.*, 2007), or diabetes might develop as a result of insulin resistance caused by vitamin D deficiency, as it is known that insulin resistance is a major factor in the pathogenesis of type 2 diabetes (Knekt *et al.*, 2008).

Thus, due to a dearth of studies conducted in Jordan, our objective in this research was to study the association between vitamin D deficiency, body mass index and insulin resistance among the Jordanian population with a hypothesis that vitamin D deficiency would contribute to obesity and insulin resistance.

2. Materials and methods

This is a cross-sectional study that was designed to determine the relationship between vitamin D deficiency, body mass index (BMI), and insulin resistance among the Jordanian population. The protocol for this study was approved by the Institutional Review Board committee (IRB) at the Hashemite University, Zarqa, Jordan.

205 apparently healthy participants were recruited in the study from the Hashemite University, Zarqa, Jordan,

during the period of mid-March till mid-April 2019. Participants who agreed to be part of the study signed a consent form and their data were collected using a questionnaire. Selection of participants was based on the inclusion and exclusion criteria listed in Table 1 below.

Table 1. Participant inclusion and exclusion criteria

Exclusion Criteria	Inclusion Criteria
Aged less than 18 years	Aged 18 and above
Vitamin D supplements intake	Adults with no health issues (apparently healthy)
Calcium supplements intake	No history of previous vitamin D supplements intake
Multivitamin supplements intake	
Diabetes Mellitus type 1 and 2	
Thyroid disease	
Gallbladder disease	
Kidney disease	
Liver disease	

Participants were requested to fast 10-12 hours prior to blood collection. Five to seven milliliters of venous blood samples were obtained from each participant in a plain tube with gel (Greiner bio-one, Austria). Samples were allowed to coagulate at room temperature, after which they were centrifuged at 3500 rpm for 5 minutes using a laboratory clinical centrifuge (HettichZentrifugen, Germany). Serum samples were separated into 1.5 ml microcentrifuge tubes using disposable plastic Pasteur pipettes (two tubes for each sample) that were properly labeled and kept at -20 °C until being analyzed. Height, weight, hip circumference, and waist circumference were measured for each participant in duplicate and the mean for each reading was calculated. Body mass index (BMI) was calculated according to the following formula:

BMI= Weight in kilograms / Height in meters² (Ness-Abramof and Apovian, 2008). BMI values are classified according to the World Health Organization (WHO) as follows:

Normal: BMI < 25 kg/m²

Overweight: BMI 25 - 29.9 kg/m²

Obese: BMI ≥ 30 kg/m²

Waist to hip ratio (WHR) was calculated according to the following formula:

W/H= Waist circumference / Hip circumference.

Serum level of vitamin D was measured using enzyme-linked immunosorbent assay technique (ELISA), using 25-OH Vitamin D Total ELISA kit (Diasource, Belgium). 25-OH vitamin D levels ≥ 50 nmol/L are considered sufficient, 25- 49 nmol/L are insufficient, and levels < 25 nmol/L are deficient (Wolpowitz and Gilcrest, 2006). Serum samples were analyzed for glucose using glucose oxidase method on automated biochemistry analyzer (Mindray, China). Normal glucose levels are less than 110 mg/dl. The insulin test was done using TOSOH analyzer (Japan). The ST AIA-PACK IRI is a two-site immunoenzymometric assay which is performed entirely in the ST AIA-PACK IRI test cups. Normal level for

fasting insulin is 2.6 - 10.0 $\mu\text{U/mL}$. Homeostasis model assessment of insulin resistance (HOMA-IR) index is considered a simple and reproducible method for determining insulin resistance (Singh and Saxena, 2010). Fasting blood glucose and insulin levels were used to calculate HOMA-IR according to the following formula:

$$\text{HOMA-IR} = \frac{\text{serum insulin level } (\mu\text{U/mL}) * \text{blood glucose (mmol/L)}}{22.5} \text{ (Singh et al., 2013).}$$

Cut-off point of HOMA-IR ≥ 1.9 indicates insulin resistance (Ghasemi et al., 2015).

2.1. Statistical analysis

Collected data were summarized using Excel sheets and statistical analysis was performed using Statistical Package for Social Sciences software (SPSS). Data was analyzed using a two-independent t- test. Vitamin D was considered deficient if it was below 25 nmol/L, while a BMI of over 25 was considered obese, and a reading of over 1.9 indicated HOMA insulin resistance.

3. Results and discussion

3.1. 3.1. Vitamin D and BMI

205 students were enrolled in this study. BMI data were obtained for 200 students (5 were absent). 115 (57.5 %) had a BMI below 25 kg/m^2 , and 85 (42.5 %) had a BMI above 25 kg/m^2 . 33 students (16.5%) were vitamin D deficient with normal body weight, while 36 students (18%) with vitamin D deficiency were overweight or obese.

Vitamin D deficiency was present in 71 of the students (34.6%), and 134 (65.4%) had normal vitamin D levels, from the total of 205 students.

The data described in Tables 2 and 3 provide sufficient evidence (P value= 0.044) to conclude that body mass index for vitamin D deficient students is significantly greater than normal students. With 95% confidence, vitamin D deficiency increases mean BMI by a value between 0.03 and 2.6 kg/m^2 .

According to our results, vitamin D deficiency significantly increased (P = 0.044) with body mass index (Tables 2 and 3). This finding is consistent with the results of Arunabh et al. (2003), who reported that 25(OH)D levels are inversely related to body mass index and body fat content in healthy women, and Gannagé-Yared et al. (2009) who showed that 25(OH)D concentrations are inversely associated with BMI in a group of healthy non-obese young adults. The results of Chiu et al. (2004) also showed an inverse relationship between BMI and 25(OH)D concentrations in healthy young adults, but no relation between 25(OH)D and waist to hip ratio (WHR). Muscogiuri et al. (2010) also concluded that there is a significant correlation between 25(OH)D and BMI, as did Liu et al. (2008).

Lower 25-hydroxyvitamin D levels are associated with higher BMI, as reported by Vilarrasa et al. (2007), who showed that 25(OH)D concentrations decreased with the increase of body mass index. Lagunova et al. (2009) reported a similar pattern of a significant decrease in 25(OH)D levels with the increase in BMI. A study by Garanty-Bogacka et al. (2011) showed that vitamin D deficiency is associated with higher body mass and increased fat content in adolescents, while Poomthavorn et

al. (2012) reported no association between 25(OH)D and BMI in obese Thai adolescents and children.

In a population-based study, Jorde et al. (2010) also confirmed the strong negative association between serum levels of 25(OH)D and BMI. They also investigated the relationship between BMI and the improvement of 25(OH)D serum levels after vitamin D supplementation and concluded that the increase in 25(OH)D levels are also inversely correlated with BMI. In clinical application, this finding means people with higher BMI would need higher doses of vitamin D supplementation to correct its deficiency (Lee et al., 2009).

It is thought that the increase in body mass index that is accompanied with an increase in fat tissue causes sequestration of vitamin D in the adipose tissue and limits its bioavailability (Earthman et al., 2012). This possibility was investigated in a study by Wortsman et al. (2000). They exposed obese and non-obese subjects to UV light to induce vitamin D synthesis and found that the increase in vitamin D levels were 57% less in obese subjects compared to non-obese, although the percentage of producing vitamin D from previtamin D was similar in both groups. This indicates that obesity did not affect the production of vitamin D from the skin, but subcutaneous fat tissue in obese subjects might have sequestered the synthesized vitamin D. Furthermore, oral doses of vitamin D given to both groups resulted in less bioavailability with the increase in BMI, further supporting the sequestering of vitamin D in the body fat. This explanation could be supported by the results of some studies that reported an increase in 25-hydroxyvitamin D concentrations following weight loss (Tzotzas et al., 2010; Reinehr et al., 2007).

Another proposed explanation of the relationship between vitamin D deficiency, body mass index, and obesity, is the limited sun exposure or time spent outdoors. The only way to activate the chemical reaction that results in vitamin D production is for sunlight to reach your skin directly.

Additional proposed causes of low 25-hydroxyvitamin D levels seen in obesity is the increased catabolism of vitamin D, that is mediated by the enzyme 24-hydroxylase, which is expressed by adipose tissue. Another possible cause is reduced synthesis of 25-hydroxyvitamin D from liver in obese individuals as a result of non-alcoholic fatty liver disease that is associated with obesity (Earthman et al., 2012).

Although vitamin D deficiency is more prevalent in obesity, the causal direction of the relationship is still undetermined (Rosen et al., 2012). However, the results of a major analysis of multiple cohorts that tried to find the direction of causality suggested that higher body mass index leads to lower 25-hydroxyvitamin D concentrations (Vimalleswaran et al., 2013).

The current study found no significant association between vitamin D deficiency and increased waist to hip ratio (WHR). This might be due to the lack of high WHR in the studied group, since none of the students fell into the WHR range that is considered high.

Table 2. Distribution of Vitamin D Normal and Vitamin D Deficient Students according to BMI

Vitamin D	BMI		Total
	Normal ¹	Obese ²	
Normal ³	82 (41%)	49 (24.5%)	131
Deficient ⁴	33 (16.5%)	36 (18%)	69
Total	115 (57.5%)	85 (42.5%)	200

¹BMI < 25Kg/m²²BMI > 25Kg/m²³Vitamin D > 25 nmol/L⁴Vitamin D < 25 nmol/L**Table 3.** Results of BMI according to Vitamin D Status

Vitamin D	Insulin		Total
	Normal ¹	Resistant	
Normal ²	75 (37%)	59 (29%)	134
Deficient ³	23 (11%)	48 (23%)	71
Total	98(48 %)	107(52 %)	205

¹Vitamin D > 25 nmol/L²Vitamin D < 25 nmol/L

3.2. Vitamin D and Insulin Resistance

205 students were enrolled in this study. HOMA-IR index results were elevated in 107 students (52%), and normal in 98(48%).

Vitamin D deficiency was present in 71 of the students (34.6%), and 134 (65.4%) had normal vitamin D levels. 23 students (11%) were vitamin D deficient with normal HOMA-IR, while 48 students (23%) were vitamin D deficient with elevated HOMA-IR.

The data described in Tables 4 and 5 provides sufficient evidence (P value= 0.046) to conclude that insulin resistance for vitamin D deficient patients is significantly greater than for normal patients. With 95% confidence, vitamin D deficiency increases mean insulin resistance (HOMA-IR) by a value between 0.01 and 0.8.

Our results showed that there was a significant association between 25-hydroxyvitamin D levels and HOMA-IR (P = 0.046) (as shown in Tables 4 and 5), where vitamin D deficiency caused an increase in insulin resistance. These findings are consistent with those of Chiu *et al.* (2004) who reported an increase in insulin resistance risk in subjects with low 25-hydroxyvitamin D levels. Subjects who participated in this study were healthy with normal glucose tolerance. Also, a study by Liu *et al.* (2008) of non-diabetic adults revealed that 25(OH)D concentrations were inversely associated with fasting glucose, fasting insulin, and HOMA-IR, which means that low 25(OH)D levels is associated with increased insulin resistance. Abdelkarem, El-Sherif, and Gomaa (2016) also reported similar results in their research on female university students from Saudi Arabia. Gannagé-Yared *et al.* (2009) explored the association on a group of healthy non-obese university students in Lebanon and found that 25(OH)D concentrations were inversely correlated with HOMA-IR values.

Alemzadeha, Kichlerb, Babara, and Calhoun's (2008) research on obese children and adolescents with mean age

13 years old, reported that vitamin D deficiency was associated with increased insulin resistance independent of body obesity. However, their results are not consistent with those of Poomthavorn *et al.* (2012) who found no relationship between 25(OH)D levels and insulin sensitivity, or even between 25(OH)D and body mass index in obese children and adolescents.

Muscogiuri *et al.* (2010) reported a significant correlation between 25(OH)D with body mass index and insulin sensitivity. They found that low 25(OH)D levels are associated with decreased insulin sensitivity, and the lowest concentrations of 25(OH)D were associated with higher degrees of insulin resistance. Also, higher BMI was associated with lower concentrations of 25(OH)D. In this study, they attributed the increase in insulin resistance seen in lower levels of 25(OH)D to be the result of increased BMI, rather than being caused by low 25(OH)D.

Several mechanisms were proposed to explain the relationship between vitamin D and insulin resistance, and how vitamin D deficiency affects it. It is known that vitamin D is essential for normal secretion of insulin from β pancreatic cells (Chiu *et al.*, 2004; Rosen *et al.*, 2012), and its deficiency inhibits insulin secretion and induces glucose intolerance (Bouillon *et al.*, 2008). Vitamin D enhances the synthesis of various proteins within the cells and accelerates the transformation of proinsulin into insulin (Chiu *et al.*, 2004). It also stimulates the expression of insulin receptors in target tissues leading to enhanced glucose uptake by peripheral tissues and increased insulin responsiveness (Pittas *et al.*, 2007).

Insulin secretion is a calcium-dependent process. Vitamin D facilitates insulin secretion indirectly by regulating extracellular calcium and calcium influx to β cells. Any disturbance in the intracellular calcium levels or its influx toward the cell will impair β cells' function (Muscogiuri *et al.*, 2014; Pittas *et al.*, 2007). Calcium is equally important in cells and tissue that responds to insulin to regulate their glucose uptake and intracellular processes. Any alteration in intracellular levels of ionized calcium in insulin target tissues may lead to insulin resistance in these tissues, due to impaired insulin signal transduction, which in turn affects glucose transporter-4 function (Pittas *et al.*, 2007).

Low levels of vitamin D cause an increase in parathyroid hormone (PTH) levels. High PTH will affect intracellular free calcium concentrations in cells, including pancreatic cells, which in turn will decrease insulin sensitivity and impair glucose tolerance (Mezza *et al.*, 2012).

Another proposed mechanism involves the immunomodulatory effect of vitamin D. Vitamin D regulates the production and function of cytokines. Inadequate vitamin D status may result in inflammatory response, which may lead to insulin resistance, but this hypothesis is still debatable (Liu *et al.*, 2008; Muscogiuri *et al.*, 2014; Pittas *et al.*, 2007).

Increasing 25(OH) levels by supplementation to satisfactory level would lead to good outcomes. Some studies have reported an increase in insulin secretion by 60% after correcting 25(OH) levels (Holick, 2008). Von Hurst *et al.* (2010) reported that the treatment of vitamin D deficiency would improve insulin sensitivity and reduce its resistance, but other studies showed no improvement in

insulin resistance or any of the obesity parameters (Tai *et al.*, 2008; Wamberg *et al.*, 2013).

Whether vitamin D supplementation results in improved insulin sensitivity or not, vitamin D deficiency should be treated, and improving vitamin D levels to satisfactory levels will not lead to negative outcomes.

Table 4. Distribution of Vitamin D Normal and Vitamin D Deficient Students according to Insulin Resistance

BMI (kg/m ²)	Vitamin D	
	Deficient ¹	Normal ²
Minimum	20.22	17.46
Maximum	40.22	46.43
Mean	25.85	24.51
Standard Deviation	4.17	4.94
Missing data	2	3

¹2.6 - 10.0 µU/mL

²Vitamin D > 25 nmol/L

³Vitamin D < 25nmol/L

Table 5: Results of HOMA-IR Index according to Vitamin D Status

HOMA-IR Index	Vitamin D	
	Deficient ¹	Normal ²
Minimum	1.08	0.39
Maximum	10.47	12.52
Mean	2.51	2.10
Standard Deviation	1.33	1.53

¹Vitamin D < 25 nmol/L

²Vitamin D > 25 nmol/L

4. Conclusion

Our study showed that vitamin D deficiency caused an increase in BMI and an increase in insulin resistance measured by homeostatic model assessment of insulin resistance (HOMA-IR). However, this study showed no association between vitamin D deficiency and waist to hip ratio.

The obtained results uncovered that the Jordanian population has a high rate of vitamin D deficiency which might highly correlate with increasing rates of insulin resistance among them. As a preventative procedure for insulin resistance and increased BMI, we recommend that individuals take a regular vitamin D test and take the needed vitamin D supplement as soon as deficiency or insufficiency is detected with consultation with physicians.

References

Abdelkarem HM, El-Sherif MA and Gomaa SB. 2016. Vitamin D status and insulin resistance among young obese Saudi females. *Saudi Med J*, **37**(5): 561-566.

Alemzadeh R, Kichler J, Babar G and Calhoun M. 2008. Hypovitaminosis D in obese children and adolescents: relationship with adiposity, insulin sensitivity, ethnicity, and season. *Metabolism*, **57**(2): 183-191.

Arunabh S, Pollack S, Yeh J, and Aloia JF. 2003. Body fat content and 25-hydroxyvitamin D levels in healthy women. *J. Clin. Endocrinol. Metab.*, **88**(1): 157-161.

Batieha A, Khader Y, Jaddou H, Hyassat D, Batieha Z, Khateeb M, and Ajlouni K. 2011. Vitamin D status in Jordan: dress style and gender discrepancies. *Ann. Nutr. Metab.*, **58**(1): 10-18.

Bouillon R, Carmeliet G, Verlinden L, van Etten E, Verstuyf A, Luderer H F and Demay M. 2008. Vitamin D and human health: lessons from vitamin D receptor null mice. *Endocr. Rev.*, **29**(6): 726-776.

Chiu KC, Chu A, Go VLW and Saad MF. 2004. Hypovitaminosis D is associated with insulin resistance and β cell dysfunction. *Am. J. Clin. Nutr.*, **79**(5): 820-825.

DeLuca HF. 2004. Overview of general physiologic features and functions of vitamin D. *Am. J. Clin. Nutr.*, **80**(6): 1689S-1696S.

Drincic AT, ArmasLA, VanDiest EE and Heaney RP. 2012. Volumetric dilution, rather than sequestration best explains the low vitamin D status of obesity. *Obesity*, **20**(7):1444-1448.

Earthman CP, Beckman LM, Masodkar K and Sibley SD. 2012. The link between obesity and low circulating 25-hydroxyvitamin D concentrations: considerations and implications. *Int. J. Obes.*, **36**(3): 387-396.

Gannagé-Yared MH, Chedid R, Khalife S, Azzi E, Zoghbi F and Halaby G. 2009. Vitamin D in relation to metabolic risk factors, insulin sensitivity and adiponectin in a young Middle-Eastern population. *Eur. J. Endocrinol.*, **160**(6): 965-971.

Garanty-Bogacka B, Syrenicz M, Goral J, Krupa B, Syrenicz J, Walczak M and Syrenicz A. 2011. Serum 25-hydroxyvitamin D (25-OH-D) in obese adolescents. *Endokrynol Pol*, **62**(6): 506-511.

Ghasemi A, Tohidi M, Derakhshan A, Hashemina M, Azizi F and Hadaegh F. 2015. Cut-off points of homeostasis model assessment of insulin resistance, beta-cell function, and fasting serum insulin to identify future type 2 diabetes: Tehran Lipid and Glucose Study. *Acta Diabetol.*, **52**(5): 905-915.

Gharaibeh MA and Stoecker BJ. 2009. Assessment of serum 25 (OH) D concentration in women of childbearing age and their preschool children in Northern Jordan during summer. *Eur. J. Clin. Nutr.*, **63**(11): 1320-1326.

Holick, M. F. (2008). Diabetes and the vitamin D connection. *Curr. Diab. Rep.*, **8**(5): 393-398.

Holick MF. 2012. Nutrition: D-iabetes and D-eath D-efying vitamin D. *Nat. Rev. Endocrinol.*, **8**(7): 388-390.

Hyppönen E and Boucher BJ. 2018. Adiposity, vitamin D requirements, and clinical implications for obesity-related metabolic abnormalities. *Nutr. Rev.*, **176**(9): 687-692.

Jorde R, Sneve M, Emaus N, Figenschau Y, and Grimnes G. 2010. Cross-sectional and longitudinal relation between serum 25-hydroxyvitamin D and body mass index: the Tromsø study. *Eur. J. Nutr.*, **49**(7): 401-407.

Knekt P, Laaksonen M, Mattila C, Härkänen T, Marniemi J, Heliövaara M and Reunanen A. 2008. Serum vitamin D and subsequent occurrence of type 2 diabetes. *Epidemiology*, **19**(5): 666-671.

Kong J and Li YC. 2006. Molecular mechanism of 1, 25-dihydroxyvitamin D3 inhibition of adipogenesis in 3T3-L1 cells. *Am. J. Physiol. Endocrinol. Metab.*, **290**(5): E916-E924.

Lagunova Z, Porojnicu AC, Lindberg F, Hexeberg S and Moan J. 2009. The dependency of vitamin D status on body mass index, gender, age and season. *Anticancer Res.*, **29**(9): 3713-3720.

Lee P, Greenfield JR, Seibel MJ, Eisman JA, and Center JR. 2009. Adequacy of vitamin D replacement in severe deficiency is dependent on body mass index. *Am. J. Med.*, **122**(11): 1056-1060.

- Liu E, Meigs JB, Pittas AG, McKeown NM, Economos CD, Booth SL and Jacques PF. 2008. Plasma 25-hydroxyvitamin D is associated with markers of the insulin resistant phenotype in nondiabetic adults. *J Nutr*, **139**(2): 329-334.
- Looker AC. 2005. Body fat and vitamin D status in black versus white women. *J. Clin. Endocrinol. Metab.*, **90**(2): 635-640.
- Mathieu C, Gysemans C, Giulietti A and Bouillon R. 2005. Vitamin D and diabetes. *Diabetologia*, **48**(7): 1247-1257.
- Melmed S, Polonsky KS, Larsen PR and Kronenberg H M. 2016. **Williams Textbook of Endocrinology**. 13th edition. Elsevier.
- Mezza T, Muscogiuri G, Sorice GP, Prioletta A, Salomone E, Pontecorvi A and Giaccari, Andrea. 2012. Vitamin D deficiency: a new risk factor for type 2 diabetes. *Ann. Nutr. Metab.*, **61**(4): 337-348.
- Muscogiuri G, Mitri J, Mathieu C, Badenhoop K, Tamer G, Orio F and Pittas A. 2014. Mechanisms in endocrinology: vitamin D as a potential contributor in endocrine health and disease. *Eur. J. Endocrinol.*, **171**(3): R101-R110.
- Muscogiuri G, Sorice GP, Prioletta A, Policola C, Della Casa S, Pontecorvi A and Giaccari A. 2010. 25-Hydroxyvitamin D concentration correlates with insulin-sensitivity and BMI in obesity. *Obesity*, **18**(10): 1906-1910.
- Nichols EK, Khatib IMD, Aburto NJ, Serdula MK, Scanlon KS, Wirth JP and Sullivan KM. 2015. Vitamin D status and associated factors of deficiency among Jordanian children of preschool age. *Eur. J. Clin. Nutr.*, **69**(1): 90-95.
- Nichols EK, Khatib IMD, Aburto NJ, Sullivan KM, Scanlon KS, Wirth JP and Serdula, MK. 2012. Vitamin D status and determinants of deficiency among non-pregnant Jordanian women of reproductive age. *Eur. J. Clin. Nutr.*, **66**(6): 751-756.
- Pfotenhauer KM and Shubrook JH. 2017. Vitamin D Deficiency, Its Role in Health and Disease, and Current Supplementation Recommendations. *J. Osteopath. Med.*, **117**(5): 301-305.
- Pittas AG, Lau J, Hu FB, and Dawson-Hughes B. 2007. The role of vitamin D and calcium in type 2 diabetes. A systematic review and meta-analysis. *J. Clin. Endocrinol. Metab.*, **92**(6): 2017-2029.
- Poomthavorn P, Saowan S, Mahachoklertwattana P, Chailurkit L and Khlairit P. 2012. Vitamin D status and glucose homeostasis in obese children and adolescents living in the tropics. *Int. J. Obes.*, **36**(4): 491-495.
- Reineh T, de Sousa G, Alexy U, Kersting M and Andler W. 2007. Vitamin D status and parathyroid hormone in obese children before and after weight loss. *Eur. J. Endocrinol.*, **157**(2): 225-232.
- Rosen CJ, Adams JS, Bikle DD, Black DM, Demay MB, Manson JE and Kovacs C S. 2012. The nonskeletal effects of vitamin D: an Endocrine Society scientific statement. *Endocr. Rev.*, **33**(3): 456-492.
- Tai K, Need AG, Horowitz M and Chapman IM. 2008. Glucose tolerance and vitamin D: Effects of treating vitamin D deficiency. *Nutrition*, **24**(10): 950-956.
- Shoelson SE, Herrero L and Naaz A. 2007. Obesity, inflammation, and insulin resistance. *Gastroenterology*, **132**(6): 2169-2180.
- Singh Y, Garg MK, Tandon N and Marwaha RK. 2013. A study of insulin resistance by HOMA-IR and its cut-off value to identify metabolic syndrome in urban Indian adolescents. *J. Clin. Res. Pediatr. Endocrinol.*, **5**(4): 245-251.
- Teegarden D. and Donkin SS. 2009. Vitamin D: emerging new roles in insulin sensitivity. *Nutr. Res. Rev.*, **22**(1): 82-92.
- Tsiaras WG and Weinstock MA. 2011. Factors influencing vitamin D status. *Acta Derm. Venereol.*, **91**(2): 115-124.
- Tzotzas T, Papadopoulou FG, Tziomalos K, Karras S, Gastaris K, Perros P and Krassas GE. 2010. Rising serum 25-hydroxy-vitamin D levels after weight loss in obese women correlate with improvement in insulin resistance. *J. Clin. Endocrinol. Metab.*, **95**(9): 4251-4257.
- Vanlint S. 2013. Vitamin D and obesity. *Nutrients*, **5**(3): 949-956.
- Vilarrasa N, Maravall J, Estepa A, Sanchez R, Masdevall C, Navarro MA and Gómez JM. 2007. Low 25-hydroxyvitamin D concentrations in obese women: their clinical significance and relationship with anthropometric and body composition variables. *J. Endocrinol. Invest.*, **30**(8): 653-658.
- Vimaleswaran KS, Berry DJ, Lu C, Tikkanen E, Pilz S, Hiraki LT and Wood AR. 2013. Causal relationship between obesity and vitamin D status: bi-directional Mendelian randomization analysis of multiple cohorts. *PLoS Med.*, **10**(2): e1001383.
- Von Hurst PR, Stonehouse W. and Coad J. 2010. Vitamin D supplementation reduces insulin resistance in South Asian women living in New Zealand who are insulin resistant and vitamin D deficient - a randomised, placebo-controlled trial. *Br. J. Nutr.*, **103**(4): 549-555.
- Wacker M and Holick M. 2013. Vitamin D - effects on skeletal and extraskelatal health and the need for supplementation. *Nutrients*, **5**(1): 111-148.
- Wamberg L, Kampmann U, Stødkilde-Jørgensen H, Rejnmark L, Pedersen SB and Richelsen B. 2013. Effects of vitamin D supplementation on body fat accumulation, inflammation, and metabolic risk factors in obese adults with low vitamin D levels—results from a randomized trial. *Eur. J. Intern. Med.*, **24**(7): 644-649.
- Wimalawansa SJ. 2018. Associations of vitamin D with insulin resistance, obesity, type 2 diabetes, and metabolic syndrome. *J. Steroid Biochem. Mol. Biol.*, **175**: 177-189.
- Wortsman J, Matsuoka LY, Chen TC, Lu Z and Holick M F. 2000. Decreased bioavailability of vitamin D in obesity. *Am. J. Clin. Nutr.*, **72**(3): 690-693.

The Growth Response and Digestive Enzyme Activity of Juvenile African Catfish (*Clarias gariepinus*) Exposed to Artificial Light at Night (ALAN) Spectral

Gabriel A. Dedeke¹, Festus O. Kehinde^{2,*} and Ife A. George¹

¹Department of Pure and Applied Zoology, College of Biosciences, Federal University of Agriculture Abeokuta, Nigeria; ²Department of Animal and Environmental Biology, Faculty of Natural Science, Prince Abubakar Audu University Anyigba, Nigeria

Received: February 10, 2023; Revised: May 30, 2023; Accepted: June 8, 2023

Abstract

Artificial light in various spectral is a relatively new development for modifying the environment of fish. According to research, light has a spectral and species-specific effect on fish. As a result, the goal of this study was to see how different visible light colors affected *Clarias gariepinus* growth and digestive enzymes. 105 Juvenile fish (body length 10.00 ± 0.55 cm, initial weight 8.67 ± 0.62 g) were randomly exposed in triplicate to the following LEDs: Red (RL), Blue (BL), Green (GL), and Yellow (Y). Total Darkness (TD) and Ambient Light (AL) were used as controls. The fish were exposed for 12 hours overnight for 50 days. At five-day intervals, the fish's body weights were measured with an electric weighing scale (0.01g sensitivity); head length (cm), tail length (cm), and total body length (cm) were measured with a graduated measuring plastic box. The variables listed below were computed: Weight Gain (WG), Daily Weight Gain (DWG), Daily Growth Rate (DGR), Specific Growth Rate (SGR), Percentage Weight Gain (PWG), Food Conversion Ratio (FCR), Length Gain (LG), Daily Length Gain (DLG), Survival Rate (SR) and Condition Factor are some of the metrics used to calculate weight gain. Standard methods were used to measure the activities of digestive enzymes (proteinase and amylase). ANOVA was used to compare the acquired means, and Duncan's multiple range tests were used to further separate the means. Fish reared in YL had significantly higher WG, DWG, DGR, PWG, DLG, LG, and CF levels. SR of fish reared under TD conditions was the lowest, but it was significantly ($P < 0.05$) higher in fish reared under YL and RL conditions. Fish exposed to YL had significantly higher FCR and CF than those exposed to the other light treatments and the Control. The digestive enzyme activities were significantly ($P < 0.05$) reduced during the light treatment. Finally, nighttime artificial light exposure had a significant impact on juvenile catfish growth performance and digestive enzymes, with yellow light eliciting better growth performance.

Keywords: ALAN Spectral, catfish, Growth Performance, digestive enzymes, *Clarias gariepinus*.

1. Introduction

Fish provide some nutritional values for humans such as high levels of protein (Kakoolaki *et al.*, 2013), essential amino acids, and easy metabolism by humans of all ages (Ariño *et al.*, 2013). Fish is rich in long chain polyunsaturated fatty acids, Omega-3, which are protective against cardiovascular disorders in human (Duran and Talas, 2009). The environment where fish is raised is as vital as most of the body physiology is strongly affected by the environment. Rapid growth in human activity leads to continual expansions in industrialization (Caglar *et al.*, 2017) which has an effect on the amount of artificial light entering the aquatic environment and its possible effects on aquatic resources, the effects of which are still mostly unknown.

Light as *zeitgebers*, or time givers, has a large impact on the overall activities of living things. Photoperiod is a critical factor that influences many physiological responses in fish. The use of artificial light in various spectra to modify the environment of fish is a relatively new development. The modification of the fish environment by light has been found to be beneficial to some fishes and

detrimental to others. Some fish physiological responses have been reported to be influenced by artificial light. Light, for example, has been shown to influence fish feeding and swimming behavior (Rotllant *et al.*, 2003), hormone levels (Boeuf and Le Bail, 1998), basal body metabolism (Almaza'n *et al.*, 2004), and skin pigmentation. Photoperiod also influences growth, locomotor activity, metabolic rates, body pigmentation, sexual maturation, and reproduction in fish, according to Biswas *et al.* (2002ab; 2005). Light and background color have been found to impede the detection of feed and the success of feeding of cultured fish in natural settings (Henne and Watanabe, 2003), which in turn influences the overall fitness of the fish. Rainbow trout (*Oncorhynchus mykiss*) larvae grew the fastest when lighting and backdrop color were adjusted to create a contrast in the background for easy identification.

Furthermore, only a few studies looked at the effect of light spectrum on fish; the majority, however, focused on the effects of photoperiod and light intensity. Hybrid catfish and Africa catfish, for example, had the best growth performance in total darkness when raised under different photoperiods (Almazán *et al.*, 2004; Mustapha *et al.*, 2012; Orina *et al.*, 2016). As a result of these findings,

it has been suggested that Africa catfish be raised in complete darkness. However, the physiology of fish, like that of higher vertebrates, may be affected by the light spectrum (Karakatsouli *et al.*, 2008).

Furthermore, results from some of the studies revealed that raising fish under different light colors or wavelengths has an impact on both growth performance and the chemical composition of some fish. Elsbaay (2016), for example, reported that Nile tilapia, *Oreochromis niloticus*, exposed to blue light had the best growth performance and that blue light increased amino acid concentration more than other light colors. When exposed to red light, rainbow trout, *O. mykiss*, performed best. Blue light has also been shown to promote the growth and other physiological responses of juvenile Beluga whales, *Huso huso*. Because data on the effect of light spectral on African catfish, *Clarias gariepinus*, is still limited, and it is assumed that they perform better in total darkness (Britz and Pienaar, 2009; Ruchin, 2019), this study aims to add to the existing literature by investigating how LED light wavelengths in the visible spectrum may affect the growth and digestive enzymes of *C. gariepinus*. The Africa cat fish was chosen for this study because it is a popular species in Africa and other parts of the world (Handajani *et al.*, 2021).

2. Materials and Methods

2.1. Experimental Site and Housing

The study was carried out in the animal house of the Department of Pure and Applied Zoology, Federal University of Agriculture Abeokuta (FUNAAB), Ogun State.

2.2. Experimental Animal

FUNAAB fish farm provided fish stock (105 in number and 6 weeks old) for the study. The fish were brought to the animal house and acclimatized for seven days in natural conditions.

2.3. Construction of Water Circulation System

For this study, eighteen 30-liter transparent plastic containers were used. 15 of them were wrapped in aluminum foil to prevent external light from passing through and to increase total internal reflection, allowing the radiated light to concentrate within the container. To ensure effective drainage of used water, a water tap was attached to the base of each plastic container. The entire set of plastic containers was linked to a 2000-liter Storex® water tank to ensure a steady supply of clean water to replace the used ones.

2.4. Illumination System

Red, blue, green, and yellow Light Emitting Diode (LED) bulbs were used in three replicates each. The LED bulbs have a power rating of 3 watts and were connected in series via electric flexible cables to a 500-watt solar power system to ensure an uninterrupted power supply during the study period. Each container's inner cover was gummed up with bulbs. Aside from saving energy, these bulbs emit no heat, preventing heat discharge to the fish. Although the exact wavelength of the various light colors used could not be determined, the intensity of the light was measured using a light meter.

2.5. Experimental design

A completely random design was used for distributing fish into various containers. One hundred and five juvenile African catfish (*Clarias gariepinus*) were used; initial weight was 8.67 ± 0.62 g and initial length of $10.00 \pm .55$ cm. They were distributed randomly among the various light treatments and the control. There were fifteen fish per treatment in a replicate of three and five fish per replicate. The exposure took place at night (7 p.m.–7 a.m.) during the period that the Africa catfish are most active. All the fish experienced ambient light during the day except those in total darkness (Figure 1). The exposure is as indicated: ambient light (12L:12D), blue light (12L:12B), green light (12L:12G), yellow light (12L:12Y), red light (12L:12R), and total darkness (0L:24D). The exposure lasted for 50 days, after which the study was terminated. The ethical guidelines for animal experimentation (regulation CEE 86/609) were strictly followed during the experiment.

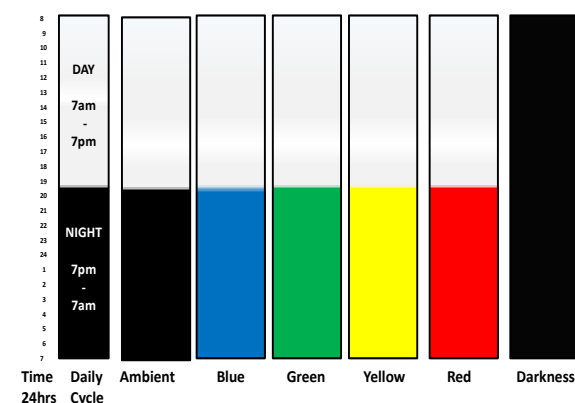


Figure 1. Showing the various light treatment indicating the period of exposure

2.6. Sanitation

Sanitation was done daily by removing remnants of food through the use of rubber hose. Complete changing of used water was usually done every 3 days in order to reduce the ammonia waste.

2.7. The measurement weight and length growth

The body weight and length were measured weekly using an electric weighing scale, and the values were recorded to two decimal places in terms of sensitivity (0.01 g) and one decimal place in terms of meter rule (0.1 cm), respectively. Three catfish were chosen at random from each replicate (for a total of nine fish per treatment), and their weight and length were recorded. The fish was placed in a calibrated transparent container, and its total length was measured.

2.8. Measurement of digestive enzyme

At the end of day 50, three fish from each treatment were randomly selected and sacrificed. The fish tissue was collected, homogenized, and the supernatant was collected for amylase and proteinase analysis.

2.8.1. Measurement of the total amylase (α and β) activity

Sodium acetate buffer of 1/10 M with a pH 5.0 was introduced to 1 ml of the supernatant. The solution obtained was then incubated at 27 °C for 1hr. The action of the enzyme was halted by adding 2 mL of DNSA reagent. The resultant-colored solution gotten was then heated for 5

minutes. The solution was thereafter diluted with distilled water to make up a volume of 10 ml, and this was chilled under running water. The optical density of the solution at 540 nm was compared with a blank. The blank contained 1 ml of identically tested boiling enzyme extract. The amount of reducing sugar produced was calculated. A standard curve for maltose was used to calculate the amount of reducing sugar that was produced (Swain and Dekker, 1966).

2.8.2. Analysis of proteinase activity

The procedure for producing enzyme extracts was the same as that used to produce total amylase extracts, with the exception that the extracting solution was 20 ml of 0.05 M sodium phosphate buffer with a pH 6.0. By adding two milliliters of soluble casein and 0.05 M soluble phosphate buffer with a pH 6.0 to the reaction mixture in order to precipitate unhydrolyzed casein, the Lowry Folin technique was used to measure the proteinase activity in the enzyme extracts (Osborne and Voogt, 1978). The ensuring suspension was centrifuged. A total of 5 ml of 2 % Na₂CO₃, 0.05 ml of 2.7% sodium potassium tartrate, 0.05 ml of 1 % CuSO₄, and 3 ml of 0.2 NaOH were poured into 1 ml of the supernatant. Folin-ciocalteu reagent of 0.5 ml was added to the solution formed after 10 minutes, and the mixture was thereafter left for 30 minutes at 30 °C and shook periodically. At 700 nm, the optical density of the mixture was evaluated in comparison to a blank that contained 1 ml of identically processed boiling enzyme extract. Using a standard curve of different tyrosine concentrations, proteinase activity was estimated (Somkuti and Babel, 1967).

2.9. Data Analysis

Descriptive analysis and linear regression of the gathered data were performed using Excel. ANOVA was used to compare the acquired means, and Duncan's multiple range tests were used to further separate the means. Utilizing SPSS version 22, the analysis was carried out.

3. Results

3.1. The trend of weight increases in African catfish exposed to different light spectral at night

Figure 2 depicts the gradual changes in body weight of African catfish exposed to various light conditions. The regression analysis revealed that the weight change increased significantly ($P < 0.05$) over time, but at a different rate. Fish exposed to YL had the highest R² value (0.97), followed by fish exposed to red light (0.96), and the lowest was recorded in fish exposed to ambient light, the control condition.

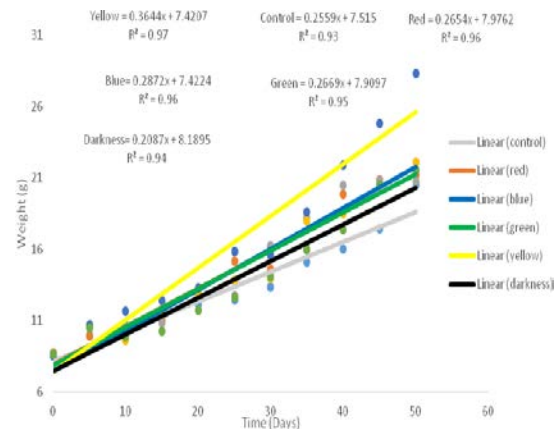


Figure 2. Trend in change in weight of juvenile African catfish exposed to different light spectral over the period of 50 days

3.2. Growth performance (weight basis) of African catfish exposed to different light spectra

Table 1 depicts the effect of various light spectral levels. Fish raised in total darkness gained weight at the same rate ($P > 0.05$) as those raised in ambient light, blue, green, and red light. Yellow light has a significant ($P < 0.05$) effect on final body weight, total body weight, weight gain, daily weight gain, daily growth rate, and percentage weight gain. Food conversion ratio was similar ($P > 0.05$) in catfish exposed to yellow, red, green, and blue lights, as well as darkness, but significantly higher ($P < 0.05$) than in ambient conditions. The fish exposed to yellow light had the highest condition factor (2.220 ± 0.35), but it was not significantly ($P > 0.05$) different from the control (1.490 ± 0.20).

Table 1. Weight Growth indices of African catfish exposed to various light spectral.

LT	Control	Blue	Green	Yellow	Red	Darkness
I W (g)	8.890 ± 0.300 ^a	8.880 ± 0.200 ^a	8.408 ± 0.278 ^a	8.880 ± 0.290 ^a	8.995 ± 0.225 ^a	8.990 ± 0.310 ^a
F W (g)	22.735 ± 2.185 ^a	23.715 ± 2.955 ^a	24.345 ± 2.225 ^a	33.490 ± 5.160 ^b	23.935 ± 2.735 ^a	24.380 ± 2.840 ^a
T B W (g)	152.670 ± 5.200 ^a	168.680 ± 8.050 ^a	168.490 ± 8.090 ^a	196.600 ± 14.760 ^b	166.320 ± 5.590 ^a	157.575 ± 4.535 ^a
F C R	0.047 ± 0.002 ^b	0.043 ± 0.002 ^{ab}	0.043 ± 0.002 ^{ab}	0.040 ± 0.003 ^a	0.042 ± 0.001 ^{ab}	0.043 ± 0.003 ^{ab}
W G (g)	14.255 ± 2.295 ^a	15.050 ± 2.970 ^a	15.605 ± 2.155 ^a	24.955 ± 5.215 ^b	15.150 ± 2.710 ^a	15.890 ± 3.030 ^a
D W G (g)	0.285 ± 0.045 ^a	0.300 ± 0.060 ^a	0.315 ± 0.045 ^a	0.495 ± 0.105 ^b	0.305 ± 0.055 ^a	0.320 ± 0.060 ^a
D G R (g)	3.395 ± 0.575 ^a	3.485 ± 0.695 ^a	3.600 ± 0.500 ^a	5.860 ± 1.230 ^b	3.470 ± 0.630 ^a	3.800 ± 0.770 ^a
S G R (g)	0.850 ± 0.110 ^a	0.850 ± 0.120 ^a	0.890 ± 0.090 ^a	1.155 ± 0.175 ^a	0.845 ± 0.105 ^a	0.900 ± 0.130 ^a
% W G	169.830 ± 28.730 ^a	174.405 ± 34.745 ^a	179.950 ± 25.030 ^a	293.325 ± 61.615 ^b	173.480 ± 1.510 ^a	189.885 ± 38.405 ^a
C F	1.490 ± 0.20 ^a	1.820 ± 0.23 ^a	1.805 ± 0.22 ^a	2.220 ± 0.35 ^a	1.580 ± 0.56 ^a	1.630 ± 0.61 ^a

Note, Means with the same superscript along the column are significantly different ($P < 0.05$)

LT = Light treatment; I W = Initial Weight; F W = Final Weight; T B W = Total Body Weight; F C R = Food Conversion Ratio; W G = Weight gain; D W G = Daily Weight Gain; D G R = Daily Growth Rate; S G R = Specific Growth Rate; C F = Condition Factor

3.3. Length growth indices of African catfish exposed to different light conditions

Table 2 displays the length growth indices of African catfish exposed to various light conditions. Exposure to different light conditions had no effect on the FL, LG,

Table 2: Length Growth Indices of *Clarias gariepinus* on Exposure to Different Light Conditions

LT	IL (cm)	FL (cm)	TL (cm)	LG (cm)	% LG (cm)	DLGR (cm)
Ambient	10.6±.7 ^{ab}	14.3±1.3 ^a	136.1±3.4 ^a	4.0±1.0 ^a	139.0±11.1 ^a	2.7±.4 ^a
Blue	10.7±.4 ^{ab}	14.3±1.3 ^a	138.2±5.6 ^{ab}	3.6±1.0 ^a	134.1±9.4 ^a	2.7±.4 ^a
Green	10.6±.7 ^{ab}	14.7±1.2 ^a	138.6±4.9 ^{ab}	4.1±1.4 ^a	138.2±14.9 ^a	2.8±.3 ^a
Yellow	10.2±.4 ^a	15.7±2.2 ^a	142.5±6.8 ^b	5.5±2.3 ^a	153.1±23.0 ^a	3.0±.5 ^a
Red	10.5±.5 ^{ab}	14.7±2.5 ^a	137.1±3.3 ^a	4.2±2.8 ^a	141.1±28.3 ^a	2.8±.6 ^a
Darkness	11.0±.5 ^b	14.8±1.3 ^a	137.6±3.0 ^{ab}	3.8±1.2 ^a	134.8±10.8 ^a	2.8±.3 ^a

Note, means with different superscript along the column are significantly different ($P < 0.05$)

LT = Light Treatment; IL = Initial length; FL = Final Length; TL = Total length; LG = Length Gain; DLGR = Daily Length Growth Rate

3.4. Percentage Digestive Enzyme of African Catfish Exposed to Different Light Spectra.

3.4.1. Amylase of African catfish exposed to different light spectra.

The percentage of digestive enzyme (amylase) in African catfish exposed to different light treatments was significantly ($P < 0.05$) different (Figure 3). The light treatment significantly reduced the activity of amylase as compared with the control (16.3 % ambient and 12.6 % total darkness). The least significant value was reported in the catfish exposed to yellow and green lights (4.3 % and 5.5 %, respectively).

3.4.2. Proteinase percentage of juvenile African catfish exposed to different light spectra.

There was marked ($P < 0.05$) difference in the percentage of proteinase in African catfish exposed to different light treatments. The *C. gariepinus* under yellow and green lights had the least significant ($P < 0.05$) values (1.8 % and 2.0 %, respectively) as compared to the control (ambient 10.5 % and total darkness 7.9 %).

Figure 3. Amylase and proteinase percentage of juvenile African catfish exposed to different light spectral.

3.5. Comparison of the final body weight and digestive enzymes functions of the cat fish exposed to different light wavelengths

Figure 4 depicts a comparison of final body weight and digestive enzyme activity. Except for red light, there is an inverse relationship between digestive enzymes and body weight that is proportional to the wavelength of the light.

LG%, or DLGR ($P > 0.05$). Meanwhile, catfish exposed to yellow light had significantly ($P < 0.05$) longer tail length than those exposed to ambient and red light but were similar ($P > 0.05$) to those exposed to blue, green, and darkness.

The enzymes' activities decreased as the wavelength increased. The growth indicator, on the other hand, was found to increase as the wavelength of the light increased.

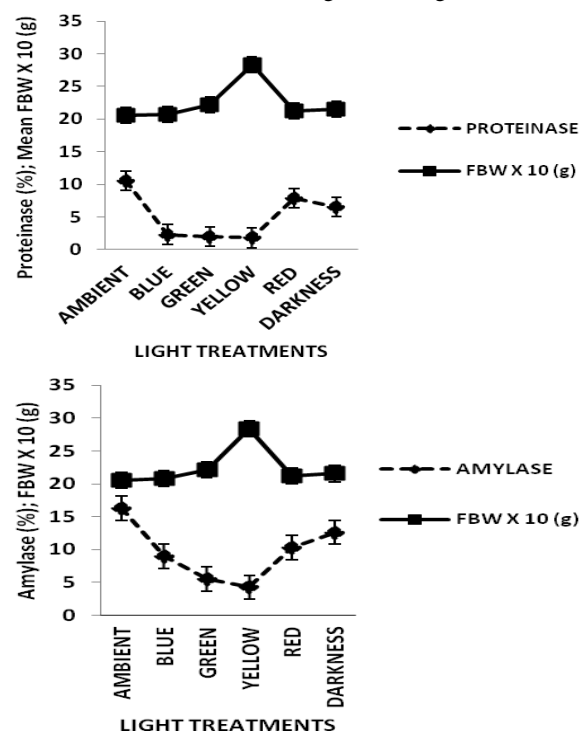


Figure 4. Comparison between the final body weights (FBW) and the digestive enzymes (Proteinase A, and Amylase B) functions of catfish exposed to light of various wavelengths

3.6. Survival rate of African catfish (*Clarias gariepinus*) exposed to different light condition.

In terms Survival rate, result showed that fish reared under yellow and red lights had the highest survival rate of 80.95 %, while those of blue, green and ambient condition had 61.90 %. Those under dark condition gave the lowest survival rate (52.38 %). This implies that the highest percentage of death rate was recorded in those under dark condition, while those under yellow and light spectral survived best (Figure 5).

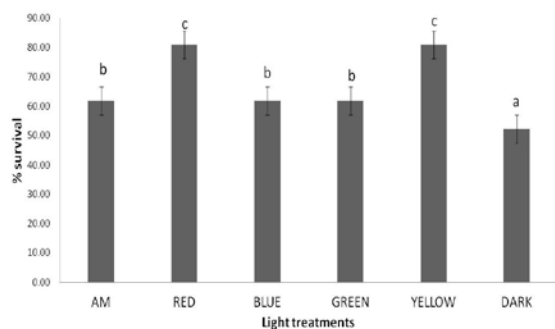


Figure 5 . Survival rate of juvenile African catfish (*Clarias gariepinus*) exposed to different light spectral for the period of 50 days.

Mean with dissimilar superscript are significantly different ($p < 0.05$)

4. Discussion

This study investigated how changing light wavelengths affected the development and digestive enzyme activity of *C. gariepinus*. The influence of photoperiod on *C. gariepinus* physiological processes has been studied. According to reports, the various life stages of *C. gariepinus* thrive best in absolute darkness as opposed to ambient light. Throughout this investigation, the same correlation was detected between ambient light and darkness.

The growth indicators demonstrated in this study that *C. gariepinus* responds favorably to yellow light. The outcome is congruent with what has been seen elsewhere. Shittu (2015) found the same phenomenon in *C. gariepinus* exposed to yellow light, with the exception that he utilized fluorescent bulbs instead of LEDs in his investigation. In accordance with this study, Sallehudin *et al.* (2017a) demonstrated that when African catfish were exposed to various light hues for fourteen days, yellow light promoted the greatest growth. Some studies on the impact of light hue on the growth performance of various fish have produced contradictory findings. For instance, the growth performance of Nile tilapia, *Oreochromis niloticus*, was greatest when exposed to red light (Lopez-Betancur *et al.*, 2020), although Elsbaay (2013; 2016) indicated that blue light was more effective. Nasir and Farmer (2017) found the optimum growth performance for Common carp, *Cyprinus carpio*, under red light, and Ruchin *et al.* (2002) under green light. In addition, Dadfar *et al.* (2017) showed that the weight parameters of rainbow trout, *O. mykiss*, were greater under yellow and white lighting as opposed to Karakatsouli *et al.* (2008), who stated that *O. mykiss* performed best under red light. The juvenile Beluga, *Huso huso*, performed best under blue light (Banan *et al.*, 2010), while Snakehead performed best when exposed to green light.

It is still unclear how colored light affects fish in general and Catfish specifically in terms of growth performance. In order to determine whether there is a direct relationship between the color of the light and the activity of the enzymes, this study examined the effect of colored light on the function of the digestive system. How well food is absorbed during digestion has been shown to be significantly influenced by the actions of the digestive enzymes (Sanchez-Muros *et al.*, 2013). According to Fereshteh *et al.* (2016), pancreatic enzyme activities increase along with photoperiod, which improves the

growth performance of juvenile rainbow trout. This implied that the light diet might have an impact on how well the digestive enzymes work. According to this study, enzyme activity decreased when exposed to light and then increased as the light's wavelength increased. The enzyme activity and growth efficiency under yellow light had a complete inverse relationship. One would think that since yellow light exposure produced the best growth results, the enzyme's activity would be at its peak, but the opposite was true. If the enzymes' activity had been found to be higher in the presence of yellow light, one might have hypothesized that the upregulation of the enzymes would result in greater digestion, which would then produce more energy and promote greater growth. However, since the enzyme's activity was now markedly diminished by yellow light, the growth performance could no longer be directly linked to food digestion, which would increase the energy available. The growth response observed under the yellow light must be caused by something other than food since the activity of the enzymes does not directly correlate with growth, and this other cause is still unknown.

In addition, Sallehudin *et al.* (2017b) reported that Africa catfish exposed to yellow light showed less aggression as compared to other light colors. Since the same authors had reported better growth performance under yellow light in their earlier work (Sallehudin *et al.*, 2017a), then the assumption one can make is that the energetic cost on aggressive behavior might have been channeled on building of the muscles and the skeletal system hence, the better growth performance observed. There is a need for more investigations to know the mechanism by which light colors help enhance growth performance in fish.

5. Conclusion

Weight and length of juvenile African catfish (*C. gariepinus*) were affected by monochromatic lights. Yellow light improved daily growth rate, weight gain, and length gain in juvenile *C. gariepinus*. Yellow and red lights increase the survival rate of *C. gariepinus*. Blue, green, and yellow lights reduced the activities of amylase and protease.

6. Recommendation

We want to recommend that the actual wavelength of yellow light that will elicit the best response be examined. Also, the proximate analysis of the fish should be evaluated so as to know the part of the fish's nutrition that may be affected due to the exposure. It will also be of interest to evaluate the amino acid and lipid profiles of the fish after the exposure so as to ascertain the nutritional value of the fish after the exposure.

References

- Almaza'n RP Schrama JW and Verreth JAJ. 2004. Behavioral responses under different feeding methods and light regimes of the African catfish (*Clarias gariepinus*) juveniles, *Aquac.*, **231**:47–359.
- Appelbaum S and Kamler E. 2000. Survival, growth, metabolism and behavior of *Clarias gariepinus* (Burchell 1822) early stages under different light conditions. *Aquac Eng.*, **22**, 269–287.

- Ariño A Beltrán JA Herrera A and Roncalés P. 2013. Fish and seafood: Nutritional Value, In: Benjamin C (Eds.), **Encyclopedia of Human Nutrition (Third Edition)**, Elsevier, pp. 254-261.
- Banan A Kalbassi MR Bahmani M and Sadati MAY. 2010. Effects of colored light and tank color on growth indices and some physiological parameters of juvenile beluga (*Huso huso*). *J. Appl. Ichthyol.*, **27**: 565–570.
- Biswas AK Endo M and Takeuchi T. 2002b. Effects of different photoperiod cycles on metabolic rate and energy loss of both fed and unfed young tilapia *Oreochromis niloticus*: part I. *Fish Sci.*, **68**: 465–477.
- Biswas AK Morita T Yoshizaki G Maita M and Takeuchi T. 2005. Control of reproduction in Nile tilapia *Oreochromis niloticus* (L.) by photoperiod manipulation. *Aquac.*, **243**: 229–239.
- Biswas AK and Takeuchi T. 2002a. Effects of different photoperiod cycles on metabolic rate and energy loss of both fed and unfed adult tilapia. *Oreochromis niloticus*: part II. *Fish Sci.*, **68**: 543–553.
- Boeuf G and LeBail PY. 1998. Does light have an influence on fish growth? *Aquac.*, **177**: 129–152.
- Britz PJ and Pienaar AG. 2009. Laboratory experiments on the effect of light and cover on the behaviour and growth of African catfish, *Clarias gariepinus* (Pisces: Clariidae). *J. Zool.*, **227**(1): 43–62.
- Caglar M Canpolat O and Selamoglu Z. 2019. Determination of some heavy metal levels in three freshwaterfish in Keban Dam Lake (Turkey) for public consumption. *Iran. J. Fish. Sc.* **18**(1): 188-198.
- Cao J Liu W Wang Z Xie D Jia L and Chen Y. 2008. Green and Blue Monochromatic Lights Promote Growth and Development of Broilers Via Stimulating Testosterone Secretion and Myofiber Growth. *J Appl Poult Res*, **17**: 211–218.
- Dadfar F Bahaoddini A Esmaeili HR and Dorota FB. 2017. The effects of different artificial light colors on the growth rate of embryo and juvenile rainbow trout *Oncorhynchus mykiss* (WALBAUM, 1792)*. *Pol. J. Natur. Sc.*, **32**(1): 179–189.
- Diyani L Long Z Mingyao Y Huadong Y Huailiang X Jessica S Trask DG Smith ZZ and Qing Z. 2014. The effect of monochromatic light-emitting diodes on reproductive traits of laying hens. *J Appl Poult Res*, **23**: 367–375.
- Duran A and Talas ZSJ. 2009. Biochemical changes and sensory assessment on tissues of carp (*Cyprinus carpio*, Linnaeus 1758) during sale conditions. *Fish Physiol. Biochem.*, **35**: 709-714.
- Elsbaay AM. 2013. Effects of Photoperiod and Different Artificial Light Colors on Nile Tilapia Growth Rate. *J. Agric. Vet. Sci.*, **3**(3): 05-12.
- Elsbaay AM. 2016. Impacts of illumination time and color on tilapia outgrowth and fish flesh quality. *Misr J. Ag. Eng.*, **33**(3): 1109 – 1126.
- Fereshteh D Aminollah B Hamid RE and Dorota F. 2017. The effects of different artificial light colors on the growth rate of embryo and juvenile rainbow trout *Oncorhynchus mykiss*. *J. Nat. Sci.*, **32**(1): 179–189.
- Handajani H Adhywirawan G Andriawan S Prasetyo D and Mavuso BR. 2021. Evaluation of Efficiency of *Echinodorus palaefolius* (J.F. Macbr.) Involved in the *Clarias gariepinus* (Burchell, 1822) Culture for Water Quality Recovery and Fish Growth Support. *Jordan J. Biol. Sci.*, **14**(5): 959 – 964.
- Henne JP and Watanabe WO. 2003. Effects of light intensity and salinity on growth, survival, and whole-body osmolality of larval southern flounder *Paralichthys lethostigma*. *JWAS*, **34**: 450–465.
- Imanpoor MR and Abdollahi M. 2011. Effects of tank color on growth, stress response and skin color of juvenile Caspian kutum (*Rutilus frisii Kutum*). *Glob Vet*, **6**(2): 118–125.
- Kakoolaki S Talas ZS Cakir O Ciftci O and Ozdemir I. 2013. Role of Propolis on Oxidative Stress in Fish Brain. *Basic Clin. Neurosci.* **4**(2): 47-52.
- Karakatsouli N Papoutsoglou SE Panopoulos G Papoutsoglou ES Chadio S and Kalogiannis D. 2008. Effects of light spectrum on growth and stress response of rainbow trout *Oncorhynchus mykiss* reared under recirculating system conditions. *Aquac Eng*, **38**: 36-42.
- Kim B Lee D and Chun K. 2018. Effects of Led light color on fish growth in aquaculture. *J. Appl. Eng. Sci.*, **13**(3): 3321- 3325.
- Lopez-Betancur D Moreno I Guerrero-Mendez C Gómez-Meléndez D Macias M de J and Olvera-Olvera C. 2020. Effects of Colored Light on Growth and Nutritional Composition of Tilapia, and Biofloc as a Food Source. *Appl. Sci.*, **10**: 362-375.
- Mustapha MK Okafor BU Olaoti KS and Oyelakin OK. 2012. Effects of three different photoperiods on the growth and body coloration of juvenile African catfish, *Clarias gariepinus* (Burchell). *Arch. Pol. Fish*, **20**: 55-59.
- Nasir NAN and Farmer KW. 2017. Effects of different artificial light colors on the growth of juveniles common carp (*Cyprinus carpio*). *Mesopo. Environ. J.*, **3**(3): 79-86.
- Orina PS Rasowo J Oyoo-Okoth E Musa S Munguti JM and Charo-Karisa H. 2016. Combined effects of photoperiod and temperature on growth and survival of African catfish (*Clarias gariepinus*, Burchell 1822) larvae under laboratory conditions, *J. Appl. Aquac.*, **28**(1): 17-25.
- Osborne DR and Voogt P. 1978. Calculation of Caloric Value. In: "Analysis of Nutrients in Foods". Academic Press, New York, pp. 23-34.
- Rotllant J Tort L Monteroc D Pavlidis M Martinez M Bonga SEW and Balme PHM. 2003. Background color influence on the stress response in cultured red porgy *Pagrus pagrus*. *Aquac.*, **223**: 129–139.
- Ruchin AB. 2019. Rearing carp (*Cyprinus carpio*) in different light: mini review. *AAACL Bioflux*, **12**(5): 1850- 1865
- Ruchin AB Vechkanov VS Kuznetsov VA. 2002. Growth and feeding intensity of young Carp *Cyprinus carpio* under different constant and variable monochromatic illuminations. *J Ichthyol.*, **42**: 191–199.
- Sallehudin MF Yusoff NA Tan NH Saad S and Mukai Y. 2017a. Optimum light wavelength and light intensity for rearing juvenile African Catfish (*Clarias gariepinus*). *Int. J. Aqu. Sci.*, **8**(2): 107-112.
- Sallehudin MF Yusoff NA Tan NH Saad S and Mukai Y. 2017b. Aggressive Behaviour of African Catfish *Clarias gariepinus* juveniles under different light intensities and light wavelengths. *Malays. Appl. Biol.*, **46**(4): 7–13
- Sánchez-Muros MJ Gómez-Milán E Barroso FG and Manzano-Agugliaro F. 2013. Daily and Annual Variation in Digestive Enzymes - Amylase and Basic and Acid Proteases - in Gilt-head Sea Bream, *Sparus aurata*. *JWAS*, **44**(1): 105–114.
- Shittu, 2015. Growth performance and melatonin concentration in catfish, *Clarias gariepinus*. BSc thesis, Department of Pure and Applied Zoology. FUNAAB, Nigeria.
- Somkuti GA and Babel FJ. 1967. Condition influencing the synthesis of Acid protease by *Mucor pusillus*ltd. *ASM*, 1309-1312.
- Swain RR and Dekker EE. 1966. Seed germination studies. 3. Properties of a cell-free amino acid incorporating system from pea cotyledons; possible origin of cotyledonary alpha- amylase. *Plant physiol.*, **44**(3): 319-25.

Generation and Evaluation of Gold-binding Peptide Fused Protein A

Thuy-Dung Doan-Tran^{1,3,4}, Thanh-Tan Nguyen^{1,2,3,4}, and Hieu Tran-Van^{1,2,3,4,*}

¹Department of Molecular and Environmental Biotechnology, Faculty of Biology and Biotechnology, University of Science Ho Chi Minh City, Vietnam; ²Laboratory of Biosensors, Faculty of Biology and Biotechnology, University of Science Ho Chi Minh City, Vietnam; ³Laboratory of Molecular Biotechnology, University of Science, Ho Chi Minh City, Vietnam; ⁴Vietnam National University, Ho Chi Minh City, Vietnam

Received: December 31, 2022; Revised: March 9, 2023; Accepted: April 4 2023

Abstract

Immobilizing antibodies onto the surface of gold nanoparticles (AuNPs) in an oriented manner is essential to achieve high sensitivity and detection limits in immunoassays and biosensors. In this research, the two-domain protein proAx1-Au-binding was generated as the result of the fusion between staphylococcal protein A and a gold-binding peptide (GBP). This novel protein allows the fragment antigen-binding (Fab) region of captured antibodies to be exposed while binding stably to the gold surface. In this present study, we successfully constructed the recombinant pET22b-proAx1-Au-binding plasmid. The expression of proAx1-Au-binding was induced by Isopropyl β-D-1-thiogalactopyranoside (IPTG) and then confirmed by Tricine-SDS-PAGE and Western Blot. The gold-binding ability of this novel protein was evaluated and the result showed that proAx1-Au-binding had a higher affinity for AuNPs than protein A alone, thereby enhancing antibody immobilization onto AuNPs. This study laid the groundwork for facilitating the preparation of any target-specific antibody-AuNPs.

Keywords: antibody immobilization, gold nanoparticle, gold-binding peptide, immunoassay, protein A

1. Introduction

Gold nanoparticles (AuNPs) have been gaining tremendous attraction in recent years for their potential applications in various fields, especially in biomedicine. This is due to their advantageous size as well as their interesting physical, chemical, and optical properties (Dreaden *et al.*, 2012). The size of AuNPs is in the nanoscale, which is 1-100 nm (Bakshi *et al.*, 2014). Despite their small size, they have a high surface-to-volume ratio which allows them to be conjugated with a wide range of biomolecules (Akbarzadeh Khiavi *et al.*, 2019; Bhumkar *et al.*, 2007; Deka *et al.*, 2017; Kumari *et al.*, 2020; Lin *et al.*, 2021; Rahme *et al.*, 2019; Thomas and Klibanov, 2003). This leads to the development of novel complexes which possess characteristics of both AuNPs and their conjugating partners. Among various types of biomolecules, proteins with diverse structural and functional properties are the most focused, especially antibodies since gold nanoparticle-antibody (AuNP-Ab) conjugates are promising for many diagnostic applications such as biosensing, immunoassay, etc. (Lin *et al.*, 2021)

Two main strategies for conjugating antibodies to AuNPs are non-covalent mode (based on hydrophobic and ion interaction) and covalent mode (based on EDC/NHS reactions, thiol derivatives, and linkers) (Jazayeri *et al.*, 2016). While being relatively simple, the non-covalent method has major weaknesses including weak binding and random orientation of antibodies on particles' surfaces,

reducing immunoassay sensitivity (Saha *et al.*, 2014). Conversely, the covalent mode helps to achieve strong and oriented immobilization. However, this method is labor-intensive and involves chemical modification of antibodies, which can potentially affect the structure and function of those molecules (Katz and Willner, 2004).

The new approach to immobilizing antibodies to AuNPs' surface utilizing gold binding peptides (GBPs) could overcome the limitation of existing methods. These GBPs have a natural affinity with gold material; therefore, they can act as linkers to connect desired molecules with AuNPs. With a high level of modularity in molecular design, GBPs could be fused with different biomolecules through gene engineering to become bi-functional linkers that display both gold-binding qualities as well as characteristics of the fusion partner (Lee *et al.*, 2021; Park *et al.*, 2006). While GBPs can adsorb onto the gold surface easily, they do not bind antibodies; hence, the peptide and another molecule with a natural affinity for antibodies need to be fused. Protein A, originally found in *Staphylococcus aureus*, is probably the most ideal fusion partner in this case since it is capable of binding to the fragment crystallizable (Fc) region of immunoglobulins, especially IgG, from a large number of species (Moks *et al.*, 1986). This property allows the Fab region of antibodies to point outward increasing interaction with antigens. The AuNP-Ab complex conjugated via GBP-protein A fusion protein is expected to be stable, highly interactive with antigens, and therefore considerably

* Corresponding author. e-mail: tvhieu@hcmus.edu.vn.

improve the limit of detection as well as the sensitivity of biosensors and bioassays.

There were previous studies that have conjugated antibodies to AuNPs using protein A-GBP fusion proteins. However, oftentimes the whole protein A was used to generate the fusion protein (Koet *et al.*, 2009). Although protein A consists of five homologous domains and each domain is able to bind IgGs, previous studies showed that each protein A can only bind with approximately two to three IgG molecules (Janset *et al.*, 2009). This means that each fusion protein of gold-binding peptides and protein A can only bind up to three IgG molecules. In this study, a protein A-GBP fusion protein was generated by fusing GBPs with the domain Eof protein A, which has the highest affinity for the Fc region as well as the second-lowest affinity for the Fab region of antibodies, making it the ideal fusion partner for generating the fusion protein (Jansson *et al.*, 1998). This novel fusion protein is expected to be smaller in size while having a strong affinity for antibodies compared to previous protein A-GBP fusion proteins. Our study aims to immobilize antibodies onto AuNPs in an oriented manner using this novel fusion protein (Fig. 1). The gold-binding capability of this fusion protein was evaluated. Antibody immobilization using this fusion protein was also carried out and compared with other conventional strategies.

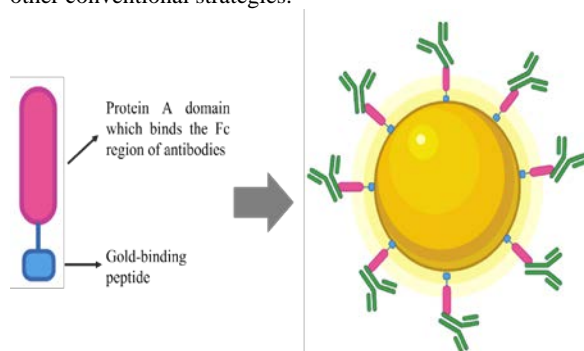


Figure 1. Schematic of immobilization of antibodies onto AuNPs using protein A-GBP fusion protein.

2. Materials and Methods

2.1. Reagents and equipment

Reagents and equipment are listed: proAx1-Au-binding coding template G-block and primers (PHUSA BioChem, Vietnam); restriction enzymes, T4 DNA ligase, and buffers (Thermo Fisher Scientific, USA); MyTaq Red Mix (2X) (Bioline, UK); EZ-10 Spin Column DNA Minipreps Kit (Biobasic, Canada); PCR P25 instrument (PHUSA BioChem, Vietnam); ENDURO™ Gel XL Electrophoresis System (Labnet International); Mini-PROTEAN Electrophoresis System (BIO-RAD, USA); ThermoBioMate 3 Spectrophotometer (Thermo Fisher Scientific, USA); Fluorescence microscope (Nikon, Japan); Horseradish peroxidase (HRP)-conjugated 6*His, His-Tag Monoclonal antibody (ProteinTech, USA); DCNovations Colloidal Gold Conjugation Kit (DCN Dx, USA); GFP-Fc protein; chemicals (Merck, USA), otherwise stated.

2.2. Strains and plasmids

The *E. coli* strain DH5 α was used as a host for the manipulation of recombinant DNA. The *E. coli* strain BL21(DE3) was used for recombinant protein expression. The *E. coli* strain BL21(DE3) carrying pET22b-*proAx1* plasmids was used to express the recombinant protein proAx1 (Tran-Nguyen *et al.*, 2021). The pET22b plasmid used to construct the proAx1-Au-binding expression vector is under the control of T7 promoter and carries an ampicillin resistance gene for screening of transformants and a His-tag sequence (Novagen).

2.3. Construction of pET22b-*proAx1*-Au-binding plasmid

The Au-binding peptide HGKTQATSGTIQS was used in this study (Verde *et al.*, 2009). The DNA coding sequence of the domain E of staphylococcal protein A was obtained from NCBI (GenBank: X61307.1). The DNA coding sequences of domain E and the GBP were fused and optimized for later expressing steps in *E. coli*. The complete *E. coli* optimized, coding region of the *proAx1*-Au-binding gene, was obtained from the G-block template (PhuSa Biochem, Vietnam) by polymerase chain reaction (PCR) with gene-specific primers containing a restriction site of *Nde*I at 5' end and a restriction site of *Hind*III at 3' end. All designed primers are listed in Table 1. The PCR reaction (50 μ l total volume) composed of 25 μ l of MyTaq Red Mix, 1 μ l of protein-coding templates (approximately 1000 ng), and 2 μ l of each primer (10 pmol/ml). The PCR amplification process was performed under the following conditions: an initial denaturation step at 95°C for 3 min; followed by 35 cycles of 95°C for 15 sec, 55°C for 15 sec, 72°C for 30 sec, and a final extension step at 72°C for 6 min. The size of the PCR product was analyzed on agarose gel electrophoresis (1.5%).

The digestion of the pET22b plasmid and the *proAx1*-Au-binding gene with *Hind*III/*Nde*I restriction enzymes was simultaneously carried out in a single reaction for 4 hr for complete digestion (Le-Dao *et al.*, 2022; Mohammad and Soukkarieh, 2022). Digested products were ligated using T4 DNA ligase, then transformed into competent *E. coli* DH5 α cells by heat shock method for the construction of the pET22b-*proAx1*-Au-binding plasmid. Five recombinant clones that grew on LB agar plates containing 100 μ g/ml ampicillin (LB-Amp100) were selected and tested by colony PCR with the same procedure mentioned above to confirm the insertion of the *proAx1*-Au-binding gene into pET22b plasmids.

Table 1 Primer sequences used in this study.

Primer	Sequence
216F-Nde	<u>C</u> ATATGGACAACAAATTCACAAAGAAC
418R-HindIII	AAGCTT <u>G</u> CTCTGAATGGTGCCGCTGGTCG
T7 pro	CGAAATTAATACGACTCACTATAGG
T7 ter	GGTTATGCTAGTTATTGCTCAGCG

Underlined letters indicate the restriction enzyme.

2.4. Expression of the recombinant *proAx1*-Au-binding protein

The recombinant pET22b-*proAx1*-Au-binding plasmid was cloned in *E. coli* BL21(DE3) with the same procedure. The production of proAx1-Au-binding was induced using IPTG (final concentration 0.5 mM) at 37°C for 4 hr. Transformed *E. coli* BL21(DE3) cells bearing the pET22b

plasmid were similarly induced to serve as the control sample. The induced *E. coli* BL21(DE3) cells were lysed in 20 mM PBS buffer (3.8 mM NaH_2PO_4 , 16.2 mM Na_2HPO_4 , pH 7.4) by sonication (30%, 3 min) to extract total protein and then centrifuged at 13,000 rpm/min for 20 min to obtain supernatant containing soluble proteins and insoluble cell pellets.

2.5. Protein expression analysis with SDS-PAGE and Western Blot

The analysis of Au-binding-proAx1 expression was carried out simultaneously with proAx1 - one of the five homologous domains of staphylococcal protein A - expressed with the same procedure mentioned above. Sample buffer (0.375 M Tris (pH 6.8), SDS 12%, Glycerol 60%, 0.6M DTT, Bromophenol Blue 0.06%, dH_2O) was added to protein samples and heated at 100 °C for 15 min. before being analyzed with Tricine-SDS-PAGE.

Cloning in expression vector pET22b allowed recombinant proteins to be expressed as His-tagged proteins, which could be detected by Western blotting using His-tag antibodies. Protein samples were subjected to Tricine-SDS-PAGE on a 20% gel, after which the unstained gel was transferred to the nitrocellulose membrane and probed with HRP-conjugated His-tag antibodies at dilution of 1:50,000.

2.6. Evaluation of the gold-binding ability

2.6.1. Preparation of AuNPs

Before immobilization, AuNPs were cleaned using 10 mM MES buffer and 10 mM acetate buffer (5.499 mM acetic acid, 4.501 mM sodium acetate, pH 4.5). The colloidal gold solution was first centrifuged at 13,000 rpm/min for 10 min and the pellet of AuNPs was then resuspended in 10 mM MES buffer. The AuNPs were subsequently centrifuged/resuspended one more time before changing into 10 mM acetate buffer (pH 4.5). Similar centrifugation/resuspension cycles were performed with 10 mM acetate buffer (pH 4.5).

2.6.2. Immobilization of proAx1 and proAx1-Au-binding onto AuNPs

The total protein extract from cultured cells expressing proAx1 and proAx1-Au-binding was obtained by lysing cells in 10 mM acetate buffer (pH 4.5). The protein bands of proAx1 and proAx1-Au-binding were quantified based on the result of Tricine-SDS-PAGE with Coomassie staining using ImageJ. The total protein extracts of proAx1 and proAx1-Au-binding were analyzed by Bradford assay to quantify the total protein concentration and then adjusted to achieve an equal molecular amount of proAx1 and proAx1-Au-binding before being incubated with the same amount of prepared AuNPs. The incubation was carried out for 1 hr at 4°C. Excess proteins were removed by centrifugation at 13,000 rpm/min for 10 min. After centrifugation, the supernatant was collected and the pellet was resuspended in 10 mM acetate buffer (pH 4.5). To further wash weakly bound proteins from AuNPs, the centrifugation/resuspension cycle mentioned above was repeated three times. After the final wash, the AuNP-protein precipitates were boiled for 10 min at 100°C in sample buffer to release the protein from the AuNPs. The immobilization of proteins onto AuNPs was then evaluated by Tricine-SDS-PAGE with silver staining.

2.7. Evaluation of the antibody-capturing ability

To evaluate the antibody-capturing ability of the AuNP-protein conjugates, GFP-Fc protein was used in place of normal antibodies since GFP-Fc proteins contain the Fc domain to which protein A bound specifically and the GFP domain which allows fluorescence visualization (Al-Homsi *et al.*, 2012; Nguyen *et al.*, 2021). The final AuNP-protein conjugates obtained after immobilizing proteins onto the AuNPs and washing, as well as AuNPs alone, were incubated with GFP-Fc proteins for 1 hr at 4°C in 10 mM acetate buffer (pH 4.5). After incubation, the same centrifugation/resuspension cycles used in the gold-immobilization step were performed to remove excess and weakly-bound GFP-Fc. The final AuNP-protein-GFP-Fc conjugates were analyzed using fluorescence microscopy. The fluorescence signal of each sample was quantified using ImageJ, function Measure. The minimum threshold was set so that the raw signal of unconjugated AuNPs would not contribute to the signal obtained from the samples which were conjugated with GFP-Fc. The particles with an area above 120,000 square pixels which was significantly bigger compared to the average size of most particles in the samples, hence they were treated as unwanted impurities and excluded from the signal quantification. T-tests were then used to determine whether there was any statistical difference between the fluorescence signal obtained from each sample.

3. Result

3.1. Cloning of the proAx1-Au-binding gene

The *proAx1-Au-binding* gene was successfully amplified by PCR using gene-specific primers. A band of approximately 246 bp, which was the size of the *proAx1-Au-binding* gene, could be observed from the electropherogram (Fig.2A, lane 2). Linearization of the pET22b plasmid was achieved using *NdeI/HindIII* restriction enzymes. The digested product gave a single linear band of approximately 5,493 bp (Fig.2B, lane 4). The *proAx1-Au-binding* gene was successfully cloned into pET22b plasmids in a correct orientation. The result of colony PCR with 416F-*NdeI*/T7 terprimers showed a band of approximately 400 bp from three out of five screened transformants, which was the expected size of the PCR product (Fig.2C, lane 3, 5, 6).

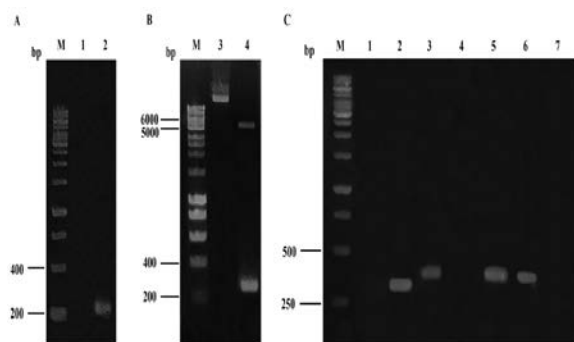


Figure 2. Construction of pET22b-*proAx1-Au-binding* plasmid. (A) PCR amplification of *proAx1-Au-binding*. M, DNA ladder; 1, negative control; 2, *proAx1-Au-binding* gene. (B) *proAx1-Au-binding* gene and pET22b plasmid were digested with *NdeI/HindIII* restriction enzymes. M, ladder; 3, plasmid pET22b; 4, digested products. (C) Screening of transformants carrying pET22b-*proAx1-Au-binding*. M, DNA ladder; 1, negative control; 2, PCR amplification of pET22b plasmids with T7 pro/T7 ter; 3-7, colony PCR of transformants with 416F-Nde/T7 ter.

3.2. Expression of *proAx1-Au-binding*

The *proAx1-Au-binding* and *proAx1* proteins were expressed in *E. coli* BL21(DE3). Bacterial lysate of *E. coli* BL21(DE3) containing pET22b-*proAx1-Au-binding* plasmid after induction with IPTG (final concentration 0.5 mM) at 37°C for 4 hr revealed an over-expressed protein band of approximately 8.9 kDa (Fig.3A, lane 3, 4), which was the predicted size of *proAx1-Au-binding* and higher than the expression band of *proAx1* (approximately 6 kDa) (Fig.3A, lane 2). There was no similar over-expressed band detected in the control lane (Fig.3A, lane 1). Both *proAx1* and *proAx1-Au-binding* were detected in the Western blot experiment employing His-tag antibodies. The result showed corresponding signals to the suspected bands in Tricine-SDS-PAGE (Fig.3B). This further confirmed that *proAx1* and *proAx1-Au-binding* were successfully expressed. As for protein solubility, *proAx1-Au-binding* was mainly expressed in soluble form as expected (Fig.3A-B, lane 4), while *proAx1* was already confirmed to be expressed in soluble form with the same expression condition as previously reported (Tran-Nguyen *et al.*, 2021).

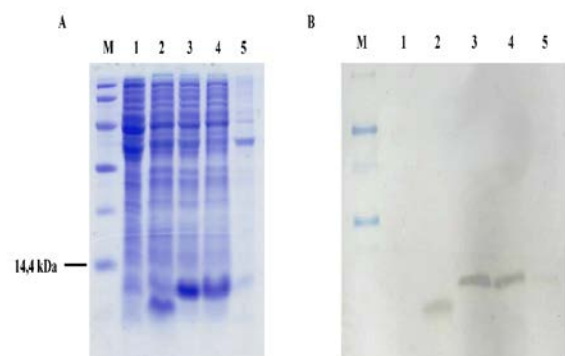


Figure 3. Protein expression analysis of *proAx1* and *proAx1-Au-binding*. (A) SDS-PAGE; (B) Western Blot. M, protein molecular weight ladder; 1: total cellular protein expressed in *E. coli* BL21(DE3) carrying pET22b as a control; 2, total cellular protein of *proAx1*; 3-5, total cellular protein, soluble fraction, insoluble fraction of *proAx1-Au-binding*.

3.3. Immobilization of proteins onto the surface of AuNPs

The immobilization of *proAx1* and *proAx1-Au-binding* onto the surface of AuNPs was facilitated by incubating the mixture of proteins and AuNPs in 10 mM acetate buffer of pH 4.5 at 4°C followed by several washing cycles of centrifugation and resuspension. The supernatant samples of each step were collected to be analyzed by Tricine-SDS-PAGE with silver staining. The result showed that the number of proteins in the mixture surpassed the binding capacity of AuNPs. Thus, unbound proteins remained in the supernatant after centrifugation (Fig. 4, lane 2, 5). The precipitate lanes revealed a major protein band of *proAx1-Au-binding* while no protein band of *proAx1* was observed, which indicated that there was little to no *proAx1* in the final AuNP-protein complex (Fig.4, lane 3, 9). This proved that the binding of *proAx1* to AuNPs was not stable while *proAx1-Au-binding*, which was the fusion of protein A and GBP, was still bound strongly to AuNPs even after being challenged by several washing steps. The result indicated that *proAx1-Au-*

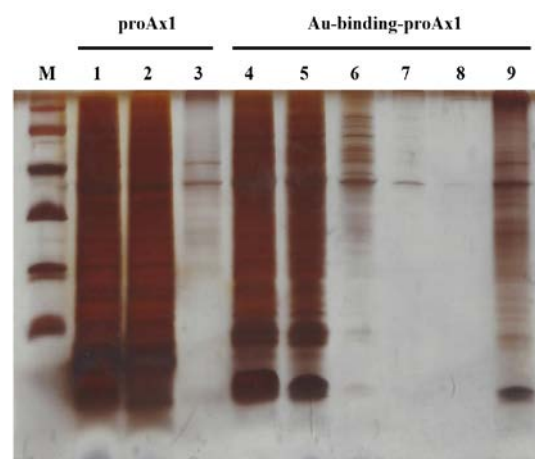


Figure 4. Immobilizing of *proAx1* and *proAx1-Au-binding* onto AuNPs. M, ladder; 1, 4, total protein; 2, 5, supernatant obtained after incubation; 3, 9, final precipitate; 6-8, supernatant of threewashing cycles.

3.4. Evaluation of antibodies immobilized onto AuNPs

Two strategies of immobilizing antibodies onto gold surfaces via *proAx1* and *proAx1-Au-binding* were evaluated. After the final wash in the gold-binding assay, the AuNP-protein conjugates were incubated with GFP-Fc and then washed in 10 mM acetate buffer (pH 4.5). The final conjugates obtained were analyzed with fluorescence spectroscopy and ImageJ (Fig. 5A). The fluorescent signal quantification result showed that the immobilization via *proAx1-Au-binding* strategy gave the highest signal of $48,078,802.67 \pm 10,842,323.01$, which indicated the successful capture of GFP-Fc. Meanwhile, the immobilization via *proAx1* strategy showed much less signal of $28,661,414.33 \pm 5,162,967.87$, since little to no *proAx1* was presented in the initial conjugates, as demonstrated in the silver staining analysis. The direct absorption strategy giving the lowest signal of $15,547,923.67 \pm 2,640,668.05$ also proved that most of the

uncaptured GFP-Fc remained in the supernatant after centrifugation, so the fluorescent signal was obtained mainly owing to the binding of GFP-Fc to proteins. The t-test results (all two-tailed) indicated that there was a statistical difference between each pair of samples with p-values < 0.05 (Fig. 5B). These results demonstrated that the strategy to immobilize antibodies onto AuNPs via the two-domain protein proAx1-Au-binding was much more effective compared to immobilizing via protein A or direct absorption.

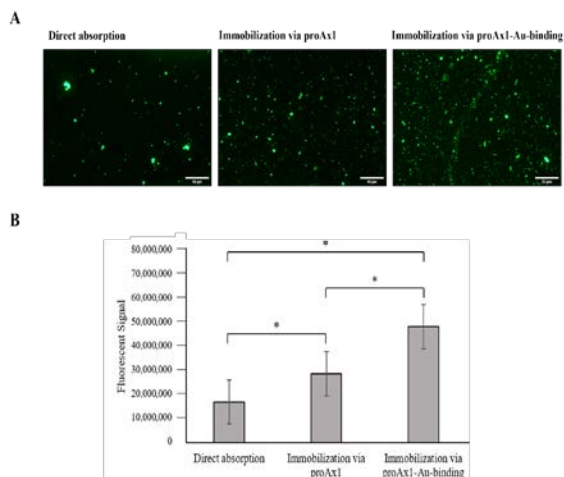


Figure 5. Visualization of GFP-Fc immobilization by fluorescence microscope (A) (x20 magnification; scale-bar: 50 μ m) and the comparison of the fluorescent signal of GFP-Fc immobilizing strategies (B). Data represent three replications and are expressed as mean \pm standard deviation. *p < 0.05.

4. Discussion

The novel fusion protein proAx1-Au-binding has a gold-binding domain and a protein A domain which captures the Fc region of antibodies and, therefore, allows the Fab region to freely interact with antigens. The soluble expression of recombinant protein proAx1-Au-binding in *E. coli* BL21(DE3) was achieved with 0.5 mM IPTG and an induction temperature of 37 °C for 4 hr. ProAx1-Au-binding was shown to bind better to AuNPs than proAx1 in pH 4.5 and the binding remained even after several cycles of washing, which is important when dealing with low-pH samples in immunoassays (Foley *et al.*, 2020; Isanga *et al.*, 2017). The improved gold-binding ability of protein A after being fused with a GBP is consistent with a previous publication in which protein A was also fused with another material-binding protein and thus displayed a higher affinity for that particular material compared to unmodified protein A (Tran-Nguyen *et al.*, 2021). This proves that protein A can be fused with different material-binding proteins/peptides to improve its binding capability to different materials (Faccio, 2018). Furthermore, other GBPs can be screened and genetically modified to obtain higher affinity to gold surfaces so that protein A-GBP fusion proteins could be immobilized even more effectively and stably onto AuNPs in different extreme conditions (Hnilova *et al.*, 2008).

The immobilization of antibodies via protein A-GBP fusion protein was shown to be more effective than other strategies, thus proving that the fusion with GBP did not affect the antibody-binding capability of protein A (Faccio,

2018). This novel strategy is expected to help orientate any antibody with affinity to protein A easily and stably toward the gold surface without chemical modification of antibodies (Jazayeri *et al.*, 2016). However, to guarantee the potential applications of protein A-GBP fusion protein in immunoassays and biosensors, the antigen-capture efficiency of this novel strategy would need to be further assessed.

5. Conclusion

In this work, a two-domain protein (proAx1-Au-binding) has been constructed to provide a new strategy for effective oriented immobilization of antibodies onto AuNPs. We successfully cloned the *proAx1-Au-binding* gene which encodes the two-domain protein proAx1-Au-binding. The gold-binding ability of proAx1-Au-binding was assessed and compared with a protein A domain (proAx1). ProAx1-Au-binding showed a higher binding capacity to AuNPs than proAx1 in pH 4.5. The strategy to immobilize antibodies onto AuNPs through proAx1-Au-binding also greatly improved the immobilizing efficiency compared to other conventional methods which were direct absorption and immobilizing via protein A. In conclusion, the results showed that the two-domain proAx1-Au-binding was a promising tool for the immobilization of antibodies onto the gold surface.

Acknowledgment

Thanh-Tan Nguyen was funded by the Master, PhD Scholarship Programme of Vingroup Innovation Foundation (VINIF), code VINIF.2022.ThS.077.

References

- Akbarzadeh Khiavi M, Safary A, Aghanejad A, Barar J, Rasta SH, Golchin A, Omidi Y and Somi MH. 2019. Enzyme-conjugated gold nanoparticles for combined enzyme and photothermal therapy of colon cancer cells. *Colloids Surf A: Physicochem Eng.*, **572**: 333-344.
- Al-Homsi L, Al-Assad J, Kweider M, Al-Okla S and Abbady AJJBS. 2012. Construction of pRSET-sfGFP plasmid for fusion-protein expression, purification and detection. *Jordan J Biol Sci.*, **5(4)**: 279-288.
- Bakshi S, He ZL and Harris WG. 2014. Natural Nanoparticles: Implications for Environment and Human Health. *Crit Rev Environ Sci Technol.*, **45(8)**: 861-904.
- Bhumkar DR, Joshi HM, Sastry M and Pokharkar VB. 2007. Chitosan Reduced Gold Nanoparticles as Novel Carriers for Transmucosal Delivery of Insulin. *Pharm Res.*, **24(8)**: 1415-1426.
- Deka J, Mojumdar A, Parris P, Onesti S and Casalis L. 2017. DNA-conjugated gold nanoparticles based colorimetric assay to assess helicase activity: a novel route to screen potential helicase inhibitors. *Sci Rep.*, **7(1)**.
- Dreaden EC, Alkilany AM, Huang X, Murphy CJ and El-Sayed MA. 2012. The golden age: gold nanoparticles for biomedicine. *Chem Soc Rev.*, **41(7)**: 2740-2779.
- Faccio G. 2018. From Protein Features to Sensing Surfaces. *Sensors*, **18(4)**: 1204.
- Foley MM, Brown CO, Westring CG, Danielson PB and McKiernan HE. 2020. Effects of organic acids and common household products on the occurrence of false positive test results

- using immunochromatographic assays. *Forensic Sci Int.*, **308**: 110165.
- Hnilova M, Oren EE, Seker UOS, Wilson BR, Collino S, Evans JS, Tamerler C and Sarikaya M. 2008. Effect of Molecular Conformations on the Adsorption Behavior of Gold-Binding Peptides. *Langmuir*, **24(21)**: 12440-12445.
- Isanga J, Tochi BN, Mukunzi D, Chen Y, Liu L, Kuang H and Xu C. 2017. Development of a specific monoclonal antibody assay and a rapid testing strip for the detection of apramycin residues in food samples. *Food Agric Immunol.*, **28(1)**: 49-66.
- Jans H, Liu X, Austin L, Maes G and Huo Q. 2009. Dynamic light scattering as a powerful tool for gold nanoparticle bioconjugation and biomolecular binding studies. *Anal Chem.*, **81(22)**: 9425-9432.
- Jansson B, Uhlén M and Nygren P-Å. 1998. All individual domains of staphylococcal protein A show Fab binding. *FEMS Immunol Med Microbiol.*, **20(1)**: 69-78.
- Jazayeri MH, Amani H, Pourfatollah AA, Pazoki-Toroudi H and Sedighimoghaddam B. 2016. Various methods of gold nanoparticles (GNPs) conjugation to antibodies. *Sens Biosensing Res.*, **9**: 17-22.
- Katz E and Willner I. 2004. Integrated nanoparticle-biomolecule hybrid systems: synthesis, properties, and applications. *Angew Chem Int Ed Engl.*, **43(45)**: 6042-6108.
- Ko S, Park TJ, Kim HS, Kim JH and Cho YJ. 2009. Directed self-assembly of gold binding polypeptide-protein A fusion proteins for development of gold nanoparticle-based SPR immunosensors. *Biosens Bioelectron.*, **24(8)**: 2592-2597.
- Kumari Y, Singh SK, Kumar R, Kumar B, Kaur G, Gulati M, Tewari D, Gowthamarajan K, Karri V, Ayinkamiye C, Khurshed R, Awasthi A, Pandey NK, Mohanta S, Gupta S, Corrie L, Patni P, Kumar R and Kumar R. 2020. Modified apple polysaccharide capped gold nanoparticles for oral delivery of insulin. *Int J Biol Macromol.*, **149**: 976-988.
- Le-Dao H-A, Le-Nguyen Y-V and Tran-Van HJJJoBS. 2022. Prokaryotic Expression of Murine Cellular Prion Protein for In vitro Evaluation. *Jordan J Biol Sci.*, **15(3)**.
- Lee H, Lee EM, Reginald SS and Chang IS. 2021. Peptide sequence-driven direct electron transfer properties and binding behaviors of gold-binding peptide-fused glucose dehydrogenase on electrode. *iScience*, **24(11)**: 103373.
- Lin X, O'Reilly Beringhs A and Lu X. 2021. Applications of Nanoparticle-Antibody Conjugates in Immunoassays and Tumor Imaging. *AAPS J.*, **23(2)**.
- Mohammad E and Soukkarieh CJJJoBS. 2022. A simple and cost Effectively Method for Production of Recombinant of Full Length of Human Placenta-Specific Protein using E. coli BL21 strain. *Jordan J Biol Sci.*, **15(5)**.
- Moks T, Abrahmsén L, Nilsson B, Hellman U, Sjöquist J and Uhlén M. 1986. Staphylococcal protein A consists of five IgG-binding domains. *Eur J Biochem.*, **156(3)**: 637-643.
- Nguyen TT, Vo-Nguyen HV and Tran-Van H. 2021. Prokaryotic expression of chimeric GFP-hFc protein as a potential immune-based tool. *Mol Biol Res Commun.*, **10(3)**: 105-108.
- Park TJ, Lee SY, Lee SJ, Park JP, Yang KS, Lee KB, Ko S, Park JB, Kim T, Kim SK, Shin YB, Chung BH, Ku SJ, Kim DH and Choi IS. 2006. Protein nanopatterns and biosensors using gold binding polypeptide as a fusion partner. *Anal Chem.*, **78(20)**: 7197-7205.
- Rahme K, Guo J and Holmes JD. 2019. Bioconjugated Gold Nanoparticles Enhance siRNA Delivery in Prostate Cancer Cells. *Methods Mol Biol.*, **1974**: 291-301.
- Saha B, Evers TH and Prins MW. 2014. How antibody surface coverage on nanoparticles determines the activity and kinetics of antigen capturing for biosensing. *Anal Chem.*, **86(16)**: 8158-8166.
- Thomas M and Klivanov AM. 2003. Conjugation to gold nanoparticles enhances polyethylenimine's transfer of plasmid DNA into mammalian cells. *Proc Natl Acad Sci U S A.*, **100(16)**: 9138-9143.
- Tran-Nguyen TS, Ngo-Luong DT, Nguyen-Phuoc KH, Tran TL and Tran-Van H. 2021. Simultaneously targeting nitrocellulose and antibody by a dual-headed protein. *Protein Expr Purif.*, **177**: 105764.
- Verde AV, Acres JM and Maranas JK. 2009. Investigating the Specificity of Peptide Adsorption on Gold Using Molecular Dynamics Simulations. *Biomacromolecules.*, **10(8)**: 2118-2128.

Evaluating the Mood and Memory-enhancing Effects of *Punicagranatum* Seeds (Pomegranate) Extract using an Animal Model

Abdelrahim Alqudah^{1,*†}, Esam Y. Qnais^{2†}, Omar Gammoh³, Mohammed Alqudah⁴

¹Department of Clinical Pharmacy and Pharmacy Practice, Faculty of Pharmaceutical Sciences, The Hashemite University, Zarqa, Jordan;

²Department of Biology and Biotechnology, Faculty of Science, The Hashemite University, Zarqa, Jordan; ³Department of Clinical Pharmacy and Pharmacy Practice, Faculty of Pharmacy, Yarmouk University, Irbid, Jordan; ⁴Physiology Department, School of Medicine and Biomedical Sciences, Arabian Gulf University, Manama, Bahrain

Received: July 31, 2023; Revised: September 12, 2023; Accepted: September 17, 2023

Abstract

The research aimed to elucidate the neurological benefits of *Punicagranatum* seeds (Pomegranate), which have been traditionally touted for their therapeutic properties. To understand their impact, the study systematically examined the seeds' effects on key neurological functions: anxiety, depression, memory, and motor coordination. Through a series of experiments, the seeds were observed to significantly reduce anxiety levels, alleviate depressive symptoms, and enhance memory performance. The efficacy of these seeds might be attributed to their rich content of bioactive compounds, including isoflavones, triterpenes, and antioxidants. Since, there is an increasing demand for natural remedies and a shift towards holistic wellness, the potential therapeutic applications of *Punicagranatum* seeds cannot be understated. If these promising results can be consistently replicated in more extensive clinical trials, the seeds could be harnessed to develop innovative, natural treatments for neurological disorders.

Keywords: Anxiety, Depression, Memory, *Punicagranatum*, Mice.

1. Introduction

The seeds of *Punicagranatum* (Pomegranate) are known to contain high levels of polyphenols, such as flavonoids, anthocyanin's, hydroxybenzoic acids, hydroxycinnamic acids, and tannins (Venkata *et al.*, 2011). Additionally, these seeds serve as rich sources of various fatty acids, particularly unsaturated fatty acids, including linoleic, oleic, palmitic, stearic, linoleic, arachidic, and palmitoleic acids (Elfalleh *et al.*, 2011). Several studies have provided evidence of the diverse health benefits associated with *Punicagranatum* seeds, including in vivo anti-inflammatory, anti-cancer, antimicrobial, and antioxidant properties (Fourati *et al.*, 2020). Furthermore, *Punicagranatum* seeds have a notable magnesium content (14mg/100g), which has been observed to function as an N-methyl-D-aspartate (NMDA) receptor blocker, effectively relieving nerve pain and exhibiting a euglycemic effect on diabetes by reducing the occurrence of type 2 diabetes in healthy individuals (Dumlu and Gürkan, 2007). Furthermore, research has indicated that the daily consumption of 400 mg of magnesium oxide can function as a muscle relaxant, potentially easing anxiety by inducing relaxation in patients (Guerra, Volpe and Mao, 2009).

Dementia specifically impairs a person's ability to carry out daily activities, thereby affecting decision-making. To

gauge the extent of dementia, it is customary to assess an individual's ability for new learning and memory utilizing specific models. Learning is the initial stage of forming new memories in the brain, built upon past experiences. It encompasses processes like encoding, storing, retrieving, and retaining information in memory, as well as the possibility of forgetting it (Okano *et al.*, 2000). Short-term memory pertains to temporarily holding information without the need for repetition, whereas long-term memory involves retaining data over an extended period through repetition. The typical learning process relies on neurotransmitters like dopamine, acetylcholine, and 5-hydroxytryptamine (5HT), which stimulate various brain regions, including the hippocampus, amygdala, and sensory, visual, and auditory cortices of the cerebral cortex (Wiltgen *et al.*, 2006). Additionally, certain anxiolytic and antidepressant medications can influence learning, memory, or induce amnesia.

The primary treatment options for managing dementia are cholinesterase inhibitors and dopamine agonists (O'Lunaigh and Lawlor, 2008). These medications are widely acknowledged as effective approaches. Among various neurodegenerative disorders, Alzheimer's disease (AD) is characterized by progressive dementia, often stemming from the loss of cholinergic neurons or reduced acetylcholine levels. In the management of AD, the primary approach involves the use of acetylcholinesterase (AChE) inhibitors, which work by

* Corresponding author. e-mail: Abdelrahim@hu.edu.jo.

† The two authors contributed equally to this work

elevating acetylcholine levels in the brain. Herbal remedies have been traditionally preferred in medical practices to address various ailments, as they contain bioactive compounds known to provide therapeutic benefits.

Depression refers to a psychological state marked by enduring and contrasting indicators of unhappiness, guilt, exhaustion, diminished focus, lack of interest, reduced self-assurance, and disturbances in eating or sleeping habits. For a diagnosis to be made, these symptoms of depression need to persist for a period longer than two weeks. Each type exhibits unique characteristics and may necessitate specific approaches to treatment and overall management. The Diagnostic and Statistical Manual recognizes various forms of depression, such as persistent depressive disorder, major depression, situational or seasonal affective disorder, postpartum depression, bipolar depression, psychotic depression, premenstrual dysphoric disorder, and atypical depression (Rihmer and Gonda, 2011).

The importance of this research line lies in the potential ability of *Punicagranatum* to act either as a dietary supplement or as an adjuvant to the existing therapies for mood and dementia disorders. Therefore, the objective of the current work is to evaluate the anxiolytic, antidepressant and the memory enhancing properties of *Punicagranatum* seeds using various animal models.

2. Materials and Methods

2.1. Collection of Seeds and Extraction

In May 2020, the *Punicagranatum* seeds were gathered from Irbid, located in North of Jordan. The plant material was authenticated by a botanist. To ensure future reference, a voucher specimen was sent to the Herbarium at Hashemite University in Zarqa, Jordan, where it was assigned the Herbarium number HU.No. 6257. To prepare the seeds of *Punicagranatum* for further use, 500g of seeds was soaked in 1.5 L of ethanol for a duration of 21 days. During the maceration process, the seeds were kept in airtight ambered bottles. Subsequently, the solvent was filtered and evaporated, resulting in an extract. This extract was then stored at 4°C until it underwent freeze-drying for future utilization.

2.2. Experimental Design

The study involved a group of healthy 12-weeks age male mice weighing 25-30g bred at the Department of Biology in Hashemite University's animal house. Following a one-week acclimatization period, the mice were separated into six groups, each comprising 10 mice. They were housed in polycarbonate cages with food and water freely available at a constant temperature of $25 \pm 2^\circ\text{C}$. The control group received 5% Dimethyl sulfoxide (DMSO), while two other groups were given standard drugs: diazepam at a dose of 3 mg/kg (Cheng *et al.*, 2013) and imipramine at a dose of 30 mg/kg (Podolan *et al.*, 2019). The remaining test groups were orally administered ethanol extracts of *Punicagranatum* at doses of 50, 100, and 200 mg/kg for 21 days by oral gavage. All administrations of DMSO, standard drugs, and seed extracts took place once daily between 12 am and 1 pm. To assess the behavioral impact, different models for anxiety, depression, and memory were employed on days 8 and 21

of the study. The behavioral sessions were recorded using a mobile camera running the Android operating system.

2.3. Models for Memory

2.3.1. Passive Avoidance Test

As a rapid method for evaluating fear-based avoidance memory in mice, the Passive Avoidance Test (PAT) is employed. The setup consists of both light and dark compartments, including a grid floor and a guillotine gate. The dark area is connected to a mild electric current source for delivering mild electric shocks (Cho *et al.*, 2003). In the habituation phase, the mice are introduced to the illuminated section for 300 seconds on the first and second days. They faced the dark area with the guillotine door open. If the mice enter the dark compartment during this phase, the door is closed, and a 0.6 mA foot shock lasting 0.5 seconds is given through the grid floor.

In the testing phase, the mice are reintroduced to the apparatus after specific intervals: eight days and twenty-one days. This allows for the assessment of short-term and long-term memories. During testing, the mice are placed in the illuminated section with the gate open, giving them unrestricted access to the dark avoidance section. The duration taken for the mice to re-enter the dark area while successfully avoiding the electric shock is recorded, with a maximum cutoff time of 300 seconds.

2.3.2. Morris Water Maze Test

The aim of this test was to evaluate spatial learning and memory acquisition, specifically those dependent on the hippocampus, in both short-term and long-term contexts. The experimental apparatus used was a rectangular water pool measuring 60 cm \times 30 cm, with a fixed central platform of size 15 cm \times 13 cm submerged in the water and hidden by a non-transparent material. The water temperature was maintained at 25°C. During the training sessions, the platform was visible by keeping the water level below it. The mice were placed into the pool and allowed to find the platform. Four training sessions were conducted on consecutive days, enabling the mice to gradually improve their ability to locate the platform within a shorter time. On the eighth and twenty-first days, the mice were tested again to assess their spatial learning capabilities. Improvement in spatial learning was determined by a decrease in the time taken to find the platform (Gallivan and Schmitzer-Torbert, 2018).

2.4. Motor Skilled Learning and Coordination

2.4.1. Effects on Motor Coordination through Rotarod

In the present investigation, the impact of anxiety-reducing drugs on motor coordination was evaluated using a rotarod apparatus. This apparatus comprises a plastic rod measuring 8 cm \times 3 cm, enclosed for safety purposes. Initially, mice were subjected to training on stationary rods, involving four consecutive trials. The test sessions occurred on the 8th and 21st days after administering ethanol extracts, at two different speeds: 10 and 30 rpm. The time taken for the mice to remain on the rotating rod before falling off, known as "latency time," was recorded, with a maximum limit of 180 seconds. An increase in the duration spent on the rotating rod indicated an enhancement in muscular activity. It is important to mention that drugs with an impact on neuromuscular

coordination, like diazepam, typically lead to a reduction in the latency time for mice to stay on the rotating rod.(Asgharzade *et al.*, 2015).

2.4.2. Stationary Rod Test

The educational capacity was assessed using the Stationary Rod Test (SRT), which involved elevated steel rods with a netted base. The mice were initially trained by walking on the elevated rod with the netted stage. Daily training was conducted over four consecutive days, with each trial lasting 120 seconds. After completing the training, DMSO (a solvent), standard drugs, and *Punicagranatum* seed extracts were orally administered for 21 days. On the eighth and twenty-first days, the time taken by the animals to reach the stage was observed to evaluate short and long-term motor skill learning(Lundquist *et al.*, 2022).

2.5. Models for Anxiety

2.5.1. Light and Dark Test

To evaluate the anxiolytic effects of seed extracts, this study employed a model using the preference of animals to occupy the lighter compartment as an indicator. The experimental setup comprised two identical in volume compartments, each measuring 20 cm × 20 cm × 35 cm (height). One compartment was made brighter by illuminating it with a 100 V bulb, while the other compartment was made darker using dark glasses. The mice were initially introduced to the darker zone and allowed to freely move between the two compartments through a small gate placed in between. Test sessions lasting 5 minutes were conducted, during which the mice could freely explore both compartments. The researchers measured the time spent by the mice in the light compartment, calculated the percentage of time spent there, and counted the number of transitions made between compartments. An increase in the percentage of time spent in the light area was considered an indication of anxiolytic activity(Bourin and Hascoët, 2003).

2.5.2. Elevated Plus Maze (EPM)

Afterwards, mice underwent Elevated Plus Maze (EPM) testing on the eighth and twenty-first days of dosing. The EPM apparatus consisted of two open arms measuring 50 cm × 10 cm and two closed arms measuring 50 cm × 10 cm × 38 cm, all connected to a central area measuring 10 cm × 10 cm. The maze was elevated to a height of 50 cm from the ground. Mice were placed in the central area facing one of the open arms, and their behavior was observed and recorded during a 5-minute test session. The recorded behaviors included the number of entries into both the open and closed arms, as well as the time spent by the mice in each arm.

An increase in the time spent in the open area and the number of entries into the open arm were considered indicative of anxiolytic activity.(Contreras *et al.*, 2014).To calculate the anxiety index, the researchers used the following formula:

$$\text{Anxiety Index} = 1 - (\text{time in open arm} / \text{total time}) + (\text{entries of open arm} / \text{total entries}).$$

If the anxiety index result fell between 0.6 and 1.0, this indicates the presence of anxiety in mice, while a decrease in the index reflects an anxiolytic effect.

2.5.3. Head Dip Test

The test employed a white square wooden box with dimensions of 35 cm × 45 cm × 45 cm, featuring three equally spaced and sized holes on each side. Mice were placed inside the box for a 5-minute session, and the number of head dips through the holes was recorded on the 8th and 21st days of the study (Kliethermes and Crabbe, 2006). An increase in the number of head dips in this model indicated a rise in anxiety, while a decrease in head dipping pointed to the anxiolytic effect of the extracts(Solangi and Najam, 2013).

2.5.4. Open Field Test Apparatus

The open field test (OFT) is a widely used apparatus for evaluating various behaviors in rodents, such as anxiety, memory, exploration, and depression. It consists of a transparent plexiglass cube measuring 75 cm × 75 cm × 40 cm, with a marked floor divided into 25 boxes, each measuring 15 cm × 15 cm. The central area is a 30 cm × 30 cm square. During the test, mice are placed in the center of the apparatus and allowed to explore for a 10-minute session(Crupi *et al.*, 2010; Russo *et al.*, 2013). Several parameters were measured during the test to assess the behavior of the mice, including the total distance covered, the number of entries into the central area, the duration of time spent in the central area, the frequency of rearing (standing on hind legs), and the duration of rearing. The test is informative as it provides insights into the mouse's motor activity, anxiety levels, exploratory behavior, and cognitive functions. An increase in the time spent in the center or the number of center entries suggests anxiolytic (anti-anxiety) activity. Moreover, an increase in the frequency or duration of rearing behavior indicates heightened exploratory and cognitive behavior, as well as a reduction in anxiety. Recent research has also associated an increase in rearing behavior with potential antidepressant effects(Bee and Maheshwari, 2019).

2.6. Models for Depression

2.6.1. Forced Swim Test

The aim of the test was to assess the antidepressant effects of seed extracts on the 21st day. For the experiment, a rectangular plexiglass container measuring 46 cm × 20 cm was used. Depression was induced in mice during the initial 2-minute session using the learned helplessness phenomenon. The last 4 minutes of immobility time exhibited by the mice were recorded as an indicator of antidepressant activity(Aiello *et al.*, 2015; Planchez *et al.*, 2019). Immobility was defined as the absence of movement in mice, except for instances where mice needed to keep their heads out of the water. The percentage reduction in immobility time was used as a measure to evaluate the antidepressant effect of the extracts(Adachi *et al.*, 2022).

2.6.2. Tail Suspension Test

On the 21st day, the tail suspension method was utilized to assess the antidepressant effect. The animals were suspended upside down using tape attached to their tails for a duration of 6 minutes(Steru *et al.*, 1985). During the initial 2 minutes, depression was induced through the learned helplessness phenomenon. The immobility time observed during the last 4 minutes was indicative of antidepressant activity. Immobility time was measured by

evaluating the absence of movement in mice attempting to upright themselves. The percentage reduction in immobility time was used to gauge the degree of antidepressant effect caused by the extracts (Planchez *et al.*, 2019; Adachi *et al.*, 2022).

2.7. Statistical Analysis

The statistical analysis of the results was conducted using the SPSS statistical software package version 26. All values were presented as Mean \pm SEM (Standard Error of the Mean). To analyze the data, a one-way analysis of variance (ANOVA) was initially employed. Subsequently, a post hoc Dunnett test was conducted to compare specific groups to the control group. The significance levels for the post hoc analysis were set at $P < 0.05$ and $P < 0.1$, indicating statistically significant differences between groups.

3. Results

3.1. Effect on Memory and Learning

3.1.1. Passive Avoidance Test

Figure 1 presents findings related to the impact of *Punicagranatum* seed extract on memory and learning, assessed through the Passive Avoidance Test (PAT). The 50 mg/kg dose of *Punicagranatum* showed a significant increase in latency time on the 8th day. The 100 mg/kg dose displayed a notable increase in reaction time on the 8th day and the 21st day. Furthermore, the 200 mg/kg dose resulted in a significant increase in latency time on the 21st day, and remarkably, an extremely significant increase on the 8th day. In contrast, the administration of diazepam at 3 mg/kg led to a significant decrease in latency time on both the 8th and 21st days. Conversely, imipramine at 30 mg/kg showed a significant increase in latency time on the 8th and 21st days.

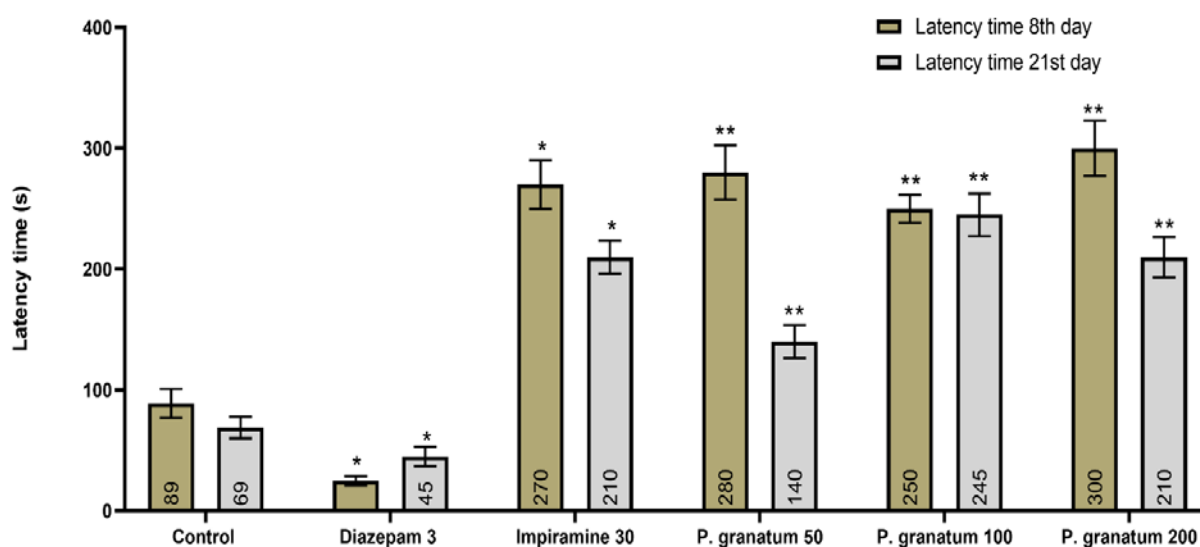


Figure 1: Impact of *Punica granatum* seeds' extract on memory (passive avoidance test). * $P < 0.05$, indicating a substantial difference compared to the control group, and ** $P < 0.01$, indicating a highly substantial difference compared to the control group.

3.1.2. Water Maze Test

Figure 2 presents the effects of *Punicagranatum* seed extract on memory and learning, as evaluated through the water maze test. The results indicated that doses of *Punicagranatum* at 50 mg/kg and 100 mg/kg significantly reduced the time taken to reach the central hidden stage on the 8th day and the time taken to reach the central stage on the 21st day. Moreover, the 200 mg/kg dose of *Punicagranatum* also led to a significant reduction in the

time to reach the stage on the 8th day and a substantial reduction on the 21st day. Conversely, the group treated with Diazepam at 3 mg/kg showed a significant increase in the time taken to reach the central hidden stage on both the 8th and 21st days. Meanwhile, the group given imipramine at 30 mg/kg exhibited a notable decrease in the time taken to reach the central hidden stage on the 8th and 21st days, compared to the untreated group.

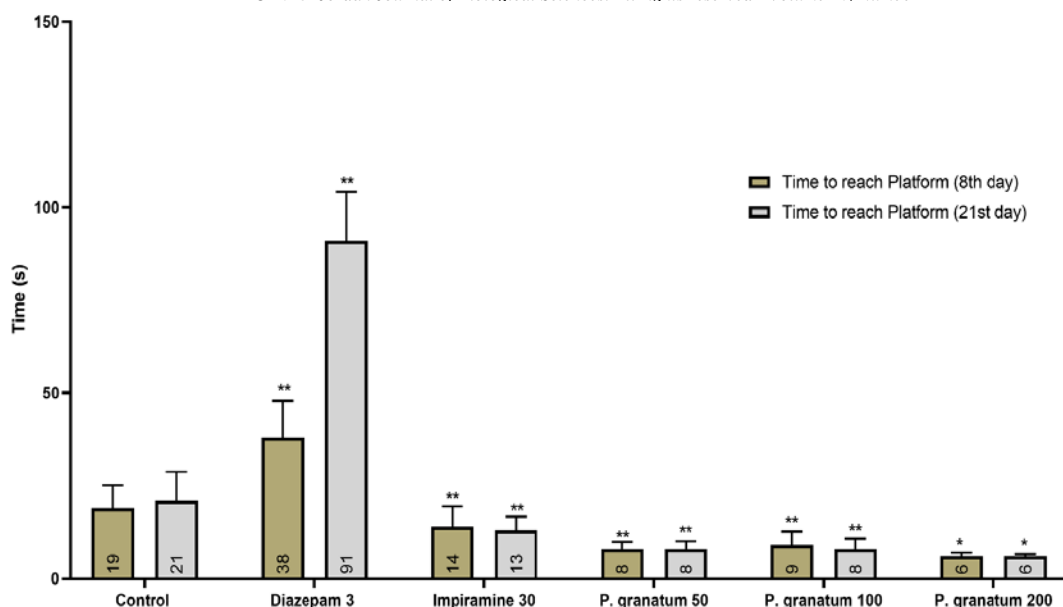


Figure 2: Impact of *Punica granatum* seeds' extract on the memory (water maze test). *P < 0.05, indicating a substantial difference compared to the control group, and **P < 0.01, indicating a highly substantial difference compared to the control group.

3.2. Effects on Motor Coordination and Motor Skilled Learning

3.3.1. Rotarod Test

According to table 1, the administration of Punicagranatum at doses of 100 mg/kg and 200 mg/kg resulted in a significant increase in fall time on the 21st day at low speed. Additionally, these Punicagranatum groups exhibited a highly significant increase in fall time on both the 8th and 21st days at high speed, in comparison to the untreated mice.

Table 1. Impact of *Punica granatum* seeds' extract on motor coordination by rotarod.

Groups/doses (mg/kg)	Fall time(s) on 10 rpm		Fall time(s) on 30 rpm	
	8 th day	21 st day	8 th day	21 st day
n=10				
Control	131.5 ± 5.3	121.5 ± 8.1	7.35 ± 1.1	5.22 ± 0.4
<i>P. granatum</i> 50mg/kg	152.2 ± 6.7	157.3 ± 7.9	22.1 ± 1.4**	28.3 ± 1.3**
<i>P. granatum</i> 100mg/kg	169.1 ± 7.2	172.1 ± 9.3*	26.4 ± 0.9**	29.9 ± 2.7**
<i>P. granatum</i> 200mg/kg	162.2 ± 4.9	163.4 ± 7.4*	36.1 ± 1.7**	36.5 ± 3.1**
Diazepam 3mg/kg	20.4 ± 2.1*	37.3 ± 3.2**	5.1 ± 0.3*	4.8 ± 0.5**
Imipramine 30mg/kg	128.1 ± 6.3	150.1 ± 5.3	27.4 ± 1.4*	29.3 ± 2.5**

The results were reported as average ± SEM (Standard Error of the Mean). The statistical significance was denoted as follows: *P < 0.05, indicating a substantial difference compared to the control group, and **P < 0.01, indicating a highly substantial difference compared to the control group.

On the other hand, Diazepam at 3 mg/kg demonstrated a highly significant reduction in fall time on the 8th day at both speeds (rpm), and there was also a highly significant reduction in fall time on the 21st day at both speeds.

Furthermore, imipramine at 20 mg/kg showed a highly significant increase in fall time on both the 8th and 21st days at high speed.

3.3.2. Stationary Rod Test

Figure 3 provides insights into the effects of *Punicagranatum* seed extract on memory and learning, evaluated through the Stationary Rod Test. The group administered *Punicagranatum* at a dose of 50 mg/kg showed a significant reduction in the time taken to reach the elevated stage on the 8th day, and a substantial reduction on the 21st day. Similarly, the group receiving *Punicagranatum* at a dose of 100 mg/kg exhibited a highly significant reduction in the time to achieve the elevated stage on both the 8th and 21st days.

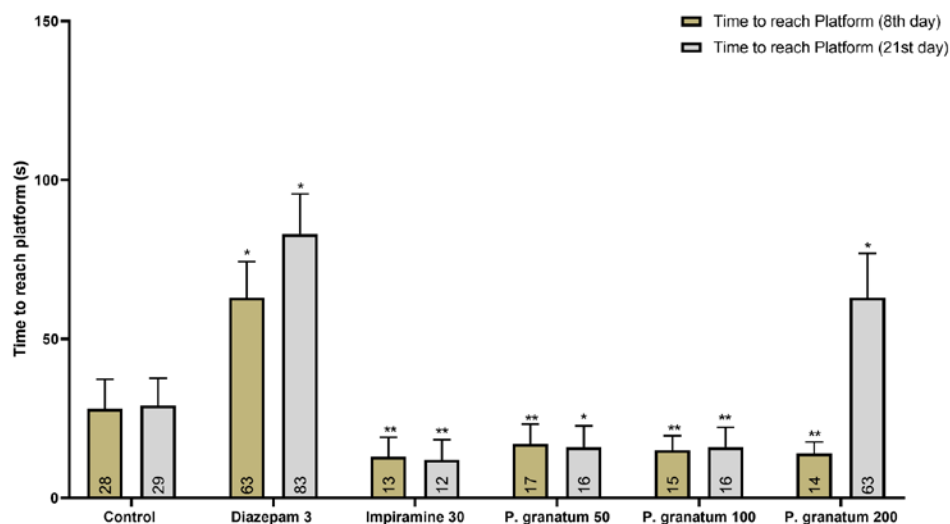


Figure 3: Impact of *Punica granatum* seeds extract on motor skilled learning and memory (stationary rod). * $P < 0.05$, indicating a substantial difference compared to the control group, and ** $P < 0.01$, indicating a highly substantial difference compared to the control group.

In contrast, *Punicagranatum* at a dose of 200 mg/kg showed a significant reduction in the time to reach the stage on the 8th day but a notable increase in the time to reach the stage on the 21st day, in comparison to the reference group.

Animals treated with diazepam at 3 mg/kg demonstrated a substantial increase in the time taken to reach the elevated stage on both the 8th and 21st days, while those given imipramine at 30 mg/kg exhibited a significant reduction in the time to reach the elevated stage on both the 8th and 21st days, compared to the control group.

3.4. Effect on Anxiety

3.4.1. Light and Dark Model

In terms of the effects on anxiety, table 2 presents information on the impact of *Punicagranatum* seed extract in the light and dark models.

Punica granatum seed extract at a dose of 50 mg/kg demonstrated a highly significant increase in transitions on the 8th and 21st days, and it also exhibited a significantly increased percentage of time spent in the light area on the 21st day compared to the reference group.

Punicagranatum at doses of 100 and 200 mg/kg showed an extremely substantial increase in the percentage of time spent in the light area on both the 8th and 21st days. Furthermore, the group administered *Punicagranatum* at a dose of 100 mg/kg demonstrated a highly significant increase in transitions on the 8th day compared to the untreated group.

Animals treated with diazepam at 3 mg/kg exhibited a greatly substantial increase in the percentage of time spent in the light area and transitions on both the 8th and 21st days.

Additionally, animals given imipramine at 30 mg/kg showed a significant increase in transitions on the 8th day.

These results suggest that *Punicagranatum* seed extract may have anxiolytic effects, as indicated by increased time spent in the light area and increased transitions, particularly at higher doses. Diazepam also demonstrated

anxiolytic effects, while imipramine showed mixed effects on anxiety-related behaviors.

Table 2. The impact of *Punica granatum* seeds' extract on anxiety by light and dark model.

Groups/doses (mg/kg)	Number of transition		Time in light (%)	
	8 th day	21 st day	8 th day	21 st day
n=10				
Control	1.4 ± 0.3	2.2 ± 0.4	6.3 ± 0.9	9.5 ± 1.3
<i>P. granatum</i> 50mg/kg	5.8 ± 0.7**	6.6 ± 1.1**	32.2 ± 5.1	37.7 ± 2.1**
<i>P. granatum</i> 100mg/kg	4.5 ± 0.4**	4.4 ± 0.5	54.4 ± 4.7**	51.5 ± 5.1**
<i>P. granatum</i> 200mg/kg	3.4 ± 0.4	3.2 ± 0.3	39.4 ± 6.5**	40.2 ± 3.2**
Diazepam 3mg/kg	4.8 ± 0.5	0.9 ± 0.4	27.7 ± 3.1**	49.9 ± 4.9**
Imipramine 30mg/kg	5.1 ± 0.7*	3.2 ± 0.7	12.1 ± 1.5	7.2 ± 1.2

The results were reported as average ± SEM (Standard Error of the Mean). The statistical significance was denoted as follows: * $P < 0.05$, indicating a substantial difference compared to the control group, and ** $P < 0.01$, indicating a highly substantial difference compared to the control group.

3.4.2. Elevated plus Maze

Table 3 presents the findings regarding the impact of *Punicagranatum* seed extracts on anxiety using the elevated plus maze test.

The administration of *Punicagranatum* at doses of 100 and 200 mg/kg resulted in a highly significant and significant increase in the amount of time spent in the open area on the 8th and 21st days, respectively. Moreover, these two groups displayed a significant increase in transitions on the 8th day. Additionally, the 100 and 200 mg/kg doses exhibited a significantly reduced amount of time spent in the closed arms on the 8th and 21st days, respectively, along with a substantial decrease in transitions. Furthermore, the anxiety index was notably reduced on the 8th and 21st days with the administration of *Punicagranatum* at 100 and 200 mg/kg, respectively.

Table 3. The impact of *Punica granatum* seeds' extract on anxiety (elevated plus maze).

Groups/doses (mg/kg)	Open arm's time (seconds)		Closed arm's time (seconds)		Closed-arm entries (times)		Open arm entries (times)		Anxiety index	
	8 th day	21 st day	8 th day	21 st day	8 th day	21 st day	8 th day	21 st day	8 th day	21 st day
n=10										
Control	10 ± 1.4	25 ± 4.1	290 ± 33.2	275 ± 31.7	2.5 ± 0.3	3.9 ± 1.1	3.5 ± 0.5	3.7 ± 0.6	0.73	0.69
<i>P. granatum</i> 50mg/kg	60 ± 6.2	20 ± 2.1	240 ± 18.7	280 ± 13.1	4.1 ± 0.7	3.1 ± 0.3	7.1 ± 0.8	3.9 ± 0.8	0.51	0.75
<i>P. granatum</i> 100mg/kg	182 ± 18**	85 ± 5.6*	118 ± 11.2**	215 ± 20.2*	4.2 ± 0.2	4.1 ± 0.6	9.1 ± 0.8**	6.7 ± 0.9	0.32	0.58
<i>P. granatum</i> 200mg/kg	208 ± 23**	89 ± 9.2*	92 ± 7.2**	211 ± 22.1*	2.6 ± 0.2	4.5 ± 0.5	8.1 ± 0.6**	8.5 ± 0.7	0.31	0.49
Diazepam 3mg/kg	175 ± 32.1**	197 ± 22.1**	125 ± 8.3**	103 ± 9.5**	2.7 ± 0.3	5.3 ± 0.4*	4.9 ± 0.5	9.1 ± 1.1*	0.48	0.26
Imipramine 30mg/kg	30 ± 5.1	42 ± 13.3	270 ± 24.7	258 ± 15.6	4.9 ± 0.6	4.8 ± 0.3	6.2 ± 0.3	7.2 ± 0.7	0.6	0.68

The results were reported as average ± SEM (Standard Error of the Mean). The statistical significance was denoted as follows: *P < 0.05, indicating a substantial difference compared to the control group, and **P < 0.01, indicating a highly substantial difference compared to the control group.

Animals treated with diazepam at a dose of 3 mg/kg showed a significantly higher amount of time spent in the open arm on the 8th and 21st days, while also displaying an increased number of transitions on the 21st day.

Imipramine at a dose of 30 mg/kg resulted in an increased amount of time spent in the open arm compared to the reference group.

Overall, the seed extract of *Punicagranatum* at doses of 100 and 200 mg/kg on the 8th day exhibited a significant reduction in the anxiety index, following the established standard. The effects of *Punicagranatum* seed extracts on anxiety using the elevated plus maze test were summarized in Table 6.

3.4.3. Head Dip Test

Table 4 provides a summary of the impact of *Punicagranatum* seed extract on the number of head dips.

The administration of *Punicagranatum* at a dosage of 100 mg/kg resulted in a highly significant decrease in the number of head dips on the 21st day. Similarly, the group receiving *Punicagranatum* at a dosage of 200 mg/kg exhibited an extremely substantial reduction in head dips on both the 8th and 21st days.

Animals treated with diazepam at a dosage of 3 mg/kg showed a significant reduction in head dips on the 8th day, as well as a greatly substantial reduction on the 21st day.

Furthermore, animals administered imipramine at a dosage of 30 mg/kg demonstrated a highly significant reduction in head dips compared to the untreated group.

These results suggest that *Punicagranatum* seed extract may have an effect on exploratory behavior, as indicated by the reduction in head dips. Diazepam and imipramine also showed significant effects on head dipping behavior in the mice.

Table 4. The impact of *Punica granatum* seeds' extract on head dips.

Groups/doses (mg/kg)	Number of head dips	
	8 th day	21 st day
n=10		
Control	32.1 ± 1.3	30.3 ± 1.2
<i>P. granatum</i> 50mg/kg	27.8 ± 1.7	26.3 ± 0.9
<i>P. granatum</i> 100mg/kg	25.3 ± 1.3	16.2 ± 0.4**
<i>P. granatum</i> 200mg/kg	23.4 ± 1.8*	16.7 ± 0.7**
Diazepam 3mg/kg	40.5 ± 1.5*	22.2 ± 0.8**
Imipramine 30mg/kg	20.1 ± 1.3**	16.3 ± 0.3**

The results were reported as average ± SEM (Standard Error of the Mean). The statistical significance was denoted as follows: *P < 0.05, indicating a substantial difference compared to the control group, and **P < 0.01, indicating a highly substantial difference compared to the control group.

3.4.4. Open Field Test

Table 5 presents the effects of *Punicagranatum* seed extract on anxiety using the open field test (OFT).

When administered at a dose of 50 mg/kg, *Punicagranatum* showed a highly significant increase in the total distance traveled on the 8th day. Additionally, there were significant and highly significant increases in center entries on the 8th and 21st days, respectively. Moreover, the duration of rearing exhibited significant and highly significant increments on the 8th and 21st days compared to the reference group.

Punicagranatum at doses of 100 and 200 mg/kg demonstrated an extremely substantial increase in the total distance traveled on the 8th day. Furthermore, there were highly significant increments in center entries, center time, as well as the number and duration of rearing on both the 8th and 21st.

Animals treated with diazepam at a dose of 3 mg/kg displayed a significant reduction in the total distance traveled on the 21st day. Additionally, there was a highly significant increase in center entries and center time on the 21st day, along with a significant reduction in the number and duration of rearing.

Imipramine at a dose of 30 mg/kg exhibited an extremely significant reduction in center entries on the 21st day, and an extremely significant increase in the number of rearing on both the 8th and 21st days.

Table 5. Outcome of *Punica granatum* seeds' extract in open field test.

Groups/doses (mg/kg)	Total distance travelled (cm)		No. of center entries		Centre time(s)		No. of rearing		Duration of rearing (s)	
	8 th day	21 st day	8 th day	21 st day	8 th day	21 st day	8 th day	21 st day	8 th day	21 st day
n=10										
Control	1910 ± 75	2311 ± 20	2.5 ± 0.2	2.6 ± 0.2	3.1 ± 0.4	3.2 ± 0.4	4.1 ± 0.3	10 ± 0.9	4.4 ± 0.2	12 ± 0.8
<i>P. granatum</i> 50mg/kg	3025 ± 18**	2150 ± 16	5.6 ± 0.3*	8.3 ± 0.7**	4.9 ± 0.9	7.5 ± 1.3	5.1 ± 0.8	11 ± 0.8	15.1 ± 1.3**	20.5 ± 1.4*
<i>P. granatum</i> 100mg/kg	2701 ± 30*	2480 ± 22	7.1 ± 0.9**	8.9 ± 0.8**	13.4 ± 1.2**	14.1 ± 0.8**	15.2 ± 1.2**	22.1 ± 1.3**	16.2 ± 0.8*	30.1 ± 2.2**
<i>P. granatum</i> 200mg/kg	2855 ± 21**	2472 ± 30	6.9 ± 0.8**	10.5 ± 1.1**	14.3 ± 0.9**	18.1 ± 0.7**	22.3 ± 2.1**	22.4 ± 2.4**	13.5 ± 1.2**	31.3 ± 4.2**
Diazepam 3mg/kg	2533 ± 25	1387 ± 18*	6.4 ± 0.4	11.1 ± 1.3**	5.2 ± 0.3	18.1 ± 0.7**	3.1 ± 0.1	2.2 ± 0.3**	3.1 ± 0.2	6.5 ± 0.8*
Imipramine 30mg/kg	1871 ± 17	1618 ± 19	3.2 ± 0.2	5.9 ± 0.6**	4.3 ± 0.2	21.2 ± 1.9**	14.2 ± 1.1**	18.9 ± 1.2**	9.2 ± 1.1	12.1 ± 2.4

The results were reported as average ± SEM (Standard Error of the Mean). The statistical significance was denoted as follows: *P < 0.05, indicating a substantial difference compared to the control group, and **P < 0.01, indicating a highly substantial difference compared to the control group.

3.5. Effect on Depression

Two models were utilized in the assessment of the antidepressant research. In the course of this evaluation, all the mice involved in the study demonstrated survival. Not a single mouse experienced drowning when subjected to the forced swim test or the tail flick method.

3.5.1. Forced Swim Test

Table 6 presents the findings regarding the impact of *Punicagranatum* seed extract on immobility time in the forced swim test (FST) as a measure of antidepressant activity.

Punica granatum seed extract at doses of 50, 100, and 200 mg/kg exhibited remarkably significant reductions in immobility time on the 21st day, resulting in percentage reductions of 22%, 29%, and 40%, respectively, compared to the untreated group.

Furthermore, imipramine at a dose of 30 mg/kg displayed the highest antidepressant activity among the

treatments, with a 47% reduction in immobility time compared to the control group in the forced swim test (FST).

3.5.2. Tail Suspension Test

Table 6 presents the findings regarding the impact of *Punicagranatum* seed extract on immobility time in the forced swim test (FST) as a measure of antidepressant activity.

In comparison to the control group, *Punica granatum* seed extract at doses of 50, 100, and 200 mg/kg exhibited highly significant reductions in immobility time on the 21st day. The percent reduction in immobility time was measured at 25%, 27%, and 37%, respectively.

Similarly, Imipramine administered at a dose of 30 mg/kg demonstrated an extremely substantial reduction in immobility time, reaching a percent reduction of 47% on the 21st day when compared to the reference group.

Table 6. Effect of *Punica granatum* seeds' extract on depression by forced swim test and tail suspension test.

Groups/doses (mg/kg)	Forced swim test		Tail suspension test	
	Immobility time (seconds) 21 st day	Reduction immobility (%)	Immobility time (seconds) 21 st day	Reduction immobility (%)
n=10				
Control	199 ± 3.1	-----	209 ± 5.3	-----
<i>P. granatum</i> 50mg/kg	155 ± 8.1**	22	156 ± 2.1**	25
<i>P. granatum</i> 100mg/kg	143 ± 7.1**	29	153 ± 2.7**	27
<i>P. granatum</i> 200mg/kg	120 ± 6.1**	40	132 ± 4.3**	37
Diazepam 3mg/kg	210 ± 12.3	6	220 ± 5.2	5
Imipramine 30mg/kg	105 ± 7.3**	47	110 ± 6.6**	47

The results were reported as average ± SEM (Standard Error of the Mean). The statistical significance was denoted as follows: *P < 0.05, indicating a substantial difference compared to the control group, and **P < 0.01, indicating a highly substantial difference compared to the control group.

4. Discussion

Herbal medicines are becoming increasingly important in the prevention and treatment of various disorders due to their rich content of secondary metabolites. In this context, the present study aimed to explore the pharmacological potential of *Punicagranatum* seeds. The focus was on its ability to alleviate anxiety and depression, as well as its impact on memory improvement.

To assess the antidepressant effects of *Punicagranatum* seeds in mice, the forced swimming and tail suspension tests were employed. The results showed that the extracts demonstrated their most potent antidepressant effects at a dose of 200 mg/kg, comparable to the effects of imipramine, a well-known antidepressant medication. This positive impact could be attributed to the presence of active metabolites like polyphenols and β -carotene, which are known to influence the central nervous system and play a role in alleviating depressive symptoms. These findings suggest the potential of *Punicagranatum* as a natural alternative for treating depression. (CNS)(Kistlera *et al.*, 2015).

According to Bekir *et al.*, (2013), the ethanol seeds of *Punica granatum* seeds extract has been identified as a cholinesterase inhibitor, implying its potential to provide neuroprotective effects. This is significant as cholinesterase is associated with cognitive impairment through the breakdown of acetylcholine. Increased acetylcholinesterase (AChE) activity in the brain accelerates acetylcholine breakdown, elevating the risk of dementia progression. As a result, there is growing interest in developing cholinesterase inhibitors to manage cognitive impairment. In addition, there is a desire for agents that inhibit butyrylcholinesterase (BChE) activity in humans. The disruption of monoaminergic neurotransmission by monoamine oxidase (MAO) inhibitors has been linked to neurodegenerative diseases such as Parkinson's and Alzheimer's (Youdim and Riederer, 2004; Bolea *et al.*, 2013). Therefore, the inhibition of MAO activities through suitable agents, particularly from plants, presents a potentially beneficial therapeutic approach for addressing cognitive impairment. Prior studies have consistently demonstrated the significant inhibitory effects of plant extracts on MAO activity. The present study suggests that the tested *Punicagranatum* extracts may also possess this ability to inhibit MAO activity (Yildiz *et al.*, 2014), thus contributing to their potential neuroprotective properties. These findings underscore the promise of *Punicagranatum* as a natural source for the development of neuroprotective compounds.

In a study conducted by Arora *et al.*, (2020), *Cucurbita moschata* seed extracts exhibited significant anxiolytic activity at a dose of 200 mg/kg. This effect was comparable to the standard drug alprazolam in both experimental models. Furthermore, the ethanol seeds at the same dose led to changes in motor coordination. The suggested mechanism for these effects was an increase in chloride ion influx, indicating a potential involvement of γ -Aminobutyric acid type A (GABAA) receptors in the extracts' action. Given these findings, it is reasonable to speculate that *Punica granatum* seeds might produce a similar pattern of effects, potentially showing anxiolytic

properties and influencing motor coordination. Yet, this needs more investigation.

The memory-suppressing impact of antidepressant and anxiolytic medications has been previously noted (Nicolas and Ruby, 2020). The focus has shifted towards exploring alternative treatments that offer beneficial outcomes without undesirable consequences. Thus, this particular investigation sought to assess the cognitive-enhancing properties of *Punica granatum* seeds through three distinct models: the stationary rod, passive avoidance, and water maze tests. In all three models employed, the seeds derived from *Punica granatum* seeds displayed a noteworthy improvement in memory retrieval, both in the short-term and long-term, when compared to the control group.

Punica granatum seeds widely recognized for its effectiveness in improving various diseases, primarily due to the presence of diverse secondary polyphenolic compounds like quercetin (Saparbekova *et al.*, 2023). These metabolites have been attributed to multiple biological activities associated with *Punicagranatum* seeds. Notably, *Punica granatum* seeds exhibits strong antioxidant properties, which can be attributed to its significant content of β -carotene. This compound not only boosts immunity but also helps reduce the risk of developing conditions like cancer and the progression of heart disease.

Previous research has indicated the potential benefits of utilizing pomegranate peel to enhance cognitive functions and provide neuroprotection (Adiga *et al.*, 2010; Harakeh *et al.*, 2020). For instance, in a study conducted by Adiga *et al.* (2010), supplementation of rat diets with pomegranate peel seeds (at a dosage of 100 mg/kg) for a duration of two weeks resulted in improved spatial learning and memory, even in the presence of impairment caused by diazepam. Similarly, Harakeh *et al.* (2020) found that administering a solution of pomegranate peel seeds (at a dosage of 50 mg/kg) along with ellagic acid for a period of four weeks led to improvements in memory deficits and degenerative changes in a rat model of Alzheimer's disease induced by $AlCl_3$. Another study conducted by H. Ahmed *et al.*, (2014) demonstrated that pomegranate seeds at dosages of 100 and 200 mg/kg exhibited cognitive-enhancing effects, potentially through the reduction of Amyloid- β Precursor (A β) aggregates in the hippocampus. Additionally, Fatima *et al.* (2017), demonstrated that oral consumption of *Punica granatum* seeds at a dosage of 500 mg/kg showed ameliorating effects on scopolamine-induced cognitive dysfunction, particularly in the passive avoidance response.

Although the findings of this study are of value, some have limitations that should be mentioned. The results of this study are behavioral observations; some markers should be measured in the brain homogenate such as biogenic amines to validate the effect of seeds extract on these markers. Also, same group of mice were assessed at two different time points, different group should be assessed at each time point.

5. Conclusion

This study sheds light on the considerable potential of *Punicagranatum* seeds in addressing neurological concerns. Not only do they offer relief from anxiety and depression, but they also bolster memory function. These

outcomes are possibly due to the seeds' abundance in bioactive compounds.

6. Future work and recommendations

While this research has shown promising results, it would be beneficial to extend the experiments to a more diverse group of test subjects. This includes different age groups, ethnic backgrounds, and health conditions, to ascertain the universality of the benefits. Furthermore, a longitudinal study observing the prolonged intake of Punica granatum seeds and its impact on neurological functions would offer insights into its long-term benefits and potential side effects. Moreover, comparing the effects of Punica granatum seeds with established pharmaceutical treatments for anxiety, depression, and memory-related issues will help to contextualize their efficacy in the broader medical landscape. Additionally, it would help to investigate if combining Punica granatum seeds with other natural remedies can enhance or modify their neurological benefits.

7. Data Availability

The supporting data for this research article can be obtained by making a reasonable request to either the corresponding author or the first author of the study.

8. Ethical Approval

This study received approval from the Institutional Review Board at the Hashemite University, Zarqa, Jordan, with the assigned approval number IRB No.: 18/2020/2021.

9. Conflicts of Interest

The authors of this research article declare that they have no conflicting interests.

References

- Adachi, N. *et al.* (2022) 'Kamikihito rescued depressive-like behaviors and hippocampus neurogenesis in chronic restraint stress rats', *J. Tradit. Complement. Med.*, 12(2), pp. 172–179. Available at: <https://doi.org/10.1016/J.JTCME.2021.08.001>.
- Adiga, S. *et al.* (2010) 'Effect of Punica granatum peel extract on learning and memory in rats', *Asian Pac. J. Trop. Med.*, 3(9), pp. 687–690. Available at: [https://doi.org/10.1016/S1995-7645\(10\)60166-6](https://doi.org/10.1016/S1995-7645(10)60166-6).
- Aiello, M. *et al.* (2015) 'Relationship between simultaneously acquired resting-state regional cerebral glucose metabolism and functional MRI: A PET/MR hybrid scanner study', *Neuroimage*, 113, pp. 111–121. Available at: <https://doi.org/10.1016/J.NEUROIMAGE.2015.03.017>.
- Arora, I. *et al.* (2020) 'Study of anxiolytic and motor coordination activity of Cucurbita moschata and its possible mechanism through GABA receptors', *Obes. Med.*, 18, p. 100204. Available at: <https://doi.org/10.1016/J.OBMED.2020.100204>.
- Asgharzade, S., Rabiei, Z. and Rafieian-Kopaei, M. (2015) 'Effects of Matricaria chamomilla extract on motor coordination impairment induced by scopolamine in rats', *Asian Pac. J. Trop. Biomed.*, 5(10), pp. 829–833. Available at: <https://doi.org/10.1016/J.APJT.2015.06.006>.
- Bee, R. and Maheshwari, K.K. (2019) 'Evaluation of antidepressant activity of acyranthosperaby using open field test in rats', *World J. Pharm. Res.* www.wjpr.net, 8, p. 1183. Available at: <https://doi.org/10.20959/wjpr20196-14912>.
- Bekir, J. *et al.* (2013) 'Assessment of antioxidant, anti-inflammatory, anti-cholinesterase and cytotoxic activities of pomegranate (Punica granatum) leaves', *Food Chem. Toxicol.*, 55, pp. 470–475. Available at: <https://doi.org/10.1016/J.FCT.2013.01.036>.
- Bolea, I., Gella, A. and Unzeta, M. (2013) 'Propargylamine-derived multitarget-directed ligands: Fighting Alzheimer's disease with monoamine oxidase inhibitors', *J. Neural Transm.*, 120(6), pp. 893–902. Available at: <https://doi.org/10.1007/S00702-012-0948-Y/FIGURES/6>.
- Bourin, M. and Hascoët, M. (2003) 'The mouse light/dark box test', *Eur. J. Pharmacol.*, 463(1–3), pp. 55–65. Available at: [https://doi.org/10.1016/S0014-2999\(03\)01274-3](https://doi.org/10.1016/S0014-2999(03)01274-3).
- Cheng, L. *et al.* (2013) 'Evaluation of anxiolytic-like effect of aqueous extract of asparagus stem in mice', *J. Evid Based Complementary Altern Med.*, 2013. Available at: <https://doi.org/10.1155/2013/587260>.
- Cho, J. *et al.* (2003) 'Antioxidant and memory enhancing effects of purple sweet potato anthocyanin and cordyceps mushroom extract', *Arch. Pharm. Res.*, 26(10), pp. 821–825. Available at: <https://doi.org/10.1007/BF02980027/METRICS>.
- Contreras, C.M. *et al.* (2014) 'Myristic Acid Produces Anxiolytic-Like Effects in Wistar Rats in the Elevated Plus Maze', *Biomed Res. Int.*, 2014. Available at: <https://doi.org/10.1155/2014/492141>.
- Crupi, R. *et al.* (2010) 'Melatonin treatment mimics the antidepressant action in chronic corticosterone-treated mice', *J. Pineal Res.*, 49(2), pp. 123–129. Available at: <https://doi.org/10.1111/J.1600-079X.2010.00775.X>.
- Dumlu, M.U. and Gürkan, E. (2007) 'Elemental and Nutritional Analysis of Punica granatum from Turkey', <https://home.liebertpub.com/jmf>, 10(2), pp. 392–395. Available at: <https://doi.org/10.1089/JMF.2006.295>.
- Elfalleh, W. *et al.* (2011) 'Fatty acids from Tunisian and Chinese pomegranate (Punica granatum L.) seeds', 62(3), pp. 200–206. Available at: <https://doi.org/10.3109/09637486.2010.526932>.
- Fatima, F. *et al.* (2017) 'A study of the neuroprotective role of Punica granatum and rosuvastatin in scopolamine induced cognitive deficit in rats', *Int J Basic Clin Pharmacol.*, 6(7), p. 1773. Available at: <https://doi.org/10.18203/2319-2003.ijbcp20172747>.
- Fourati, M. *et al.* (2020) 'Bioactive Compounds and Pharmacological Potential of Pomegranate (Punica granatum) Seeds - A Review', *Plant Foods Hum Nutr.*, 75(4), pp. 477–486. Available at: <https://doi.org/10.1007/S11130-020-00863-7/TABLES/1>.
- Gallivan, L.M. and Schmitzer-Torbert, N. (2018) 'A Low-Cost Morris Water Maze for Undergraduate Research: Construction and Demonstration in a Rat Model of Obesity-Induced Diabetes', *J. Undergrad. Neurosci. Educ.*, 16(2), p. A143. Available at: <https://pmc/articles/PMC6057760/> (Accessed: 5 July 2023).
- Guerrera, M.P., Volpe, S.L. and Mao, J.J. (2009) 'Therapeutic Uses of Magnesium', *Am Fam Physician.*, 80(2), pp. 157–162. Available at: <https://www.aafp.org/pubs/afp/issues/2009/0715/p157.html> (Accessed: 5 July 2023).

- H. Ahmed, A. *et al.* (2014) 'Pomegranate Extract Modulates Processing of Amyloid- β Precursor Protein in an Aged Alzheimer Disease Animal Model', *Curr. Alzheimer Res.*, 11(9), 834-843. Available at: <https://doi.org/10.2174/1567205011666141001115348>.
- Harakeh, S. *et al.* (2020) 'Pomegranate peel extract lessens histopathologic changes and restores antioxidant homeostasis in the hippocampus of rats with aluminium chloride-induced Alzheimer's disease', *Asian Pac. J. Trop. Med.*, 13(10), pp. 456-463. Available at: <https://doi.org/10.4103/1995-7645.291039>.
- Kistler, L. *et al.* (2015) 'Gourds and squashes (*Cucurbita* spp.) adapted to megafaunal extinction and ecological anachronism through domestication', *Proc. Natl. Acad. Sci. U.S.A.*, 112(49), pp. 15107-15112. Available at: https://doi.org/10.1073/PNAS.1516109112/SUPPL_FILE/PNAS.1516109112.SD04.RTF.
- Kliethermes, C.L. and Crabbe, J.C. (2006) 'Pharmacological and genetic influences on hole-board behaviors in mice', *Pharmacol Biochem Behav.*, 85(1), pp. 57-65. Available at: <https://doi.org/10.1016/J.PBB.2006.07.007>.
- Lundquist, A.J. *et al.* (2022) 'Knockdown of Astrocytic Monocarboxylate Transporter 4 in the Motor Cortex Leads to Loss of Dendritic Spines and a Deficit in Motor Learning', *Mol. Neurobiol.*, 59(2), pp. 1002-1017. Available at: <https://doi.org/10.1007/S12035-021-02651-Z/FIGURES/7>.
- Nicolas, A. and Ruby, P.M. (2020) 'Dreams, Sleep, and Psychotropic Drugs', *Front. Neurol.*, 11, p. 507495. Available at: <https://doi.org/10.3389/FNEUR.2020.507495/BIBTEX>.
- O'Lunaigh, C. and Lawlor, B. (2008) 'Drugs that affect competence', *Competence Assessment in Dementia*, pp. 41-50. Available at: https://doi.org/10.1007/978-3-211-72369-2_5/COVER.
- Okano, H., Hirano, T. and Balaban, E. (2000) 'Learning and memory', *Proc. Natl. Acad. Sci. U.S.A.*, 97(23), pp. 12403-12404. Available at: <https://doi.org/10.1073/PNAS.210381897>.
- Planchez, B., Surget, A. and Belzung, C. (2019) 'Animal models of major depression: drawbacks and challenges', *J. Neural Transm.* 2019 126:11, 126(11), pp. 1383-1408. Available at: <https://doi.org/10.1007/S00702-019-02084-Y>.
- Podolan, M. *et al.* (2019) 'A single injection of imipramine affected proliferation in the hippocampus of adult Swiss mice depending on the route of administration, doses, survival time and lodging conditions', *J. Chem. Neuroanat.*, 100, p. 101655. Available at: <https://doi.org/10.1016/J.JCHEMNEU.2019.101655>.
- Rihmer, Z. and Gonda, X. (2011) 'Antidepressant-resistant depression and antidepressant-associated suicidal behaviour: The role of underlying bipolarity', *Depress Res Treat.*, 2011. Available at: <https://doi.org/10.1155/2011/906462>.
- Russo, E. *et al.* (2013) 'Lamotrigine positively affects the development of psychiatric comorbidity in epileptic animals, while psychiatric comorbidity aggravates seizures', *Epilepsy Behav.*, 28(2), pp. 232-240. Available at: <https://doi.org/10.1016/J.YEBEH.2013.05.002>.
- Saparbekova, A.A. *et al.* (2023) 'Potential of phenolic compounds from pomegranate (*Punica granatum* L.) by-product with significant antioxidant and therapeutic effects: A narrative review', *Saudi J. Biol. Sci.*, 30(2), p. 103553. Available at: <https://doi.org/10.1016/J.SJBS.2022.103553>.
- Solangi, M.A. and Najam, R. (2013) 'A review of pharmacognostical, phytochemical and pharmacological properties of *Lagenaria siceraria*: a miracle herb.', *Int. j. biomed. adv. res.*, 4(5), pp. 266-274.
- Steru, L. *et al.* (1985) 'The tail suspension test: A new method for screening antidepressants in mice', *J. Psychopharmacol.*, 85(3), pp. 367-370. Available at: <https://doi.org/10.1007/BF00428203/METRICS>.
- Venkata, C., Prakash, S. and Prakash, I. (2011) 'Bioactive Chemical Constituents from Pomegranate (*Punica granatum*) Juice, Seed and Peel-A Review', *Int. j. res. chem. environ.*, 1, pp. 1-18. Available at: www.ijrce.org (Accessed: 5 July 2023).
- Wiltgen, B.J. *et al.* (2006) 'Context Fear Learning in the Absence of the Hippocampus', *J. Neurosci.*, 26(20), pp. 5484-5491. Available at: <https://doi.org/10.1523/JNEUROSCI.2685-05.2006>.
- Yildiz, O. *et al.* (2014) 'Total monoamine oxidase (MAO) inhibition by chestnut honey, pollen and propolis', <http://dx.doi.org/10.3109/14756366.2013.843171>, 29(5), pp. 690-694. Available at: <https://doi.org/10.3109/14756366.2013.843171>.
- Youdim, M.B.H. and Riederer, P.F. (2004) 'A review of the mechanisms and role of monoamine oxidase inhibitors in Parkinson's disease', *Neurology*, 63(7 suppl 2), pp. S32-S35. Available at: https://doi.org/10.1212/WNL.63.7_SUPPL_2.S32.

Extraction of *Klebsiella pneumoniae* and *Candida albicans* Biofilm and Studying their Cytotoxic Effects on Human Lymphocytes

Batol Imran Dheeb^{1, *}, Sara Najim Abdulla¹, Safaa AL-Deen Ahmed Shanter AL-Qaysi², Basma M.Al-Sarraj³, Mohammed Sami Farhan⁴

¹ University of Samarra/College of Applied Sciences/Department of Pathological Analysis; ²University of Baghdad/College of Sciences (For Women)/Department of Biology; ³University of Baghdad/College of Sciences/Department of Biotechnology; ⁴University of Tikrit/College of Sciences/Department of Biology

Received: June 19, 2023; Revised: September 5, 2023; Accepted: September 10, 2023

Abstract

The microbial polymeric biofilm matrix belongs to a single microbial species or multiple microbial species that are directly or indirectly responsible for over 80% of all microbial infections. A six-month laboratory study was conducted to extract the biofilms from *Klebsiella pneumoniae* and *Candida albicans* isolates to study their properties and their toxic effects on blood lymph. The results showed that treating 20 samples of *K. pneumoniae* and 100 samples of *C. albicans* biofilms with gentamicin and fluconazole antibiotics led to the inhibition of biofilm production for all the studied isolates by 74.9% and 64.32%, respectively. The results of screening electron microscopy (SEM) showed that the diameters of some *K. pneumoniae* cells ranged from 0.18-0.47 μm , while the diameters of *C. albicans* cells ranged from 121.82-133.89 nm. Fourier-Transform Infrared Spectroscopy (FTIR) of biofilm revealed the presence of compounds in the matrix of the biofilm of *K. pneumoniae*, such as mannans and carboxylate (C=O), indicating the presence of sugar acids, proteins, and hydrocarbons. The results of the analysis of the biofilm produced by *C. albicans* showed a high percentage of sugars, as well as carboxyl and 2' acetyl. The Biofilm produced by *K. pneumoniae* inhibited the lymphocytes by 34.8% from the 150 μL sample. The lymphocytes showed higher inhibitory activity against *C. albicans* alone and against the combined biofilm of *C. albicans* and *K. pneumoniae*, where the highest percentage of inhibition reached 74.82% and 69.5% for the two treatments, respectively, at a sample volume of 100 μL . This leads to the conclusion that the biofilms of *K. pneumoniae* and *C. albicans* are responsible for over 80% of microbial infections. The use of antibiotics such as gentamicin and fluconazole led to the inhibition of biofilm production by up to 74.9% and 64.32% respectively, indicating the effectiveness of antibiotics in controlling biofilm growth.

Keywords: Human lymphocyte, Extraction, Fungal-Bacterial biofilm, scanning electron microscope, FTIR, Co-infection, *Klebsiella, candida*

1. Introduction

The respiratory system is exposed to many different diseases resulting from bacterial, viral, and fungal infections which usually occur by inhaling air through the respiratory tract. It is followed by an exudative effusion containing red and white blood cells, large phagocytic cells, fibrin, and biologically active microbes that may reach the bloodstream in sufficient numbers, causing septicemia with the possibility of metastatic abscesses in distant organs such as the brain and kidney (Nelson, 2001; Ibrahim *et al.*, 2017).

Biofilms are complex surface-attached communities of microorganisms held together by self-produced polymer matrixes mainly composed of polysaccharides, secreted proteins, and extracellular DNAs. A biofilm can consist of a single microbial species or a combination of different species of bacteria, protozoa, archaea, algae, filamentous

fungi, and yeast that could be strongly attached to each other or to biotic or abiotic surfaces (Muhammad *et al.*, 2020). The microbial biofilms by which complex microbial cells are surrounded are found in diverse locations and ecosystems (Hall-Stoodley *et al.*, 2012; Nouri *et al.*, 2015) with a very diverse potential as in biological wastewater treatment (Rassinat *et al.*, 2015; Geladari *et al.*, 2019), biotechnological productions of chemicals or drugs, and bioremediation of soils and groundwater purification processes (Flemming *et al.*, 2016; Abdullah *et al.*, 2019).

From a pathological perspective, they are behind tremendous problems in the infections and the diseases they cause to their hosts (Rather *et al.*, 2021). The human microflora, consisting of bacteria, fungi, and viruses, invariably show that they produce polymicrobial biofilms that are even more complex to manage than monomicrobial ones (Anju *et al.*, 2022, Costa-Orlandi *et al.*, 2017, Hashim *et al.*, 2023).

* Corresponding author. e-mail: Batoolmran@yahoo.com.

Polymicrobial biofilm-related infections complicate the diagnosis and treatment and cause a higher mortality rate compared to single-species biofilm infections. Particularly, infections caused by fungal-bacterial biofilms are serious public health concerns (Galdiero *et al.* 2021, Anju *et al.* 2022).

A recent review summarizes an insight into biofilm structure, diffusion, and advection, i.e. mass transport. Due to these diverse impacts and implications, biofilms are the subject of interdisciplinary research, encompassing biology, chemistry, analytics, and engineering (Herrling, 2019). However, biofilms still need to be further studied and understood. In biological systems, biofilms that produce a matrix of highly hydrated extracellular polymeric substances (EPS) cause infections with high resistance to conventional drugs (Galdero *et al.* 2021), especially those -biofilms- caused by both fungi and bacteria. Recent estimates suggest that biofilm-associated infections are directly or indirectly responsible for over 80% of all microbial infections in humans (Nobile and Johnson, 2015).

Klebsiellapneumonia species, which are Gram-negative rods, remain one of the most significant causes of bloodstream infections in patients with immunity-related issues. One of the *K. pneumoniae* several intrinsic factors responsible for its ability to cause infection is its ability to produce biofilms on medical devices. It contains two types of antigens, namely the Somatic antigen (O), and the Capsular antigen (K), segregating the strains into 8 and 88 serological patterns respectively (Greenwood *et al.*, 2007). The colonies of this bacteria are characterized by their large size, exhibiting pink color when grown on MacConkey agar due to their ability to ferment lactose, and by their mucoid consistency due to the presence of the capsule. These bacteria colonies also tend to be raised above the medium and have a regular spherical shape (Todar, 2007). The bacteria have been a major cause of death among enteric bacteria with drug-resistant cases. The biofilm forming ability allows it to colonize the host tissues and medical devices, survive in hostile environments, and resist antibiotics and host immune response (Tutelyan *et al.*, 2022).

Samples of mixed-species infections often exhibit the presence of *C. albicans* and *K. pneumoniae*, especially from those found in the bloodstream and oral infections or respiratory diseases.

Fungal infections caused by molds are a leading cause of death among immunocompromised patients (Baddley *et al.* 2003) such as aspergillosis, which is caused by the *Aspergillus* sp. Another notable fungus, *Candida* sp. causes systemic mycoses, especially in immunocompromised patients. Factors that contribute to their growth on mucosal surfaces include exposure to moisture, availability of glucose as a food source, and little competition from commensal bacteria, as well as dysfunction of epithelial and lymphoid cells (Brooks *et al.*, 2001). *C. albicans* is a member of the human digestive and reproductive flora, with a prevalence of 40% to 60% in healthy adults (Erdogan and Rao, 2015). It is usually a commensal organism but, can become pathogenic in susceptible hosts. It is one of the few *Candida* species that causes human candidiasis resulting from fungal overgrowth (Martins *et al.*, 2014; Erdogan and Rao, 2015).

Many *in vivo* and *in vitro* studies have shown that different bacteria and fungi have complex interactions in mixed-species biofilms in human health which is a phenomenon that shows how bacterial infections may play a modulatory role in fungal infections (Bandara *et al.*, 2009). Maione *et al.* (2021) pointed out that although infections associated with mixed-species biofilms including *C. albicans* and *K. pneumoniae* have certain clinical significance, the description of interactions between *C. albicans* and *K. pneumoniae* in mixed-species biofilms is limited to a few observations.

Biofilms exhibit several characteristics that are very important to their survival strategy. Some general characteristics of biofilms include three-dimensional structure, presence of one or more microbial species, adherence to each other, adhesion to surfaces, and adherence to solid/liquid, or liquid/air interfaces. Although the extracellular matrix produced by the cells forming biofilms is a critically important factor for their structural integrity, the chemistry and physiology of biofilms can fluctuate depending on the resident microbes, and the surrounding environment (McCarty *et al.*, 2014).

The nature of biofilm structure and physiological features also endow organisms with an inherent resistance to antimicrobial agents. Although the defense mechanisms of biofilms against antimicrobials are not yet clearly understood, some possible causes have been suggested by several scientists (Sánchez-Gómez *et al.*, 2015).

The current study aims to extract and study the biofilms produced by *K. pneumoniae* and *C. albicans* and to determine their effects on lymphocytes. The objective of this study was evaluating the *ex vivo* biofilm formation potential of *Candida* and *Klebsiella*, and examining the produced biofilm's toxicity toward lymphocytes.

2. Materials and Methods

A laboratory study was conducted from September/2022 to February/2023 at the laboratories of the Department of Biology, College of Science, University of Baghdad, and the University of Al-Nahrain Center/ Al-Nahrain University. This study included 120 samples.

2.1. Collection of yeast samples:

100 yeast isolates which include *C. albicans*, *C. glabrata*, *C. kefyr*, *C. krusei*, *C. parapsilosis*, *C. rangosa*, and *C. tropicalis* were collected from Al-Tib Hospital and Yarmouk Hospital in Baghdad province, all isolates were collected from individuals with respiratory diseases. The isolates were identified using biochemical, and physiological tests, and the Vitek2 Compact system (Aubertine *et al.*, 2006).

2.2. Collection of bacterial samples:

Klebsiella spp. isolates were obtained from educational laboratories in Al-Tib City/Baghdad from 20 patients admitted with infections in the respiratory system. The isolates were diagnosed using the Vitek2 Compact system (Aubertine *et al.*, 2006).

2.3. Culture and identification of isolates:

Some steps were taken to check and confirm the microbial diagnosis as follows (Ellen *et al.* 1994):

Activating isolates on agricultural media: Isolates taken from the respiratory tract of the 120 patients were cultured

and grown on solid Sabouraud Dextrose Agar (SDA). The cultured plates were incubated at 37 °C for 2-4 days. To reactivate them, three replicates were made for each isolate, and the characteristics of the surface colonies were observed included morphological characteristic shape, color, diameter, and height the growing colony on cornmeal agar, these isolates were transferred to a chromo-agar medium and incubated at 37 °C for 48–72 hours (Hospentha *et al.*, 2006). microscopical characteristic studied when staining the yeast on glass slide, mixed with a drop of lactophenol cotton blue to observe the chlamydo spores and yeast cells (Ellis *et al.*, 2007). The ability of *Candida* spp. to develop biofilms:

The ability of *Candida* isolates to develop biofilms was tested using Congo Red Agar (CRA) medium, as described by Oliveira and Cunha (2010). inoculating "young colonies at the age of 24 hrs ,SDA medium" on Concho red medium using planning method, then the culture were incubated in aerobic conditions at a temperature of 37 C for 24 hrs. biofilm-forming isolates are black color.

2.4. The ability of *Klebsiella* to develop biofilms:

The ability of *Klebsiella* spp. isolates to form biofilms were detected using the microtiter plate method according to Adriana *et al.* (2013), as follows: -

2.5. Preparation of Biofilm:

The Yeast and bacteria used in the study were stimulated by growing them on culture media. Nutrient broth with 2% sucrose and SD broth with 2% sucrose was prepared. The fungi were grown in Sabaroud broth with 2% sucrose and the bacteria were grown in Nutrient broth with 2% sucrose. Then, catheters were placed in the media to aid in the isolation of the biofilm. Incubation was carried out for 4 days at a temperature of 37 °C. The culture media was poured off and 2-3 mL of normal saline was added to dissolve the biofilm attached to the walls and bottom of the conical flask (Adriana *et al.* 2013).The biofilm suspension and normal saline were placed in closed test tubes and subjected to sonication to kill the bacteria and fungi (the bacterial suspension was sonicated for one and a half hours, while the fungal suspension was sonicated for two hours). After that, the emulsion was cultivated on the media in Step 2 to ensure that it was free of bacteria and yeasts and that there was no growth. Different volumes of biofilms (150,100,50,25) were obtained and the suspension was prepared to study their effects on lymphoid cells.

2.6. Collection of Blood Samples to isolate lymphocytes:

The source of blood was a healthy 30-year-old male donor. Ten milliliters of blood was collected into sterile 5 mL tubes containing EDTA anticoagulant, and this blood was used for isolating lymphocytes. Lymphocytes were isolated according to the method described by Rafael and Vaclav (2000). Two hundred microliters of the isolated lymphocytes was taken and added to a plate, then the bacterial and fungal biofilm was diluted with PBS and filtered using 0.22-micron filters. Different volumes of the filtered biofilm were added to the plate (150-100-50-25 microliters) and incubated at 37°C for 24 hours in an incubator containing 5% CO₂. Then, MTT dye was added to the plate and incubated for 4 hours, followed by measurement of the results using an ELISA reader.

2.7. FTIR Spectroscopy Analysis:

FTIR spectral analysis is a fast and non-destructive technique that relies on the principle that atoms in molecules that are not closely bound absorb energy when exposed to infrared radiation (between 300 and 4000 cm⁻¹). The FTIR spectrum gave us information about the molecular structure of the sample and type of bond . This analysis was performed following the method described by Mostafa *et al.* (2012), where an appropriate amount of the biofilms was mixed with Potassium Bromide (KBr) and transferred to an FTIR spectrometer within the wavelength range of (400-4000) nanometers.

2.8. Scanning Electron Microscopy (SEM) studies:

The SEM samples were washed in a phosphate-buffered saline (PBS) solution and fixed with 1.5% glutaraldehyde in 0.2 M sodium cacodylate buffer, pH=7.4, for 24 hours at 48°C on a rotary shaker. The samples were then dehydrated through a graded series of acetone solutions (70, 80, 90, 96, and 100% acetone) for 20 minutes at room temperature. The critical-point-dried samples were then oriented, mounted on a metal stud, and coated with gold using a Polaron 5000 Sputtering System (Watford, England) before imaging. The samples were examined under a Japanese-made JSM6400 scanning electron microscope (JEOL) with digital imaging capabilities. The images were collected at an accelerating voltage of 15 kV, a filament current of 555 µA, and a working distance of 10 mm². All images were numbered as high-resolution TIFF files and then converted to high-quality JPEG files using Adobe Photoshop 7.0 (Kaniaet *al.*, 2010). The detection of biofilm formation was assessed in 40 samples employing Congo Red Agar medium following (Oliveira and Cunha, 2010,Dheebet *al.*,2022).

3. Results and Discussion

3.1. Detection of biofilm production using Congo Red Agar:

Out of the 40 isolates tested, 40% were found to produce a biofilm on the medium. This result agrees with the study conducted by Saxenaet *al.* (2014), who reported a biofilm-producing isolate rate of 41.8% on Congo Red Agar medium. However, the results do not agree with those of (Khalaf, 2016, Awad *et al.*,2020), where the biofilm-producing isolate rate was 51.6%.

These results were obtained by observing the colony morphology on Congo Red Agar medium (Figure 1) as described by (Oliveira and Cunha, 2010). Biofilm-producing isolates appear as dry, black, or shiny colonies, while non-producing isolates appear as light pink colonies. The color change in colonies that occurred in the later stages of the incubation period might be due to the presence of secondary metabolites. The use of 5% sucrose or glucose is described as a key factor in determining the production of exopolysaccharides using nutrient-rich media (Oliveira and Cunha, 2010). The color change might also be due to the direct binding of Congo Red dye to certain sugars that make up certain complexes (Hassan *et al.*, 2011).



Figure 1. A biofilm-producing isolate of *C. albicans* is shown in bright black color on the surface of Congo Red Agar medium.

The effect of the antibiotic gentamicin on the biofilm production of *K. pneumoniae* isolates Table (1) shows the mean values of biofilm production from twelve *K. pneumoniae* strains and the inhibitory effect of gentamicin on biofilm production efficiency at 0%, 25%, 50%, and 75% concentrations. Isolate A12 had the highest significant ($P < 0.05$) biofilm production of 0.503 nm, while strain A6 had the lowest rate of 0.292 nm. A 75% concentration of gentamicin resulted in a 74.9% decrease in biofilm production to 0.187 nm compared to the control

Table 1. Effects of concentration gentamicin on biofilm production in *K. pneumoniae* bacteria.

Biofilm Conc. (%)	control	25	50	75	Biofilms average
<i>K.pneumoniae</i> isolates					
A1	0.728 cde	0.626 def	0.217 j	0.202 j	0.443 ab
A2	0.690 c-f	0.430 gh	0.196 j	0.197 j	0.378 b-e
A3	0.768 bed	0.321 hij	0.188 j	0.175 j	0.363 b-f
A4	0.737 cde	0.400 hi	0.194 j	0.163 j	0.374 b-f
A5	0.596 ef	0.242 ij	0.209 j	0.165 j	0.303 ef
A6	0.559 fg	0.207 j	0.226 j	0.177 j	0.292 f
A7	0.662 def	0.228 j	0.220 j	0.210 j	0.330 def
A8	0.718 c-f	0.273 hij	0.215 j	0.168 j	0.343 c-f
A9	0.776 bed	0.293 hij	0.204 j	0.172 j	0.361 c-f
A10	0.949 a	0.320 hij	0.185 j	0.210 j	0.416 bc
A11	0.904 ab	0.313 hij	0.185 j	0.157 j	0.390 bcd
A12	0.848 abc	0.724 cde	0.195 j	0.245 ij	0.503 a
Concentration average	0.745 a	0.365 b	0.203 c		

*Means with the same letter are not significantly different according to the Duncan test ($P \leq 0.05$).

3.2. Effect of the antifungal fluconazole on the biofilms produced by *C. albicans*

The data presented in Table 2 exhibits the average biofilm production of twelve strains of *C. albicans* and the effect of 0, 25, 50, and 75% concentrations of fluconazole on the efficiency of biofilm production. It is observed that isolate A12 recorded the highest significant ($P < 0.05$) biofilm production of 0.608 nm, while strain A6 recorded the lowest rate of 0.349 nm. Regarding the effects of fluconazole, a concentration rate of 75% led to a decrease in biofilm production to 0.223 nm, a decrease of 64.32% compared to the control treatment which recorded a

treatment, which recorded a biofilm production rate of 0.745 units. The interaction between *K. pneumoniae* strain production and the effect of gentamicin showed that strain A10 had the highest biofilm production of 0.949 nm. in control treatments, while isolate A11 had the lowest production of 0.157 nm. in the treatment of 75% concentration of gentamicin.

These results are consistent with those obtained by Cadavid and Echeverri (2019), who studied the gentamicin sensitivity of mature *K. pneumoniae* biofilms and found that adding gentamicin (1.0 $\mu\text{g/mL}$) to the mature biofilm formed in the presence of inhibitors (2-hydroxycinnamic acid and 3-methyl-2(5H)-furanone) led to a reduction of the remaining biofilm by 42.51% and 33.82%, respectively. The biofilms of *K. pneumoniae* isolates examined in this study showed a significant decrease in production efficiency due to exposure to several antibiotics, including gentamicin (Geladariet al., 2019). In an earlier study, *K. pneumoniae* biofilms in the laboratory revealed that the isolates were widely resistant to gentamicin; however, these isolates formed relatively low-mass biofilms (Naparsteket al. 2014). The differences in the abilities of the studied isolates to form biofilms were the cause of their sensitivity to antibiotics. Moreover, the thick matrix outside the cell impedes the spread of antibiotics, leading to decreased antibiotic activity (Flemminget al., 2016).

biofilm production rate of 0.625 units. The interaction between *C. albicans* strains biofilm production and the effect of the antifungal fluconazole showed that isolate A12 had the highest biofilm production among the control treatments, reaching 1.117 nm, while the lowest production of 0.121 nm was recorded for isolate A6 in the 75% fluconazole concentration treatment.

The results of the present study indicate that continuous flow (60 ml per hour) of liquid through growing biofilms of *C. albicans* enhances matrix synthesis to a degree that significantly increases resistance to fluconazole. The biofilms of *C. albicans* grown under steady flow were

completely sensitive to the effects of fluconazole when exposed to high concentrations of the drugs. This is attributed to the sensitivity of the biofilm produced by *C.*

albicans due to high drug penetration rates through these biofilms (Al-Fattani and Douglas, 2006; Dheebet *al.*, 2015).

Table 2. Effects of concentration fluconazole on the production of biofilms by *C. albicans* isolates.

Biofilms Conc. (%)	control	25	50	75	Biofilms average
<i>C. albicans</i> isolates					
A1	0.668 b	0.396 k-n	0.339 n-r	0.264 s-v	0.417 cd
A2	0.641 bc	0.370 l-p	0.272 r-v	0.169 way	0.363 f
A3	0.563 def	0.381 l-o	0.318 o-s	0.247 s-v	0.377 of
A4	0.485 g-j	0.444 i-l	0.341 n-r	0.211 vwx	0.370 f
A5	0.613 bcd	0.385 l-o	0.316 o-t	0.211 vwx	0.381 of
A6	0.502 f-i	0.417 j-m	0.358 m-p	0.121 y	0.349 f
A7	0.465 h-k	0.418 j-m	0.351 m-q	0.300 p-u	0.383 def
A8	0.667 b	0.527 e-h	0.370 l-p	0.242 tuv	0.451 b
A9	0.648 bc	0.524 e-h	0.226 u-x	0.227 u-x	0.406 cde
A10	0.539 e-h	0.475 hij	0.255 s-v	0.164 xy	0.358 f
A11	0.590 cde	0.482 g-j	0.375 l-o	0.240 uvw	0.4218 bc
A12	1.117 a	0.551 d-g	0.486 g-j	0.279 q-v	0.608 a
Concentration average	0.625 a	0.447 b	0.334 c	0.223 d	

*Means with the same letter are not significantly different according to the Duncan test ($P \leq 0.05$).

3.3. Biofilm examination using electron microscopy:

The present study employed a scanning electron microscope (SEM) by Japanese-made JSM6400 scanning electron microscope (JEOL), to examine and visualize the composition of biofilms on surfaces (Figure 2).

At low magnification, irregular formations packed on a flat surface were observed, and at high magnification (Figure 2- K1 and C1) these formations showed bacterial cells with disk-shaped and round shape outlines (Figure 2 K1).

In addition to the bacterial colonies, scattered *C. albicans* cells were observed, most of which had round cell-like structures (Figure 1C). Some surface areas showed scaffolds of bacterial cells and yeast-like single-celled fungal cells (Figure 2- K3 and C3). Bacterial cells were visualized on the external surface at a single-cell level (Figure 1- K4 and C4). Dense formations of microorganisms were observed in some areas, with disk-shaped structures of bacterial cells and single-celled yeast-like cells. Although differences in bacterial and yeast growth can be observed, overall, the biofilm of the

pathogens showed abundant growth and dense colonization of the surface under SEM, as single-type cells of *C. albicans* and *K. pneumoniae* were well-cohesive and evenly distributed on the surface (Figure 2- K2 and C2).

Yeast buds were also seen clustered either in pairs or in groups with some recently formed yeast. Both the biofilm of *C. albicans* and *K. pneumoniae* showed increasing numbers of cellular layers with a recognizable extracellular matrix, and the biofilms of both pathogens were relatively thick and multilayered, although the extracellular matrix was barely visible (Figure 2- K4 and C4).

The diameters of some *K. pneumoniae* cells ranged from 0.18-0.47 nanometers (Figure 1- K2), while the diameters of *C. albicans* cells ranged from 121.82-133.89 nanometers (Figure 1- C5). However, in the visual examination using SEM, the biofilm showed few layers of cells, along with abundant cellular debris, alongside morphologically altered and degraded yeast cells (Figure 2- K2 and C2). Interestingly, most of the bacteria were observed adhering to the surface.

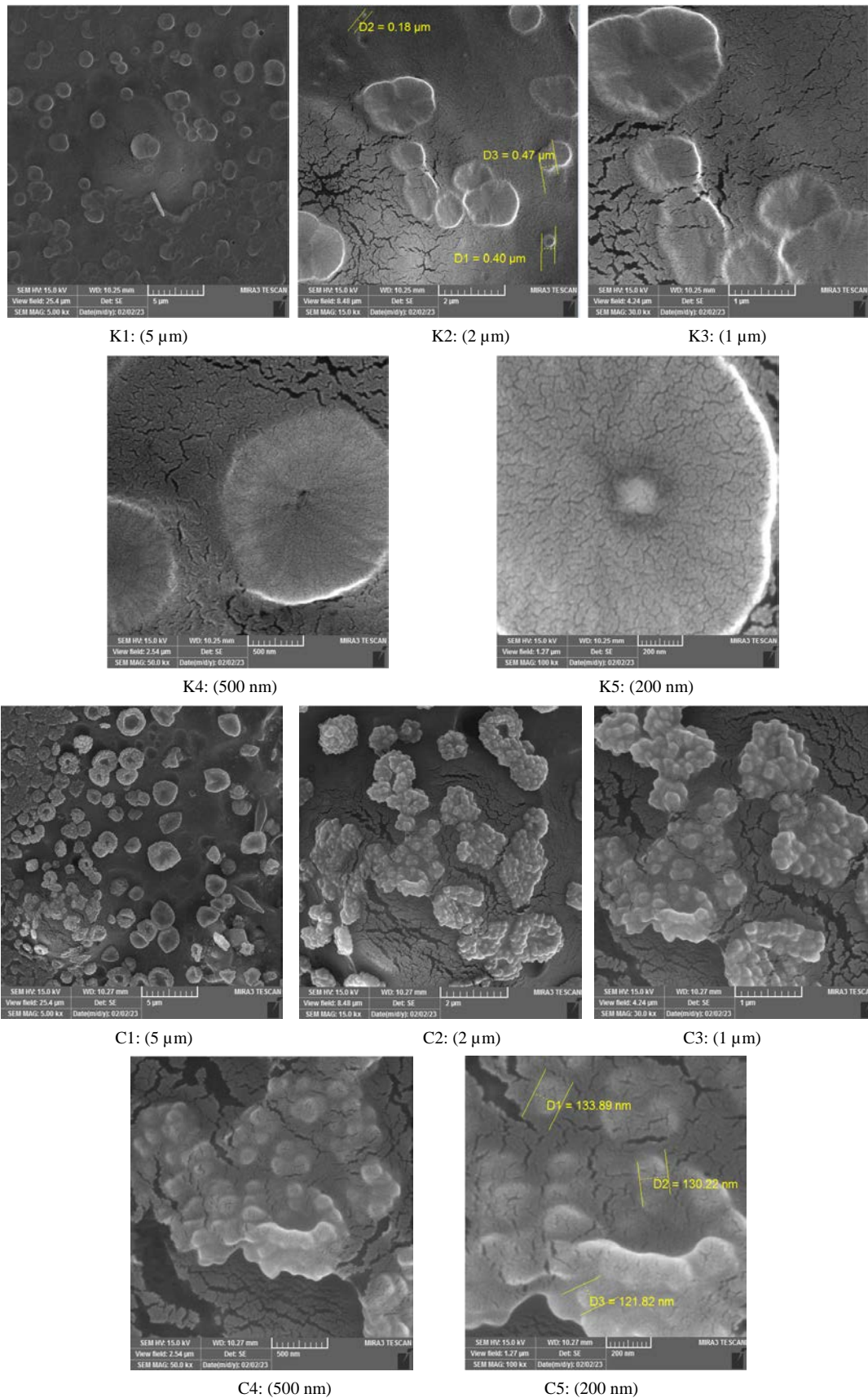


Figure 2. SEM results of the biofilms of *K. pneumoniae* bacteria and *C. albicans*.

Quantitatively, lower numbers of *K. pneumoniae* clusters were observed compared to *C. albicans*, and a thin and sparse biofilm was formed by fewer *K. pneumoniae* cells after initial colonization. In addition, there were

variable-shaped exploding vacuoles of *C. albicans*, and the biofilm showed a greater thickness compared to *K. pneumoniae*. Both *C. albicans* and *K. pneumoniae* biofilms showed an organized structure to an acceptable degree,

where the yeast was evenly distributed with minimal extracellular material, dead cells, and cellular debris. The mature biofilm showed distinct and thick layered structures (Figure 2- K2 and C2). The presence of dark areas within the biofilm can also be explained by the water channels present, as well as the heterogeneous production of matrix and different external sugars within the biofilm.

3.4. Biofilms analysis using Fourier transform infrared spectroscopy (FTIR)

FTIR spectral analysis was recently used in microbial biofilm tests (Tugarova *et al.*, 2017, Abed *et al.*, 2022) owing to its advantages of use. The study used the strains that showed the highest activities in producing and manufacturing biofilm to analyze the components of the biofilm produced by *C. albicans* and *K. pneumoniae*.

Figure (3) shows the results of FTIR analysis of the biofilms produced by *K. pneumoniae* bacteria. The results indicate a distinctive absorption band at the frequency of 3425 cm^{-1} (O-H stretching), as well as an intense band at 1647 cm^{-1} (C=O stretching of carboxylate). Medium bands were observed at the frequency of 526 , 543 , and 570 cm^{-1} (β 1-6 of Mannans), 1060 , 1074 , and 1120 cm^{-1} (β 1-3 of Glucose), 1409 and 1461 cm^{-1} (Bending of $-\delta\text{CH}_2$, δCH_3 from proteins-amide III), and 2981 cm^{-1} (C-H stretching). The remaining bands were weak.

The FTIR spectroscopic appearance obtained in the mid and far infrared regions revealed the absorption of

many compounds present in the biofilm matrix of *K. pneumoniae*. The obtained spectral ranges showed associations with Mannans at low wavelengths (Singh *et al.*, 2019). The band of the C=O carboxyl which was observed indicates the presence of sugar acids and a broad range of proteins (amide II) (Lal *et al.*, 2010; Hussain *et al.*, 2017). The absorption of the carbonyl amide bond is attributed to the presence of γ -lactone and ketone carbonyls (Wu *et al.*, 2011; Hussein *et al.*, 2019). These results confirm the presence of the lactone ring in biofilm-producing strains. The obtained spectra were very broad and, in some cases, overlapped with other ranges due to the presence of other compounds (El-Hilali *et al.*, 2016; Rosa *et al.*, 2016).

The presence of carboxyl groups may provide some adaptive advantages regarding the isolation of divalent cations' needs. The carboxyl group may also act as functional parts to generate new or modified polymers, which may enhance bacterial infection or virulence or both (Dheeb *et al.*, 2014; Baum *et al.*, 2009). The C-H stretching also indicates the movement or vibration of the carbon-hydrogen bond in the bacterial biofilms. With this vibration, the bond between the C and H atoms expands and contracts several times per second regularly, and this vibration can reveal certain molecular properties such as its structure and chemical composition (Singh *et al.*, 2019; Dheeb *et al.*, 2019, Hashim *et al.*, 2023).

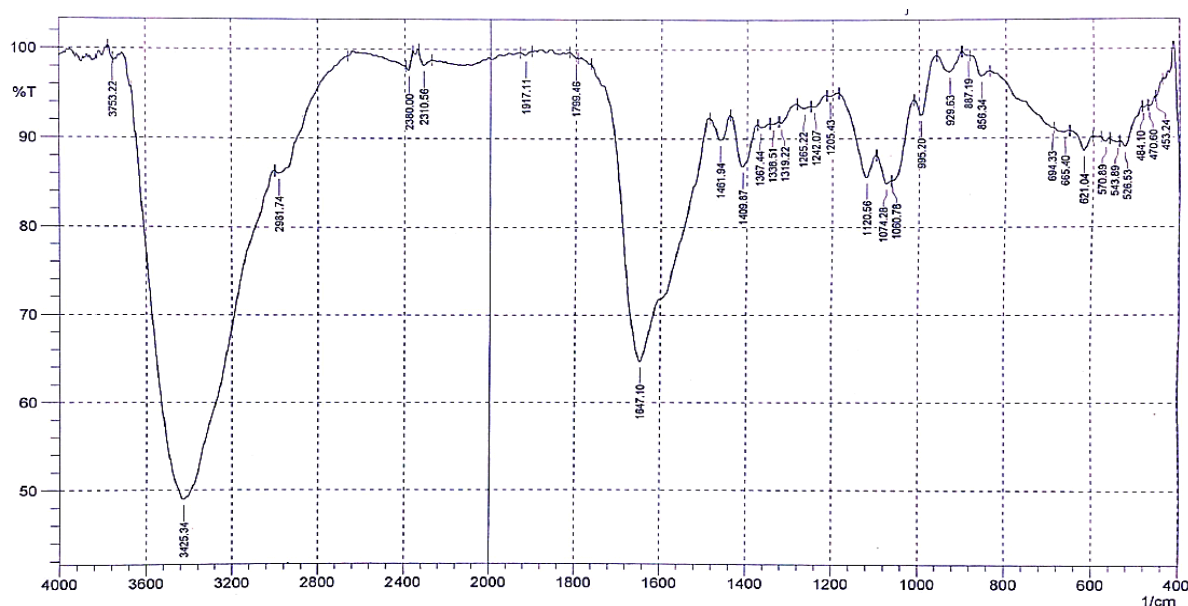


Figure 3. Analysis of the biofilm of *K. pneumoniae* bacteria using FTIR infrared spectroscopy, at spectral bands $400 - 4000\text{ cm}^{-1}$.

FTIR spectroscopy allows for the comparison of the spectra of biofilms produced by *C. albicans* yeast. The FTIR spectra of the biofilm (Figure 4) exhibit distinctive absorption bands at frequencies of 3411 and 3429 cm^{-1} (O-H stretching), as well as intense bands at a frequency of 1641 cm^{-1} (C=O stretching of carboxylate) and a frequency of 1112 cm^{-1} (Glucose-Acetyl group compounds). The plotted data also revealed moderate bands at frequencies of 1053 and 1076 cm^{-1} (Glucose β 1-3) and 1384 cm^{-1} (C-C ring stretching), while the remaining bands had weak intensities.

The high absorption peaks indicate the chemical compounds (carbohydrates) present in the biofilm

produced by *C. albicans*. The asymmetrical stretching of the carboxyl group indicates the presence of uronic acids, while the presence of acetyl group peaks indicates the presence of 20 acetyl groups, which ultimately reveal the presence of acetylated uronic acids (Lal *et al.*, 2010; Dahham *et al.*, 2019). The presence of carboxyl groups might provide some adaptive advantages in terms of isolating divalent cations for their needs. Moreover, the carboxyl group may also act as functional parts for generating new or modified polymers, which may enhance the pathogenesis of bacterial infections or fungi, or both (Baum *et al.*, 2009; Singh *et al.*, 2019, Salih *et al.*, 2023).

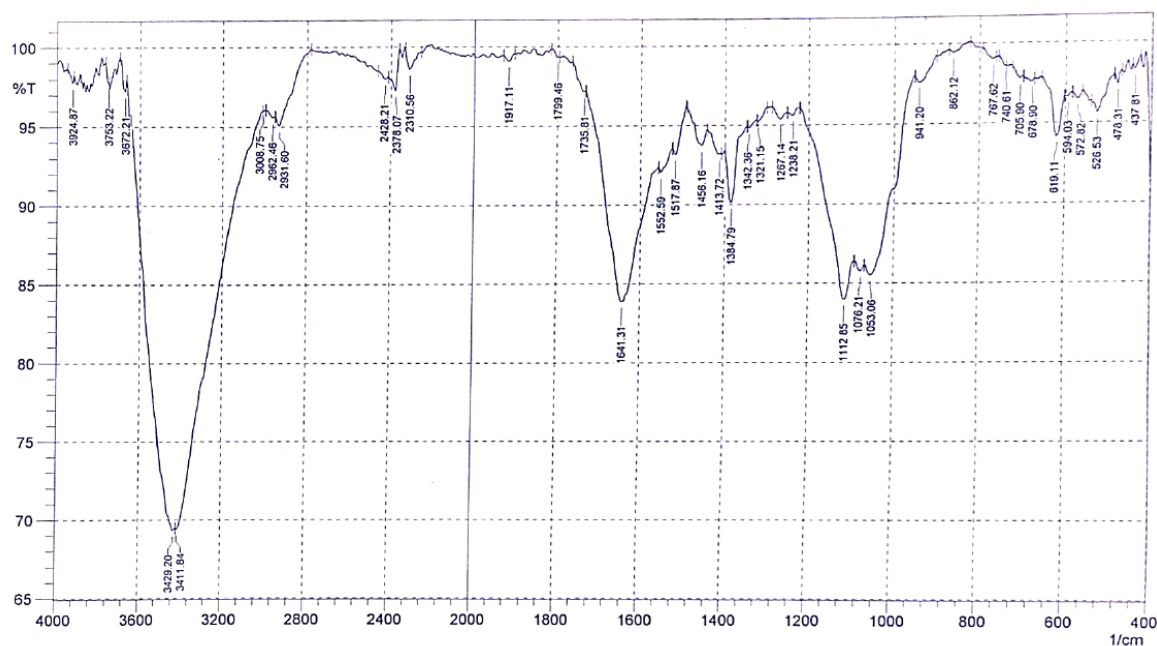


Figure 4. Analysis of the biofilm of *C. albicans* using FTIR infrared spectroscopy, at spectral bands 400 - 4000 cm^{-1} .

3.5. The effect of *K. pneumoniae* and *C. albicans* biofilms on lymphocytes:

The biofilms of pathogenic microorganisms might affect the ability of the immune system to recognize and fight them. For example, some pathogens like *C. albicans* can alter the structure of their biofilm to hide them from the immune system, making them less susceptible to targeting (Abdulbaqi *et al.*, 2018; Pontes *et al.*, 2022). Clinically, infections related to multi-microbial biofilms lead to a complicated diagnosis and inappropriate treatment which might cause a much higher mortality rate compared to mono-species biofilm infections, especially those caused by mixed fungal and bacterial biofilms. The latter type of biofilm has become a major public health problem through its transmission via medical devices such as urinary catheters (Bander *et al.*, 2015; Rodrigues *et al.*, 2019).

The percentage of cytotoxicity increased with increasing concentrations. The highest volume (100 $\mu\text{L}/\text{mL}$) of biofilm of *C. albicans* showed the highest inhibition of 74.82%, while the lowest concentrations showed 71.4%, 60.1%, and 55.2% of inhibition,

respectively, compared with the negative control as shown in the Table (3).

As for *K. pneumoniae*, the results in Table (3) show that the cytotoxicity percentage increased with increasing concentrations where the highest volume (150 $\mu\text{L}/\text{mL}$) of biofilm *K. pneumoniae* showed the highest inhibition of 34.8%, while the lowest concentrations showed 31.9%, 30.03% and 26.08% of inhibition, respectively, compared with the negative control as shown in the Table (3).

According to the results in Table (3), the biofilm mixture of the bacteria and fungus used in the study showed the highest inhibition of 69.5% at a volume of (100 $\mu\text{L}/\text{mL}$).

Due to the high heterogeneity of human microbial flora (bacteria, fungi, and viruses), polymicrobial biofilms are often co-isolated from the body. In these microbial consortia, various types of interactions can occur between microorganisms, such as mutualism, antagonism, and coexistence, making polymicrobial biofilms more complex to manage than mono-microbial ones (Dheeb *et al.*, 2016, Costa-Orlandiet *et al.*, 2017; Al-Tekreeti *et al.*, 2017).

Table 3. Inhibitory effect of lymphocytes on the individual and combined biofilm volumes of *C. albicans* and *K. pneumoniae*.

Volumes of biofilm (μL)	<i>K. pneumoniae</i>		<i>C. albicans</i>		<i>K. pneumoniae</i> + <i>C. albicans</i>	
	Control	Growth inhibition (%)	Control	Growth inhibition (%)	Control	Growth inhibition (%)
150		34.8 a		71.40 b		65.51 b
100	2.024	31.9 b	1.549	74.82 a	0.751	69.5 a
50		30.03 c		60.10 c		26.63 c
25		26.08 d		55.20 d		5.85 d

*Means with the same letter are not significantly different according to the Duncan test ($P \leq 0.05$).

The results of cytotoxicity of *C. albicans* biofilm confirm that when using the volume of 150 μL which led to the highest inhibition of lymphocytes, at the same time 100 μL for *C. albicans*, it gave the highest inhibition of

lymphocytes. Whereas, when the combination biofilm of *C. albicans* and *K. pneumoniae* the inhibition rate of lymphocyte was higher in terms of volume 100 μL .

References

- Abdulbaqi, N. J. and Dheeb, B. I. and Irshad, R. 2018. Expression of Biotransformation and Antioxidant Genes in the Liver of Albino Mice after Exposure to Aflatoxin B1 and an Antioxidant Sourced from Turmeric (*Curcuma longa*). *Jordan J of Biol Sci*; **11(2)**:89 – 93.
- Abdullah, H.I., Hammadi, S.Y., Hussein, A.S., Dheeb, B.I. 2019. Investigation of genetic diversity and relationships among the clinical candida species using random amplified polymorphic DNA (RAPD) analysis. *Research Journal of*, **14**(Special Issue 1), pp. 6–13.
- Abed, S.M., Farhan, M.G., Madhloom, N.K., Dheeb, D.I. 2022. Magnetic Field Exposure to Clinical Isolates of *Acinetobacter baumannii*. *Biomed Pharmacol J*; **15(4)**.
- Adriana, M.N.; Gloria, M.D.; David, S.P.; Jose, A.V.; Patricia, M.B. and Antonio, A.R. 2013. Comparison of biofilm and attachment mechanisms of aphytopathological and clinical isolate of *Klebsiellapneumoniae Subsp.pneumoniae*. *J. Scientific World*. **6P**.
- Al-Fattani, M. A., and Douglas, L. J. 2006. Biofilm matrix of *Candida albicans* and *Candida tropicalis*: chemical composition and role in drug resistance. *J of medical microbiology*, **55(8)**: 999-1008.
- Al-Tekreeti, A. R., Al-Halbosi, M. M. F., Dheeb, B. I., Hashim, A. J. and Al-Zuhairi, A. F. H. 2017. Molecular identification of clinical Candida isolates by simple and randomly amplified polymorphic DNA-PCR. *Arab J Sci Eng*. **017-2762-1**.
- Anju, V. T., Busi, S., Imchen, M., Kumavath, R., Mohan, M. S., Salim, S. A., ... and Dyavaiah, M. 2022. Polymicrobial Infections and Biofilms: Clinical Significance and Eradication Strategies. *Antibiotics*, **11(12)**:1731.
- Aubertine, C. L., Rivera, M., Rohan, S. M., and Larone, D. H. 2006. Comparative study of the new colorimetric VITEK 2 yeast identification card versus the older fluorometric card and CHROMagar Candida as a source medium with the new card. *J of clinical microbiol*, **44(1)**, 227-228.
- Awad, F.M., Al-Samarrai, A.H.M., Dheeb, B.I. 2020. Study of the inhibitory effects of rheum ribes extracts on a pathogenic fungi and cancer cell line. *Plant Archives*, **20(1)**, pp. 3161–3168.
- Baddley, J.W.; Pappas, P. G.; Smith, A.C. and Maser, S.A. 2003. Epidemiology of *Aspergillus terreus* at a university hospital. *J. Clin. Microbiol.*, **41(12)**: 5525- 5529.
- Bandara, H. M., Yau, J. Y., Watt, R. M., Jin, L. J. and Samaranyake, L. P. 2009. Escherichia coli and its lipopolysaccharide modulate in vitro Candida biofilm formation. *J Med Microbiol* **58**, 1623–1631.
- Bander, K. I., Mohammed, S. H., Thalij, K. M. and Dheeb, B.I. 2015. Survey Study of the Allergic Fungi in Kirkuk Area and Use Molecular Detection for Identification. *I J S: B A R*. **19(1)**:383-397.
- Baum, M. M., Kainović, A., O’Keeffe, T., Pandita, R., McDonald, K., Wu, S. 2009. Characterization of structures in biofilms formed by *Pseudomonas fluorescens* isolated from soil. *BMC Microbiol*. **9**:103.
- Brooks, G. F.; Butel, J.S. and Morse, S.A. 2001. Jawetz, **Melnick, and Adelberg’s Medical Microbiology**. 20thed. Lange Medical Books, McGraw-Hill Company, New York, USA.
- Cadavid, E., and Echeverri, F. 2019. The search for natural inhibitors of biofilm formation and the activity of the autoinductor C6-AHL in *Klebsiella pneumoniae* ATCC 13884. *Biomolecules*, **9(2)**, 49.
- Costa-Orlandi, C. B., Sardi, J. C., Pitangui, N. S., De Oliveira, H. C., Scorzoni, L., Galeane, M. C. and Mendes-Giannini, M. J. S. 2017. Fungal biofilms and polymicrobial diseases. *Journal of Fungi*, **3(2)**, 22.
- Dahham, MT, Omar, AF, Dheeb BI. 2019. Synergistic effect of tea tree oil on fungi causing vaginal thrush in pregnant women. *J of Bio Res C*; **13 (2)**:35-44.
- Dheeb BI, Al-dujayli SMA, Ibrahim IM, Abbas QA. 2019. Study the Antifungal Activity of ZnS:Mn Nanoparticles Against Some Isolated Pathogenic Fungi. *J of Phy: Conference Series*, **1178**, 46–52.
- Dheeb, B. I. 2014. Immunohistochemical study of Tumor Necrosis Factor -alpha(TNF- α) expression in lung, liver, and spleen during aspergillosis infection. *BMC genomics*. **15 (2)**: 71.
- Dheeb, B.I., Al-Mashhadani, I.I., Ismail, E.N., Majeed, S.M. and Majeed, D.M., 2014. A study of the Expression of Aflatoxin B1 Regulatory Gene in Clinical and Environmental *Aspergillus flavus* using Real-time PCR. *IJS: BAR*, **17(1)**:417-427.
- Dheeb, B.I., Al-Mudallal, N.H., Salman, Z.A., Ali, M., Nouri, M.A., Hussain, H.T. and Abdulredha, S.S., 2015. The inhibitory effects of human, camel and cow's milk against some pathogenic fungi in Iraq. *Jordan J of Biol Sci*, **14 (3)**:pp1-5.
- Dheeb, B.I., Hashim, S.S., Hussein, H.S., Hamada, T.A. 2022. Study of TGF- β Immune Marker Expression in Mice Exposed to Candida Spp. *AIP Conference Proceedings*. **2(9)**:45-51
- Dheeb, B.I., Al-Halbosi, M.M.F., Al Lihabi, R.K., Khashman, B.M. 2016. The effects of *Rubus idaeus* extract on normal human lymphocytes and cancer cell line. *BMC genomics*. **17 (6)**:18.
- El-Hilali, F., El-Hilali, H., Dheeb, B.I., Traore, B.M. and Messouak, M., 2016. Blood Transfusion Utility During Cardiopulmonary Bypass and Correlation with Key-Biochemical Laboratory Findings: A New Approach to Identify Preventive and Risk Factors (1-Year Practice at University Hospital Hassan-II of Fez). *Biochem Anal Biochem* **5(3)**:54-60.
- Ellen, J.B.; Lance, R.P. and Sydney, M.F. 1994. Bailey and Scott’s Diagnostic Microbiology, **9th ed. Mosby-year book**, Inc. st – Louis, Missouri, USA.
- Ellis, D.; Stephan, D.; Helen, A.; Rosemary, H. and Roben, B. 2007. Description of Medical Fungi. **2nd ed. Ltd. Australia**: 23-40.
- Emmons, C. W.; Binford, C. H. and Utz, J. P. 1974. Candidiasis. *In Medical Mycology*. Lea and Febiger ed. 2nd ed. Philadelphia. **Ch. 14**: 167-182.
- Erdogan, A., and Rao, S. S. 2015. Small intestinal fungal overgrowth. *Current gastroenterology reports*, **17(4)**:1-7.
- Flemming, HC, Wingender J, Szewzyk U, Steinberg P, Rice SA, Kjelleberg S. 2016. Biofilms: an emergent form of bacterial life. *Nat Rev Microbiol*; **14**:563–575.
- Galdiero, E., Ricciardelli, A., D’Angelo, C., de Alteriis, E., Maione, A., Albarano, L., and Parrilli, E. 2021. Pentadecanoic acid against *Candida albicans*-*Klebsiella pneumoniae* biofilm: Towards the development of an anti-biofilm coating to prevent polymicrobial infections. *Research in Microbiology*; **172**:(7-8).
- Geladari, A., Simitsopoulou, M., Antachopoulos, C., and Roilides, E. 2019. Dose-dependent synergistic interactions of colistin with rifampin, meropenem, and tigecycline against carbapenem-resistant *Klebsiella pneumoniae* biofilms. *Antimicrobial agents and chemotherapy*; **63(3)**: 7-18.
- Greenwood, D.; Slack, R. C. B.; Peutherer, J. F. and Barer, M. R. 2007. *Medical Microbiology. A Guide to Microbial Infections: Pathogenesis, Immunity, Laboratory Diagnosis, and Control*. 6thed. Churchill Livingstone.

- Hall-Stoodley, L., Stoodley P., Kathju S., Hoiby N., Moser C., Costerton J W. 2012. Towards diagnostic guidelines for biofilm-associated infections. *FEMS Immunol Med Microbiol.* **65**: 127-145.
- Hassan A, Usman J, Kaleem F, Omair M, Khalid A, Iqbal M. 2011. Evaluation of different detection methods of biofilm formation in the clinical isolates. *Braz J Infect Dis*; **15**:305-11.
- Hashim S. S, Mahmood Z. F, Abdulateef S. F, Dheeb B. I. 2023. Evaluation Cytotoxicity Effects of Centaurea Cineraria Extracts Against some of Cancer Cell Lines. *Biomed Pharmacol J.* **16**(1).
- Herrling, M. P. S. Lackner, H. Nirschl, H. Hornand G. Guthausen. 2019. in Annual Reports on NMR Spectroscopy, ed. G.A. Webb, Academic Press; Elsevier Science and Technology, Oxford, 163–213.
- Hospenthal, Beckius, M.I., Floyd, K.I.; Horvath. 2006. Presumptive identification of *Candida* species than *C. albicans*, *C. krusei*, and *C. tropicalis* with the chromogenic medium CHROMagar *Candida*; **3**(5):1-10.
- Hussain AF, Sulaiman GM, Dheeb BI, Hashim AJ. 2018. Histopathological changes and expression of transforming growth factor beta (TGF- β 3) in mice exposed to gliotoxin. *Journal of K S U – Science.* **27**, 193–197.
- Hussein, A., Sulaiman, G. and Hashim, A.J., 2017. Improving conditions for gliotoxin production by local isolates of *Aspergillus fumigatus*. *Journal of b r c*; **11**(1):14-24.
- Hussein, H.S., Dheeb, B.I. and Hamada, T.A., 2019. Studying the candida resistance and sensitivity for some antifungals. *Journal of B R C*; **13**(2) :26-34.
- Ibrahim, I.M., Ali, I.M., Dheeb, B.I., Abas, Q.A., Ramizy, A., Eisa, M.H. and Aljameel, A.I., 2017. Antifungal activity of wide band gap Thioglycolic acid capped ZnS: Mn semiconductor nanoparticles against some pathogenic fungi. *Materials Science and Engineering: C*; **73**:665-669.
- Lal, P., Sharma, D., Pruthi, P., and Pruthi, V. 2010. Exopolysaccharide analysis of biofilm-forming *Candida albicans*. *J. Appl. Microbiol.* **109**, 128–136.
- Maione, A., de Alteriis, E., Carraturo, F., Galdiero, S., Falanga, A., Guida, M., ... and Galdiero, E. 2021. The membranotropic peptide gH625 to combat mixed *Candida albicans*/*Klebsiella pneumoniae* biofilm: Correlation between in vitro anti-biofilm activity and in vivo antimicrobial protection. *Journal of Fungi*; **7**(1): 26.
- Martins, N., Ferreira, I. C., Barros, L., Silva, S., and Henriques, M. 2014. Candidiasis: predisposing factors, prevention, diagnosis, and alternative treatment. *Mycopathologia*; **177**(5):223-240.
- McCarty, S., Woods, E., and Percival, S. L. 2014. Biofilms: From concept to reality. In *Biofilms in Infection Prevention and Control*. 143-163 Academic Press.
- Mostafa, M.H., Eman H. I., Fatma, E. 2012. Biosynthesis of Au nanoparticles using olive leaf extract, *Arabian J of Chem*; **1** 5: 431–437.
- Muhammad MH, Idris AL, Fan X, Guo Y, Yu Y, Jin X, Qiu J, Guan X, and Huang T .2020. Beyond Risk: Bacterial Biofilms and Their Regulating Approaches. *Front. Microbiol.* **11**:928. doi: 10.3389/fmicb.2020.00928.
- Naparstek, L, Carmeli Y, Navon-Venezia S, Banin E. 2014. Biofilm formation and susceptibility to gentamicin and colistin of extremely drug-resistant KPC-producing *Klebsiella pneumoniae*. *J Antimicrob Chemother*; **69**:1027–1034.
- Nelson, S. 2001. Novel Nonantibiotic therapies for pneumonia. *Cytochin. Host defence. Chest.*, **119**: 4195- 4255.
- Nobile, CJ, Johnson AD. 2015. *Candida albicans* biofilms and human disease. *Annu Rev Microbiol*; **69**:71–92.
- Nouri, M.A., Al-Halbosiy, M.M., Dheeb, B.I. and Hashim, A.J., 2015. Cytotoxicity and genotoxicity of gliotoxin on human lymphocytes in vitro. *Journal of King Saud University-Science*; **27**(3):193-197.
- Oliveira, A.; Cunha, M.L. 2010. Comparison of methods for the detection of biofilm production in coagulase-negative Staphylococci. *BMC. Res*; **3**:260.
- Pontes, J. T. C. D., Toledo Borges, A. B., Roque-Borda, C. A., and Pavan, F. R. 2022. Antimicrobial peptides as an alternative for the eradication of bacterial biofilms of multi-drug resistant bacteria. *Pharmaceutics*; **14**(3): 642.
- Rassin, N.K., Al-judy, N.J. and Dheeb, B.I., 2015. Molecular Identification of *Aspergillus fumigatus* Using ISSR and RAPD Markers. *Iraqi J of Sci*, **56**(4):2788-2797.
- Rather, M.A., K. Gupta, P. Bardhan, M. Borah, A. Sarkar, K. S. H. Eldiehy, S. Bhuyan, M. Mandal. 2021. Microbial biofilm: A matter of grave concern for human health and food industry, *Journal of Basic Microbiology* : 1-16.
- Rodrigues, M. E., Gomes, F., and Rodrigues, C. F. 2019. *Candida* spp./bacteria mixed biofilms. *Journal of Fungi*; **6**(1): 5.
- Rosa, B., Victor, T., Ricardo, V. R., Alfredo, M., and Octavio, A. 2016. Anti-biofilm activity of ibuprofen and diclofenac against some biofilm-producing *Escherichia coli* and *Klebsiella pneumoniae* uropathogens. *African J of Microb Res*; **10**(40): 1675-1684.
- Salih, I.I., Seddiq, S.H., Hashim, S.S., Dheeb, B.I. 2022. Application of Omics and Proteomics in Fungi. *AIP Conference Proceedings*; **4**(2):34-35.
- Sánchez-Gómez, S., Ferrer-Espada, R., Stewart, P. S., Pitts, B., Lohner, K., and Martínez de Tejada, G. 2015. Antimicrobial activity of synthetic cationic peptides and lipopeptides derived from human lactoferricin against *Pseudomonas aeruginosa* planktonic cultures and biofilms. *BMC Microb*; **15**:1-11.
- Singh, A. K., Yadav, S., Chauhan, B. S., Nandy, N., Singh, R., Neogi, K., ... and Prakash, P. 2019. Classification of clinical isolates of *Klebsiella pneumoniae* based on their in vitro biofilm-forming capabilities and elucidation of the biofilm matrix chemistry with special reference to the protein content. *Frontiers in Microbiol*; **10**:669.
- Todar, K. 2007. The mechanism of bacterial pathogenicity. *Todars Textbook of Bacteriology. Wisconsin- Madison. Inc. United States of America.*
- Tugarova, A. V., Scheludko, A. V., Dyatlova, Y. A., Filip'echeva, Y. A., and Kamnev, A. A. 2017. FTIR spectroscopic study of biofilms formed by the rhizobacterium *Azospirillum brasilense* Sp245 and its mutant *Azospirillum brasilense* Sp245.1610. *Journal of Molec St.* **1140**, 142-147.
- Tutelyan, A.V.; Shlykova, D.S.; Voskanyan, S.L.; Gaponov, A.M.; Pisarev, V.M. 2022. Molecular Epidemiology of Hypervirulent *K. pneumoniae* and Problems of Health-Care Associated Infections. *Bull. Exp. Biol. Med.*, **172**:507–522.
- Wu, M.-C., Lin, T.-L., Hsieh, P.-F., Yang, H.-C., and Wang, J.-T. 2011. Isolation of genes involved in biofilm formation of a *Klebsiella pneumoniae* strain causing pyogenic liver abscess. *PLoS One* ;**6**: e23500.
- Wu, Y., Du, S., Johnson, J. L., Tung, H. Y., Landers, C. T., Liu, Y., and Corry, D. B. 2019. Microglia and amyloid precursor protein coordinate control of transient *Candida cerebritis* with memory deficits. *Nature communications*; **10**(1): 1-15.

Jordan Journal of Biological Sciences

An International Peer – Reviewed Research Journal

Published by the Deanship of Scientific Research, The Hashemite University, Zarqa, Jordan



Name: الاسم:

Specialty: التخصص:

Address: العنوان:

P.O. Box: صندوق البريد:

City & Postal Code: المدينة: الرمز البريدي:

Country: الدولة:

Phone: رقم الهاتف:

Fax No.: رقم الفاكس:

E-mail: البريد الإلكتروني:

Method of payment: طريقة الدفع:

Amount Enclosed: المبلغ المرفق:

Signature: التوقيع:

Cheque should be paid to Deanship of Research and Graduate Studies – The Hashemite University.

I would like to subscribe to the Journal

For

- One year
- Two years
- Three years

One Year Subscription Rates		
	Inside Jordan	Outside Jordan
Individuals	JD10	\$70
Students	JD5	\$35
Institutions	JD 20	\$90

Correspondence

Subscriptions and sales:

The Hashemite University
P.O. Box 330127-Zarqa 13115 – Jordan
Telephone: 00 962 5 3903333
Fax no. : 0096253903349
E. mail: jjbs@hu.edu.jo

المجلة الأردنية للعلوم الحياتية Jordan Journal of Biological Sciences (JJBS)

<http://jjbs.hu.edu.jo>

المجلة الأردنية للعلوم الحياتية: مجلة علمية عالمية محكمة ومفهرسة ومصنفة، تصدر عن الجامعة الهاشمية وبدعم من صندوق دعم البحث العلمي والإبتكار – وزارة التعليم العالي والبحث العلمي.

هيئة التحرير

رئيس التحرير

الأستاذ الدكتور

الجامعة الهاشمية، الزرقاء، الأردن

مساعد رئيس التحرير

الدكتور مهند عليان مساعدة

الجامعة الهاشمية، الزرقاء، الأردن

الأعضاء:

الأستاذ الدكتور خالد محمد خليفات

جامعة مؤتة

الاستاذ الدكتور ليث ناصر العيطان

جامعة العلوم و التكنولوجيا الأردنية

الأستاذ الدكتورة طارق حسن النجار

الجامعة الأردنية / العقبة

الأستاذ الدكتور وسام محمد هادي الخطيب

الجامعة اليرموك

الاستاذ الدكتور عبد اللطيف علي الغزاوي

الجامعة الهاشمية

الاستاذ الدكتور نضال احمد عودات

جامعة البلقاء التطبيقية

فريق الدعم:

المحرر اللغوي

الدكتور شادي نعامنة

تنفيذ وإخراج

م. مهند عقده

ترسل البحوث الى العنوان التالي:

رئيس تحرير المجلة الأردنية للعلوم الحياتية

الجامعة الهاشمية

ص.ب , 330127 , الزرقاء, 13115 , الأردن

هاتف: 0096253903333

E-mail: jjbs@hu.edu.jo, Website: www.jjbs.hu.edu.jo



المملكة الأردنية الهاشمية



المجلة الأردنية



للعلوم الحياتية

مجلة علمية عالمية محكمة

تصدر بدعم من صندوق دعم البحث العلمي و الابتكار



<http://jjbs.hu.edu.jo/>